INSTYTUT PODSTAWOWYCH PROBLEMÓW TECHNIKI

POLSKA AKADEMIA NAUK

ROZPRAWA DOKTORSKA

Piezoelektryczne polimerowe nanowłókna jako inteligentne podłoża komórkowe do zastosowań w inżynierii tkankowej

Piezoelectric polymeric nanofibers as smart scaffolds for tissue engineering applications

mgr inż. Angelika Zaszczyńska

Praca wykonana w Samodzielnej Pracowni Polimerów i Biomateriałów

pod kierunkiem Prof. dr hab. inż. Pawła Łukasza Sajkiewicza

Promotor pomocniczy: dr inż. Arkadiusz Dominik Gradys

WARSZAWA 2025

Z głęboką wdzięcznością pragnę złożyć serdeczne podziękowania wszystkim Osobom, które wniosły swój wkład w powstanie niniejszej rozprawy doktorskiej.

Przede wszystkim wyrażam najserdeczniejsze podziękowania

Panu Profesorowi Pawłowi Łukaszowi Sajkiewiczowi

Mojemu Mentorowi i Opiekunowi Naukowemu.

Za nieocenione wsparcie, inspirujące wskazówki, cierpliwość oraz mądrość, które towarzyszyły mi przez cały okres realizacji badań. Jego zaangażowanie, otwartość i życzliwość były dla mnie nieustającym źródłem motywacji i naukowej inspiracji.

Panu Doktorowi Arkadiuszowi Gradysowi

Za cenne uwagi, dzielenie się wiedzą i niezliczoną ilość godzin spędzonych na dyskusjach naukowych.

Pani Profesor Dorocie Kołbuk-Konieczny

Za motywację, istotne rady i wsparcie podczas prowadzenia badań.

Koleżankom i Kolegom za inspirujące rozmowy, wspólną naukę i wspaniałą atmosferę.

Narzeczonemu za nieoceniony humor, wsparcie, cierpliwość i wyrozumiałość.

Wszystkim Bliskim, którzy we mnie wierzyli.

Rodzicom

Streszczenie

W niniejszej rozprawie doktorskiej przedstawiono rezultaty badań piezoelektrycznych nanowłóknistych podłoży do hodowli komórkowych, z perspektywą ich zastosowania w inżynierii tkankowej, zwłaszcza w regeneracji ubytków układu nerwowego i kostnego. W ramach badań opracowano i zoptymalizowano proces elektroprzędzenia, kontrolując właściwości końcowe włókien z poli(fluorku winylidenu) (PVDF) oraz poli(L-laktydu) (PLLA), a także z dodatkami piezoelektrycznego hydroksyapatytu (nHA) lub nanocząstek złota (AuNPs). Kluczowym aspektem badań było określenie wpływu masy cząsteczkowej oraz wybranych istotnych parametrów procesu, takich jak prędkość obrotowa kolektora, szybkość podawania roztworu czy stężenie polimeru, na ukierunkowanie i morfologię włókien oraz ich właściwości piezoelektryczne i odpowiedź biologiczną.

Badania wykazały, że odpowiedni dobór parametrów elektroprzędzenia umożliwia otrzymanie jednorodnych włókien bez defektów strukturalnych (np. korali), zdolnych do generowania sygnałów elektrycznych. Badania metodami FTIR, WAXS i DSC pozwoliły określić kluczowe zależności pomiędzy strukturą a właściwościami włókien. Wykazano, że wprowadzenie dodatków, takich jak piezoelektryczny nHA i AuNPs, znacząco wpłynęło na poprawę właściwości piezoelektrycznych włókien poprzez wzrost zawartości faz piezoelektrycznych, stopnia krystaliczności oraz polarności powierzchni, co prowadzi do poprawy ich właściwości piezoelektrycznych.

Przeprowadzona analiza zwilżalności, energii swobodnej powierzchni oraz sorpcji wody pozwoliła wykazać, że zmiana ułożenia nanowłókien i wprowadzenie dodatków poprawiają biokompatybilność podłoży. Wysoka zwilżalność i zwiększona porowatość włókien PVDF i PLLA z dodatkami sprzyjają proliferacji komórek. Wyniki badań *in vitro* potwierdziły, że opracowane podłoża nie są cytotoksyczne oraz wykazują zdolność do wspierania wzrostu fibroblastów, osteoblastów, komórek macierzystych i komórek nerwowych. Obserwacje mikroskopowe wykazały, że ułożenie włókien ma istotny wpływ na organizację i migrację komórek, co sugeruje potencjalne zastosowanie ukierunkowanych nanowłókien w inżynierii tkankowej, zwłaszcza w regeneracji tkanki kostnej i nerwowej.

Podsumowując, praca dostarcza innowacyjnych wyników w zakresie projektowania i wytwarzania nanowłóknistych podłoży komórkowych o wysokiej piezoelektryczności, stanowiących perspektywiczny materiał do zastosowań w inżynierii tkanki kostnej i nerwowej. Uzyskane wyniki mogą stanowić fundament dla dalszych badań nad zastosowaniem nanomateriałów w medycynie regeneracyjnej, umożliwiając opracowanie inteligentnych i biokompatybilnych implantów wspomagających procesy naprawcze organizmu.

Abstract

In this doctoral dissertation, comprehensive research was conducted on nanofibrous cell scaffold with piezoelectric properties, intended for applications in tissue engineering, particularly in the regeneration of the nervous and skeletal systems. The electrospinning process was developed and optimized, enabling the controlled fabrication of poly(vinylidene fluoride) (PVDF) and poly(L-lactide) (PLLA) fibers with piezoelectric hydroxyapatite (nHA) and gold nanoparticles (AuNPs) addition. A key aspect of the study was determining the influence of the molecular weight of the polymer, as well as the process parameters, such as collector rotation speed, solution feed rate and concentration of the polymer, on fiber alignment and morphology, piezoelectric properties, and biocompatibility.

The studies demonstrated that appropriate selection of electrospinning parameters allows for the formation of fibers with high uniformity and free from structural defects (e.g., beads), while simultaneously enhancing their ability to generate electrical signals. Structural analysis using FTIR, WAXS, and DSC enabled the identification of key relationships between the molecular structure of the fibers and their functional properties. It was shown that the introduction of additives, such as piezoelectric nHA and AuNPs, significantly influences the content of piezoelectric phases, crystallinity degree, and polarization of nanofibers, leading to an enhancement of their piezoelectric properties.

Furthermore, a detailed analysis of wettability, surface energy, and water absorption was conducted, demonstrating that modifications in fiber alignment and the introduction of additives can improve biocompatibility. High wettability and increased porosity of PVDF and PLLA fibers with nHA addition promote cell adhesion and proliferation. The *in vitro* studies confirmed that the developed scaffolds exhibit no cytotoxicity and have the ability to support the growth of fibroblasts, osteoblasts, stromal cells and neural cells. Microscopic observations revealed that fiber alignment has a significant impact on cell organization and migration, suggesting the potential application of aligned nanofibers in tissue engineering, particularly in bone and neural tissue regeneration.

In summary, this study provides innovative solutions in the design and fabrication of nanofibrous cell scaffolds with high piezoelectricity, constituting a promising material for applications in bone and neural tissue engineering. The obtained results may serve as a foundation for further research on the application of nanomaterials in regenerative medicine, enabling the development of smart and bioactive implants that support the body's repair processes.

Spis treści

Lista skrótów

Ac	Aceton
ADSC	Komórki macierzyste pochodzące z ludzkiej tkanki tłuszczowej (*ang. human adipose-derived stromal cells)*
ANOVA	Jednoczynnikowa analiza wariancji (*ang. analysis of variance*)
ATR	Osłabione wewnętrzne odbicie *(ang. attenuated total reflection)*
AuNPs	Nanocząstki złota
DMEM	Zmodyfikowana pożywka Dulbecco Eagle
DMF	Dimetyloformamid (N,N′-dimetyloformamid)
DSC	Różnicowa kalorymetria skaningowa (a*ng. differential scanning calorimetry*)
ECM	Macierz zewnątrzkomórkowa (*ang. extracellular matrix*)
FM	Mikroskop fluorescencyjny
FTIR	Fourierowska spektroskopia w podczerwieni (*ang. Fourier transform infrared spectroscopy*)
FWHM	Szerokość połówkowa (*ang. full width at half maximum*)
HFIP	Heksafluoroizopropanol (1,1,1,3,3,3-hexafluoro-2-propanol)
hiPSC-NSC	Hodowla neuralnych komórek macierzystych wyprowadzonych z indukowanych pluripotencjalnych komórek macierzystych (*ang. human induced pluripotent stem cell-derived neural stem cell culture*)
L929	Linia komórkowa fibroblastów mysich
MG-63	Linia osteoblastopodobnych komórek ludzkich
M_w	Średnia wagowa masa cząsteczkowa
M_n	Średnia liczbowa masa cząsteczkowa
nHA	Hydroksyapatyt
PBS	Sól fizjologiczna buforowana fosforanami (*ang. phosphate-buffered saline*)
PLLA	Poli(L-laktyd) (*ang. poly(L-lactide*))
PVDF	Poli(fluorek winylidenu) (*ang. poly(vinylidene fluoride*))
SEM	Skaningowa mikroskopia elektronowa (*ang. scanning electron microscopy*)
SEM-EDS	Spektroskopia dyspersjna energii (*ang. energy dispersive spectroscopy*)
SFE	Energia swobodna powierzchni (*ang. surface free energy*)
TCP	Płytka hodowlana (*ang. tissue culture plate*)
T_g	Temperatura zeszklenia *(ang. glass transition temperature)*
THF	Tetrahydrofuran
WAXS	Szerokokątowe rozpraszanie rentgenowskie (*ang. wide-angle X-ray scattering*)
WCA	Kąt zwilżania wody (*ang. water contact angle*)
w/w	Proporcje wagowe

1. Wstęp

Współczesna medycyna stoi przed ogromnym wyzwaniem związanym z leczeniem i regeneracją uszkodzonych narządów oraz tkanek, takich jak tkanka nerwowa, skóra czy kości [1]. Zwiększająca się liczba pacjentów z urazami, powikłaniami pooperacyjnymi i chorobami intensyfikuje zapotrzebowanie na wprowadzanie nowocześniejszych metod leczenia, które będą bezpieczniejsze, skuteczniejsze oraz bardziej dostosowane do indywidualnych potrzeb pacjenta. W odpowiedzi na współczesne wyzwania inżynieria tkankowa (*ang. tissue engineering*) wyłania się jako dynamiczna i interdyscyplinarna dziedzina nauki na styku chemii, biologii, fizyki oraz nauki o materiałach [2].

W 1993 roku Profesor Robert Langer i Doktor Joseph Vacanti na łamach czasopisma *Science* zdefiniowali termin „inżynieria tkankowa" jako „interdyscyplinarna dziedzina, wykorzystująca podstawy inżynierii i nauk biologicznych w celu pozyskania biologicznych zamienników, które przywracają, utrzymują lub poprawiają funkcjonowanie organu" [3]. Zgodnie z definicją biomateriał to taka kombinacja substancji naturalnych lub syntetycznych, innych niż leki, które w dowolnym czasie mogą być wykorzystane do zastąpienia tkanki bądź organu, jednocześnie przejmując jego funkcję [4]. Inżynieria tkankowa koncentruje się na tworzeniu materiałów, które funkcjonalnie i strukturalnie odwzorowują naturalne środowisko komórkowe, czyli macierz zewnątrzkomórkową (ECM, *ang. extracellular matrix*) (Rys. 1). Zadaniem takich struktur jest tymczasowe wspieranie komórek poprzez zapewnienie im odpowiednich warunków do namnażania oraz tworzenia nowej, żywej tkanki. Macierz zewnątrzkomórkowa złożona jest m.in. z włókien białkowych, takich jak kolagen i elastyna, które pełnią funkcje takie jak przyłączanie komórek oraz przekazywanie sygnałów bioelektrycznych. Struktury ECM (Rys. 1) reagują na bodźce z otoczenia, takie jak bodźce mechaniczne, deformacje czy zmiany ciśnienia, przekształcając je w sygnały biochemiczne lub elektryczne, które wpływają na zachowanie komórek. Przekazywanie tych sygnałów może regulować kluczowe procesy komórkowe, takie jak migracja, proliferacja, różnicowanie czy apoptoza. W przypadku niektórych tkanek, zwłaszcza nerwowej i kostnej, właściwości elektroprzewodzące i elektroaktywne ECM mają szczególne znaczenie dla utrzymania funkcji fizjologicznych oraz procesów regeneracji. Inspirowane architekturą i właściwościami ECM polimerowe, piezoelektryczne podłoża komórkowe, odwzorowujące jej trójwymiarową organizację i charakterystykę biologiczną, uczestniczą również w przekazywaniu sygnałów bioelektrycznych. Celem opracowywania takich podłoży komórkowych jest nie tylko

odtworzenie ich struktury, lecz także przywrócenie zdolności ECM do dynamicznego przekazywania sygnałów międzykomórkowych.

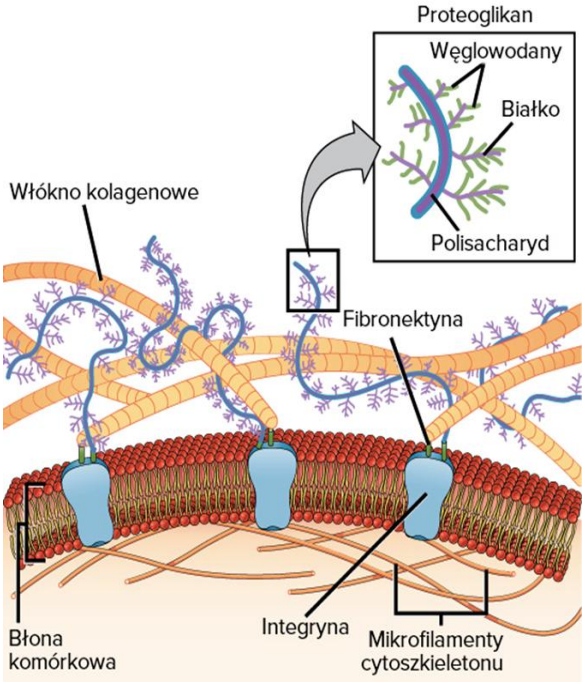

Rys 1. Schematyczny rysunek macierzy zewnątrzkomórkowej (ECM) [5].

W ostatnich latach w dziedzinie inżynierii tkankowej zaobserwowano wzrost zainteresowania naukowego i technologicznego badaniami nad rozwojem kompozytów [6], hydrożeli [7] oraz projektowaniem inteligentnych materiałów (*ang. smart materials*) [8–10]. Inteligentne materiały są opracowywane tak, aby reagowały na bodźce zewnętrzne (fizyczne, chemiczne, mechaniczne), zachowując się w ten sposób podobnie do naturalnych tkanek organizmu ludzkiego [11]. Jednym z rodzajów inteligentnych materiałów są materiały piezoelektryczne, które mogą generować sygnały elektryczne w odpowiedzi na przyłożony bodziec zewnętrzny (np. naprężenie), stanowiąc responsywne, mechanoelektryczne systemy transdukcji [12]. Przewiduje się, że materiały te mogą skutecznie stymulować ścieżki sygnałowe, a tym samym wspomagać regenerację tkanek w uszkodzonym obszarze. Podłoża komórkowe stanowią rodzaj biomateriału powszechnie badanego i stosowanego w inżynierii tkankowej [13]. Podłoża komórkowe powinny spełniać odpowiednie wymagania, obejmujące bioaktywność i biozgodność, odpowiednią porowatość i strukturę przestrzenną oraz morfologię sprzyjającą namnażaniu komórek. Dodatkowo, w przypadku podłoży piezoelektrycznych, istotna jest wysoka piezoelektryczność [14,15].

Piezoelektryczność (*gr. piezein – „ściskać”*) to zjawisko generowania potencjału elektrycznego pod wpływem naprężenia mechanicznego jako bodźca zewnętrznego. Zjawisko piezoelektryczności zostało odkryte w 1880 roku przez Pierre'a i Jacques'a Curie [16]. Udowodniono, że przyłożone w określonym kierunku naprężenie mechaniczne powoduje powstanie proporcjonalnego napięcia elektrycznego na powierzchni badanego materiału [17]. Zjawiska piezoelektryczności są obserwowane w organizmach ludzi i zwierząt, na przykład w układzie nerwowym, DNA, ścięgnie Achillesa (kolagenie), kościach i zębinie, a nawet w skórze [18]. W 1940 roku Martin [19] opisał pierwsze zjawiska piezoelektryczności w tkankach biologicznych, obserwując powstawanie napięcia elektrycznego w wiązce wełny ściśniętej pomiędzy dwiema płytami mosiężnymi.

Głównym składnikiem wełny, a także włosów i rogów, jest keratyna występująca w formie tzw. α-helisy. Wysoka piezoelektryczność keratyny wynika z jej uporządkowanej architektury, usztywnionej przez wiązania wodorowe pomiędzy grupami aminowymi i karbonylowymi (Rys. 2) [20–25].

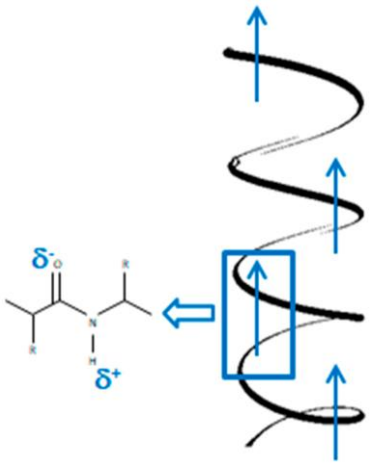

Rys. 2. Schemat trwałej polaryzacji w α-helisie [26].

W celu zapewnienia wysokiej aktywności komórek, w szczególności komórek kostnych i nerwowych, niezbędna jest obecność ładunków elektrycznych [27]. Jako że materiały piezoelektryczne mają naturalną zdolność do generowania ładunków elektrycznych, cecha ta stanowi jedną z ich głównych zalet. Zjawisko to jest zgodne ze współczesnym podejściem w inżynierii tkankowej, skierowanym na opracowanie technologii minimalnie inwazyjnych oraz wykorzystujących materiały inteligentne [28]. Celem tych działań jest ograniczenie konieczności przeprowadzania skomplikowanych

i czasochłonnych zabiegów chirurgicznych, przy jednoczesnym skróceniu czasu rekonwalescencji.

Polimery piezoelektryczne: poli(fluorek winylidenu) (PVDF, *ang. poly(vinylidene fluoride)*) oraz poli(L-laktyd) (PLLA, *ang. poly(L-lactide)*), które były przedmiotem badań opisywanych w niniejszej rozprawie, są znane z wysokiej piezoelektryczności, łatwości przetwarzania oraz korzystnych właściwości biologicznych, co czyni je doskonałymi kandydatami do zastosowania jako inteligentne podłoża komórkowe.

Piezoelektryczne podłoża komórkowe mogą być formowane za pomocą procesu elektroprzędzenia w postaci nano- i submikronowych włóknin. Nanowłókniste podłoża są w stanie skutecznie naśladować włóknistą strukturę ECM. W przypadku piezoelektrycznych nanowłókien kluczowe znaczenie ma ich zdolność do generowania ładunków elektrycznych, które mogą stymulować aktywność biologiczną komórek. W tym celu konieczne jest zwiększenie efektywność piezoelektrycznej nanowłókien jako biomateriałów poprzez modyfikację zarówno badanego układu materiałowego, jak i parametrów procesu wytwarzania. Biorąc pod uwagę obecne zapotrzebowania inżynierii tkankowej, a także specyfikę układu kostnego i nerwowego, połączenie nanowłókien z nanocząstkami stanowi obiecujące podejście w projektowaniu materiałów przeznaczonych do regeneracji uszkodzonych tkanek.

Zarówno PVDF, jak i PLLA mogą występować w kilku różnych fazach krystalicznych. PVDF jest termoplastycznym, polimorficznym polimerem, który może krystalizować w co najmniej pięciu różnych fazach: α, β, γ, δ i ε (Rys. 3). Najważniejszą odmianą polimorficzną, ze względu na najwyższe właściwości piezoelektryczne, ferroelektryczne i piroelektryczne jest faza β, a w mniejszym stopniu - faza γ [29]. Natomiast PLLA wykazuje złożony polimorfizm z trzema głównymi formami krystalicznymi: α, β i γ, w zależności od warunków przygotowania [30]. Oprócz tych trzech głównych faz krystalicznych, w PLLA zaobserwowano dwie nieuporządkowane modyfikacje formy α, oznaczone α′ i α″. Zgodnie z literaturą, modyfikacja α′ charakteryzuje się nieuporządkowaniem konformacyjnym oraz luźnym sposobem upakowania łańcuchów, co sprawia, że uznaje się ją za mezofazę (kryształy Condis) [31].

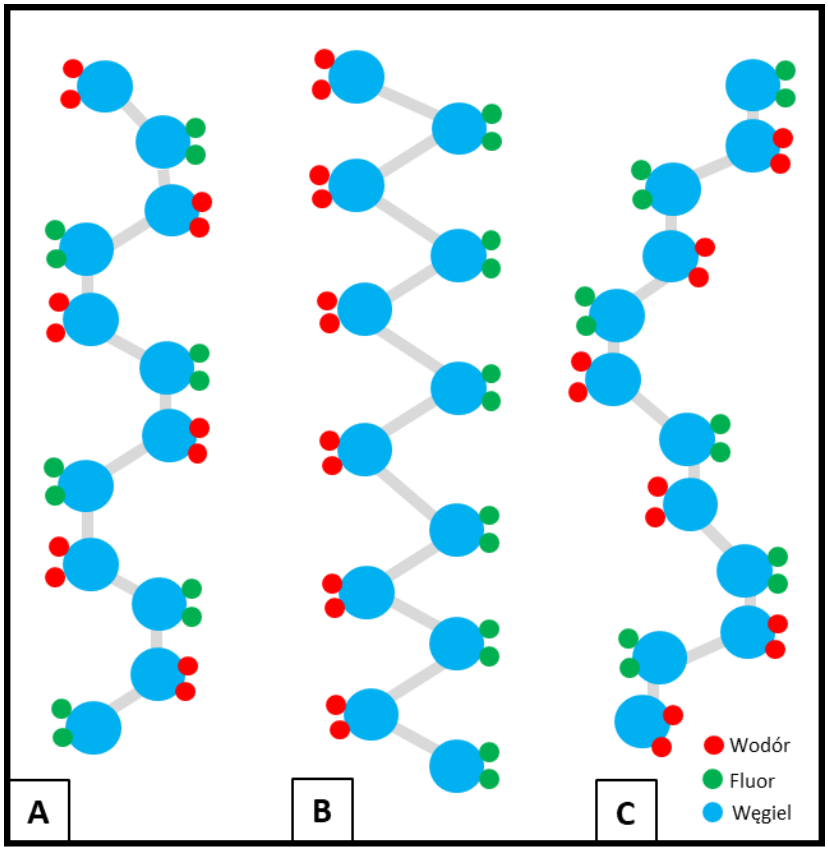

Rys. 3. Schematyczne przedstawienie konformacji łańcucha faz w PVDF; (A) - faza α, (B) - faza β i (C) - faza γ [32].

Od lat 80. XX wieku wiadomo, że uzyskanie określonej fazy krystalicznej w PVDF jest możliwe przy użyciu wybranych metod. Do najważniejszych z tych metod należy zaliczyć krystalizację ze stopu lub z roztworu, wygrzewanie (także pod wysokim ciśnieniem), ciągnienie mechaniczne oraz polaryzację elektryczną w polu zewnętrznym. Dotychczas wykazano, że najbardziej piezoelektryczną fazę β można uzyskać poprzez dobór odpowiednich rozpuszczalników, takich jak dimetyloformamid (DMF) lub dimetyloacetamid (DMAC) [33], a także poprzez deformację rozciągającą [34,35], wygrzewanie pod bardzo wysokim ciśnieniem [36] oraz polaryzację w silnym polu elektrycznym [37]. Proces elektroprzędzenia sprzyja również zwiększeniu zawartości faz piezoelektrycznych [38], dzięki współwystępowaniu zjawisk polaryzacji elektrycznej, deformacji mechanicznej oraz możliwości zastosowania odpowiednich rozpuszczalników. Ta stosunkowo prosta i tania technika umożliwia formowanie włókien nano- i submikronowych, których właściwości znacznie różnią się od właściwości materiałów formowanych metodami tradycyjnymi [39]. Ponadto nanowłókna, pod względem morfologicznym, naśladują ECM, zapewniając komórkom odpowiednie mikrośrodowisko do wzrostu.

W literaturze można znaleźć doniesienia na temat wpływu procesu elektroprzędzenia na strukturę czystego PVDF [40] i PLLA [41], jednak nadal brakuje systematycznych badań obejmujących wpływ poszczególnych parametrów na właściwości piezoelektryczne. Wiadomo, że formowanie włókien w polu elektrycznym sprzyja orientacji łańcuchów makrocząsteczek, co z kolei sprzyja powstawaniu faz piezoelektrycznych [42].

W przypadku PVDF zawartość polarnej fazy β jest znacznie wyższa w elektroprzędzonych włóknach w porównaniu do odlewanej folii [43]. Jednak efekt ten nie został szeroko zbadany z punktu widzenia parametrów elektroprzędzenia. Zawartość faz polarnych w nanowłóknach zależy m.in. od prędkości obrotowej kolektora stosowanego podczas formowania włókien. Efekt ten jest spowodowany odkształceniem mechanicznym, o którym wiadomo, że sprzyja tworzeniu się fazy polarnej [44,45]. Przegląd literatury udowodnił potrzebę systematycznych badań nad warunkami powstawania faz piezoelektrycznych w nano- i submikronowych włóknach oraz nad ich wpływem na odpowiedź komórkową. Obecność faz piezoelektrycznych, w połączeniu z odpowiednią morfologią włókien i ich stosunkowo wysoką elastycznością, stwarza perspektywy zastosowania tego materiału w inżynierii tkankowej. Obecność faz piezoelektrycznych ma szczególne znaczenie w kontekście bioelektrycznej stymulacji układu kostnego i nerwowego, co stwarza potencjał dla skutecznej regeneracji uszkodzonych tkanek [46]. Ponadto dodanie nanocząstek może poprawić właściwości fizykochemiczne [47], zwiększyć zawartość faz piezoelektrycznych [48], wykazywać działanie przeciwbakteryjne [49], a także wpływać na wzmocnienie odpowiedzi biologicznej analizowanych materiałów [50].

W niniejszej rozprawie opisano rezultaty systematycznych badań nad zaawansowanymi, inteligentnymi materiałami nanowłóknistymi, składającymi się z piezoelektrycznych polimerów PVDF i PLLA oraz nad wpływem dodatku nanocząstek hydroksyapatytu (nHA) i złota (AuNPs) na ich właściwości piezoelektryczne. Zaproponowane materiały wybrano ze względu na ich komplementarne właściwości: PVDF charakteryzuje się wysoką piezoelektrycznością, stabilnością chemiczną oraz zdolnością do elektroaktywnej stymulacji komórek, natomiast PLLA cechuje się biodegradowalnością, bioresorbowalnością i wysoką biozgodnością sprzyjającą adhezji i proliferacji komórek. W połączeniu z dodatkiem nHA, który zwiększa bioaktywność i właściwości osteokonduktywne, oraz AuNPs poprawiającymi właściwości biologiczne, uzyskane nanowłókniste kompozyty stanowią odpowiednie materiały do zastosowań jako podłoża komórkowe w inżynierii tkankowej, w szczególności do regeneracji komórek kostnych i nerwowych (Rys. 4).

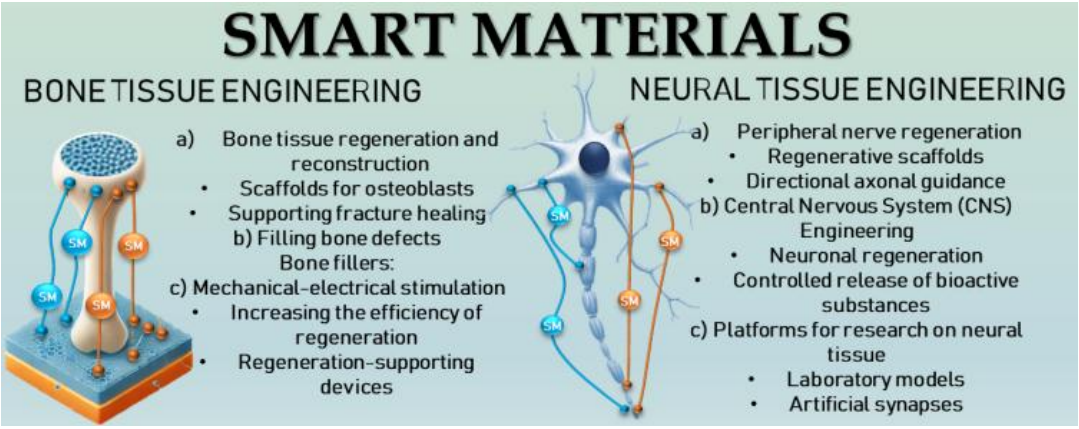

Rys. 4. Schematyczna ilustracja zastosowania biomateriałów piezoelektrycznych do regeneracji tkanki kostnej i nerwowej [51].

Główną zaletą tego systemu materiałowego jest połączenie biokompatybilności i biodegradowalności z możliwością naśladowania naturalnej struktury i właściwości kości oraz tkanek nerwowych, a także właściwości piezoelektrycznych. W niniejszej rozprawie zaproponowano proces elektroprzędzenia umożliwiający precyzyjne formowanie włóknin o zróżnicowanym ułożeniu nanowłókien - od losowego po ukierunkowane. Przeanalizowano wpływ wybranych istotnych parametrów procesowo-materiałowych na morfologię włókien oraz wpływ dodatków na zawartość faz piezoelektrycznych, piezoelektryczność oraz odpowiedź komórkową. W dostępnej literaturze istnieje niewiele prac dotyczących analizy piezoelektryczności materiałów polimerowych w formie nanowłóknistych podłoży komórkowych z dodatkami, w kontekście właściwości piezoelektrycznych obserwowanych w naturalnej kości i komórkach nerwowych. Ponadto brakuje danych dotyczących wpływu ułożenia włókien na właściwości piezoelektryczne w kontekście wzrostu i przeżywalności komórek.

Niniejsza rozprawa stanowi cykl 6 publikacji, w których przedstawiono rezultaty badań przeprowadzonych w ciągu kilkuletniej pracy naukowej.

Dwa pierwsze artykuły w cyklu mają charakter przeglądowy i pełnią rolę wprowadzenia do zagadnień poruszanych w rozprawie. W publikacjach dokonano analizy aktualnego stanu wiedzy z zakresu piezoelektrycznych materiałów polimerowych wykorzystywanych w regeneracji tkanek kostnych i nerwowych. Szczególną uwagę poświęcono zagadnieniu piezoelektryczności oraz jej potencjalnemu zastosowaniu w projektowaniu podłoży komórkowych, z uwzględnieniem jej wpływu na procesy naprawcze tkanek. Omówiono również istniejące strategie formowania podłoży oraz ich wpływ na odpowiedź biologiczną. Na podstawie przeprowadzonych analiz możliwe było

sformułowanie głównych kierunków badawczych podjętych w kolejnych pracach eksperymentalnych.

W artykułach nr 3 i 4 przedstawiono wyniki badań wstępnych, których celem była optymalizacja procesu elektroprzędzenia włókien z PVDF pod kątem ich zastosowania w inżynierii tkankowej. Badania koncentrowały się na zależnościach pomiędzy warunkami procesu a strukturą i właściwościami włókien, ze szczególnym uwzględnieniem ich ukierunkowania oraz powstawania faz piezoelektrycznych. Określono wpływ masy cząsteczkowej, stężenia polimeru oraz kilku kluczowych parametrów procesu na zawartość faz β i γ, odpowiedzialnych za właściwości piezoelektryczne włókien. Uzyskane wyniki umożliwiły określenie warunków sprzyjających formowaniu włókien o pożądanej morfologii i właściwościach biologicznych. Sformułowane wnioski stanowiły ukierunkowanie dalszych badań, obejmujących również modyfikację materiałów.

W artykułach nr 5 i 6 przedstawiono kulminacyjną część badań rozprawy, potwierdzając postawioną hipotezę dotyczącą potencjału piezoelektrycznych podłoży komórkowych do zastosowań w inżynierii tkankowej. W artykule nr 5 opisano opracowanie biodegradowalnych podłoży z PLLA z dodatkiem nHA o optymalnej morfologii, silnej odpowiedzi piezoelektrycznej oraz wysokiej biozgodności, tym samym wykazując ich przydatność do regeneracji ubytków kostnych.

W artykule nr 6 opisano z kolei sposób otrzymywania podłoży z PVDF, w tym z dodatkiem nHA oraz z naniesionymi ultradźwiękowo na powierzchnię włókien AuNPs. Analizując wpływ dodatków na właściwości strukturalne i biologiczne, szczególną uwagę poświęcono znaczeniu ukierunkowania włókien z punktu widzenia poprawy regeneracji komórek kostnych i nerwowych oraz synergii pomiędzy materiałami w kontekście stymulacji komórkowej. Otrzymane wyniki potwierdziły hipotezę badawczą, że odpowiednio opracowane piezoelektryczne podłoża komórkowe mogą stanowić skuteczne narzędzie wspomagające procesy regeneracyjne w komórkach kostnych i nerwowych.

2. Cele pracy

Główny cel pracy:

Celem niniejszej rozprawy było opracowanie nanowłóknistych podłoży komórkowych o optymalnych właściwościach piezoelektrycznych i biologicznych, przeznaczonych do zastosowań w inżynierii tkankowej, szczególnie w regeneracji tkanki kostnej i nerwowej.

Cele szczegółowe:

W celu realizacji założenia, konieczny był dobór optymalnych materiałów oraz dodatków wraz z ich stężeniami i proporcjami, określenie rodzaju procesu wytwarzania oraz wybór parametrów istotnych z punktu widzenia wybranych właściwości, a także dobór odpowiednich metod badawczych i metodologii w celu charakterystyki próbek.

Do badań wybrano polimery przejawiające właściwości piezoelektryczne: poli(fluorek winylidenu) (PVDF) i poli(L-laktyd) (PLLA) oraz metodę elektroprzędzenia (*ang. electrospinning*) do formowania włóknistych podłoży dla komórek. Głównymi parametrami materiałowymi były masa cząsteczkowa i stężenie polimeru, natomiast parametrami procesowymi - prędkość obrotowa kolektora, napięcie przyłożone podczas procesu oraz szybkość podawania roztworu.

- Na wstępie kluczowy był dobór odpowiednich parametrów procesu, umożliwiających wytworzenie jednorodnych, pozbawionych defektów włókien, co osiągnięto, dobierając parametry procesu takie jak: stężenie polimeru, szybkość podawania roztworu, napięcie elektryczne oraz odległość igły od kolektora. Następnie, zbadanie wpływu prędkości obrotowej kolektora na orientację włókien, a do dalszych systematycznych badań wybrano dwie wartości prędkości, umożliwiające otrzymanie podłoża o prawie losowym oraz wyraźnie ukierunkowanym ułożeniu włókien.
- Drugą istotną częścią pracy były systematyczne badania w zakresie inżynierii materiałowej mające na celu wyznaczenie szeregu istotnych właściwości otrzymanych włókien oraz wykonanych z nich podłoży z perspektywy wybranych parametrów procesu. Określenie m.in. stopienia krystaliczności, zawartości faz piezoelektrycznych, ukierunkowania włókien i współczynnika piezoelektryczności, a także porowatość, zwilżalność, energię swobodną powierzchni oraz sorpcję wody włóknin.
- Trzecie zadanie badawcze polegało na ocenie wpływu morfologii, ukierunkowania włókien, a także właściwości piezoelektrycznych włóknin na ich właściwości biologiczne,

a ponadto na ocenieniu cytotoksyczności oraz stopnia proliferacji komórek w warunkach eksperymentalnych *in vitro*.

Dodatkowym celem badawczym była ocena wpływu wybranych dodatków w kontekście efektywności piezoelektrycznej podłoży oraz ich właściwości biologicznych. Jako dodatków użyto piezoelektrycznego hydroksyapatytu (nHA) oraz nanocząstek złota (AuNPs). W ramach realizacji tego zadania skupiono się na następujących kwestiach:

- Pierwszą kwestią było określenie wpływu dodatków na morfologię, głównie rozkład orientacji włókien, piezoelektryczność, zwilżalność, krystaliczność i zawartość faz piezoelektrycznych.
- Następną kwestią była optymalizacja zawartości dodatków z perspektywy efektywności biologicznej podłoży, ocenianej w badaniach komórkowych *in vitro*.
- Ostatnim wiążącym etapem pracy było całościowe określenie oraz ocena zależności pomiędzy odpowiedzią komórkową a piezoelektrycznością, rodzajem polimeru i dodatku oraz orientacją włókien.

3. Hipoteza badawcza

Przy wykorzystaniu polimerów przejawiających właściwości piezoelektryczne oraz procesu elektroprzędzenia, możliwe jest wytworzenie nanowłóknistego, biozgodnego podłoża do hodowli komórkowej, które może znaleźć zastosowanie w inżynierii tkankowej do regeneracji tkanki nerwowej i kostnej.

4. Materiały

4.1. Materiały piezoelektryczne

Polimery piezoelektryczne są stosunkowo nową klasą materiałów, umożliwiających generowanie ładunków elektrycznych pod wpływem bodźca zewnętrznego, np. stymulacji mechanicznej bez konieczności stosowania dodatkowych źródeł energii lub elektrod [52]. Dodatkowo, z punktu widzenia biomedycznego, polimery te charakteryzują się biokompatybilnością, co jest bardzo istotne w kontekście nowoczesnych implantów stosowanych w medycynie regeneracyjnej [53]. Kolejną zaletą polimerów piezoelektrycznych jest ich stosunkowo łatwa przetwarzalność, odróżniająca je od materiałów nieorganicznych [54]. Przykładowe zastosowania polimerów piezoelektrycznych przedstawiono na rysunku 5.

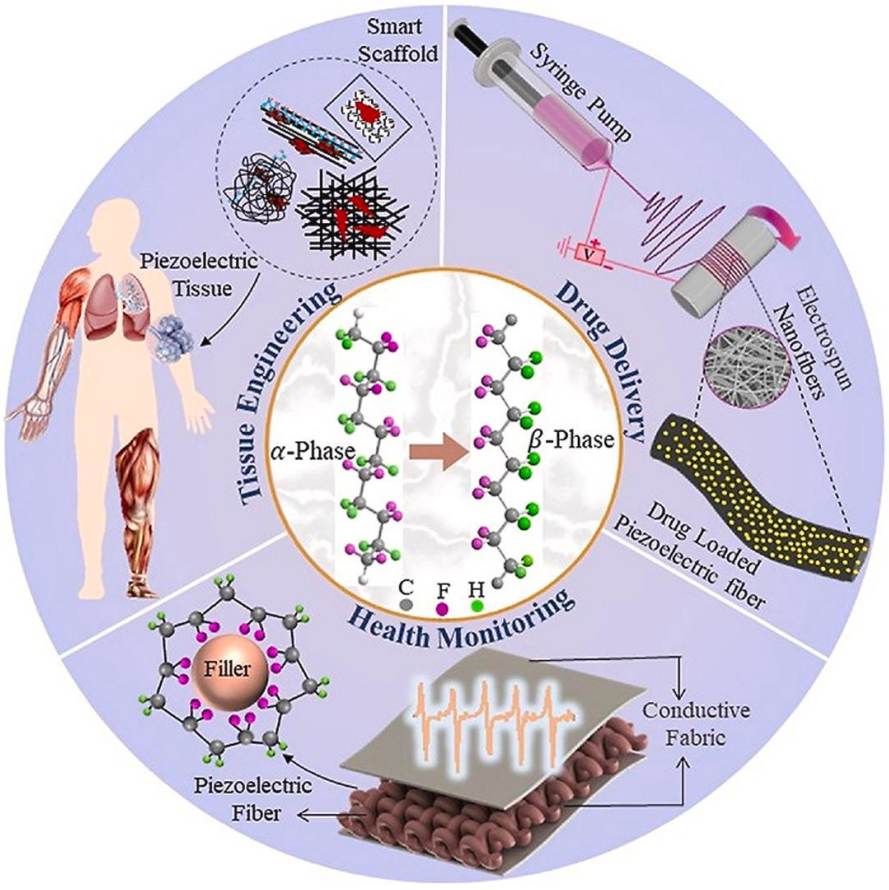

Rys. 5. Przykładowe zastosowania polimerów piezoelektrycznych [55].

4.1.1. Poli(fluorek winylidenu)

PVDF zastosowany w niniejszych badaniach w pracy 3, 4 i 6 jest niebiodegradowalnym, termoplastycznym polimerem o liniowej budowie łańcucha. Struktura chemiczna jednostki meru została przedstawiona na rysunku 6.

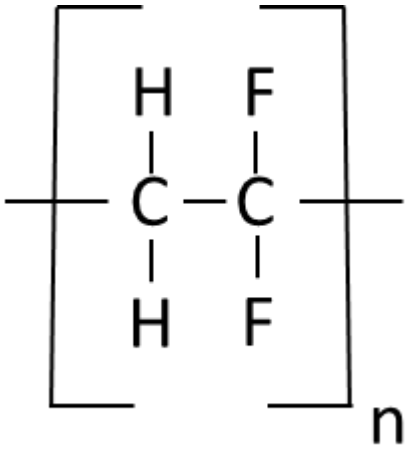

Rys. 6. Struktura chemiczna meru poli(fluorku winylidenu).

Segmenty łańcuchów makrocząsteczek PVDF mogą przyjmować odmienne konformacje, co skutkuje powstawaniem zróżnicowanych momentów dipolowych. Silny moment elektryczny wynika z dużej różnicy elektroujemności między atomami fluoru a atomami wodoru. Gdy łańcuchy polimeru są ułożone w kryształy z równoległym układem dipoli, ich dipole sumują się, co skutkuje powstawaniem niezerowego momentu dipolowego netto [56–58]. Taki układ cząsteczkowy występuje w fazach β, γ i δ, przy czym faza β wykazuje najsilniejszy moment dipolowy, ze względu na konformację typu *TTT* (*trans-trans-trans*). Dla innych konformacji łańcucha, takich jak *TGTG-* i T_3GT_3G-, równoległy układ momentów dipolowych (odpowiednio w fazach δ i γ), prowadzi do niższej polaryzacji wypadkowej łańcucha. Natomiast w przypadku antyrównoległego ułożenia dipoli przy tych samych konformacjach moment dipolowy netto jest równy zeru, jak to ma miejsce w fazach α i ε [59].

Różne metody pozwalają zwiększyć zawartość faz piezoelektrycznych, m.in. rekrystalizacja w stanie stopionym [60], polaryzacja w wysokim polu elektrycznym [61], zastosowanie wysokiego ciśnienia [62], rozciąganie mechaniczne [63] oraz dodawanie nanocząstek [64]. W niniejszych badaniach przyjęto założenie, że pole orientujące w procesie elektroprzędzenia sprzyja powstawaniu konformacji łańcuchów o silnych momentach dipolowych *TTT* i T_3GT_3G-. W celu zwiększenia ilości faz piezoelektrycznych PVDF badano

wpływ wysokich prędkości obrotowych kolektora podczas procesu elektroprzędzenia, a także wpływ dodatku nanocząstek (piezoelektrycznego nHA).

4.1.2. Poli(L-laktyd)

W niniejszej rozprawie, w pracy 5, zastosowano polimorficzny PLLA, który może przyjmować trzy formy krystaliczne: α, β i γ (Rys. 7) [65]. Dodatkowo w PLLA mogą występować również dwie odmiany o obniżonym stopniu uporządkowania, określane jako α′ i α″. Fazy te określa się jako quasi-heksagonalne o zaburzonym uporządkowaniu rotacyjnym i podłużnym [66]. Polimer ten jest biodegradowalny, biokompatybilny i może być stosowany jako resorbowalne wypełnienie ubytków kostnych oraz nerwowych. Piezoelektryczność PLLA wynika z obecności izotaktycznych łańcuchów polimerowych, które mogą tworzyć uporządkowane struktury krystaliczne zdolne do polaryzacji. Źródłem momentów elektrycznych są grupy karbonylowe i eterowe, charakteryzujące się asymetrycznym rozkładem ładunków. Pod wpływem naprężeń mechanicznych, takich jak rozciąganie lub ściskanie, dipole te ulegają przemieszczeniu, co prowadzi do powstania różnicy potencjałów elektrycznych [67]. Podczas procesu elektroprzędzenia łańcuchy PLLA ulegają reorientacji, co skutkuje przesunięciem ładunków elektrycznych. W efekcie tworzy się dipolowy moment elektryczny, prowadzący do generowania napięcia na powierzchni nanowłókien. PLLA został wybrany do badań ze względu na swoje właściwości piezoelektryczne, biokompatybilność, możliwość przetwarzania [68] oraz biodegradowalność [69].

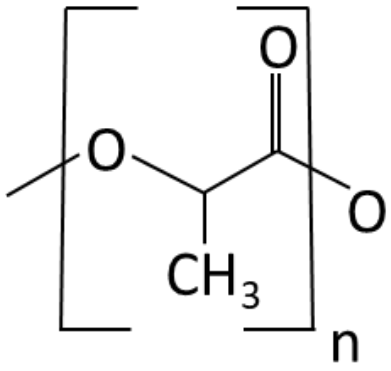

Rys. 7. Struktura chemiczna meru poli(L-laktydu) [70].

4.1.3. Hydroksyapatyt

Hydroksyapatyt (nHA) zastosowany w badaniach opisanych w pracach 5 i 6, stanowi główny składnik mineralny kości oraz zębów u ludzi i zwierząt [71–73], współwystępując ze składnikiem organicznym (kolagenem) oraz komórkami kostnymi [74]. nHA krystalizuje w postaci licznych płytek (lub igłowatych nanokryształów) zlokalizowanych w szczelinach włókienek tropokolagenu, co prowadzi do wzmocnienia struktury tkanki kostnej [75]. Ze względu na swoją aktywność biologiczną, nHA jest szeroko stosowanym biomateriałem w medycynie do wytwarzania implantów kostnych i stomatologicznych (jako wypełniacz i materiał powłokowy) [76]. Struktura krystaliczna nHA należy do układu heksogalnego (grupa przestrzenna $P6_3/m$), w której grupy hydroksylowe (-OH) są uporządkowane wzdłuż osi krystalograficznej *c*. Ułożenie to pozwala na aktywny przepływ protonów wzdłuż tej osi, co prowadzi do wytworzenia wewnętrznej polaryzacji dipolowej i ładunku powierzchniowego. W wyniku przyłożenia bodźca zewnętrznego (np. ściskania) w kryształach nHA zachodzi do przesunięcia grup fosforanowych i jonów wapnia, powoduje to powstanie różnicy potencjałów, czyli zjawiska piezoelektryczności [77]. Piezoelektryczna odpowiedź nHA może wpływać na aktywność potencjałów w błonach komórkowych komórek osteoblastycznych, ale również neuronów, przyczyniając się do stymulacji procesów regeneracyjnych. Właściwości te sprawiają, że nHA, jako dodatek do podłoża komórkowego, może działać jako bioaktywne, elektroresponsywne wzmocnienie w nanowłóknach polimerowych [78].

4.2. Nanocząstki złota

Nanocząstki złota (AuNPs) użyte do badań w pracy 6 są szeroko znane ze swojej biokompatybilności, łatwości kontroli rozmiaru i kształtu oraz powtarzalności procesu wytwarzania [79,80]. AuNPs stanowią obiecujący materiał do zastosowania w inżynierii tkanki kostnej ze względu na udokumentowaną w literaturze poprawę właściwości regeneracyjnych kości po urazach [81]. AuNPs wspierają regenerację kości poprzez regulację różnicowania osteogenicznego, hamując aktywność osteoklastów [82,83]. Ponadto AuNPs są intensywnie badane pod kątem ich potencjalnego zastosowania w leczenia osteoporozy [84]. W przypadku układu nerwowego AuNPs wykorzystywane są w terapiach wspomaganych nanocząsteczkami jako innowacyjne platformy wspierające proces regeneracji nerwów obwodowych [85]. W ciągu ostatnich dziesięciu lat wzrosła liczba badań w zakresie wykorzystania AuNPs w inżynierii tkankowej i medycynie regeneracyjnej, co potwierdza analiza bazy danych

PubMed. AuNPs charakteryzują się wysokim przewodnictwem elektrycznym wynikającym z obecności elektronów swobodnych, co umożliwia efektywną transmisję sygnałów elektrycznych w obrębie materiału. Ich obecność w strukturze polimerowej sprzyja uporządkowaniu dipoli molekularnych poprzez lokalne wzmocnienie pola elektrycznego, co z kolei może prowadzić do zwiększenia polarności i wzmocnienia właściwości dielektrycznych i piezoelektrycznych podłoży [86]. AuNPs wpływają na poprawę interakcji z płynami biologicznymi, ponieważ wpływają na zwiększenie hydrofilowości [87].

5. Metody badawcze

5.1. Formowanie włóknin - proces elektroprzędzenia

Metoda formowania włókien w procesie elektroprzędzenia została opatentowana w 1934 roku w Stanach Zjednoczonych [88]. Największy rozwój tej metody zaobserwowano na przełomie lat 80. i 90. XX wieku, kiedy opracowano i skomercjalizowano materiały filtracyjne w przemyśle włókienniczym [89]. Układ aparaturowy jest stosunkowo prosty, natomiast zjawiska zachodzące w trakcie formowania włókien są na tyle złożone, że proces zależy od wielu czynników, nie tylko parametrów materiałowo-procesowych, lecz także od warunków zewnętrznych, takich jak temperatura i wilgotność.

Piezoelektryczne, polimerowe podłoża komórkowe w formie włóknin formowano metodą elektroprzędzenia z roztworu, stosując odpowiednie rozpuszczalniki. Roztwór polimeru umieszczano w strzykawce z igłą podłączoną do źródła wysokiego napięcia. Roztwór polimeru podawano ze stałą szybkością (rzędu mililitrów na godzinę) za pomocą pompy o wysokiej dokładności. Pomiędzy igłą a uziemionym (lub o ujemnym potencjale) kolektorem powstają siły elektrostatyczne. Wraz ze wzrostem natężenia pola elektrycznego osiągany jest punkt krytyczny, w którym siła elektrostatyczna przewyższa napięcie powierzchniowe roztworu polimeru. Kropla polimeru wydłuża się, formując stożek nazywany stożkiem Taylora. Następnie z wierzchołka stożka Taylora zostaje wyrzucony naładowany strumień cieczy. Początkowo strumień ten przemieszcza się w sposób prostoliniowy. Na skutek odpychania się jednoimiennych ładunków elektrostatycznych gromadzących się na powierzchni strumienia, traci on stabilność, formując spiralną trajektorię i finalnie osadza się na kolektorze w postaci bardzo cienkich włókien tworzących włókninę (Rys. 8).

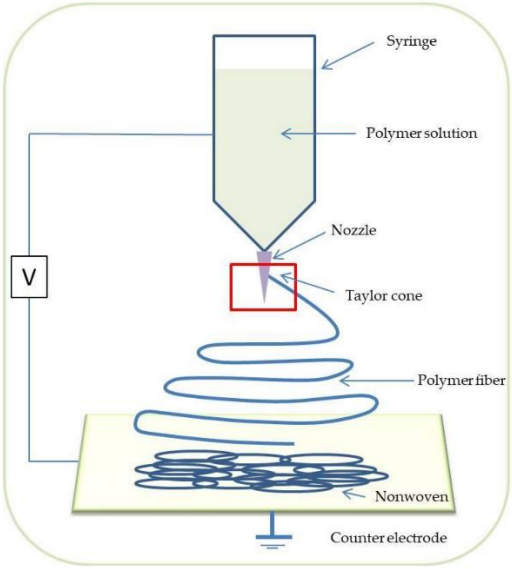

Rys. 8. Schemat procesu elektroprzędzenia [90].

Elektroprzędzone włókniny formowano z roztworów polimerów piezoelektrycznych o wybranych stężeniach i rozpuszczonych w odpowiednich rozpuszczalnikach.

Polimer piezoelektryczny PVDF (M_w = 180 000 g/mol, 400 000 g/mol, 530 000 g/mol) rozpuszczano w odpowiedniej ilości rozpuszczalnika (DMF lub DMF/Ac). W celu uzyskania wizualnie jednorodnego roztworu mieszano go w temperaturze 50°C przez 24 godziny. PLLA (M_w = 330 000 g/mol) rozpuszczano w HFIP w temperaturze pokojowej i pozostawiono na noc w celu pełnego rozpuszczenia. Następnie roztwory domieszkowano, dodając nanocząstki nHA w wybranych stężeniach. Dodatkowo roztwory poddano działaniu ultradźwięków przez 20 minut, aby zapobiec agregacji nanocząstek nHA (myjka ultradźwiękowa EMAG, EMMI-D60, Niemcy).

Proces elektroprzędzenia przeprowadzano w komercyjnej komorze przędzalniczej (Fluidnatek LE-50, Bioinicia, Walencja, Hiszpania) oraz w komorze wykonanej samodzielnie przez pracowników SPPiB (Rys. 9). Komory składają się z zasilacza wysokiego napięcia, pompy strzykawkowej z igłą oraz uziemionego kolektora, na którym osadzają się nanowłókna. W komorze wytwarzane jest silne pole elektrostatyczne, niezbędne do formowania włókien. Roztwór polimerowy podawano przy użyciu precyzyjnej pompy infuzyjnej, umożliwiającej kontrolę szybkości podawania. Komora zapewnia bezpieczeństwo użytkownika oraz umożliwia kontrolę warunków zewnętrznych, takich jak temperatura i wilgotność. Włókna zbierano w postaci nanowłóknistych mat na obracającym się kolektorze, stosując różne prędkości obrotowe. Próbki o losowym ułożeniu włókien formowano z prędkością

100-200 obr./min., natomiast próbki o ukierunkowanym ułożeniu włókien przy prędkości 2000 obr./min.

Rys. 9. Komory przędzalnicze wykorzystywane w procesie elektroprzędzenia w artykułach 3-6. Komora wykonana samodzielnie przez pracowników SPPiB (z lewej); komora umożliwiająca dodatkowo regulację warunków zewnętrznych (temperatura i wilgotność) LE-50 Fluidnatek firmy Bioinicia (z prawej).

Próbki z dodatkiem nanocząstek złota otrzymywano metodą osadzania ultradźwiękowego. Proces sonifikacji przeprowadzano z wydajnością 80% na urządzeniu Hielscher UP200Ht (Teltow, Niemcy). Osadzania prowadzono w określonych odstępach czasu (2 x 2 min). Następnie próbki dokładnie płukano wodą i suszono.

Szczegółowe informacje dotyczące formowania włóknin znajdują się w publikacjach 3-6: *Influence of process-material conditions on the structure and biological properties of electrospun polyvinylidene fluoride fibers), Enhanced Electroactive Phases of Poly(vinylidene Fluoride) Fibers for Tissue Engineering Applications), Poly(L-lactide)/nano-hydroxyapatite piezoelectric scaffolds for tissue engineering, On the Structural and Biological Effects of Hydroxyapatite and Gold nano-scale Particles in Poly(vinylidene fluoride) Smart Scaffolds for Bone and Neural Tissue Engineering.*

5.2. Pomiar lepkości roztworów

Lepkość roztworów polimerowych mierzono przy użyciu wiskozymetru rotacyjnego HADV-III Ultra (Brookfield, Middleboro, MA, USA) o konfiguracji stożek-płytka. Pomiary wykonano przy różnych szybkościach ścinania, a także przy stałej szybkości ścinania wynoszącej ≈33 1/s. Stałą szybkość ścinania wybrano ponieważ, odpowiada ona oszacowanej wartości szybkości ścinania wewnątrz igły podczas procesu elektroprzędzenia. Pomiary przeprowadzano na etapie przygotowywania roztworów w celu określenia ich stabilności. Szczegółowe informacje dotyczące przeprowadzania badań lepkości i ich analiza znajdują się w publikacji 3: *Influence of process-material conditions on the structure and biological properties of electrospun polyvinylidene fluoride fibers.*

5.3. Skaningowa mikroskopia elektronowa

Skaningowa mikroskopia elektronowa (SEM, Jeol, JSM-6010PLUS/LV InTouchScope™, Akishima, Tokio, Japonia) została użyta do obrazowania morfologii włókien oraz architektury włóknin. Przed pomiarem badane próbki napylano złotem (grubość warstwy 6-10 nm; Smart Coater, JEOL, Tokyo, Japan).

Analiza architektury nanowłóknistych podłoży została przeprowadzona przy użyciu oprogramowania ImageJ (wersja oprogramowania 1.52q). Przeprowadzono 100 pomiarów średnicy włókien i określono ich rozkład przy użyciu funkcji Gaussa.

Wpływ prędkości obrotowej kolektora na ukierunkowanie włókien oceniano przy użyciu wybranych metod. Do analizy wykorzystano tzw. wtyczkę „kierunkowość" w oprogramowaniu ImageJ. Rozkład orientacji aproksymowano funkcją Gaussa przy użyciu oprogramowania Origin 2021b (OriginLab Corporation, Northampton, USA). Stopień ukierunkowania włókien oceniono na podstawie szerokości połówkowej (FWHM, *ang. Full Width at Half Maximum*) - parametru funkcji Gaussa używanej do aproksymacji rozkładu orientacji. Dla każdej próbki wartości FWHM uśredniono na podstawie pięciu obrazów. Współczynnik orientacji określono przy użyciu współczynnika anizotropii α, gdzie $\alpha = 1$ oznacza idealne ukierunkowanie włókien, a $\alpha = 0$ oznacza brak ukierunkowania włókien.

Szczegółowe informacje dotyczące przeprowadzonych badań przy użyciu SEM oraz analiza obrazów przedstawiono w publikacjach 3-6: *Influence of process-material conditions on the structure and biological properties of electrospun polyvinylidene fluoride*

fibers, Enhanced Electroactive Phases of Poly(vinylidene Fluoride) Fibers for Tissue Engineering Applications, Poly(L-lactide)/nano-hydroxyapatite piezoelectric scaffolds for tissue engineering, On the Structural and Biological Effects of Hydroxyapatite and Gold nano-scale Particles in Poly(vinylidene fluoride) Smart Scaffolds for Bone and Neural Tissue Engineering.

5.4. Pomiar porowatości i średniego rozmiaru porów

Oszacowanie porowatości oraz średniego rozmiaru porów przeprowadzano mierząc masę i wymiary zewnętrzne podłoży komórkowych. W pierwszym etapie dokonano dokładnego pomiaru masy każdej próbki za pomocą precyzyjnej wagi laboratoryjnej (waga analityczna XA 52.R2, Radwag, Polska). Następnie wyznaczano wymiary zewnętrzne zważonych próbek, co pozwoliło na obliczenie ich objętości całkowitej. Na tej podstawie wyliczano gęstość pozorną, rozumianą jako stosunek masy próbki do jej całkowitej objętości. Następnie porównano gęstość pozorną do gęstości właściwej materiału litego co pozwalało na wyznaczenie porowatości, którą wyrażano jako procentowy udział objętości porów w całkowitej objętości próbki. Średni rozmiar porów oszacowano na podstawie zależności pomiędzy średnicą włókien a porowatością materiału. Szczegółowe informacje dotyczące przeprowadzonych badań porowatości i wyznaczania średniego rozmiaru porów włóknin znajdują się w publikacjach 4-6: *Enhanced Electroactive Phases of Poly(vinylidene Fluoride) Fibers for Tissue Engineering Applications, Poly(L-lactide)/nano-hydroxyapatite piezoelectric scaffolds for tissue engineering, On the Structural and Biological Effects of Hydroxyapatite and Gold nano-scale Particles in Poly(vinylidene fluoride) Smart Scaffolds for Bone and Neural Tissue Engineering.*

5.5. Pomiar zwilżalności próbek

Zwilżalność próbek oceniano przy użyciu metody statycznego kąta zwilżania wodą. Pomiary wykonywano za pomocą goniometru Data Physics OCA 15EC (Filderstadt, Niemcy). Kroplę wody destylowanej (2 µl) umieszczano w temperaturze pokojowej na powierzchni próbki mierząc kąt zwilżania wodą po upływie 3 sekund. Każdy pomiar powtórzono 10-krotnie dla każdego rodzaju materiału, a wynik uśredniono. Szczegółowe informacje dotyczące przeprowadzonych badań znajdują się w publikacjach 5 i 6: *Poly(L-lactide)/nano-hydroxyapatite piezoelectric scaffolds for tissue engineering, On the Structural and Biological*

Effects of Hydroxyapatite and Gold nano-scale Particles in Poly(vinylidene fluoride) Smart Scaffolds for Bone and Neural Tissue Engineering.

5.6. Wyznaczenie energii swobodnej powierzchni i polarności powierzchni

Energię swobodną powierzchni (SFE, *ang. surface free energy*) określono przy użyciu metody Kaelble-Owens-Wendt'a. Do obliczenia użyto wyników z pomiarów przeprowadzonych z wykorzystaniem trzech cieczy: dijodometanu, wody i formamidu. SFE wyznaczono z użyciem oprogramowania SCA20 (Data Physics Instruments GmbH, Filderstadt, Niemcy). Wynik uśredniono na podstawie 10 pomiarów. Do obliczenia polarności powierzchni podłoży komórkowych wykorzystano metodę Wu. Szczegółowe informacje dotyczące przeprowadzonych badań znajdują się w publikacjach 5 i 6: *Poly(L-lactide)/nano-hydroxyapatite piezoelectric scaffolds for tissue engineering, On the Structural and Biological Effects of Hydroxyapatite and Gold nano-scale Particles in Poly(vinylidene fluoride) Smart Scaffolds for Bone and Neural Tissue Engineering.*

5.7. Ocena zdolności podłoży komórkowych do sorpcji wody

Zdolność do sorpcji wody oceniono poprzez pomiar zdolności próbek do wchłaniania wody. Każdą próbkę podzielono na fragmenty o wymiarach 2 x 1 cm, a następnie zanurzono w wodzie dejonizowanej. Po upływie 60 s próbki wyjmowano, delikatnie osuszano bibułką i ważono (waga analityczna XA 52.R2, Radwag, Polska). Procedurę tę powtarzano przez 10 min. Szczegółowe informacje dotyczące przeprowadzonych badań znajdują się w publikacjach 5 i 6: *Poly(L-lactide)/nano-hydroxyapatite piezoelectric scaffolds for tissue engineering, On the Structural and Biological Effects of Hydroxyapatite and Gold nano-scale Particles in Poly(vinylidene fluoride) Smart Scaffolds for Bone and Neural Tissue Engineering.*

5.8. Spektroskopia w podczerwieni

Badania budowy molekularnej warstw powierzchniowych piezoelektrycznych podłoży komórkowych zostały wykonane przy użyciu spektrometru (Bruker, Vertex 70, Mannheim, Niemcy) z przystawką ATR (*ang. Attenuated Total Reflection, Fourier Transform Infrared Spectroscopy*). Wyniki uśredniono z pomiaru pięciu niezależnych próbek. Próbki skanowano w zakresie od 400 cm^{-1} do 4000 cm^{-1} z rozdzielczością 2 cm^{-1}, wykonując łącznie 32 skany.

Dodatkowo, za pomocą spektroskopii potwierdzano obecność nanocząstek nHA oraz AuNPs, a także określano zawartość faz piezoelektrycznych we włóknach. Szczegółowe informacje dotyczące przeprowadzonych badań znajdują się w publikacjach 3-6: *Influence of process-material conditions on the structure and biological properties of electrospun polyvinylidene fluoride fibers, Enhanced Electroactive Phases of Poly(vinylidene Fluoride) Fibers for Tissue Engineering Applications, Poly(L-lactide)/nano-hydroxyapatite piezoelectric scaffolds for tissue engineering, On the Structural and Biological Effects of Hydroxyapatite and Gold nano-scale Particles in Poly(vinylidene fluoride) Smart Scaffolds for Bone and Neural Tissue Engineering.*

5.9. Spektroskopia dyspersyjna energii

Do potwierdzenia obecności nanocząstek nHA oraz AuNPs w piezoelektrycznych podłożach została wykorzystana również metoda spektroskopii dyspersyjnej energii (SEM-EDS, *ang. energy dispersive spectroscopy*, JSM-6010PLUS/LV InTouchScope™, JEOL, Tokio, Japonia). Próbki mierzono przy następujących parametrach: napięcie przyspieszające równe 8 kV, odległość robocza = 10 mm, prąd sondy = 500 pA i czas pomiaru 30 min. Szczegółowe informacje dotyczące przeprowadzonych badań znajdują się w publikacjach 5 i 6: *Poly(L-lactide)/nano-hydroxyapatite piezoelectric scaffolds for tissue engineering, On the Structural and Biological Effects of Hydroxyapatite and Gold nano-scale Particles in Poly(vinylidene fluoride) Smart Scaffolds for Bone and Neural Tissue Engineering.*

5.10. Różnicowa kalorymetria skaningowa

Analizę termiczną próbek wykonano przy użyciu skaningowego kalorymetru różnicowego Pyris 1 (Perkin Elmer, Waltham, MA, USA) wyposażonego w Intracooler 2P. Przed analizą próbki suszono próżniowo (suszarka próżniowa, Menmert, Hiszpania) w temperaturze otoczenia przez co najmniej 24 godziny w celu usunięcia pozostałości rozpuszczalnika. Próbki o masie 6-8 mg badano w standardowych aluminiowych naczynkach w atmosferze azotu.

Analiza termiczna podłoży komórkowych PVDF, a także PVDF z dodatkiem nHA i AuNPs o losowym i ukierunkowanym ułożeniu włókien obejmowała określenie temperatury i ciepła topnienia oraz wyznaczenie krystaliczności. Analiza efektów cieplnych wymagała rozdzielenia pików (dekonwolucji) przy użyciu funkcji asymetrycznej podwójnej sigmoidy.

Szczegółowe informacje dotyczące przeprowadzonych badań znajdują się w publikacji 6: *On the Structural and Biological Effects of Hydroxyapatite and Gold nano-scale Particles in Poly(vinylidene fluoride) Smart Scaffolds for Bone and Neural Tissue Engineering.*

Analiza termiczna podłoży komórkowych PLLA, a także PLLA z dodatkiem nHA o losowym i ukierunkowanym ułożeniu włókien nakierowana była głównie na zbadanie wpływu parametrów procesu elektroprzędzenia i składu materiału na temperaturę zeszklenia. Szczegółowe informacje dotyczące przeprowadzonych badań znajdują się w publikacji 5: *Poly(L-lactide)/nano-hydroxyapatite piezoelectric scaffolds for tissue engineering.*

5.11. Szerokokątowe rozpraszanie promieniowania rentgenowskiego

Badania struktury nadcząsteczkowej próbek metodą szerokokątowego rozpraszania promieniowania rentgenowskiego (WAXS, *ang. Wide Angle X-ray Scattering*) przeprowadzono przy użyciu dyfraktometru Bruker D8 Discover (Manheim, Niemcy). Pomiary przeprowadzono przy użyciu promieniowania CuKα o długości fali $\lambda = 1{,}5406$ Å. Profile WAXS zarejestrowano przy użyciu jednowymiarowego i wysoko czułego detektora Lynx Eye 1-D. Szczegółowe informacje dotyczące przeprowadzonych badań włóknin z PLLA oraz z dodatkiem nHA znajdują się w publikacji 5: *Poly(L-lactide)/nano-hydroxyapatite piezoelectric scaffolds for tissue engineering.*

W przypadku badań włóknin z PVDF, a także PVDF z dodatkiem nHA i AuNPs, profile WAXS analizowano przy użyciu nieliniowej metody dopasowania najmniejszych kwadratów z funkcją Gaussa prowadzącą do dekonwolucji refleksów dyfrakcyjnych, umożliwiając określenie krystaliczności całkowitej oraz zawartości faz piezoelektrycznych. Szczegółowe informacje dotyczące przeprowadzonych badań znajdują się w publikacji 6: *On the Structural and Biological Effects of Hydroxyapatite and Gold nano-scale Particles in Poly(vinylidene fluoride) Smart Scaffolds for Bone and Neural Tissue Engineering.*

5.12. Pomiar współczynnika piezoelektryczności

Pomiary współczynnika piezoelektryczności dla elektroprzędzonych włóknin PVDF i PLLA zostały wykonane przy użyciu specjalistycznego miernika d_{33} o wysokiej precyzji (miernik d_{33} YE2730A, Sinocera, Chiny). Urządzenie umożliwia pomiar na podstawie odpowiedzi prądowej generowanej w materiale piezoelektrycznym. Każda próbka została zmierzona 5 razy, następnie wyniki uśredniono. Szczegółowe informacje dotyczące badania

znajdują się w publikacjach 4 i 5: *Enhanced Electroactive Phases of Poly(vinylidene Fluoride) Fibers for Tissue Engineering Applications, Poly(L-lactide)/nano-hydroxyapatite piezoelectric scaffolds for tissue engineering.*

5.13. Ocena odpowiedzi komórkowej

Do oceny odpowiedzi komórkowej użyto czterech typów komórek:

5.13.1. Badania *in vitro* z użyciem fibroblastów L929

W przypadku podłoży z PVDF, ocenę odpowiedzi komórkowej oparto o wyniki testów biologicznych z użyciem komórek mysich - fibroblastów L929 (SigmaAldrich, Saint Louis, MO, USA). Proces hodowli komórek przeprowadzono w 48-dołkowych płytkach hodowlanych przez okres 7 dni. Aktywność metaboliczną komórek oceniono za pomocą testu MTT (SigmaAldrich, Saint Louis, MO, USA). W eksperymentach stymulacyjnych komórki fibroblastów L929 hodowane na podłożach piezoelektrycznych PVDF, poddawano działaniu ultradźwięków przez 30 minut, raz dziennie. Zastosowano bodziec ultradźwiękowy o mocy 20 mW/cm^2, 80 mW/cm^2 i częstotliwości 1,7 MHz. Obrazowanie morfologii komórek przeprowadzono przy użyciu skaningowej mikroskopii elektronowej (SEM, JSM-6010PLUS/LV InTouchScope™, JEOL, Tokio, Japonia). Próbkami kontrolnymi były podłoża komórkowe hodowane bez stymulacji ultradźwiękowej. Szczegółowe informacje dotyczące badania znajdują się w publikacji 3: *Influence of process-material conditions on the structure and biological properties of electrospun polyvinylidene fluoride fibers.*

5.13.2. Badania *in vitro* z użyciem ludzkich komórek osteblastopodobnych linii MG-63

W przypadku włóknin z PLLA, badania odpowiedzi komórkowej wykonano z użyciem linii ludzkich komórek osteoblastopodobnych MG-63 (SigmaAldrich, Saint Louis, MO, USA). Komórki hodowano w odpowiednim medium i inkubowano w środowisku 5% CO_2 w temperaturze 37°C. W celu oceny żywotności komórek wykonano test PrestoBlue™ (Thermo Fisher Scientific, Basingstoke, Wielka Brytania) po 3 i 5 dniach hodowli. Do weryfikacji morfologii komórek MG-63 w bezpośrednim kontakcie zastosowano mikroskopię fluorescencyjną (barwienie immunohistochemiczne). Obrazy uzyskano przy użyciu mikroskopu Leica (AM TIRF MC, Niemcy). Szczegółowe informacje dotyczące

badania znajdują się w publikacji 5: *Poly(L-lactide)/nano-hydroxyapatite piezoelectric scaffolds for tissue engineering.*

5.13.3. Badania *in vitro* z użyciem komórek macierzystych pochodzących z tkanki tłuszczowej człowieka

W przypadku podłoży z PVDF, wykonano również badania z użyciem komórek macierzystych pochodzących z ludzkiej tkanki tłuszczowej (ADSC, *ang. human adipose-derived stromal cells*), które uzyskano zgodnie z ustalonym protokołem opisanym wcześniej [91] i hodowano na podłożach piezoelektrycznych elektroprzędzonych z różnymi prędkościami obrotowymi kolektora. W celu przeprowadzenia testu żywotności komórek, wysterylizowane promieniowaniem UV podłoża umieszczono w 96-dołkowej płytce hodowlanej, a komórki wysiewano bezpośrednio na powierzchnię. Próbki inkubowano w temperaturze 37°C w 5% CO_2 przez 21 dni. Test PrestoBlue™ (Thermo Fisher Scientific, Basingstoke, Wielka Brytania) wykonano w celu zbadania aktywności metabolizmu komórkowego po 3, 14 i 21 dniach. Test Fluoroskan Ascent (Thermo Fisher Scientific, Wielka Brytania) użyto do pomiaru emisji światła o długości fali 620 nm i 530 nm. Obserwacje włókien i morfologii komórek przeprowadzono przy użyciu skaningowej mikroskopii elektronowej (SEM, JSM-6010PLUS/LV InTouchScope™, JEOL, Tokio, Japonia). Szczegółowe informacje dotyczące przeprowadzonych badań znajdują się w publikacji 4: *Enhanced Electroactive Phases of Poly(vinylidene Fluoride) Fibers for Tissue Engineering Applications.*

5.13.4. Badania *in vitro* z użyciem neuralnych komórek macierzystych wyprowadzonych z indukowanych pluripotencjalnych komórek macierzystych

Neuralne komórki macierzyste uzyskano z linii ludzkich indukowanych pluripotencjalnych komórek macierzystych (hiPSC-NSC, *ang. human induced pluripotent stem cell-derived neural stem cell culture*) zgodnie z protokołem opisanym wcześniej [92], z pewnymi modyfikacjami. Komórki z ludzkiej linii indukowanych pluripotencjalnych komórek macierzystych (Gibco, Thermo Fisher Scientific, Wielka Brytania) hodowano w odpowiednim medium. W celu indukcji neuronalnej komórki przemywano w PBS i pasażowano. Następnie komórki przeniesiono do naczyń hodowlanych pokrytych Geltrexem (Thermo Fisher Scientific, Wielka Brytania). Po 24 godzinach medium zastąpiono medium

PSC (Neural Induction Medium, Thermo Fisher Scientific, Wielka Brytania), a komórki hodowano przez 7 dni. W 7. dniu indukcji neuronowej, komórki pasażowano przy użyciu Accutase do płytek 6-dołkowych pokrytych Geltrexem w medium do ekspansji neuronowej. Komórki utrzymywano w tych warunkach i pasażowano co tydzień. Komórki z pasażu 6 wykorzystano do dalszych eksperymentów.

Komórki hiPSC-NSC wysiewano na podłożach PVDF w medium do ekspansji neuronów. Następnego dnia próbki przeniesiono do nowego naczynia hodowlanego i hodowano przez okres 7 dni. W dniu 7. komórki na podłożach PVDF przemywano i utrwalano. Po usunięciu roztworu permeabilizującego, próbki utrwalano przez 1 godzinę w temperaturze pokojowej. Następnie komórki inkubowano przez noc w temperaturze 4°C z przeciwciałami pierwotnymi. Przed obrazowaniem za pomocą mikroskopu konfokalnego (LSM510, Zeiss, Germany) próbki przemywano w PBS, poddawano kontrastowaniu barwnikiem przez 15 minut w celu uwidocznienia jąder komórkowych oraz umieszczano w medium fluorescencyjnym. Szczegółowe informacje dotyczące przeprowadzonych badań znajdują się w publikacji 6: *On the Structural and Biological Effects of Hydroxyapatite and Gold nano-scale Particles in Poly(vinylidene fluoride) Smart Scaffolds for Bone and Neural Tissue Engineering*

5.14. Analiza statystyczna

Analiza statystyczna została przeprowadzona dla $p<0,05$ przy użyciu oprogramowania GraphPad Prism 8.0.1 (GraphPad, Boston, MA, USA). W razie potrzeby przeprowadzono dwukierunkową analizę wariancji z testem wielokrotnych porównań Tukeya. Wartość p poniżej 0,05 uznano za statystycznie istotną. Szczegółowe informacje dotyczące analizy statystycznej znajdują się w publikacjach 4-6: *Enhanced Electroactive Phases of Poly(vinylidene Fluoride) Fibers for Tissue Engineering, Poly(L-lactide)/nano-hydroxyapatite piezoelectric scaffolds for tissue engineering, On the Structural and Biological Effects of Hydroxyapatite and Gold nano-scale Particles in Poly(vinylidene fluoride) Smart Scaffolds for Bone and Neural Tissue Engineering.*

6. Publikacje włączone w cykl rozprawy doktorskiej

1. **Zaszczynska, A.**, Sajkiewicz, P., Gradys, A. Piezoelectric Scaffolds as Smart Materials for Neural Tissue Engineering. *Polymers*, Vol.12, No.1, pp.161-1-25, **2020**.

2. **Zaszczyńska A.**, Zabielski K., Gradys A. D., Kowalczyk T., Sajkiewicz P. Ł., Piezoelectric Scaffolds as Smart Materials for Bone Tissue Engineering, *Polymers*, ISSN: 2073-4360, DOI: 10.3390/polym16192797, Vol.16, No.19, pp.2797-1-30, **2024**.

3. **Zaszczyńska A.**, Sajkiewicz P.Ł., Gradys A., Tymkiewicz R., Urbanek O., Kołbuk D., Influence of process-material conditions on the structure and biological properties of electrospun polyvinylidene fluoride fibers, *BULLETIN OF THE POLISH ACADEMY OF SCIENCES: TECHNICAL SCIENCES*, Vol.68, No.3, pp.627-633, **2020**.

4. **Zaszczyńska A.**, Gradys A.D., Ziemiecka A., Szewczyk P., Tymkiewicz R., Lewandowska-Szumieł M., Stachewicz U., Sajkiewicz P.Ł., Enhanced Electroactive Phases of Poly(vinylidene Fluoride) Fibers for Tissue Engineering Applications, *International Journal of Molecular Sciences*, Vol.25, No.9, pp.4980-1-25, **2024**.

5. **Zaszczyńska A.**, Gradys A. D., Kołbuk-Konieczny D., Zabielski K., Szewczyk P., Stachewicz U., Sajkiewicz P. Ł., Poly(L-lactide)/nano-hydroxyapatite piezoelectric scaffolds for tissue engineering, *Micron*, ISSN: 0968-4328, DOI: 10.1016/j.micron.2024.103743, Vol.188, pp.103743-1-15, **2025**.

6. **Zaszczyńska, A.**, Zychowicz, M., Kołbuk, D., Denis, P.; Gradys, A.; Sajkiewicz, P.Ł. On the Structural and Biological Effects of Hydroxyapatite and Gold Nano-Scale Particles in Poly(Vinylidene Fluoride) Smart Scaffolds for Bone and Neural Tissue Engineering. *Molecules*, DOI: 10.3390/molecules30051041, 30, 1041, **2025**.

Tabela 1. Dane bibliograficzne artykułów włączonych w rozprawę doktorską na dzień 20.11.2025r.

Numer publikacji	**Rok wydania**	**IF (2025)**	**Punkty MNiSW (2024)**	**Liczba cytowań (Scopus)**	**Liczba cytowań (Web of Science)**
1.	2020	4.7	100	129	119
2.	2024	4.7	100	21	19
3.	2020	1.2	100	16	15
4.	2024	4.9	140	9	11
5.	2025	2.2	100	4	3
6.	2025	4.6	140	1	1

7. Podsumowanie publikacji włączonych w cykl rozprawy doktorskiej

7.1. Piezoelectric scaffolds as smart materials for neural tissue engineering

Przeprowadzono przegląd literatury, którego celem było przedstawienie aktualnego stanu badań nad piezoelektrycznymi nanowłóknistymi podłożami komórkowymi oraz ocena ich potencjalnego zastosowania w inżynierii tkanki nerwowej. Dodatkowym celem było określenie wpływu ukierunkowania włókien i dodatków (np. nHa) na właściwości fizykochemiczne oraz piezoelektryczność materiału, analiza interakcji nanowłókien z komórkami w warunkach *in vitro*, w kontekście ich cytotoksyczności i proliferacji. Najistotniejszym efektem przeglądu była ocena możliwości zastosowania używanych obecnie materiałów w biomedycynie, szczególnie w kontekście przyspieszenia regeneracji tkanki nerwowej poprzez stymulację piezoelektryczną.

Na wstępie omówiono zaburzenia oraz uszkodzenia ośrodkowego (CNS) i obwodowego (PNS) układu nerwowego, które prowadzą do trwałych dysfunkcji sensorycznych i motorycznych. Ograniczona zdolność organizmu człowieka do samodzielnej regeneracji tych tkanek sprawia, że skuteczne terapie wciąż pozostają wyzwaniem. To skłania badaczy do poszukiwania nowych biomateriałów wspierających regenerację uszkodzonych neuronów. Jednym z obiecujących podejść jest zastosowanie piezoelektrycznych podłoży komórkowych, które mogą generować sygnały elektryczne pod wpływem działania bodźca zewnętrznego. Materiały te dobrze naśladują naturalne środowisko biologiczne i mogą wspomagać różnicowanie komórek nerwowych. Tkanki biologiczne, takie jak kości, ścięgna czy nerwy, wykazują naturalną piezoelektryczność, co pozwala przypuszczać, że sztucznie wytworzone materiały o tej właściwości będą wspierały regenerację tych tkanek. Co istotne, piezoelektryczność podłoży oznacza brak konieczności stosowania elektrod i źródeł zasilania, co czyni je niezwykle atrakcyjnymi do zastosowań w inżynierii tkanki nerwowej.

Następnie przedstawiono budowę układu nerwowego oraz charakterystykę neuronów. Szerzej omówiono elektryczne właściwości komórek nerwowych odpowiedzialnych za transmisję sygnałów elektrycznych. Podsumowując, wskazano kluczowe cechy materiałów, z uwzględnieniem technik formowania podłoży komórkowych oraz ich zalet i ograniczeń. Podkreślono rosnące zapotrzebowanie na inteligentne podłoża komórkowe reagujące na bodźce zewnętrzne i zdolne do generowania oraz przekazywania sygnałów bioelektrycznych, które zachowują się analogicznie do sygnałów tkanek natywnych

i zapewniają odpowiednie funkcje fizjologiczne. Materiały piezoelektryczne są szczególnie obiecujące, gdyż mogą generować sygnały elektryczne w odpowiedzi na przyłożone naprężenie, wywołane nawet przez migrację komórek lub ruchy ciała.

Przeprowadzono analizę literatury eksperymentalnej dotyczącej badań nad materiałami piezoelektrycznymi i ich odpowiedzią komórkową, przedstawiającą aktualne trendy w stosowaniu podłoży piezoelektrycznych do regeneracji układu nerwowego oraz ich główne zalety i wady. Szczególną uwagę poświęcono inteligentnym polimerowym podłożom komórkowym oraz stosowanym dodatkom. Zwrócono uwagę na metodę elektroprzędzenia, która umożliwia wytwarzanie nanowłókien z PVDF, który, przy wysokiej zawartości fazy β, odznacza się wysokimi właściwościami piezoelektrycznymi.

Stwierdzono, że obecne strategie terapeutyczne stosowane przy regeneracji nerwów są bardzo ograniczone, dlatego też piezoelektryczne podłoża komórkowe mogą stanowić przełomową technologię. W przeciwieństwie do klasycznych biomateriałów, umożliwiają one nieinwazyjną stymulację bioelektryczną, naśladując naturalne sygnały nerwowe. Zauważono, że do tak zaawansowanego zadania zastosowanie tylko jednego materiału polimerowego może być niewystarczające. Postawiono tezę, że zastosowanie połączenia różnych materiałów polimerowych w formie nanowłókien, na przykład PVDF z odpowiednimi dodatkami, może skuteczniej podnieść właściwości piezoelektryczne i poprawić odpowiedź biologiczną podłoży w porównaniu z aktualnie stosowanymi rozwiązaniami.

Artykuł przeglądowy umożliwił wybór materiałów o określonych, kluczowych właściwościach z perspektywy układu nerwowego, które następnie zostały systematycznie zbadane w toku niniejszej pracy doktorskiej.

7.2. Piezoelectric Scaffolds as Smart Materials for Bone Tissue Engineering

Przeprowadzono przegląd literatury, którego celem było przedstawienie aktualnego stanu wiedzy na temat materiałów piezoelektrycznych i ich zastosowania w inżynierii tkanki kostnej. W artykule skoncentrowano się na analizie właściwości piezoelektrycznych biomateriałów oraz ich zdolności do generowania sygnałów elektrycznych. Przedstawiono istniejące wyniki dotyczące wpływu ułożenia włókien na właściwości piezoelektryczne podłoży komórkowych i ich oddziaływanie na regenerację kości.

W artykule przeglądowym omówiono rolę piezoelektryczności w inżynierii tkanki kostnej oraz możliwości zastosowania różnych materiałów piezoelektrycznych, które odgrywają kluczową rolę w proliferacji i różnicowaniu komórek kostnych.

W ostatnich latach zauważono znaczący wzrost zainteresowania materiałami piezoelektrycznymi w inżynierii tkankowej kości. Szczególną uwagę poświęcono polimerom syntetycznym, takim jak PVDF i PLLA, a także ich modyfikacjom poprzez domieszkowanie materiałami takimi jak hydroksyapatyt, nanorurki węglowe czy tytanian baru. Zaobserwowano, że zastosowanie powyższych materiałów pozwala na uzyskanie satysfakcjonujących właściwości biologicznych oraz piezoelektrycznych, co czyni je obiecującymi kandydatami do zastosowań w biomedycynie. Omówiono również znaczenie bioelektryczności w regeneracji tkanki kostnej, w tym wpływ sygnałów elektrycznych na gojenie i remodelowanie kości. Przedstawiono doniesienia o pozytywnym wpływie ładunków elektrycznych w kościach na proliferację i wzrost komórek oraz o korzystnym oddziaływaniu ukierunkowania włókien na piezoelektryczność podłoży komórkowych. Stwierdzono, że korzystne jest dążenie do właściwości piezoelektrycznych implantowanych materiałów możliwie jak najbardziej zbliżonych do właściwości naturalnych kości.

Następnie szeroko omówiono naturalne i syntetyczne polimery piezoelektryczne, ich właściwości oraz potencjalne zastosowania biomedyczne. Wskazano, że naturalne polimery wykazują się ograniczoną stabilnością oraz znaczną degradacją, co może ograniczać ich długoterminowe zastosowanie w inżynierii tkankowej. Z kolei w przypadku polimerów syntetycznych zauważono, że mogą one umożliwić bardziej precyzyjne dobranie właściwości piezoelektrycznych oraz zapewnić większą stabilność biomateriałów. Stwierdzono, że z uwagi na złożoność zagadnienia konieczne są dalsze badania w celu optymalizacji formowania materiałów piezoelektrycznych i ich integracji z komórkami kostnymi. Skoncentrowano się na dyskusji wyników aktualnych badań, analizując wpływ struktury, morfologii i właściwości fizykochemicznych elektroprzędzonych włóknin na ich potencjał w inżynierii tkankowej oraz wpływ dodatków i ukierunkowania włókien. Wykazano, że odpowiednia modyfikacja składu materiałowego może pozwolić na uzyskanie podłoży o zwiększonej biozgodności, piezoelektryczności i potencjale regeneracyjnym w odniesieniu do tkanki kostnej oraz tkanki nerwowej.

Podsumowując, piezoelektryczne biomateriały są obiecującym rozwiązaniem w inżynierii tkanki kostnej, gdyż mogą generować sygnały elektryczne, które wspierają regenerację tkanek, imitując naturalne procesy zachodzące w organizmie. Przyszłe badania powinny koncentrować się na poprawie biokompatybilności i biodegradowalności piezoelektrycznych polimerów, opracowaniu nowych kompozytów o lepszych właściwościach piezoelektrycznych, optymalizacji metod wytwarzania inteligentnych podłoży oraz integracji piezoelektrycznych biomateriałów z metodami stymulacji zewnętrznej.

W odpowiedzi na te zagadnienia przyjęto, że piezoelektryczne podłoże komórkowe na bazie PLLA, zmodyfikowane dodatkiem piezoelektrycznego nHA, stanowi perspektywiczną kombinację materiałową. Parametry tego podłoża można regulować poprzez zastosowanie elektroprzędzenia przy różnych prędkościach odbioru, co umożliwia precyzyjne dostosowanie podłoża komórkowego do określonych potrzeb.

7.3. Influence of process-material conditions on the structure and biological properties of electrospun polyvinylidene fluoride fibers

Piezoelektryczność PVDF wynika z obecności faz polarnych, w szczególności fazy β, której powstawanie zależy od warunków procesu elektroprzędzenia. Elektroprzędzone włókna PVDF o podwyższonych właściwościach piezoelektrycznych mogą pełnić funkcję inteligentnych podłoży komórkowych.

Celem badań opisanych w niniejszym artykule było opracowanie i optymalizacja procesu elektroprzędzenia piezoelektrycznego polimeru PVDF, a także określenie wpływu prędkości obrotowej kolektora na morfologię, zawartość faz piezoelektrycznych oraz właściwości biologiczne. W szczególności analizowano wpływ struktury na interakcję komórek z podłożem oraz wpływ zawartości faz piezoelektrycznych na odpowiedź komórkową.

Przed procesem elektroprzędzenia przeprowadzono pomiary lepkości roztworów polimerowych. Ustalono, że efekt rozrzedzania ścinaniem występuje jedynie w przypadku roztworu o najwyższym stężeniu, natomiast roztwory o niższych stężeniach zachowują się jak płyny newtonowskie. Efekt rozrzedzania ścinaniem jest najprawdopodobniej związany z efektywną orientacją cząsteczek przy wyższych szybkościach ścinania. Analiza zmian lepkości w funkcji czasu, prowadzona od momentu przygotowania roztworu, wykazała, że niezależnie od użytego stężenia polimeru roztwory pozostają stabilne.

Proces formowania włókien PVDF prowadzono z roztworów o szeroko zróżnicowanym stężeniu, co pozwoliło na określenie optymalnych parametrów oraz wyznaczenie okna procesowego gwarantującego stabilność procesu i uzyskanie jednorodnych włókien bez defektów morfologicznych, takich jak tzw. koraliki.

Analiza morfologii z użyciem obrazów SEM wykazała, że najwyższej jakości włókna, pozbawione defektów struktury, otrzymano z roztworu o stężeniu 22%, który został następnie wybrany do dalszych badań. Włókna formowano przy różnych prędkościach obrotowych kolektora w celu uzyskania zarówno losowego, jak i ukierunkowanego ułożenia. Analiza

morfologii włókien wykazała, że wraz ze wzrostem prędkości obrotowej kolektora średnica włókien ulega zmniejszeniu, a rozkład średnic opisuje krzywa Gaussa. Ponadto wykazano, że rozkład orientacji włókien staje się węższy (szerokość połówkowa rozkładu maleje) wraz ze wzrostem prędkości kolektora. W pracy wykazano, że wzrost prędkości obrotowej kolektora w procesie elektroprzędzenia prowadzi do zwiększenia stopnia ukierunkowania włókien.

Do obliczenia zawartości faz piezoelektrycznych (faza β i faza γ) w podłożach komórkowych zastosowano spektroskopię FTIR-ATR. Wykazano, że zwiększenie prędkości obrotowej kolektora prowadzi nie tylko do zwiększenia stopnia ukierunkowania włókien oraz zmniejszenia ich średnicy, ale także do istotnego wzrostu zawartości faz piezoelektrycznych. Dalsza analiza ujawniła, że próbki o losowym ułożeniu włókien zawierają jedynie 0,6% faz piezoelektrycznych, natomiast w próbkach o ukierunkowanym ułożeniu wartość ta osiągnęła 94,5%.

Badania *in vitro* przeprowadzono z wykorzystaniem mysich fibroblastów linii L929. Dodatkowo komórki poddano stymulacji ultradźwiękowej, przy czym jako próbki kontrolne zastosowano podłoża bez stymulacji. We wszystkich przypadkach przeżywalność komórek przekraczała 70%, co, zgodnie z normą ISO 10993-5, wskazuje, że analizowane próbki nie wykazują cytotoksyczności. Zaobserwowano, że włókna o ukierunkowanym ułożeniu i poddane stymulacji ultradźwiękowej charakteryzowały się wyższą przeżywalnością komórek w porównaniu z włóknami niestymulowanymi. Po siedmiodniowej hodowli fibroblasty na powierzchni włókien PVDF wykazywały wydłużoną i spłaszczoną morfologię, co sugeruje korzystną interakcję komórek z podłożem komórkowym.

Uzyskane wyniki są niezwykle obiecujące i wskazują na potencjał elektroprzędzonych włókien PVDF jako innowacyjnych podłoży komórkowych. Wykazano, że poprzez precyzyjny dobór parametrów procesu możliwe jest uzyskanie podłoży komórkowych o zwiększonych właściwościach piezoelektrycznych oraz poprawionej odpowiedzi komórkowej. Takie inteligentne materiały mogą w przyszłości wpłynąć na rozwój inżynierii tkankowej, szczególnie w zakresie regeneracji tkanki nerwowej i kostnej, eliminując konieczność stosowania zewnętrznej stymulacji. Wyniki te mogą stanowić podstawę do dalszych badań nad zaawansowanymi biomateriałami aktywnymi, które w połączeniu z nowoczesnymi technologiami medycznymi mogą prowadzić do nowych rozwiązań w medycynie regeneracyjnej.

7.4. Enhanced Electroactive Phases of Poly(vinylidene Fluoride) Fibers for Tissue Engineering Applications

Celem badań przedstawionych w artykule była analiza wpływu masy cząsteczkowej polimerów piezoelektrycznych oraz parametrów procesu elektroprzędzenia na zwiększenie właściwości piezoelektrycznych i odpowiedzi komórkowej. Badania miały doprowadzić do uzyskania optymalnych parametrów procesu elektroprzędzenia, pozwalających na uzyskanie pożądanej morfologii, dużej zawartości faz piezoelektrycznych, a tym samym wartości współczynnika piezoelektryczności oraz zwiększonej odpowiedzi biologicznej, z perspektywy materiału odpowiedniego do zastosowań w inżynierii tkankowej. W pracy badano wpływ masy cząsteczkowej PVDF, ułożenia włókien oraz parametrów procesu elektroprzędzenia na zawartość faz piezoelektrycznych, wartość współczynnika piezoelektryczności oraz odpowiedź komórkową, badaną z wykorzystaniem ludzkich stromalnych komórek macierzystych.

Przeprowadzono proces formowania podłoży komórkowych przy różnych parametrach procesu, takich jak prędkość obrotowa kolektora, szybkość podawania roztworu oraz przyłożone napięcie, w wyniku czego wytworzono 24 różne próbki, które poddano analizie pod kątem morfologii, ułożenia włókien oraz zawartości faz piezoelektrycznych.

Pierwsza grupa podłoży komórkowych została wytworzona z polimerów o różnej masie cząsteczkowej (M_w = 180 000 g/mol, 530 000 g/mol) z zastosowaniem zróżnicowanej prędkości obrotowych kolektora podczas procesu elektroprzędzenia. Analiza morfologii włókien przeprowadzona za pomocą mikroskopii SEM potwierdziła otrzymanie jednorodnych, bezdefektowych nanowłókien o równomiernej średnicy. Stwierdzono, że średnica włókien zmniejsza się wraz ze wzrostem prędkości obrotowej kolektora, jak również, że przy dużych prędkościach obrotowych kolektora średnica włókien nie zależy od masy cząsteczkowej polimeru, natomiast przy małych prędkościach obserwuje się wyraźny wpływ masy cząsteczkowej na średnicę włókien. Wywnioskowano, że gęstość splątań i długość łańcucha w polimerze mają znaczenie w warunkach relatywnie małego naprężenia rozciągającego działającego na włókna przy małych prędkościach obrotowych kolektora. Przy dużej prędkości obrotowej kolektora siły rozciągające eliminują ograniczenia wynikające z lepkości, umożliwiając tworzenie cieńszych włókien dzięki działaniu intensywnego naprężenia mechanicznego.

Wpływ prędkości obrotowej kolektora na ukierunkowanie nanowłókien PVDF określono ilościowo przy użyciu wskaźnika anizotropii (α), którego wartość wzrastała

wraz ze wzrostem prędkości obrotowej kolektora. Porównanie wartości wskaźnika anizotropii dla różnych mas cząsteczkowych wykazało jedynie niewielki wzrost ukierunkowania włókien dla dużej masy cząsteczkowej. Ilościową analizę zawartości faz piezoelektrycznych przeprowadzono z użyciem spektroskopii FTIR-ATR. Wraz ze wzrostem prędkości obrotowej kolektora, powodującej wzrost sił rozciągających, stwierdzono wzrost zawartości faz piezoelektrycznych.

Kolejną grupę próbek poddano analizie wpływu napięcia przyłożonego podczas procesu elektroprzędzenia. Badania prowadzono przy ustalonej, dużej prędkości obrotowej kolektora. Stwierdzono, że zawartość faz piezoelektrycznych osiąga maksimum przy wartości 22 kV, która sprzyja rozciąganiu i orientowaniu się łańcuchów polimerowych. Po przekroczeniu tej wartości siły elektrostatyczne są zbyt wysokie, co powoduje destabilizację strugi i powstawanie kropli polimeru, a w rezultacie zmniejszenie zawartości faz piezoelektrycznych.

W przypadku wpływu szybkości podawania roztworu polimeru na proces elektroprzędzenia najniższa szybkość przepływu (0,5 ml/h) okazała się niewystarczająca do utworzenia stabilnej strugi polimeru. Stwierdzono, że zawartość faz piezoelektrycznych osiąga maksimum przy szybkości przepływu 0,8 ml/h. Gdy szybkość przepływu osiąga wartość 1,5 ml/h, proces staje się niestabilny, ze względu na osłabienie sił rozciągających strugę roztworu polimeru.

Uzyskane wyniki wyraźnie wskazują na korelację współczynnika piezoelektryczności z zawartością faz piezoelektrycznych. Zależność tę wykazano, badając zawartość faz piezoelektrycznych metodą spektroskopii FTIR-ATR. Stwierdzono ponadto, że współczynnik piezoelektryczności wzrasta wraz ze wzrostem prędkości obrotowej kolektora, niezależnie od masy cząsteczkowej polimeru. Zaobserwowano, że wpływ prędkości obrotowej kolektora jest większy w przypadku dużej masy cząsteczkowej i prowadzi do wyższego współczynnika piezoelektryczności.

Badania biologiczne wykazały brak cytotoksyczności oraz zwiększoną przeżywalność ludzkich stromalnych komórek macierzystych hodowanych na podłożach o zwiększonych właściwościach piezoelektrycznych. Najwyższe wartości proliferacji uzyskano dla podłoży formowanych przy prędkości obrotowej 2000 obr./min. Morfologię komórek oceniono za pomocą mikroskopii SEM w 3. i 21. dniu hodowli. Korzystne rozpłaszczanie się komórek obserwowano we wszystkich próbkach. Najgęstsza warstwa komórkowa, prawdopodobnie zawierająca również macierz zewnątrzkomórkową wytworzoną przez komórki, została zaobserwowana w próbce o najwyższych właściwościach piezoelektrycznych po 21. dniu

hodowli. Uzyskane wyniki wykazały korzystny wpływ faz piezoelektrycznych na adhezję komórek do podłoża, co było widoczne w ich wysokiej proliferacji i optymalnej morfologii.

Badania pozwoliły na pogłębione zrozumienie mechanizmów fundamentalnego procesu formowania faz piezoelektrycznych w PVDF, wykazując ich ścisły związek z masą cząsteczkową i parametrami procesu elektroprzędzenia. Określono optymalne parametry formowania włókien, umożliwiające uzyskanie maksymalnej zawartości faz piezoelektrycznych. Wykazano, że wysoka zawartość faz piezoelektrycznych, powodująca relatywnie dużą piezoelektryczność, nie wpływa negatywnie na cytotoksyczność próbek. Wartość współczynnika piezoelektryczności formowanych podłoży wynosiła około 4-4,5 pC/N^{-1}, podczas gdy ludzka kość charakteryzuje się właściwościami piezoelektrycznymi na poziomie 0,7-2,3 pC/N^{-1}.

7.5. Poly(L-lactide)/nano-hydroxyapatite piezoelectric scaffolds for tissue engineering

Celem badań przedstawionych w artykule było opracowanie piezoelektrycznego, biodegradowalnego i nanowłóknistego podłoża komórkowego na bazie PLLA zawierającego nHA, charakteryzującego się jednorodną i regularną morfologią nanowłókien, podwyższonymi właściwościami piezoelektrycznymi oraz zwiększoną odpowiedzią komórkową. Przy wykorzystaniu procesu elektroprzędzenia wytworzono piezoelektryczne włókna PLLA z dodatkiem nHA o losowym i ukierunkowanym ułożeniu włókien, a następnie oceniono wpływ ułożenia włókien oraz obecności nHA na zawartość faz piezoelektrycznych i właściwości piezoelektryczne. Ponadto przeprowadzono badania *in vitro* z wykorzystaniem ludzkich komórek osteoblastopodobnych MG63 w celu określenia cytotoksyczności, przeżywalności komórek oraz analizę morfologii hodowli na opracowanych materiałach.

W procesie elektroprzędzenia zastosowano optymalne parametry procesu ustalone na podstawie wcześniejszych badań, stosując różne prędkości obrotowe kolektora. Zastosowanie mniejszych prędkości obrotowych prowadziło do powstania próbek o losowym ułożeniu włókien, natomiast przy dużej prędkości obrotowej kolektora uzyskano próbki charakteryzujące się ukierunkowanym ułożeniem włókien.

Analiza morfologii za pomocą mikroskopii SEM wykazała, że włókna charakteryzowały się jednolitą strukturą, bez widocznych defektów ani aglomeratów nHA. Stwierdzono, że zwiększenie prędkości obrotowej kolektora powoduje zmniejszenie średnicy włókien zarówno w czystych próbkach, jak i w próbkach domieszkowanych nHA. Analiza

obrazów SEM wykazała, że obecność dodatku nHA nie wpływa na średnicę włókien, natomiast analiza SEM-EDS potwierdziła obecność nHA wewnątrz nanowłókien PLLA. Stwierdzono, że większa prędkość obrotowa kolektora prowadzi do większego ukierunkowania włókien, określonego ilościowo za pomocą wskaźnika anizotropii (α). Dodatkowo, stwierdzono wpływ dodatku nHA na wzrost porowatości włókien o około 5%. Z kolei, badania zwilżalności wykazały, że dodatek nHA zwiększa hydrofilowość podłoży z PLLA. Pomiar kąta zwilżania wykazał, że obecność nHA obniża kąt zwilżania dla wszystkich analizowanych cieczy (woda, formamid, dijodometan), przy czym największy efekt zaobserwowano w przypadku włókien o ułożeniu ukierunkowanym.

Analiza energii swobodnej powierzchni (SFE) metodą Kaelble-Owensa-Wendt'a wykazała wpływ dodatku nHA na wzrost SFE nanowłóknistych podłoży z PLLA. Szczególnie istotny wzrost zaobserwowano w przypadku włókien ukierunkowanych PLLA/nHA. Zwiększenie wartości SFE wynikało głównie z wyższego udziału składowej oddziaływań polarnych, co wskazuje na lepszą interakcję z wodnymi środowiskami biologicznymi. Badania zdolności sorpcji wody wykazały, że dodatek nHA zwiększa zdolność włókien do wchłaniania wody. Najwyższą sorpcję odnotowano dla włóknin PLLA/nHA o ukierunkowanym ułożeniu. Z punktu widzenia inżynierii tkankowej jest to korzystne, ponieważ może poprawić transport substancji odżywczych oraz wspomagać proliferację komórek.

Analiza wykonana metodą spektroskopii FTIR-ATR potwierdziła obecność nHA wewnątrz nanowłókien PLLA oraz pozwoliła ocenić potencjalne interakcje chemiczne między składnikami kompozytu. Widma FTIR czystego PLLA wykazały charakterystyczne pasma dla tego polimeru, w tym pasma związane z drganiami grup estrowych, grup metylowych oraz mostków estrowych. W przypadku włókien PLLA/nHA dodatkowo zaobserwowano pasma charakterystyczne dla nHA, w tym pasma związane z jonami fosforanowymi. Nie zaobserwowano pasma przy 921 cm^{-1}, które jest związane z krystaliczną fazą PLLA, co wskazuje na amorficzność PLLA we włóknach. Ponadto brak istotnych przesunięć pasm nHA wskazuje na brak silnych oddziaływań chemicznych między PLLA a nHA.

Badania metodą WAXS potwierdziły amorficzność otrzymanych włókien PLLA, pokazując brak ostrych refleksów dyfrakcyjnych PLLA oraz obecność dodatku krystalicznego nHA. Analiza amorficznego halo dla PLLA wykazała jego bimodalny kształt, sugerując współistnienie klasycznej składowej nieuporządkowanej fazy α oraz części struktury wykazującej słabe uporządkowanie, prawdopodobnie pochodzącej od fazy α'. Stwierdzono, że dodatek nHA nie wpływa na krystalizację PLLA podczas procesu elektroprzędzenia. Podsumowując, elektroprzędzone włókna PLLA, niezależnie od ułożenia i obecności nHA,

pozostawały w stanie amorficznym, ze słabym uporządkowaniem charakterystycznym dla fazy α'. Wyniki te korelują z analizą DSC, w której wykazano intensywną krystalizację próbek dopiero po przekroczeniu temperatury zeszklenia (T_g), co może wskazywać na istnienie słabo uporządkowanej struktury stanowiącej obszar sprzyjający zimnej krystalizacji, zachodzącej bezpośrednio po przekroczeniu T_g.

Badania metodą różnicowej kalorymetrii skaningowej (DSC) zostały przeprowadzone w celu określenia właściwości cieplnych podłoży z PLLA oraz oceny wpływu dodatku nHA na ich stabilność termiczną i procesy krystalizacji. W zakresie temperatur poniżej 50°C obserwowano liniowy wzrost pojemności cieplnej (C_p), natomiast w przedziale 50-80°C, po przekroczeniu T_g, zarejestrowano dwa efekty cieplne: endotermiczny (relaksacja naprężeń) oraz silny egzotermiczny efekt zimnej krystalizacji. W zakresie 80-150°C zarejestrowano dodatkowy szeroki efekt egzotermiczny, prawdopodobnie związany z rekrystalizacją i/lub przemianami polimorficznymi fazy α' w bardziej uporządkowaną fazę α. Powyżej 160°C zaobserwowano silny efekt endotermiczny związany z topnieniem kryształów, które pojawiły się podczas ogrzewania, osiągając maksimum przy 180-190°C. Istotnym spostrzeżeniem było to, że próbki PLLA/nHA wykazywały mniejszą zdolność do krystalizacji oraz niższą entalpię topnienia w porównaniu z czystym PLLA. Stopień krystaliczności czystego PLLA wynosił ok. 70%, natomiast PLLA/nHA ok. 40%, co wskazuje na to, że obecność nHA ogranicza mobilność łańcuchów polimerowych i hamuje proces krystalizacji. Ponadto włókniny PLLA/nHA wykazywały niższą pojemność cieplną w stanie amorficznym w porównaniu z czystym PLLA, co potwierdza zmniejszoną mobilność łańcuchów polimerowych w obecności nHA.

Badania współczynnika piezoelektryczności przeprowadzono w celu oceny wpływu ukierunkowania włókien oraz dodatku nHA na właściwości piezoelektryczne elektroprzędzonych podłoży komórkowych z PLLA. Wyniki wykazały, że zarówno ukierunkowanie włókien, jak i wprowadzenie dodatku nHA znacząco zwiększały wartość współczynnika piezoelektryczności. Próbka PLLA/nHA o losowym ułożeniu włókien osiągnęła wartość 4,42±0,13 pC/N^{-1}, natomiast próbka PLLA/nHA o ukierunkowanym ułożeniu włókien wykazała najwyższą wartość 4,68±0,08 pC/N^{-1}. Zaobserwowany wzrost właściwości piezoelektrycznych można wyjaśnić dwoma czynnikami: większą orientacją dipoli piezoelektrycznych w przypadku włókien ukierunkowanych, co umożliwia efektywniejszą konwersję energii mechanicznej w energię elektryczną, oraz wpływem nHA, który sam wykazuje właściwości piezoelektryczne i może wzmacniać efekt piezoelektryczny PLLA.

Badania *in vitro* przeprowadzono w celu oceny cytotoksyczności oraz osteokonduktywności piezoelektrycznych podłoży komórkowych z wykorzystaniem ludzkiej linii osteoblastów MG-63, analizując ich przeżywalność, proliferację oraz morfologię po 3. i 5. dniu hodowli. Wszystkie testowane podłoża wykazały brak cytotoksyczności, spełniając wymagania normy ISO 10993-5 dotyczące materiałów biomedycznych. Przeżywalność osteoblastów wynosiła ponad 70% dla wszystkich próbek, przy czym najwyższą proliferację komórek zaobserwowano na podłożach PLLA/nHA z włóknami o ułożeniu ukierunkowanym. Obserwacje przy użyciu mikroskopii fluorescencyjnej wykazały, że osteoblasty na wszystkich próbkach wykazywały prawidłową rozpłaszczoną morfologię. Na próbkach o losowym ułożeniu włókien komórki również przyjmowały rozpłaszczony kształt. Na podłożach PLLA/nHA zaobserwowano lepsze przyleganie komórek oraz bardziej rozbudowaną strukturę cytoszkieletu, co wskazuje na korzystny wpływ nHA na interakcje komórka-materiał. Ukierunkowanie włókien wspomagało organizację i migrację komórek.

Badania potwierdziły, że opracowane nanowłókniste podłoża komórkowe z PLLA z dodatkiem nHA wykazują właściwości sprzyjające zastosowaniom w inżynierii tkanki kostnej. W szczególności wykazano, że zarówno ukierunkowane ułożenie włókien, jak i obecność nHA wpływają na kluczowe parametry fizykochemiczne, piezoelektryczne oraz biologiczne materiału. Ukierunkowane włókna wykazywały bardziej uporządkowaną strukturę, co zwiększało ich piezoelektryczność i sprzyjało korzystnym interakcjom z komórkami. Próbki o losowym ułożeniu włókien tworzyły bardziej porowatą i nieregularną sieć, co mogło wspierać wielokierunkowy wzrost tkanki, ale ich właściwości piezoelektryczne były niższe. Otrzymane wyniki jednoznacznie wskazują, że ukierunkowane nanowłókna oraz obecność dodatku nHA stanowią szczególnie obiecujący biomateriał do regeneracji kości dzięki połączeniu biodegradowalności, piezoelektryczności oraz wysokiej bioaktywności.

7.6. On the Structural and Biological Effects of Hydroxyapatite and Gold nano-scale Particles in Poly(vinylidene fluoride) Smart Scaffolds for Bone and Neural Tissue Engineering

Celem badań przedstawionych w artykule było opracowanie piezoelektrycznego i nanowłóknistego podłoża komórkowego formowanego z PVDF o dużej masie cząsteczkowej (M_w = 530 000 g/mol), o losowym i ukierunkowanym ułożeniu włókien, a także z dodatkiem piezoelektrycznego nanohydroksyapatytu (nHA) lub powierzchniowo bioaktywnymi nanocząstkami złota (AuNPs). Badania obejmowały ocenę morfologii, zwilżalności, energii

swobodnej powierzchni i polarności, sorpcji wody i zawartości faz piezoelektrycznych z perspektywy materiału odpowiedniego do zastosowań w inżynierii tkankowej. Badania biologiczne obejmowały ocenę odpowiedzi komórkowej z użyciem ludzkich komórek osteoblastopodobnych (MG63) i komórek pochodzących z hodowli neuralnych komórek macierzystych wyprowadzonych z indukowanych pluripotencjalnych komórek macierzystych (hiPSC-NSC) w celu wykluczenia cytotoksyczności i oceny przeżywalności, a także ocenę morfologii hodowli *in vitro* na proponowanych materiałach.

Analiza morfologii próbek metodą mikroskopii SEM potwierdziła otrzymanie podłoży o jednorodnej strukturze pozbawionej defektów. Podobnie jak w publikacjach 7.3, 7.4 i 7.5., zwiększenie prędkości obrotowej kolektora skutkowało zwiększeniem ukierunkowanego ułożenia włókien oraz zmniejszeniem ich średnicy we wszystkich typach próbek. Włączenie dodatków do struktury włókien nie powodowało znaczących zmian w ich średnicy, natomiast zwiększyło porowatość próbek. Obecność dodatków potwierdzono przy użyciu spektroskopii SEM-EDS.

Przeprowadzono badania sorpcji wody, kąta zwilżania oraz energii swobodnej powierzchni (SFE). Najwyższą zdolność sorpcyjną wykazywały próbki zawierające nHA, zarówno o losowym, jak i ukierunkowanym ułożeniu włókien. Wzrost sorpcji wody w próbkach o ukierunkowanym ułożeniu włókien przypisywano z bardziej uporządkowaną strukturą, która zwiększała dostępność powierzchni dla wody. Zwilżalność próbek o ukierunkowanym ułożeniu włókien była wyższa, a dodatkowo obecność nHA i AuNPs w strukturze włókien zwiększała ten efekt. SFE była najwyższa dla próbki o ukierunkowanym ułożeniu włókien, a wprowadzenie dodatków prowadziło do dalszego jej wzrostu.

Badania metodą spektroskopii FTIR-ATR potwierdziły obecność nanocząstek nHA (drgania zginające i rozciągające grup fosforanowych przy 565 cm^{-1} i 601 cm^{-1}) oraz AuNPs (drgania rozciągające wiązań Au-O przy 525 cm^{-1} i 612 cm^{-1}). Przeprowadzono również analizę ilościową zawartości faz piezoelektrycznych PVDF. Zidentyfikowano obecność fazy α (490, 766, 1402, 1432 cm^{-1}), fazy β (510, 600, 840, 1280 cm^{-1}) oraz fazy γ (812, 840, 1234 cm^{-1}). Wykazano, że zawartość fazy β była wyższa w przypadku włókien formowanych przy prędkości kolektora 2000 obr./min. w porównaniu z włóknami otrzymanymi przy 100 obr./min. Ponadto zaobserwowano, że dodatek nHA zwiększał zawartość faz piezoelektrycznych zarówno w próbkach o losowym, jak i ukierunkowanym ułożeniu włókien. Najsilniejszy efekt odnotowano w przypadku próbek o ukierunkowanym ułożeniu włókien. Zmniejszenie zawartości faz piezoelektrycznych w próbkach z dodatkiem AuNPs może wynikać z lokalnego nagrzewania podczas procesu sonifikacji, co mogło

prowadzić do częściowej transformacji faz β i γ w fazę α. Zagadnienie to wymaga dalszych badań. Stwierdzono również, że wzrost prędkości obrotowej kolektora powodował istotne zwiększenie ilości faz piezoelektrycznych, przy jednoczesnym zmniejszaniu średnicy włókien. Zjawisko to można wytłumaczyć wzrostem sił rozciągających, które sprzyjają orientacji łańcuchów polimerowych w nanowłóknach. Na podstawie otrzymanych wyników oceniono, że mniejsza porowatość próbek sprzyja większej zawartości faz piezoelektrycznych, przy jednoczesnym zmniejszeniu średnicy włókien. Na podstawie przeprowadzonych badań stwierdzono, że stabilność faz β i γ jest większa w materiałach uporządkowanych i bardziej porowatych, gdzie występuje ograniczona migracja i deformacja łańcuchów polimerowych.

Profile WAXS zostały wykorzystane do oszacowania krystaliczności podłoży komórkowych, zawartości faz α i β, a także obecności nHA i AuNPs. Całkowitą krystaliczność próbek określono na około 30%. Dodanie nHA znacząco zwiększało zawartość fazy β. Z kolei stymulacja ultradźwiękami prowadziła do wzrostu zawartości fazy α. Ponadto wyższa prędkość obrotowa kolektora (włókna ukierunkowane) prowadziła do zwiększenia zawartości fazy β we włóknach PVDF i PVDF/Au, ale nie wpływała znacząco na zawartość faz we włóknach PVDF/nHA. Zawartość faz α i β uzyskana z analizy WAXS była zgodna z wynikami spektroskopii FTIR-ATR.

Badania DSC przeprowadzono w celu określenia temperatury i ciepła topnienia oraz wyznaczenia krystaliczności. W analizowanych próbkach wyróżniono trzy charakterystyczne efekty termiczne: P1 (~60°C) - przypisany do rozpadu kryształów o najmniejszej doskonałości, który jest typowy dla PVDF przechowywanego w warunkach pokojowych; P2 (~166°C) - odpowiadający topnieniu kryształów faz α i β, obecnych we wszystkich badanych próbkach i P3 (~171°C) - odpowiadający topnieniu kryształów fazy γ, występującej w próbkach PVDF i PVDF/Au, natomiast nieobecnej w PVDF/nHA. Sonifikacja w próbkach o ukierunkowanym ułożeniu włókien z dodatkiem AuNPs doprowadziła do nieznacznego zmniejszenia ilości fazy γ, przy jednoczesnym wzroście liczby wadliwych kryształów wtórnych, co potwierdzono wzrostem wielkości piku P1. W próbkach o losowym ułożeniu włókien sonifikacja spowodowała nieznaczny wzrost ilości kryształów α powstających z wadliwych kryształów wtórnych, co znalazło odzwierciedlenie w zmniejszeniu wielkości piku P1.

Przyjmując teoretyczną wartość równowagowej entalpii topnienia, ΔH_0 = 104,5 J/g, krystaliczność próbek określono na ok. 60%, co stanowi wartość niemal dwukrotnie wyższą niż ta uzyskana metodą analizy profili WAXS (ok. 30%). Tak duża rozbieżność jest zaskakująca, tym bardziej że analiza krystaliczności granulatu PVDF wyniosła

odpowiednio 53,5% (WAXS) i 55,8% (DSC). Zjawisko to można wytłumaczyć dużym stopniem zdefektowania struktury krystalicznej, wynikającym z ekstremalnie szybkiego odparowywania rozpuszczalnika. Struktura ta o relatywnie niskiej krystaliczności była rejestrowana bezpośrednio w badaniach WAXS prowadzonych w temperaturze pokojowej. Z kolei w analizach DSC krystaliczność wyznaczana jest na podstawie ciepła topnienia kryształów zarówno tych, które powstają w trakcie elektroprzędzenia, jak i tych, które mogą powstawać podczas ogrzewania próbki z niedoskonałych struktur krystalicznych jako rezultat dążenia do osiągnięcia równowagi termodynamicznej. Skutkuje to pozornie wyższą krystalicznością wyznaczaną metodą DSC.

Analiza *in vitro* z użyciem komórek MG-63 potwierdziła brak cytotoksyczności nanowłóknistych podłoży PVDF. Przeżywalność komórek wynosiła powyżej 70%, co spełnia kryteria normy ISO 10993-5 dla materiałów nietoksycznych. Stwierdzono istotny wpływ ułożenia włókien (określanego na podstawie wartości FWHM) oraz zawartości faz piezoelektrycznych na przeżywalność komórek MG-63. Najwyższą przeżywalność odnotowano dla próbek z dodatkiem nHA i ukierunkowanym ułożeniem włókien, które charakteryzowały się jednocześnie najwyższą zawartością fazy β. W próbkach o losowym ułożeniu włókien komórki wykazywały niższą proliferację, co może być związane z mniej korzystną morfologią i niższą zawartością faz piezoelektrycznych. Natomiast w przypadku próbek o ukierunkowanym ułożeniu włókien komórki wykazywały charakterystyczne rozpłaszczanie i ukierunkowanie wzdłuż włókien.

Wstępne eksperymenty *in vitro* z wykorzystaniem komórek hiPSC-NSC przeprowadzono w celu oceny różnicowania komórek oraz ich zachowania na elektroprzędzonych nanowłóknistych matach formowanych z czystego PVDF oraz PVDF z dodatkiem nHA, przy losowym i ukierunkowanym ułożeniu włókien. Komórki hodowane na powierzchni nanowłókien różnicowały się w neurony, co potwierdzono obecnością markera beta-tubuliny III. Wpływ ukierunkowania włókien na morfologię komórek był stosunkowo niewielki, co może wynikać z obecności dodatkowej powłoki białkowej macierzy zewnątrzkomórkowej, naniesionej na maty nanowłókniste, niezbędnej do zapewnienia odpowiedniej adhezji komórek. W próbkach o ukierunkowanym ułożeniu włókien zaobserwowano jednak wyższy stopień kierunkowego różnicowania komórek neuronalnych w porównaniu z próbkami o losowym ich ułożeniu. Kwestia, czy ukierunkowanie włókien skuteczniej wspiera formowanie sieci neuronowych oraz wydłużanie aksonów, pozostaje otwarta i wymaga dalszych, bardziej szczegółowych badań.

Podsumowując, wykazano, że wprowadzenie dodatku nHA do elektroprzędzonych włókien PVDF i duża prędkość obrotowa kolektora, nie tylko zwiększają ukierunkowane ułożenie wlókien, ale również sprzyjają powstawaniu faz piezoelektrycznych. Włókna o losowym ułożeniu mogą lepiej odwzorowywać strukturalną złożoność naturalnej macierzy kostnej, natomiast włókna o wysokim stopniu ukierunkowania mogą być szczególnie odpowiednie w kierowaniu regeneracją nerwów, co podkreśla wielofunkcyjny charakter opracowanego materiału. Przeprowadzone badania potwierdzają, że opracowane kompozyty piezoelektryczne mogą stać się obiecującymi materiałami w inżynierii tkankowej, szczególnie w trudnych zagadnieniach regeneracyjnych, takich jak naprawa kości i układu nerwowego.

8. Wnioski

Potwierdzono hipotezę badawczą, że przy wykorzystaniu polimerów przejawiających właściwości piezoelektryczne, możliwe jest wytworzenie metodą elektroprzędzenia nanowłóknistych i biozgodnych podłoży sprzyjających efektywnemu wzrostowi komórek, umożliwiając ich zastosowanie w inżynierii tkankowej, w szczególności do regeneracji tkanki nerwowej i kostnej.

W szczególności stwierdzono, że:

- Najwyższe właściwości piezoelektryczne podłoży uzyskuje się w warunkach sprzyjających silnej orientacji makrocząsteczek polimeru, przy czym dla PVDF prowadzi to do krystalizacji faz o konformacjach piezoelektrycznych, podczas gdy dla PLLA mamy do czynienia z pojawieniem się konformacji piezoelektrycznej w fazie amorficznej, która może lokalnie indukować powstawanie słabo uporządkowanej fazy α'.

- Wzrost ukierunkowania włókien oraz dodatek nHA prowadzą do wzrostu piezoelektryczności podłoży, podnosząc przeżywalność komórek.

- Zastosowanie dodatków nHA i AuNPs zwiększa hydrofilowość podłoży poprawiając tym samym ich odpowiedź biologiczną.

- Szeroki zakres aplikacyjny opracowanej technologii umożliwia wytworzenie zarówno włókien o losowym ułożeniu, które bardziej naśladują strukturalną złożoność naturalnej macierzy kostnej, jak i włókien ukierunkowanych, które wydają się szczególnie odpowiednie dla zastosowań w inżynierii tkanki nerwowej.

9. Elementy wkładu oryginalnego

Elementem wkładu oryginalnego w dziedzinę przedmiotu jest opracowanie metody otrzymywania nanowłókien polimerowych o kontrolowanej zawartości faz piezoelektrycznych i precyzyjnie sterowanym ułożeniu włókien za pomocą zoptymalizowanego procesu elektroprzędzenia. Po raz pierwszy wykazano, że optymalizacja parametrów procesu takich jak napięcie pola elektrycznego, prędkość obrotowa kolektora oraz prędkość podawania roztworu w połączeniu z odpowiednim doborem masy cząsteczkowej polimeru, umożliwia znaczące zwiększenie właściwości piezoelektrycznych polimerów PVDF i PLLA. Wyniki przeprowadzonych badań stanowią poszerzenie wiedzy na temat wpływu struktury, morfologii, ułożenia włókien na bioaktywność i funkcjonalność nanowłókien, szczególnie w kontekście ich potencjalnych zastosowań w inżynierii tkankowej.

Pomimo, że dotychczasowe prace w literaturze odnoszą się do pewnych wybranych zagadnień piezoelektryczności [93–95], wciąż brakowało systematycznych badań w kontekście ułożenia włókien i ich wpływu na piezoelektryczność. W pracy po raz pierwszy systematycznie oceniono wpływ masy cząsteczkowej polimerów oraz ich stężenia na właściwości piezoelektryczne i morfologię włókien PVDF oraz PLLA. Wykazano, że zastosowanie odpowiednich warunków wytwarzania umożliwia formowanie włókien o wysokim stopniu jednorodności, pozbawionych defektów, z jednoczesnym zwiększeniem ich właściwości piezoelektrycznych. Określono optymalne parametry elektroprzędzenia umożliwiające uzyskanie włóknin o kontrolowanym ukierunkowaniu włókien, co jest kluczowe dla ich funkcjonalności w zastosowaniach biomedycznych.

Nowatorskim elementem pracy było również uzyskanie wyników wpływu dodatków (nHA, AuNPs) na strukturę i właściwości piezoelektryczne włóknin polimerowych oraz opracowanie optymalnych parametrów procesu formowania takich materiałów z perspektywy ich piezoelektryczności i właściwości biologicznych w kontakcie z komórkami. Dodatkowo, pozyskano wyniki kompleksowej analizy oddziaływań międzycząsteczkowych, struktury nadcząsteczkowej oraz właściwości cieplnych włókien przy wykorzystaniu metod FTIR, WAXS oraz DSC. Dzięki temu, określono dokładne zależności pomiędzy parametrami procesu, a strukturą i właściwościami nanowłókien, co stanowi istotne uzupełnienie dotychczasowych badań literaturowych. Wykazano, że dodatek piezoelektrycznego hydroksyapatytu oraz nanocząstek złota istotnie wpływa na stopień krystaliczności i polarność powierzchni, co prowadzi do zwiększenia ich właściwości piezoelektrycznych. W rozprawie po raz pierwszy otrzymano wyniki badań dotyczących systematycznej oceny wpływu struktury

nadcząsteczkowej, ułożenia włókien i obecności dodatków na współczynnik piezoelektryczności, wskazując najbardziej korzystne konfiguracje materiałowe. Oryginalnym aspektem pracy były także wyniki badań *in vitro* z wykorzystaniem różnych typów linii komórkowych (L929, MG-63, ADSC oraz hiPSC-NSC), jak również wyniki eksperymentów biologicznych w warunkach stymulacji ultradźwiękowej.

10. Literatura

1. Garkal, A.; Bangar, P.; Avachat, A.; Pandit, A.; Paryani, M.; Sami, A.; Patel, J.; Butani, S.; Mehta, T. Biodegradable Polymers in Tissue Engineering and Regenerative Medicine. In *Handbook of Biodegradable Polymers*; Jenny Stanford Publishing, 2024 ISBN 978-1-03-269330-9.
2. Yuan, X.; Zhu, W.; Yang, Z.; He, N.; Chen, F.; Han, X.; Zhou, K. Recent Advances in 3D Printing of Smart Scaffolds for Bone Tissue Engineering and Regeneration. *Advanced Materials* **2024**, *36*, 2403641, doi:10.1002/adma.202403641.
3. Vacanti, J.P.; Langer, R. Tissue Engineering: The Design and Fabrication of Living Replacement Devices for Surgical Reconstruction and Transplantation. *The Lancet* **1999**, *354*, S32–S34, doi:10.1016/S0140-6736(99)90247-7.
4. Mirjankar, M.R.; Ganeshka, M.P.; Gaddigal, A.T.; Shivappa, P.; Poojari, P.B.; Pattar, S.V.; Goder, P.H.; Kamanavalli, C.M. Use of Biomaterials in the Field of Biomedical Engineering: Current Trends, Challenges, and Opportunities in Implementations. In *Computational Approaches in Biomaterials and Biomedical Engineering Applications*; CRC Press, 2024 ISBN 978-1-03-269988-2.
5. Https://Pl.Khanacademy.Org/.
6. Álvarez-Chimal, R.; Arenas-Alatorre, J.Á.; Álvarez-Pérez, M.A. Nanoparticle-Polymer Composite Scaffolds for Bone Tissue Engineering. A Review. *European Polymer Journal* **2024**, *213*, 113093, doi:10.1016/j.eurpolymj.2024.113093.
7. Khan, M.U.A.; Stojanović, G.M.; Abdullah, M.F.B.; Dolatshahi-Pirouz, A.; Marei, H.E.; Ashammakhi, N.; Hasan, A. Fundamental Properties of Smart Hydrogels for Tissue Engineering Applications: A Review. *International Journal of Biological Macromolecules* **2024**, *254*, 127882, doi:10.1016/j.ijbiomac.2023.127882.
8. Wu, S.; Gai, T.; Chen, J.; Chen, X.; Chen, W. Smart Responsive in Situ Hydrogel Systems Applied in Bone Tissue Engineering. *Front. Bioeng. Biotechnol.* **2024**, *12*, 1389733, doi:10.3389/fbioe.2024.1389733.
9. Jana, S.; Stöbener, D.; Hoogenboom, R. Thermoresponsive “Smart” Polymer Systems for Drug Delivery, Gene Therapy and Tissue Engineering. In *Smart Systems in Biotechnology*; CRC Press, 2024 ISBN 978-1-00-332891-9.
10. Aishwarya, B.K.; V, R.; Singh, N.; Mathew, L.; Dhamija, K.; Fallah, M.H.; Kalra, R. Biodegradable Polymer Biomaterials for Tissue Engineering Applications: A Critical Review. *E3S Web of Conf.* **2024**, *529*, 01051, doi:10.1051/e3sconf/202452901051.

11. Aflori, M. Smart Nanomaterials for Biomedical Applications—A Review. *Nanomaterials* **2021**, *11*, 396, doi:10.3390/nano11020396.
12. Rajabi, A.H.; Jaffe, M.; Arinzeh, T.L. Piezoelectric Materials for Tissue Regeneration: A Review. *Acta Biomaterialia* **2015**, *24*, 12–23, doi:10.1016/j.actbio.2015.07.010.
13. Yadav, S.; Khan, J.; Yadav, A. Applications of Scaffolds in Tissue Engineering: Current Utilization andFuture Prospective. *CGT* **2024**, *24*, 94–109, doi:10.2174/0115665232262167231012102837.
14. Wang, C.; Zhou, Y. Sacrificial Biomaterials in 3D Fabrication of Scaffolds for Tissue Engineering Applications. *J Biomed Mater Res* **2024**, *112*, e35312, doi:10.1002/jbm.b.35312.
15. Wu, Y.; Zou, J.; Tang, K.; Xia, Y.; Wang, X.; Song, L.; Wang, J.; Wang, K.; Wang, Z. From Electricity to Vitality: The Emerging Use of Piezoelectric Materials in Tissue Regeneration. *Burns & Trauma* **2024**, *12*, tkae013, doi:10.1093/burnst/tkae013.
16. Curie, J.; Curie, P. Développement par compression de l'électricité polaire dans les cristaux hémièdres à faces inclinées. *Bulletin de Minéralogie* **1880**, *3*, 90–93, doi:10.3406/bulmi.1880.1564.
17. Yang, M.-M.; Zhu, T.-Y.; Renz, A.B.; Sun, H.-M.; Liu, S.; Gammon, P.M.; Alexe, M. Auxetic Piezoelectric Effect in Heterostructures. *Nat. Mater.* **2024**, *23*, 95–100, doi:10.1038/s41563-023-01736-5.
18. Singh, J.; Rani, S.; Rohini; Parida, A. Generation of Piezoelectricity from the Human Body. In Proceedings of the 2014 Annual International Conference on Emerging Research Areas: Magnetics, Machines and Drives (AICERA/iCMMD); IEEE: Kottayam, July 2014; pp. 1–5.
19. Martin, R.M. Piezoelectricity. *Phys. Rev. B* **1972**, *5*, 1607–1613, doi:10.1103/PhysRevB.5.1607.
20. Shamos, M.H.; Lavine, L.S. Piezoelectricity as a Fundamental Property of Biological Tissues. *Nature* **1967**, *213*, 267–269, doi:10.1038/213267a0.
21. Wojnar, R. Piezoelectric Phenomena in Biological Tissues. In *Piezoelectric Nanomaterials for Biomedical Applications*; Ciofani, G., Menciassi, A., Eds.; Nanomedicine and Nanotoxicology; Springer Berlin Heidelberg: Berlin, Heidelberg, 2012; pp. 173–185 ISBN 978-3-642-28043-6.
22. Fukada, E. Electrical Phenomena in Biorheology. *BIR* **1982**, *19*, 15–27, doi:10.3233/BIR-1982-191-205.

23. Athenstaedt, H. Pyroelectric and Piezoelectric Behaviour of Human Dental Hard Tissues. *Archives of Oral Biology* **1971**, *16*, 495–501, doi:10.1016/0003-9969(71)90194-4.
24. De Rossi, D.; Domenici, C.; Pastacaldi, P. Piezoelectric Properties of Dry Human Skin. *IEEE Trans. Elect. Insul.* **1986**, *EI-21*, 511–517, doi:10.1109/TEI.1986.349102.
25. Ingber, D.E. The Architecture of Life. *Scientific American* **1998**, *278*, 48–57.
26. Zaszczynska, A.; Sajkiewicz, P.; Gradys, A. Piezoelectric Scaffolds as Smart Materials for Neural Tissue Engineering. *Polymers* **2020**, *12*, 161, doi:10.3390/polym12010161.
27. Aguilar, M.R.; San Román, J. Introduction to Smart Polymers and Their Applications. In *Smart Polymers and their Applications*; Elsevier, 2019; pp. 1–11 ISBN 978-0-08-102416-4.
28. Piskin, E. Biodegradable Polymers as Biomaterials. *Journal of Biomaterials Science, Polymer Edition* **1995**, *6*, 775–795, doi:10.1163/156856295X00175.
29. Lim, J.Y.; Kim, S.; Seo, Y. Enhancement of β-Phase in PVDF by Electrospinning.; Cleveland, Ohio, USA, 2015; p. 070006.
30. Eling, B.; Gogolewski, S.; Pennings, A.J. Biodegradable Materials of Poly(l-Lactic Acid): 1. Melt-Spun and Solution-Spun Fibres. *Polymer* **1982**, *23*, 1587–1593, doi:10.1016/0032-3861(82)90176-8.
31. Zaszczyńska, A.; Gradys, A.; Kołbuk, D.; Zabielski, K.; Szewczyk, P.K.; Stachewicz, U.; Sajkiewicz, P. Poly(L-Lactide)/Nano-Hydroxyapatite Piezoelectric Scaffolds for Tissue Engineering. *Micron* **2025**, *188*, 103743, doi:10.1016/j.micron.2024.103743.
32. Zaszczyńska, A.; Gradys, A.; Ziemiecka, A.; Szewczyk, P.K.; Tymkiewicz, R.; Lewandowska-Szumieł, M.; Stachewicz, U.; Sajkiewicz, P.Ł. Enhanced Electroactive Phases of Poly(Vinylidene Fluoride) Fibers for Tissue Engineering Applications. *IJMS* **2024**, *25*, 4980, doi:10.3390/ijms25094980.
33. Wu, L.; Jin, Z.; Liu, Y.; Ning, H.; Liu, X.; Alamusi; Hu, N. Recent Advances in the Preparation of PVDF-Based Piezoelectric Materials. *Nanotechnology Reviews* **2022**, *11*, 1386–1407, doi:10.1515/ntrev-2022-0082.
34. Salimi, A.; Yousefi, A.A. Analysis Method. *Polymer Testing* **2003**, *22*, 699–704, doi:10.1016/S0142-9418(03)00003-5.
35. Li, L.; Zhang, M.; Rong, M.; Ruan, W. Studies on the Transformation Process of PVDF from α to β Phase by Stretching. *RSC Adv.* **2014**, *4*, 3938–3943, doi:10.1039/C3RA45134H.
36. Ren, J.-Y.; Ouyang, Q.-F.; Ma, G.-Q.; Li, Y.; Lei, J.; Huang, H.-D.; Jia, L.-C.; Lin, H.; Zhong, G.-J.; Li, Z.-M. Enhanced Dielectric and Ferroelectric Properties of

Poly(Vinylidene Fluoride) through Annealing Oriented Crystallites under High Pressure. *Macromolecules* **2022**, *55*, 2014–2027, doi:10.1021/acs.macromol.1c02436.

37. Debili, S.; Gasmi, A.; Bououdina, M. Synergistic Effects of Stretching/Polarization Temperature and Electric Field on Phase Transformation and Piezoelectric Properties of Polyvinylidene Fluoride Nanofilms. *Appl. Phys. A* **2020**, *126*, 309, doi:10.1007/s00339-020-03492-8.
38. Ji, D.; Lin, Y.; Guo, X.; Ramasubramanian, B.; Wang, R.; Radacsi, N.; Jose, R.; Qin, X.; Ramakrishna, S. Electrospinning of Nanofibres. *Nat Rev Methods Primers* **2024**, *4*, 1, doi:10.1038/s43586-023-00278-z.
39. Li, Y.; Zhu, J.; Cheng, H.; Li, G.; Cho, H.; Jiang, M.; Gao, Q.; Zhang, X. Developments of Advanced Electrospinning Techniques: A Critical Review. *Adv Materials Technologies* **2021**, *6*, 2100410, doi:10.1002/admt.202100410.
40. Cozza, E.S.; Monticelli, O.; Marsano, E.; Cebe, P. On the Electrospinning of PVDF: Influence of the Experimental Conditions on the Nanofiber Properties. *Polymer International* **2013**, *62*, 41–48, doi:10.1002/pi.4314.
41. Maleki, H.; Gharehaghaji, A.A.; Moroni, L.; Dijkstra, P.J. Influence of the Solvent Type on the Morphology and Mechanical Properties of Electrospun PLLA Yarns. *Biofabrication* **2013**, *5*, 035014, doi:10.1088/1758-5082/5/3/035014.
42. Keirouz, A.; Wang, Z.; Reddy, V.S.; Nagy, Z.K.; Vass, P.; Buzgo, M.; Ramakrishna, S.; Radacsi, N. The History of Electrospinning: Past, Present, and Future Developments. *Adv Materials Technologies* **2023**, *8*, 2201723, doi:10.1002/admt.202201723.
43. Xin, Y.; Zhu, J.; Sun, H.; Xu, Y.; Liu, T.; Qian, C. A Brief Review on Piezoelectric PVDF Nanofibers Prepared by Electrospinning. *Ferroelectrics* **2018**, *526*, 140–151, doi:10.1080/00150193.2018.1456304.
44. Ghasemi-Mobarakeh, L.; Kolahreez, D.; Ramakrishna, S.; Williams, D. Key Terminology in Biomaterials and Biocompatibility. *Current Opinion in Biomedical Engineering* **2019**, *10*, 45–50, doi:10.1016/j.cobme.2019.02.004.
45. Damaraju, S.M.; Wu, S.; Jaffe, M.; Arinzeh, T.L. Structural Changes in PVDF Fibers Due to Electrospinning and Its Effect on Biological Function. *Biomed. Mater.* **2013**, *8*, 045007, doi:10.1088/1748-6041/8/4/045007.
46. Hoop, M.; Chen, X.-Z.; Ferrari, A.; Mushtaq, F.; Ghazaryan, G.; Tervoort, T.; Poulikakos, D.; Nelson, B.; Pané, S. Ultrasound-Mediated Piezoelectric Differentiation of Neuron-like PC12 Cells on PVDF Membranes. *Sci Rep* **2017**, *7*, 4028, doi:10.1038/s41598-017-03992-3.

47. Kim, S.-H.; Ha, J.-W.; Lee, S.G.; Sohn, E.-H.; Park, I.J.; Kang, H.S.; Yi, G.-R. Fluorinated Titania Nanoparticle-Induced Piezoelectric Phase Transition of Poly(Vinylidene Fluoride). *Langmuir* **2019**, *35*, 8816–8822, doi:10.1021/acs.langmuir.9b00546.
48. Marino, A.; Battaglini, M.; De Pasquale, D.; Degl'Innocenti, A.; Ciofani, G. Ultrasound-Activated Piezoelectric Nanoparticles Inhibit Proliferation of Breast Cancer Cells. *Sci Rep* **2018**, *8*, 6257, doi:10.1038/s41598-018-24697-1.
49. Issa, A.; Al-Maadeed, M.; Luyt, A.; Ponnamma, D.; Hassan, M. Physico-Mechanical, Dielectric, and Piezoelectric Properties of PVDF Electrospun Mats Containing Silver Nanoparticles. *C* **2017**, *3*, 30, doi:10.3390/c3040030.
50. Kushwah, M.; Sagar, R.; Rogachev, A.A.; Gaur, M.S. Dielectric, Pyroelectric and Polarization Behavior of Polyvinylidene Fluoride (PVDF) - Gold Nanoparticles (AuNPs) Nanocomposites. *Vacuum* **2019**, *166*, 298–306, doi:10.1016/j.vacuum.2019.05.010.
51. Zaszczyńska, A.; Zychowicz, M.; Kołbuk, D.; Denis, P.; Gradys, A.; Sajkiewicz, P.Ł. On the Structural and Biological Effects of Hydroxyapatite and Gold Nano-Scale Particles in Poly(Vinylidene Fluoride) Smart Scaffolds for Bone and Neural Tissue Engineering. *Molecules* **2025**, *30*, 1041, doi:10.3390/molecules30051041.
52. Ribeiro, C.; Correia, D.M.; Ribeiro, S.; Sencadas, V.; Botelho, G.; Lanceros-Méndez, S. Piezoelectric Poly(Vinylidene Fluoride) Microstructure and Poling State in Active Tissue Engineering. *Engineering in Life Sciences* **2015**, *15*, 351–356, doi:10.1002/elsc.201400144.
53. Samui, A.B. Introduction to Smart Polymers. In *Smart Polymers*; CRC Press, 2022.
54. Nair, L.S.; Laurencin, C.T. Biodegradable Polymers as Biomaterials. *Progress in Polymer Science* **2007**, *32*, 762–798, doi:10.1016/j.progpolymsci.2007.05.017.
55. Mokhtari, F.; Azimi, B.; Salehi, M.; Hashemikia, S.; Danti, S. Recent Advances of Polymer-Based Piezoelectric Composites for Biomedical Applications. *Journal of the Mechanical Behavior of Biomedical Materials* **2021**, *122*, 104669, doi:10.1016/j.jmbbm.2021.104669.
56. Furukawa, T. Piezoelectricity and Pyroelectricity in Polymers. *IEEE Trans. Elect. Insul.* **1989**, *24*, 375–394, doi:10.1109/14.30878.
57. Ribeiro, C.; Sencadas, V.; Correia, D.M.; Lanceros-Méndez, S. Piezoelectric Polymers as Biomaterials for Tissue Engineering Applications. *Colloids and Surfaces B: Biointerfaces* **2015**, *136*, 46–55, doi:10.1016/j.colsurfb.2015.08.043.

58. Fukada, E. History and Recent Progress in Piezoelectric Polymers. *IEEE Transactions on Ultrasonics, Ferroelectrics, and Frequency Control* **2000**, *47*, 1277–1290, doi:10.1109/58.883516.
59. Esterly, D.M.; Love, B.J. Phase Transformation to B-poly(Vinylidene Fluoride) by Milling. *J Polym Sci B Polym Phys* **2004**, *42*, 91–97, doi:10.1002/polb.10613.
60. Wang, J.; Li, H.; Liu, J.; Duan, Y.; Jiang, S.; Yan, S. On the α → β Transition of Carbon-Coated Highly Oriented PVDF Ultrathin Film Induced by Melt Recrystallization. *J. Am. Chem. Soc.* **2003**, *125*, 1496–1497, doi:10.1021/ja029352r.
61. Kaura, T.; Nath, R.; Perlman, M.M. Simultaneous Stretching and Corona Poling of PVDF Films. *J. Phys. D: Appl. Phys.* **1991**, *24*, 1848–1852, doi:10.1088/0022-3727/24/10/020.
62. Ramanathan, A.K.; Headings, L.M.; Dapino, M.J. Design Optimization of Flexible Piezoelectric PVDF Unimorphs for Surface Pressure Transducer Applications. In Proceedings of the Smart Structures and NDE for Energy Systems and Industry 4.0; Niezrecki, C., Meyendorf, N.G., Gath, K., Eds.; SPIE: Denver, United States, March 18 2019; p. 6.
63. Ellingford, C.; Smith, H.; Yan, X.; Bowen, C.; Figiel, Ł.; McNally, T.; Wan, C. Electrical Dual-Percolation in MWCNTs/SBS/PVDF Based Thermoplastic Elastomer (TPE) Composites and the Effect of Mechanical Stretching. *European Polymer Journal* **2019**, *112*, 504–514, doi:10.1016/j.eurpolymj.2019.01.029.
64. Zhang, S.; Jia, Z.; Liu, T.; Wei, G.; Su, Z. Electrospinning Nanoparticles-Based Materials Interfaces for Sensor Applications. *Sensors* **2019**, *19*, 3977, doi:10.3390/s19183977.
65. Kalish, J.P.; Aou, K.; Yang, X.; Hsu, S.L. Spectroscopic and Thermal Analyses of A′ and α Crystalline Forms of Poly(l-Lactic Acid). *Polymer* **2011**, *52*, 814–821, doi:10.1016/j.polymer.2010.12.042.
66. Cho, T.-Y.; Strobl, G. Temperature Dependent Variations in the Lamellar Structure of Poly(l-Lactide). *Polymer* **2006**, *47*, 1036–1043, doi:10.1016/j.polymer.2005.12.027.
67. Capuana, E.; Lopresti, F.; Ceraulo, M.; La Carrubba, V. Poly-l-Lactic Acid (PLLA)-Based Biomaterials for Regenerative Medicine: A Review on Processing and Applications. *Polymers* **2022**, *14*, 1153, doi:10.3390/polym14061153.
68. Xu, L.; Zhang, Q.K.; Hu, Z.; Hua, C.; Xue, L.; Lu, P.; Zhang, F.; Zhang, Y.; Xiong, J. Fully Biodegradable Piezoelectric Nanogenerator Based on Cellulose/PLLA Electrospun Fibers with High-Performance for Mechanical Energy Harvesting. *Colloids and Surfaces A: Physicochemical and Engineering Aspects* **2025**, *706*, 135813, doi:10.1016/j.colsurfa.2024.135813.

69. Gholami, K.; Seyedjafari, E.; Mahdavi, F.S.; Naghdipoor, M.; Mesbah, G.; Zahmatkesh, P.; Akbarzadehmoallemkolaei, M.; Baghdadabad, L.Z.; Pandian, S.K.; Meilika, K.N.; et al. The Effect of Multilayered Electrospun PLLA Nanofibers Coated with Human Amnion or Bladder ECM Proteins on Epithelialization and Smooth Muscle Regeneration in the Rabbit Bladder. *Macromolecular Bioscience* **2024**, *24*, 2300308, doi:10.1002/mabi.202300308.
70. Soni, P.N.; Mandal, D. Piezoelectric, Triboelectric and Magnetoactive Materials for Tissue Engineering. In *Stimuli-Responsive Materials for Tissue Engineering*; Lanceros-Méndez, S., Ribeiro, C., Silván, U., Eds.; Wiley, 2024; pp. 35–90 ISBN 978-3-527-35047-6.
71. Kulinets, I. Biomaterials and Their Applications in Medicine. In *Regulatory Affairs for Biomaterials and Medical Devices*; Elsevier, 2015; pp. 1–10 ISBN 978-0-85709-542-8.
72. Bystrov, V.S. Piezoelectricity and Pyroelectricity in Hydroxyapatite. *Ferroelectrics* **2019**, *541*, 25–29, doi:10.1080/00150193.2019.1574638.
73. Weiner, S.; Price, P.A. Disaggregation of Bone into Crystals. *Calcif Tissue Int* **1986**, *39*, 365–375, doi:10.1007/BF02555173.
74. Epple, M.; Ganesan, K.; Heumann, R.; Klesing, J.; Kovtun, A.; Neumann, S.; Sokolova, V. Application of Calcium Phosphatenanoparticles in Biomedicine. *J. Mater. Chem.* **2010**, *20*, 18–23, doi:10.1039/B910885H.
75. Kay, M.I.; Young, R.A.; Posner, A.S. Crystal Structure of Hydroxyapatite. *Nature* **1964**, *204*, 1050–1052, doi:10.1038/2041050a0.
76. Kanzaki, N.; Onuma, K.; Ito, A.; Teraoka, K.; Tateishi, T.; Tsutsumi, S. Direct Growth Rate Measurement of Hydroxyapatite Single Crystal by Moire Phase Shift Interferometry. *J. Phys. Chem. B* **1998**, *102*, 6471–6476, doi:10.1021/jp981512r.
77. Nakamura, S.; Takeda, H.; Yamashita, K. Proton Transport Polarization and Depolarization of Hydroxyapatite Ceramics. *Journal of Applied Physics* **2001**, *89*, 5386–5392, doi:10.1063/1.1357783.
78. Bystrov, V.S.; Coutinho, J.; Avakyan, L.A.; Bystrova, A.V.; Paramonova, E.V. Piezoelectric, Ferroelectric, Optoelectronic Phenomena in Hydroxyapatite by First-Principles and with Various Defects. **2019**, *1*.
79. Ghosh, P.; Han, G.; De, M.; Kim, C.; Rotello, V. Gold Nanoparticles in Delivery Applications☆. *Advanced Drug Delivery Reviews* **2008**, *60*, 1307–1315, doi:10.1016/j.addr.2008.03.016.

80. Duncan, B.; Kim, C.; Rotello, V.M. Gold Nanoparticle Platforms as Drug and Biomacromolecule Delivery Systems. *Journal of Controlled Release* **2010**, *148*, 122–127, doi:10.1016/j.jconrel.2010.06.004.
81. Li, H.; Pan, S.; Xia, P.; Chang, Y.; Fu, C.; Kong, W.; Yu, Z.; Wang, K.; Yang, X.; Qi, Z. Advances in the Application of Gold Nanoparticles in Bone Tissue Engineering. *J Biol Eng* **2020**, *14*, 14, doi:10.1186/s13036-020-00236-3.
82. Lee, D.; Heo, D.N.; Kim, H.-J.; Ko, W.-K.; Lee, S.J.; Heo, M.; Bang, J.B.; Lee, J.B.; Hwang, D.-S.; Do, S.H.; et al. Inhibition of Osteoclast Differentiation and Bone Resorption by Bisphosphonate-Conjugated Gold Nanoparticles. *Sci Rep* **2016**, *6*, 27336, doi:10.1038/srep27336.
83. Ko, W.-K.; Heo, D.N.; Moon, H.-J.; Lee, S.J.; Bae, M.S.; Lee, J.B.; Sun, I.-C.; Jeon, H.B.; Park, H.K.; Kwon, I.K. The Effect of Gold Nanoparticle Size on Osteogenic Differentiation of Adipose-Derived Stem Cells. *Journal of Colloid and Interface Science* **2015**, *438*, 68–76, doi:10.1016/j.jcis.2014.08.058.
84. Heo, D.N.; Ko, W.-K.; Moon, H.-J.; Kim, H.-J.; Lee, S.J.; Lee, J.B.; Bae, M.S.; Yi, J.-K.; Hwang, Y.-S.; Bang, J.B.; et al. Inhibition of Osteoclast Differentiation by Gold Nanoparticles Functionalized with Cyclodextrin Curcumin Complexes. *ACS Nano* **2014**, *8*, 12049–12062, doi:10.1021/nn504329u.
85. Shi, S.; Ou, X.; Cheng, D. Nanoparticle-Facilitated Therapy: Advancing Tools in Peripheral Nerve Regeneration. *IJN* **2024**, *Volume 19*, 19–34, doi:10.2147/IJN.S442775.
86. Duman, H.; Akdaşçi, E.; Eker, F.; Bechelany, M.; Karav, S. Gold Nanoparticles: Multifunctional Properties, Synthesis, and Future Prospects. *Nanomaterials* **2024**, *14*, 1805, doi:10.3390/nano14221805.
87. Ghaziof, S.; Shojaei, S.; Mehdikhani, M.; Khodaei, M.; Jafari Nodoushan, M. Electro-Conductive 3D Printed Polycaprolactone/Gold Nanoparticles Nanocomposite Scaffolds for Myocardial Tissue Engineering. *Journal of the Mechanical Behavior of Biomedical Materials* **2022**, *132*, 105271, doi:10.1016/j.jmbbm.2022.105271.
88. Henry, P.H. Method of Producing Artificial Threads 1934.
89. Greiner, A.; Wendorff, J.H. Electrospinning: A Fascinating Method for the Preparation of Ultrathin Fibers. *Angew Chem Int Ed* **2007**, *46*, 5670–5703, doi:10.1002/anie.200604646.
90. Zaszczyńska, A.; Moczulska-Heljak, M.; Gradys, A.; Sajkiewicz, P. Advances in 3D Printing for Tissue Engineering. *Materials* **2021**, *14*, 3149, doi:10.3390/ma14123149.

91. Mrozikiewicz-Rakowska, B.; Szabłowska-Gadomska, I.; Cysewski, D.; Rudziński, S.; Płoski, R.; Gasperowicz, P.; Konarzewska, M.; Zieliński, J.; Mieczkowski, M.; Sieńko, D.; et al. Allogenic Adipose-Derived Stem Cells in Diabetic Foot Ulcer Treatment: Clinical Effectiveness, Safety, Survival in the Wound Site, and Proteomic Impact. *International Journal of Molecular Sciences* **2023**, *24*, 1472, doi:10.3390/ijms24021472.
92. Buzanska, L. The Collagen Scaffold Supports hiPSC-Derived NSC Growth and Restricts hiPSC. *Front Biosci* **2019**, *11*, 105–121, doi:10.2741/s529.
93. Yousry, Y.M.; Yao, K.; Chen, S.; Liew, W.H.; Ramakrishna, S. Mechanisms for Enhancing Polarization Orientation and Piezoelectric Parameters of PVDF Nanofibers. *Adv Elect Materials* **2018**, *4*, 1700562, doi:10.1002/aelm.201700562.
94. He, Z.; Rault, F.; Lewandowski, M.; Mohsenzadeh, E.; Salaün, F. Electrospun PVDF Nanofibers for Piezoelectric Applications: A Review of the Influence of Electrospinning Parameters on the β Phase and Crystallinity Enhancement. *Polymers* **2021**, *13*, 174, doi:10.3390/polym13020174.
95. Motamedi, A.S.; Mirzadeh, H.; Hajiesmaeilbaigi, F.; Bagheri-Khoulenjani, S.; Shokrgozar, M.A. Piezoelectric Electrospun Nanocomposite Comprising Au NPs/PVDF for Nerve Tissue Engineering. *J Biomedical Materials Res* **2017**, *105*, 1984–1993, doi:10.1002/jbm.a.36050.

PUBLIKACJE NAUKOWE WŁĄCZONE DO ROZPRAWY DOKTORSKIEJ

polymers

MDPI

Review

Piezoelectric Scaffolds as Smart Materials for Neural Tissue Engineering

Angelika Zaszczynska *, Paweł Sajkiewicz and Arkadiusz Gradys

Institute of Fundamental Technological Research, Polish Academy of Sciences, Pawinskiego 5b St., 02-106 Warsaw, Poland; psajk@ippt.pan.pl (P.S.); argrad@ippt.pan.pl (A.G.)

* Correspondence: azasz@ippt.pan.pl

Received: 29 November 2019; Accepted: 5 January 2020; Published: 8 January 2020

Abstract: Injury to the central or peripheral nervous systems leads to the loss of cognitive and/or sensorimotor capabilities, which still lacks an effective treatment. Tissue engineering in the post-injury brain represents a promising option for cellular replacement and rescue, providing a cell scaffold for either transplanted or resident cells. Tissue engineering relies on scaffolds for supporting cell differentiation and growth with recent emphasis on stimuli responsive scaffolds, sometimes called smart scaffolds. One of the representatives of this material group is piezoelectric scaffolds, being able to generate electrical charges under mechanical stimulation, which creates a real prospect for using such scaffolds in non-invasive therapy of neural tissue. This paper summarizes the recent knowledge on piezoelectric materials used for tissue engineering, especially neural tissue engineering. The most used materials for tissue engineering strategies are reported together with the main achievements, challenges, and future needs for research and actual therapies. This review provides thus a compilation of the most relevant results and strategies and serves as a starting point for novel research pathways in the most relevant and challenging open questions.

Keywords: neural tissue engineering; piezoelectric scaffolds; smart materials; polymers

1. Introduction

The nervous system is the most complicated system in the body affecting the sensory and motor functions, when the system is damaged. Injuries of the central nervous system (CNS), i.e., brain and spinal cord, lead usually to permanent disability due to severe limitations for spontaneous regeneration of the CNS [1–9], leading to considerable socio-economic problems. For instance, 577 cases of traumatic brain injuries (TBI) per 100,000 people per year occurred in the U.S. alone, while, in Europe, the number of patients with diagnosed TBI was estimated at 262 per 100,000 [10]. Spinal cord injuries (SCI) are predominantly associated with irreversible loss of motor functions. In the U.S., 39 per 100,000 people were estimated to be SCI victims every year, mostly due to traffic accidents, jumping in pools, and falling from heights, while in Europe, the amount of SCI cases was 15 per 100,000 per year [11]. Regeneration of damaged neural tissue is often hindered by the presence of internal factors, such as tumor and scar tissue formation, which blocks its reconstruction. Up to date, there is no effective therapy for TBI and SCI, and surgery is able to inhibit lesion spreading only, while drug therapies have been so far focused mostly on pain relief. Hence, the current goal of CNS tissue engineering is to design a biomaterial enabling the effective outgrowth and differentiation of neural stem cells [12–14].

In recent decades, there has been increasing interest in research related to the development of smart materials [15]. Such materials are generally designed to respond to external stimuli (physical, chemical, mechanical) and behave similar to natural body tissues. One type of such smart materials is piezoelectric scaffolds, which can generate electrical signals in response to the applied stress [16]. Furthermore, they can stimulate the signaling pathways and thereby enhance the tissue regeneration

at the impaired site. This applies especially to neural tissue, where the electrical charges are crucial for cellular activity. The major advantage of such piezoelectric scaffolds is that electrical potential can be generated non-invasively under the influence of mechanical forces, without the need to use invasive electrodes [17,18].

It is known that obtaining piezoelectric scaffolds is possible using various paths, involving solvent casting, TIPS (thermally induced phase separation), freeze drying, or solution blowing [19]. One of most simple and effective methods of fabricating scaffolds in the form of ultrafine fibers with diameters ranging from a few nanometers to several micrometers is electrospinning. This relatively new method uses electric force applied in the form of a very high electrostatic field to draw charged threads from polymer solutions or melts up to the fiber. The process of electrospinning depends on various parameters, which are usually divided into three groups related to the process, material, and ambient parameters. This quite simple and inexpensive technique enables the formation of nano and submicron fibers, the properties of which differ substantially from the ones observed in the bulk materials [20].

For neural tissue engineering, a broad spectrum of synthetic and natural polymers has been studied in the form of electrospun scaffolds [21–30]. Nerve regeneration is a localized and complex biological phenomenon that makes the treatment of patients suffering from nervous system injuries difficult. Therefore, the application of piezoelectric polymers as nerve guidance conduits allows direct delivery of electrical stimulation of the cell's ingrowth with its electrical activity during mechanical deformation without the need for an external power source. Recent investigations have proven that neurons are extremely sensitive to electrical signals [30–39].

The aim of this paper is to summarize the studies on piezoelectric materials used for neural tissue engineering. The most used materials for neural tissue engineering strategies are reported together with the main achievements, challenges, and future needs for research and actual therapies. This review provides thus a compilation of the most relevant results and strategies and serves as a starting point for novel research pathways in the most relevant and challenging open questions.

2. Mechanotransduction and Piezoelectricity in Living Organisms

Mechanotransduction is any of the various mechanisms through which cells sense and convert mechanical stimuli into electrochemical activity. The well known direct element on the way between external stress transmitted through the extracellular matrix and the cells are s.c. stress activated channels, being membrane proteins capable of responding to mechanical stimuli, i.e., opening or closing, generating selective ion fluxes inside the cell, resulting in a cascade of signaling processes [40–43]. Other types of transmembrane ion channels are voltage gated channels, which are activated by changes in the electrical membrane potential near the channel (Figure 1) [44–46]. They play a key role in excitable cells such as neuronal and muscle tissues, allowing rapid and coordinated depolarization in response to triggering voltage change. Found along the axon and at the synapse, voltage gated ion channels directionally propagate electrical signals. Voltage gated ion channels are usually ion specific, for instance to sodium (Na+), potassium (K+), calcium (Ca2+), and chloride (Cl−) ions. In the case of voltage gated channels, the natural piezoelectricity of the body elements is important for the generation of electrical charges under mechanical stress [47–50].

Mechanotransduction influences many aspects of biological functions. Nerves and neural stem cells (NSC) are sensitive to their surrounding environment, and they interact with this environment through cell surface receptors. Niche features such as substrate bound molecules, extracellular matrix (ECM) proteins, and properties such as stiffness and topography affect cell adhesion, survival, proliferation, migration, morphology, and differentiation [51–58].

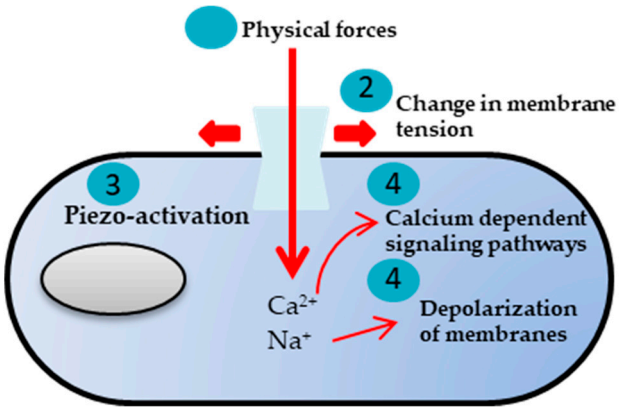

Figure 1. Various mechanical stimuli exerted on the cell induce changes in plasma membrane tension, eliciting piezo-channel openings (adapted from [59]).

The unique features of the nervous system present challenges to bioengineering research addressing nerve injuries. The nervous system is classified into the central nervous system (CNS) containing brain and spinal cord and the peripheral nervous system (PNS) created by the nerves leaving the CNS (Figure 2). The PNS somatic system transmits sensory and motor information for the CNS, while the autonomic one controls automatic functions (e.g., heart beating, blood pressure) [60–62].

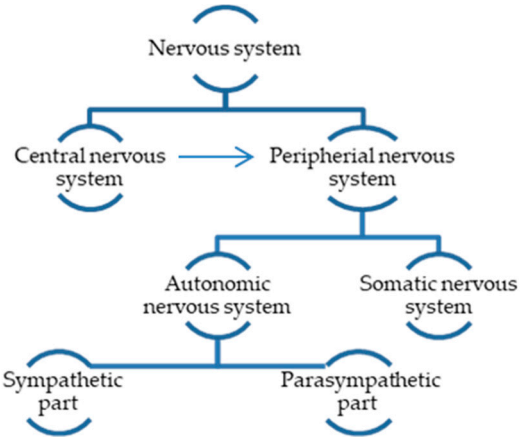

Figure 2. Classification of the nervous system.

The basic functional units in the nervous system having specific electrical properties are neurons and neuroglia (Figure 3), which enable effective transmission of the signals [63,64]. The plasma membrane in a non-excited state is characterized by the resting potential, the value of which is usually around −70 mV [65–67].

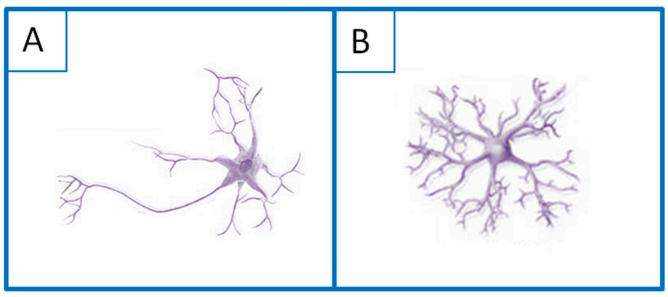

Figure 3. Schematic illustration of the basic units of the nervous tissue: (**A**) neuron and (**B**) neuroglia.

The electrical properties of the neural cells are described by transmission of electrical signals. This phenomenon strongly affects cell behavior via activated ion influx/efflux across the cell membrane. Another phenomenon connected with the transmission of the signals in nerve cells is the action potential. This potential can be dispersed along the axon, which next releases the neurotransmitter (presynaptic ending), and the potential is spread further. A method to activate the action potential is the application of an electrical signal across the neuron. When a dendrite receives an electrical stimulus, the Na+ channels open, and the potential changes from −70 mV to −55 mV. When the potential changes up to +30 mV, the depolarization process starts. Next, the Na+ channels close, and the K+ ones open, completing the depolarization process. When the potential reaches a value around −90 mV, hyperpolarization begins, and the next step is the repolarization of the membrane, which allows receiving another stimulus through the neuron (Figure 4). After the hyperpolarization, the Na+ and K+ channels restore the potential state at the level of −70 mV [68].

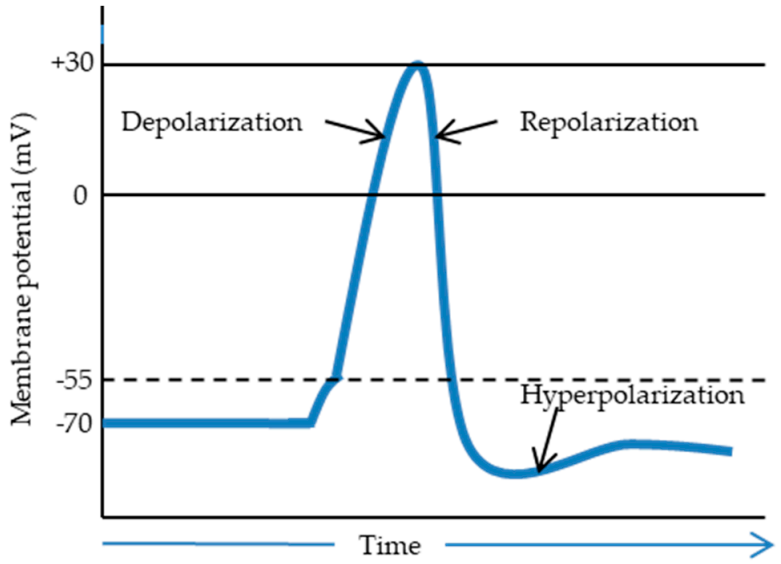

Figure 4. Potential difference in neural transmission as a function of time (adapted from [69]).

Signal transmission is the integral objective of neurons; hence, they are influenced by electrical stimuli. Many research groups have tried to explain the effect of electric stimulation on nerve regeneration. One group described the general effect of electrical stimulation on neurons [70]. Another group studied the activation of the growth controlling transport processes across the plasma membrane and the electrophoretic accumulation of the surface molecules responsible for neurite growth or cell substratum adhesion [70]. Freeman et al. [71] suggested that changes in ionic currents comprise a possible phenomenon that can affect nerve cells, while another thesis [72] described the effect of electrical stimulation on the synthesis of protein and stimulation of the neurite outgrowth in vitro. Furthermore, the authors in [73] postulated that pheochromocytoma in rat neuronal cells (PC12 cells) was electrically activated, while in [74], it was shown that the electrical stimulation increased the adsorption of fibronectin, which explains the enhanced neurite extension on electrically stimulated polypyrrole films. Additionally, nerve cells in the presence of electrical stimulation showed an extensively elongated morphology. In general, tensile/compression forces acting on the piezoelectric scaffolds generate the electrical stimulation and transfer it to the surrounding cells, promoting the cell signaling pathways, responsible for growth factor synthesis (Figure 5) [75].

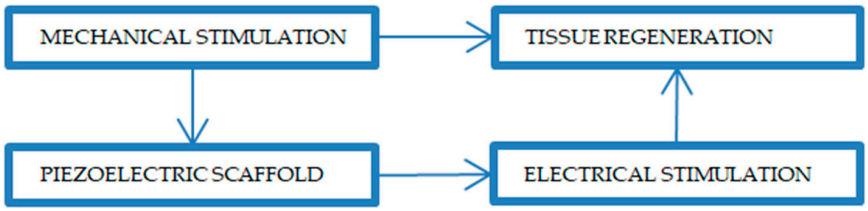

Figure 5. Representative scheme of tissue regeneration in response to the mechanical and electrical stimulation on the piezoelectric scaffold.

In 1940, Martin [76] reported the first piezoelectric phenomena in biological tissues, when he observed electric potentials from a bundle of wool compressed by two brass plates. The main component of hair, horns, and wool is keratin in the form of an alpha-helix. It is known that the piezoelectricity of this tissue is due to the highly ordered arrangement and natural polarization of the alpha-helices, which are stabilized by hydrogen bonds between the hydrogen in the amine group and the oxygen in the carbonyl group [77–82] (Figure 6).

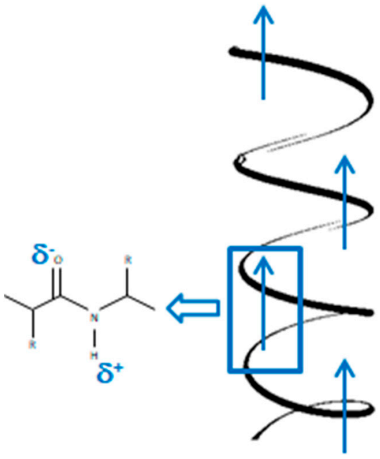

Figure 6. Scheme of permanent polarization in the α-helix.

The results of investigations on the piezoelectric properties of biological tissues have been extensively reported [83–85]. The piezoelectric phenomenon has been confirmed in a variety of biological tissues, such as bone and tendons, due to the presence of highly ordered crystalline fibrillar structures such as collagen, chitin, and elastin [86–90].

The piezoelectric effect, by definition, is described by four piezoelectric coefficients d, e.g., and h:

$$d = (\delta D/\delta X)^E = (\delta x/\delta E)^X \quad (1)$$

$$e = (\delta D/\delta x)^E = -(\delta X/\delta E)^x \quad (2)$$

$$g = -(\delta E/\delta X)^D = (\delta x/\delta D)^X \quad (3)$$

$$h = -(\delta E/\delta x)^D = -(\delta X/\delta D)^x \quad (4)$$

which relate the electrical variables: D (electric displacement) and E (electric field) with the mechanical variables: X (stress) and x (strain). The first terms in Equations (1)–(4) describe the direct piezoelectric effect, while the second terms the converse piezoelectric effect. The subscripts relate to zero constraints of E, D, X, or x. Moreover, each of the coefficients d, e, g, and h is a third rank tensor expressed as a 3 × 6 matrix. The piezoelectric coefficients are indicated in the scheme in Figure 7, along with the coefficients ε (dielectric permittivity) and c (elastic constant) relating to each other the electrical variables D and E as well as the mechanical variables X and x, respectively.

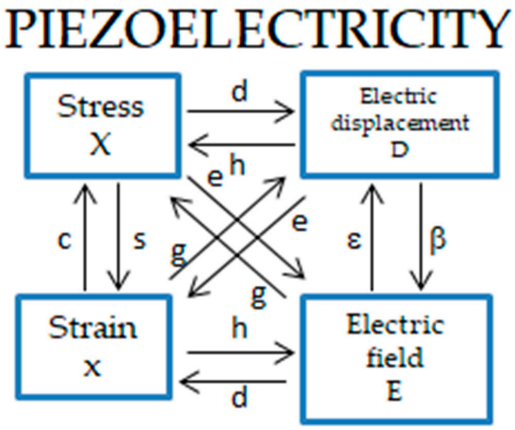

Figure 7. Definition of the piezoelectric coefficients (adapted from [91]).

The ratios of the coefficients ε and c at zero constraints of x, X, E, and D, as indicated by superscripts, define the electromechanical coupling coefficient, K, as given by:

$$\varepsilon^x/\varepsilon^X = c^E/c^D = 1 - K^2 \quad (5)$$

which characterizes the efficiency of the conversion of mechanical energy to electrical energy and vice versa in the direct and converse piezoelectric effect, respectively. The piezoelectric coefficients may be determined through the direct and converse effects or the piezoelectric resonance, providing directly d, e, g, and h coefficients or the efficiency coefficient K, respectively. The results are complementary, as they cover the low (below audio) and the high frequency ranges (above 10 kHz) [91].

The piezoelectric effect is exhibited in all of the amino acid crystals, excluding alpha glycine alone. The piezoelectric coefficients found in biological materials are generally low, typically in the range of 0.1–10 pm/V (the converse effect) with the values for collagen as low as 0.2–2.0 pC/N (the direct effect). The piezoelectric properties for the most relevant natural materials are reported in Table 1.

Table 1. Natural polymers with the piezoelectric response.

Natural Polymers		Piezoelectric Coefficient −d14 (pC/N)	Ref.
Collagen	Skin	0.2	[92]
	Bone	0.7	[92]
	Tendon	2.0	[93]
Keratin	Horn	1.8	[94]
	Wool	0.1	[94]
Fibrin	Salmon DNA	0.07	[93]

3. Scaffolds: Stimuli Responsive (Piezoelectric) vs. Passive

It is generally perceived that the tissue engineering scaffolds should mimic natural existing extracellular matrix (ECM), having similarities as much as possible to the native tissues they are intended to replace in terms of the chemical composition, morphology, physical and mechanical properties, as well as biocompatibility and biodegradability. In detail, the fundamental requirements, that need to be taken into account during scaffold designing are: scaffold biocompatibility, appropriate degradation time in the case of biodegradable materials, the presence of interconnected pores in an appropriate size range, scaffold thickness, mechanical properties, and convenience of use during a surgical procedure [95,96].

It is well known that ECM is a highly dynamic structure; it is constantly being remodeled, either enzymatically or non-enzymatically, and its molecular components are subjected to various modifications. However, most of the recent artificial scaffolds remain passive, i.e., non-stimuli

responsive to the external changes of the environment (static scaffolds) [97]. Moreover, conventional static scaffolds, even conductive, largely disturb the natural signaling pathways, due to their rigidity towards the signal conduction. Thus, there is a high need for smart, stimuli responsive scaffolds, which can generate and transfer the bioelectric signals analogously to the native tissues for appropriate physiological functions. Piezoelectric materials can generate electrical signals in response to the applied stress, which can be imposed even by attachment and migration of cells or body movements [98]. Using piezoelectric materials as tissue engineering scaffolds enables electrical stimulation without the need for electrodes, an external source of electricity, or implanting batteries. Such scaffolds should possess proper architecture and mechanical properties in addition in order to support cell adhesion, proliferation, and differentiation. The size of pores should be controllable and adjusted in order to enable diffusion of the metabolite, but also for appropriate cell adhesion to the biomaterial. Ninety percent porosity and a pore size in the range of 10–100 μm seem to be the most suitable for neuron growth. Scaffolds characterized by 85–90% porosity may be obtained by the electrospinning technique [99]. Such porosity is reported as supporting cellular migration and controlled diffusion of cells, metabolites, and medium, being important for cells organization, differentiation, and survival [100,101].

Obtaining a scaffold that would be biocompatible, biodegradable, conducting, and resistant to infection in order to provide neurite outgrowth is a complex task [102]. Successful nerve regeneration requires tissue engineered scaffolds not only for mechanical support of growing neurites and impediment of the ingrowth of fibrous scar tissues, but also to send biological signals to guide the axonal growth cone to the distal stump. Polymers are in general that materials that have been extensively used for creating suitable scaffolds for neural tissue [103].

Table 2 summarizes the main works on the application of piezoelectric potential scaffold materials and their applications.

Table 2. Piezoelectric materials in nerve tissue engineering.

Material Type	Scaffold Design	Cells Type Used	Ref.
Polyvinylidene Fluoride (PVDF)	Film *	Spinal cord neurons	[104]
	Film *	Mouse neuroblastoma cells	[105]
	Channels	Mouse sciatic nerve model	[106]
	Tubes	Wistar rats	[107]
	Membranes	Neuronal cells	[108]
	Films	Stem cells	[109]
	Nanosheets *	Rat neuronal cell line	[110]
	Fibers *	Osteoblasts MG-63 cells	[111]
	Fibers	Mesenchymal stem cells	[112]
Poly[(vinylidene fluoride-co-trifluoroethylene] (PVDF-TrFE)	Fibers	Poietics normal human neural progenitors	[113]
		Dorsal root ganglion	[114]
	Films	Poietics normal human neural progenitors	[113]
	Membranes *	Osteoblasts SaOS-2 cells	[115]
	Tubes	In vivo implementation: rat sciatic nerves	[116]
	Fibers *	Preosteoblasts	[117]
Poly(3,4ethylenedioxythiophene) (PEDOT)	Films	Fibroblast growth factor (bFGF)	[118]
	Films *	-	[119]
	Films *	Neural stem cells	[120]
	Films	Neural stem cells	[121]
	Nanofibers *	Brain neuroglioma cells	[122]
Polylactic acid (PLLA)	Fibers	Sprague–Dawley rats	[123]
		PLLA blends for vascular differentiation in vitro	[124]
		Neural differentiation and growth in vitro	[125,126]
		PLLA blends for bone formation in vitro	[127]
	+PANi fibers *	Nerve stem cells	[128]
Poly(3-hydroxybutyrate-co-3-hydroxyvalerate) (PHBV)	Fibers *	Human mesenchymal stem cell	[129]
Collagen	Fibers	Schwann cells	[130]
	3D gel matrices	Embryonic rat cerebral cortices	[131]
BaTiO3	+PVDF matrix	Osteoblasts	[132]

* Tests conducted with electrical/mechanical stimulation.

4. Application of Piezoelectric Biomaterials in Neural Tissue Engineering

4.1. Piezoceramics

The earliest studied piezoelectric material group is the piezoceramics. The first applications were dated since around 1950, and since then, they have been widely used in the industry [133]. Wersing et al. [134] conducted the pioneering study on porous piezoceramics, as well as provided the basics in the theory and initial measurements [135]. Currently, there is a great need for lead-free piezoelectric materials, but the most practical ceramics are still based on lead zirconate titanate. Rat cortical neurons cultured on PZT slides coated with poly-L-lysine grew significantly longer axons, despite a decrease in cell number. Furthermore, the frequency and amplitude of the excitatory postsynaptic currents increased, suggesting that piezoelectricity could have augmented neuronal activity [136]. It is worth mentioning that piezoceramics are used for medical applications, especially medical actuators, transducers, and sensors. Due to allergic reactions, piezoceramics are not used in pure solution for medical implants. The innovative systems for medical applications are composites based on polymer matrices, with ceramic fillers, in the form of fibers [137–139]. To achieve bone defect repair, Lopes et al. [140] incorporated barium titanate nanoparticles into polymer matrix, which induced relatively high spontaneous polarization. Moreover, this system is characterized by reduced fragility and can be used as electroactive scaffolds [141].

4.1.1. Barium Titanate

The first piezoelectric effects in ceramics were discovered during poling of BT and led to the wide use of this material group, also as an addition in scaffolds, especially in medical applications [142,143]. Piezoceramics based on barium titanate exhibit low toxicity compared to lead based piezoelectric materials. For their high strain, they are among the most investigated groups of piezoceramics. BT nanoparticles have demonstrated cytocompatibility, even at higher concentrations of 100 µg/mL [144]. Ciofani et al. [145] demonstrated that PLGA matrix with the addition of BT nanoparticles supports the cell proliferation and attachment of osteocytes and osteoblasts. Additionally, the incorporation of barium titanate nanoparticles into the polymeric matrix improves the mechanical properties of the composite scaffold [146] and promotes cellular activity in tissue engineering applications [147].

4.1.2. Boron Nitride

Boron nitride (BN) based nanomaterials play a significant role in nanotechnology owing to their conductivity, mechanical strength, and high thermal stability [148,149]. The most known boron nitride piezo-materials are in the shape of nanotubes, and with increased cytocompatibility, they can be used in tissue engineering [150] and drug delivery, due to their high piezoelectric properties [151–155]. It has been proven that boron nitride nanotubes have a positive influence on the adhesion of cells [156]. Among all the properties of boron nitride nanotubes (BNNTs), their excellent piezoelectricity is the most important for using them as nanovectors to deliver electrical or mechanical signals within cells [157].

4.1.3. Zinc Oxide

Zinc oxide based piezoceramics are widely used due to their asymmetric hexagonal wurtzite structure and polar crystal surface. They have found application as piezoelectric nanogenerators, because of the easy fabrication [158]. ZnO in the shape of nanostructures is biocompatible [159]. It has been suggested that with ZnO size, its cytotoxicity increases, which has an influence on the levels of reactive oxygen species, reduces the mitochondrial membrane potential, and induces the production of interleukin in human cells. Additionally, it has been reported that chemical modification can reduce toxicity, providing a way for use in biomedical applications [160,161].

4.2. Piezopolymers

Piezoelectric polymers are a relatively new class of materials allowing the formation of electrical charges under mechanical stimulation in the absence of additional energy sources or electrodes [162]. Additionally, which is very important from the biomedical point of view, polymers are able to meet the requirements of biocompatibility and biodegradability, which is very crucial for new types of implants in regenerative medicine [163]. Further, their big advantage is the very high processing flexibility, which differentiates them from inorganic materials [164].

4.2.1. Synthetic Polymers

Polyvinylidene Fluoride

Among various piezoelectric polymers, PVDF is widely investigated, primarily because of its high piezoelectricity, processability, good chemical resistance, thermal stability, and good mechanical properties as compared to other piezoelectric polymers. PVDF may exist in at least five crystalline polymorphic phases, among which the β-phase shows the highest piezoelectricity, which reaches 20 pC/N (Figure 8) [165,166].

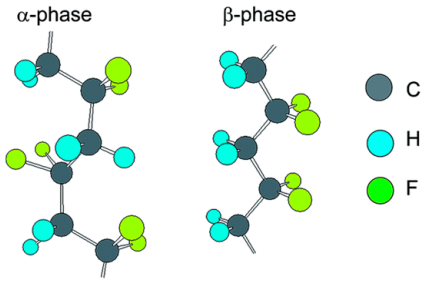

Figure 8. Structures of alpha and beta PVDF.

PVDF macromolecules may take various chain conformations and arrangement of CH_2–CF_2 molecular dipoles, resulting in various net dipole moments. A strong electric moment in the PVDF monomer unit arises from the strong electro-negativity of fluorine atoms as compared to hydrogen atoms. In the case that polymer chains are packed into crystals to form parallel dipoles, the crystal has a non-zero net dipole moment [89–94]. Such a molecular arrangement is observed in the β, γ, and δ phases, the first one showing the strongest dipole moment, due to the all-trans conformation. In the case of other chain conformations: TGTG- and T_3GT_3G-, parallel dipole moment arrangement, as in the δ and γ phases, respectively, leads to lower polarity; in the case of the same conformations, antiparallel chain dipole arrangement leads to the zero net dipole moment as in the α and ϵ phases [167].

The piezoelectricity of PVDF is phase content dependent, which hinges on the processing conditions. Obtaining a particular crystal phase is possible using various paths, involving melt or solution crystallization, annealing (also at high pressure), mechanical drawing, or electrical poling. The presence of polar phases is very important, in particular, due to its bioelectrical effect of the stimulation of the nervous system, holding promise for effective tissue regeneration [168,169].

As regards the most polar β-phase, it may be obtained, for example, by annealing at very high pressure from the α-phase, by poling at a very high electrical field from the α-phase or δ-phase [170] or drawing from the γ-phase [171]. In order to increase the content of polar phases, various methods are reported: melt-recrystallization [172], poling under a high electric field [173], application of high pressure [174], mechanical stretching [175], and the addition of nanoparticles, graphene, and nanowires [176].

The desire to use PVDF in piezoelectric scaffolds in tissue engineering requires the use of fabrication techniques that allow obtaining the proper morphology and high polar phase content responsible for the high piezoelectricity [177]. One of the promising fabrication techniques to fulfil both expectations is

the electrospinning technique. Many publications were devoted to electrospinning of PVDF nanofibers from solution [178], determining the effect of processing parameters on the structure and properties of nanofibers and the characteristics of nonwoven nanofiber [179]. The content of the β-phase in PVDF was studied from the point of view of the applied voltage and rotation speed of the rotational collector. The collector rotational speed relates to the mechanical deformation, which is known to promote the formation of the polar phase [180]. Liu et al. [181] formed nanofibers with different rotational speeds of the collector: 900, 1100, 1300, 1500, 1700 and 1900 rpm. XRD diffraction showed a peak around 20.6–20.9 deg, which belonged to the β-phase, while the α-phase peaks disappeared. They received piezoelectric PVDF fibers with a small diameter, smooth surface morphology, and appropriate β-phase at a velocity of 1900 rpm. Recent works support the view that increasing of the rotational speed of the collector induces a higher content of the piezoelectric β-phase [182–184].

The hydrophobicity of PVDF is a problematic issue in neural tissue engineering. In order to reduce it, numerous research works have been conducted. In order to enhance the hydrophilic, as well as mechanical and electrical properties, PVDF has been modified by the addition of different nanostructures: nanoparticles [185–187], inorganic nanoparticles [188,189], nanotubes [190], and also by the addition of different polymers such as polyethylene glycol (PEG) [191] and polyvinyl alcohol (PVA) [192]. The addition of nanoparticles, especially metallic ones, improves the chemical, physical, and optical properties [193], while diamond nanoparticles have no significant impact on neuroblastoma cell morphology [194]. The incorporation of these nanostructures into a polymer piezoelectric scaffold can positively affect the nerve tissue. Additionally, modification of the surface can increase the neuron length and number of synaptic connections [195,196].

Arinzeh et al. [113,114] tested the piezoelectric scaffolds' potential for promoting in vitro neural differentiation of human neural stem cells, thus demonstrating their applicability in neural tissue engineering. The authors in [197] extended the above studies by applying mechanical vibration, while generating electric fields to induce the piezoelectric effect in piezopolymers. The activation of the piezoelectric effect can be achieved by choosing various sources of mechanical stimulation, including vibration plates, sound, and ultrasound (US) [198,199]. Hoop et al. [85] investigated the influence of the piezoelectric PVDF substrate on supporting neural differentiation under dynamic stimulation. The results showed that the applied ultrasonic waves were sufficient to induce polarization in piezoelectric PVDF sheets and resulted in differentiation of PC12 cells. Piezoelectric PVDF can influence neuronal differentiation and neurite outgrowth of mouse neuroblastoma cells [200]. Electric fields have been shown to influence the growth and orientation of neurons in vitro, whereas the electric field was generated via electrodes [201]. Other studies have been reported successful neural stimulation in various piezoelectric systems, especially piezoelectric micro- and nano-fibers [202,203].

It was shown that the long term application of piezoelectric stimulation on neurons induces the number, length, and branching of neural cells with respect to non-stimulation conditions. No effects on neurite regeneration were observed when vibrations were applied to non-piezoelectric materials (e.g., mechanical stimulation of neurons) [204–206].

Poly-Vinylidene Fluoride-Trifluoroethylene

Among the piezoelectric materials, this copolymer demonstrated the highest electroactive properties with a piezoelectric coefficient as high as 30 pC/N [207]. PVDF-TrFE forms the β-phase through copolymerization without the need for mechanical stretching or drawing [208]. In the case of additional annealing, mechanical stretching, or electrical poling, it is possible to further increase the crystallinity and alignment of the CF2 dipoles, thereby inducing higher piezoelectricity as compared to homopolymer PVDF, dependent on the TrFE content [209]. Electrospun PVDF-TrFE fibrous scaffolds showed higher crystallinity and β-phase content as compared to the starting powder material for neural and bone tissue engineering [101–104]. PVDF-TrFE and barium titanate piezoelectric composite membrane has been reported as a charge generator to promote bone regeneration [106].

PVDF-TrFE piezoelectric fibrous scaffolds were used to study their influence on neural repair. Many investigations reported a positive influence of PVDF-TrFE scaffolds on nerve cell growth and differentiation [210]. Lee et al. [114] fabricated a PVDF-TrFE piezoelectric electrospun scaffold with different orientations of the fibers, randomly and aligned. It was shown that the scaffold with aligned fibers had the highest potential in neural tissue engineering, especially in neurite outgrowth of dorsal root ganglion neurons. It was observed that PVDF-TrFE scaffolds can promote the formation of mature neural cells exhibiting neuron-like characteristics, while aligned fibers can promote primary neuron extension and can direct the neurite outgrowth [211].

Nerve guidance channels may be built using PVDF-TrFE for neural regeneration [212]. In this study, poled (negatively charged and positively charged) and unpoled channels were used. After four weeks, it was observed that the positively poled channels increased the number of regenerated nerves.

In muscle regeneration, the charge at the surface of PVDF films influences the cell proliferation [213]. However, until now, studies with specific dynamic conditions for piezoelectric PVDF-TrFE with mechanical or electrical stimulation have not been conducted.

Poly-3-Hydroxybutyrate-3-Hydroxyvalerate

PHBV is a polyester with a low piezoelectric coefficient (1.2 pC/N) [214]. It is a thermoplastic produced by many bacteria as an intracellular reservoir of carbon and energy. This polyester is also biodegradable, biocompatible, and exhibits strong mechanical properties, which allow using PHBV as a scaffold in biomedicine and as a biosensor [215,216]. PHBV has a comparable piezoelectric potential to that of bone, which can facilitate bone growth and healing [217,218]; thus, it can be used in the form of a composite with the addition of hydroxyapatite for bone tissue engineering. PHBV has been studied for neural tissue engineering, as a support for neuronal cell growth and axon dendrite polarization [219]. In the form of electrospun aligned PHBV fibers, with the addition of collagen, it can be used as a substrate for nerve tissue engineering [220–222].

Poly-L-Lactic Acid

Poly-L-lactic acid is a biodegradable and biocompatible polymer, with a piezoelectric coefficient of −10 pC/N [223]. Fukada et al. demonstrated that implantation of PLLA can promote bone growth in the response of its piezoelectric polarization [93]. PLLA with a structure similar to natural ECM may be used as a biomaterial in various biomedical applications [224]. Aligned PLLA nanofibrous scaffolds coated with graphene oxide promote neural cell growth [225]. Finally, the addition of iron oxide nanoparticles supports extending neurites along electrospun PLLA microfibers [226,227].

4.2.2. Natural Biopolymers

Natural polymers are gaining more importance in tissue engineering because of their biodegradability and low toxicity. In general, many biopolymers exhibit piezoelectricity. As an example, we show some polysaccharides and proteins with relatively strong piezoelectricity.

Cellulose

Cellulose with a piezoelectric coefficient of 0.10 pC/N is a widely investigated natural polymeric material. Cellulose is a linear homopolymer of glucose with high biocompatibility [228–234]. It is used in different shapes and forms: membrane sponges, microspheres, and non-woven, woven, or knitted textiles. Cellulose has been investigated in the tissue engineering of bones [235,236], cartilage [237], for connective tissue formation [238], as a drug delivery system [239], and as a scaffold for growing functional cardiac cell constructs in vitro [240]. One of the important derivatives of cellulose is methylcellulose (MC), presenting in general good solubility in water, particularly at low temperatures, being dependent on the degree of methyl substitution and the distribution of methoxy groups. Collectively, these data indicate that MC is well suited as a biocompatible injectable scaffold for the repair of brain defects [241–243]. Gelatin coated nanoparticles contained in cellulose acetate/PLA

scaffolds showed higher cell viability than uncoated scaffolds, and they acted as a nerve guidance conduit for sciatic nerve defects in vitro and in vivo [244], while a gelatin/chitosan/PEDOT hybrid scaffold enhanced the neurite growth of PC12 cells and promoted neuron-like cell adhesion and proliferation [245].

Chitin and Chitosan

Chitin is a natural polysaccharide with a piezoelectric structure with a low piezoelectric coefficient in the range from 0.2 to 1.5 pC/N [246]. It is a natural component of the cuticles of crustaceans, insects, and mollusks. Since it is hydrophilic and biocompatible, chitin is used for biomedical applications, promoting cell adhesion, proliferation, and differentiation [247].

Chitosan is a biodegradable and biocompatible linear polysaccharide obtained by partial deacetylation of chitin. It has been extensively investigated for the preparation of porous scaffolds for cartilage tissue engineering [248]. However, the low mechanical properties of scaffolds prepared from chitosan make its clinical application problematic. An effective method to overcome chitosan's drawbacks is to blend it with synthetic polymers [249–252]. Skop et al. designed biocompatible chitosan microspheres for the delivery of neural stem cells and growth factors for CNS injuries [253]; another group designed chitosan particles loaded with the drug piperine, reported to have neuroprotective potential against Alzheimer's disease, which successfully targeted specific areas of the brain [254]. Chitosan nanoparticles have also been developed for intranasal delivery of therapeutic agents to the brain [255,256]. Aligned PCL/chitosan fibers supported PC12 cells adhesion and growth, enhancing neurite extension along the fiber orientation [257]. PLGA/chitosan scaffolds guided neuronal differentiation for peripheral nerve regeneration both in vitro and in vivo [258,259].

Collagen

This is a natural piezoelectric material with a piezoelectric coefficient in the range from 0.2 to 2.0 pC/N [260]. Research has been reported on the application of collagen scaffolds in bone healing [261–264]. Furthermore, collagen-calcium phosphate composites have been reported for cartilage tissue engineering [265]. Similarly, collagen-hydroxyapatite piezoelectric composite scaffolds have been proven to be suitable for cellular growth [266]. Collagen scaffolds with the addition of chitosan have been tested in adipose tissue regeneration. Adipocytes were seeded, and the in vitro cytocompatibility and in vivo biocompatibility of scaffolds was confirmed experimentally [267]. An interesting application of collagen is entubulation, hence the use of magnetically aligned type I collagen gel, achieved by exposing the forming collagen gel to a high strength magnetic field, as a filler for collagen tubes. This method was successful in small peripheral nerve lesions, improving nerve regeneration significantly in a 6 mm nerve gap in mice [268] and guiding neurite elongation and Schwann cell invasion in vitro [269] and in vivo [270].

5. Conclusions and Future Perspectives

Recently, smart materials have been of great interest for scientists and physicians, because of the many opportunities to use them as candidates for developing the next generation of biomedical devices, transient implants, and drug delivery vehicles. Considering smart scaffolds for tissue repair and regeneration, piezoelectric materials have recently been of particular interest as they can deliver electrical stimulus without an external power source. There is no doubt that the bioelectric signals produced by piezoelectric scaffolds can regenerate and repair the tissues by definite pathways similar to the natural processes occurring within the natural extracellular matrix (ECM). The combination of morphology together with the chemical, mechanical, and electrical properties of the scaffolds is crucial for the success in tissue regeneration. Electrical charges are particularly important in neural tissue engineering, in which electric pulses can stimulate neurite directional outgrowth to fill gaps in nervous tissue injuries. There is no doubt that the perspective of the broader application of piezoelectric scaffolds as smart materials for neural tissue regeneration is of great importance, allowing avoiding

traditional (invasive) electrical stimulation. It was shown recently in in vitro conditions that the deformation of the piezoelectric scaffolds either by mechanical or ultrasound stimulation led to neurite extension and enhanced cell adhesion and proliferation. However, one should be aware that most of the up-to-date experiments using piezoelectric scaffolds were performed without such stimulation, which does not lead to piezoelectricity and resulting electrical charges. In such a case, the only charges that can be active from the cellular perspective are surface charges due to permanent polarization, as well as related to transient deformation caused by the contraction and protrusion of the attached cells. Nonetheless, it is crucial from the perspective of experiments with piezoelectric scaffolds to mimic the in vivo conditions with internal macro- and micro-deformations by in vitro conditions using mechanical (ultrasounds) agitation, allowing obtaining a real piezoelectric response. The next problem in the area of piezoelectric scaffolds is related to the non-biodegradability of the polymers exhibiting the highest piezoelectric coefficients, i.e., PVDF and its copolymers. Therefore, attention should be focused on biodegradable piezoelectric polymers like PHB or PLLA. An interesting alternative, which should be explored in the future, is related to the composite scaffolds containing an electro-conductive polymer like PANi in addition to a piezoelectric polymer. It was shown that the addition of an electro-conductive polymer to the piezoelectric matrix resulted in an increase in piezoelectricity. This kind of composite scaffold should be taken into account, when thinking about biodegradable piezoelectric polymers with originally relatively low piezoelectricity.

Author Contributions: Conceptualization, A.Z., P.S., and A.G.; validation, P.S. and A.G.; writing, original draft preparation, A.Z.; writing, review and editing, A.Z., P.S., and A.G.; visualization, A.Z., P.S., and A.G.; supervision, P.S., and A.G. All authors have read and agreed to the published version of the manuscript.

Funding: This research received no external funding.

Conflicts of Interest: The authors declare no conflict of interest.

References

1. Wolfenson, H.; Yang, B.; Sheetz, M.P. Steps in mechanotransduction pathways that control cell morphology. *Annu. Rev. Physiol.* **2019**, *81*, 585–605. [CrossRef] [PubMed]
2. Whalin, M.K.; Arora, S.S. Anatomy of the Brain and Spinal Cord. In *Basic Sciences in Anesthesia*; Farag, E., Argalious, M., Tetzlaff, J., Sharma, D., Eds.; Springer: New York, NY, USA, 2018; pp. 41–59.
3. Lis, A.; Szarek, D.; Laska, J. The outlook for the use of polymeric scaffolds in the reconstruction and the regeneration stimulation of traumatic brain injuries. *Polim. Med.* **2018**, *43*, 302–312.
4. Han, D.; Cheung, K.C. Biodegradable cell-seeded nanofiber scaffolds for neural repair. *Polymers* **2011**, *3*, 1684–1733. [CrossRef]
5. Balint, R.; Cassidy, N.J.; Cartmell, S.H. Conductive polymers: Towards a smart biomaterial for tissue engineering. *Acta Biomat.* **2014**, *10*, 2341–2353. [CrossRef]
6. Niemczyk, B.; Sajkiewicz, P.; Gradys, A. Injectable hydrogels as novel materials for central nervous system regeneration. *J. Neural Eng.* **2018**, *15*, 051002. [CrossRef]
7. Lis, A.; Szarek, D.; Laska, J. Biomaterials engineering strategies for spinal cord regeneration: State of the art. *Polim. Med.* **2013**, *43*, 59–80.
8. Taylor, C.A.; Bell, J.M.; Breiding, M.J.; Xu, L. Traumatic brain injury—Related emergency Department Visits, Hospitalizations, and Deaths—United States, 2007 and 2013. *MMWR Surveill. Summ.* **2017**, *66*, 1. [CrossRef]
9. Mathieu, S.; Manneville, J.B. Intracellular mechanics: Connecting rheology and mechanotransduction. *COCEBI* **2019**, *56*, 34–44. [CrossRef]
10. Delcroix, G.J.R.; Schiller, P.C.; Benoit, J.P.; MonteroMenei, C.N. Adult cell therapy for brain neuronal damages and the role of tissue engineering. *Biomaterials* **2010**, *31*, 2105–2120. [CrossRef]
11. Wang, S.; Hou, J.; Bei, J.; Zhao, Y. Tissue engineering and peripheral nerve regeneration (III)—Sciatic nerve regeneration with PDLLA nerve guide. *Sci. China* **2001**, *44*, 419–426. [CrossRef]
12. Adrian, H.; Mårten, K.; Salla, N.; Lasse, V. Biomarkers of Traumatic Brain Injury: Temporal Changes in Body Fluids. *eNeuro* **2016**, *3*, 0294-16. [CrossRef] [PubMed]

13. Weidner, N.; Rudiger, R.; Tansey, K.E. *Neurological Aspects of Spinal Cord Injury*; Springer: Cham, Switzerland, 2017; Volume 1, pp. 3–17.
14. Zhang, L.; Sirivisoot, S.; Balasundaram, G.; Webster, T.J. *Advanced Biomaterials: Fundamentals, Processing and Applications*; Basu, B., Katti, D., Kumar, A., Eds.; John Wiley & Sons, Inc.: Hoboken, NJ, USA, 2009.
15. Langlois, J.A.; Rutland-Brown, W.; Thomas, K.E. *Traumatic Brain Injury in the United States: Emergency Department Visits, Hospitalizations, and Deaths, Centers for Disease Control and Prevention*; National Center for Injury Prevention and Control: Atlanta, GA, USA, 2004.
16. Flax, J.D.; Aurora, S.; Yang, C. Engraftable human neural stem cells respond to developmental cues, replace neurons, and express foreign genes. *Nature Biotechnol.* **1998**, *16*, 1033–1438. [CrossRef] [PubMed]
17. Kordower, J.H.; Tuszynski, M.H. *CNS Regeneration: Basic Science and Clinical Advances*; Kordower, J.H., Tuszynski, M.H., Eds.; Academic: Cambridge, MA, USA, 1999; pp. 159–182.
18. Steel, E.M.; Sundararaghavan, H.G. Electrically Conductive Materials for Nerve Regeneration. In *Neural Engineering*; Springer: New York, NY, USA, 2016; pp. 145–179.
19. Zhao, P.; Gu, H.; Mi, H.; Rao, C.; Fu, J.; Turng, L.S. Fabrication of scaffolds in tissue engineering: A review. *Front. Mech. Eng.* **2018**, *13*, 107–119. [CrossRef]
20. Gao, S.; Tang, G.; Hua, D.; Xiong, R.; Han, J.; Jiang, S.; Huang, C. Stimuli-responsive bio-based polymeric systems and their applications. *J. Mater. Chem. B* **2019**, *7*, 709–729. [CrossRef]
21. Jalili-Firoozinezhad, S.; Mirakhori, F.; Baharvand, H. Nanotissue Engineering of Neural Cells. *Stem Cell Nanoeng.* **2015**, *265*, 265–283.
22. Nguyen, H.T.; Wei, C.; Chow, J.K.; Nguy, L.; Nguyen, H.K.; Schmidt, C.E. Electric field stimulation through a substrate influences Schwann cell and extracellular matrix structure. *J. Neural Eng.* **2013**, *10*, 046011. [CrossRef] [PubMed]
23. Chew, S.Y.; Wen, Y.; Dzenis, Y.; Leong, K.W. The role of electrospinning in the emerging field of nanomedicine. *Curr. Pharm. Des.* **2006**, *12*, 4751–4770. [CrossRef]
24. Murugan, R.; Ramakrishna, S. Nano-featured scaffolds for tissue engineering: A review of spinning methodologies. *Tissue Eng.* **2006**, *12*, 435–447. [CrossRef]
25. Venugopal, J.; Low, S.; Choon, A.T.; Ramakrishna, S. Interaction of cells and nanofiber scaffolds in tissue engineering. *J. Biomed. Mater. Res. B* **2008**, *84*, 34–48. [CrossRef]
26. Teo, W.E.; He, W.; Ramakrishna, S. Electrospun scaffold tailored for tissue-specific extracellular matrix. *Biotechno. J.* **2006**, *1*, 918–929. [CrossRef]
27. Barnes, C.P.; Sell, S.A.; Boland, E.D.; Simpson, D.G.; Bowlin, G.L. Nanofiber technology: Designing the next generation of tissue engineering scaffolds. *Adv. Drug Deliv. Rev.* **2007**, *59*, 1413–1433. [CrossRef]
28. Murugan, R.; Ramakrishna, S. Design strategies of tissue engineering scaffolds with controlled fiber orientation. *Tissue Eng.* **2007**, *13*, 1845–1866. [CrossRef] [PubMed]
29. Heydarkhan-Hagvall, S.; Schenke-Layland, K.; Dhanasopon, A.P.; Rofail, F.; Smith, H.; Wu, B.M.; Shemin, R.; Beygui, R.E.; MacLellan, W.R. Three-dimensional electrospun ECM-based hybrid scaffolds for cardiovascular tissue engineering. *Biomaterials* **2008**, *29*, 2907–2914. [CrossRef] [PubMed]
30. Li, W.J.; Mauck, J.A.; Cooper, X.; Yuan, R.S. Tuan Engineering controllable anisotropy in electrospun biodegradable nanofibrous scaffolds for musculoskeletal tissue engineering. *J. Biomech.* **2007**, *40*, 1686–1693. [CrossRef] [PubMed]
31. Li, W.J.; Tuli, R.; Huang, X.; Laquerriere, P.; Tuan, R.S. Multilineage differentiation of human mesenchymal stem cells in a three-dimensional nanofibrous scaffold. *Biomaterials* **2005**, *26*, 5158–5166. [CrossRef] [PubMed]
32. Yang, F.; Xu, C.Y.; Kotaki, M.; Wang, S.; Ramakrishna, S. Characterization of neural stem cells on electrospun poly(L-lactic acid) nanofibrous scaffold. *J. Biomater. Sci. Polym. Ed.* **2004**, *15*, 1483–1497. [CrossRef] [PubMed]
33. Ting, Y.; Gunawan, H.; Sugondo, A.; Chiu, C. A New Approach of Polyvinylidene Fluoride (PVDF) Poling Method for Higher Electric Response. *Ferroelectrics* **2013**, *446*, 28–38. [CrossRef]
34. Dang, Z.M.; Lin, Y.H.; Nan, C.W. Novel ferroelectric polymer composites with high dielectric constants. *Adv. Mater.* **2003**, *15*, 1625–1629. [CrossRef]
35. Bera, B.; Sarkar, M. Piezoelectricity in PVDF and PVDF Based Piezoelectric Nanogenerator: A Concept. *Int. J. Appl. Phys.* **2017**, *9*, 95–99. [CrossRef]
36. Damaraju, S.M.; Wu, S.; Jaffe, M.; Arinzeh, T.L. Structural changes in PVDF fibers due to electrospinning and its effect on biological function. *Biomed. Mater.* **2013**, *8*, 045007. [CrossRef]

37. Defteralı, Ç.; Verdejo, R.; Majeed, S.; Boschetti-de-Fierro, A.; Méndez-Gómez, H.R.; Díaz-Guerra, E.; Vuluga, D. In vitro evaluation of biocompatibility of uncoated thermally reduced graphene and carbon nanotube-loaded PVDF membranes with adult neural stem cell-derived neurons and glia. *Front. Bioeng. Biotechnol.* **2016**, *4*, 94. [CrossRef] [PubMed]
38. Young, T.H.; Lin, U.H.; Lin, D.J.; Chang, H.H.; Cheng, L.P. Immobilization of L-lysine on microporous PVDF membranes for neuron culture. *J. Biomater. Sci. Polym.* **2009**, *20*, 703–720. [CrossRef] [PubMed]
39. Bar, H.N.; Bhat, M.R.; Murthy, C.R.L. Identification of failure modes in GFRP using PVDF sensors: ANN approach. *Compos. Struct.* **2004**, *65*, 231–237. [CrossRef]
40. Fu, Y.S.; Shih, Y.T.; Cheng, Y.C.; Min, M.Y. Transformation of human umbilical mesenchymal cells into neurons in vitro. *J. Biomed. Sci.* **2004**, *11*, 652–660. [CrossRef]
41. Ning, C.; Zhou, Z.; Tan, G.; Zhu, Y.; Mao, C. Electroactive polymers for tissue regeneration: Developments and perspectives. *Prog. Polym. Sci.* **2018**, *81*, 144–162. [CrossRef]
42. Moran, H.; Cancel, L.M.; Mayer, M.A.; Qazi, H.; Munn, L.L.; Tarbell, J.M. The cancer cell glycocalyx proteoglycan glypican-1 mediates interstitial flow mechanotransduction to enhance cell migration and metastasis. *Biorheology* **2019**, *56*, 151–161. [CrossRef]
43. Gargalionis, A.N.; Basdra, E.K.; Papavassiliou, A.G. Polycystins and Mechanotransduction in Human Disease. *Int. J. Mol. Sci.* **2019**, *20*, 2182. [CrossRef]
44. Maurer, M.; Lammerding, J. The driving force: Nuclear mechanotransduction in cellular function, fate, and disease. *Annu. Rev. Biomed. Eng.* **2019**, *21*, 443–468. [CrossRef]
45. Yamada, K.M.; Sixt, M. Mechanisms of 3D cell migration. *Nat. Rev. Mol.* **2019**, *20*, 738–752. [CrossRef]
46. Chang, W.; Gu, J.G. Impairment of tactile responses and Piezo channel mechanotransduction in mice following chronic vincristine treatment. *Neurosci. Lett.* **2019**, *705*, 14–19. [CrossRef]
47. Salvi, A.M.; DeMali, K.A. Mechanisms linking mechanotransduction and cell metabolism. *COCEBI* **2018**, *54*, 114–120. [CrossRef] [PubMed]
48. Pariy, I.O.; Ivanova, A.A.; Shvartsman, V.V.; Lupascu, D.C.; Sukhorukov, G.B.; Ludwig, T.; Surmenev, R.A. Piezoelectric Response in Hybrid Micropillar Arrays of Poly (Vinylidene Fluoride) and Reduced Graphene Oxide. *Polymers* **2019**, *11*, 1065. [CrossRef] [PubMed]
49. Ruan, L.; Yao, X.; Chang, Y.; Zhou, L.; Qin, G.; Zhang, X. Properties and Applications of the β Phase Poly (vinylidene fluoride). *Polymers* **2018**, *10*, 228. [CrossRef] [PubMed]
50. Guilak, F.; Cohen, D.M.; Estes, B.T.; Gimble, J.M.; Liedtke, W.; Chen, C.S. Control of stem cell fate by physical interactions with the extracellular matrix. *Cell Stem Cell* **2009**, *5*, 17–26. [CrossRef] [PubMed]
51. Lee, M.R.; Kwon, K.W.; Jung, H.; Kim, H.N.; Suh, K.Y.; Kim, K.; Kim, K.S. Direct differentiation of human embryonic stem cells into selective neurons on nanoscale ridge/groove pattern arrays. *Biomaterials* **2010**, *31*, 4360–4366. [CrossRef] [PubMed]
52. McBeath, R.; Pirone, D.M.; Nelson, C.M.; Bhadriraju, K.; Chen, C.S. Cell shape, cytoskeletal tension, and RhoA regulate stem cell lineage commitment. *Dev. Cell* **2004**, *6*, 483–495. [CrossRef]
53. Verkhratsky, A.; Ho, M.S.; Parpura, V. Evolution of Neuroglia. In *Neuroglia in Neurodegenerative Diseases*; Springer: New York, NY, USA, 2019; pp. 15–44.
54. Georges, P.C.; Miller, W.J.; Meaney, D.F.; Sawyer, E.S.; Janmey, P.A. Matrices with compliance comparable to that of brain tissue select neuronal over glial growth in mixed cortical cultures. *Biophys. J.* **2006**, *90*, 3012–3018. [CrossRef]
55. Doetsch, F. A niche for adult neural stem cells. *Curr. Opin. Genet. Dev.* **2003**, *13*, 543–550. [CrossRef]
56. Alenghat, F.J.; Ingber, D.E. Mechanotransduction: All signals point to cytoskeleton, matrix, and integrins. Science's STKE: Signal transduction knowledge environment. *Sci. Signal.* **2002**, *119*, pe6. [CrossRef]
57. Kjellman, C.; Lidman, J.; Ljungström, K. Nilsson, Piezoelectric Sensor in a Living Organism for Fluid Pressure Measurement. U.S. Patent 6,886,411, 3 May 2005.
58. Wada, Y.; Hayakawa, R. Piezoelectricity and pyroelectricity of polymers. *Jpn. J. Appl. Phys.* **1976**, *15*, 2041. [CrossRef]
59. Parpaite, T.; Coste, B. Piezo channels. *Curr. Biol.* **2017**, *27*, R250–R252. [CrossRef] [PubMed]
60. Liu, Y.; Gao, J.; Peng, M.; Meng, H.; Ma, H.; Cai, P.; Si, G. A review on central nervous system effects of gastrodin. *Front. Pharmacol.* **2018**, *9*, 24. [CrossRef] [PubMed]

61. Piccoli, A.; Rossettini, G.; Cecchetto, S.; Viceconti, A.; Ristori, D.; Turolla, A.; Testa, M. Effect of attentional focus instructions on motor learning and performance of patients with central nervous system and musculoskeletal disorders: A systematic review. *J. Funct. Morphol. Kinesiol.* **2018**, *3*, 40. [CrossRef]
62. Schulte, F.; Kunin-Batson, A.S.; Olson-Bullis, B.A.; Banerjee, P.; Hocking, M.C.; Janzen, L.; Krull, K.R. Social attainment in survivors of pediatric central nervous system tumors: A systematic review and meta-analysis from the Children's Oncology Group. *J. Cancer Surviv.* **2019**, *13*, 921–931. [CrossRef]
63. Saheb, N.; Mekid, S. Fiber-Embedded Metallic Materials: From Sensing towards Nervous Behavior. *Materials* **2015**, *8*, 7938–7961. [CrossRef]
64. Stavoe, A.K.; Holzbaur, E.L. Autophagy in Neurons. *Annu. Rev. Cell Dev. Biol.* **2019**, *35*, 477–500. [CrossRef]
65. Swenarchuk, L.E. Nerve, Muscle, and Synaptogenesis. *Cells* **2019**, *8*, 1448. [CrossRef]
66. Martí, D.; Brunel, N.; Ostojic, S. Correlations between synapses in pairs of neurons slow down dynamics in randomly connected neural networks. *Phys. Rev. E* **2018**, *97*, 062314. [CrossRef]
67. Van Driesche, S.J.; Martin, K.C. New frontiers in RNA transport and local translation in neurons. *Dev. Neurobiol.* **2018**, *78*, 331–339. [CrossRef]
68. Zhao, W.; Cui, W.; Xu, S.; Cheong, L.Z.; Wang, D.; Shen, C. Direct study of the electrical properties of PC12 cells and hippocampal neurons by EFM and KPFM. *Nanoscale Adv.* **2019**, *1*, 537–545. [CrossRef]
69. Averbeck, B.B.; Lee, D. Coding and transmission of information by neural ensembles. *Trends Neurosci.* **2004**, *27*, 225–230. [CrossRef]
70. Patel, N. Orientation of neurite growth by extracellar electric fields. *J. Neurosci.* **1982**, *2*, 483–496. [CrossRef]
71. Freeman, J.A.; Manis, P.B.; Snipes, G.J. Steady growth cone currents revealed by a novel circularly vibrating probe: A possible mechanism underlying neurite growth. *J. Neurosci.* **1985**, *13*, 257–283. [CrossRef] [PubMed]
72. Sisken, B.F.; Kanje, M.; Lundborg, G.; Herbst, E.; Kurtz, W. Stimulation of rat sciatic nerve regeneration with pulsed electromagnetic fields. *Brain Res.* **1989**, *485*, 309–316. [CrossRef]
73. Kimura, K.; Yanagida, Y.; Haruyama, T.; Kobatake, E.; Aizawa, M. Gene expression in the electrically stimulated differentiation of PC12 cells. *J. Biotechnol.* **1998**, *63*, 55–65. [CrossRef]
74. Kotwal, A.; Schmid, C.E. Electrical stimulation alters protein adsorption and nerve cell interactions with electrically conducting biomaterials. *Biomaterials* **2001**, *22*, 1055–1064. [CrossRef]
75. Ghasemi-Mobarakeh, L.; Prabhakaran, M.P.; Morshed, M.; Nasr-Esfahani, M.H.; Baharvand, H.; Kiani, S.; Ramakrishna, S. Application of conductive polymers, scaffolds and electrical stimulation for nerve tissue engineering. *J. Tissue Eng. Regen. Med.* **2011**, *5*, 17–35. [CrossRef]
76. Martin, R.M. Piezoelectricity. *Phys. Rev. B* **1972**, *5*, 1607. [CrossRef]
77. Shamos, M.H.; Lavine, L.S. Piezoelectricity as a fundamental property of biological tissues. *Nature* **1967**, *213*, 267–269. [CrossRef]
78. Telega, J.J.; Wojnar, R. Piezoelectric effects in biological tissues. *J. Theor. Appl. Mech.* **2002**, *40*, 723–759.
79. Fukada, E. Electrical phenomena in biorheology. *Biorheology* **1982**, *19*, 15–27. [CrossRef] [PubMed]
80. Athenstaedt, H. Pyroelectric and piezoelectric behaviour of human dental hard tissues. *Arch. Oral Biol.* **1971**, *16*, 495–501. [CrossRef]
81. De Rossi, D.; Domenici, D.; Pastacaldi, P. Piezoelectric Properties of Dry Human Skin. *IEEE Trans. Electr. Insul.* **1985**, *21*, 511–517. [CrossRef]
82. Ingber, D.E. The architecture of life. *Sci. Am.* **1998**, *278*, 48–57. [CrossRef]
83. Reyes-Gasga, J.; Galindo-Mentle, M.; Brès, E.; Vargas-Becerril, N.; Orozco, E.; Rodríguez-Gómez, A.; García-García, R. Detection of the piezoelectricity effect in nanocrystals from human teeth. *J. Phys. Chem. Solids* **2020**, *136*, 109140. [CrossRef]
84. Udovč, L.; Spreitzer, M.; Vukomanović, M. Towards hydrophilic piezoelectric poly-L-lactide films: Optimal processing, post-heat treatment and alkaline etching. *Polym. J.* **2019**, 1–13. [CrossRef]
85. Hoop, M.; Chen, X.; Ferrari, A.; Fajer, M.; Gagik, G.; Theo, T.; Dimos, P.; Bradley, N.; Salvador, P. Ultrasound-mediated piezoelectric differentiation of neuron-like PC12 cells on PVDF membranes. *Sci. Rep.* **2017**, *7*, 4028. [CrossRef]
86. Ahn, A.C.; Grodzinsky, A.J. Relevance of collagen piezoelectricity to "Wolff's Law": A critical review. *Med. Eng. Phys.* **2009**, *31*, 733–741. [CrossRef]
87. Lang, S.B. Pyroelectric Effect in Bone and Tendon. *Nature* **1966**, *212*, 704–705. [CrossRef]
88. Anderson, J.C.; Eriksson, C. Electrical properties of wet collagen. *Nature* **1968**, *218*, 166–168. [CrossRef]

89. Anderson, J.C.; Eriksson, C. Piezoelectric properties of dry and wet bone. *Nature* **1970**, *227*, 491–492. [CrossRef] [PubMed]
90. Fukada, E. Piezoelectricity in polymers and biological materials. *Ultrasonics* **1968**, *6*, 229–234. [CrossRef]
91. Furukawa, T. Piezoelectricity and pyroelectricity in polymers. *IEEE Tran. Electr. Insul.* **1989**, *24*, 375–394. [CrossRef]
92. Puppi, D.; Chiellini, F.; Piras, A.; Chiellini, E. Polymeric materials for bone and cartilage repair. *Prog. Polym. Sci.* **2010**, *35*, 403–440. [CrossRef]
93. Ribeiro, C.; Sencadas, V.; Correia, D.M.; Lanceros-Méndez, S. Piezoelectric polymers as biomaterials for tissue engineering applications. *Colloids Surf. B Biointerfaces* **2015**, *136*, 46–55. [CrossRef]
94. Fukada, E. History and recent progress in piezoelectric polymers. *IEEE Trans. Ultrason. Ferroelectr. Freq. Control* **2000**, *47*, 1277–1290. [CrossRef]
95. Zhong, Y.; Bellamkonda, R. V Biomaterials for the central nervous system. *J. R. Soc. Interface* **2008**, *5*, 957–975. [CrossRef]
96. Jeznach, O.; Kołbuk, D.; Sajkiewicz, P. Injectable hydrogels and nanocomposite hydrogels for cartilage regeneration. *J. Biomed. Mater. Res. A* **2018**, *106*, 2762–2776. [CrossRef]
97. Brown, B.N.; Badylak, S.F. Extracellular matrix as an inductive scaffold for functional tissue reconstruction. *Transl. Res.* **2014**, *163*, 268–285. [CrossRef]
98. Ravichandran, R.; Astrand, C.; Patra, H.K.; Turner, A.P.; Chotteau, V.; Phopase, J. Intelligent ECM mimetic injectable scaffolds based on functional collagen building blocks for tissue engineering and biomedical applications. *RSC Adv.* **2017**, *7*, 21068–21078. [CrossRef]
99. Miguel, S.P.; Sequeira, R.S.; Moreira, A.F.; Cabral, C.C.; Mendonça, A.G.; Ferreira, P.; Correia, I.J. An overview of electrospun membranes loaded with bioactive molecules for improving the wound healing process. *Eur. J. Pharm. Biopharm.* **2019**, *139*, 1–22. [CrossRef] [PubMed]
100. Okamoto, M. The role of scaffolds in tissue engineering. In *Handbook of Tissue Engineering Scaffolds*; Elsevier: Amsterdam, The Netherlands, 2019; Volume 1, pp. 23–49.
101. Morgado, P.I.; Aguiar-Ricardo, A.; Correia, I.J. Asymmetric membranes as ideal wound dressings: An overview on production methods, structure, properties and performance relationship. *J. Membr. Sci.* **2015**, *490*, 139–151. [CrossRef]
102. Subramanian, A.; Krishnan, U.M.; Sethuraman, S. Development of biomaterial scaffold for nerve tissue engineering: Biomaterial mediated neural regeneration. *J. Biomed. Sci.* **2009**, *16*, 108. [CrossRef] [PubMed]
103. Shapiro, F. Overview of Deformities. In *Pediatric Orthopedic Deformities*; Springer: Cham, Switzerland, 2016; Volume 1, pp. 159–254.
104. Royo-Gascon, N.; Wininger, M.; Scheinbeim, J.I.; Firestein, B.L.; Craelius, W. Piezoelectric substrates promote neurite growth in rat spinal cord neurons. *Ann. Biomed. Eng.* **2013**, *41*, 112–122. [CrossRef] [PubMed]
105. Valentini, R.F.; Vargo, T.G.; Gardella, J.A., Jr.; Aebischer, P. Electrically charged polymeric substrates enhance nerve fibre outgrowth in vitro. *Biomaterials* **1992**, *13*, 183–190. [CrossRef]
106. Aebischer, P.; Valentini, R.F.; Dario, P.; Domenici, C.; Galletti, P.M. Piezoelectric guidance channels enhance regeneration in the mouse sciatic nerve after axotomy. *Brain Res.* **1987**, *436*, 165–168. [CrossRef]
107. Delaviz, H.; Faghihi, A.; Delshad, A.A.; Hadi Bahadori, M.; Mohamadi, J.; Roozbehi, A. Repair of peripheral nerve defects using a polyvinylidene fluoride channel containing nerve growth factor and collagen gel in adult rats. *Cell J.* **2011**, *13*, 137–142.
108. Young, T.H.; Chang, H.H.; Lin, D.J.; Cheng, L.P. Surface modification of microporous PVDF membranes for neuron culture. *J. Membr. Sci.* **2010**, *350*, 32–41. [CrossRef]
109. Ariga, K.; Jia, X.; Song, J.; Hsieh, C.T.; Hsu, S.H. Materials Nanoarchitectonics as Cell Regulators. *ChemNanoMat* **2019**, *5*, 692–702. [CrossRef]
110. Ai, J.; Kiasat-Dolatabadi, A.; Ebrahimi-Barough, S.; Ai, A.; Lotfibakhshaiesh, N.; Norouzi-Javidan, A.; Aghayan, H.R. Polymeric scaffolds in neural tissue engineering: A review. *Arch Neurosci.* **2014**, *1*, 15–20. [CrossRef]
111. Abzan, N.; Kharaziha, M.; Labbaf, S. Development of three-dimensional piezoelectric polyvinylidene fluoride-graphene oxide scaffold by non-solvent induced phase separation method for nerve tissue engineering. *Mater. Design* **2019**, *167*, 107636. [CrossRef]

112. Khorshidi, S.; Ansari, S.; Naghizadeh, Z.; Akbari, N.; Karkhaneh, A.; Haghighipour, N. Concurrent effects of piezoelectricity and hydrostatic pressure on chondrogenic differentiation of stem cells. *Mater. Lett.* **2019**, *246*, 71–75. [CrossRef]
113. Lee, Y.S.; Arinzeh, T.L. The influence of piezoelectric scaffolds on neural differentiation of human neural stem/progenitor cells. *Tissue Eng. A* **2012**, *18*, 2063–2072. [CrossRef] [PubMed]
114. Lee, Y.S.; Collins, G.; Arinzeh, T.L. Neurite extension of primary neurons on electrospun piezoelectric scaffolds. *Acta Biomater.* **2011**, *7*, 3877–3886. [CrossRef]
115. Genchi, G.G.; Sinibaldi, E.; Ceseracciu, L.; Labardi, M.; Marino, A.; Marras, S.; Ciofani, G. Ultrasound-activated piezoelectric P (VDF-TrFE)/boron nitride nanotube composite films promote differentiation of human SaOS-2 osteoblast-like cells. *Nanomedicine* **2018**, *14*, 2421–2432. [CrossRef]
116. Fine, E.G.; Valentini, R.F.; Bellamkonda, R.; Aebischer, P. Improved nerve regeneration through piezoelectric vinylidenefluoride-trifluoroethylene copolymer guidance channels. *Biomaterials* **1991**, *12*, 775–780. [CrossRef]
117. Wang, A.; Hu, M.; Zhou, L.; Qiang, X. Self-Powered Well-Aligned P (VDF-TrFE) Piezoelectric Nanofiber Nanogenerator for Modulating an Exact Electrical Stimulation and Enhancing the Proliferation of Preosteoblasts. *Nanomaterials* **2019**, *9*, 349. [CrossRef]
118. Collazos-Castro, J.E.; Polo, J.L.; Hernández-Labrado, G.R.; Padial-Cañete, V.; García-Rama, C. Bioelectrochemical control of neural cell development on conducting polymers. *Biomaterials* **2010**, *31*, 9244–9255. [CrossRef]
119. Ludwig, K.A.; Uram, J.D.; Yang, J.; Martin, D.C.; Kipke, D.R. Chronic neural recordings using silicon microelectrode arrays electrochemically deposited with a poly (3, 4-ethylenedioxythiophene)(PEDOT) film. *J. Neural. Eng.* **2006**, *3*, 59–70. [CrossRef]
120. Pires, F.; Ferreira, Q.; Rodrigues, C.A.; Morgado, J.; Ferreira, F.C. Neural stem cell differentiation by electrical stimulation using a cross-linked PEDOT substrate: Expanding the use of biocompatible conjugated conductive polymers for neural tissue engineering. *Biochim. Biophys. Acta* **2015**, *1850*, 1158–1168. [CrossRef]
121. Sebaa, M.; Nguyen, T.Y.; Dhillon, S.; Garcia, S.; Liu, H. The effects of poly (3, 4-ethylenedioxythiophene) coating on magnesium degradation and cytocompatibility with human embryonic stem cells for potential neural applications. *J. Biomed. Mater. Res. A* **2015**, *103*, 25–37. [CrossRef]
122. Du, L.; Li, T.; Jin, F.; Wang, Y.; Li, R.; Zheng, J.; Feng, Z.Q. Design of high conductive and piezoelectric poly (3, 4-ethylenedioxythiophene)/chitosan nanofibers for enhancing cellular electrical stimulation. *J. Colloid Interface Sci.* **2020**, *559*, 65–75. [CrossRef] [PubMed]
123. Evans, G.R.; Brandt, K.; Niederbichler, A.D.; Chauvin, P.; Hermann, S.; Bogle, M.; Patrick, C.W. Clinical long-term in vivo evaluation of poly (L-lactic acid) porous conduits for peripheral nerve regeneration. *J. Biomater. Sci. Polym.* **2000**, *11*, 869–878. [CrossRef] [PubMed]
124. Jia, L.; Prabhakaran, M.P.; Qin, X.; Ramakrishna, S. Stem cell differentiation on electrospun nanofibrous substrates for vascular tissue engineering. *Mater. Sci. Eng. C* **2013**, *33*, 4640–4650. [CrossRef] [PubMed]
125. Yang, F.; Murugan, R.; Ramakrishna, S.; Wang, X.; Ma, Y.X.; Wang, S. Fabrication of nano-structured porous PLLA scaffold intended for nerve tissue engineering. *Biomaterials* **2004**, *25*, 1891–1900. [CrossRef]
126. Yang, F.; Murugan, R.; Wang, S.; Ramakrishna, S. Electrospinning of nano/micro scale poly (L-lactic acid) aligned fibers and their potential in neural tissue engineering. *Biomaterials* **2005**, *26*, 2603–2610. [CrossRef]
127. Prabhakaran, M.P.; Venugopal, J.; Ramakrishna, S. Electrospun nanostructured scaffolds for bone tissue engineering. *Acta Biomater.* **2009**, *5*, 2884–2893. [CrossRef]
128. Prabhakaran, M.P.; Ghasemi-Mobarakeh, L.; Jin, G.; Ramakrishna, S. Electrospun conducting polymer nanofibers and electrical stimulation of nerve stem cells. *J. Biosci. Bioeng.* **2011**, *112*, 501–507. [CrossRef]
129. Jacob, J.; More, N.; Mounika, C.; Gondaliya, P.; Kalia, K.; Kapusetti, G. The Smart Piezoelectric Nanohybrid of Poly-(3-hydroxybutyrate-co-3-hydroxyvalerate) and Barium Titanate for Stimulated Cartilage Regeneration. *ACS Appl. Bio Mater.* **2019**, *2*, 4922–4931. [CrossRef]
130. De Guzman, R.C.; Loeb, J.A.; VandeVord, P.J. Electrospinning of matrigel to deposit a basal lamina-like nanofiber surface. *J. Biomater. Sci. Polym. Ed.* **2010**, *21*, 1081–1101. [CrossRef]
131. O'Shaughnessy, T.J.; Lin, H.J.; Ma, W. Functional synapse formation among rat cortical neurons grown on three-dimensional collagen gels. *Neurosci. Lett.* **2003**, *340*, 169–172. [CrossRef]
132. Shuai, C.; Liu, G.; Yang, Y.; Yang, W.; He, C.; Wang, G.; Peng, S. Functionalized BaTiO3 enhances piezoelectric effect towards cell response of bone scaffold. *Colloids Surf. B.* **2020**, *185*, 110587. [CrossRef] [PubMed]

133. Mercadelli, E.; Sanson, A.; Galassi, C. Porous Piezoelectric Ceramics. In *Piezoelectric Ceramics*; Suaste-Gomez, E., Ed.; InTech: Rijeka, Croatia, 2010; pp. 111–129.
134. Wersing, W.; Lubitz, K.; Mohaupt, J. Dielectric, elastic and piezoelectric properties of porous PZT ceramics. *Ferroelectrics* **1986**, *68*, 77–97. [CrossRef]
135. Ringgaard, E.; Lautzenhiser, F.; Bierregaard, L.; Zawada, T.; Molz, E. Development of porous piezoceramics for medical and sensor applications. *Materials* **2015**, *8*, 8877–8889. [CrossRef] [PubMed]
136. Xue, C.; Hu, N.; Gu, Y.; Yang, Y.; Liu, Y.; Liu, J.; Ding, F.; Gu, X. Joint Use of a Chitosan/PLGA Scaffold and MSCs to Bridge an Extra Large Gap in Dog Sciatic Nerve. *Neurorehabil. Neural Repair* **2012**, *26*, 96–106. [CrossRef]
137. Carville, N.C.; Collins, L.; Manzo, M.; Gallo, K.; Lukasz, B.I.; McKayed, K.K.; Rodriguez, B.J. Biocompatibility of ferroelectric lithium niobate and the influence of polarization charge on osteoblast proliferation and function. *J. Biomed. Mater. Res. A* **2015**, *103*, 2540–2548. [CrossRef]
138. Furuya, K.; Morita, Y.; Tanaka, K.; Katayama, T.; Nakamachi, E. Acceleration of osteogenesis by using barium titanate piezoelectric ceramic as an implant material. In Proceedings of the International Society for Optics and Photonics, San Diego, CA, USA, 3–7 May 2011; Volume 7975, p. 79750U.
139. Ball, J.P.; Mound, B.A.; Nino, J.C.; Allen, J.B. Biocompatible evaluation of barium titanate foamed ceramic structures for orthopedic applications. *J. Biomed. Mater. Res. A* **2014**, *102*, 2089–2095. [CrossRef]
140. Lopes, H.B.; Santos, T.D.S.; De Oliveira, F.S.; Freitas, G.P.; De Almeida, A.L.; Gimenes, R.; Beloti, M.M. Poly (vinylidene-trifluoroethylene)/barium titanate composite for in vivo support of bone formation. *J. Biomater. Appl.* **2014**, *29*, 104–112. [CrossRef]
141. Zhang, X.; Zhang, C.; Lin, Y.; Hu, P.; Shen, Y.; Wang, K.; Liu, Y. Nanocomposite membranes enhance bone regeneration through restoring physiological electric microenvironment. *ACS Nano* **2016**, *10*, 7279–7286. [CrossRef]
142. Roberts, S. Dielectric and piezoelectric properties of barium titanate. *Phys. Rev.* **1947**, *71*, 890. [CrossRef]
143. Baxter, F.R.; Bowen, C.R.; Turner, I.G.; Dent, A.C. Electrically active bioceramics: A review of interfacial responses. *Ann. Biomed. Eng.* **2010**, *38*, 2079–2092. [CrossRef] [PubMed]
144. Ciofani, G.; Ricotti, L.; Canale, C.; D'Alessandro, D.; Berrettini, S.; Mazzolai, B.; Mattoli, V. Effects of barium titanate nanoparticles on proliferation and differentiation of rat mesenchymal stem cells. *Colloids Surf. B Biointerfaces* **2013**, *102*, 312–320. [CrossRef]
145. Ciofani, G.; Ricotti, L.; Mattoli, V. Preparation, characterization and in vitro testing of poly (lactic-co-glycolic) acid/barium titanate nanoparticle composites for enhanced cellular proliferation. *Biomed. Microdevices* **2011**, *13*, 255–266. [CrossRef] [PubMed]
146. Ivanova, O.; Williams, C.; Campbell, T. Additive manufacturing (AM) and nanotechnology: Promises and challenges. *Rapid Prototyp. J.* **2013**, *19*, 353–364. [CrossRef]
147. Jacob, J.; More, N.; Kalia, K.; Kapusetti, G. Piezoelectric smart biomaterials for bone and cartilage tissue engineering. *Inflamm. Regen.* **2018**, *38*, 2. [CrossRef]
148. Matassi, F.; Nistri, L.; Paez, D.C.; Innocenti, M. New biomaterials for bone regeneration. *Clin. Cases Miner. Bone Metab.* **2011**, *8*, 21.
149. Ahmad, P.; Khandaker, M.U.; Khan, Z.R.; Amin, Y.M. Synthesis of boron nitride nanotubes via chemical vapour deposition: A comprehensive review. *Mater. Sci. Eng. R.* **2010**, *70*, 92–111. [CrossRef]
150. Lahiri, D.; Rouzaud, F.; Richard, T.; Keshri, A.K.; Bakshi, S.R.; Kos, L.; Agarwal, A. Boron nitride nanotube reinforced polylactide–polycaprolactone copolymer composite: Mechanical properties and cytocompatibility with osteoblasts and macrophages in vitro. *Acta Biomater.* **2010**, *6*, 3524–3533. [CrossRef]
151. Lahiri, D.; Singh, V.; Benaduce, A.P.; Seal, S.; Kos, L.; Agarwal, A. Boron nitride nanotube reinforced hydroxyapatite composite: Mechanical and tribological performance and in-vitro biocompatibility to osteoblasts. *J. Mech. Behav. Biomed.* **2011**, *4*, 44–56. [CrossRef]
152. Li, X.; Zhi, C.; Hanagata, N.; Yamaguchi, M.; Bando, Y.; Golberg, D. Boron nitride nanotubes functionalized with mesoporous silica for intracellular delivery of chemotherapy drugs. *Chem. Commun.* **2013**, *49*, 7337–7339. [CrossRef]
153. Ciofani, G.; Danti, S.; Genchi, G.G.; Mazzolai, B.; Mattoli, V. Boron nitride nanotubes: Biocompatibility and potential spill-over in nanomedicine. *Small* **2013**, *9*, 1672–1685. [CrossRef] [PubMed]

154. Li, X.; Hanagata, N.; Wang, X.; Yamaguchi, M.; Yi, W.; Bando, Y.; Golberg, D. Multimodal luminescent-magnetic boron nitride nanotubes@ NaGdF 4: Eu structures for cancer therapy. *Chem. Commun.* **2014**, *50*, 4371–4374. [CrossRef]
155. Weng, Q.; Wang, B.; Wang, X.; Hanagata, N.; Li, X.; Liu, D.; Golberg, D. Highly water-soluble, porous, and biocompatible boron nitrides for anticancer drug delivery. *ACS Nano* **2014**, *8*, 6123–6130. [CrossRef] [PubMed]
156. Wang, J.; Lee, C.H.; Yap, Y.K. Recent advancements in boron nitride nanotubes. *Nanoscale* **2010**, *2*, 2028–2034. [CrossRef] [PubMed]
157. Ciofani, G.; Raffa, V.; Menciassi, A.; Cuschieri, A. Boron nitride nanotubes: An innovative tool for nanomedicine. *Nano Today* **2009**, *4*, 8–10. [CrossRef]
158. Rasmussen, J.W.; Martinez, E.; Louka, P.; Wingett, D.G. Zinc oxide nanoparticles for selective destruction of tumor cells and potential for drug delivery applications. *Expert Opin. Drug Deliv.* **2010**, *7*, 1063–1077. [CrossRef]
159. Goel, S.; Kumar, B. A review on piezo-/ferro-electric properties of morphologically diverse ZnO nanostructures. *J. Alloys Compd.* **2019**, *816*, 152491. [CrossRef]
160. Yin, Y.; Lin, Q.; Sun, H.; Chen, D.; Wu, Q.; Chen, X.; Li, S. Cytotoxic effects of ZnO hierarchical architectures on RSC96 Schwann cells. *Res. Lett.* **2012**, *7*, 439. [CrossRef]
161. Safaei, M.; Sodano, H.A.; Anton, S.R. A review of energy harvesting using piezoelectric materials: State-of-the-art a decade later (2008–2018). *Smart Mater. Struct.* **2019**, *28*, 113001. [CrossRef]
162. Ribeiro, C.; Correia, D.M.; Ribeiro, S.; Sencadas, V.; Botelho, G.; Lanceros-Méndez, S. Piezoelectric poly (vinylidene fluoride) microstructure and poling state in active tissue engineering. *Eng. Life Sci.* **2015**, *15*, 351–356. [CrossRef]
163. Aguilar, M.R.; San Román, J. Introduction to smart polymers and their applications. In *Smart Polymers and Their Applications*; Woodhead Publishing: Sawston, UK, 2019; pp. 1–11.
164. Piskin, E. Biodegradable polymers as biomaterials. *J. Biomater. Sci. Polym. Ed.* **1995**, *6*, 775–795. [CrossRef] [PubMed]
165. Sajkiewicz, P. Crystallization behaviour of poly(vinylidene fluoride). *Eur. Polym. J.* **1999**, *35*, 1581–1590. [CrossRef]
166. Gradys, A.; Sajkiewicz, P.; Adamovsky, S.; Minakov, A.A.; Schick, C. Crystallization of poly(vinylidene fluoride) during ultra-fast cooling. *Thermochim. Acta* **2007**, *461*, 153–157. [CrossRef]
167. Esterly, D.M.; Love, B.J. Phase transformation to β-poly (vinylidene fluoride) by milling. *J. Polym. Sci. B Polym. Phys.* **2004**, *42*, 91–97. [CrossRef]
168. Cozza, E.S.; Monticelli, O.; Marsano, E.; Cebe, S. On the Electrospinning of PVDF: Influence of the Experimental Conditions on the Nanofiber Properties. *Polym. Int.* **2013**, *62*, 41–48. [CrossRef]
169. Yu, L.; Cebe, P. Crystal polymorphism in electrospun composite nanofibers of poly (vinylidene fluoride) with nanoclay. *Polymer* **2009**, *50*, 2133–2141. [CrossRef]
170. El Mohajir, B.E.; Heymans, N. Changes in structural and mechanical behaviour of PVDF with processing and thermomechanical treatments. 1. Change in structure. *Polymer* **2001**, *42*, 5661–5667. [CrossRef]
171. Imamura, R.; Silva, A.B.; Gregorio, R., Jr. γ→ β Phase transformation induced in poly (vinylidene fluoride) by stretching. *J. Appl. Polym. Sci.* **2008**, *110*, 3242–3246. [CrossRef]
172. Wang, J.; Li, H.; Liu, J.; Duan, Y.; Jiang, S.; Yan, Y. On the α→β Transition of Carbon Coated Highly Oriented PVDF Ultrathin Film Induced by Melt Recrystallization. *J. Am. Chem. Soc.* **2003**, *125*, 1496–1497. [CrossRef]
173. Kaura, T.; Nath, R.; Perlman, M.M. Simultaneous stretching and corona poling of PVDF films. *J. Phys. D: Appl. Phys.* **1991**, *24*, 1848. [CrossRef]
174. Ramanathan, A.K.; Headings, L.M.; Dapino, M.J. Design optimization of flexible piezoelectric PVDF unimorphs for surface pressure transducer applications. In *Smart Structures and NDE for Energy Systems and Industry 4.0*; International Society for Optics and Photonics: Bellingham, WA, USA, 2019; Volume 10973, p. 1097307.
175. Ellingford, C.; Smith, H.; Yan, X.; Bowen, C.; Figiel, Ł.; McNally, T.; Wan, C. Electrical dual-percolation in MWCNTs/SBS/PVDF based thermoplastic elastomer (TPE) composites and the effect of mechanical stretching. *Eur. Polym. J.* **2019**, *112*, 504–514. [CrossRef]
176. Zhang, S.; Jia, Z.; Liu, T.; Wei, G.; Su, Z. Electrospinning Nanoparticles-Based Materials Interfaces for Sensor Applications. *Sensors* **2019**, *19*, 3977. [CrossRef] [PubMed]

177. Li, Y.; Liao, C.; Tjong, S.C. Electrospun Polyvinylidene Fluoride-Based Fibrous Scaffolds with Piezoelectric Characteristics for Bone and Neural Tissue Engineering. *Nanomaterials* **2019**, *9*, 952. [CrossRef] [PubMed]
178. Yu, L.; Zhou, P.; Wu, D.; Wang, L.; Lin, L.; Sun, D. Shoepad nanogenerator based on electrospun PVDF nanofibers. *Microsyst. Technol.* **2019**, *25*, 3151–3156. [CrossRef]
179. Ribeiro, C.; Costa, C.M.; Correia, D.M.; Nunes-Pereira, J.; Oliveira, J.; Martins, P.; Lanceros-Méndez, S. Electroactive poly (vinylidene fluoride)-based structures for advanced applications. *Nat. Protoc.* **2018**, *13*, 681. [CrossRef] [PubMed]
180. Fortunato, M.; Cavallini, D.; De Bellis, G.; Marra, F.; Tamburrano, A.; Sarto, F.; Sarto, M.S. Phase Inversion in PVDF Films with Enhanced Piezoresponse Through Spin-Coating and Quenching. *Polymers* **2019**, *11*, 1096. [CrossRef]
181. Liu, Z.H.; Pan, C.T.; Lin, L.W.; Huang, J.C.; Ou, Z.Y. Direct-write PVDF nonwoven fiber fabric energy harvesters via the hollow cylindrical near-field electrospinning process. *Smart Mater. Struct.* **2013**, *23*, 025003. [CrossRef]
182. Zaarour, B.; Zhu, L.; Jin, X. Controlling the surface structure, mechanical properties, crystallinity, and piezoelectric properties of electrospun PVDF nanofibers by maneuvering molecular weight. *Soft Mater.* **2019**, *17*, 181–189. [CrossRef]
183. Singh, R.K.; Lye, S.W.; Miao, J. PVDF Nanofiber Sensor for Vibration Measurement in a String. *Sensors* **2019**, *19*, 3739. [CrossRef]
184. Khalifa, M.; Janakiraman, S.; Ghosh, S.; Venimadhav, A.; Anandhan, S. PVDF/halloysite nanocomposite-based non-wovens as gel polymer electrolyte for high safety lithium ion battery. *Polym. Compos.* **2019**, *40*, 2320–2334. [CrossRef]
185. Liang, S.; Kang, Y.; Tiraferri, A.; Giannelis, E.P.; Huang, X.; Elimelech, M. Highly hydrophilic polyvinylidene fluoride (PVDF) ultrafiltration membranes via postfabrication grafting of surface-tailored silica nanoparticles. *ACS Appl. Mater. Interfaces* **2013**, *5*, 6694–6703. [CrossRef] [PubMed]
186. Mandal, D.; Henkel, K.; Schmeißer, D. The electroactive β-phase formation in poly (vinylidene fluoride) by gold nanoparticles doping. *Materials Lett.* **2012**, *73*, 123–125. [CrossRef]
187. Li, J.H.; Shao, X.S.; Zhou, Q.; Li, M.Z.; Zhang, Q.Q. The double effects of silver nanoparticles on the PVDF membrane: Surface hydrophilicity and antifouling performance. *App. Surf. Sci.* **2013**, *265*, 663–670. [CrossRef]
188. Liang, S.; Xiao, K.; Mo, Y.; Huang, X. A novel ZnO nanoparticle blended polyvinylidene fluoride membrane for anti-irreversible fouling. *J. Membr. Sci.* **2012**, *394*, 184–192. [CrossRef]
189. Teow, Y.H.; Ahmad, A.L.; Lim, J.K.; Ooi, B.S. Preparation and characterization of PVDF/TiO2 mixed matrix membrane via in situ colloidal precipitation method. *Desalination* **2012**, *295*, 61–69. [CrossRef]
190. Zhang, J.; Xu, Z.; Mai, W.; Min, C.; Zhou, B.; Shan, M.; Qian, X. Improved hydrophilicity, permeability, antifouling and mechanical performance of PVDF composite ultrafiltration membranes tailored by oxidized low-dimensional carbon nanomaterials. *J. Mater. Chem. A* **2013**, *1*, 3101–3111. [CrossRef]
191. Song, H.; Shao, J.; He, Y.; Liu, B.; Zhong, X. Natural organic matter removal and flux decline with PEG–TiO2-doped PVDF membranes by integration of ultrafiltration with photocatalysis. *J. Membr. Sci.* **2012**, *405*, 48–56. [CrossRef]
192. Li, N.; Xiao, C.; An, S.; Hu, X. Preparation and properties of PVDF/PVA hollow fiber membranes. *Desalination* **2010**, *250*, 530–537. [CrossRef]
193. Gayen, A.L.; Mondal, D.; Roy, D.; Bandyopadhyay, P.; Manna, S.; Basu, R.; Nandy, P. Improvisation of electrical properties of PVDF-HFP: Use of novel metallic nanoparticles. *J. Mater. Sci.: Mater.* **2017**, *28*, 14798–14808. [CrossRef]
194. Jaleh, B.; Sodagar, S.; Momeni, A.; Jabbari, A. Nanodiamond particles/PVDF nanocomposite flexible films: Thermal, mechanical and physical properties. *Mater. Res. Express* **2016**, *3*, 085028. [CrossRef]
195. Fraczek-Szczypta, A. Carbon nanomaterials for nerve tissue stimulation and regeneration. *Mater. Sci. Eng. C* **2014**, *34*, 35–49. [CrossRef]
196. Tsonos, C.; Pandis, C.; Soin, N.; Sakellari, D.; Myrovali, E.; Kripotou, S.; Siores, E. Multifunctional nanocomposites of poly (vinylidene fluoride) reinforced by carbon nanotubes and magnetite nanoparticles. *Express Polym. Lett.* **2015**, *9*. [CrossRef]
197. Lorber, B.; Hsiao, W.K.; Hutchings, I.M.; Martin, K.R. Adult rat retinal ganglion cells and glia can be printed by piezoelectric inkjet printing. *Biofabrication* **2013**, *6*, 015001. [CrossRef] [PubMed]

198. Inaoka, T.; Shintaku, H.; Nakagawa, T.; Kawano, S.; Ogita, H.; Sakamoto, T.; Ito, J. Piezoelectric materials mimic the function of the cochlear sensory epithelium. *Proc. Natl. Acad. Sci. USA* **2011**, *108*, 18390–18395. [CrossRef] [PubMed]
199. Gao, Y.; Wang, Z.L. Electrostatic potential in a bent piezoelectric nanowire. The fundamental theory of nanogenerator and nanopiezotronics. *Nano Lett.* **2007**, *7*, 2499–2505. [CrossRef] [PubMed]
200. Walsh, J.F.; Manwaring, M.E.; Tresco, P.A. Directional neurite outgrowth is enhanced by engineered meningeal cell-coated substrates. *Tissue Eng.* **2005**, *11*, 1085–1094. [CrossRef] [PubMed]
201. Asano, T.; Kubo, T.; Nishikitani, Y. Electrochemical properties of dye-sensitized solar cells fabricated with PVDF-type polymeric solid electrolytes. *J. Photochem. Photobiol.* **2004**, *164*, 111–115. [CrossRef]
202. Marino, A.; Arai, S.; Hou, Y.; Sinibaldi, E.; Pellegrino, M.; Chang, B.; Mazzolai, V.; Mattoli Suzuki, M.; Ciofani, G. Piezoelectric nanoparticle-assisted wireless neuronal stimulation. *ACS Nano* **2015**, *9*, 7678–7689. [CrossRef]
203. Genchi, G.G.; Ceseracciu, L.; Marino, A.; Labardi, M.; Marras, S.; Pignatelli, F.; Bruschini, L.; Mattoli, V.; Ciofani, G. P(VDF-TrFE)/BaTiO3 nanoparticle composite films mediate piezoelectric stimulation and promote differentiation of SH-SY5Y neuroblastoma cells. *Adv. Healthc. Mater.* **2016**, *5*, 1808–1820. [CrossRef]
204. Weber, N.; Lee, Y.S.; Shanmugasundaram, S.; Jaffe, M.; Arinzeh, T.L. Characterization and in vitro cytocompatibility of piezoelectric electrospun scaffolds. *Acta Biomater.* **2010**, *6*, 3550–3556. [CrossRef]
205. De Ruiter, G.C.; Malessy, M.J.; Yaszemski, M.J.; Windebank, A.J.; Spinner, R.J. Designing ideal conduits for peripheral nerve repair. *Neurosurg. Focus.* **2009**, *26*, E5. [CrossRef] [PubMed]
206. Ichihara, S.; Inada, Y.; Nakamura, T. Artificial nerve tubes and their application for repair of peripheral nerve injury: An update of current concepts. *Injury* **2008**, *39*, 29–39. [CrossRef] [PubMed]
207. Ji, Y.; Jin, R.; Zhang, X.; Bouchilaoun, R.; Fan, J.; Zhao, R.; Yang, H. Electric polarizations in PVDF-TrFE nanorods under lateral nanoshaping. *Int. J. Appl.* **2019**, *126*, 174108. [CrossRef]
208. Wan, C.; Bowen, C.R. Multiscale-structuring of polyvinylidene fluoride for energy harvesting: The impact of molecular-, micro- and macro-structure. *J. Mater. Chem. A* **2017**, *5*, 3091–3128. [CrossRef]
209. Sun, F.C.; Dongare, A.M.; Asandei, A.D.; Alpay, S.P.; Nakhmanson, S. Temperature dependent structural, elastic, and polar properties of ferroelectric polyvinylidene fluoride (PVDF) and trifluoroethylene (TrFE). *copolymers. J. Mater. Chem. C* **2015**, *3*, 8389–8396. [CrossRef]
210. Belkas, J.S.; Shoichet, M.S.; Midha, R. Peripheral nerve regeneration through guidance tubes. *Neurol. Res.* **2004**, *26*, 151–160. [CrossRef]
211. Boni, R.; Ali, A.; Shavandi, A.; Clarkson, A.N. Current and novel polymeric biomaterials for neural tissue engineering. *J Biomed. Sci.* **2018**, *25*, 90. [CrossRef]
212. Fine, E.G.; Valentini, R.F.; Bellamkonda, R.; Aebischer, P. Influence of surface texture of polymeric sheets throught piezoelectric vinylidenefluoride-trifluoroethylene copolymer guidance channels. *Biomaterials* **1991**, *12*, 259–263. [CrossRef]
213. Martins, P.M.; Ribeiro, S.; Ribeiro, C.; Sencadas, V.; Gomes, A.C.; Gama, F.M.; Lanceros-Méndez, S. Effect of poling state and morphology of piezoelectric poly(vinylidene fluoride) membranes for skeletal muscle tissue engineering. *RSC Adv.* **2013**, *3*, 17938–17944. [CrossRef]
214. Ke, S.; Huang, H.; Ren, L.; Wang, Y. Nearly constant dielectric loss behavior in poly (3-hydroxybutyrate-co-3-hydroxyvalerate) biodegradable polyester. *J. Appl. Phys.* **2009**. [CrossRef]
215. Numata, K.; Abe, H.; Doi, Y. Enzymatic processes for biodegradation of poly (hydroxyalkanoate) s crystals. *Can. J. Chem.* **2008**, *86*, 471–483. [CrossRef]
216. Willerth, S.M.; Sakiyama-Elbert, S.E. Approaches to neural tissue engineering using scaffolds for drug delivery. *Adv. Drug Deliv. Rev.* **2007**, *59*, 325–338. [CrossRef] [PubMed]
217. Wu, Q.; Wang, Y.; Chen, G.Q. Medical application of microbial biopolyesters polyhydroxyalkanoates. *Artif. Cells Blood Substit. Immobil. Biotechnol.* **2009**, *37*, 1–12. [CrossRef] [PubMed]
218. Misra, S.K.; Valappil, S.P.; Roy, I.; Boccaccini, A.R. Polyhydroxyalkanoate (PHA)/inorganic phase composites for tissue engineering applications. *Biomacromolecules* **2006**, *7*, 2249–2258. [CrossRef]
219. Prabhakaran, M.P.; Vatankhah, E.; Ramakrishna, S. Electrospun aligned PHBV/collagen nanofibers as substrates for nerve tissue engineering. *Biotechnol Bioeng.* **2013**, *110*, 2775–2784. [CrossRef]
220. Rahman, M.S.; Tsuchiya, T. Enhancement of chondrogenic differentiation of human articular chondrocytes by biodegradable polymers. *Tissue Eng.* **2001**, *7*, 781–790. [CrossRef]

221. Chen, W.; Tong, Y.W. PHBV microspheres as neural tissue engineering scaffold support neuronal cell growth and axon–dendrite polarization. *Acta Biomater.* **2012**, *8*, 540–548. [CrossRef]
222. Rivera-Briso, A.L.; Serrano-Aroca, A. Poly(3-Hydroxybutyrate-co-3-Hydroxyvalerate): Enhancement Strategies for Advanced Applications. *Polymers* **2018**, *10*, 732. [CrossRef]
223. Sencadas, V.; Ribeiro, C.; Heredia, A.; Bdikin, I.K.; Kholkin, A.L.; Lanceros-Méndez, S. Local piezoelectric activity of single poly (L-lactic acid)(PLLA) microfibers. *Appl. Phys. A* **2012**, *109*, 51–55. [CrossRef]
224. Jin, L.; Feng, Z.Q.; Zhu, M.L.; Wang, T.; Leach, M.K.; Jiang, Q. A novel fluffy conductive polypyrrole nano-layer coated PLLA fibrous scaffold for nerve tissue engineering. *J. Biomed. Nanotechnol.* **2012**, *8*, 779–785. [CrossRef]
225. Zhang, K.; Zheng, H.; Liang, S.; Gao, C. Aligned PLLA nanofibrous scaffolds coated with graphene oxide for promoting neural cell growth. *Acta Biomater.* **2016**, *37*, 131–142. [CrossRef] [PubMed]
226. Zuidema, J.M.; Provenza, C.; Caliendo, T.; Dutz, S.; Gilbert, R.J. Magnetic NGF-releasing PLLA/iron oxide nanoparticles direct extending neurites and preferentially guide neurites along aligned electrospun microfibers. *ACS Chem. Neurosci.* **2015**, *6*, 1781–1788. [CrossRef] [PubMed]
227. Venugopal, J.; Zhang, Y.Z.; Ramakrishna, S. Electrospun nanofibres: Biomedical applications. Proceedings of the institution of mechanical engineers. *N J. Nanoeng. Nanosyst.* **2004**, *218*, 35–45.
228. Philipp, B.; Bock, W.; Schierbaum, F. Application of polysaccharides and their derivatives as supporting materials and auxiliary substances in medicine and nutrition. *J. Polym. Sci. Polym. Symp.* **1979**, *66*, 83–100. [CrossRef]
229. Franz, G. Polysaccharides in pharmacy. *Adv. Polym. Sci.* **1986**, *76*, 1–30.
230. Miyamoto, T.; Takahashi, S.I.; Ito, H.; Inagaki, H.; Noishiki, Y. Tissue biocompatibility of cellulose and its derivatives. *J. Biomed. Mater. Res.* **1989**, *23*, 125–133. [CrossRef]
231. Ikada, Y. Biomedical applications of cellulose membranes. In *Cellulose: Structural and Functional Aspects*; Kennedy, J.F., Phillips, G.O., Williams, P.A., Eds.; Ellis Horwood: Chichester, UK, 1989; pp. 447–455.
232. Barbié, C.; Chauveaux, D.; Barthe, X.; Baquey, C.; Poustis, J. Biological behaviour of cellulosic materials after bone implantation: Preliminary results. *Clin. Mater.* **1990**, *5*, 251–258. [CrossRef]
233. Gross, U.; Muller-Mai, C.; Voigt, C. The tissue response on cellulose cylinders after implantation in the distal femur of rabbits. In Proceedings of the Fourth World Biomaterials Congress, Berlin, Germany, 19–24 May 1992; p. 192.
234. Märtson, M.; Viljanto, J.; Hurme, T.; Saukko, P. Biocompatibility of cellulose sponge with bone. *Eur. Surg. Res.* **1998**, *30*, 426–432. [CrossRef]
235. Bhatnagar, A.; Sain, M. Processing of cellulose nanofiber-reinforced composites. *J. Reinf. Plast. Comp.* **2005**, *24*, 1259–1268. [CrossRef]
236. Fricain, J.C.; Granja, P.L.; Barbosa, M.A.; De Jéso, B.; Barthe, N.; Baquey, C. Cellulose phosphates as biomaterials. In vivo biocompatibility studies. *Biomaterials* **2002**, *23*, 971–980. [CrossRef]
237. Svensson, A.; Nicklasson, E.; Harrah, T.; Panilaitis, B.; Kaplan, D.L.; Brittberg, M.; Gatenholm, P. Bacterial cellulose as a potential scaffold for tissue engineering of cartilage. *Biomaterials* **2005**, *26*, 419–431. [CrossRef] [PubMed]
238. Märtson, M.; Viljanto, J.; Laippala, P.; Saukko, P. Connective tissue formation in subcutaneous cellulose sponge implants in the rat. *Eur. Surg. Res.* **1998**, *30*, 419–425. [CrossRef] [PubMed]
239. Fundueanu, G.; Constantin, M.; Esposito, E.; Cortesi, R.; Nastruzzi, C.; Menegatti, E. Cellulose acetate butyrate microcapsules containing dextran ion-exchange resins as self-propelled drug release system. *Biomaterials* **2005**, *26*, 4337–4347. [CrossRef] [PubMed]
240. Entcheva, E.; Bien, H.; Yin, L.; Chung, C.Y.; Farrell, M.; Kostov, Y. Functional cardiac cell constructs on cellulose-based scaffolding. *Biomaterials* **2004**, *25*, 5753–5762. [CrossRef]
241. Tate, M.C.; Shear, D.A.; Hoffman, S.W.; Stein, D.G.; LaPlaca, M.C. Biocompatibility of methylcellulose-based constructs designed for intracerebral gelation following experimental traumatic brain injury. *Biomaterials* **2001**, *22*, 1113–1123. [CrossRef]
242. Hoseini, S.M.; Khosravi-Darani, K.; Mozafari, M.R. Nutritional and medical applications of spirulina microalgae. *Mini Rev. Med. Chem.* **2013**, *13*, 1231–1237. [CrossRef]
243. Granja, P.L.; Barbosa, M.A.; Pouységu, L.; De Jéso, B.; Rouais, F.; Baquey, C. Cellulose phosphates as biomaterials. Mineralization of chemically modified regenerated cellulose hydrogels. *J. Mater. Sci.* **2001**, *36*, 2163–2172. [CrossRef]

244. Naseri-Nosar, M.; Salehi, M.; Hojjati-Emami, S. Cellulose acetate/poly lactic acid coaxial wet-electrospun scaffold containing citalopram-loaded gelatin nanocarriers for neural tissue engineering applications. *Int. J. Biol. Macromol.* **2017**, *103*, 701–708. [CrossRef]
245. Wang, S.; Sun, C.; Guan, S.; Li, W.; Xu, J.; Ge, D.; Ma, X. Chitosan/gelatin porous scaffolds assembled with conductive poly (3, 4-ethylenedioxythiophene) nanoparticles for neural tissue engineering. *J. Mat. Chem. B* **2017**, *5*, 4774–4788. [CrossRef]
246. Koide, S.S. Chitin-chitosan: Properties, benefits and risks. *Nutr. Res.* **1998**, *18*, 1091–1101. [CrossRef]
247. Rinaudo, M. Chitin and chitosan: Properties and applications. *Prog. Polym. Sci.* **2006**, *31*, 603–632. [CrossRef]
248. Madihally, S.V.; Matthew, H.W. Porous chitosan scaffolds for tissue engineering. *Biomaterials* **1999**, *20*, 1133–1142. [CrossRef]
249. Ohkawa, K.; Cha, D.; Kim, H.; Nishida, A.; Yamamoto, H. Electrospinning of chitosan. *Macromol. Rapid Commun.* **2004**, *25*, 1600–1605. [CrossRef]
250. Izzo, D.; Palazzo, B.; Scalera, F.; Gullotta, F.; Lapesa, V.; Scialla, S.; Gervaso, F. Chitosan scaffolds for cartilage regeneration: Influence of different ionic crosslinkers on biomaterial properties. *Int. J. Polym. Mater.* **2019**, *68*, 936–945. [CrossRef]
251. Maged, A.; Abdelkhalek, A.A.; Mahmoud, A.A.; Salah, S.; Ammar, M.M.; Ghorab, M.M. Mesenchymal stem cells associated with chitosan scaffolds loaded with rosuvastatin to improve wound healing. *Eur. J. Pharm. Sci.* **2019**, *127*, 185–198. [CrossRef]
252. Xue, Y.; Wu, M.; Liu, Z.; Song, J.; Luo, S.; Li, H.; Chen, F. In vitro and in vivo evaluation of chitosan scaffolds combined with simvastatin-loaded nanoparticles for guided bone regeneration. *J. Mater. Sci. Mater. Med.* **2019**, *30*, 47. [CrossRef]
253. Skop, N.B.; Calderon, F.; Levison, S.W.; Gandhi, C.D.; Cho, C.H. Heparin crosslinked chitosan microspheres for the delivery of neural stem cells and growth factors for central nervous system repair. *Acta Biomater.* **2013**, *9*, 6834–6843. [CrossRef]
254. Elnaggar, Y.S.R.; Etman, S.M.; Abdelmonsif, D.A. Intranasal Piperine-Loaded Chitosan Nanoparticles as Brain-Targeted Therapy in Alzheimer's Disease: Optimization, Biological Efficacy, and Potential Toxicity. *J. Pharm. Sci.* **2015**, *104*, 3544–3556. [CrossRef]
255. Raj, R.; Wairkar, S.; Sridhar, V.; Gaud, R. Pramipexole dihydrochloride loaded chitosan nanoparticles for nose to brain delivery: Development, characterization and in vivo anti-Parkinson activity. *Int. J. Biol. Macromol.* **2018**, *109*, 27–35. [CrossRef]
256. Liu, S.H.; Ho, P.C. Intranasal administration of brain-targeted HP-β-CD/chitosan nanoparticles for delivery of scutellarin, a compound with protective effect in cerebral ischaemia. *J. Pharm. Pharmacol.* **2017**, *69*, 1495–1501. [CrossRef]
257. Cooper, A.; Bhattarai, N.; Zhang, M. Fabrication and cellular compatibility of aligned chitosan–PCL fibers for nerve tissue regeneration. *Carbohydr. Polym.* **2011**, *85*, 149–156. [CrossRef]
258. Kuo, Y.C.; Yeh, C.F.; Yang, J.T. Differentiation of bone marrow stromal cells in poly(lactide-co-glycolide)/chitosan scaffolds. *Biomaterials* **2009**, *30*, 6604–6613. [CrossRef] [PubMed]
259. Marchesano, V.; Gennari, O.; Mecozzi, L.; Grilli, S.; Ferraro, P. Effects of lithium niobate polarization on cell adhesion and morphology. *ACS Appl. Mater. Interfaces.* **2015**, *7*, 18113–18119. [CrossRef] [PubMed]
260. Tiffany, A.; Harley, B.A. Sequestration of biomolecules for controlled delivery in mineralized collagen scaffolds. In 42nd Society for Biomaterials Annual Meeting and Exposition 2019: The Pinnacle of Biomaterials Innovation and Excellence. *Soc. Biomater.* **2019**, *40*, 1526–7547.
261. Sallent, I.; Capella-Monsonís, H.; Zeugolis, D.I. Production and Characterization of Chemically Cross-Linked Collagen Scaffolds. In *Collagen*; Humana Press: New York, NY, USA, 2019; pp. 23–38.
262. Mohee, L.; Offeddu, G.S.; Husmann, A.; Oyen, M.L.; Cameron, R.E. Investigation of the intrinsic permeability of ice-templated collagen scaffolds as a function of their structural and mechanical properties. *Acta Biomater.* **2019**, *83*, 189–198. [CrossRef]
263. Liu, Y.; Nelson, T.; Chakroff, J.; Cromeens, B.; Johnson, J.; Lannutti, J.; Besner, G.E. Comparison of polyglycolic acid, polycaprolactone, and collagen as scaffolds for the production of tissue engineered intestine. *J. Biomed. Mater. Res. B* **2019**, *107*, 750–760. [CrossRef]
264. Lei, X.; Gao, J.; Xing, F.; Zhang, Y.; Ma, Y.; Zhang, G. Comparative evaluation of the physicochemical properties of nano-hydroxyapatite/collagen and natural bone ceramic/collagen scaffolds and their osteogenesis-promoting effect on MC3T3-E1 cells. *Regen. Biomater.* **2019**, *6*, 361–371. [CrossRef]

265. Radhakrishnan, S.; Nagarajan, S.; Bechelany, M.; Kalkura, S.N. Collagen Based Biomaterials for Tissue Engineering Applications: A Review. In *Processes and Phenomena on the Boundary between Biogenic and Abiogenic*; Nature; Springer: Cham, Switzerland, 2020; pp. 3–22.
266. Eltom, A.; Zhong, G.; Muhammad, A. Scaffold Techniques and Designs in Tissue Engineering Functions and Purposes: A Review. *Adv. Mater. Sci. Eng.* **2019**. [CrossRef]
267. Mohseni, M.; Castro, N.J.; Dang, H.P.; Nguyen, T.D.; Ho, H.M.; Tran, M.P.N.; Tran, P.A. Adipose tissue regeneration: Scaffold—Biomaterial strategies and translational perspectives. In *Biomaterials in Translational Medicine*; Academic Press: Cambridge, MA, USA, 2019; pp. 291–330.
268. Ceballos, D.; Navarro, X.; Dubey, N.; Wendelschafer-Crabb, G.; Kennedy, W.R.; Tranquillo, R.T. Magnetically Aligned Collagen Gel Filling a Collagen Nerve Guide Improves Peripheral Nerve Regeneration. *Exp. Neurol.* **1999**, *158*, 290–300. [CrossRef]
269. Dubey, N.; Letourneau, P.C.; Tranquillo, R.T. Guided Neurite Elongation and Schwann Cell Invasion into Magnetically Aligned Collagen in Simulated Peripheral Nerve Regeneration. *Exp. Neurol.* **1999**, *158*, 338–350. [CrossRef]
270. Eguchi, Y.; Ogiue-Ikeda, M.; Ueno, S. Control of orientation of rat Schwann cells using an 8-T static magnetic field. *Neurosci. Lett.* **2003**, *351*, 130–132. [CrossRef]

polymers

MDPI

Review

Piezoelectric Scaffolds as Smart Materials for Bone Tissue Engineering

Angelika Zaszczyńska, Konrad Zabielski, Arkadiusz Gradys, Tomasz Kowalczyk * and Paweł Sajkiewicz

Institute of Fundamental Technological Research, Polish Academy of Sciences, Pawińskiego 5B, 02-106 Warsaw, Poland; azasz@ippt.pan.pl (A.Z.); kzab@ippt.pan.pl (K.Z.); argrad@ippt.pan.pl (A.G.); psajk@ippt.pan.pl (P.S.)

* Correspondence: tkowalcz@ippt.gov.pl

Abstract: Bone repair and regeneration require physiological cues, including mechanical, electrical, and biochemical activity. Many biomaterials have been investigated as bioactive scaffolds with excellent electrical properties. Amongst biomaterials, piezoelectric materials (PMs) are gaining attention in biomedicine, power harvesting, biomedical devices, and structural health monitoring. PMs have unique properties, such as the ability to affect physiological movements and deliver electrical stimuli to damaged bone or cells without an external power source. The crucial bone property is its piezoelectricity. Bones can generate electrical charges and potential in response to mechanical stimuli, as they influence bone growth and regeneration. Piezoelectric materials respond to human microenvironment stimuli and are an important factor in bone regeneration and repair. This manuscript is an overview of the fundamentals of the materials generating the piezoelectric effect and their influence on bone repair and regeneration. This paper focuses on the state of the art of piezoelectric materials, such as polymers, ceramics, and composites, and their application in bone tissue engineering. We present important information from the point of view of bone tissue engineering. We highlight promising upcoming approaches and new generations of piezoelectric materials.

Keywords: piezoelectricity; scaffolds; smart scaffolds; PVDF; PLLA; PVDF-TRFE; collagen; keratin; tissue engineering; bone tissue engineering; smart medicine; regenerative medicine

check for updates

Citation: Zaszczyńska, A.; Zabielski, K.; Gradys, A.; Kowalczyk, T.; Sajkiewicz, P. Piezoelectric Scaffolds as Smart Materials for Bone Tissue Engineering. *Polymers* **2024**, *16*, 2797. https://doi.org/10.3390/polym16192797

Academic Editor: Xufeng Dong

Received: 26 August 2024
Revised: 26 September 2024
Accepted: 29 September 2024
Published: 2 October 2024

1. Introduction

Piezoelectric materials (PMs) are smart materials (SMs) that can generate electrical signals in response to applied factors. In 1880, Pierre and Jacques Curie discovered piezoelectricity through deformation, resulting in a shift in ions or charges. This phenomenon includes electricity generation and electric polarization changes [1].

PMs dedicated to bone tissue engineering (BTE) have been gaining attention since 2016 [2]. Generally, the biological properties of the selected material depend on its ability to mimic human tissues [3], and in piezoelectric materials, the electric stimuli are crucial [4]. External electrical stimulation, electrical fields, and bioelectrical signals are important factors due to their contribution to bone repair. PMs can deliver electrical signals without external stimuli and increase the bone's ability to regenerate [5–8]. Also, these specific types of materials are known for the converse piezoelectric effect. Thus, electromechanical behavior can be managed by physiological electrical changes as mechanical signals appear. There is an increasing amount of research on the use of piezoelectric nanomaterials in bone tissue engineering. Especially since 2016, the number of publications has increased dramatically. The state of the-art shows the need for novel materials to restore bone fractures [9].

Piezoelectric, ferroelectric, and pyroelectric signals are the bioelectrical signals that occur in a naturally living bone. It has been proven that these factors influence the healing,

remodeling, and growth of bone structures [10,11]. Bioelectricity in the living bone was found to be connected with the non-centrosymmetry and piezoelectricity of collagen molecules [12]. The electric field in bones supports cell proliferation and growth. It has been noted that the polarity of the piezoelectric charges depends on the direction of bone deformation or mechanical stress, with positive and negative piezoelectric charges (Figure 1). The piezoelectric constant (d_{33}) of bone has been found to range from 0.7 to 2.3 pC/N^{-1} [13].

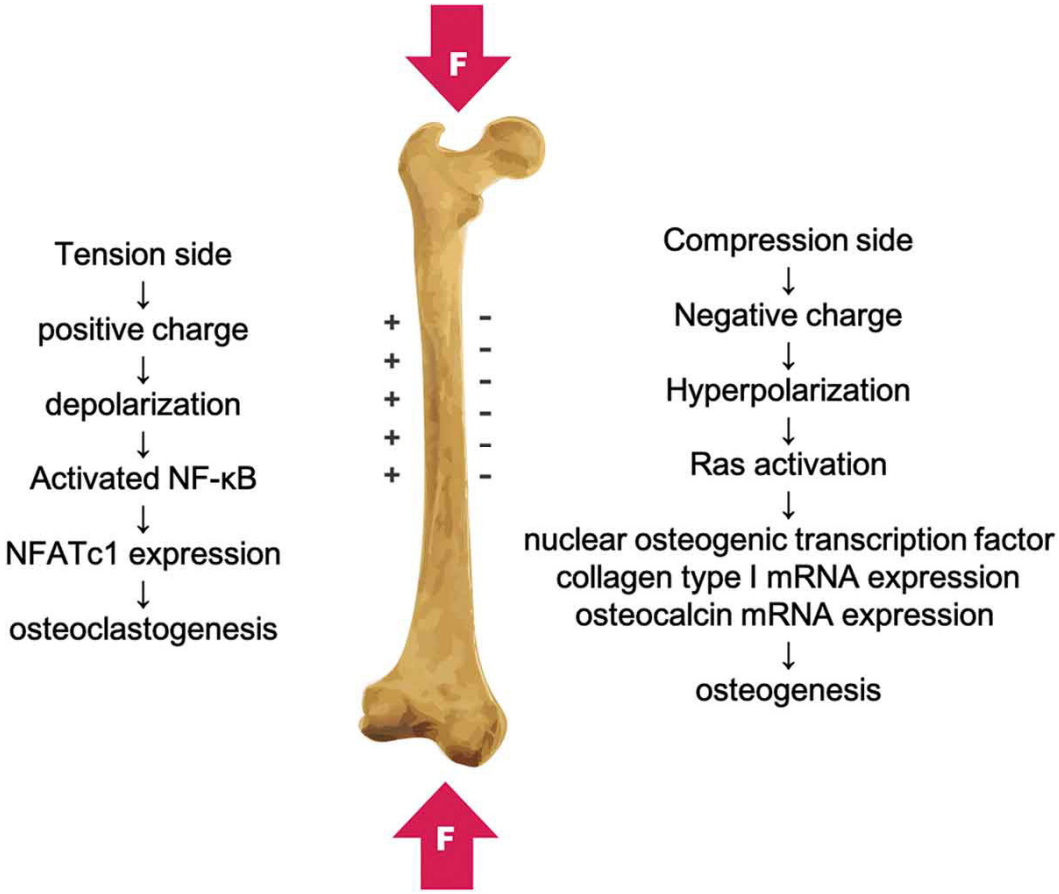

Figure 1. The piezoelectricity in bone caused by mechanical deformation with positive and negative charges. Reprinted with permission from Ref. [14]. Copyright 2019, Taylor and Francis Group.

The piezoelectric potential of human bone during walking is around 300 μV [15]. Information about the piezoelectric and dielectric properties of bone (trabecular and cortical) and articular cartilage is shown in Table 1.

Table 1. Piezoelectric coefficient, relative permittivity, and conductivity of bone and articular cartilage.

	Bone		Articular Cartilage	Ref.
	Cortical	Trabecular		
Piezoelectric Coefficient (d_{33}) [pC/N^{-1}]	0.7–2.3		0.2–0.7	[16]
Relative Permittivity	1.45×10^2	2.49×10^2	1.39×10^3	[17]
Conductivity (S/m)	0.02	0.079	1.14 ± 0.11	[18]

PMs generate electrical charges on the surface under an external stimulus, similarly to bone. It was reported that polarized surfaces can improve the osteogenic properties of natural bone [19]. Also, piezoelectric implants promote bone tissue repair [20]. Imple-

menting the piezoelectric scaffold into the bone defect causes electrical stimulation through physiological loads [21]. During activation of the cell membrane, calcium channels are open, providing hyperpolarization.

Figure 2 illustrates the calcium ion (Ca^{2+}) signal transduction pathway and several additional signaling pathways triggered by both electrical and mechanical stimulation. When mechanical forces are applied to a piezoelectric scaffold, they generate electrical signals that, in turn, activate voltage-gated Ca^{2+} channels. This leads to an increase in intracellular Ca^{2+} concentration, subsequently initiating the activation of calcium-modulated protein (calmodulin). Calmodulin, in turn, triggers the activation of calcineurin, a calcium- and calmodulin-dependent serine/threonine protein phosphatase. Once activated, calcineurin dephosphorylates NF-AT (nuclear factor of activated T-cells), causing it to translocate to the nucleus, where it collaborates with other associated proteins as transcription factors. Furthermore, mechanical stimulation itself can activate mechanoreceptors within the cell membrane, ultimately initiating the activation of protein kinase C (PKC) and mitogen-activated protein kinase (MAPK) signaling cascades. These cascades contribute to the synthesis of proteoglycan and the inhibition of interleukin-1 (IL-1), which is responsible for the degradation of proteoglycan [22].

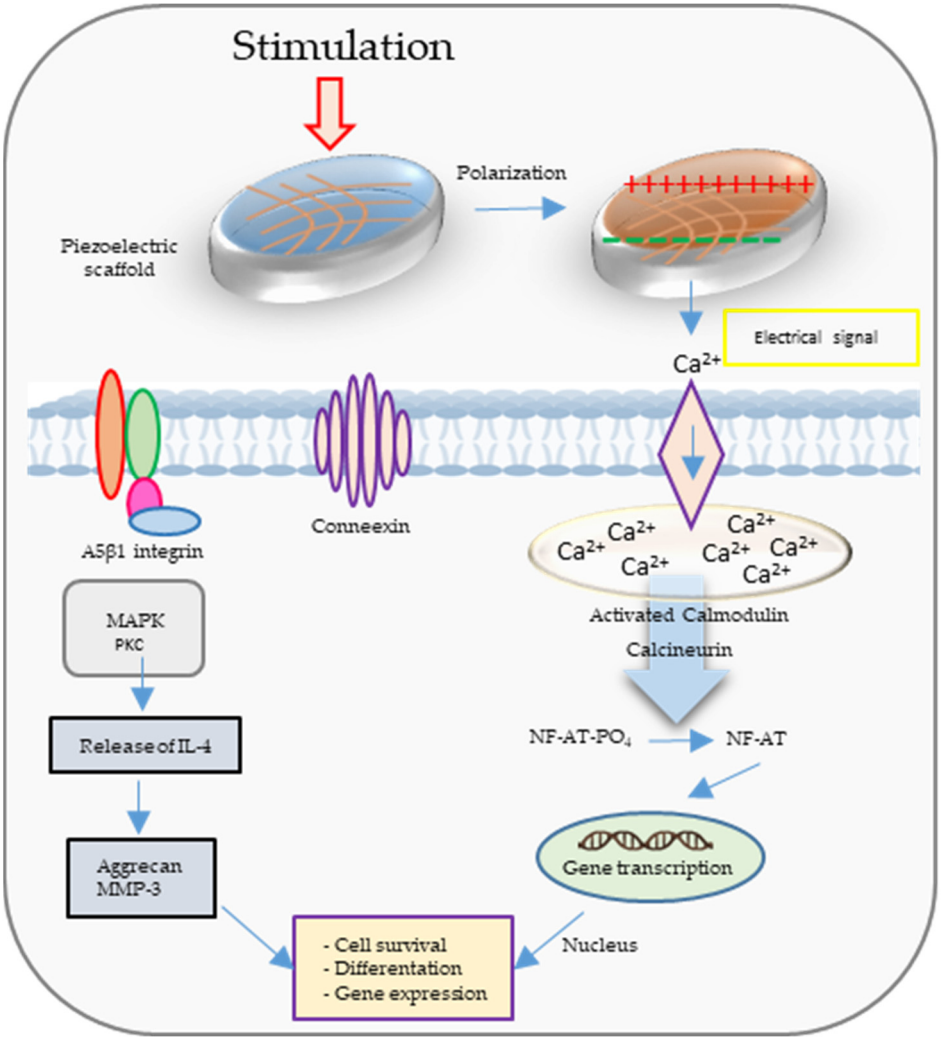

Figure 2. The calcium ion (Ca^{2+}) signal transduction pathway and several additional signaling pathways are activated through electrical and mechanical stimulation.

The role of intracellular Ca^{2+} ions is significant in cellular proliferation [23]. Hence, it can be deduced that the use of piezoelectric biocompatible scaffolds may lead to early

restoration of damaged tissue compared to their non-piezoelectric counterparts [24]. Liu et al. [25] examined the osseointegration of various implants by implanting positively polarized bismuth ferrite perovskites membrane–strontium titanate, a negatively polarized strontium titanate membrane–strontium titanate implant, and a non-polarized strontium titanate implant into rat femurs. At the interface of the oppositely charged strontium titanate and bismuth ferrite perovskites implant (+75 mV) and the electronegative bone defect surface (−52 to −87 mV), an inherent electric field was formed [26]. Consequently, this electric field promoted greater osseointegration compared to the strontium titanate and the bismuth ferrite perovskites implant and non-polarized strontium titanate surfaces.

Given the aforementioned context, this review provides an overview of the fundamental concepts, origins, and implications of piezoelectricity in natural bone. Furthermore, it explores the potential of different piezoelectric bioceramics and biopolymers to emulate the electromechanical characteristics observed in living bone. The discussion also addresses the challenges associated with processing and achieving the desired combination of piezoresponse properties, along with potential solutions. Additionally, an objective examination of the beneficial effects of polarized piezoelectric substrates on enhancing biocompatibility is included.

2. The Role of Piezoelectricity in Bone Tissue Engineering

In 1940, Martin [27,28] observed the initial manifestation of biological piezoelectricity. This occurred during the discovery of electric potentials emanating from compressed wool enclosed in shellac between two brass plates. Mammalian hair, wool, horn, and hoof primarily consist of α-keratin, characterized by a spiral α-helix structure [29]. The piezoelectric properties of these tissues stem from the orderly arrangement of α-helices, promoting inherent polarization [30]. The α-helix, a right-handed coil, achieves stability through hydrogen bonds between the amine and carbonyl groups. As depicted in Figure 3, the helical structure aligns amino acid dipoles, resulting in a substantial and enduring polarization [31].

The piezoelectric properties of bone were first reported by Yasuda in 1954 [32]. Subsequently, Yasuda and Fukada [33] conducted experiments on boiled bone and determined that the piezoelectric response was not attributed to living cells. They concluded that the application of shear on collagen within bone was responsible for its piezoelectric behavior. Bone is a composite material comprising densely packed collagen fibrils aligned with hydroxyapatite particles [34]. Collagen, the most abundant protein in mammals, possesses a triple helix structure known as the "triple helix" [35].

In 1892, Julius Wolff [36] proposed that bone adapts its structure in response to mechanical stress, known as "Wolff's Law". This principle is evidenced by the denser bone found in the arms of tennis players who hold rackets and the bone loss observed in astronauts. The discovery of piezoresponse in dry bone [32,37] led to the suggestion that piezoelectricity could explain the process of bone growth and resorption in response to stress. One of the pioneers in investigating the biological effects of piezoelectricity, Bassett [38], observed that periodically deformed chick embryonic tibiae produced large periosteal chondroid masses after seven days, unlike undeformed samples. He described Wolff's Law as a negative feedback loop: the applied load on bone induces strain in less dense regions, while denser and stiffer regions remain unstrained. The strain is converted into an electric field that aligns macromolecules and ions in the extracellular matrix, stimulating bone remodeling by cells until the signal is deactivated.

As piezoelectric measurements expanded to include wet bone [39] and wet collagen [40], which represent physiological conditions, discrepancies were observed in the amplitude and behavior of stress-generated potentials between wet and dry samples, and it was discovered that the induced electric potential and the relaxation time are dependent on the induced potential, which is significantly higher in wet samples. Various hypotheses were proposed to explain these inconsistencies, including the p–n junction characteristic of apatite–collagen [41], which suggested that bone exhibited piezoelectric behavior in

one direction and piezoresistive behavior in another. However, a widely accepted notion suggested that while piezoelectricity accounted for stress-induced potentials in dry bone, the mechanism responsible for wet bone was the streaming potential [42,43]. According to the streaming potential theory, the stress-generated potential in wet bone was a result of the flow of ion-containing interstitial fluid through the bone under pressure. This theory gained prominence after Pienkowski et al. [44] reported that the conductivity of the saturating fluid significantly influenced the amplitude and polarity of the generated potentials, and the longer relaxation time was attributed to the fluid's viscosity.

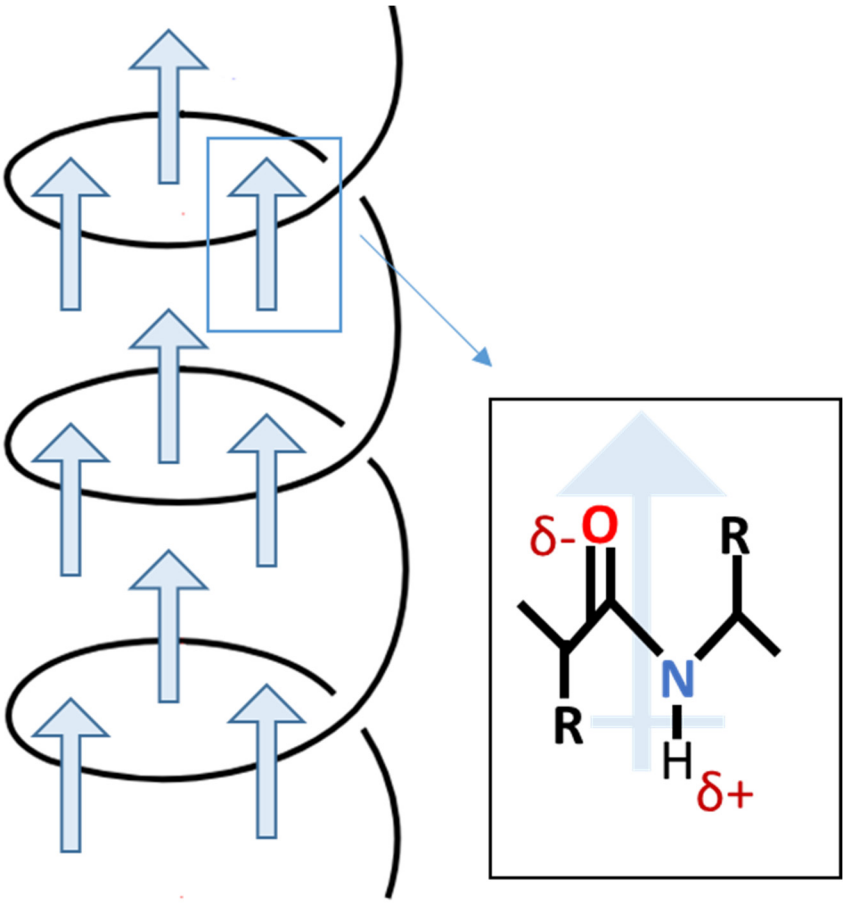

Figure 3. Scheme of permanent polarization in α-helix.

A more recent theory of mechanosensation in bone proposes that applied stress on bone is translated into biochemical signals through the flow of interstitial fluid into the canaliculi–lacunae space, which supplies bone cells with nutrients and conveys shear stress to cells [45]. Despite these new theories, the debate continues regarding the exclusion of piezoelectricity entirely from mechanosensation.

$$V = \frac{\zeta P \kappa}{4\pi\sigma\eta} \quad (1)$$

where ζ, P, κ, σ, and η are the zeta potential, the pressure on the bone, the dielectric permittivity, the conductivity, and the viscosity of the interstitial fluid, respectively.

3. Overview of Piezoelectric Materials for Bone Tissue Engineering

Piezoelectric polymers can be divided into natural and synthetic. Figure 4 shows selected piezoelectric materials along with the piezoelectric coefficient (d_{33}).

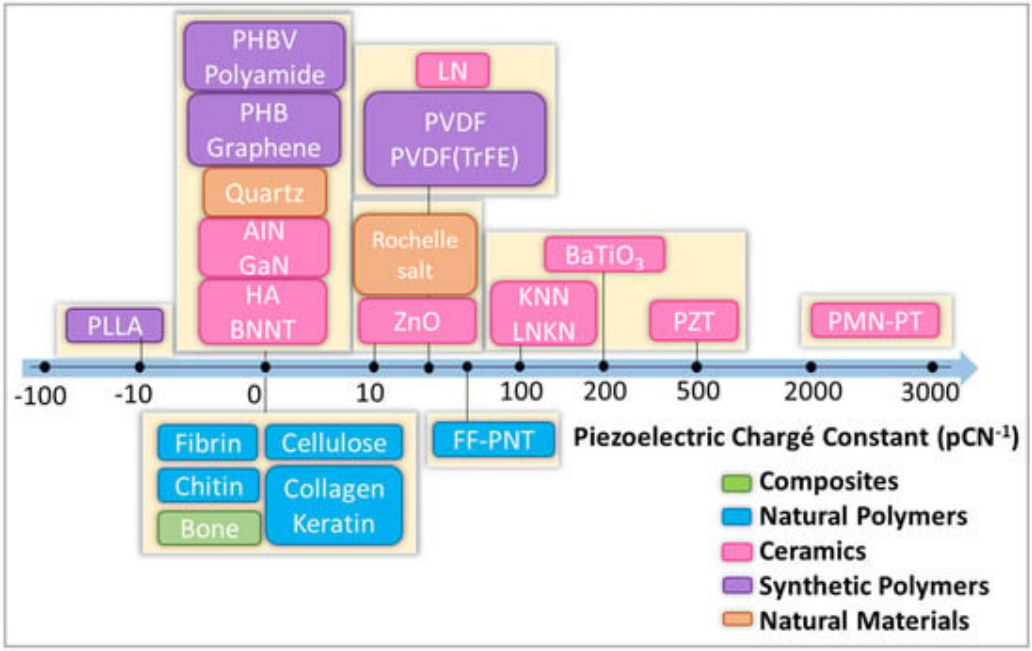

Figure 4. Scheme with classification of selected natural and synthetic piezoelectric materials. HA: hydroxyapatite. Zinc oxide (ZnO), boron nitride (BN), gallium nitride (GaN), poly(vinylidene fluoride-trifluoro ethylene) P(VDF-TrFE), poly(vinylidene fluoride) (PVDF), poly(l-lactic acid) (PLLA), polyhydroxybutyrate (PHB). Reprinted from ref. [46].

3.1. Natural Polymers

Among the natural polymers are two groups important from the point of view of piezoelectricity: polysaccharides and proteins. Piezoelectric polysaccharides are, e.g., chitosan and cellulose, and piezoelectric proteins are, e.g., keratin, collagen, and fibrin. Table 2 shows piezoelectric coefficients in various types of natural materials.

Table 2. The piezoelectric coefficient for different natural piezoelectric materials.

Type of Material	Piezoelectric Materials	Piezoelectric Coefficient	Ref.
Polysaccharides	Chitosan	d_{33} = 18.4 pCN^{-1}	[47]
	Chitin (nanofibers)	d_{33} = 9.49 pCN^{-1}	[48]
	Cellulose	d_{33} = 19.3 ± 2.9 pCN^{-1}	[49]
Proteins	Collagen	d_{14} = 12 p N^{-1}	[50]
	Keratin	d_{14} = 1.8 pCN^{-1}	[51]
	Silk	d_{14} = 5–1.5 pCN^{-1}	[52]
	Fish swim bladder (FSB)	d_{33} = 22 pCN^{-1}	[53]

3.1.1. Chitosan

Chitosan, a naturally occurring polysaccharide polymer with piezoelectric properties, was examined in a comprehensive review by Martino [54]. Studies have shown that polymer scaffolds derived from chitosan possess a range of beneficial features suitable for orthopedic implants, including osteoconductivity, porosity, ease of shaping, antibacterial properties, and minimal foreign body response. Preliminary investigations have documented the piezoelectric sensitivity of chitosan [55], and the current study presents the development of a vibration sensor leveraging chitosan's piezoelectricity, with the maximum d_{33} coefficient of chitosan amounting to 18.4 pCN^{-1} [47,56]. Chitosan, while regenerating bone defects, may also have antibacterial properties (see Figure 5).

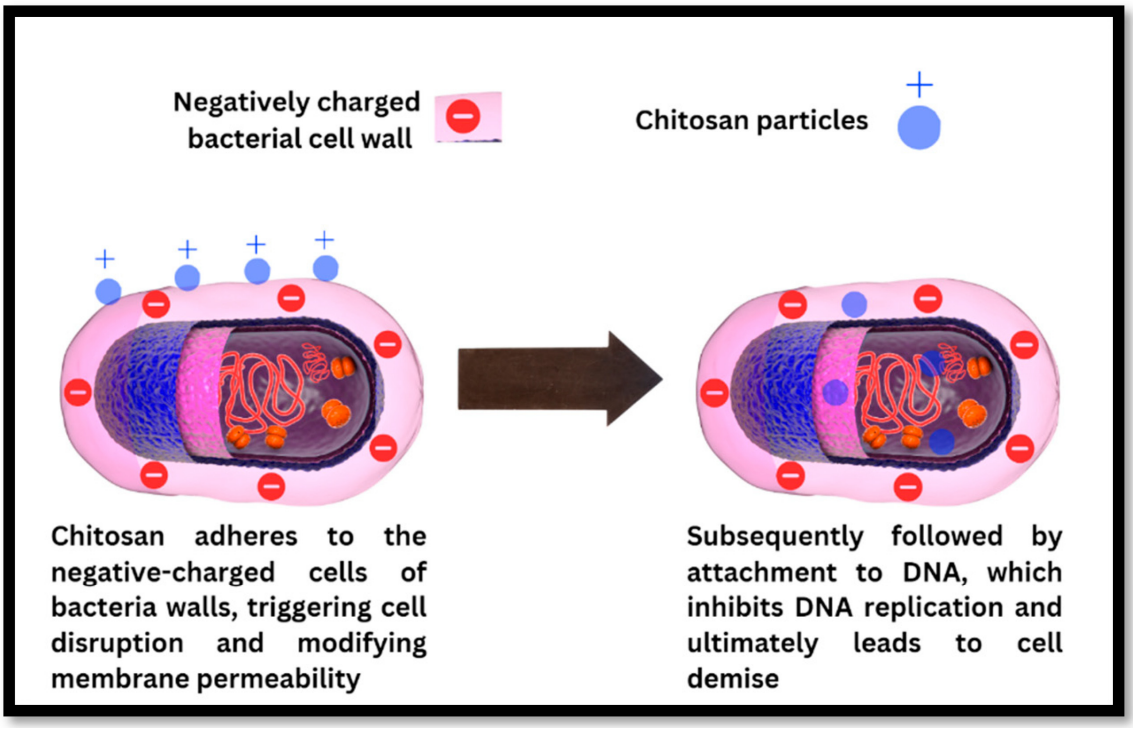

Figure 5. The antibacterial mechanism of chitosan particles involves disrupting the bacterial cell wall, binding to bacterial DNA, and inhibiting DNA replication, ultimately resulting in bacterial cell death. Reprinted from ref. [57].

3.1.2. Cellulose

Cellulose, an inherent polysaccharide polymer with piezoelectric properties, emerges as a promising option for bone tissue applications owing to its exceptional biocompatibility and robust mechanical strength. In a study by Zaborowska [58], it was found that employing a microporous cellulose scaffold led to a considerably greater proliferation of MC3T3-E1 osteoblast cells compared to the nanoporous scaffold. Research studies have provided evidence of cellulose's capacity to enhance cellular adhesion, specifically for chondrocytes, osteocytes, endothelial cells, and smooth muscle cells [59]. As a result, cellulose is regarded as a suitable piezoelectric material for applications in both bone and cartilage tissue engineering [60].

3.1.3. Keratin

Keratin has been utilized to create diverse scaffold architectures suitable for tissue engineering applications. These include hydrogels [61], films [62], sponges [63], microcapsules, and dense materials [64]. Various fabrication techniques, such as solvent casting, lyophilization, electrospinning, and 3D printing, have been employed to produce these keratin-based structures [65]. Furthermore, keratin's cell recognition domains have been observed to facilitate the attachment of different cell types, including osteoblasts [66].

3.1.4. Collagen

The application of collagen scaffolds in bone healing has been previously reported [67]. Additionally, the effectiveness of collagen–hydroxyapatite piezoelectric composite scaffolds in promoting cellular growth and facilitating bone healing has been demonstrated [68]. Moreover, collagen–calcium phosphate composite scaffolds have been explored for cartilage tissue engineering. Studies involving these scaffolds have shown an average filling ratio of the defect area with newly formed cartilage tissue at weeks eight and twenty to be approximately 81% and 96%, respectively [69]. Nonetheless, it is important to acknowledge certain limitations of these scaffolds, including low mechanical stiffness, rapid degradation,

and potential toxicity associated with the use of crosslinking agents. Collagen under stress reduces the hydraulic permeability and increases the stiffness [70], which can be improved through electrical stimulation [71]. Table 3 summarizes information about natural piezoelectric materials and their applications in bone tissue engineering (BTE).

Table 3. Natural piezoelectric materials and their applications in bone tissue engineering.

Materials	Advantages	Description and Application	Ref.
Chitosan	-biocompatible -antibacterial -biodegradable -high porosity -non-cytotoxic	Bone tissue engineering	[72]
		Chitosan/alginate hydrogels containing parathyroid hormone (PTH), peptide, and hydroksyapatite (HA) dedicated to cranial bone regeneration.	[73]
		Chitosan-coated poly(trimethylene carbonate)/oleic-acid-treated HA/PLA/vancomycin hydrochloride microsphere scaffold used in BTE.	[74]
Cellulose	-biocompatible -non-cytotoxic -high tensile strength -biodegradable	A cellulose porous scaffold was prepared through incorporation of paraffin wax with bacterial cellulose via a fermentation process for a higher osteoblast response.	[58]
Keratin	-structural integrity -biocompatibility -biodegradability -bioactivity	Keratin-based biomaterials in orthopedic tissue engineering.	[75]
		Electrospun poly(3-hydroxybutyrate)/keratin scaffold for bone tissue engineering focused on the osteogenic activity of the scaffolds, which is enhanced in the presence of keratin.	[76]
		Silk fibroin/wool keratin composite scaffold with a hierarchical fibrous and porous structure formed through electrospinning with potential use in meniscal repair and healing bone injuries.	[77]
Collagen	-biocompatibility -biodegradability -bioactivity	Preparation of 3D porous microsphere of collagen/BMP-2/bacterial cellulose through the reverse-phase suspension regeneration method to promote biocompatibility, osteogenic differentiation, proliferation, and adhesion of mice cells in 3D scaffolds.	[78]
		Composites made from the piezoelectric component of bone, collagen (fibrilar bovine collagen type I), used to fabricate materials for bone substitutes.	[79]
		A scaffold combination of collagen and hydroxyapatite that exhibits osteoconductive properties.	[80]

3.2. Synthetic Polymers

Piezoelectric synthetic polymers have unique electrical properties that can be used to stimulate bone tissue cells. Thanks to the ability to convert mechanical energy into electrical signals, these polymers are used in the creation of tissue scaffolds that not only mechanically support bone regeneration but also provide electrical stimulation that mimics the natural conditions of the cellular microenvironment [81,82]. The piezoelectric coefficient data for different synthetic piezoelectric materials are shown in Table 4.

Table 4. The piezoelectric coefficient for different synthetic piezoelectric materials.

Type of Material	Piezoelectric Materials	Piezoelectric Coefficient	Ref.
Polymers	Polyvinylidene fluoride (PVDF)	d_{31} = 23 pCN^{-1}	[78]
	Polyvinylidene fluoride–trifluoroethylene (PVDF-TrFE)	d_{33} = 38 pCN^{-1}	[79]
	Poly (l-lactic acid) (PLLA)	d_{14} = 9.82 pCN^{-1}	[83]
	Polyhydroxybutyrate (PHB)	d_{14} = 1.6–2 pCN^{-1}	[14]
	Poly(3-hydroxybutyrate-co-3-hydroxyvalerate) (PHBV)	d_{14} = 1.3 pCN^{-1}	[14]
	Glycine–polyvinyl alcohol (PVA)	d_{33} = 5.3 pCN^{-1}	[84]
Peptide	Poly-γ-benzyl-L-glutamate (PBLG)	d_{33} = 25 pCN^{-1}	[85]
	Poly-γ-methyl-L-glutamate (PMLG)	d_{14} = 2 pCN^{-1}	[83]

3.2.1. Polyvinylidene Fluoride (PVDF)

PVDF is a water-insoluble polymer that has gained a lot of attention in a broad range of fields due to its electroactive properties as well as its high chemical and thermal stability. The crystalline phase of PVDF can include five different polymorphs (i.e., α, β, γ, δ, ε) (Figure 6), and their presence is dictated mostly by processing method conditions [86]. PVDF usually crystallizes in the form of α phase due to its thermodynamic stability. However, β and γ phases are very often desired because of their electroactive properties, such as piezoelectricity, pyroelectricity, and ferroelectricity [87,88]. These properties are related to the conformation of their chains, where the γ phase shows a worse piezoelectric effect than the β phase due to a gauche bond existing in every fourth repeating unit [89]. It has been known for some time that β-PVDF induces cellular proliferation and differentiation, especially under dynamic conditions, which is one of the reasons why PVDF is considered a promising material for BTE [90]. This section focuses on advances made in the field of PVDF for application in BTE, and it reviews articles published mainly since 2018 to date, acting as a follow-up to the review by Tandon et al. [2].

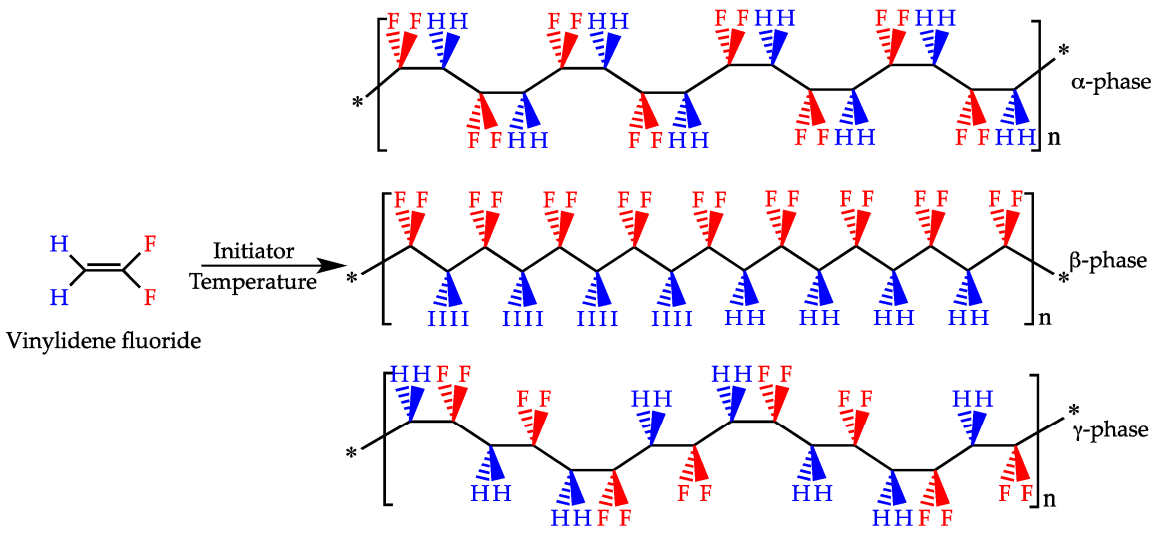

Figure 6. Polymerization of the vinylidene flyuoride monomer with various PVDF chain conformations of α-phase (non-polar) and β- and γ-phases (polar). Reprinted From Ref. [91].

Recently, great advances have been made to address one of the main limiting factors to the widespread use of PVDF in BTE, which is its hydrophobic profile. Kitsara et al. used oxygen plasma treatment for electrospun and solvent-cast scaffolds and proved that the enhanced hydrophilic profile of PVDF can be maintained even up to two years, resulting in better cell spreading and interaction with the scaffold [92]. Hydrophilicity was also improved through spin coating of PVDF onto the TiO_2 nanotube surface of titanium, which halved the contact angle after PVDF polarization and promoted mineralization, but maintaining these properties long-term is questionable due to the loss of negative charge [93]. A different approach to address poor cell–scaffold interaction due to the hydrophilicity of PVDF was proposed, in which PVDF membranes were coated with elastin-like recombinants containing l-arginyl-glycyl-l-aspartic acid sequence (RGD) motifs, and it improved MSCs' adhesion and proliferation [94]. As mentioned previously, the β phase is the most desirable for BTE, and during the electrospinning process, a fraction of this phase can be increased by adjusting the accelerating voltage towards higher values [95]. Therefore, to obtain a significant amount of β phase, the piezoelectricity and the molecular weight can be increased. The surface is shown in Figure 7.

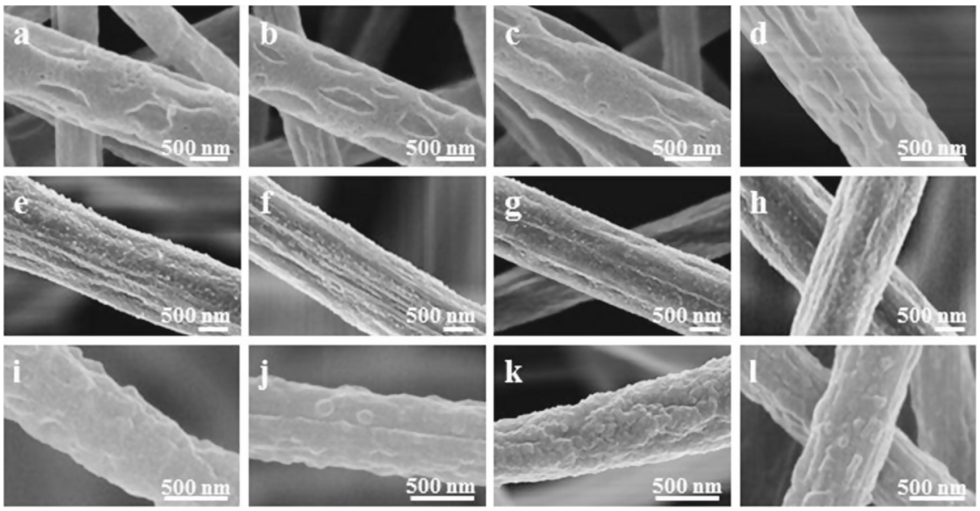

Figure 7. SEM microstructures with PVDF electrospun fibers' morphology with various applied voltages during the electrospinning process; (**a**,**e**,**i**)—6 kV; (**b**,**f**,**j**)—12 kV; (**c**,**g**,**k**)—18 kV; (**d**,**h**,**l**)—24 kV. Reprinted with permission from ref. [96]. Copyright 2019, IOP Publishing Group.

Recently, Lee et al. produced a three-dimensional cotton-like scaffold by changing the relative humidity and compared different post-treatment methods (i.e., heating, cooling, quenching) to increase the β-PVDF content, from which cooling showed the best results [97]. A comparison of 2D and 3D structures was conducted for solvent casting methods at different temperatures, and although the room temperature process resulted in higher amounts of β-PVDF and crystallinity, their hydrophobicity was greater compared to high-temperature solvent casting [98]. Surprisingly, their results also showed that 2D films promote cell proliferation better than 3D scaffolds. Mirzaei et al. came to different conclusions when comparing 2D films with 3D electrospun fibers and showed that the latter is better at improving the osteogenic differentiation of induced pluripotent stem cells (iPSCs) [99]. Different studies tested a freeze-extraction method to produce PVDF membranes with controlled microporosity. However, their control samples (glass slides) showed better proliferation of MSCs than the obtained membranes [100]. Szewczyk et al. showed that the surface potential of PVDF electrospun fibers has a significant effect on the mineralization rate and cell attachment, and it can be controlled through polarity during the electrospinning process [101]. Moreover, it was shown that Kelvin probe force microscopy is a viable method to measure the surface potential of electrospun fibers.

Studies on PVDF copolymers and composites have been focused mainly on difficulties with the fabrication of scaffolds with proper topography and spatial morphology and maintaining sufficient piezoelectric properties. For example, poly(vinylidene fluoride-hexafluoropropylene) (PVDF-HFP) copolymer was used to produce a termite-like scaffold using the wet electrospinning method, which resulted in improved electric output and promoted NIH 3T3 cell migration and attachment in comparison to regular electrospun fibers [102]. On the other hand, Zhou et al. fabricated electrochemically polypyrrole (PPy) nanocones on the surface of the PVDF membrane, which enhanced bone marrow mesenchymal stem cells' (BMSCs) spreading, adhesion, and osteogenic differentiation [103]. Cell stimulation can be realized through the pulsed electromagnetic field (PEMF) method, and it was shown that the presence of conductive polymer polyaniline (PANI) in the electrospun PVDF fibers not only improves biocompatibility and osteoinductivity of copolymer but also enhances the effect that PEMF has on dental pulp stem cells' (DPSCs) osteogenic differentiation [104].

3.2.2. Poly(Vinylidene Fluoride-Trifluoroethylene) (PVDF-TRFE)

This polymer is a copolymer composed of vinylidene fluoride (VDF) and trifluoroethylene (TrFE). Among the various polymers, this particular copolymer has demonstrated the

highest piezoelectric coefficient (30 pCN-1) [33,105]. Research indicates that the copolymer exhibits cytocompatibility and exerts a positive influence on cell adhesion and proliferation. Notably, it possesses regenerative capabilities for various tissue types, including bone, skin, cartilage, and tendons [106,107]. Electrospun nanofibrous scaffolds based on the PVDF-TrFE copolymer have shown remarkable efficiency in the regeneration of bone, cartilage, and others [108]. In addition, PVDF and PVDF-TrFE have been blended with natural polymers, such as starch or cellulose, to develop suitable scaffold structures for tissue repair and regeneration, especially in the field of bone tissue engineering. Blending starch or cellulose produces a porous structure that supports tissue growth [109]. Scientists [110] showed increased bone growth when a thin film of PVDF-TrFE with 10 vol% $BaTiO_3$ piezoelectric composite, thermally treated at 1200 °C for 4 h, was implanted into the tibiae of male rabbits for 21 days. The formation of new bone was stimulated through electrical signals generated from the strained piezoelectric membrane during the rabbits' physical activity. Lopes et al. [111] conducted a comparison between the P(VDF-TrFE) 10 vol% $BaTiO_3$ piezoelectric composite and polytetrafluoroethylene (PTFE) to evaluate new bone formation by implanting them in rat calvarial defects for 4 and 8 weeks. Their findings suggest that the piezoelectricity and hydrophilicity of the P(VDF-TrFE)–$BaTiO_3$ composite enhance the protein binding affinity, leading to increased osteogenesis. Light microscopy and micro-CT images demonstrated significant hard tissue growth and connective tissue formation at the interface of the implanted piezoelectric membrane in both implants. Scientists [112] have discovered that the responses of bone marrow macrophages (BMDMs) and bone marrow mesenchymal stem cells (BMSCs) to PMMA-coated PVDF-TRFE scaffolds can be controlled by changing certain parameters, such as the surface potential, which in turn enables targeted bone regeneration (see various parameters in Figure 8).

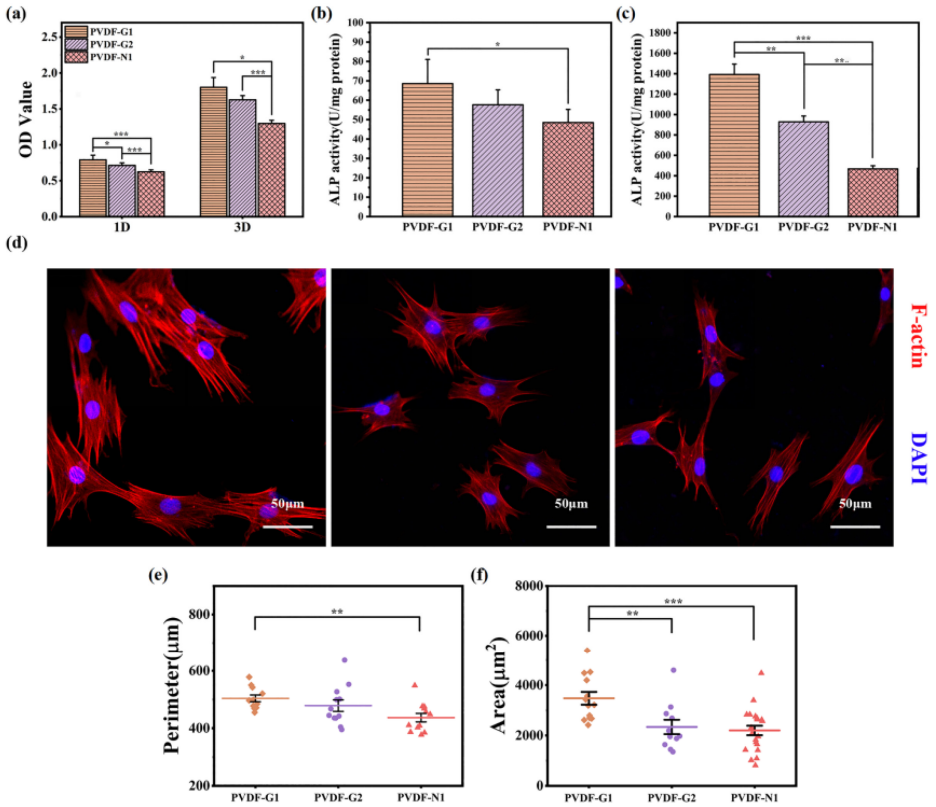

Figure 8. Selected parameters of scaffolds. (**a**) The adhesion (day 1) proliferation (day 3) behaviors of MSCs on PVDF-TrFE; (**b**,**c**) ALP activity of MSCs using PVDF-TrFE after 7 and 14 days. (**d**) Microstructures of CLSM of MSCs on PVDF-TrFE after 3 days. (**e**,**f**) Cytomorphometric tests of MSCs on PVDF-TrFE for 3 days. Reproduced with permission from the publisher, reference [112].

3.2.3. Barium Titanate ($BaTiO_3$, BT) as PVDF Dopant

In the literature, one of the most commonly found constituents of PVDF composites is barium titanate ($BaTiO_3$, BT), mainly due to its outstanding ferroelectric properties, high dielectric constant, and decent biocompatibility [113]. Recently, a PVDF/BT composite was fabricated for the purpose of testing whether electrical stimulation in the form of a monophasic direct current, a square waveform, and a biphasic waveform has a direct effect on hMSCs' differentiation. The presented results show that the biphasic waveform does not induce osteogenic differentiation, whereas square wave stimulation does show osteogenic lineage commitment with lower reactive oxygen species (ROS) compared to direct current stimulation [114]. Similar studies explored a composite made from PVDF/BT with a multi-walled carbon nanotube (MWCNT) addition and its combined effect with direct current stimulation of MC3T3-E1 cells, which resulted in a significant improvement in cell proliferation, migration, and osteogenic differentiation in comparison to an unstimulated composite and PVDF control samples [115]. On the other hand, it was shown that PVDF-TrFE/BT membranes combined with MSCs injection are a viable approach for bone repair in the presence of osteoporosis; however, in vivo studies did not result in full bone repair [116]. Freitas et al. showed in their paper the importance of cell sources used with the PVDF-TrFE/BT membrane for bone repair, and only MSCs from bone marrow enhanced bone formation, while MSCs from adipose tissue did not show significant improvement [117]. An in-depth analysis of the biological processes that occur during MSCs osteogenesis induced through a piezoelectric PVDF/BT composite was conducted, and it was noted that the transformation of physical signals into intracellular mechanotransduction is the main driving factor for the improvement of osteogenesis [118]. The homogeneous distribution of BT filler in a polymeric matrix poses a significant challenge, and functionalization with polydopamine has been proposed as a possible approach [119]. Composites obtained through the selective laser sintering (SLS) method with functionalized BT showed not only homogenous distribution, which resulted in an 11% increase in β-PVDF's presence and more than tripled the voltage output, but also improved mechanical properties of the scaffold. A follow-up study by the same researchers introduced Ag nanoparticles onto the surface of functionalized BT nanoparticles, thus increasing the conductivity and voltage output of a PVDF composite, as well as providing it with antibacterial properties [120]. A similar but different approach was presented recently, in which PVDF was functionalized with polydopamine and later combined with BT to produce a bioactive coating on a bioinert Ti_6Al_4V alloy. Functionalization of PVDF increased the fraction of β-PVDF by 91%, and combining it with BT further enhanced β-PVDF's presence by 96% [121]. Qi et al. produced core–shell BT nanoparticles through functionalization with polydopamine and high-temperature carbonization, which were combined with PVDF and turned into scaffolds through the SLS method [122]. The results show that carbon-coated BT nanoparticles promote β phase formation and increase composite conductivity and its mechanical properties.

3.2.4. Carbon-Based Materials (GO, MXene) as PVDF Dopants

Graphene oxide (GO) is known for its outstanding conductive properties and has been utilized in several studies as an addition to PVDF. The presence of GO in PVDF scaffolds produced through SLS resulted in higher tensile and compressive strength but also enhanced the transformation of PVDF from α to β phase through fluorine and carbonyl group interactions [123]. The same composite system was used for the fabrication of electrospun fibers, and although cell studies showed improvement in iPSCs' osteogenic differentiation in comparison to pure PVDF, their mechanical properties were significantly worse [123]. Other studies tried to improve electrospun fibers of PVDF/GO composite by blending it with PVA, which increased the tensile strength almost tenfold and more than doubled the tensile strain and modulus [124]. Moreover, this ternary system of PVDF/PVA/GO showed better osteoinductive properties, cell proliferation, and alkaline phosphatase (ALP) activity in comparison to PVDF/GO and PVDF/PVA. Fu et al. used a different approach and incorporated MXenes into the electrospinning solution of PVDF, which improved the

mechanical properties, promoted bone regeneration in vivo, increased the β phase content, and also increased the contact angle, making fibers more hydrophobic [125].

3.2.5. Zinc-Based Materials as PVDF Dopants

Zinc-based materials have garnered interest in bone tissue engineering due to their great antibacterial properties. The addition of zinc oxide (ZnO) into electrospun PVDF fibers promoted β phase formation, significantly improved its mechanical properties, and provided the scaffold with antibacterial properties, which were better when piezo-excitation was applied by Li et al. [126]. Their in vitro studies on human osteoblasts resulted in lower cell density after three days without piezo-excitation in comparison to the control group, but with stimulation, cell density was higher for the tested composite. Similar results were obtained by Xi et al., who conducted studies on the same composite in comparable conditions [127]. An interesting approach was recently proposed in which a hybrid system composed of PVDF piezoelectric nanofibers with ZnO nanorods and polycaprolactone (PCL) nanofibers with dexamethasone-loaded chitosan nanoparticles were fabricated using a dual electrospinning method [128]. The obtained results showed that increasing the content of ZnO nanorods simultaneously increases β phase content and that the hybrid scaffold induces osteogenic differentiation of mouse bone marrow stromal stem cells (mBMSCs) and improves their proliferation. On the other hand, Chen et al. used zinc-based metal–organic frameworks (ZIF-8) and, through shear milling and salt leaching methods, produced PVDF/ZIF-8 foams, which were able to generate 10 V outputs without polarization and showed angiogenic, osteogenic, and antibacterial activity [129].

3.2.6. Hydroxyapatite (HA) as PVDF Dopant

One of the most popular groups of materials applied in BTE is calcium phosphates. For example, studies conducted on electrospun PVDF fibers with the addition of hydroxyapatite (HA) showed no cytotoxicity; apatite growth was observed, but the presence of HA slightly decreased the amount of β phase [130]. Other studies used a different approach and first produced electrospun PVDF fibers, which were later treated with plasma, and HA was electrodeposited on their surface [131]. Obtained scaffolds showed a highly hydrophilic character due to plasma treatment. They possessed antibacterial properties, and they promoted MG63 cell proliferation. However, no significant improvement was observed in comparison to reference samples. PVDF coating on the anodized surface of titanium was modified with HA, which decreased the contact angle by 66% for 20% HA content, and enhanced mineralization was observed [132]. Malherbi et al. produced PVDF/β-TCP/HA discs and showed that under oscillating electric fields, the apatite growth rate is increased in SBF in comparison to no stimulation [133]. In other studies, Ca-P-Si-derived material was combined with PVDF, and through the phase separation–hydration method, porous scaffolds were produced that did not show cytotoxicity, had mechanical properties similar to cancellous bone, and promoted HA deposition and osteoblast redifferentiation. However, studies have compared scaffolds with different contents of calcium phosphate silicate (Ca-P-Si) and lack reference to pure PVDF scaffolds [134]. Ma et al. fabricated a PVDF-HFP scaffold through dipping and phase separation methods, which were modified with calcium phosphate (CaP). The resulting scaffolds showed a hydrophilic profile, promoted bone repair in rats, and were capable of generating electrical signals through body movement [135]. PVDF has limited biodegradation in the physiological environment, and to address this issue, PVDF/HA electrospun fibers were produced with the addition of PCL to the electrospinning solution [136]. Although these scaffolds showed cytocompatibility, cell proliferation was worse in comparison to PCL after three days, and only a small increase in ALP activity was observed. Moreover, degradation studies were not included despite being one of the main reasons for PCL addition. In a different approach, polycaprolactone–tricalcium phosphate (PCL-TCP) films were coated in PVDF through a self-polarization technique, which resulted in enhanced osteoinduction through the synergistic effect of polycaprolactone/tricalcium phosphate/poly(vinylidene fluoride)

(PCL/TCP/PVDF) piezoelectricity and PEMF stimulation [137]. Alimohammadi et al. used PVDF to improve the bioactivity of sulfonated PEEK and further modified it with HA and carbon nanofibers, which resulted in an improved hydrophilic profile, apatite formation, and MG-63 cell attachment and proliferation [138]. Because the fabrication of PVDF scaffolds with a developed spatial structure is difficult, a UV-curable poly(glycerol azelaic acid)-g-glycidyl methacrylate (PGAz-g-GMA) resin was used and modified with PVDF, HA, and Cloisite Na+ [139]. These scaffolds proved to be mechanically compliant with cancellous bone tissue, the hydrophilic profile was improved due to nanofillers, and the attachment and proliferation of MG-63 cells were observed.

3.2.7. Cobalt Ferrite ($CoFe_2O_4$, CFO) as PVDF Dopant

A few studies have tried to incorporate CFO into PVDF to produce magnetoactive scaffolds. Fernandes et al. used a solvent casting method to develop a porous PVDF/CFO scaffold with the help of a nylon template, which was later removed [140]. The addition of CFO slightly increased the β phase fraction and decreased contact angle, and it showed improved cell proliferation with magnetic stimulation. Other studies have focused on providing magnetoelectric properties for injectable methacrylated gellan gum (GGMA) hydrogel through the incorporation of CFO/PVDF spheres in its structure; however, the obtained scaffold showed worse cell viability in comparison to control samples [141]. Recently, PVDF/CFO spheres were produced using the electrospraying method and introduced into gelatin hydrogel for the purpose of guiding MSCs towards osteogenic differentiation, but magnetic stimulation was shown to have a minimal effect in this regard [94].

3.2.8. Poly(L-Lactic Acid) (PLLA)

PLLA is the second most popular piezoelectric polymer utilized in BTE. One of the main advantages that PLLA has over PVDF is that it is biodegradable; however, similarly to PVDF, it also suffers from hydrophobicity, which hinders scaffold–cell interaction. Moreover, its piezoelectric properties are usually weaker than those of PVDF, which is why it is less commonly found in the literature. Nevertheless, in recent years, several noteworthy advances have been made.

The fused deposition modeling (FDM) method was used to fabricate computer-designed PLLA scaffolds with high porosity, and mechanical testing has shown that the obtained properties are similar to those of trabecular bone [142]. Moreover, scaffolds maintained piezoelectric properties after the 3D printing process, but crystallinity was lower in comparison to the initial filament. Similarly to what has been shown for PVDF, the voltage polarization applied during the electrospinning process has a direct effect on the surface potential and piezoelectricity of PLLA fibers [143]. Positive polarization resulted in better MG-63 cell adhesion and spreading. In a different study, PLLA electrospun fibers were used in pairs with externally controlled ultrasound to stimulate stem cells in vitro and induce bone growth in vivo [144]. The synergistic effect of the scaffold and the stimulation exhibited positive outcomes in both situations. Tai et al. showed that the fiber diameter and heat treatment of electrospun PLLA fibers affect the voltage output. Heat treatment above the glass transition temperature of PLLA simultaneously increases longitudinal and decreases transverse voltage output. They also showed that neurogenic differentiation of stem cells was improved for orthogonal piezoelectricity, whereas osteogenic differentiation was improved for shear piezoelectricity [145]. The novel approach proposed by Lai et al. produced an electrospun PLLA scaffold with extracellular vesicles for the treatment of cartilage defects [146]. Piezoelectric stimulation improved the migration and proliferation of chondrocytes and increased the retention of extracellular vesicles. Liu et al. conducted studies on PLLA scaffolds designed for a cartilage–bone interface in which gradient polarization was applied [147]. This approach resulted in scaffolds with gradient piezoelectric properties in which stronger piezoelectricity guided MSCs towards osteogenic differentiation, whereas weaker piezoelectricity guided them towards chondrogenic differentiation. In a different study by the same first author, the PLLA scaffold was tested in vivo to eval-

uate the effect of exercise on cartilage regeneration [148]. Although the presence of the scaffold improved cartilage healing in rabbits, the results regarding the impact of exercise are inconclusive. As mentioned previously, the hydrophobicity of PLLA is a significant obstacle towards functional BTE scaffolds, and thus plasma treatment was applied with argon (Ar) and oxygen (O_2) on electrospun membranes, which had no significant impact on the physicochemical properties of PLLA but increased the surface roughness and decreased the contact angle [149].

On the other hand, piezoelectric stimulation has been shown to provide antibacterial properties. Ando et al. produced PLLA yarns and tested them against Staphylococcus Aureus, which proved their antibacterial properties during mechanical deformation [150]. However, the mechanism through which bacteria are killed was not fully explained. Their studies were later expanded by Gazevoda et al., who obtained similar results on nanotextured films but showed that the impact of reactive oxygen species and pH changes is insignificant and bactericidal properties are attributed to the piezo stimulation [151].

3.2.9. Barium Titanate (BT) as PLLA Dopant

Antibacterial and anti-inflammatory properties were obtained for PLLA solvent-cast membranes through the addition of electrospun BT nanofibers co-doped with Ca/Mn [152]. PLLA scaffolds showed increased electroactivity, osteogenesis, and mineral deposition in the presence of nanofiller. Other authors have addressed the issue of dielectric differences between ceramic BT and PLLA by introducing graphene oxide into this composite [153]. They produced scaffolds using the SLS method and showed that the addition of GO improved the output voltage and the current and promoted cell proliferation and differentiation, especially when stimulated with ultrasounds. The orientation of PLLA/BT electrospun fibers has been shown to affect the differentiation of BMSCs and the electrical properties of the scaffold [154]. Randomly oriented PLLA fibers generally showed better properties by promoting osteogenic differentiation and higher dielectric permittivity, which was further improved by the presence of BT, which simultaneously decreased the contact angle and increased the surface roughness. In a recent study, the effects of BT morphology (i.e., nanoparticles, nanosheets, nanotextured rods, microblocks) incorporated into PLLA film were evaluated. The results showed that high-aspect-ratio structures of the filler are preferable for obtaining highly crystalline PLLA, which translated into better cellular proliferation [155].

3.2.10. Hydroxyapatite (HA) as PLLA Dopant

In the literature, there is an abundance of reports regarding PLLA/HA composites; however, the majority of these studies focus either on piezoelectric properties for non-biomedical applications (e.g., energy harvesting [156,157]) or strictly on the aspect of cellular scaffolds for BTE, excluding the piezoelectric effect [158–160]. We have failed to find a study that evaluates both of these for the same PLLA/HA platform. HA dopants for the PLLA were tested in vivo to produce plates for the fixation of bone fractures [161]. Subcutaneous implantation of PLA/HA [162] scaffolds in mice showed good tolerance of all scaffolds and tissue growth. Samples containing HA showed a lower inflammatory response after 14 days of implantation compared to PLA samples (see Figure 9).

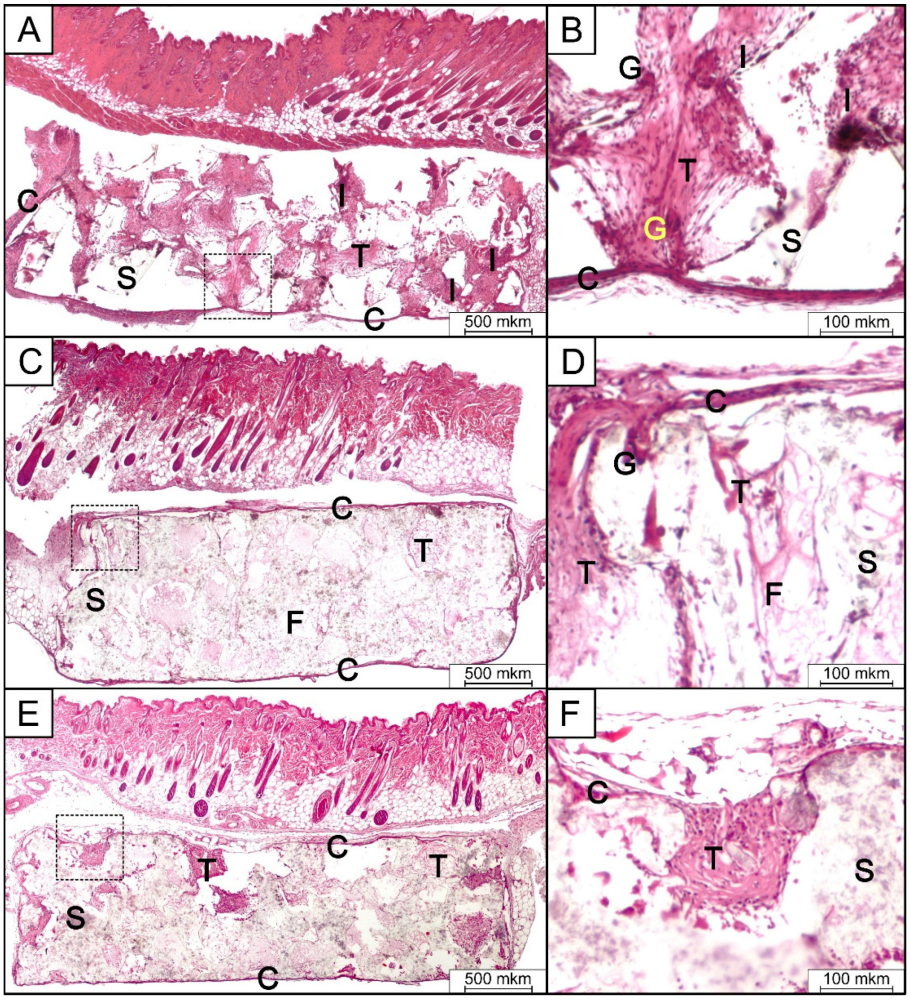

Figure 9. Micrographs of H&E-stained tissue sections from the subcutaneous implantation area in group 1 (PLA) (**A**,**B**), group 2 (PLA/HA 15%) (**C**,**D**), and group 3 (PLA/HA 20%) (**E**,**F**) after 14 days of implantation. S—scaffold; C,T—connective tissue; F—collagen fibers; I—inflammatory infiltrates; G—giant multinucleated cell. (Reproduced with the permission from the publisher, reference [162]).

3.2.11. Carbon-Based Materials (GO, MXene) as PLLA Dopants

A different study incorporated graphene oxide (rGO) into PLLA and modified produced electrospun fibers with perylene-3,4,9,10-tetracarboxylic dianhydride (PDA) to increase the attachment of chondrocytes [163]. The results showed that not only piezoelectricity but also the degradation profile have a direct effect on clonal mouse embryonic cell line (ATDC5) cell differentiation. Pariy et al. also modified PLLA electrospun fibers with rGO but focused their studies on its effect on piezoelectricity, which was increased in and out of plane 2.3 and 15.4 times, respectively [164]. Moreover, they showed that the piezoresponse of the PLLA composite is dependent on the molecular structure. Other authors showed that coating PLLA electrospun fibers with PANI and carbon nanotubes (CNTs) deteriorates the mechanical properties but lowers the electrical resistance and increases the voltage output [165]. The addition of conductive components improved human-bone-marrow-derived mesenchymal stem cells' (hBMMSCs) proliferation and osteogenic differentiation only when stimulated through ultrasonication. Ramasamy et al. decided to go a step further and incorporate into the PLLA fibers two pluronic F-127 (PL) functionalized fillers, with one improving conductivity (PL-MWCNT's) and the other improving piezoelectricity (PL-BN) [166]. This complex system resulted in increased mechanical properties and an improvement in wettability and electroactivity, and it promoted

MC3T3-E1 cell adhesion and proliferation. Table 5 summarizes information about synthetic piezoelectric materials and their applications in BTE.

Table 5. Synthetic piezoelectric materials and their applications in bone tissue engineering.

Materials	Advantages	Description and Application	Ref.
Polyvinylidene fluoride (PVDF)	-easy to process -high piezoelectric coefficient -non-cytotoxic -flexible -biocompatible	Application in bone tissue engineering.	[27]
		PVDF scaffold largely promoted the osteogenic differentiation of human-adipose-derived stem cells.	[167]
		Actuator device based on PVDF with effective stimulation properties for bone growth.	[168]
		Bone formation in vitro.	[95]
		Osteogenic differentiation in vitro.	[169]
		In vivo tests of β-PVDF polymer samples were conducted through implantation in rats' bones.	[170]
		Significant increase in cell viability compared to control samples.	[171]
Polyvinylidene fluoride trifluoroethylene (PVDF-TrFE)	-high piezoelectric coefficient -flexible -non-cytotoxic -biocompatible	Faster bone regeneration and higher osteogenic properties of bone cells.	[172]
		Piezoelectric fibers promoted the MSCs' chondrogenic differentiation and the osteogenic differentiation of MSCs.	[173]
		Cartilage tissue engineering.	[83]
		Bone, cardiac, neural, skin TE, cartilage.	[14,174,175]
Poly (l-lactic acid) (PLLA)	-biocompatible -elastomeric behavior -biodegradable -non-cytotoxic -corrosion resistance -easy to process	In vitro PLLA blends for bone regeneration.	[176]
		Bone regeneration in vivo.	[177]
		Electrospun P(LLA-CL) type I collagen for BTE.	[178]
		Electrospun PLLA with freeze-dried collagen promotes the osteogenic differentiation of seeded MSCs in vitro. In vivo tests on damaged rabbits' bones enhanced AC formation.	[179]
		Electrospun PLLA, PCL, and PLLA/PCL scaffolds were seeded with MSCs. All scaffolds promoted the chondrogenic differentiation of MSCs.	[180]
		Cartilage, vascular, medical devices (e.g., screws), skin, bone, and neural TE, wound dressing, and drug delivery.	[72,181,182]
PHB/PHBV	-biodegradable -biosynthesized -resistant to UV radiation -low moisture permeability -good moisture resistance -provides an odor barrier	Proliferation and differentiation of rabbit bone marrow cells.	[183]
		Multiple applications in BTE.	[69]
		Higher cell proliferation and differentiation on PHB/HA scaffolds compared to the PHB samples.	[184]

3.3. Other Piezoelectric Polymeric Materials

As previously described, PVDF and PLLA are the most commonly found piezoelectric polymers in the literature for use in BTE. However, two alternatives have been proposed to date that might be suitable for scaffold design. This section will briefly characterize them by showing their advantages and disadvantages, but it will also mention the most significant advances.

Poly(3-hydroxybutyrate) (PHB) is a part of the polyhydroxyalkanoate family, biodegradable bacterial polyesters that have been found to be used in different branches of medicine [185–187]. PHB is considered to be highly biocompatible due to its degradation product being a natural metabolite, and it does not induce inflammatory reactions. Moreover, it possesses piezoelectric properties, which are attributed to the presence of a polar oxygen group linked with an asymmetric carbon [188]. However, PHB has a low degradation rate, it may contain contaminants causing adverse effects, it is hydrophobic and brittle, and its piezoelectric coefficient is significantly lower than that of PVDF and PLLA [189]. Nevertheless, several studies have explored the viability of PHB, its blends, and composites, mostly in the form of electrospun fibers [190,191] but also as 3D-printed scaffolds [6,192], hot-pressed films [193], solvent-casted films [194,195], and lyophilized films [196].

Polyamide-11 (PA-11) is a synthetic polymer with better piezoelectric and mechanical properties than PHB, but its non-biodegradable character limits its application in BTE. PA-11 can crystallize into five different phases, from which the polar pseudo-hexagonal γ phase exhibits the highest piezoelectricity [197]. Despite the popularity of polyamides in the biomedical field, very few researchers have decided to study PA-11 for BTE. In 2007, Wang et al. produced a PA/HA composite scaffold through the phase inversion method and showed that the obtained structures are characterized by exceptional mechanical properties, promote MSCs' osteoblastic differentiation, and induce bone formation in vivo [198]. However, the study did not consider the piezoelectric aspect of polyamide. A more recent study produced piezoelectric PA-11 nanoparticles for ultrasound stimulation of stem cells towards osteogenic differentiation [197]. In their paper, the authors stated that synthesized particles are endocytosed by stem cells and exhibit great potential in regulating their fate under stimulation. Despite the fact that PA-11 is not biodegradable, its potential is underappreciated, and it is expected that in the upcoming years, more researchers will include it in their studies either as a standalone scaffold or as a bioactive coating for inert implants.

4. Stimulation and Biological Properties of Piezoelectric Materials

The introduction of piezoelectric material stimulation into tissue engineering opens up perspectives for more effective and precise therapies in the healing and regeneration processes of bone tissue. Determining how mechanical stimulation of these materials can affect cells and tissues, with a particular emphasis on bone tissue regeneration processes, is crucial for improving the quality of treatment [2].

Multiple stimulation factors can activate the piezoelectric properties of scaffolds. It was reported that cells, through adhesion to the surface of the scaffold, can exert enough strain to cause polarization and an electrical response [135]. Moreover, the surface polarity of piezoelectric material can affect the conformation of adsorbed proteins from the extracellular matrix (ECM), thus possibly improving adhesion and osteogenic differentiation [123].

Optimizing the piezoelectric effect of biomaterials for biomedical applications requires careful adjustment of many material and process parameters that affect their mechanical and electrical properties [2]. In the context of tissue regeneration, such as bone, piezoelectric biomaterials can convert mechanical stimuli into electrical signals that support natural biological processes. The key is to optimize the piezoelectric effect, which starts with the selection of the appropriate material depending on the application. More specifically, piezoelectric composites that combine the flexibility of polymers with the higher piezoelectricity of inorganic materials can be an interesting choice. The structure of the piezoelectric material also plays a role [199]. The orientation of the fibers (e.g., [46]) can increase their ability

to generate electrical signals. Appropriate mechanical properties are also important so that the material has mechanical properties similar to bone tissue, which prevents damage to the newly formed tissue. The introduction of appropriate additives [200] and the adjustment of the biodegradation rate [201] also play a key role. Only through a comprehensive approach is it possible to obtain biomaterials that will effectively support regenerative processes while offering long-term stability and biocompatibility.

Mechanical stimulation is the simplest stimulus that also naturally occurs during movement and can be easily applied to a scaffold. Piezoelectric scaffolds induce better attachment, proliferation, and differentiation of cells under dynamic culturing conditions [90,98,103]. On the other hand, in vivo studies have shown that piezoelectric scaffolds perform significantly better during regular exercises, which improves overall chondrogenic differentiation and cartilage formation in rabbits [148]. The combination of electrical stimulation (ES) and conductive polymers, which strengthen the local electrical field, has been known to improve osteogenic activity. This synergistic effect favors mineral nucleation and protein absorption, accelerates the transport of Ca^{2+} ions into the cells, and upregulates the mitochondrial activity [202–206]. Bhaskar et al. constructed an in-house 12-well plate device to study the effects of electrical stimulation on cell culture and showed that ES promotes cell migration, spreading, and attachment on the piezoelectric PVDF/BT/MWCNT scaffold in comparison to a lack of stimulation [115]. The effect of the waveform on osteogenesis was recently evaluated by Panda et al. [114]. It was found that the direct current causes higher levels of intracellular ROS and induces early osteogenesis in MSCs, whereas the square wave produces lower levels of ROS and affects late osteogenesis. On the other hand, one study showed that the PVDF scaffold does not induce apatite nucleation in simulated body fluid (SBF) with and without ES, but PVDF/HA composite does [133,186]. It can be concluded that electrical stimulation can positively affect bone regeneration [23,207] and control the movement of tested cells [208].

Negatively charged PVDF scaffolds [167] promoted the osteogenic differentiation of human-adipose-derived stromal cells. Combining mechanical stimuli with biochemical stimuli successfully replicates the biomimetic microenvironment of the human body. These findings were validated by in vivo studies in which PVDF films were tested for their osteogenic properties in Wistar rats by analyzing new bone formation in a bone defect model [170]. After four weeks, significantly more defect closure and bone remodeling were observed (Figure 10). In this case, the mechanical stimuli were provided by the movements of the rats.

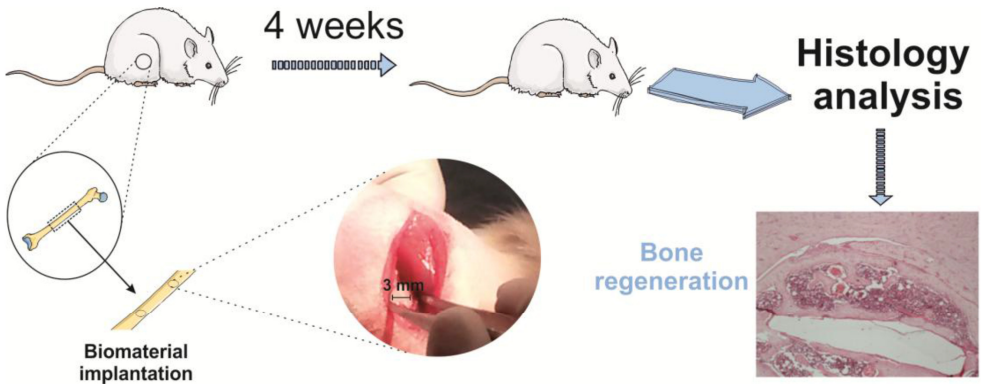

Figure 10. A visual depiction of the biomaterial implantation surgical protocol and a typical image of Hematoxylin and Eosin (H&E) staining showing the healing defects four weeks post-implantation on a poled β-PVDF film. Reproduced with permission [170].

The electromagnetic field (EMF) is another stimulus that can be considered in combination with a piezoelectric scaffold to improve overall performance. Although there are reports stating that it can have a negative impact on different physiological processes, the extremely low-frequency EMF shows therapeutic potential in bone tissue treatment [209,210].

Mirzaei et al. showed that the dental pulp stem cells seeded on piezoelectric scaffolds have better attachment and viability, and protein adsorption is increased, when EMF is applied [104,211].

In the literature, ultrasound stimulation has shown promising results in bone and cartilage tissue engineering. Chen et al. conducted in vivo studies by implanting PVDF/ZIF-8 foam into femur defects of rats [129]. The piezoelectric component was activated through ultrasonic stimulation for 20 min at 1000 Hz three times a day. This resulted in improved angiogenesis and osteogenesis, as well as upregulated ions transported into the cells. Cell adhesion, proliferation, and differentiation on PVDF composite scaffolds were also significantly improved when ultrasounds were applied [119,120,123]. Similar results were also obtained for piezoelectric PLLA scaffolds [155]. Das et al. conducted extensive in vitro and in vivo studies and found that cellular osteogenesis, as well as bone defect healing, is best when both the piezoelectric scaffold and ultrasound (US) are applied synergistically [144]. The piezoelectric material can be used as a coating for metallic bone implants and, in a similar manner, also improve osteogenesis with the help of US [212]. In subsequent work, scientists investigated PVDF scaffolds in vitro with [213] and without [46] ultrasound. It has been shown that appropriate ultrasound power can increase cell proliferation; in this case, it was 80 mW.

In the context of preclinical evaluation, it was observed that polarized PVDF exhibited significantly higher osteogenic efficacy compared to a non-polarized polymer substrate when implanted into the interosseous membrane of the rat tibia for six weeks. It is indicated that enhanced bone regeneration can be attributed to piezoelectric signals generated by polarized surfaces. Polarized PVDF films and fibers facilitate enhanced bone regeneration in rat femurs compared to non-polarized PVDF [169,214].

5. Future Challenges

While contemporary tissue engineering methods have progressed significantly, there remain numerous unresolved limitations and challenges within the field, including the following.

- Effective integration of piezoelectric nanomaterials into existing bone tissue. Issues related to biomechanics and biomechanical compatibility may affect the durability and effectiveness of piezoelectric stimulation in physiological conditions.
- In vivo studies on piezoelectric scaffolds are full of challenges, such as physiological differences between animals and humans, material degradation issues, post-implant inflammation, and incomplete knowledge of bioelectric mechanisms. Further research is needed to meet these requirements.
- The biological environment in organisms is very complex. The challenge is to understand how piezoelectric nanomaterials behave in a dynamic cellular environment, taking into account various aspects, such as movement, fluid flow, and the presence of other cells.
- The immune system's response to the introduction of nanomaterials may pose a challenge. Potential side effects, immunological reactions, and long-term consequences of the use of piezoelectric nanomaterials in bone tissue must be taken into account.
- Obtaining piezoelectric materials with appropriate mechanical, electrical, and biocompatibility properties can be a challenge. It is also important that these materials are available in sufficient quantities for the potential scale of application in therapeutics and tissue engineering.
- The introduction of new technologies must take into account ethical issues as well as issues related to patient safety. Research into the long-term effects and potential risks to patient health is essential.

6. Conclusions

Research on the use of piezoelectric nanomaterials in tissue engineering shows the promising potential of piezoelectric stimulation in the process of bone regeneration. In vitro

and in vivo experiments provide evidence of the beneficial effects of these materials on the proliferation and differentiation of bone cells [82]. However, despite promising results, there are limitations related to the effective integration of piezoelectric nanomaterials into the biological environment of bone tissue. Further understanding of cellular interactions, biomechanics, and the long-term effects of stimulation is needed. One of the answers is the use of piezoelectric stimulation, which can accelerate the healing process of bone fractures and support the formation of a dense bone tissue structure. This opens up prospects for shortening the recovery time of patients and improving the effectiveness of treatment of bone injuries.

In the context of future research, it is worth considering the role of artificial intelligence in optimizing the applications of piezoelectric nanomaterials. Machine learning algorithms can support the design of materials with optimal biomechanical and biological properties.

In order to transfer this promising research from the laboratory to clinical practice, further clinical studies are necessary to evaluate the effectiveness, safety, and long-term results of the use of piezoelectric nanomaterials in bone regeneration therapy.

In the context of future research, it is necessary to focus on research on the long-term safety of using piezoelectric nanomaterials in organisms while taking into account potential side effects and the immune system's response.

Author Contributions: Conceptualization, A.Z.; validation, T.K., A.G. and P.S.; formal analysis, T.K. and P.S.; investigation, A.Z. and K.Z.; writing—original draft preparation, A.Z. and K.Z.; writing—review and editing, P.S. and T.K.; supervision, T.K., A.G. and P.S. All authors have read and agreed to the published version of the manuscript.

Funding: This research was partially funded by the EU Horizon 2020 MSCA-RISE-2018 Research and Innovation Staff Exchange Programme, project iP-OSTEO "Induced pluripotent stem cell for bone and cartilage defects" under the Marie Skłodowska-Curie grant agreement No 824007.

Institutional Review Board Statement: Not applicable.

Data Availability Statement: No new data were created or analyzed in this study. Data sharing is not applicable to this article.

Conflicts of Interest: The authors declare no conflicts of interest.

Abbreviations

Abbreviation	Full Name
ALP	alkaline phosphatase
ATDC5	clonal mouse embryonic cell line
BMP-2	bone morphogenetic protein 2
BMSCs	bone marrow mesenchymal stem cells
BTE	bone tissue engineering
CaP	calcium phosphate
Ca-P-Si	calcium phosphate silicate
CNT	carbon nanotubes
DPSCs	dental pulp stem cells
ECM	extracellular matrix
EMF	electromagnetic field
ES	electrical stimulation
FDM	fused deposition modeling
FSB	fish swim bladder
GGMA	methacrylated gellan gum
GO	graphene oxide
HA	hydroksyapatite
hBMMSCs	human-bone-marrow-derived mesenchymal stem cells
IL-1	interleukin-1
iPSCs	induced pluripotent stem cells
MAPK	mitogen-activated protein kinase

mBMSCs	mouse bone marrow stromal stem cells
MSCs	mesenchymal stem cells
MWCNT	multiwalled carbon nanotube
NF-AT	nuclear factor of activated T-cells
PANI	polyaniline
PA-11	polyamide-11
PBLG	poly-γ-benzyl-L-glutamate
PCL	polycaprolactone
PCL-TCP	polycaprolactone–tricalcium phosphate
PDA	perylene-3, 4,9, 10-tetracarboxylic dianhydride
PEMF	pulsed electromagnetic field
PHB	poly(3-hydroxybutyrate)
PHBV	poly(3-hydroxybutyrate-co-3-hydroxyvalerate)
PKC	protein kinase C
PLA	poly(lactic acid)
PLLA	poly (l-lactic acid)
PMLG	poly-γ-methyl-L-glutamate
PMs	piezoelectric materials
PPy	polypyrrole
PTH	parathyroid hormone
PVA	polyvinyl alcohol
PVDF	polyvinylidene fluoride
PVDF-HFP	poly(vinylidene fluoride-hexafluoropropylene)
PVDF-TrFE	polyvinylidene fluoride-trifluoroethylene
RGD	l-arginyl-glycyl-l-aspartic acid sequence
ROS	reactive oxygen species
SBF	simulated body fluid
SLS	selective laser sintering
SMs	smart materials
TCP	tricalcium phosphate
TE	tissue engineering
US	ultrasound
ZIF-8	zinc-based metal–organic frameworks

References

1. Curie, J.; Curie, P. Développement par compression de l'électricité polaire dans les cristaux hémièdres à faces inclinées. *Bull. Minéralogie* **1880**, *3*, 90–93. [CrossRef]
2. Tandon, B.; Blaker, J.J.; Cartmell, S.H. Piezoelectric materials as stimulatory biomedical materials and scaffolds for bone repair. *Acta Biomater.* **2018**, *73*, 1–20. [CrossRef] [PubMed]
3. Joyce, K.; Fabra, G.T.; Bozkurt, Y.; Pandit, A. Bioactive potential of natural biomaterials: Identification, retention and assessment of biological properties. *Sig. Transduct. Target. Ther.* **2021**, *6*, 122. [CrossRef] [PubMed]
4. Zaszczynska, A.; Sajkiewicz, P.; Gradys, A. Piezoelectric Scaffolds as Smart Materials for Neural Tissue Engineering. *Polymers* **2020**, *12*, 161. [CrossRef] [PubMed]
5. Zhang, X.; Zhang, C.; Lin, Y.; Hu, P.; Shen, Y.; Wang, K.; Meng, S.; Chai, Y.; Dai, X.; Liu, X.; et al. Nanocomposite Membranes Enhance Bone Regeneration Through Restoring Physiological Electric Microenvironment. *ACS Nano* **2016**, *10*, 7279–7286. [CrossRef]
6. Ribeiro, C.; Sencadas, V.; Correia, D.M.; Lanceros-Méndez, S. Piezoelectric polymers as biomaterials for tissue engineering applications. *Colloids Surf. B Biointerfaces* **2015**, *136*, 46–55. [CrossRef]
7. Wang, A.; Liu, Z.; Hu, M.; Wang, C.; Zhang, X.; Shi, B.; Fan, Y.; Cui, Y.; Li, Z.; Ren, K. Piezoelectric nanofibrous scaffolds as in vivo energy harvesters for modifying fibroblast alignment and proliferation in wound healing. *Nano Energy* **2018**, *43*, 63–71. [CrossRef]
8. Zaszczyńska, A.; Niemczyk-Soczynska, B.; Sajkiewicz, P. A Comprehensive Review of Electrospun Fibers, 3D-Printed Scaffolds, and Hydrogels for Cancer Therapies. *Polymers* **2022**, *14*, 5278. [CrossRef]
9. Zaszczyńska, A.; Moczulska-Heljak, M.; Gradys, A.; Sajkiewicz, P. Advances in 3D Printing for Tissue Engineering. *Materials* **2021**, *14*, 3149. [CrossRef]
10. Perez, R.A.; Seo, S.-J.; Won, J.-E.; Lee, E.-J.; Jang, J.-H.; Knowles, J.C.; Kim, H.-W. Therapeutically relevant aspects in bone repair and regeneration. *Mater. Today* **2015**, *18*, 573–589. [CrossRef]
11. Voog, J.; Jones, D.L. Stem Cells and the Niche: A Dynamic Duo. *Cell Stem Cell* **2010**, *6*, 103–115. [CrossRef] [PubMed]
12. Lang, S.B. Pyroelectric Effect in Bone and Tendon. *Nature* **1966**, *212*, 704–705. [CrossRef]

13. Butcher, M.T.; Espinoza, N.R.; Cirilo, S.R.; Blob, R.W. In vivo strains in the femur of river cooter turtles (*Pseudemys concinna*) during terrestrial locomotion: Tests of force-platform models of loading mechanics. *J. Exp. Biol.* **2008**, *211*, 2397–2407. [CrossRef] [PubMed]
14. Kao, F.-C.; Chiu, P.-Y.; Tsai, T.-T.; Lin, Z.-H. The application of nanogenerators and piezoelectricity in osteogenesis. *Sci. Technol. Adv. Mater.* **2019**, *20*, 1103–1117. [CrossRef]
15. Yasuda, I. Electrical Callus and Callus Formation by Electret. *Clin. Orthop. Relat. Res.* **1977**, *124*, 53. [CrossRef]
16. Kapat, K.; Shubhra, Q.T.H.; Zhou, M.; Leeuwenburgh, S. Piezoelectric Nano-Biomaterials for Biomedicine and Tissue Regeneration. *Adv. Funct. Mater.* **2020**, *30*, 1909045. [CrossRef]
17. Gorbachova, T.; Melenevsky, Y.; Cohen, M.; Cerniglia, B.W. Osteochondral Lesions of the Knee: Differentiating the Most Common Entities at MRI. *RadioGraphics* **2018**, *38*, 1478–1495. [CrossRef]
18. Raben, H.; Kämmerer, P.W.; Bader, R.; van Rienen, U. Establishment of a Numerical Model to Design an Electro-Stimulating System for a Porcine Mandibular Critical Size Defect. *Appl. Sci.* **2019**, *9*, 2160. [CrossRef]
19. Park, J.B.; von Recum, A.F.; Kenner, G.H.; Kelly, B.J.; Coffeen, W.W.; Grether, M.F. Piezoelectric ceramic implants: A feasibility study. *J. Biomed. Mater. Res.* **1980**, *14*, 269–277. [CrossRef]
20. Bauso, L.V.; La Fauci, V.; Longo, C.; Calabrese, G. Bone Tissue Engineering and Nanotechnology: A Promising Combination for Bone Regeneration. *Biology* **2024**, *13*, 237. [CrossRef]
21. Sultana, A.; Kumar Ghosh, S.; Sencadas, V.; Zheng, T.; Higgins, M.J.; Ranjan Middya, T.; Mandal, D. Human skin interactive self-powered wearable piezoelectric bio-e-skin by electrospun poly- l -lactic acid nanofibers for non-invasive physiological signal monitoring. *J. Mater. Chem. B* **2017**, *5*, 7352–7359. [CrossRef] [PubMed]
22. Riddle, R.C.; Donahue, H.J. From Streaming-Potentials to Shear Stress: 25 Years of Bone Cell Mechanotransduction. *J. Orthop. Res.* **2009**, *27*, 143–149. Available online: https://onlinelibrary.wiley.com/doi/abs/10.1002/jor.20723 (accessed on 17 January 2024). [CrossRef]
23. Murillo, G.; Blanquer, A.; Vargas-Estevez, C.; Barrios, L.; Ibáñez, E.; Nogués, C.; Esteve, J. Electromechanical Nanogenerator–Cell Interaction Modulates Cell Activity. *Adv. Mater.* **2017**, *29*, 1605048. [CrossRef] [PubMed]
24. More, N.; Kapusetti, G. Piezoelectric material—A promising approach for bone and cartilage regeneration. *Med. Hypotheses* **2017**, *108*, 10–16. [CrossRef]
25. Liu, Y.; Zhang, X.; Cao, C.; Zhang, Y.; Wei, J.; Li, Y.J.; Liang, W.; Hu, Z.; Zhang, J.; Wei, Y.; et al. Built-In Electric Fields Dramatically Induce Enhancement of Osseointegration. *Adv. Funct. Mater.* **2017**, *27*, 1703771. Available online: https://onlinelibrary.wiley.com/doi/full/10.1002/adfm.201703771 (accessed on 17 January 2024). [CrossRef]
26. Zigman, T.; Davila, S.; Dobric, I.; Antoljak, T.; Augustin, G.; Rajacic, D.; Kovac, T.; Ehrenfreund, T. Intraoperative measurement of bone electrical potential: A piece in the puzzle of understanding fracture healing. *Injury* **2013**, *44*, S16–S19. [CrossRef]
27. Rajabi, A.H.; Jaffe, M.; Arinzeh, T.L. Piezoelectric materials for tissue regeneration: A review. *Acta Biomater.* **2015**, *24*, 12–23. [CrossRef] [PubMed]
28. Martin, A.J.P. Tribo-electricity in wool and hair. *Proc. Phys. Soc.* **1941**, *53*, 186. [CrossRef]
29. Wu, D.-D.; Irwin, D.M.; Zhang, Y.-P. Molecular evolution of the keratin associated protein gene family in mammals, role in the evolution of mammalian hair. *BMC Evol. Biol.* **2008**, *8*, 241. [CrossRef]
30. Feughelman, M.; Lyman, D.; Menefee, E.; Willis, B. The orientation of the α-helices in α-keratin fibres. *Int. J. Biol. Macromol.* **2003**, *33*, 149–152. [CrossRef]
31. Alparone, A. Response electric properties of α-helix polyglycines: A CAM-B3LYP DFT investigation. *Chem. Phys. Lett.* **2013**, *563*, 88–92. [CrossRef]
32. Yasuda, I. On the piezoelectric activity of bone. *J. Jpn. Orthop. Surg. Soc.* **1954**, *28*, 267.
33. Fukada, E.; Yasuda, I. On the Piezoelectric Effect of Bone. *J. Phys. Soc. Jpn.* **1957**, *12*, 1158–1162. [CrossRef]
34. Hassenkam, T.; Fantner, G.E.; Cutroni, J.A.; Weaver, J.C.; Morse, D.E.; Hansma, P.K. High-resolution AFM imaging of intact and fractured trabecular bone. *Bone* **2004**, *35*, 4–10. [CrossRef]
35. Ramachandran, G.N.; Kartha, G. Structure of Collagen. *Nature* **1955**, *176*, 593–595. [CrossRef]
36. Wolff, J. Das Gesetz der Transformation der Knochen. *DMW-Dtsch. Med. Wochenschr.* **1893**, *19*, 1222–1224. [CrossRef]
37. Mohammadkhah, M.; Marinkovic, D.; Zehn, M.; Checa, S. A review on computer modeling of bone piezoelectricity and its application to bone adaptation and regeneration. *Bone* **2019**, *127*, 544–555. [CrossRef] [PubMed]
38. Bassett, C.A.L. Biologic significance of piezoelectricity. *Calc. Tis. Res.* **1967**, *1*, 252–272. [CrossRef] [PubMed]
39. Cochran, G.V.B.; Pawluk, R.J.; Bassett, C.A.L. 24 Electromechanical Characteristics of Bone Under Physiologic Moisture Conditions. *Clin. Orthop. Relat. Res.* **1968**, *58*, 249. [CrossRef]
40. Anderson, J.C.; Eriksson, C. Electrical Properties of Wet Collagen. *Nature* **1968**, *218*, 166–168. [CrossRef]
41. Wong, M.; Rao, L.G.; Ly, H.; Hamilton, L.; Tong, J.; Sturtridge, W.; Mcbroom, R.; Aubin, J.E.; Murray, T.M. Long-term effects of physiologic concentrations of dexamethasone on human bone-derived cells. *J. Bone Miner. Res.* **1990**, *5*, 803–813. [CrossRef] [PubMed]
42. Johnson, M.W.; Chakkalakal, D.A.; Harper, R.A.; Katz, J.L. Comparison of the electromechanical effects in wet and dry bone. *J. Biomech.* **1980**, *13*, 437–442. [CrossRef]
43. Gross, D.; Williams, W.S. Streaming potential and the electromechanical response of physiologically-moist bone. *J. Biomech.* **1982**, *15*, 277–295. [CrossRef]

44. Pienkowski, D.; Pollack, S.R. The Origin of Stress-Generated Potentials in Fluid-Saturated Bone. *J. Orthop. Res.* **1983**, *1*, 30–41. Available online: https://onlinelibrary.wiley.com/doi/abs/10.1002/jor.1100010105 (accessed on 18 January 2024). [CrossRef]
45. IJMS | Free Full-Text | Runx2 and Polycystins in Bone Mechanotransduction: Challenges for Therapeutic Opportunities. Available online: https://www.mdpi.com/1422-0067/25/10/5291 (accessed on 25 June 2024).
46. Zaszczyńska, A.; Gradys, A.; Ziemiecka, A.; Szewczyk, P.K.; Tymkiewicz, R.; Lewandowska-Szumieł, M.; Stachewicz, U.; Sajkiewicz, P.Ł. Enhanced Electroactive Phases of Poly(vinylidene Fluoride) Fibers for Tissue Engineering Applications. *Int. J. Mol. Sci.* **2024**, *25*, 4980. [CrossRef]
47. Praveen, E.; Murugan, S.; Jayakumar, K. Investigations on the existence of piezoelectric property of a bio-polymer—Chitosan and its application in vibration sensors. *RSC Adv.* **2017**, *7*, 35490–35495. [CrossRef]
48. Amin Hoque, N.; Thakur, P.; Biswas, P.; Minarul Saikh, M.; Roy, S.; Bagchi, B.; Das, S.; Pratim Ray, P. Biowaste crab shell-extracted chitin nanofiber-based superior piezoelectric nanogenerator. *J. Mater. Chem. A* **2018**, *6*, 13848–13858. [CrossRef]
49. Wang, J.; Carlos, C.; Zhang, Z.; Li, J.; Long, Y.; Yang, F.; Dong, Y.; Qiu, X.; Qian, Y.; Wang, X. Piezoelectric Nanocellulose Thin Film with Large-Scale Vertical Crystal Alignment. *ACS Appl. Mater. Interfaces* **2020**, *12*, 26399–26404. [CrossRef] [PubMed]
50. Denning, D.; Kilpatrick, J.I.; Fukada, E.; Zhang, N.; Habelitz, S.; Fertala, A.; Gilchrist, M.D.; Zhang, Y.; Tofail, S.A.M.; Rodriguez, B.J. Piezoelectric Tensor of Collagen Fibrils Determined at the Nanoscale. *ACS Biomater. Sci. Eng.* **2017**, *3*, 929–935. [CrossRef]
51. Fukada, E. History and recent progress in piezoelectric polymers. *IEEE Trans. Ultrason. Ferroelectr. Freq. Control* **2000**, *47*, 1277–1290. [CrossRef]
52. Horan, R.L.; Antle, K.; Collette, A.L.; Wang, Y.; Huang, J.; Moreau, J.E.; Volloch, V.; Kaplan, D.L.; Altman, G.H. In vitro degradation of silk fibroin. *Biomaterials* **2005**, *26*, 3385–3393. [CrossRef] [PubMed]
53. Ghosh, S.K.; Mandal, D. Efficient natural piezoelectric nanogenerator: Electricity generation from fish swim bladder. *Nano Energy* **2016**, *28*, 356–365. [CrossRef]
54. Di Martino, A.; Sittinger, M.; Risbud, M.V. Chitosan: A versatile biopolymer for orthopaedic tissue-engineering. *Biomaterials* **2005**, *26*, 5983–5990. [CrossRef] [PubMed]
55. Hänninen, A.; Rajala, S.; Salpavaara, T.; Kellomäki, M.; Tuukkanen, S. Piezoelectric Sensitivity of a Layered Film of Chitosan and Cellulose Nanocrystals. *Procedia Eng.* **2016**, *168*, 1176–1179. [CrossRef]
56. Prokhorov, E.; Luna-Bárcenas, G.; Yáñez Limón, J.M.; Gómez Sánchez, A.; Kovalenko, Y. Chitosan-ZnO Nanocomposites Assessed by Dielectric, Mechanical, and Piezoelectric Properties. *Polymers* **2020**, *12*, 1991. [CrossRef]
57. Mawazi, S.M.; Kumar, M.; Ahmad, N.; Ge, Y.; Mahmood, S. Recent Applications of Chitosan and Its Derivatives in Antibacterial, Anticancer, Wound Healing, and Tissue Engineering Fields. *Polymers* **2024**, *16*, 1351. [CrossRef]
58. Zaborowska, M.; Bodin, A.; Bäckdahl, H.; Popp, J.; Goldstein, A.; Gatenholm, P. Microporous bacterial cellulose as a potential scaffold for bone regeneration. *Acta Biomater.* **2010**, *6*, 2540–2547. [CrossRef]
59. Murizan, N.I.S.; Mustafa, N.S.; Ngadiman, N.H.A.; Mohd Yusof, N.; Idris, A. Review on Nanocrystalline Cellulose in Bone Tissue Engineering Applications. *Polymers* **2020**, *12*, 2818. [CrossRef]
60. Janmohammadi, M.; Nazemi, Z.; Salehi, A.O.M.; Seyfoori, A.; John, J.V.; Nourbakhsh, M.S.; Akbari, M. Cellulose-based composite scaffolds for bone tissue engineering and localized drug delivery. *Bioact. Mater.* **2023**, *20*, 137–163. [CrossRef]
61. Hill, P.S.; Apel, P.J.; Barnwell, J.; Smith, T.; Koman, L.A.; Atala, A.; Van Dyke, M. Repair of Peripheral Nerve Defects in Rabbits Using Keratin Hydrogel Scaffolds. *Tissue Eng. Part A* **2011**, *17*, 1499–1505. [CrossRef]
62. Tanabe, T.; Okitsu, N.; Yamauchi, K. Fabrication and characterization of chemically crosslinked keratin films. *Mater. Sci. Eng. C* **2004**, *24*, 441–446. [CrossRef]
63. Hamasaki, S.; Tachibana, A.; Tada, D.; Yamauchi, K.; Tanabe, T. Fabrication of highly porous keratin sponges by freeze-drying in the presence of calcium alginate beads. *Mater. Sci. Eng. C* **2008**, *28*, 1250–1254. [CrossRef]
64. Peplow, P.V.; Dias, G.J. A study of the relationship between mass and physical strength of keratin bars in vivo. *J. Mater. Sci. Mater. Med.* **2004**, *15*, 1217–1220. [CrossRef] [PubMed]
65. Placone, J.K.; Navarro, J.; Laslo, G.W.; Lerman, M.J.; Gabard, A.R.; Herendeen, G.J.; Falco, E.E.; Tomblyn, S.; Burnett, L.; Fisher, J.P. Development and Characterization of a 3D Printed, Keratin-Based Hydrogel. *Ann. Biomed. Eng.* **2017**, *45*, 237–248. [CrossRef] [PubMed]
66. Duncan, W.J.; Greer, P.F.; Lee, M.H.; Loch, C.; Gay, J.H. Wool-Derived Keratin Hydrogel Enhances Implant Osseointegration in Cancellous Bone. *J. Biomed. Mater. Res. Part B Appl. Biomater.* **2018**, *106*, 2447–2454. Available online: https://onlinelibrary.wiley.com/doi/full/10.1002/jbm.b.34047 (accessed on 18 January 2024). [CrossRef]
67. Rocha, L.B.; Goissis, G.; Rossi, M.A. Biocompatibility of anionic collagen matrix as scaffold for bone healing. *Biomaterials* **2002**, *23*, 449–456. [CrossRef]
68. Silva, C.C.; Thomazini, D.; Pinheiro, A.G.; Aranha, N.; Figueiró, S.D.; Góes, J.C.; Sombra, A.S.B. Collagen–hydroxyapatite films: Piezoelectric properties. *Mater. Sci. Eng. B* **2001**, *86*, 210–218. [CrossRef]
69. Köse, G.T.; Korkusuz, F.; Özkul, A.; Soysal, Y.; Özdemir, T.; Yildiz, C.; Hasirci, V. Tissue engineered cartilage on collagen and PHBV matrices. *Biomaterials* **2005**, *26*, 5187–5197. [CrossRef]
70. Ahn, A.C.; Grodzinsky, A.J. Relevance of collagen piezoelectricity to "Wolff's Law": A critical review. *Med. Eng. Phys.* **2009**, *31*, 733–741. [CrossRef]
71. Dubey, A.K.; Mukhopadhyay, A.; Basu, B. *Interdisciplinary Engineering Sciences: Concepts and Applications to Materials Science*; CRC Press: Boca Raton, FL, USA, 2020; ISBN 978-1-00-002741-9.

72. Zheng, T.; Huang, Y.; Zhang, X.; Cai, Q.; Deng, X.; Yang, X. Mimicking the electrophysiological microenvironment of bone tissue using electroactive materials to promote its regeneration. *J. Mater. Chem. B* **2020**, *8*, 10221–10256. [CrossRef]
73. Zou, Z.; Wang, L.; Zhou, Z.; Sun, Q.; Liu, D.; Chen, Y.; Hu, H.; Cai, Y.; Lin, S.; Yu, Z.; et al. Simultaneous incorporation of PTH(1–34) and nano-hydroxyapatite into Chitosan/Alginate Hydrogels for efficient bone regeneration. *Bioact. Mater.* **2021**, *6*, 1839–1851. [CrossRef]
74. He, J.; Hu, X.; Cao, J.; Zhang, Y.; Xiao, J.; Peng, L.J.; Chen, D.; Xiong, C.; Zhang, L. Chitosan-coated hydroxyapatite and drug-loaded polytrimethylene carbonate/polylactic acid scaffold for enhancing bone regeneration. *Carbohydr. Polym.* **2021**, *253*, 117198. [CrossRef] [PubMed]
75. Diwan, H.; Sah, M.K. Exploring the potential of keratin-based biomaterials in orthopedic tissue engineering: A comprehensive review. *Emergent Mater.* **2023**, *6*, 1441–1460. [CrossRef]
76. Naderi, P.; Zarei, M.; Karbasi, S.; Salehi, H. Evaluation of the effects of keratin on physical, mechanical and biological properties of poly (3-hydroxybutyrate) electrospun scaffold: Potential application in bone tissue engineering. *Eur. Polym. J.* **2020**, *124*, 109502. [CrossRef]
77. Yang, J.; Wang, H.; Zhou, Y.; Duan, L.; Schneider, K.H.; Zheng, Z.; Han, F.; Wang, X.; Li, G. Silk Fibroin/Wool Keratin Composite Scaffold with Hierarchical Fibrous and Porous Structure. *Macromol. Biosci.* **2023**, *23*, 2300105. [CrossRef] [PubMed]
78. Zhang, W.; Wang, X.; Li, X.; Zhang, L.; Jiang, F. A 3D porous microsphere with multistage structure and component based on bacterial cellulose and collagen for bone tissue engineering. *Carbohydr. Polym.* **2020**, *236*, 116043. [CrossRef]
79. Molecular Mechanism of Polarization and Piezoelectric Effect in Super-Twisted Collagen | ACS Biomaterials Science & Engineering. Available online: https://pubs.acs.org/doi/abs/10.1021/acsbiomaterials.6b00021 (accessed on 18 January 2024).
80. Zanfir, A.V.; Voicu, G.; Busuioc, C.; Jinga, S.I.; Albu, M.G.; Iordache, F. New Coll–HA/BT composite materials for hard tissue engineering. *Mater. Sci. Eng. C* **2016**, *62*, 795–805. [CrossRef]
81. Liu, S.; Zhang, L.; Li, Z.; Gao, F.; Zhang, Q.; Bianco, A.; Liu, H.; Ge, S.; Ma, B. Materials-Mediated In Situ Physical Cues for Bone Regeneration. *Adv. Funct. Mater.* **2024**, *34*, 2306534. [CrossRef]
82. Zhang, J.; Zhuang, Y.; Sheng, R.; Tomás, H.; Rodrigues, J.; Yuan, G.; Wang, X.; Lin, K. Smart stimuli-responsive strategies for titanium implant functionalization in bone regeneration and therapeutics. *Mater. Horiz.* **2024**, *11*, 12–36. [CrossRef]
83. Jacob, J.; More, N.; Kalia, K.; Kapusetti, G. Piezoelectric smart biomaterials for bone and cartilage tissue engineering. *Inflamm. Regen.* **2018**, *38*, 2. [CrossRef]
84. Yang, F.; Li, J.; Long, Y.; Zhang, Z.; Wang, L.; Sui, J.; Dong, Y.; Wang, Y.; Taylor, R.; Ni, D.; et al. Wafer-scale heterostructured piezoelectric bio-organic thin films. *Science* **2021**, *373*, 337–342. [CrossRef] [PubMed]
85. Farrar, D.; Ren, K.; Cheng, D.; Kim, S.; Moon, W.; Wilson, W.L.; West, J.E.; Yu, S.M. Permanent Polarity and Piezoelectricity of Electrospun α-Helical Poly(α-Amino Acid) Fibers. *Adv. Mater.* **2011**, *23*, 3954–3958. Available online: https://onlinelibrary.wiley.com/doi/full/10.1002/adma.201101733 (accessed on 18 January 2024). [CrossRef] [PubMed]
86. Ruan, L.; Yao, X.; Chang, Y.; Zhou, L.; Qin, G.; Zhang, X. Properties and Applications of the β Phase Poly(vinylidene fluoride). *Polymers* **2018**, *10*, 228. [CrossRef]
87. Husain, M.; Singh, R.; Pabla, B.S. On 3D Printing of PVDF Composite- Based Sensors for Biomedical Applications. *Natl. Acad. Sci. Lett.* **2024**, *47*, 147–152. [CrossRef]
88. Yuan, X.; Shi, J.; Kang, Y.; Dong, J.; Pei, Z.; Ji, X. Piezoelectricity, Pyroelectricity, and Ferroelectricity in Biomaterials and Biomedical Applications. *Adv. Mater.* **2024**, *36*, 2308726. [CrossRef] [PubMed]
89. Song, R.; Yang, D.; He, L. Effect of surface modification of nanosilica on crystallization, thermal and mechanical properties of poly(vinylidene fluoride). *J. Mater. Sci.* **2007**, *42*, 8408–8417. [CrossRef]
90. Rodrigues, M.T.; Gomes, M.E.; Mano, J.F.; Reis, R.L. β-PVDF Membranes Induce Cellular Proliferation and Differentiation in Static and Dynamic Conditions. *MSF* **2008**, *587–588*, 72–76. [CrossRef]
91. Cardoso, V.F.; Correia, D.M.; Ribeiro, C.; Fernandes, M.M.; Lanceros-Méndez, S. Fluorinated Polymers as Smart Materials for Advanced Biomedical Applications. *Polymers* **2018**, *10*, 161. [CrossRef]
92. Kitsara, M.; Blanquer, A.; Murillo, G.; Humblot, V.; De Bragança Vieira, S.; Nogués, C.; Ibáñez, E.; Esteve, J.; Barrios, L. Permanently hydrophilic, piezoelectric PVDF nanofibrous scaffolds promoting unaided electromechanical stimulation on osteoblasts. *Nanoscale* **2019**, *11*, 8906–8917. [CrossRef]
93. Wu, C.; Tang, Y.; Mao, B.; Yan, X.; Pu, Y.; Zhao, K. Improved hydrophilicity and durability of polarized PVDF coatings on anodized titanium surfaces to enhance mineralization ability. *Colloids Surf. B Biointerfaces* **2021**, *205*, 111898. [CrossRef]
94. Guillot-Ferriols, M.; Del Barrio, A.; Costa, C.M.; Lanceros Méndez, S.; Rodríguez-Cabello, J.C.; Gómez Ribelles, J.L.; Santos, M.; Gallego Ferrer, G. Effective elastin-like recombinamers coating on poly(vinylidene) fluoride membranes for mesenchymal stem cell culture. *Eur. Polym. J.* **2021**, *146*, 110269. [CrossRef]
95. Damaraju, S.M.; Wu, S.; Jaffe, M.; Arinzeh, T.L. Structural changes in PVDF fibers due to electrospinning and its effect on biological function. *Biomed. Mater.* **2013**, *8*, 045007. [CrossRef] [PubMed]
96. Zaarour, B.; Zhu, L.; Jin, X. Maneuvering the secondary surface morphology of electrospun poly (vinylidene fluoride) nanofibers by controlling the processing parameters. *Mater. Res. Express* **2019**, *7*, 015008. [CrossRef]
97. Lee, J.C.; Park, C.H.; Kim, C.S. Amplified piezoelectric response with β-phase formation in PVDF blended 3D cotton type nanofibers for osteogenic differentiation. *J. Ind. Eng. Chem.* **2023**, *118*, 155–163. [CrossRef]

98. Silva, C.A.; Fernandes, M.M.; Ribeiro, C.; Lanceros-Mendez, S. Two- and three-dimensional piezoelectric scaffolds for bone tissue engineering. *Colloids Surf. B Biointerfaces* **2022**, *218*, 112708. [CrossRef] [PubMed]
99. Mirzaei, A.; Moghadam, A.S.; Abazari, M.F.; Nejati, F.; Torabinejad, S.; Kaabi, M.; Enderami, S.E.; Ardeshirylajimi, A.; Darvish, M.; Soleimanifar, F.; et al. Comparison of osteogenic differentiation potential of induced pluripotent stem cells on 2D and 3D polyvinylidene fluoride scaffolds. *J. Cell. Physiol.* **2019**, *234*, 17854–17862. [CrossRef]
100. Morales-Román, R.M.; Guillot-Ferriols, M.; Roig-Pérez, L.; Lanceros-Mendez, S.; Gallego-Ferrer, G.; Gómez Ribelles, J.L. Freeze-extraction microporous electroactive supports for cell culture. *Eur. Polym. J.* **2019**, *119*, 531–540. [CrossRef]
101. Szewczyk, P.K.; Metwally, S.; Karbowniczek, J.E.; Marzec, M.M.; Stodolak-Zych, E.; Gruszczyński, A.; Bernasik, A.; Stachewicz, U. Surface-Potential-Controlled Cell Proliferation and Collagen Mineralization on Electrospun Polyvinylidene Fluoride (PVDF) Fiber Scaffolds for Bone Regeneration. *ACS Biomater. Sci. Eng.* **2019**, *5*, 582–593. [CrossRef]
102. Muenwacha, T.; Weeranantanapan, O.; Chudapongse, N.; Diaz Sanchez, F.J.; Maensiri, S.; Radacsi, N.; Nuansing, W. Fabrication of Piezoelectric Electrospun Termite Nest-like 3D Scaffolds for Tissue Engineering. *Materials* **2021**, *14*, 7684. [CrossRef]
103. Zhou, Z.; Yu, P.; Zhou, L.; Tu, L.; Fan, L.; Zhang, F.; Dai, C.; Liu, Y.; Ning, C.; Du, J.; et al. Polypyrrole Nanocones and Dynamic Piezoelectric Stimulation-Induced Stem Cell Osteogenic Differentiation. *ACS Biomater. Sci. Eng.* **2019**, *5*, 4386–4392. [CrossRef]
104. Mirzaei, A.; Saburi, E.; Enderami, S.E.; Barati Bagherabad, M.; Enderami, S.E.; Chokami, M.; Shapouri Moghadam, A.; Salarinia, R.; Ardeshirylajimi, A.; Mansouri, V.; et al. Synergistic effects of polyaniline and pulsed electromagnetic field to stem cells osteogenic differentiation on polyvinylidene fluoride scaffold. *Artif. Cells Nanomed. Biotechnol.* **2019**, *47*, 3058–3066. [CrossRef] [PubMed]
105. Orkwis, J.A.; Wolf, A.K.; Shahid, S.M.; Smith, C.; Esfandiari, L.; Harris, G.M. Development of a Piezoelectric PVDF-TrFE Fibrous Scaffold to Guide Cell Adhesion, Proliferation, and Alignment. *Macromol. Biosci.* **2020**, *20*, 2000197. [CrossRef] [PubMed]
106. Valentini, R.F. Negatively Charged Polymeric Electret Implant. U.S. Patent No. 5,759,205, 2 June 1998.
107. Wu, S.; Chen, M.-S.; Maurel, P.; Lee, Y.; Bunge, M.B.; Arinzeh, T.L. Aligned fibrous PVDF-TrFE scaffolds with Schwann cells support neurite extension and myelination in vitro. *J. Neural Eng.* **2018**, *15*, 056010. [CrossRef] [PubMed]
108. Arinzeh, T.; Collins, G.; Lee, Y.-S. A Piezoelectric Scaffold for Nerve Growth and Repair. 2018. Available online: https://researchwith.njit.edu/en/publications/a-piezoelectric-scaffold-for-nerve-growth-and-repair (accessed on 25 June 2024).
109. Pereira, J.D.A.S.; Camargo, R.C.T.; Filho, J.C.S.C.; Alves, N.; Rodriguez-Perez, M.A.; Constantino, C.J.L. Biomaterials from blends of fluoropolymers and corn starch—Implant and structural aspects. *Mater. Sci. Eng. C* **2014**, *36*, 226–236. [CrossRef]
110. Gimenes, R.; Zaghete, M.A.; Bertolini, M.; Varela, J.A.; Coelho, L.O.; Silva, N.F., Jr. Composites PVDF-TrFE/BT used as bioactive membranes for enhancing bone regeneration. In Proceedings of the Smart Structures and Materials 2004: Electroactive Polymer Actuators and Devices (EAPAD), San Diego, CA, USA, 14–18 March 2004; SPIE: San Diego, CA, USA, 2004; Volume 5385, pp. 539–547.
111. Lopes, H.B.; de Santos, T.S.; de Oliveira, F.S.; Freitas, G.P.; de Almeida, A.L.; Gimenes, R.; Rosa, A.L.; Beloti, M.M. Poly(vinylidene-trifluoroethylene)/barium titanate composite for in vivo support of bone formation. *J. Biomater. Appl.* **2014**, *29*, 104–112. [CrossRef]
112. Luo, Q.; He, X.; Duan, X.; Liu, H.; Zhou, Z.; Cheng, K. A Facile Synthesis of P(VDF-TrFE)-Coated-PMMA Janus Membranes for Guided Bone Regeneration. *Coatings* **2022**, *12*, 1947. [CrossRef]
113. Sood, A.; Desseigne, M.; Dev, A.; Maurizi, L.; Kumar, A.; Millot, N.; Han, S.S. A Comprehensive Review on Barium Titanate Nanoparticles as a Persuasive Piezoelectric Material for Biomedical Applications: Prospects and Challenges. *Small* **2023**, *19*, 2206401. [CrossRef]
114. Panda, A.K.; Sitaramgupta, V.S.N.; Pandya, H.J.; Basu, B. Electrical stimulation waveform-dependent osteogenesis on PVDF/$BaTiO_3$ composite using a customized and programmable cell stimulator. *Biotech. Bioeng.* **2022**, *119*, 1578–1597. [CrossRef]
115. Bhaskar, N.; Kachappilly, M.C.; Bhushan, V.; Pandya, H.J.; Basu, B. Electrical field stimulated modulation of cell fate of pre-osteoblasts on PVDF/BT/MWCNT based electroactive biomaterials. *J. Biomed. Mater. Res.* **2023**, *111*, 340–353. [CrossRef]
116. Almeida, A.L.G.; Freitas, G.P.; Lopes, H.B.; Gimenes, R.; Siessere, S.; Sousa, L.G.; Beloti, M.M.; Rosa, A.L. Effect of stem cells combined with a polymer/ceramic membrane on osteoporotic bone repair. *Braz. Oral. Res.* **2019**, *33*, e079. [CrossRef]
117. Freitas, G.P.; Lopes, H.B.; Almeida, A.L.G.; Abuna, R.P.F.; Gimenes, R.; Souza, L.E.B.; Covas, D.T.; Beloti, M.M.; Rosa, A.L. Potential of Osteoblastic Cells Derived from Bone Marrow and Adipose Tissue Associated with a Polymer/Ceramic Composite to Repair Bone Tissue. *Calcif. Tissue Int.* **2017**, *101*, 312–320. [CrossRef] [PubMed]
118. Bone Piezoelectricity-Mimicking Nanocomposite Membranes Enhance O: Ingenta Connect. Available online: https://www.ingentaconnect.com/contentone/asp/jbn/2021/00000017/00000006/art00006 (accessed on 18 January 2024).
119. Shuai, C.; Liu, G.; Yang, Y.; Yang, W.; He, C.; Wang, G.; Liu, Z.; Qi, F.; Peng, S. Functionalized $BaTiO_3$ enhances piezoelectric effect towards cell response of bone scaffold. *Colloids Surf. B Biointerfaces* **2020**, *185*, 110587. [CrossRef] [PubMed]
120. Shuai, C.; Liu, G.; Yang, Y.; Qi, F.; Peng, S.; Yang, W.; He, C.; Wang, G.; Qian, G. A strawberry-like Ag-decorated barium titanate enhances piezoelectric and antibacterial activities of polymer scaffold. *Nano Energy* **2020**, *74*, 104825. [CrossRef]
121. Sharma, V.; Chowdhury, S.; Bose, S.; Basu, B. Polydopamine Codoped $BaTiO_{3-}$ Functionalized Polyvinylidene Fluoride Coating as a Piezo-Biomaterial Platform for an Enhanced Cellular Response and Bioactivity. *ACS Biomater. Sci. Eng.* **2022**, *8*, 170–184. [CrossRef]
122. Qi, F.; Zeng, Z.; Yao, J.; Cai, W.; Zhao, Z.; Peng, S.; Shuai, C. Constructing core-shell structured $BaTiO_3$@carbon boosts piezoelectric activity and cell response of polymer scaffolds. *Mater. Sci. Eng. C* **2021**, *126*, 112129. [CrossRef]

123. Shuai, C.; Zeng, Z.; Yang, Y.; Qi, F.; Peng, S.; Yang, W.; He, C.; Wang, G.; Qian, G. Graphene oxide assists polyvinylidene fluoride scaffold to reconstruct electrical microenvironment of bone tissue. *Mater. Des.* **2020**, *190*, 108564. [CrossRef]
124. Azadian, E.; Arjmand, B.; Ardeshirylajimi, A.; Hosseinzadeh, S.; Omidi, M.; Khojasteh, A. Polyvinyl alcohol modified polyvinylidene fluoride-graphene oxide scaffold promotes osteogenic differentiation potential of human induced pluripotent stem cells. *J. Cell. Biochem.* **2020**, *121*, 3185–3196. [CrossRef] [PubMed]
125. Fu, Y.; Huang, S.; Feng, Z.; Huang, L.; Zhang, X.; Lin, H.; Mo, A. MXene-Functionalized Ferroelectric Nanocomposite Membranes with Modulating Surface Potential Enhance Bone Regeneration. *ACS Biomater. Sci. Eng.* **2023**, *9*, 900–917. [CrossRef] [PubMed]
126. Li, Y.; Sun, L.; Webster, T.J. The Investigation of ZnO/Poly(vinylidene fluoride) Nanocomposites with Improved Mechanical, Piezoelectric, and Antimicrobial Properties for Orthopedic Applications. *J. Biomed. Nanotechnol.* **2018**, *14*, 536–545. [CrossRef]
127. Xi, Y.; Pan, W.; Xi, D.; Liu, X.; Yu, J.; Xue, M.; Xu, N.; Wen, J.; Wang, W.; He, H.; et al. Optimization, characterization and evaluation of ZnO/polyvinylidene fluoride nanocomposites for orthopedic applications: Improved antibacterial ability and promoted osteoblast growth. *Drug Deliv.* **2020**, *27*, 1378–1385. [CrossRef]
128. FotouhiArdakani, F.; Mohammadi, M.; Mashayekhan, S. ZnO-incorporated polyvinylidene fluoride/poly(ε-caprolactone) nanocomposite scaffold with controlled release of dexamethasone for bone tissue engineering. *Appl. Phys. A* **2022**, *128*, 654. [CrossRef]
129. Chen, J.; Song, L.; Qi, F.; Qin, S.; Yang, X.; Xie, W.; Gai, K.; Han, Y.; Zhang, X.; Zhu, Z.; et al. Enhanced bone regeneration via ZIF-8 decorated hierarchical polyvinylidene fluoride piezoelectric foam nanogenerator: Coupling of bioelectricity, angiogenesis, and osteogenesis. *Nano Energy* **2023**, *106*, 108076. [CrossRef]
130. Dos Santos, G.G.; Malherbi, M.S.; De Souza, N.S.; César, G.B.; Tominaga, T.T.; Miyahara, R.Y.; De Mendonça, P.D.S.B.; Faria, D.R.; Rosso, J.M.; Freitas, V.F.; et al. 4th Generation Biomaterials Based on PVDF-Hydroxyapatite Composites Produced by Electrospinning: Processing and Characterization. *Polymers* **2022**, *14*, 4190. [CrossRef] [PubMed]
131. Rodrigues, P.J.G.; Elias, C.D.M.V.; Viana, B.C.; De Hollanda, L.M.; Stocco, T.D.; De Vasconcellos, L.M.R.; Mello, D.D.C.R.; Santos, F.E.P.; Marciano, F.R.; Lobo, A.O. Electrodeposition of bactericidal and bioactive nano-hydroxyapatite onto electrospun piezoelectric polyvinylidene fluoride scaffolds. *J. Mater. Res.* **2020**, *35*, 3265–3275. [CrossRef]
132. Wu, C.; Tang, Y.; Mao, B.; Zhao, K.; Cao, S.; Wu, Z. Rapid apatite induction of polarized hydrophilic HA/PVDF bio-piezoelectric coating on titanium surface. *Surf. Coat. Technol.* **2021**, *405*, 126510. [CrossRef]
133. Malherbi, M.S.; Dias, L.C.; Lima, M.S.Z.; Ribeiro, L.G.; Freitas, V.F.; Bonadio, T.G.M.; Silva, L.M.; Souza, G.B.; Volnistem, E.A.; Rosso, J.M.; et al. Electrically stimulated bioactivity in hydroxyapatite/β-tricalcium phosphate/polyvinylidene fluoride biocomposites. *J. Mater. Res. Technol.* **2022**, *20*, 169–179. [CrossRef]
134. Gong, T.; Li, T.; Meng, L.; Chen, Y.; Wu, T.; Zhou, J.; Lu, G.; Wang, Z. Fabrication of piezoelectric Ca-P-Si-doped PVDF scaffold by phase-separation-hydration: Material characterization, in vitro biocompatibility and osteoblast redifferentiation. *Ceram. Int.* **2022**, *48*, 6461–6469. [CrossRef]
135. Ma, Z.; Hu, X.; Zhang, Y.; Li, X.; Chen, B.; An, Q.; Zhao, Y.; Zhang, Y. Biomineralized Piezoelectrically Active Scaffolds for Inducing Osteogenic Differentiation. *Chem. A Eur. J.* **2023**, *29*, e202203166. [CrossRef]
136. Akbari, N.; Khorshidi, S.; Karkhaneh, A. Effect of piezoelectricity of nanocomposite electrospun scaffold on cell behavior in bone tissue engineering. *Iran. Polym. J.* **2022**, *31*, 919–930. [CrossRef]
137. Dong, Y.; Suryani, L.; Zhou, X.; Muthukumaran, P.; Rakshit, M.; Yang, F.; Wen, F.; Hassanbhai, A.M.; Parida, K.; Simon, D.T.; et al. Synergistic Effect of PVDF-Coated PCL-TCP Scaffolds and Pulsed Electromagnetic Field on Osteogenesis. *Int. J. Mol. Sci.* **2021**, *22*, 6438. [CrossRef]
138. Alimohammadi, M.; Ramazani, S.A.A. Surface modification of polyether ether ketone implant with a novel nanocomposite coating containing poly (vinylidene fluoride) toward improving piezoelectric and bioactivity performance. *Colloids Surf. B Biointerfaces* **2023**, *222*, 113098. [CrossRef] [PubMed]
139. Fakhri, V.; Jafari, A.; Zeraatkar, A.; Rahimi, M.; Hadian, H.; Nouranian, S.; Kruppke, B.; Khonakdar, H.A. Introducing photo-crosslinked bio-nanocomposites based on polyvinylidene fluoride/poly(glycerol azelaic acid)-*g*-glycidyl methacrylate for bone tissue engineering. *J. Mater. Chem. B* **2023**, *11*, 452–470. [CrossRef] [PubMed]
140. Fernandes, M.M.; Correia, D.M.; Ribeiro, C.; Castro, N.; Correia, V.; Lanceros-Mendez, S. Bioinspired Three-Dimensional Magnetoactive Scaffolds for Bone Tissue Engineering. *ACS Appl. Mater. Interfaces* **2019**, *11*, 45265–45275. [CrossRef] [PubMed]
141. Hermenegildo, B.; Ribeiro, C.; Pérez-Álvarez, L.; Vilas, J.L.; Learmonth, D.A.; Sousa, R.A.; Martins, P.; Lanceros-Méndez, S. Hydrogel-based magnetoelectric microenvironments for tissue stimulation. *Colloids Surf. B Biointerfaces* **2019**, *181*, 1041–1047. [CrossRef]
142. Karanth, D.; Puleo, D.; Dawson, D.; Holliday, L.S.; Sharab, L. Characterization of 3D printed biodegradable piezoelectric scaffolds for bone regeneration. *Clin. Exp. Dent. Res.* **2023**, *9*, 398–408. [CrossRef]
143. Polak, M.; Berniak, K.; Szewczyk, P.K.; Karbowniczek, J.E.; Marzec, M.M.; Stachewicz, U. PLLA scaffolds with controlled surface potential and piezoelectricity for enhancing cell adhesion in tissue engineering. *Appl. Surf. Sci.* **2023**, *621*, 156835. [CrossRef]
144. Das, R.; Curry, E.J.; Le, T.T.; Awale, G.; Liu, Y.; Li, S.; Contreras, J.; Bednarz, C.; Millender, J.; Xin, X.; et al. Biodegradable nanofiber bone-tissue scaffold as remotely-controlled and self-powering electrical stimulator. *Nano Energy* **2020**, *76*, 105028. [CrossRef]
145. Tai, Y.; Yang, S.; Yu, S.; Banerjee, A.; Myung, N.V.; Nam, J. Modulation of piezoelectric properties in electrospun PLLA nanofibers for application-specific self-powered stem cell culture platforms. *Nano Energy* **2021**, *89*, 106444. [CrossRef]

146. Lai, C.; Jin, F.; Feng, Z.; Zhang, R.; Yuan, M.; Qian, L.; Zhang, L.; Wang, Y.; Zhao, J. Combining Piezoelectric Stimulation and Extracellular Vesicles for Cartilage Regeneration. *J. Tissue Eng. Regen. Med.* **2023**, *2023*, 5539194. [CrossRef]
147. Liu, Q.; Xie, S.; Fan, D.; Xie, T.; Xue, G.; Gou, X.; Li, X. Integrated osteochondral differentiation of mesenchymal stem cells on biomimetic nanofibrous mats with cell adhesion-generated piezopotential gradients. *Nanoscale* **2022**, *14*, 3865–3877. [CrossRef]
148. Liu, Y.; Dzidotor, G.; Le, T.T.; Vinikoor, T.; Morgan, K.; Curry, E.J.; Das, R.; McClinton, A.; Eisenberg, E.; Apuzzo, L.N.; et al. Exercise-induced piezoelectric stimulation for cartilage regeneration in rabbits. *Sci. Transl. Med.* **2022**, *14*, eabi7282. [CrossRef] [PubMed]
149. Correia, D.M.; Ribeiro, C.; Botelho, G.; Borges, J.; Lopes, C.; Vaz, F.; Carabineiro, S.A.C.; Machado, A.V.; Lanceros-Méndez, S. Superhydrophilic poly(l-lactic acid) electrospun membranes for biomedical applications obtained by argon and oxygen plasma treatment. *Appl. Surf. Sci.* **2016**, *371*, 74–82. [CrossRef]
150. Ando, M.; Takeshima, S.; Ishiura, Y.; Ando, K.; Onishi, O. Piezoelectric antibacterial fabric comprised of poly(l-lactic acid) yarn. *Jpn. J. Appl. Phys.* **2017**, *56*, 10PG01. [CrossRef]
151. Gazvoda, L.; Perišić Nanut, M.; Spreitzer, M.; Vukomanović, M. Antimicrobial activity of piezoelectric polymer: Piezoelectricity as the reason for damaging bacterial membrane. *Biomater. Sci.* **2022**, *10*, 4933–4948. [CrossRef]
152. Zheng, T.; Yu, Y.; Pang, Y.; Zhang, D.; Wang, Y.; Zhao, H.; Zhang, X.; Leng, H.; Yang, X.; Cai, Q. Improving bone regeneration with composites consisting of piezoelectric poly(l-lactide) and piezoelectric calcium/manganese co-doped barium titanate nanofibers. *Compos. Part B Eng.* **2022**, *234*, 109734. [CrossRef]
153. Yang, Y.; Peng, S.; Qi, F.; Zan, J.; Liu, G.; Zhao, Z.; Shuai, C. Graphene-assisted barium titanate improves piezoelectric performance of biopolymer scaffold. *Mater. Sci. Eng. C* **2020**, *116*, 111195. [CrossRef]
154. Li, Y.; Dai, X.; Bai, Y.; Liu, Y.; Wang, Y.; Liu, O.; Yan, F.; Tang, Z.; Zhang, X.; Deng, X. Electroactive $BaTiO_3$ nanoparticle-functionalized fibrous scaffolds enhance osteogenic differentiation of mesenchymal stem cells. *Int. J. Nanomed.* **2017**, *12*, 4007–4018. [CrossRef]
155. Vukomanović, M.; Gazvoda, L.; Kurtjak, M.; Maček-Kržmanc, M.; Spreitzer, M.; Tang, Q.; Wu, J.; Ye, H.; Chen, X.; Mattera, M.; et al. Filler-Enhanced Piezoelectricity of Poly- *L* -Lactide and Its Use as a Functional Ultrasound-Activated Biomaterial. *Small* **2023**, *19*, 2301981. [CrossRef]
156. Liu, W.; Shi, Y.; Sun, Z.; Zhang, L. Poling-Free Hydroxyapatite/Polylactide Nanogenerator with Improved Piezoelectricity for Energy Harvesting. *Micromachines* **2022**, *13*, 889. [CrossRef]
157. Hu, X.; Hu, Y.; Guo, Z.; Liu, S.; Zhang, Q.; Zhang, X.; Xiang, Y. High-energy conversion-efficiency direct-alternating-current hybrid generator with piezoelectric polylactide and dynamic Schottky diode. *J. Mater. Sci.* **2020**, *55*, 9014–9026. [CrossRef]
158. Santos, D.; Correia, C.O.; Silva, D.M.; Gomes, P.S.; Fernandes, M.H.; Santos, J.D.; Sencadas, V. Incorporation of glass-reinforced hydroxyapatite microparticles into poly(lactic acid) electrospun fibre mats for biomedical applications. *Mater. Sci. Eng. C* **2017**, *75*, 1184–1190. [CrossRef] [PubMed]
159. Santos, D.; Silva, D.M.; Gomes, P.S.; Fernandes, M.H.; Santos, J.D.; Sencadas, V. Multifunctional PLLA-ceramic fiber membranes for bone regeneration applications. *J. Colloid Interface Sci.* **2017**, *504*, 101–110. [CrossRef] [PubMed]
160. Nazir, F.; Abbas, L.; Iqbal, M. A comparative insight into the mechanical properties, antibacterial potential, and cytotoxicity profile of nano-hydroxyapatite and nano-whitlockite-incorporated poly-L-lactic acid for bone tissue engineering. *Appl. Nanosci.* **2022**, *12*, 47–68. [CrossRef]
161. Peng, W.; Zheng, W.; Shi, K.; Wang, W.; Shao, Y.; Zhang, D. An in vivo evaluation of PLLA/PLLA-gHA nano-composite for internal fixation of mandibular bone fractures. *Biomed. Mater.* **2015**, *10*, 065007. [CrossRef]
162. Zimina, A.; Senatov, F.; Choudhary, R.; Kolesnikov, E.; Anisimova, N.; Kiselevskiy, M.; Orlova, P.; Strukova, N.; Generalova, M.; Manskikh, V.; et al. Biocompatibility and Physico-Chemical Properties of Highly Porous PLA/HA Scaffolds for Bone Reconstruction. *Polymers* **2020**, *12*, 2938. [CrossRef]
163. Lai, Y.-H.; Chen, Y.-H.; Pal, A.; Chou, S.-H.; Chang, S.-J.; Huang, E.-W.; Lin, Z.-H.; Chen, S.-Y. Regulation of cell differentiation via synergistic self-powered stimulation and degradation behavior of a biodegradable composite piezoelectric scaffold for cartilage tissue. *Nano Energy* **2021**, *90*, 106545. [CrossRef]
164. Pariy, I.O.; Chernozem, R.V.; Chernozem, P.V.; Mukhortova, Y.R.; Skirtach, A.G.; Shvartsman, V.V.; Lupascu, D.C.; Surmeneva, M.A.; Mathur, S.; Surmenev, R.A. Hybrid biodegradable electrospun scaffolds based on poly(l-lactic acid) and reduced graphene oxide with improved piezoelectric response. *Polym. J.* **2022**, *54*, 1237–1252. [CrossRef]
165. Por Hajrezaei, S.; Haghbin Nazarpak, M.; Hojjati Emami, S.; Shahryari, E. Biocompatible and Electroconductive Nanocomposite Scaffolds with Improved Piezoelectric Response for Bone Tissue Engineering. *Int. J. Polym. Sci.* **2022**, *2022*, 4521937. [CrossRef]
166. Sekkarapatti Ramasamy, M.; Krishnamoorthi Kaliannagounder, V.; Rahaman, A.; Park, C.H.; Kim, C.S.; Kim, B. Synergistic Effect of Reinforced Multiwalled Carbon Nanotubes and Boron Nitride Nanosheet-Based Hybrid Piezoelectric PLLA Scaffold for Efficient Bone Tissue Regeneration. *ACS Biomater. Sci. Eng.* **2022**, *8*, 3542–3556. [CrossRef]
167. Ribeiro, C.; Pärssinen, J.; Sencadas, V.; Correia, V.; Miettinen, S.; Hytönen, V.P.; Lanceros-Méndez, S. Dynamic Piezoelectric Stimulation Enhances Osteogenic Differentiation of Human Adipose Stem Cells. *J. Biomed. Mater. Res. Part A* **2015**, *103*, 2172–2175. Available online: https://onlinelibrary.wiley.com/doi/full/10.1002/jbm.a.35368 (accessed on 18 January 2024). [CrossRef]
168. Reis, J.; Frias, C.; Canto e Castro, C.; Botelho, M.L.; Marques, A.T.; Simões, J.A.O.; Capela e Silva, F.; Potes, J. A New Piezoelectric Actuator Induces Bone Formation In Vivo: A Preliminary Study. *BioMed Res. Int.* **2012**, *2012*, 613403. [CrossRef]

169. Mohamed, S.S.; Zaki, H.F.; Raafat, S.N. The Effect of Clopidogrel and Ticagrelor on Human Adipose Mesenchymal Stem Cell Osteogenic Differentiation Potential: In Vitro Comparative Study. *Adv. Pharmacol. Pharm. Sci.* **2024**, *2024*, 2990670. [CrossRef] [PubMed]
170. Ribeiro, C.; Correia, D.M.; Rodrigues, I.; Guardão, L.; Guimarães, S.; Soares, R.; Lanceros-Méndez, S. In vivo demonstration of the suitability of piezoelectric stimuli for bone reparation. *Mater. Lett.* **2017**, *209*, 118–121. [CrossRef]
171. Electrosprayed Poly(vinylidene fluoride) Microparticles for Tissue Engineering Applications—RSC Advances (RSC Publishing). Available online: https://pubs.rsc.org/en/content/articlehtml/2014/ra/c4ra04581e (accessed on 18 January 2024).
172. Zhang, C.; Liu, W.; Cao, C.; Zhang, F.; Tang, Q.; Ma, S.; Zhao, J.; Hu, L.; Shen, Y.; Chen, L. Modulating Surface Potential by Controlling the β Phase Content in Poly(vinylidene fluoridetrifluoroethylene) Membranes Enhances Bone Regeneration. *Adv. Healthc. Mater.* **2018**, *7*, 1701466. Available online: https://onlinelibrary.wiley.com/doi/full/10.1002/adhm.201701466 (accessed on 18 January 2024). [CrossRef]
173. Damaraju, S.M.; Shen, Y.; Elele, E.; Khusid, B.; Eshghinejad, A.; Li, J.; Jaffe, M.; Arinzeh, T.L. Three-dimensional piezoelectric fibrous scaffolds selectively promote mesenchymal stem cell differentiation. *Biomaterials* **2017**, *149*, 51–62. [CrossRef] [PubMed]
174. Lyons, J.G.; Plantz, M.A.; Hsu, W.K.; Hsu, E.L.; Minardi, S. Nanostructured Biomaterials for Bone Regeneration. *Front. Bioeng. Biotechnol.* **2020**, *8*, 922. [CrossRef]
175. Ning, C.; Zhou, Z.; Tan, G.; Zhu, Y.; Mao, C. Electroactive polymers for tissue regeneration: Developments and perspectives. *Prog. Polym. Sci.* **2018**, *81*, 144–162. [CrossRef]
176. Prabhakaran, M.P.; Venugopal, J.; Ramakrishna, S. Electrospun nanostructured scaffolds for bone tissue engineering. *Acta Biomater.* **2009**, *5*, 2884–2893. [CrossRef]
177. Ikada, Y.; Shikinami, Y.; Hara, Y.; Tagawa, M.; Fukada, E. Enhancement of Bone Formation by Drawn Poly (L-lactide). *J. Biomed. Mater. Res.* **1996**, *30*, 553–558. Available online: https://onlinelibrary.wiley.com/doi/abs/10.1002/(SICI)1097-4636(199604)30:4%3C553::AID-JBM14%3E3.0.CO;2-I (accessed on 18 January 2024). [CrossRef]
178. Liu, S.; Wu, J.; Liu, X.; Chen, D.; Bowlin, G.L.; Cao, L.; Lu, J.; Li, F.; Mo, X.; Fan, C. Osteochondral Regeneration Using an Oriented Nanofiber Yarn-Collagen Type I/Hyaluronate Hybrid/TCP Biphasic Scaffold. *J. Biomed. Mater. Res. Part A* **2015**, *103*, 581–592. Available online: https://onlinelibrary.wiley.com/doi/full/10.1002/jbm.a.35206 (accessed on 18 January 2024). [CrossRef]
179. Zhang, S.; Chen, L.; Jiang, Y.; Cai, Y.; Xu, G.; Tong, T.; Zhang, W.; Wang, L.; Ji, J.; Shi, P.; et al. Bi-layer collagen/microporous electrospun nanofiber scaffold improves the osteochondral regeneration. *Acta Biomater.* **2013**, *9*, 7236–7247. [CrossRef] [PubMed]
180. Herrero-Herrero, M.; Alberdi-Torres, S.; González-Fernández, M.L.; Vilariño-Feltrer, G.; Rodríguez-Hernández, J.C.; Vallés-Lluch, A.; Villar-Suárez, V. Influence of chemistry and fiber diameter of electrospun PLA, PCL and their blend membranes, intended as cell supports, on their biological behavior. *Polym. Test.* **2021**, *103*, 107364. [CrossRef]
181. Chorsi, M.T.; Curry, E.J.; Chorsi, H.T.; Das, R.; Baroody, J.; Purohit, P.K.; Ilies, H.; Nguyen, T.D. Piezoelectric Biomaterials for Sensors and Actuators. *Adv. Mater.* **2019**, *31*, 1802084. [CrossRef] [PubMed]
182. Khare, D.; Basu, B.; Dubey, A.K. Electrical stimulation and piezoelectric biomaterials for bone tissue engineering applications. *Biomaterials* **2020**, *258*, 120280. [CrossRef]
183. Wang, Y.-W.; Wu, Q.; Chen, G.-Q. Attachment, proliferation and differentiation of osteoblasts on random biopolyester poly(3-hydroxybutyrate-co-3-hydroxyhexanoate) scaffolds. *Biomaterials* **2004**, *25*, 669–675. [CrossRef]
184. Wang, Y.-W.; Wu, Q.; Chen, J.; Chen, G.-Q. Evaluation of three-dimensional scaffolds made of blends of hydroxyapatite and poly(3-hydroxybutyrate-co-3-hydroxyhexanoate) for bone reconstruction. *Biomaterials* **2005**, *26*, 899–904. [CrossRef]
185. Goonoo, N.; Bhaw-Luximon, A.; Passanha, P.; Esteves, S.R.; Jhurry, D. Third generation poly(hydroxyacid) composite scaffolds for tissue engineering. *J. Biomed. Mater. Res.* **2017**, *105*, 1667–1684. [CrossRef]
186. Bretcanu, O.; Misra, S.K.; Yunos, D.M.; Boccaccini, A.R.; Roy, I.; Kowalczyk, T.; Blonski, S.; Kowalewski, T.A. Electrospun nanofibrous biodegradable polyester coatings on Bioglass®-based glass-ceramics for tissue engineering. *Mater. Chem. Phys.* **2009**, *118*, 420–426. [CrossRef]
187. Silva, M.J.; Dias, Y.J.; Zaszczyńska, A.; Robles, J.R.; Abiade, J.; Kowalczyk, T.; Kołbuk, D.; Sajkiewicz, P.Ł.; Yarin, A.L. Biocomposite-based fibrous scaffolds of natural rubber/polyhydroxybutyrate blend reinforced with 45S5 bioglass aiming at biomedical applications. *Polym. Compos.* **2023**, *45*, 1107–1127. [CrossRef]
188. Fukada, E.; Ando, Y. Piezoelectric properties of poly-β-hydroxybutyrate and copolymers of β-hydroxybutyrate and β-hydroxyvalerate. *Int. J. Biol. Macromol.* **1986**, *8*, 361–366. [CrossRef]
189. Soleymani Eil Bakhtiari, S.; Karbasi, S.; Toloue, E.B. Modified poly(3-hydroxybutyrate)-based scaffolds in tissue engineering applications: A review. *Int. J. Biol. Macromol.* **2021**, *166*, 986–998. [CrossRef] [PubMed]
190. Sheng, R.; Mu, J.; Chernozem, R.V.; Mukhortova, Y.R.; Surmeneva, M.A.; Pariy, I.O.; Ludwig, T.; Mathur, S.; Xu, C.; Surmenev, R.A.; et al. Fabrication and Characterization of Piezoelectric Polymer Composites and Cytocompatibility with Mesenchymal Stem Cells. *ACS Appl. Mater. Interfaces* **2023**, *15*, 3731–3743. [CrossRef] [PubMed]
191. Chernozem, R.V.; Surmeneva, M.A.; Surmenev, R.A. Hybrid biodegradable scaffolds of piezoelectric polyhydroxybutyrate and conductive polyaniline: Piezocharge constants and electric potential study. *Mater. Lett.* **2018**, *220*, 257–260. [CrossRef]
192. Dan, L.; Cheng, Q.; Narain, R.; Krause, B.; Pötschke, P.; Elias, A. Three-Dimensional Printed and Biocompatible Conductive Composites Comprised of Polyhydroxybutyrate and Multiwalled Carbon Nanotubes. *Ind. Eng. Chem. Res.* **2021**, *60*, 885–897. [CrossRef]

193. Malmonge, J.A.; Malmonge, L.F.; Fuzari, G.C.; Malmonge, S.M.; Sakamoto, W.K. Piezo and dielectric properties of PHB–PZT composite. *Polym. Compos.* **2009**, *30*, 1333–1337. [CrossRef]
194. Sadat-Shojai, M.; Khorasani, M.-T.; Jamshidi, A.; Irani, S. Nano-hydroxyapatite reinforced polyhydroxybutyrate composites: A comprehensive study on the structural and in vitro biological properties. *Mater. Sci. Eng. C* **2013**, *33*, 2776–2787. [CrossRef]
195. Misra, S.K.; Mohn, D.; Brunner, T.J.; Stark, W.J.; Philip, S.E.; Roy, I.; Salih, V.; Knowles, J.C.; Boccaccini, A.R. Comparison of nanoscale and microscale bioactive glass on the properties of P(3HB)/Bioglass® composites. *Biomaterials* **2008**, *29*, 1750–1761. [CrossRef] [PubMed]
196. Medvecky, L. Microstructure and Properties of Polyhydroxybutyrate-Chitosan-Nanohydroxyapatite Composite Scaffolds. *Sci. World J.* **2012**, *2012*, 537973. [CrossRef]
197. Datta, A.; Choi, Y.S.; Chalmers, E.; Ou, C.; Kar-Narayan, S. Piezoelectric Nylon-11 Nanowire Arrays Grown by Template Wetting for Vibrational Energy Harvesting Applications. *Adv. Funct. Mater.* **2017**, *27*, 1604262. [CrossRef]
198. Wang, H.; Li, Y.; Zuo, Y.; Li, J.; Ma, S.; Cheng, L. Biocompatibility and osteogenesis of biomimetic nano-hydroxyapatite/polyamide composite scaffolds for bone tissue engineering. *Biomaterials* **2007**, *28*, 3338–3348. [CrossRef]
199. Cecen, B.; Hassan, S.; Li, X.; Zhang, Y.S. Smart Biomaterials in Biomedical Applications: Current Advances and Possible Future Directions. *Macromol. Biosci.* **2024**, *24*, 2200550. [CrossRef] [PubMed]
200. Oflaz, K.; Özaytekin, İ. Analysis of electrospinning and additive effect on β phase content of electrospun PVDF nanofiber mats for piezoelectric energy harvester nanogenerators. *Smart Mater. Struct.* **2022**, *31*, 105022. [CrossRef]
201. Ali, M.; Bathaei, M.J.; Istif, E.; Karimi, S.N.H.; Beker, L. Biodegradable Piezoelectric Polymers: Recent Advancements in Materials and Applications. *Adv. Healthc. Mater.* **2023**, *12*, 2300318. [CrossRef] [PubMed]
202. Huang, Y.; Deng, H.; Fan, Y.; Zheng, L.; Che, J.; Li, X.; Aifantis, K.E. Conductive nanostructured Si biomaterials enhance osteogeneration through electrical stimulation. *Mater. Sci. Eng. C* **2019**, *103*, 109748. [CrossRef]
203. Jing, W.; Huang, Y.; Wei, P.; Cai, Q.; Yang, X.; Zhong, W. Roles of electrical stimulation in promoting osteogenic differentiation of BMSCs on conductive fibers. *J. Biomed. Mater. Res* **2019**, *107*, 1443–1454. [CrossRef]
204. Meng, S.; Zhang, Z.; Rouabhia, M. Accelerated osteoblast mineralization on a conductive substrate by multiple electrical stimulation. *J. Bone Min. Metab.* **2011**, *29*, 535–544. [CrossRef] [PubMed]
205. Shi, G.; Rouabhia, M.; Meng, S.; Zhang, Z. Electrical stimulation enhances viability of human cutaneous fibroblasts on conductive biodegradable substrates. *J. Biomed. Mater. Res.* **2008**, *84A*, 1026–1037. [CrossRef]
206. Zhu, S.; Jing, W.; Hu, X.; Huang, Z.; Cai, Q.; Ao, Y.; Yang, X. Time-dependent effect of electrical stimulation on osteogenic differentiation of bone mesenchymal stromal cells cultured on conductive nanofibers. *J. Biomed. Mater. Res.* **2017**, *105*, 3369–3383. [CrossRef] [PubMed]
207. Martino, F.; Perestrelo, A.R.; Vinarský, V.; Pagliari, S.; Forte, G. Cellular Mechanotransduction: From Tension to Function. *Front. Physiol.* **2018**, *9*, 824. [CrossRef]
208. Mycielska, M.E.; Djamgoz, M.B.A. Cellular mechanisms of direct-current electric field effects: Galvanotaxis and metastatic disease. *J. Cell Sci.* **2004**, *117*, 1631–1639. [CrossRef]
209. Maziarz, A.; Kocan, B.; Bester, M.; Budzik, S.; Cholewa, M.; Ochiya, T.; Banas, A. How electromagnetic fields can influence adult stem cells: Positive and negative impacts. *Stem Cell Res. Ther.* **2016**, *7*, 54. [CrossRef] [PubMed]
210. Saliev, T.; Mustapova, Z.; Kulsharova, G.; Bulanin, D.; Mikhalovsky, S. Therapeutic potential of electromagnetic fields for tissue engineering and wound healing. *Cell Prolif.* **2014**, *47*, 485–493. [CrossRef] [PubMed]
211. Bar, J.K.; Lis-Nawara, A.; Kowalczyk, T.; Grelewski, P.G.; Stamnitz, S.; Gerber, H.; Klimczak, A. Osteogenic Potential of Human Dental Pulp Stem Cells (hDPSCs) Growing on Poly L-Lactide-Co-Caprolactone and Hyaluronic Acid (HYAFF-11TM) Scaffolds. *Int. J. Mol. Sci.* **2023**, *24*, 16747. [CrossRef] [PubMed]
212. Cai, K.; Jiao, Y.; Quan, Q.; Hao, Y.; Liu, J.; Wu, L. Improved activity of MC3T3-E1 cells by the exciting piezoelectric BaTiO3/TC4 using low-intensity pulsed ultrasound. *Bioact. Mater.* **2021**, *6*, 4073–4082. [CrossRef] [PubMed]
213. Zaszczyńska, A.; Sajkiewicz, P.; Gradys, A.; Tymkiewicz, R.; Urbanek, O.; Kołbuk, D. Influence of process-material conditions on the structure and biological properties of electrospun polyvinylidene fluoride fibers. *Bull. Pol. Acad. Sci. Tech. Sci.* **2020**, *3*, 133368. [CrossRef]
214. Marino, A.A.; Rosson, J.; Gonzalez, E.; Jones, L.; Rogers, S.; Fukada, E. Quasi-static charge interactions in bone. *J. Electrost.* **1988**, *21*, 347–360. [CrossRef]

BULLETIN OF THE POLISH ACADEMY OF SCIENCES
TECHNICAL SCIENCES, Vol. 68, No. 3, 2020
DOI: 10.24425/bpasts.2020.133368

Influence of process-material conditions on the structure and biological properties of electrospun polyvinylidene fluoride fibers

A. ZASZCZYŃSKA[1]*, P.Ł. SAJKIEWICZ[1], A. GRADYS[1], R. TYMKIEWICZ[2], O. URBANEK[1], and D. KOŁBUK[1]

[1] Institute of Fundamental Technological Research, Polish Academy of Sciences, Laboratory of Polymers and Biomaterials, Pawińskiego 5B, 02-106 Warsaw, Poland
[2] Institute of Fundamental Technological Research, Polish Academy of Sciences, Department of Ultrasound, Pawińskiego 5B, 02-106 Warsaw, Poland

Abstract. Polyvinylidene fluoride (PVDF) is one of the most important piezoelectric polymers. Piezoelectricity in PVDF appears in polar β and γ phases. Piezoelectric fibers obtained by means of electrospinning may be used in tissue engineering (TE) as a smart analogue of the natural extracellular matrix (ECM). We present results showing the effect of rotational speed of the collecting drum on morphology, phase content and in vitro biological properties of PVDF nonwovens. Morphology and phase composition were analyzed using scanning electron microscopy (SEM) and Fourier-transform infrared spectroscopy (FTIR), respectively. It was shown that increasing rotational speed of the collector leads to an increase in fiber orientation, reduction in fiber diameter and considerable increase of polar phase content, both β and γ. In vitro cell culture experiments, carried out with the use of ultrasounds in order to generate electrical potential via piezoelectricity, indicate a positive effect of polar phases on fibroblasts. Our preliminary results demonstrate that piezoelectric PVDF scaffolds are promising materials for tissue engineering applications, particularly for neural tissue regeneration, where the electric potential is crucial.

Key words: scaffolds, electrospinning, polyvinylidene fluoride, tissue engineering.

1. Introduction

As regards the field of biomedical engineering, in recent decades, increasing scientific and technical interest has been observed in research related to development of composites [1] and hydrogels [2] as well as the design of polymers with nanofillers [3, 4] and smart materials [5]. Smart materials are generally designed to react in response to external stimuli (physical, chemical, mechanical) thus behaving similar to natural body tissues [6–8]. One type of such smart materials are piezoelectric scaffolds, which can generate electrical signals in response to the applied stress or vice versa, constituting sensitive mechano-electrical transduction systems. It is anticipated that such materials can effectively stimulate signaling pathways and thereby enhance tissue regeneration at the impaired site. Piezoelectric phenomena are observed in animal bodies, for example in DNA, the tendons, bones, skin, cartilage, ligaments and the dentin.

It is known that electrical charges are important for the activity of cells, particularly neural cells. The major advantage of piezoelectric scaffolds is that electrical potential can be generated non-invasively under the influence of a mechanical field, without the need to use invasive electrodes. State-of-the-art in tissue engineering is directed towards minimally invasive and "smart" technologies [9–13]. In these approaches, smart materials are reported to help avoid complex and long surgeries.

Since the discovery of strong piezoelectric activity in polyvinylidene fluoride (PVDF), intensive research has been conducted on this polymer. At least four different polymorphs, referred to as α, β, γ, and δ phases, depending on the processing conditions, have been reported [14, 15]. Among them, the β-phase, showing the highest piezoelectricity because of trans-trans molecular conformation in orthorhombic crystals, has been reported during the past 40 years in numerous works aiming at high level of β-phase (Fig. 1) [16].

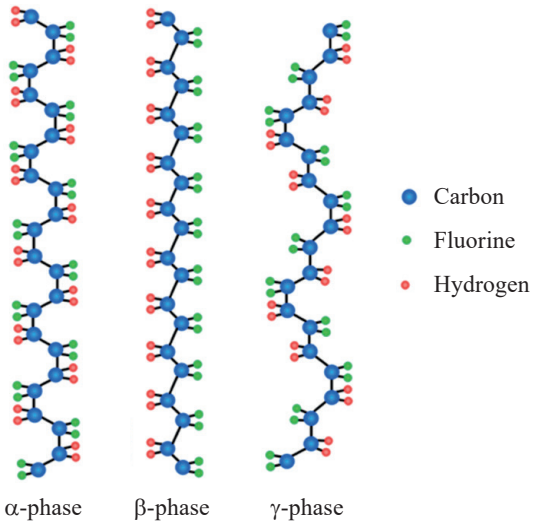

Fig. 1. Schematic representation of the chain conformation for the α, β and γ phases of PVDF

*e-mail: azasz@ippt.pan.pl

Manuscript submitted 2019-10-08, revised 2020-02-25, initially accepted for publication 2020-02-25, published in June 2020

A variety of experimental techniques, such as mechanical stretching [17], application of high pressure [18, 19], melt-quenching [20], poling under high electric field [21] and incorporating some additives (e.g. nanoparticles, nanowires, graphene) [22–26], have been investigated to induce formation of the β-phase. For piezoelectric applications, β-crystal samples must be subjected to a poling procedure to orient the CF_2 dipoles; however, they are more prone to break down under a high-electric field [27]. The presence of polar phases is very important, in particular, due to its bioelectrical effect in stimulation of the nervous system, holding promise of effective tissue regeneration [28–32]. The content of polar phases in nanofibers may also be affected by rotational speed of the collector used during electrospinning [33].

An interesting idea, reported only in few publications, is to design an innovative smart electrospun active piezoelectric scaffold for tissue engineering applications. Among polymeric materials, PVDF nanofibers have the strongest piezoelectric properties with practically no aging of piezoelectricity at the body temperature of mammals [34], rendering it biologically very attractive [35–38].

We recall the studies on the effect of rotational speed of the collecting drum on phase content, morphology and in vitro biological properties of PVDF nonwovens.

2. Materials and methods

2.1. Materials. Polyvinylidene fluoride (PVDF) nonwovens were formed using the electrospinning process from a mixture of acetone and an N,N′-dimethylformamide (DMF) solution. PVDF pellets (Kynar, $M_W = 400{,}000$ g/mol) were purchased from Arkema while high purity acetone and DMF were obtained from Merck.

Solutions of PVDF at the concentrations of 17, 19 and 22 (w/v%) were prepared by dissolving PVDF pellets in the DMF/acetone mixture of solvents at a 4:1 ratio. First, PVDF pellets were dissolved in DMF for 4 hours at 70°C, then acetone was added and the solution was mixed for 2h at room temperature to receive a homogeneous solution.

2.2. Electrospinning process. The electrospinning setup (Fig. 2) consisted of a syringe ended with a 0.3 mm needle facing a grounded rotating drum collector (4 cm radius and 12 cm in length). A high voltage generator with a positive terminal was connected to the stainless steel needle. The distance between the needle and the collector was 180 mm, flow rate of the solution was 600 µl/h. The applied voltage was in the range of 16–18 kV, which was optimum for obtaining uniform fibers and for maintaining a stable electrospinning process. Collecting of the fibers was performed at three rotational speeds of the collector: 100, 900 and 1000 rpm. The electrospinning process was conducted horizontally. After electrospinning, nonwovens were placed under a fume hood for 48 hours to remove solvent residue.

Samples were labeled with collector rotational speed and, if necessary, additional information was provided in the text or in the descriptions of figures.

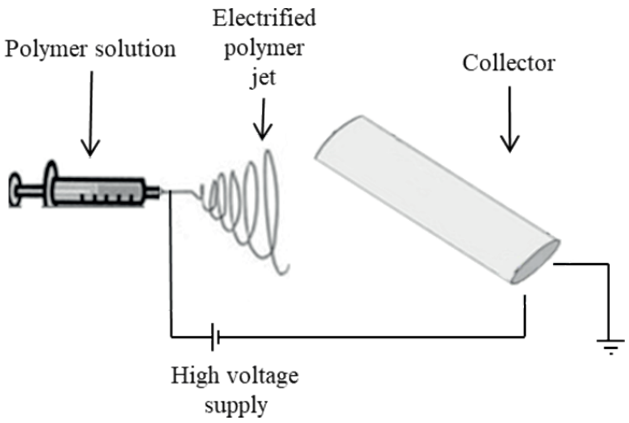

Fig. 2. Scheme of conventional electrospinning setup used with a rotating collector

2.3. Solution viscosity measurements. Solution viscosity was measured using a Brookfield HADV-III Ultra rotational viscometer with cone-plate configuration. In addition to the viscosity measurements at various shear rates, viscosity measurements at a constant shear rate ≈ 33 1/s were performed as a function of time during solution preparation in order to determine stability of the solution. The shear rate ≈ 33 1/s corresponds to the value estimated for the shear rate, inside the applied needle (1):

$$\gamma = \frac{4Q}{\pi r^3} \tag{1}$$

where Q is the volumetric flow rate (600 µL/h) and r is the inner needle radius (0.17 mm).

2.4. Scanning electron microscopy. Scanning electron microscopy (SEM) imaging was performed using scanning electron microscopy (SEM, Jeol JSM-6010PLUS/LV InTouchScope™) in order to determine the distribution of fiber orientation and diameter as a function of collector rotational speed. Before imaging, the nonwovens were coated with gold. The acceleration voltage was 10 kV. Data analysis was performed using ImageJ software. The fibers diameter distribution was determined by means of 100 measurements for each sample, using Gaussian function approximation. The fibers orientation distribution was determined using ImageJ software with a Directionality plugin. Half width was calculated using Pearson VII function for approximation of orientation distribution.

2.5. Fourier-transform infrared spectroscopy (FTIR). Fourier-transform infrared (FTIR) analysis was performed using the Perkin Elmer FTIR-ATR 100 instrument, MA, USA, and the data presented are representative of three independent samples and runs. The samples were scanned from 400 to 4000 cm^{-1} with a resolution of 2 cm^{-1} and a total of 32 scans.

The relative fraction of two polar phases, β and γ, in addition to non-polar α was determined according to the procedure

described in [38]. This method allows to determine relative amounts of the electroactive β and γ phases, F_{EA}, in terms of crystalline components in any samples such as a sample containing two phases ($\alpha + \beta$, $\alpha + \gamma$, or $\beta + \gamma$) or three phases ($\alpha + \beta + \gamma$):

$$F_{EA} = \frac{I_{840^*}}{\left(\frac{K_{840^*}}{K_{763}}\right) I_{763} + I_{840^*}} \times 100\% \tag{2}$$

where, characteristic absorption I_{840^*} and I_{763} are bands at 837–841 cm^{-1}, which can be assigned to both β and γ phases, and at 763 cm^{-1} attributed to an α phase, respectively, assuming these absorption bands follow the Beer-Lambert law with absorption coefficients of $K_{763} = 6.1 \times 10^4$ and $K_{840^*} = 7.7 \times 104$ cm^2 mol^{-1}.

Quantification of individual β and γ phases content, F(β) and F(γ), was performed by using the absorbance (peak area or peak height) of the two bands at 1275 and 1234 cm^{-1}. However, a much more preferable method is proposed by calculating the peak-to-valley height ratio between the peaks around at 1275 and 1234 cm^{-1} and their nearest valleys:

$$F(\beta) = F_{EA} \times \left(\frac{\Delta H_{\beta'}}{\Delta H_{\beta'} + \Delta H_{\gamma'}} \right) \times 100\% \tag{3}$$

$$F(\gamma) = F_{EA} \times \left(\frac{\Delta H_{\gamma'}}{\Delta H_{\beta'} + \Delta H_{\gamma'}} \right) \times 100\% \tag{4}$$

where, $\Delta H_{\beta'}$ and $\Delta H_{\gamma'}$ are the height differences (absorbance differences) between the peak present at 1275 cm^{-1} and the nearest valley present at 1260 cm^{-1}, and the peak present at 1234 cm^{-1} and the nearest valley present at 1225 cm^{-1}, respectively.

2.6. Cellular studies. Polyvinylidene fluoride (PVDF) nanofibers were subjected to in vitro cellular studies. In the stimulation experiments, L929 fibroblast cells cultured on piezoelectric PVDF scaffolds, collected at various rotational speeds of the collector, were exposed to ultrasounds for 30 minutes, once a day, for 7 days. Ultrasound stimulus with the power of 20 mW/cm^2 and 80 mW/cm^2 at the frequency of 1.7 MHz was applied (Fig. 3). In order to confirm the piezoelectric effect of the PVDF scaffolds on fibroblasts activity, piezoelectric PVDF scaffolds without ultrasonic stimulation were used as a control (0 mW/cm^2) and a fibroblasts mitochondrial activity (MTT) test was conducted.

Observations of cell morphology on fibers were conducted using SEM.

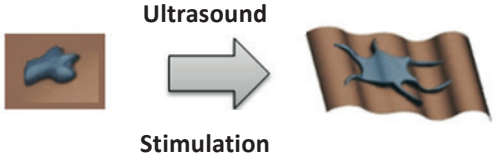

Fig. 3. Schematic illustration of the influence of ultrasound stimulation on the shape of L929 fibroblast cell

3. Results

3.1. Solution viscosity measurements. One of the most important material parameters of electrospinning is viscosity. It defines the resistance of the fluid to flow, thus stabilizing the jet. Viscosity is directly proportional to the concentration of the solution and to the molecular weight of the polymer.

From shear rate dependence in Fig. 4, it is evident that the shear thinning effect is seen only for the highest solution concentration, while for the lower concentrations the solutions behave like Newtonian fluids. The shear thinning effect is most probably related to an effective molecular orientation at higher shear rates. From the viscosity over time dependence (Fig. 5),

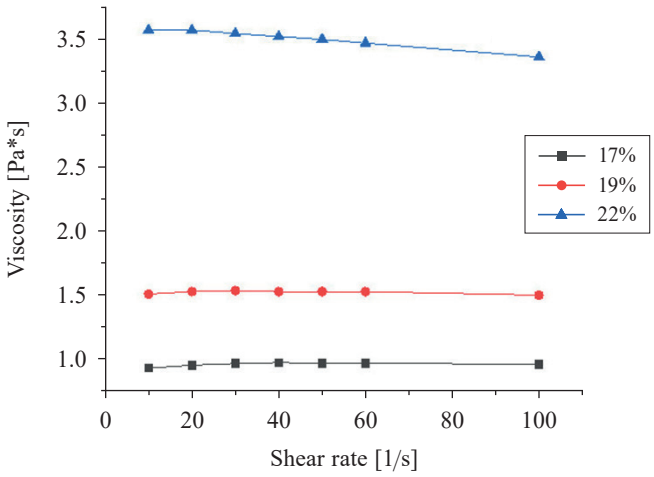

Fig. 4. Viscosity as a function of shear rate for various PVDF concentrations

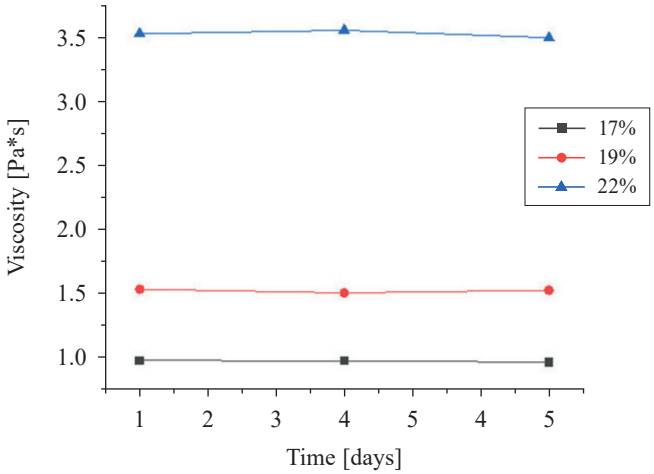

Fig. 5. Viscosity as a function of time (at shear rate = 33 1/s) for various PVDF concentrations

measured from the moment of solution preparation, it is seen that irrespective of the polymer concentration used, the solution is stable over time.

3.2. Electrospinning and morphology of fibers. All PVDF concentrations provided a stable electrospinning process, however, beadless fibers were obtained only for PVDF concentration of 22%. This solution was subjected to further studies.

In Figs. 6–8, SEM images and fiber diameter and orientation distribution for various collector rotational speeds are presented. The fiber diameter was in the range from 200 nm to 1.4 μm with the average value of 900 nm. It is seen that the average fiber diameter decreases with collector rotational speed, which is consistent with the previous results [39–44].

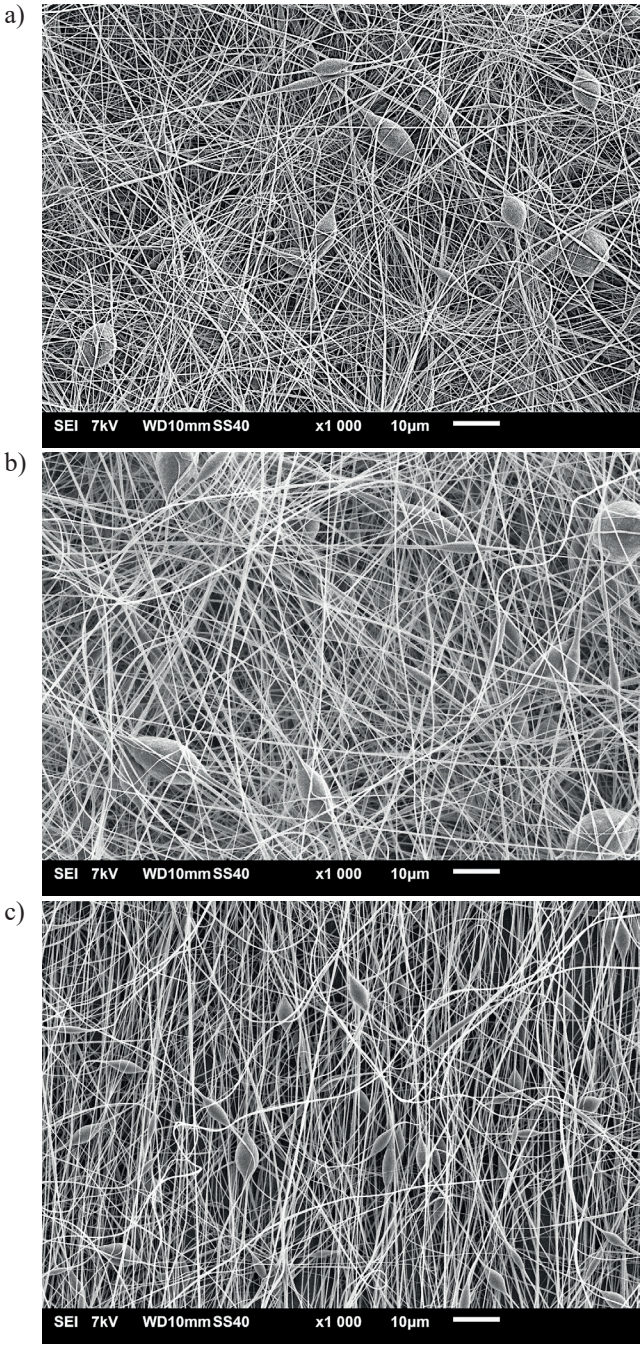

Fig. 6. SEM micrograph for nonwovens electrospun from 22% PVDF solution for different rotational speeds of the collector: a) 100 rpm, b) 900 rpm and c) 1000 rpm

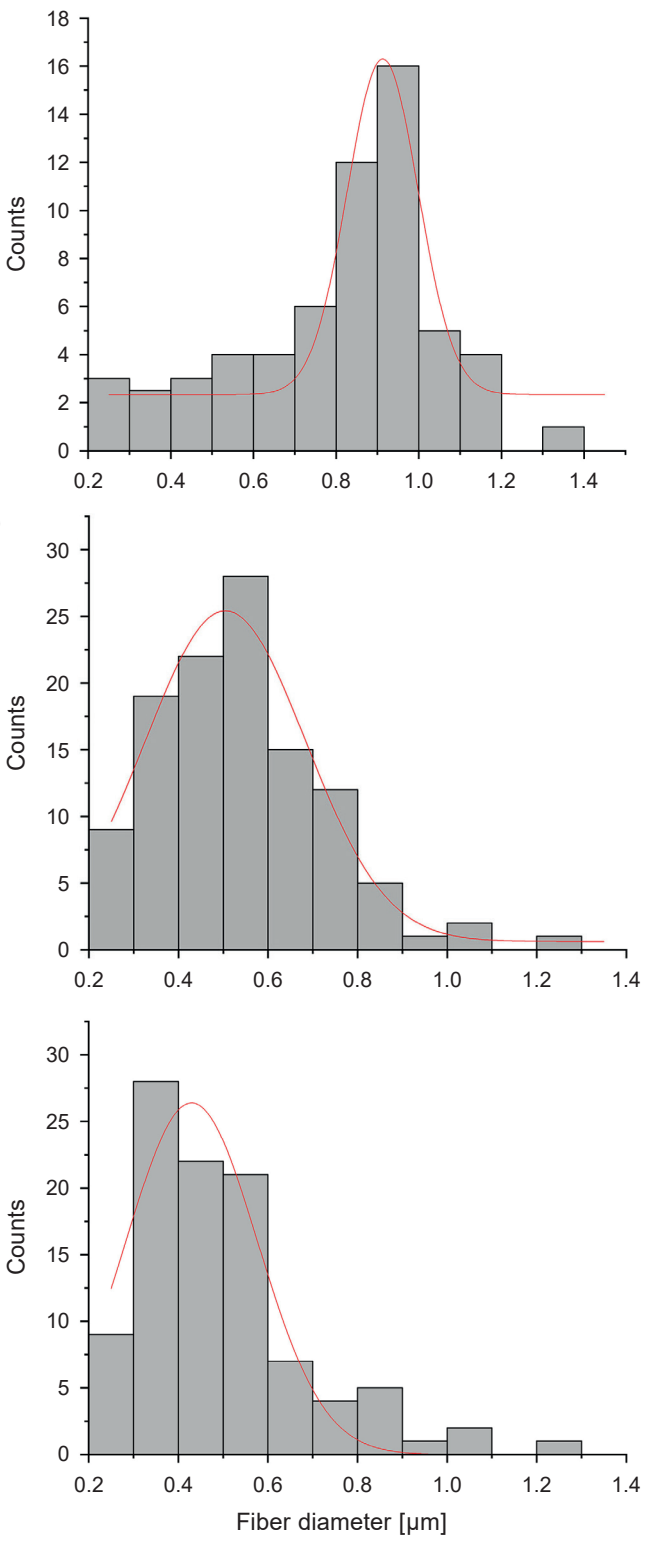

Fig. 7. Diameter distributions for nonwovens electrospun from 22% PVDF solution for different rotational speeds of the collector: a) 100 rpm, b) 900 rpm and c) 1000 rpm

This reduction is due to increasing tangential force caused by the rotating collector providing stronger mechanical stretching. From Fig. 8, it is evident that with increasing rotational speed, the fiber orientation distribution becomes narrower. The half width of the orientation distribution changes from 14.3° at 1000 rpm through 19.0° at 900 rpm to 86.1° at 100 rpm. Alignment around 90° in samples PVDF900 and PVDF1000 corresponds to the collector rotation direction.

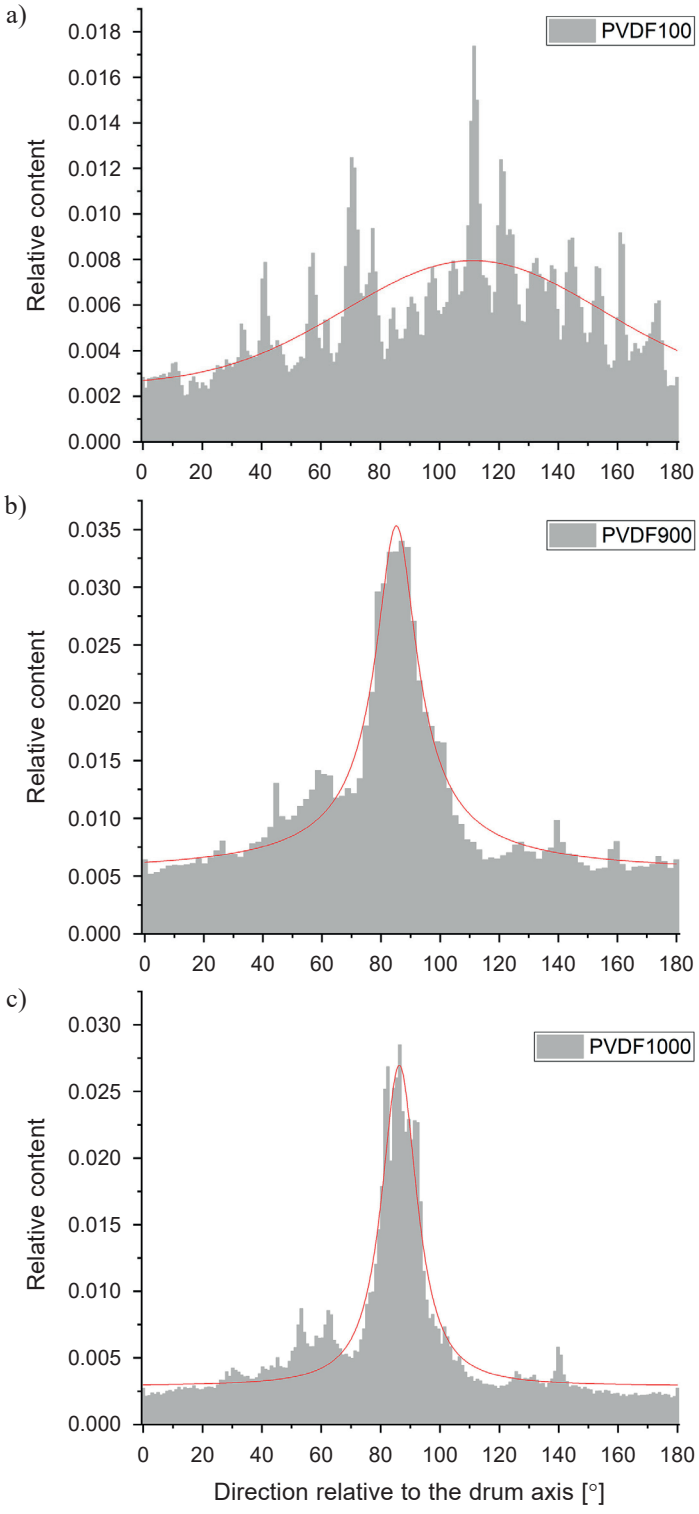

Fig. 8. Fiber orientation distribution (experimental data with numerical approximation) for nonwovens electrospun from 22% PVDF solution for different rotational speeds of the collector a) 100 rpm, b) 900 rpm and c) 1000 rpm

3.3. Fourier-transform infrared spectroscopy (FTIR). FTIR spectrum of PVDF nanofiber mats is shown in Fig. 9. Based on Equations (2–4), the relative fraction of the electroactive β and γ phases for all samples was calculated (Table 2). The randomly oriented electrospun PVDF fibers contain only 0.6% of polar phases, thus the piezoelectric effect should be negligible. At rotational speed of the collector of 900 and 1000 rpm, polar phases content is found at 76.65% and 94.48%, respectively. Thus, increasing collector rotation speed results not only in increased fiber orientation and smaller fiber diameter but also in a dramatic increase of the polar phase content.

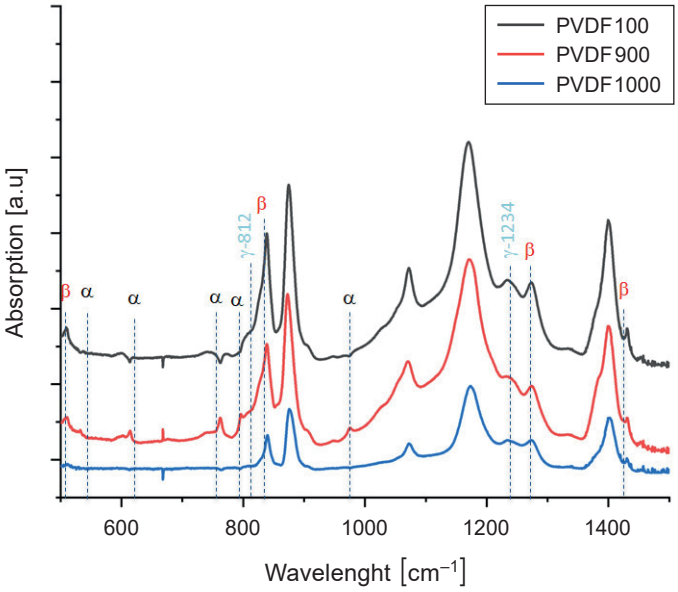

Fig 9. FTIR-ATR spectra for nonwovens spun from 22% PVDF solution. Most significant peaks corresponding to α-, β- and γ-phases are indicated

Table 2.
Relative content of polar phases in e-spun PVDF

Sample	$(F(\beta)+F(\gamma))$	$F(\beta)$	$F(\gamma)$
	[%]	[%]	[%]
PVDF100	0.60 ± 0.01	0.57 ± 0.01	0.03 ± 0.01
PVDF900	76.65 ± 0.2	72.03 ± 0.2	4.61 ± 0.2
PVDF1000	94.48 ± 0.2	55.17 ± 0.2	39.31 ± 0.2

3.4. Cellular studies. Results of MTT tests presented in Fig. 10 indicate a positive effect of polar phases on the cells via the piezoelectric effect achieved under ultrasounds stimulation. Cell viability results were in agreement with other studies that conclude that PVDF is not cytotoxic and that it allows cell

proliferation [24, 25]. Piezoelectric effect was mostly evident for samples formed at the highest collector rotational speed, allowing formation of the highest content of polar phases. The observations using SEM confirm good attachment and proliferation of the cells on the ultrasound-stimulated fiber scaffolds: on day 1, the cells had more rounded morphology, while by day 7, their morphology was more elongated and spread-out (Fig. 10).

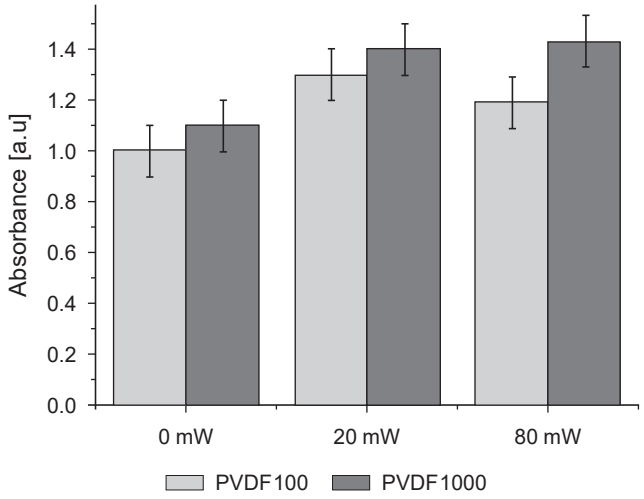

Fig. 10. Viability of L929 fibroblasts on PVDF100 and PVDF1000 samples using ultrasound stimulation with different power on day 7

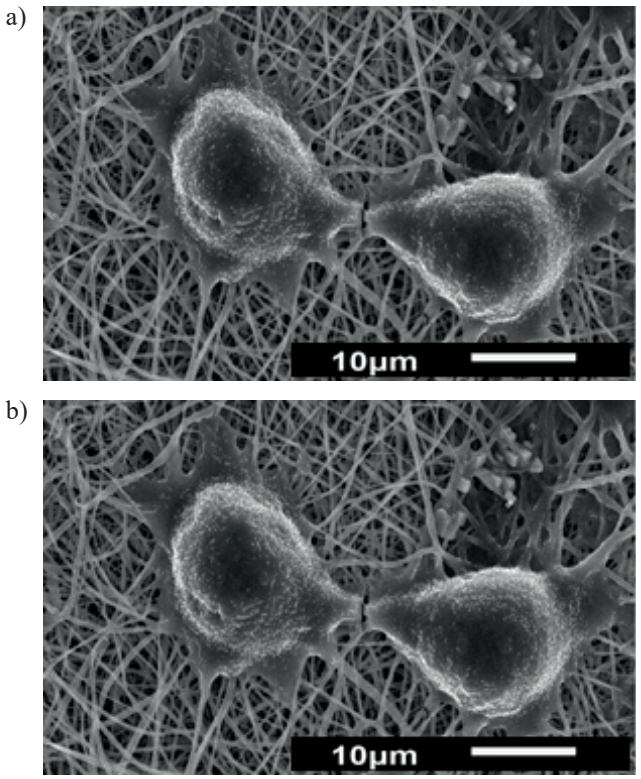

Fig. 11. SEM images of L929 fibroblasts on PVDF1000 nanofibers with power 80 mW/cm^2 a) on day 1 and b) on day 7

4. Conclusions

We showed that the application of relatively high rotational speed of the collector allows for electrospinning of thin PVDF fibers with preferred spatial arrangement and high polar phases content. Our preliminary cellular studies under in vitro conditions show that such nonwovens constitute promising smart scaffolds for tissue engineering applications, especially when stimulated by ultrasounds in order to activate their piezoelectric properties.

References

[1] T.E. Douglas, J. Schietse, A. Zima, S. Gorodzha, B.V. Parakhonskiy, D. Khalenkow, R. Shkarin, A. Ivanova, T. Baumbach, V. Weinhardt, Ch. Stevens, V. Vanhoorne, Ch. Vervaet, L. Balcaen, F. Vanhaecke, A. Slośarczyk, M. Surmaneva, R. Surmenev, and A. Skirtach, "Novel self-gelling injectable hydrogel/alpha-tricalcium phosphate composites for bone regeneration: Physiochemical and microcomputer tomographical characterization", *J. Biomed. Mater. Res. A*, 106(3), 822–828 (2018).

[2] B. Niemczyk, P. Sajkiewicz, and D. Kolbuk,"Injectable hydrogels as novel materials for central nervous system regeneration", *J. Neural Eng.* 15, 15 (2018).

[3] W. Matysiak, T. Tański, and M. Zaborowska, "Manufacturing process and characterization of electrospun PVP/ZnO NPs nanofibers", *Bull. Pol. Ac.: Tech.* 67(2), 193–200 (2019).

[4] B. Ostrowska, J. Jaroszewicz, E. Zaczynska, W. Tomaszewski, W. Swieszkowski, and K. Kurzydłowski, "Evaluation of 3D hybrid microfiber/nanofiber scaffolds for bone tissue engineering", *Bull. Pol. Ac.: Tech.* 62(3), 551–556 (2014).

[5] A. Ulatowska-Jarża, J. Pucińska, K. Wysocka-Król, I. Hołowacz, and H. Podbielska, "Nanotechnology for biomedical applications – enhancement of photodynamic activity by nanomaterials", *Bull. Pol. Ac.: Tech.* 59(3), 253–261 (2011).

[6] P. Sajkiewicz, "Crystallization behaviour of poly (vinylidene fluoride)", *Eur. Polym. J.* 35, 1581–1590 (1999).

[7] A. Gradys, P. Sajkiewicz, S. Adamovsky, A.A. Minakov, and C. Schick, "Crystallization of poly (vinylidene fluoride) during ultra-fast cooling", *Thermochimica Acta* 461, 153–157 (2007).

[8] A. Zaszczynska, P. Sajkiewicz, and A. Gradys, "Piezoelectric Scaffolds as Smart Materials for Neural Tissue Engineering", *Polymers*, 12(1), 161 (2020).

[9] Z.M. Dang, Y.H. Lin, and C.W. Nan, "Novel ferroelectric polymer composites with high dielectric constants". *Adv Mater* 15, 1625–1629 (2003).

[10] S. Yoon, A. Prabu, and K. Park, "Metal salt-induced ferroelectric crystalline phase in poly (vinylidene fluoride) films", *Macromol Rapid Commun* 29, 1316–1321 (2008).

[11] L. Yu and P. Cebe, "Crystal polymorphism in electrospun composite nanofibers of poly (vinylidene fluoride) with nanoclay", *Polymer*, 50, 2133–2141 (2009).

[12] T. Lei and L. Yu, Experiments and modelling of electrospinning process G. Zheng, "Electrospinning-induced preferred dipole orientation in PVDF fibers", *J Mater Sci* 50, 4342 (2015).

[13] T. Kowalewski and S. Błoński, Experiments and modelling of electrospinning process S. Baaral, „Experiments and modelling of electrospinning process", *Bull. Pol. Ac.: Tech*. 53(4), 385–394 (2005).

[14] A.J. Lovinger, "Annealing of poly (vinylidene fluoride) and formation of a fifth phase", *Macromolecules* 15, 40–44 (1982).

[15] R. Gregorio and M. Cestari, "Effect of crystallization temperature on the crystalline phase content and morphology of poly (vinylidene fluoride", *J. Polym. Sci. Part B Polym. Phys*. 32, 859–870 (1944).

[16] B. Bera and M. Sarkar, "Piezoelectricity in PVDF and PVDF Based Piezoelectric Nanogenerator: A Concept", *J Appl Phys* 9, 95–99 (2017).

[17] P. Sajkiewicz, A. Wasiak, and Z. Gocłowski, "Phase transitions during stretching of poly (vinylidene fluoride)", *European Polym. J.* 35(3), 423–429 (1999).

[18] K. Matsushige, K. Nagata, S. Imada, and T. Takemura, "The II-I crystal transformation of poly (vinylidene fluoride) under tensile and compressional stresses", *Polymer* 21, 1391–1397 (1980).

[19] J. Scheinbeim, C. Nakafuku, B.A. Newman, and K. Pae, "High-pressure crystallization of poly (vinylidene fluoride)", *J. Appl. Phys*., 50(6), 4399 – 4405 (1979).

[20] J. Wang, H. Li, J. Liu, Y. Duan, S. Jiang, and S. Yan, "On the α → β Transition of Carbon-Coated Highly Oriented PVDF Ultrathin Film Induced by Melt Recrystallization" *J Am Chem Soc.* 125(6), 1496–1497 (2003).

[21] Y. Ting, H. Gunawan, A. Sugondo, and Ch. Chiu, "A New Approach of Polyvinylidene Fluoride (PVDF) Poling Method for Higher Electric Response", *Ferroelectrics* 446, 28–38 (2013).

[22] S. Liang, Y. Kang, A. Tiraferri, E. Giannelis, H. Xia, and E. Menachem, "Highly Hydrophilic Polyvinylidene Fluoride (PVDF) Ultrafiltration Membranes via Postfabrication Grafting of Surface-Tailored Silica Nanoparticles", *ACS Appl Mater* 5(14), 6694–6703 (2013).

[23] D. Mandala, K. Henkelb, and D. Schmeißerb, "The electroactive β-phase formation in Poly (vinylidene fluoride) by gold nanoparticles doping", *Mater Lett* 73, 123–125 (2012).

[24] T.K. Sinha, S. Ghosh, R. Maiti, S. Jana, B. Adhikari, D. Mandal, and S.K. Ray, "Graphene-Silver-Induced Self-Polarized PVDF-Based Flexible Plasmonic Nanogenerator Toward the Realization for New Class of Self Powered Optical Sensor", *ACS Appl. Mater. Interfaces* 8(24), 14986–14993 (2016).

[25] A. Issa, M. Al-Maadeed, A. Luyt, D. Ponnamma, and M. Hassan, "Physico-Mechanical, Dielectric, and Piezoelectric Properties of PVDF Electrospun Mats Containing Silver Nanoparticles", *C—Journal of Carbon Research* 3(4), 30 (2017).

[26] F.A. He, K. Lin, D.L. Shi, H.L. Wu, H.K. Huang, J. Chen, F. Chen, and K.H. Lam, "Preparation of organosilicate/PVDF composites with enhanced piezoelectricity and pyroelectricity by stretching", *Compos Sci Technol* 137(12), 138–147 (2016).

[27] L. Jian-Hua, S. Xi-Sheng, Z. Qing, L. Mi-Zi, and Z. Qi-Qing, "The double effects of silver nanoparticles on the PVDF membrane: Surface hydrophilicity and antifouling performance", *Appl Surf Sci*. 265, 663–670 (2013).

[28] J. Sakata and M. Mochizuki, "Preparation of organic thin films by an electrospray technique I. Crystal forms and their orientation in poly (vinylidene flouride) films", *Thin Solid Films* 195, 175–184 (1991).

[29] S. Damaraju, S. Wu, M. Jaffe, and T. Arinzeh, "Structural changes in PVDF fibers due to electrospinning and its effect on biological function", *Biomed. Mater.* 8, 045007 (2013).

[30] C. Ribeiro, J. Pärssinen, V. Sencadas, V. Correia, S. Miettinen, V. Hytönen, and S. Lanceros-Méndez, "Dynamic piezoelectric stimulation enhances osteogenic differentiation of human adipose stem cells", *J. Biomed. Mater. Res.* 103, 2172–2175 (2014).

[31] M.T. Rodrigues, M.E. Gomes, J.F. Mano, and R.L. Reis, „β-PVDF Membranes Induce Cellular Proliferation and Differentiation in Static and Dynamic Conditions", *Materials Science Forum* 587–588, 72–76 (2008).

[32] M. Hoop, X.Z. Chen, A. Ferrari, F. Mushtaq, G. Ghazaryan, T. Tervoort, D. Poulikakos, B. Nelson, and S. Pané, "Ultrasound-mediated piezoelectric differentiation of neuron-like PC12 cells on PVDF membranes", *Scientific Reports* 7, 4028 (2017).

[33] L. Ghasemi-Mobarakeh, M.P. Prabhakaran, M. Morshed, M. Hossein, N.E. Hossein, B.S. Kiani, S. Al-Deyab, and S. Ramakrishna,"Application of conductive polymers, scaffolds and electrical stimulation for nerve tissue engineering", *J Tissue Eng Regen M* (2017).

[34] A.G. Kolbeck, „Aging of piezoelectricity in poly (vinylidene fluoride)", *J Polym Sci Pol Phys.* 20, 1987–2001 (1982).

[35] S.B. Rodan, Y. Imai, M.A. Thiede, G. Wesolowski, D. Thompson, Z. Bar-Shavit, S. Shull, K. Mann, and G.A. Rodan, "Characterization of a Human Osteosarcoma Cell Line (Saos-2) with Osteoblastic Properties", *Cancer Res*. 47, 4961–4966 (1987).

[36] D. Klee, Z. Ademovic, A. Bosserhoff, H. Hoecker, G. Maziolis, and H.J. Erli, "Surface modification of poly (vinylidenefluoride) to improve the osteoblast adhesio", *Biomaterials* 24, 3663–3670 (2003).

[37] W.A. Yeea, M. Kotaki, Y. Liu, and X. Lu, "Morphology, polymorphism behavior and molecular orientation of electrospun poly (vinylidene fluoride) fibers", *Polymer* 48(2), 512–521 (2007).

[38] Y. Li, Ch. Liao, and S.Ch. Tjong, "Electrospun Polyvinylidene Fluoride-Based Fibrous Scaffolds with Piezoelectric Characteristics for Bone and Neural Tissue Engineering", *Nanomaterials* (Basel) 9(7), 952 (2019).

[39] X. Cai, T. Lei, D. Sund, and L. Linde, "A critical analysis of the a, b and g phases in poly (vinylidene fluoride) using FTIR", *RSC Adv*. 7, 15382–15389 (2017).

[40] K. Chwee and T. Limbc, "Nanofiber technology: current status and emerging developments", *Prog Polym Sci.* 70, 1–17 (2017).

[41] Z.M. Huang, Y.Z. Zhang, M. Kotaki, and S. Ramakrishna, "A review on polymernanofibers by electrospinning and their applications in nanocomposites", *Compos. Sci. Technol*. 63(15), 2223–2253 (2003).

[42] E. Zussman, A. Theron, and A. Yarin, "Formation of nanofiber crossbars in electrospinning", *Appl. Phys. Lett.* 82(6), 973–975 (2003).

[43] H. Pan, L. Li, L. Hu, and X. Cui, "Continuous aligned polymer fibers produced by a modified electrospinning method", *Polymer* 47(14), 4901–4904 (2006).

[44] B. Sundaray, V. Subramanian, T. Natarajan, R.Z. Xiang, C.C. Chang, and W.S. Fann, "Electrospinning of continuous aligned polymer fibers", *Appl. Phys. Lett*. 84(7), 1222–1224 (2004).

International Journal of
Molecular Sciences

MDPI

Article

Enhanced Electroactive Phases of Poly(vinylidene Fluoride) Fibers for Tissue Engineering Applications

Angelika Zaszczyńska [1], Arkadiusz Gradys [1], Anna Ziemiecka [2], Piotr K. Szewczyk [3], Ryszard Tymkiewicz [1], Małgorzata Lewandowska-Szumieł [2,4], Urszula Stachewicz [3] and Paweł Ł. Sajkiewicz [1,*]

1 Laboratory of Polymers Biomaterials, Institute of Fundamental Technological Research, Polish Academy of Sciences, Pawińskiego 5B, 02-106 Warsaw, Poland; azasz@ippt.pan.pl (A.Z.); argrad@ippt.pan.pl (A.G.); rtym@ippt.pan.pl (R.T.)
2 Laboratory of Cell Research and Application, 02-106 Warsaw, Poland; ania.cieciuch@gmail.com (A.Z.); malgorzata.lewandowska-szumiel@wum.edu.pl (M.L.-S.)
3 Faculty of Metals Engineering and Industrial Computer Science, AGH University of Krakow, 30-059 Krakow, Poland; pszew@agh.edu.pl (P.K.S.); ustachew@agh.edu.pl (U.S.)
4 Department of Histology and Embryology, Centre for Biostructure Research, Medical University of Warsaw, Centre for Preclinical Research and Technology, 02-106 Warsaw, Poland
* Correspondence: psajk@ippt.pan.pl

Abstract: Nanofibrous materials generated through electrospinning have gained significant attention in tissue regeneration, particularly in the domain of bone reconstruction. There is high interest in designing a material resembling bone tissue, and many scientists are trying to create materials applicable to bone tissue engineering with piezoelectricity similar to bone. One of the prospective candidates is highly piezoelectric poly(vinylidene fluoride) (PVDF), which was used for fibrous scaffold formation by electrospinning. In this study, we focused on the effect of PVDF molecular weight (180,000 g/mol and 530,000 g/mol) and process parameters, such as the rotational speed of the collector, applied voltage, and solution flow rate on the properties of the final scaffold. Fourier Transform Infrared Spectroscopy allows for determining the effect of molecular weight and processing parameters on the content of the electroactive phases. It can be concluded that the higher molecular weight of the PVDF and higher collector rotational speed increase nanofibers' diameter, electroactive phase content, and piezoelectric coefficient. Various electrospinning parameters showed changes in electroactive phase content with the maximum at the applied voltage of 22 kV and flow rate of 0.8 mL/h. Moreover, the cytocompatibility of the scaffolds was confirmed in the culture of human adipose-derived stromal cells with known potential for osteogenic differentiation. Based on the results obtained, it can be concluded that PVDF scaffolds may be taken into account as a tool in bone tissue engineering and are worth further investigation.

Keywords: scaffolds; polymers; piezoelectricity; bone tissue engineering; nanofibers; regenerative medicine

Citation: Zaszczyńska, A.; Gradys, A.; Ziemiecka, A.; Szewczyk, P.K.; Tymkiewicz, R.; Lewandowska-Szumieł, M.; Stachewicz, U.; Sajkiewicz, P.Ł. Enhanced Electroactive Phases of Poly(vinylidene Fluoride) Fibers for Tissue Engineering Applications. *Int. J. Mol. Sci.* **2024**, *25*, 4980. https://doi.org/10.3390/ijms25094980

Academic Editor: Jacek Matys

Received: 4 April 2024
Revised: 26 April 2024
Accepted: 30 April 2024
Published: 2 May 2024

1. Introduction

We are witnessing a rapid aging of society. More and more people are hospitalized due to bone system diseases [1]. Despite the great achievements of modern medicine, many diseases are still not effectively treated. Approximately 1.5 million individuals suffer from bone diseases such as osteoporosis [2]. Furthermore, bone fractures represent a prevalent musculoskeletal issue necessitating hospitalization more frequently than any other condition in this category [3]. The challenges are colossal, and several solutions must be implemented to improve patient care. Intensive work on materials for medicine that will support the regeneration of bone tissue is necessary.

Bone tissue regeneration is a complex biological phenomenon. Many material requirements must be fulfilled. In the realm of biomedical engineering, there has been a growing surge of scientific and technical attention towards investigating smart materials (SM) over

the past few decades. These materials have garnered interest due to their ability to react to different external stimuli, including physical, chemical, and mechanical signals, thereby mimicking the behavior observed in natural bodily tissues [4]. One important type of SM is piezoelectric scaffolds, which can generate electrical signals in response to the applied stress. Furthermore, they can stimulate the signaling pathways and thereby enhance tissue regeneration at the impaired site [5]. Piezoelectric phenomena are observed in various molecular structures in animal bodies, for example, in DNA, collagen, and keratin, being present in multiple tissues and organs like dentin, tendons, and, most importantly, in human bones [6]. The existence of piezoelectricity in the living organism was shown first by Fukada et al. [7] in 1957 (dry and wet bones) and Basset in 1962 [8]. He described the generation of electrical potentials by bone responses to mechanical stress. It is known that electrical charges are important for the activity of cells, particularly for human adipose-derived stromal cells [9]. One significant benefit of piezoelectric scaffolds is their capacity to generate electrical potential in a non-invasive manner when subjected to mechanical forces, eliminating the requirement for invasive electrodes. In bone tissue engineering, the main properties of the scaffolds are accounted for to emulate both the morphology and function of the native tissue. Consequently, piezoelectric scaffolds can dynamically mimic the cellular microenvironment to be appropriate for a specific bone tissue engineering injury [10–12]. The presence of polar phases combined with fiber morphology and relatively high elasticity provides the perspective of using this material in bone regeneration [13]. Classification of various piezoelectric materials is shown in Figure 1.

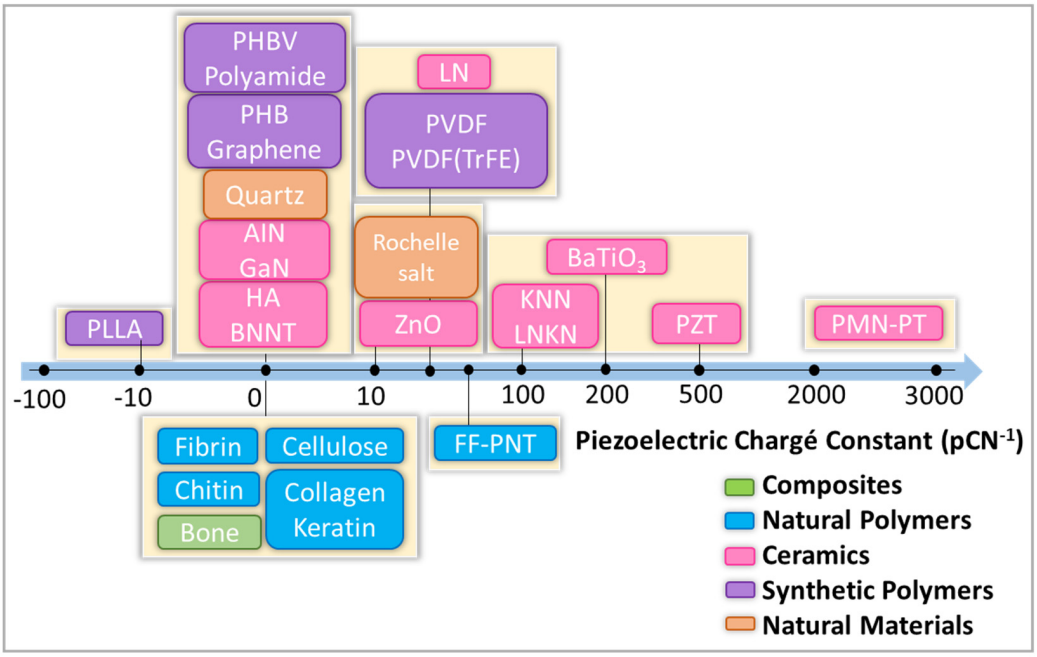

Figure 1. Classification of piezoelectric materials. P(VDF-TrFE): poly(vinylidene fluoride-trifluoro ethylene), PVDF: poly(vinylidene fluoride), PHB: polyhydroxybutyrate, PLLA: poly(l-lactic acid), gallium nitride (GaN), boron nitride (BN), zinc oxide (ZnO), HA: hydroxyapatite.

The important property of nanofibrous piezoelectric scaffolds is biocompatibility, but also topography, porosity, density, geometry [14,15], humidity [16], and electrical polarity [17]. In the last few years, several studies have shown that different techniques, such as phase separation, 3D printing, photolithography, and electrospinning, have been tested to create a unique 3D nanofibrous scaffold with appropriate features [18]. The general influence of electrospinning parameters on fiber diameter is shown in Figure 2.

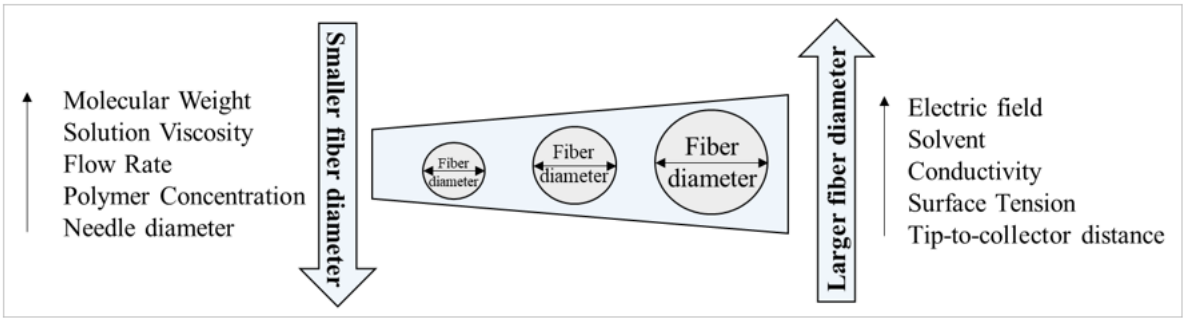

Figure 2. Schematic representation of the influence of electrospinning parameters on fiber diameter.

In tissue engineering, electrospinning is widely investigated as a scaffold for drug delivery [19], bone tissue engineering [20], cardiac tissue engineering [21], cartilage [22], soft tissue [23], or skin [24]. In addition to many advantages of electrospinning, such as the controlled architecture of the scaffolds providing similarity to ECM, cheapness, and simplicity [25], the electrospinning technique (Figure 3A) is a particularly promising method of PVDF scaffold formation because of the possibility of reaching relatively high polar form and thus piezoelectricity by optimizing electrospinning conditions [26]. The electrospinning configuration comprises a high-voltage power source, a spinneret assembly, and a grounded collector. The spinneret part contains a syringe with a needle, feed storage that is polymer solution, and a special pump, which injects solution at a constant flow rate. High voltage is connected to the tip of the metal needle, thereby generating electrostatic forces [27], which in addition to surface tension, viscoelastic force, air drag, and gravity force, result in the formation of the nanofibers from a liquid jet (Figure 3B). The main stages of the electrospinning process are the starting formation of the cone at the top of the spinneret and the development of a rectilinear jet; evaporation of solvent during the bending deformation with looped and spiral trajectories during the process; final nanofiber collections on the collector [28,29].

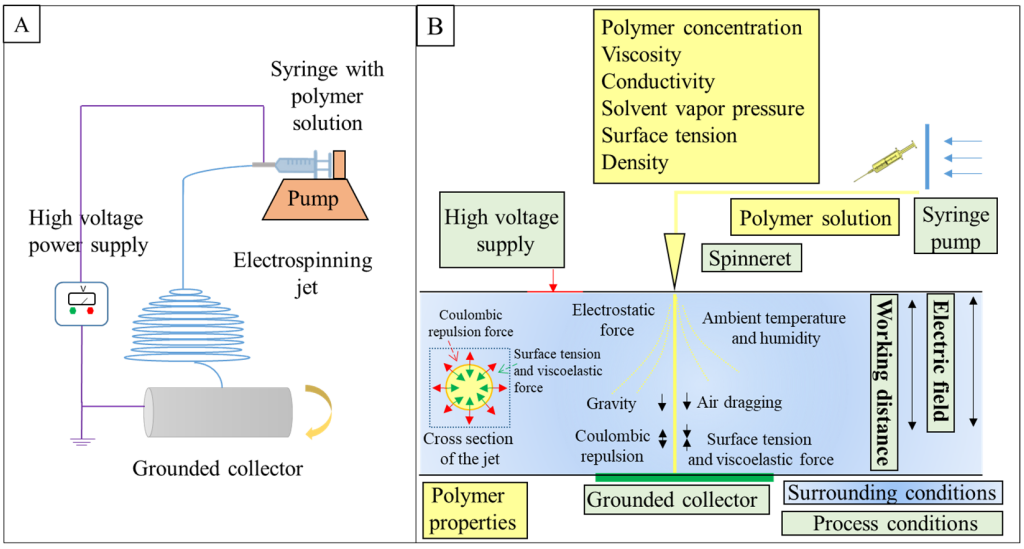

Figure 3. (**A**) Schematic illustration of electrospinning setup, (**B**) general scheme of nanofiber formation using electrospinning.

Various natural and synthetic polymers have been investigated for bone tissue engineering applications [30]. One of the most promising is piezoelectric PVDF with strong chemical resistance, biocompatibility, and optical transparency [31]. PVDF is a semi-crystalline and can crystallize in at least five different crystallographic phases: α, β, γ, δ, and ε (Figure 4). They differ in chain conformation and arrangement of CH_2–CF_2 dipoles,

resulting in various net dipole moments. A strong electric moment in the PVDF monomer unit arises because of the strong electro-negativity of fluorine atoms as compared to hydrogen atoms. In case the polymer chains are packed into crystals to form parallel dipoles, the crystal has a non-zero net dipole moment. Observations indicate distinct characteristics across the β, γ, and δ phases. The β phase exhibits the highest dipole moment, primarily attributed to its all-trans conformation. Conversely, parallel dipole arrangements are evident in alternative chain conformations such as $TGTG^-$ and $T3GT3G^-$, corresponding to lower polarity in the δ and γ phases, respectively. Conversely, identical conformations result in a net zero dipole moment due to antiparallel chain arrangements, as seen in the α and ϵ phases [32]. Thus, the most electrically important polymorphic variant due to the highest piezo-, ferro- and pyroelectric properties is the β-phase [33]. In the recent literature, the electrospinning technique has been quite frequently used for the formation of PVDF fibers. It is known that the electrospinning of PVDF from solutions generally favors the formation of polar phases [34]. It is explained by the extremely short time of solvent evaporation being equivalent to fast cooling in melt crystallization as well as the electric interactions of the polymer with the external electric field [35]. In the case of pure PVDF, Cozza et al. [36] have revealed that the content of polar β-phase is much higher in electrospun fibers than cast film. As such, systematic studies from the perspectives of polymer molecular weight and electrospinning parameters are necessary.

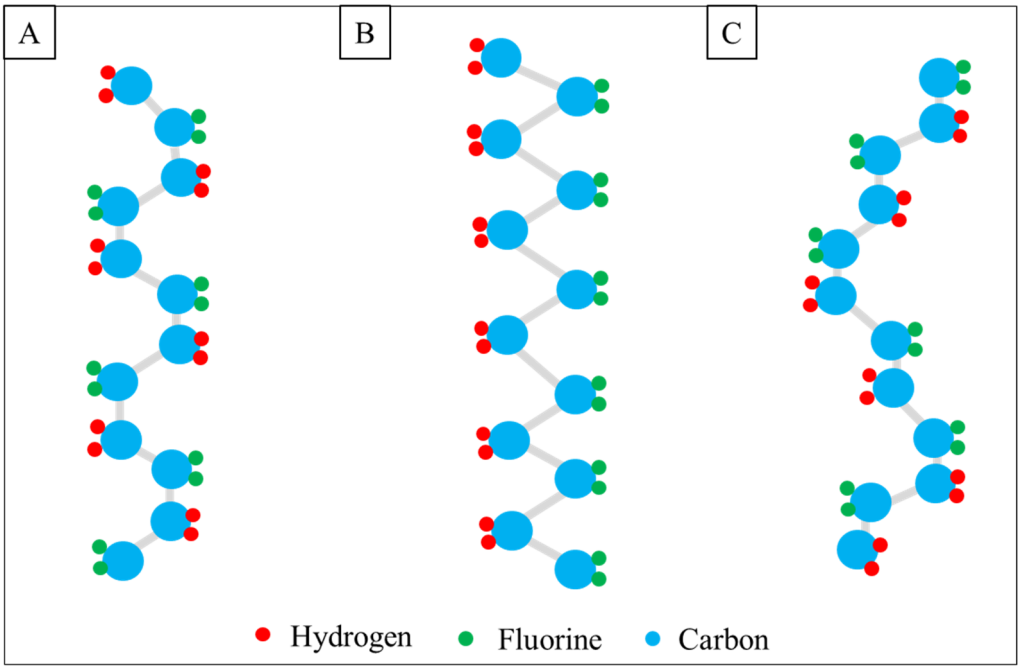

Figure 4. Schematic representation of the chain conformation of the phases in PVDF; (**A**)—α-phase, (**B**)—β-phase, and (**C**)—γ-phase.

The formation of random and aligned fiber orientation scaffolds allows the forming of connected 3D nonwovens of micro- and nano-fibers with high surface area and porosity, which should enhance cell adhesion [37]. Hence, fibrous scaffolds may offer a more conducive environment for cellular attachment and proliferation compared to non-fibrous scaffolds [38]. In this study, PVDF cell scaffolds in the form of nanofibers (lowly and highly oriented) were formed by the electrospinning technique. The effect of PVDF molecular masses, fiber spatial arrangements of fibers, and electrospinning parameters during the process on polymorph content was investigated. The aim of the research was to optimize the morphology, chemical structure, content of electroactive phases, piezoelectricity coefficient, and biocompatibility from the perspective of material suitable for BTE.

2. Results and Discussion

2.1. Morphology

SEM images of fiber mats collected at 200, 1000, and 2000 rpm of the collector speed for the two Mws (Figure 5) indicate continuous bead-free morphology of the nanofibers. It is evident from Figure 6 that the average fiber diameter decreases with increasing collector rotational speed. The reduction in diameter is particularly evident when changing rotational speed from 1000 to 2000 rpm. From Figure 7 it can be concluded that at the high rotational speed of the collector, the average diameter does not depend on the molecular weight. In contrast, at low rotational speeds of the collector, the influence of the molecular weight on the average diameter of the fibers is observed. In conditions of low rotational speed, when the fiber stretching force exerted by the collector on which the fiber is wound is low, the effect of molecular weight on the fiber diameter is visible. It is caused by the density of chain splicing, which is higher for large molecular weights, at which the viscosity is high, and the viscous resistance during fiber formation is high. As the collector rotates rapidly, the tensile (mechanical) forces eliminate any viscosity issues, and thin fibers are formed due to the significant mechanical field from the collector [39,40]. In the case of low molecular weight PVDF, the total porosity was 82 ± 0.16%, 80 ± 0.22%, and 79 ± 0.4% for PVDF1, PVDF2, and PVDF3, respectively, and the mean pore size was ~215 ± 12 nm. The porosity increased with the increase in molecular weight [41] and was 84 ± 0.11%, 83 ± 0.13%, and 81 ± 0.45% for samples PVDF4, PVDF5, and PVDF6, respectively, and the mean pore size was ~189 ± 19 nm.

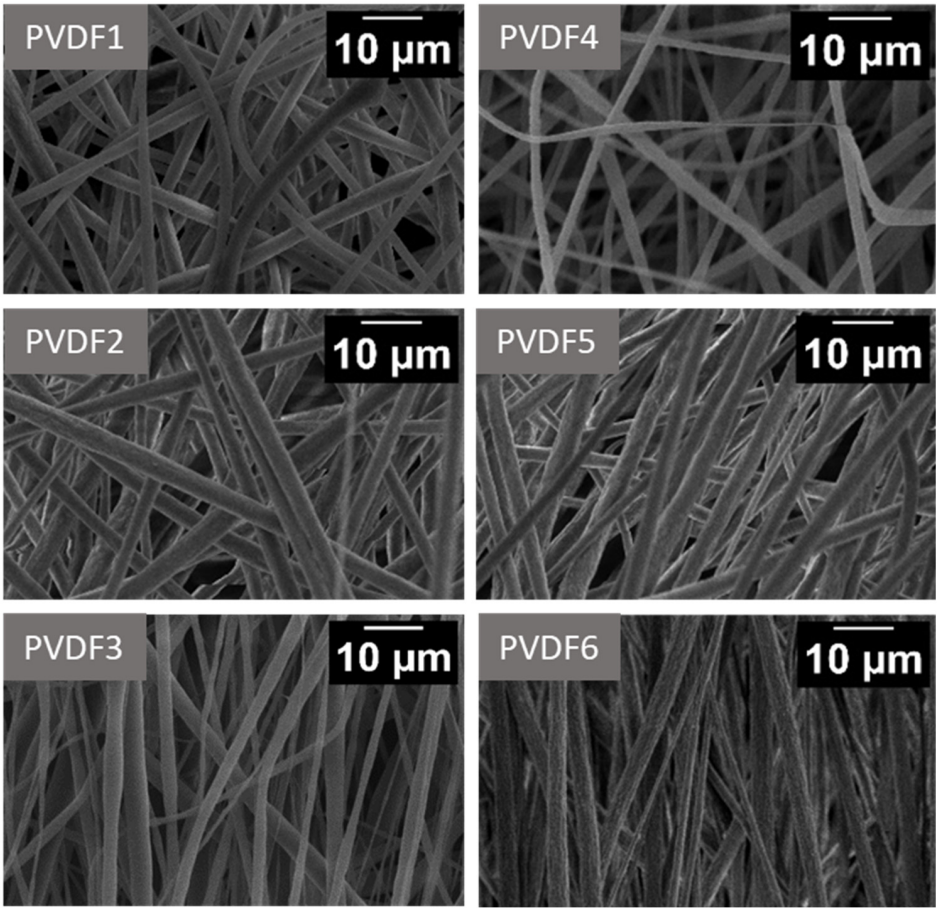

Figure 5. SEM images of electrospun fiber mats. PVDF1—180,000 g/mol, collector speed—200 rpm; PVDF2—180,000 g/mol, collector speed—1000 rpm; PVDF3—180,000 g/mol, collector speed—2000 rpm; PVDF4—530,000 gm/mol, collector speed—200 rpm; PVDF5—530,000 g/mol, collector speed—1000 rpm; PVDF6—530,000 g/mol, collector speed—2000 rpm. All samples C_p = 20%, F_R—1 mL/h (details in Table 4).

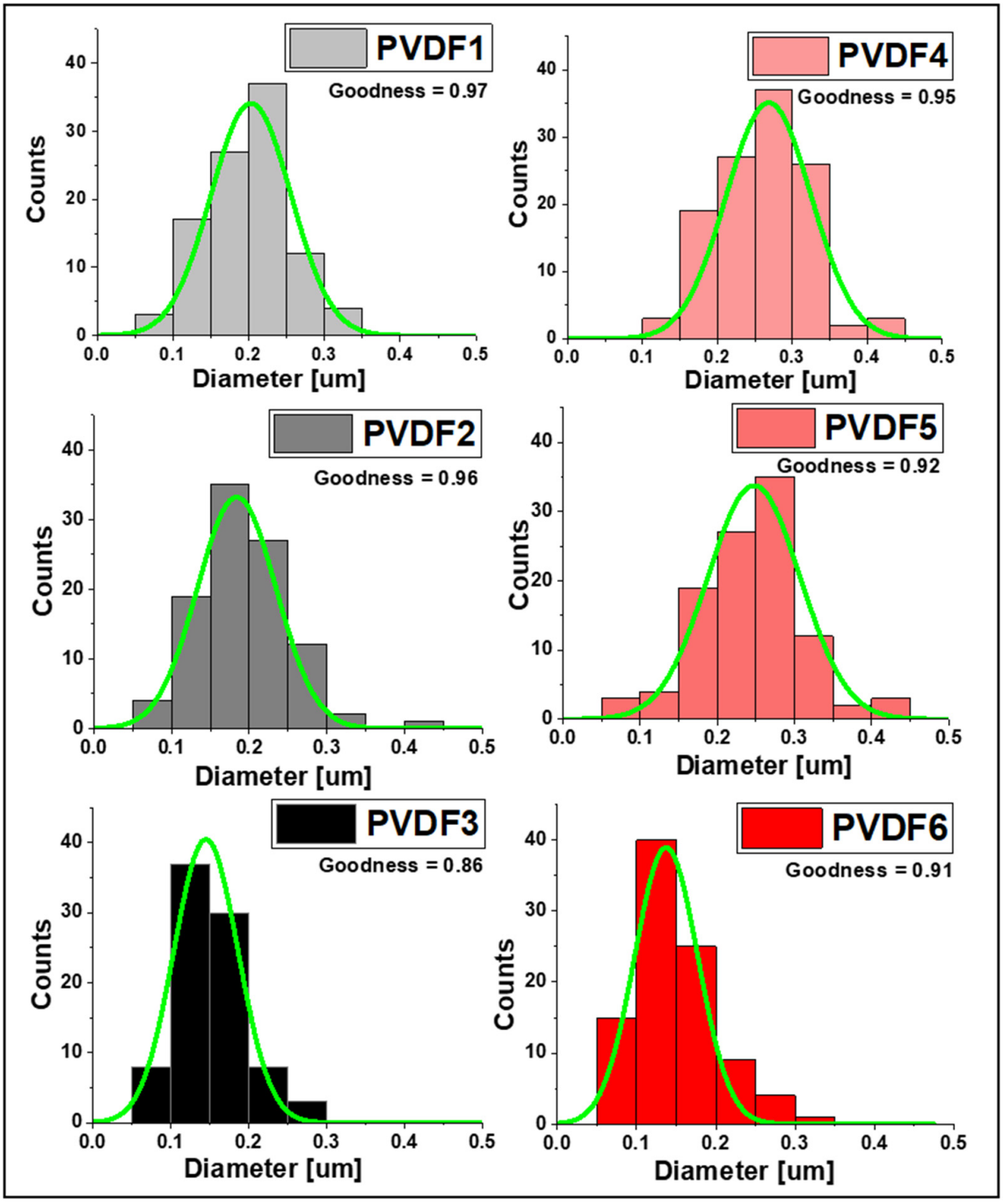

Figure 6. Histograms of the PVDF fiber diameter distribution approximated with the Gauss function. PVDF1—180,000 g/mol, collector speed—200 rpm; PVDF2—180,000 g/mol, collector speed—1000 rpm; PVDF3—180,000 g/mol, collector speed—2000 rpm; PVDF4—530,000 gm/mol, collector speed—200 rpm; PVDF5—530,000 g/mol, collector speed—1000 rpm; PVDF6—530,000 g/mol, collector speed—1000 rpm. All samples Cp = 20%, F_R—1 mL/h (details in Table 4).

Also, the average diameter is higher for PVDF6 is 148 ± 84 nm (Mw—530,000 g/mol), compared to samples with lower molecular weight (Mw—180,000 g/mol) and the same

collector speed (PVDF3 = 141 ± 62 nm). More precisely, the slight diameter reduction is connected to tangential force, which increases with molecular weight and the higher rotating speed of the collector. Generally, in random and aligned samples, the diameter of the fibers decreases with higher collector rotational speed, combined the effect of collector rotational speed and polymer molecular weight is interdependent. Additionally, the dimensions of the fibers are lower in samples with higher collector rotational speed in random and aligned orientations, which is in agreement with the literature [42]. Higher rotational speed can partially counteract the hindered elongation caused by higher molecular weight, leading to a reduction in average fiber diameter. However, the dominant factor affecting fiber diameter is often the molecular weight of the polymer.

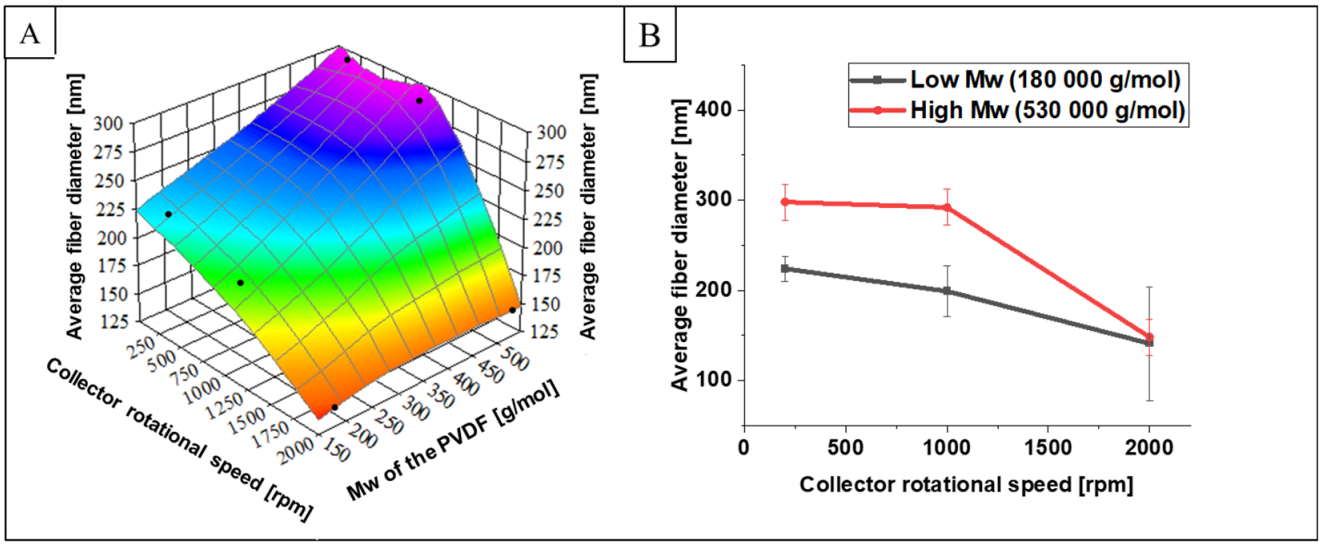

Figure 7. The relation between collector rotational speed, polymer molecular weight, and average fiber diameter (**A**), and relation between collector rotational speed and average fiber diameter (**B**). PVDF1—180,000 g/mol, collector speed—200 rpm; PVDF2—180,000 g/mol, collector speed—1000 rpm; PVDF3—180,000 g/mol, collector speed—2000 rpm; PVDF4—530,000 gm/mol, collector speed—200 rpm; PVDF5—530,000 g/mol, collector speed—1000 rpm; PVDF6—530,000 g/mol, collector speed—1000 rpm. All samples Cp = 20%, F_R—1 mL/h (details in Table 4).

The effect of collector rotational speed and polymer molecular weight on spatial arrangements of fibers can be deduced from the analysis of the orientation distribution of PVDF (Figure 8), and FWHM (Figure 9). It is evident that the fiber orientation becomes higher with the increasing speed of the rotational collector, being weakly dependent on the molecular weight. The full width at half maximum (FWHM) of the orientation of the fibers changes from 81.30 o at 200 rpm, through 27.13 at 1000 rpm, and 13.29 at 2000 rpm in PVDF for lower molecular weight PVDF, and 74.10 o at 200 rpm, through 25.19 at 1000 rpm, and 11.16 at 2000 rpm for higher molecular weight PVDF. Higher rotational speeds lead to increased tensile forces, which can enhance the stretching and alignment of the fibers [43]. To quantitatively compare the effect of the rotational speed of the collector on the arrangement of PVDF nanofibers, the anisotropy index was used (α). As the rotating speed increases from 200 to 2000 rpm, the α increases from 0.29 to 0.78 in PVDF with low molecular weight and from 0.35 to 0.84 in PVDF with higher molecular weight. It indicates clearly an increase in the nanofibers' orientation with the rotational speed of the collector. The comparison of the anisotropy index for different molecular weights shows only a small increase in orientation with increasing molecular weight.

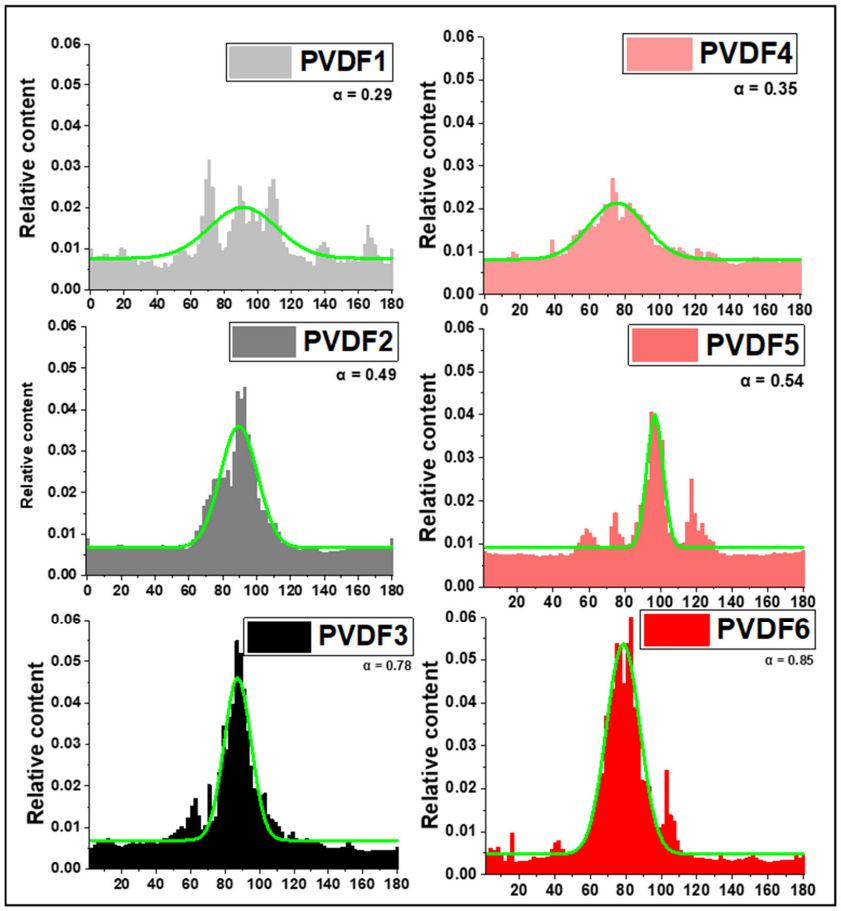

Figure 8. The distribution of PVDF nanofibers orientation, the anisotropy index (α) calculated from Equations (1) and (2). PVDF1—180,000 g/mol, collector speed—200 rpm; PVDF2—180,000 g/mol, collector speed—1000 rpm; PVDF3—180,000 g/mol, collector speed—2000 rpm; PVDF4—530,000 gm/mol, collector speed—200 rpm; PVDF5—530,000 g/mol, collector speed—1000 rpm; PVDF6—530,000 g/mol, collector speed—1000 rpm. All samples Cp = 20%, F_R—1 mL/h (details in Table 4).

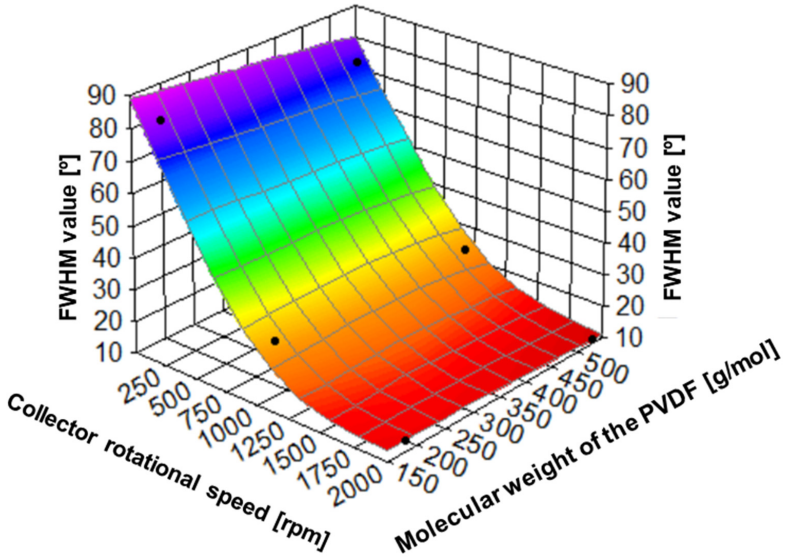

Figure 9. The relation between collector rotational speed, polymer molecular weight, and fiber alignment (expressed as FWHM values).

2.2. Influence of the Process Parameters on the Electroactive Phases Content

2.2.1. Collector Rotational Speed

Figure 10 shows the FTIR spectra of the nanofibrous samples. The bands at 490, 766, 1402, and 1432 cm^{-1} are assigned to the α phase, while the bands at 510, 600, 840, and 1280 cm^{-1} are assigned to the electroactive β-phase. Additionally, the bands at 812, 840, and 1234 cm^{-1} correspond to the electroactive γ-phase. Some of the α and β bands are overlapped with the bands coming from the γ-phase, for instance, with the band at 840 cm^{-1}. Multiple phases such as α, β, and γ phases coexist with partially overlapped bands. The relative amount of β-phase in each sample was estimated using the absorption bands at 840 and 766 cm^{-1} (corresponding to the β and α phases) and calculated from Equations (3)–(5).

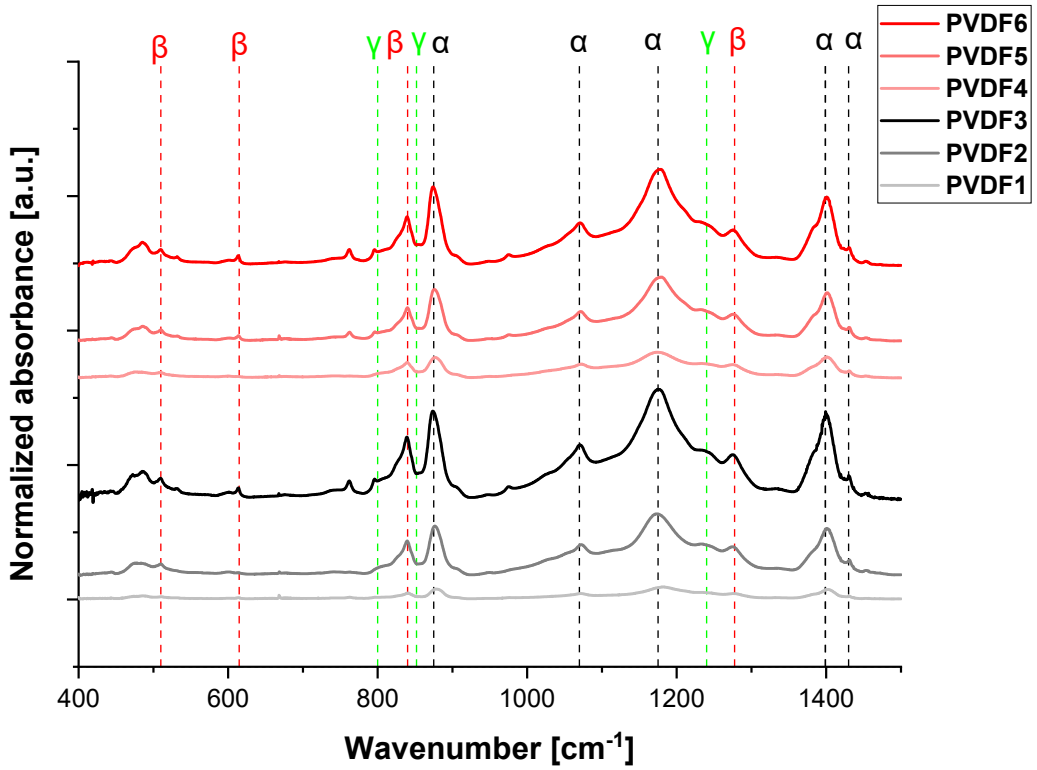

Figure 10. FTIR-ATR spectrum (400–1500 cm^{-1}) of selected samples with various molecular weights and rotational speeds of the collector. PVDF1—180,000 g/mol, collector speed—200 rpm; PVDF2—180,000 g/mol, collector speed—1000 rpm; PVDF3—180,000 g/mol, collector speed—2000 rpm; PVDF4—530,000 gm/mol, collector speed—200 rpm; PVDF5—530,000 g/mol, collector speed—1000 rpm; PVDF6—530,000 g/mol, collector speed—1000 rpm. All samples Cp = 20%, F_R—1 mL/h (details in Table 4).

It is evident from Figure 11 that the effect of the collector's rotational speed on the content of electroactive phases is strong. The electroactive phase fractions of samples from PVDF with lower molecular weight were determined to be 12, 65, and 92%, at 200, 1000, and 2000 rpm, respectively, and with higher molecular weight, 24, 72, and 91%, respectively. Such a strong increase in the content of electroactive phases with increasing collector rotational speed is related to an increase in stretching forces leading to better molecular alignment and orientation in the nanofibers. It is well known from the literature that molecular orientation induced by external fields like mechanical [44] promotes the formation of piezoelectric phases. The effect of molecular weight on the content of electroactive phases is evident only at the lowest rotational speed. The analysis of β and γ phase content (Figure 11, Table 1) indicates the gradual increase in γ phase

content with collector rotational speed and kind of saturation of β phase content above 1000 rpm.

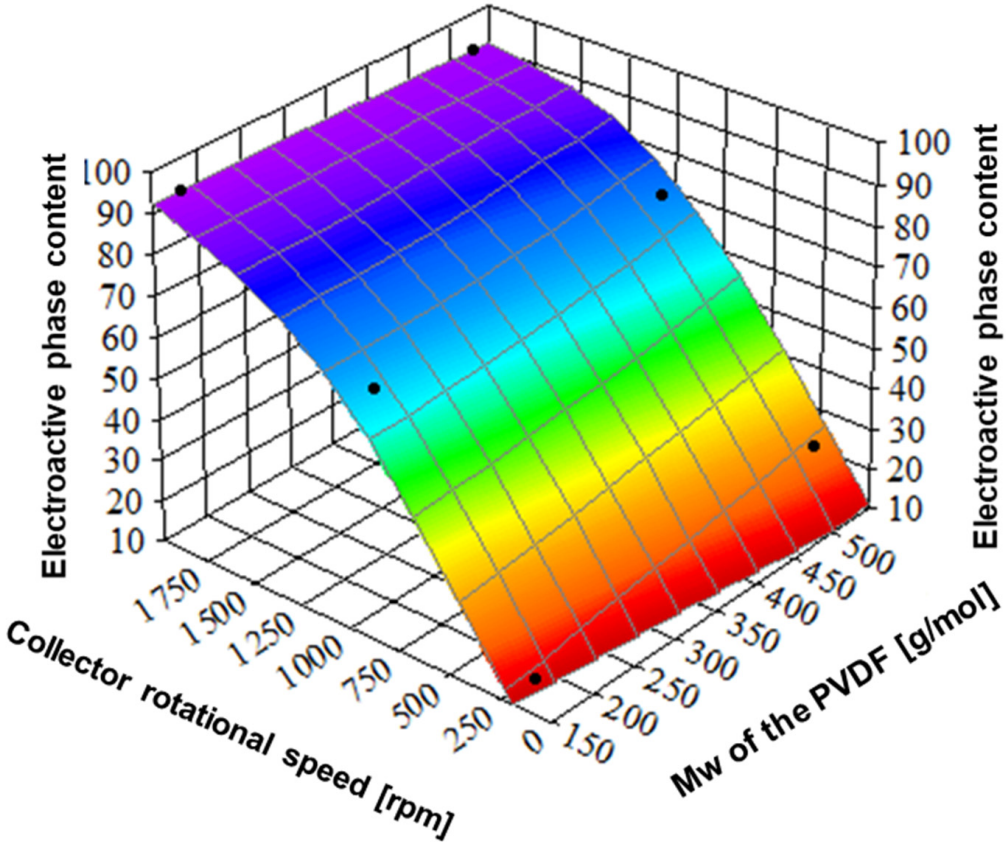

Figure 11. The relation between collector rotational speed, polymer molecular weight, and electroactive phase content. PVDF1—180,000 g/mol, collector speed—200 rpm; PVDF2—180,000 g/mol, collector speed—1000 rpm; PVDF3—180,000 g/mol, collector speed—2000 rpm; PVDF4—530,000 gm/mol, collector speed—200 rpm; PVDF5—530,000 g/mol, collector speed—1000 rpm; PVDF6—530,000 g/mol, collector speed—1000 rpm. All samples C_p = 20%, F_R—1 mL/h (details in Table 1).

Table 1. Electroactive phase content in PVDF scaffolds.

Sample ID	F(α) (%)	F(β) + F(γ) (%)	F(β) (%)	F(γ) (%)
PVDF1	88 ± 0.2	12 ± 1.2	9 ± 3	3 ± 4
PVDF2	35 ± 1.4	65 ± 0.7	52 ± 6.1	13 ± 3.3
PVDF3	8 ± 2.2	92 ± 4	47 ± 2	45 ± 4.8
PVDF4	76 ± 3	24 ± 0.4	15 ± 0.6	9 ± 4.2
PVDF5	28 ± 1.9	72 ± 2.9	57 ± 0.9	15 ± 1.3
PVDF6	11 ± 3.3	91 ± 6.3	60 ± 2	29 ± 1.2

2.2.2. Applied Voltage

In this section, the effect of applied voltage on the content of electroactive phases was investigated using the samples formed at the collector's rotational speed allowing to obtain the highest content of electroactive phases. Figure 12 shows FTIR spectra of samples electrospun at 15 kV, 22 kV, and 25 kV. It is seen from Figure 13 that there is a maximum of the electroactive phases amount around 22 kV. Additionally, there is a weak effect of molecular weight on electroactive phase content; for instance, in the case of applied voltage

15 kV, the amount of electroactive phases is 37% and 52%, for low and high molecular weight, respectively.

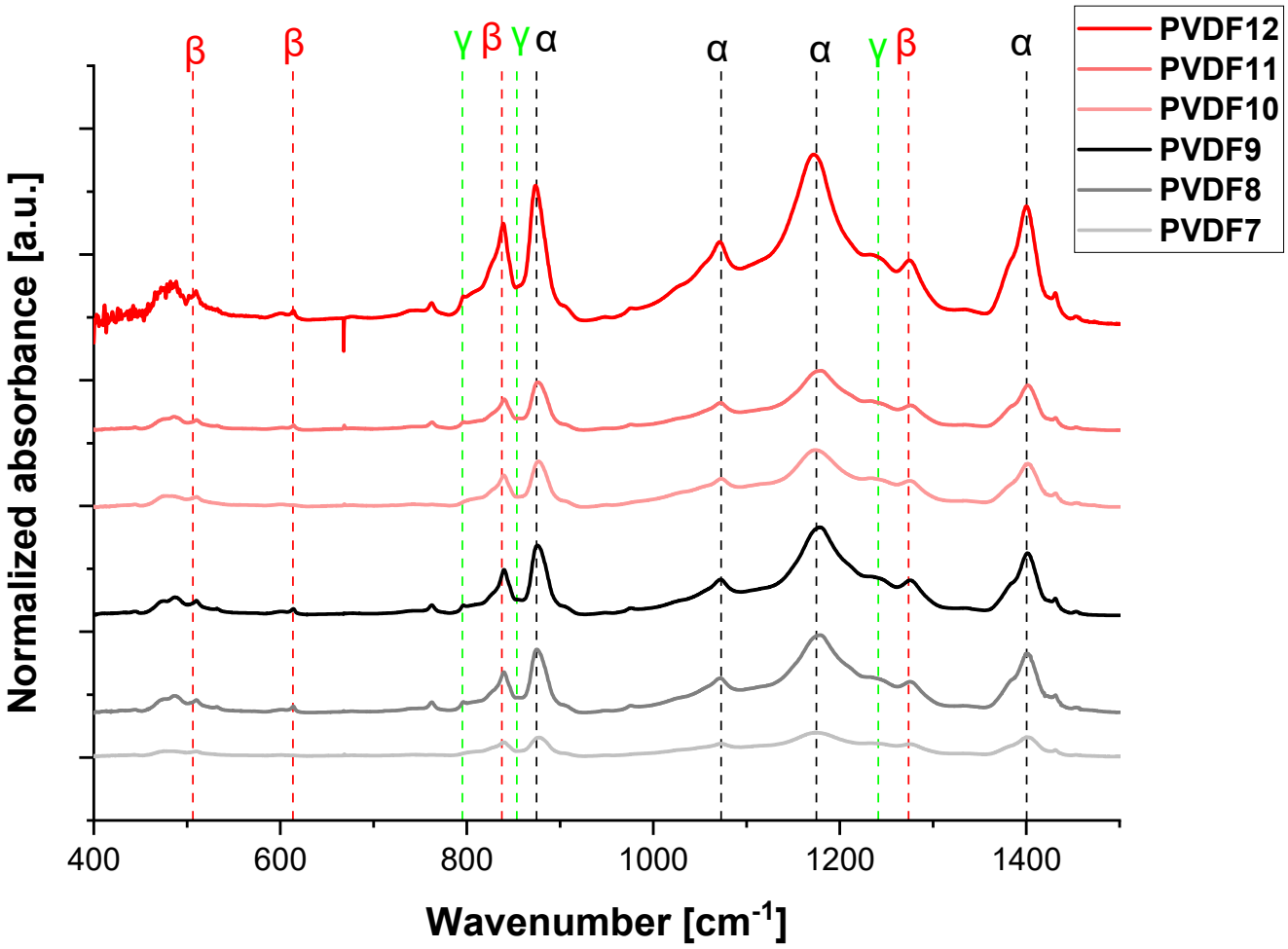

Figure 12. FTIR-ATR spectrum (400–1500 cm^{-1}) of selected samples formed with various applied voltages. PVDF7—180,000 g/mol, applied voltage—15 kV; PVDF8—180,000 g/mol, applied voltage—20 kV; PVDF9—180,000 g/mol, applied voltage—25 kV; PVDF10—530,000 gm/mol, applied voltage—15 kV; PVDF11—530,000 g/mol, applied voltage—20 kV rpm; PVDF12—530,000 g/mol, applied voltage—25 kV. All samples: Cp = 20%, F_R—1 mL/h, collector rotational speed—2000 rpm (details in Table 4).

During the electrospinning process of the PVDF, applied voltage causes the stretching and orientation of the polymer chains, promoting the formation of electroactive phases. The applied voltage is a factor of great importance in the effective stretching of the molecules and the formation of the electroactive phases [45]. It is evident from Figure 13 and Table 2 that the maximum of the phase content at 22 kV is reached by each of the electroactive phases, β, γ. The reduction in electroactive phase content above 22 kV is most probably related to disturbances of the electrospinning process and molecular orientation at the highest voltage [46]. Considering the positive effect of higher molecular weight on the formation of the electroactive phase, it can be concluded that a combination of higher applied voltage and higher molecular weight PVDF results in nanofibers with higher electroactive phase content while not exceeding the voltage at which the fibers are not effectively formed [47].

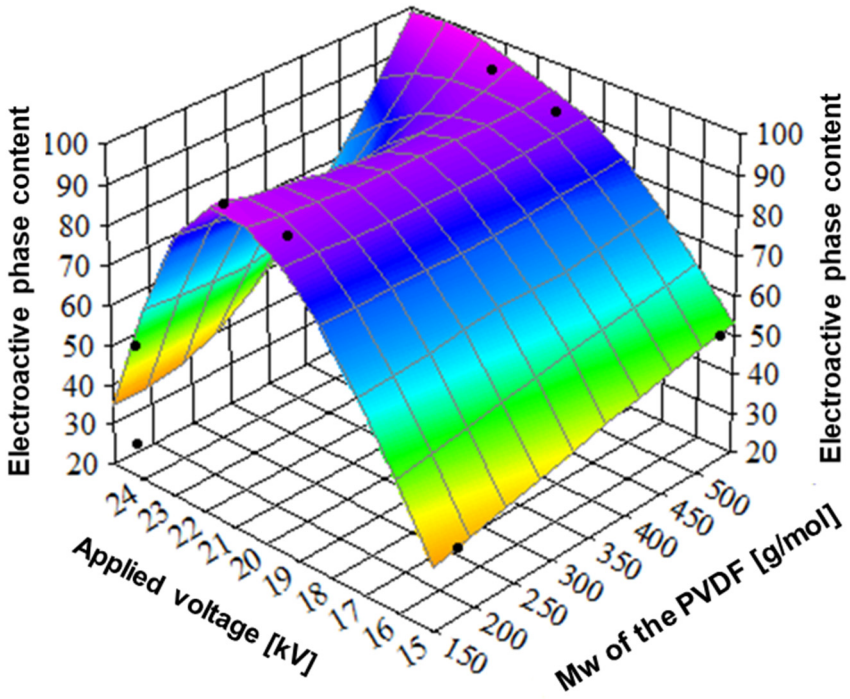

Figure 13. The relation between applied voltage, polymer molecular weight, and the sum of electroactive phase content. PVDF7—180,000 g/mol, applied voltage—15 kV; PVDF8—180,000 g/mol, applied voltage—20 kV; PVDF9—180,000 g/mol, applied voltage—25 kV; PVDF10—530,000 gm/mol, applied voltage—15 kV; PVDF11—530,000 g/mol, applied voltage—20 kV rpm; PVDF12—530,000 g/mol, applied voltage—25 kV. All samples: Cp = 20%, F_R—1 mL/h, collector rotational speed—2000 rpm (details in Table 4).

Table 2. Electroactive phase content in PVDF scaffolds.

Sample ID	F(α) (%)	F(β) + F(γ) (%)	F(β) (%)	F(γ) (%)
Applied Voltage [kV]		15 kV		
PVDF7	63 ± 2	37 ± 0.4	23 ± 2.7	14 ± 2.9
PVDF10	48 ± 0.6	52 ± 2.9	28 ± 0.6	24 ± 0.9
Applied Voltage [kV]		22 kV		
PVDF8	8 ± 3	93 ± 1.4	48 ± 0.7	45 ± 1.1
PVDF11	11 ± 6.1	95 ± 6.3	45 ± 4	50 ± 0.9
Applied Voltage [kV]		25 kV		
PVDF9	78 ± 2	22 ± 0.6	15 ± 0.9	6 ± 3.4
PVDF12	63 ± 0.9	47 ± 0.7	26 ± 1.4	21 ± 1.8

2.2.3. The Flow Rate of the Solution

Figure 14 shows the FTIR-ATR spectra for electrospun fibers using various flow rates—0.5 mL/h, 0.8 mL/h, and 1.5 mL/h. The lowest flow rate (0.5 mL/h) was insufficient to form a stable polymer jet due to excessive stretching (similar to high applied voltage) [48]. To summarize, when the stretching effect is too low, it is difficult to form the electroactive phases (F(β) + F(γ) in PVDF13 and PVDF16, 34% and 42%, respectively). When the flow rate increases, the polymer jet is more stable, and in effect, the amount of electroactive phases increases (F_R = 0.8 mL/h, F(β) + F(γ) = 89% and 96% in PVDF14 and PVDF17, respectively). It is caused by the stretching effect—when the flow rate increases, the stretching effect decreases [49]. Next, when the flow rate reaches the value of 1.5 mL/h or more, the increase in the flow rate lowers the stretching effect of the electric field, and

the effect decreases the electroactive phase content (F(β) + F(γ) = 11% and 42% in PVDF15 and PVDF18, respectively) [50]. The changing of the flow rate affects the structure of the nanofibers and, more precisely, affects the stretching of the polymer solution. The phase content vs. flow rate has a maximum similar to the applied voltage and speed of the collector (Figure 15 and Table 3).

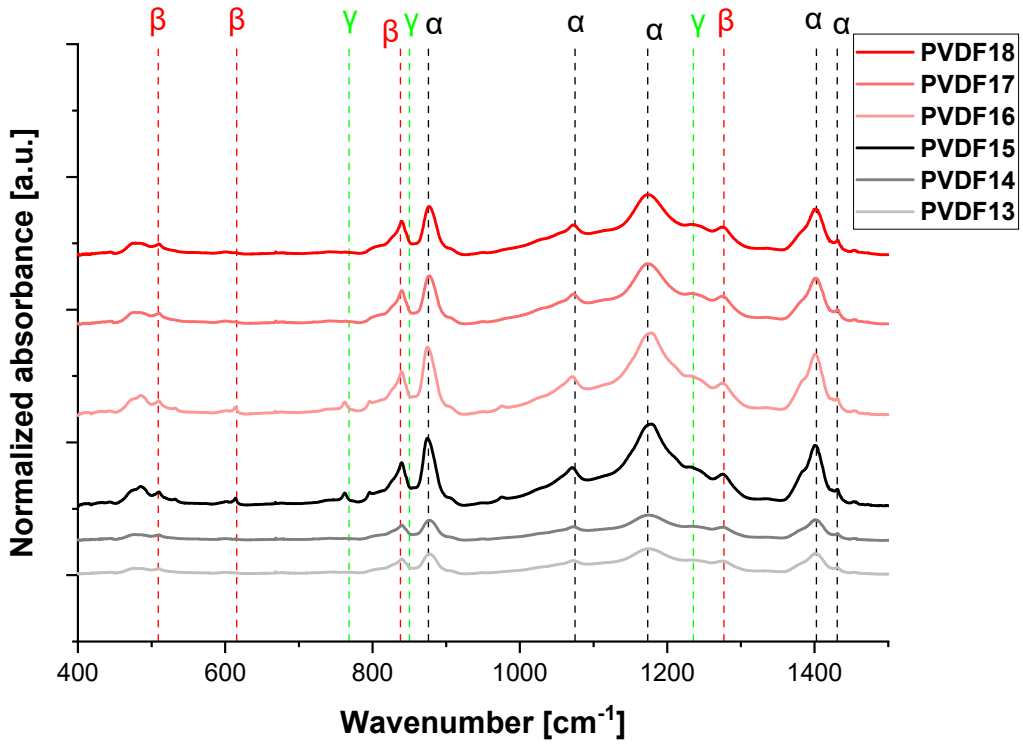

Figure 14. FTIR-ATR spectrum (400–1500 cm^{-1}) of selected samples formed with various flow rates. PVDF13—180,000 g/mol, F_R—0.5 mL/h; PVDF14—180,000 g/mol, F_R—1.0 mL/h; PVDF15—180,000 g/mol, F_R—1.5 mL/h; PVDF16—530,000 gm/mol, F_R—0.5 mL/h; PVDF17—530,000 g/mol, F_R—1.0 mL/h; PVDF18—530,000 g/mol, F_R—1.5 mL/h. All samples: Cp = 20%, collector rotational speed—2000 rpm, applied voltage—20 kV (details in Table 4).

Table 3. Electroactive phase content in PVDF scaffolds.

Sample ID	F(α) (%)	F(β) + F(γ) (%)	F(β) (%)	F(γ) (%)
Flow Rate		0.5 mL/h		
PVDF13	63 ± 2	37 ± 0.4	23 ± 2.7	14 ± 2.9
PVDF16	48 ± 0.6	52 ± 2.9	28 ± 0.6	24 ± 0.9
Flow Rate		0.8 mL/h		
PVDF14	7 ± 3	93 ± 1.4	48 ± 0.7	45 ± 1.1
PVDF17	3 ± 6.1	97 ± 6.3	47 ± 4	50 ± 0.9
Flow Rate		1.5 mL/h		
PVDF15	89 ± 2	11 ± 0.6	9 ± 0.9	7 ± 3.4
PVDF18	58 ± 0.9	42 ± 0.7	27 ±1.4	15 ± 1.8

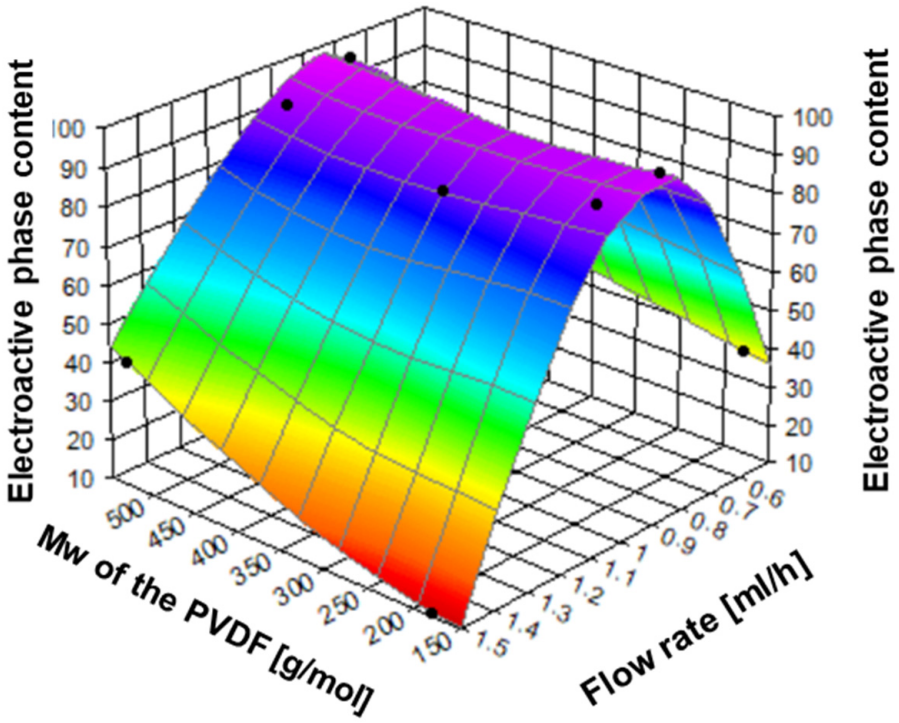

Figure 15. The relation between applied voltage, polymer molecular weight, and electroactive phase content. PVDF13—180,000 g/mol, $_{FR}$—0.5 mL/h; PVDF14—180,000 g/mol, F_R_1.0 mL/h; PVDF15—180,000 g/mol, F_R—1.5 mL/h; PVDF16—530,000 gm/mol, F_R—0.5 mL/h; PVDF17—530,000 g/mol, F_R—1.0 mL/h; PVDF18—530,000 g/mol, F_R—1.5 mL/h. All samples: Cp = 20%, collector rotational speed—2000 rpm, applied voltage—20 kV (details in Table 4).

2.3. Piezoelectric Coefficient Measurements

Measurements of the piezoelectric properties of the fibers with the highest electroactive phase content as a function of collector rotation speed and polymer molecular weight were performed (see Figure 16). Notably, regardless of the molecular weight used, the d_{33} response from the fibers increased with the rotations of the collector. It is seen that the effect of collector rotation speed is slightly larger for higher molecular weight samples, leading to higher d_{33} coefficients. For instance, the d_{33} piezoelectric coefficient for the highest rotational speed is 4.28 ± 0.08 for low molecular weight (PVDF21) and 4.52 ± 0.08 for high molecular weight (PVDF24). In contrast, the d_{33} piezoelectric coefficient for the lowest collector rotational speed is 0.9 ± 0.3 for low molecular weight (PVDF19), and 0.58 ± 0.08 for high molecular weight (PVDF22).

An increase in the piezoelectric coefficient with collector rotational speed is caused by an increase in electroactive phase content. Figure 17 illustrates the dependence of the piezoelectric coefficient on β and γ phase content determined by FTIR. Despite the relatively large data scattering, it is evident, as expected, a strong dependence of piezoelectricity on the content of both electroactive phases [51].

It is worth noticing that the increase in the piezoelectric coefficient with the collector rotational speed results in an increase in the electroactive phase content. Moreover, the dependence of the piezoelectric coefficient on the content of electroactive phases β and γ was proved based on FTIR analysis. Despite some scatter in the data, a strong dependence of piezoelectricity on the content of both electroactive phases is visible. The values of the d_{33} coefficient vary depending on the specific material and its properties, such as crystal structure, degree of polymerization, and production conditions. There are studies in the literature in which the d_{33} coefficient plays a key role, but in, e.g., electronic applications and is [52,53]. In the designed scaffolds, the goal was to increase the d_{33} factor while maintaining the cytotoxicity of the material for tissue engineering applications, and there are few such

detailed studies in the literature [54]. Moreover, human bone has piezoelectric properties lower than the designed materials and is at the level of 0.7–2.3 pC/N^{-1} [55–57]. Implanting a material with a higher piezoelectric coefficient d_{33} may result in faster regeneration of damaged bone.

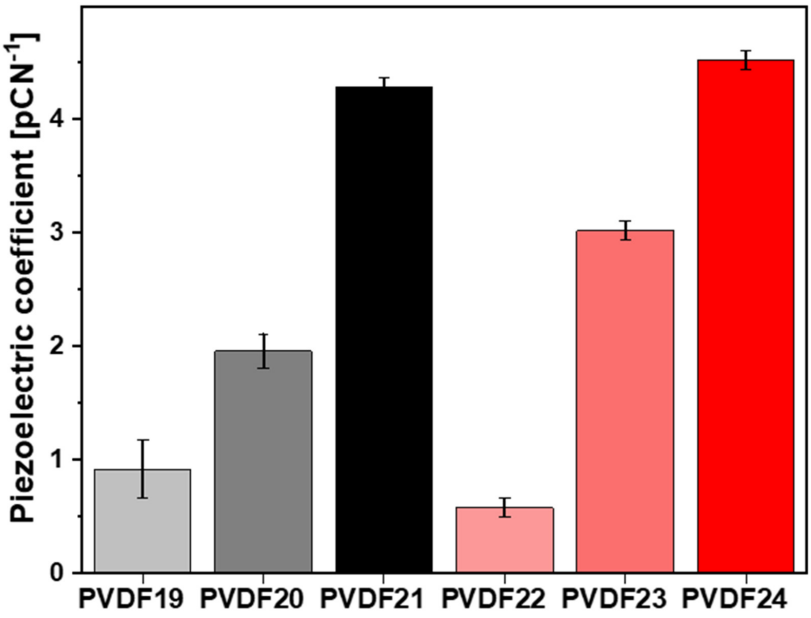

Figure 16. Results from d_{33} piezoelectric coefficient measurement of electrospun PVDF fibers. PVDF19—180,000 g/mol, collector rotational speed 200 rpm, PVDF20—180,000 g/mol, collector rotational speed—1000 rpm, PVDF21—180,000 g/mol, collector rotational speed—2000 rpm, PVDF22—530,000 g/mol, collector rotational speed—200 rpm, PVDF23—530,000 g/mol, collector rotational speed—1000 rpm, PVDF24—530,000 g/mol, collector rotational speed—2000 rpm. All samples: Cp—20%, applied voltage 22 kV, F_R—0.8 mL/h (details in Table 4).

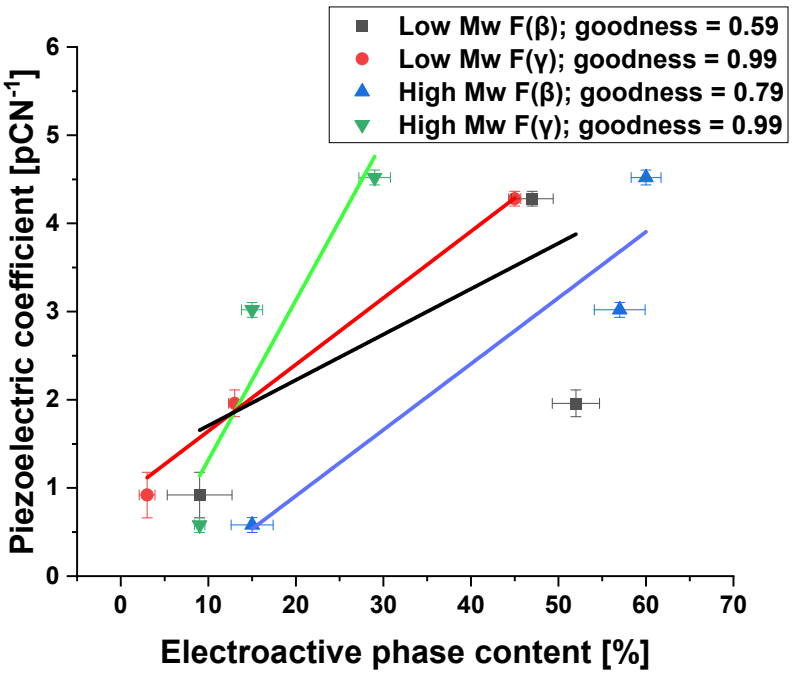

Figure 17. Dependence of the piezoelectricity coefficient d_{33} on the content of electroactive phases for low and high molecular weight PVDF.

2.4. In Vitro Study

Cell viability was assessed for ADSC cultured on scaffolds with the highest number of electroactive phases formed from PVDF (Mw—530,000 g/mol). Three types of materials, obtained by using different rotational speeds of the collector, i.e., 200 rpm, 1000 rpm, and 2000 rpm, with the same applied voltage of 22 kV and flow rate of 0.8 mL/h were taken into observation. The results of the viability assay performed on those materials are presented in Figure 18. In all cases, the growing cell number in time was observed. The highest values were obtained for the scaffolds obtained by using 2000 rpm rotational speed. For this material viability of ≥70% of the control was found regardless of the time point in culture, which confirms its cytotolerance in accordance with the ISO 10993-5.

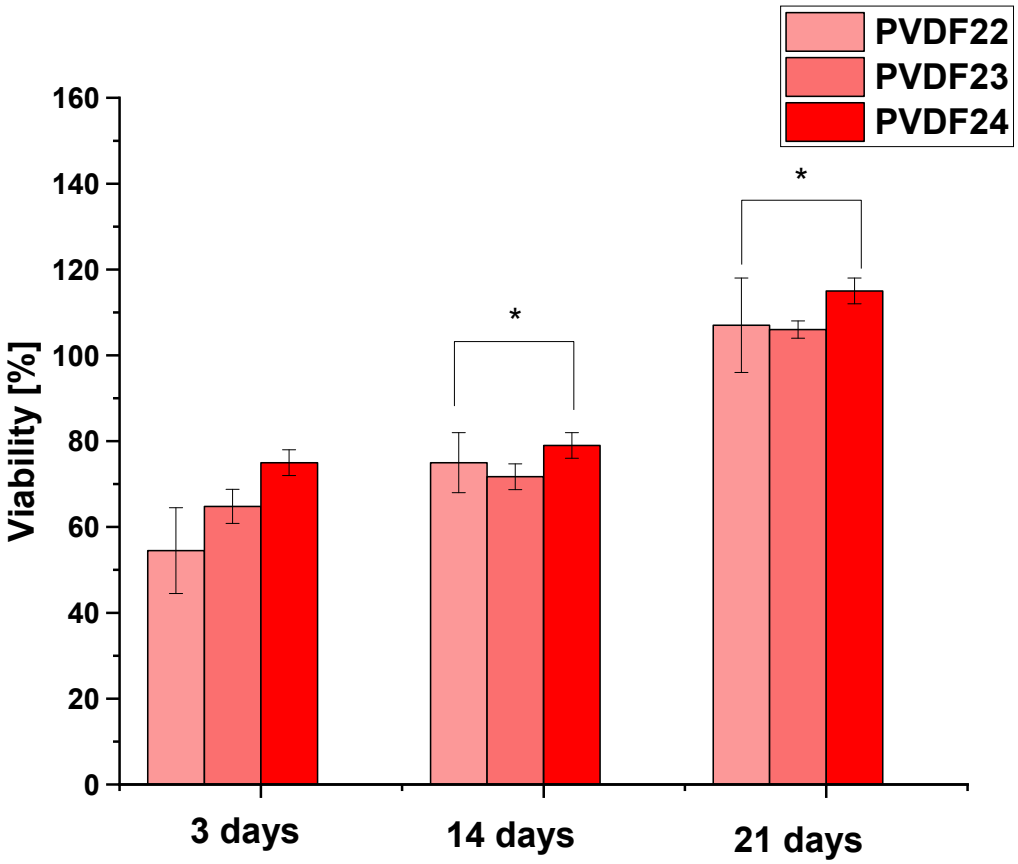

Figure 18. Cell viability of ADSC cultured on three types of PVDF samples different in rotational speeds of the collector applied—as described in Table 4, shown as the percentage of the values obtained in the control (cells cultured on tissue culture polystyrene). The data are presented as the mean value with standard deviation Statistical significance: * $p < 0.05$.

ADSCs morphology on the PVDF22, PVDF23, and PVDF24 samples, as visualized by SEM on days 3 and 21, is presented in Figure 19. Cell attachment and spreading were observed in all cases, which confirms material cytocompatibility. The densest culture—consisting of cells and, most likely, also of the extracellular matrix produced by them—was observed on the PVDF24 surface on day 21.

Cell proliferation, attachment, and spreading may be difficult on the surface of the scaffolds obtained by electrospinning as compared to the surface of the culture dish, which served as a control, because of the availability of the points for the focal adhesion formation. Nevertheless, the obtained results confirm the cytocompatibility of the investigated scaffolds, especially the PVDF24, i.e., the scaffold obtained by using the rotational speed of the collector of 2000 rpm.

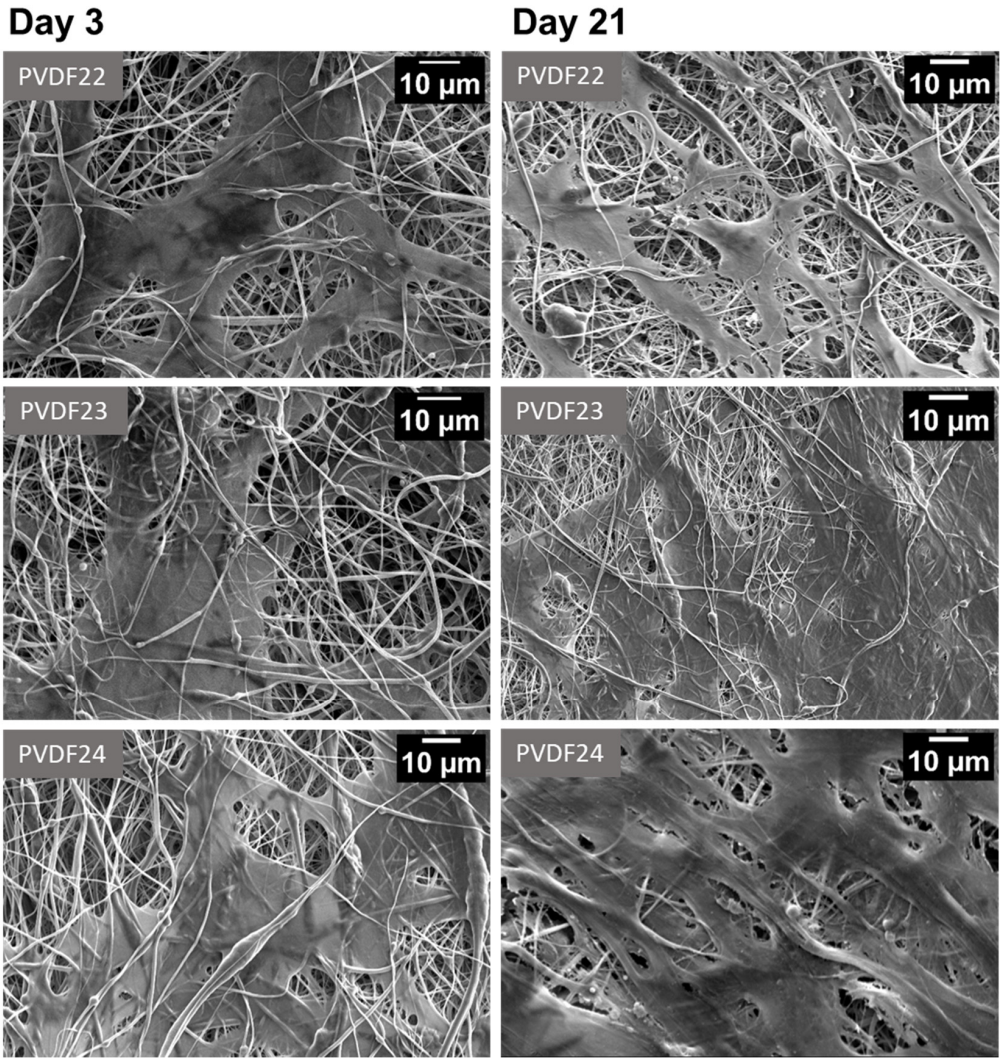

Figure 19. Representative SEM pictures of PVDF piezoelectric scaffolds cultured for 3, and 21 days. PVDF22—530,000 g/mol, collector rotational speed—200 rpm, PVDF23—530,000 g/mol, collector rotational speed—1000 rpm, PVDF24—530,000 g/mol, collector rotational speed—2000 rpm. All samples: Cp—20%, applied voltage 22 kV, F_R—0.8 mL/h (details in Table 4).

The development of nanostructured scaffolds with piezoelectric properties has shown promise in improving bone tissue regeneration [53]. Our research allows us to explore the issue of the formation and increase in the number of electroactive phases and their positive impact on the human adipose-derived stromal cells proliferation and also constitutes a good basis for determining the interactions of cells with the external environment (piezoelectric scaffold). In vitro, research on PVDF scaffolds is essential in the context of various fields of science [58], and PVDF is a material with unique properties that can be properly used to improve the lives of patients. Research on cell cultures on piezoelectric scaffolds concerns cell adhesion and proliferation [59], cytotoxicity, and the cultivation of piezoelectric scaffolds in the presence of ultrasound [60]. Recently, research has been conducted on the use of piezoelectric materials in the regeneration of vascularized bone [61]. However, there are also challenges associated with in vitro studies on PVDF scaffolds, such as controlling the electrospinning process to ensure a uniform and repeatable structure [62]. The quality of the scaffold formation is also important. Long-term studies are needed to determine the interactions of scaffolds with bone cells and the surrounding biological environment. Particularly noteworthy are ceramic nanoparticles with a high piezoelectricity coefficient (high d_{33}), which, when dispersed in a polymer matrix, can have a positive effect on increasing

the formation of piezoelectric phases while being biocompatible, which may constitute one of the systems with the most significant potential for BTE applications. In conclusion, in vitro studies on PVDF scaffolds have great potential in the field of regenerative medicine. However, further research is necessary to better understand the properties of these scaffolds and their potential clinical applications.

3. Materials and Methods

3.1. Materials

Poly(vinylidene fluoride) (PVDF) with various molecular masses, 180,000 g/mol and 530,000 g/mol (Merck, Rahway, NJ, USA) was used for the formation of the scaffold using electrospinning from *N*,*N*-Dimethylformamide (DMF), and acetone (Merck, USA) solutions.

All materials were analytical standard.

3.2. Electrospinning

The PVDF pellets from each polymer were dissolved in the solvent at a concentration of 20 wt % at 50 °C for 24 h until a visually homogeneous solution was formed. The electrospinning chamber (Fluidnatek LE-50, Bioinicia, Valencia, Spain) in a horizontal mode used for scaffold formation consisted of a syringe with the polymer solution, a needle 23G connected to the high-voltage supply with a positive potential, a pump, and a grounded collector. The fibers were collected as non-woven mats on a rotating drum (12 cm in length and 4 cm radius).

The process was provided at room temperature, 20% relative humidity, and 150 mm tip to the collector distance. The range of parameters was chosen to obtain a stable electrospinning process and continuous beadless fibers. The collected fiber mats were placed under the fume hood for 72 h for residual solvent evaporation. Table 4 describes the parameters used during electrospinning. Three sets of samples were analyzed from the perspective of the number of electroactive phases, morphology, and orientation. They were collected: (1) at various collector speeds, (2) at various applied voltages, and (3) at various flow rates. The effect of the applied voltage and of the flow rate was evaluated for the value of the collector speed 2000 rpm which led to the highest content of the electroactive phase. Then, 6 samples (PVDF19—PVDF24) were produced under favorable conditions for the formation of electroactive phases (applied voltage—22 kV, F_R—0.8 mL/h) and tested to determine the piezoelectric coefficient (d_{33}). Finally, 3 samples (PVDF22—PVDF24) with the highest number of electroactive phases (Mw—530,000 g/mol), formed at different collector rotational speeds (200 rpm, 1000 rpm, and 2000 rpm), were selected for in vitro tests.

Table 4. Sample identification.

Sample ID	Molecular Weight [g/mol]	Cp [%]	Applied Voltage [kV]	Flow Rate [ml/h]	Collector Speed [rpm]
PVDF1	180,000	20	20	1	200
PVDF2					1000
PVDF3					2000
PVDF4	530,000				200
PVDF5					1000
PVDF6					2000
PVDF7	180,000		15	1	2000
PVDF8			20		
PVDF9			25		
PVDF10	530,000		15		
PVDF11			20		
PVDF12			25		

Table 4. *Cont.*

Sample ID	Molecular Weight [g/mol]	Cp [%]	Applied Voltage [kV]	Flow Rate [ml/h]	Collector Speed [rpm]
PVDF13	180,000	20	20	0.5	2000
PVDF14				1	
PVDF15				1.5	
PVDF16	530,000			0.5	
PVDF17				1	
PVDF18				1.5	
PVDF19	180,000		22	0.8	200
PVDF20					1000
PVDF21					2000
PVDF22	530,000				200
PVDF23					1000
PVDF24					2000

3.3. Scanning Electron Microscopy (SEM)

Characterization of fiber morphology was performed using scanning electron microscopy (SEM, JSM-6010PLUS/LV InTouchScope™, JEOL, Tokyo, Japan) at an acceleration voltage of 10 kV. Prior to analysis, a layer of gold was applied to all samples. Quantitative microstructure analysis was performed using ImageJ software with the Fiji distribution plugin using Gaussian function approximation [63]. Fiber diameter was measured on 50 fibers for each fiber mat sample. The fiber diameter distribution was analyzed with the Gaussian fitting, also providing the goodness of fit using ImageJ software (1.52q software version).

The effect of the rotational speed of the collector on the fibers' orientation in the scaffold was determined using the directionality plugin to the ImageJ software. The orientation patterns were determined using the Fourier Transform on sections of the SEM images. The orientation distribution was approximated using the Gaussian function with Origin 2021b software. The degree of fiber alignment was additionally estimated using the full-width at half maximum (FWHM) of the Gaussian used for approximation of the orientation distribution. FWHM was averaged on five images for each sample.

The orientation factor was calculated using the anisotropy index α ($\alpha = 1$ for perfect alignment, and $\alpha = 0$ for random distribution), (Equations (1) and (2)) [64].

$$\Omega = \frac{1}{I_{tot}} \sum I_i \begin{vmatrix} cos^2\theta_i & sin\theta_i cos\theta_i \\ sin\theta_i cos\theta_i & sin^2\theta_i \end{vmatrix} \quad (1)$$

$$\alpha = 1 - \lambda_1/\lambda_2 \quad (2)$$

where Ω is the orientation matrix with eigenvalues of λ_1 and λ_2, I_{tot}—is the sum of the nanofiber length (nm), I_i—length of a single i-th nanofiber (nm), θ_i—the angle between the nanofiber axis and the x-axis (the direction perpendicular to the collector axis). The lengths of the nanofibers and the angles were determined from the SEM images using the Directionality plugin to the ImageJ software.

Total average porosity (p) was calculated as in our earlier research (Equation (3)) [65]:

$$p = \frac{V_t - V_f}{V_t} = \left(1 - V_f \times \frac{\rho}{m_t}\right) = \left(1 - \frac{m_f}{m_t}\right) \quad (3)$$

In this equation, m_t represents the theoretical mass of the solid sample, calculated as the product of the volume occupied by a patch V_t and the density of PVDF (1.75 g/cm^3)

while V_f and m_f denote the actual sample volume and mass, respectively. The average pore size (p) was determined using the following formula (Equation (4)):

$$P = \frac{2D}{(1-p)} \tag{4}$$

D represents the mean fiber diameter, and $(1-p)$ denotes the average total projected area of fibers per unit area, where p is approximately the total porosity.

3.4. Fourier Transform Infrared Spectroscopy (FTIR)

The content of the electroactive phases in the nonwoven scaffolds was determined using Fourier transform infrared spectroscopy (FTIR-ATR, Bruker Vertex 70, Billerica, MA, USA). The results presented are representative for five independent specimens and runs. The specimens were investigated from 400 cm^{-1} to 4000 cm^{-1} with a resolution of 2 cm^{-1}, which summarizes 32 scans.

F_{EA}, the relative content of two piezoelectric phases, β and γ, was determined in accordance to [42,66] using equation:

$$F_{EA} = \frac{I_{840^*}}{\left(\frac{K_{840^*}}{K_{763}}\right) \times I_{763} + I_{840^*}} \times 100\% \tag{5}$$

where I_{763} and I_{840^*} are the intensities of the bands at 763 cm^{-1} and 837–841 cm^{-1}, assigned to the α phase, and to both β and γ phases together, respectively. These absorption bands follow Beer–Lambert law with absorption coefficients of $K_{840^*} = 7.7 \times 10^4$ cm^2 mol^{-1}, and $K_{763} = 6.1 \times 10^4$.

The absorbance of the peak area or peak height at bands at 1234 cm^{-1} and 1275 cm^{-1} was used to quantify individual β and γ phases content, $F(\beta)$ and $F(\gamma)$. The procedure used was the calculation of the peak-to-valley height ratio between the peaks around 1234 cm^{-1} and 1275 cm^{-1}, and their nearest valleys.

$$F(\beta) = F_{EA} \times \left(\frac{\Delta H_{\beta'}}{\Delta H_{\beta'} + \Delta H_{\gamma'}}\right) \times 100\% \tag{6}$$

$$F(\gamma) = F_{EA} \times \left(\frac{\Delta H_{\gamma'}}{\Delta H_{\beta'} + \Delta H_{\gamma'}}\right) \times 100\% \tag{7}$$

where $\Delta H\beta'$ is the absorbance difference (height difference) between the peak, 1275 cm^{-1}, and the nearest valley, around 1260 cm^{-1}, and $\Delta H\gamma'$ is the peak, around 1234 cm^{-1} and the nearest valley, around 1225 cm^{-1}.

3.5. Piezoelectric Coefficient Measurements

The piezoelectric coefficients of the electrospun PVDF scaffolds were examined using a d_{33} meter (YE2730A d_{33} meter, Sinocera, Shanghai, China). This instrument is specifically designed for directly measuring the d_{33} values of piezoelectric materials. For testing, an 8 nm 80Au−20Pd layer (Q150RS, Quorum Technologies, Laughton, East Sussex, UK) was applied as an electrode on both sides of the PVDF fibers. Five measurements were conducted for each sample, and the average d_{33} value was calculated. To account for potentially low piezoelectric values of fibers resulting from the high porosity of the prepared materials, a reference sample was also tested to validate the instrument. The reference sample was a piezoelectrically poled PVDF film 110 μm thick, with a piezoelectric coefficient stated by the supplier ranging from 23 to 28 pCN^{-1}, obtained from PolyK (Philipsburg, PA 16866, USA). The sample was used as received after a 4 × 4 cm square was cut out from the polymer film. Prior to the measurements on fibers, the instrument was validated using the reference sample, which yielded a value of 25.6 ± 2.3 pCN^{-1}, falling within the manufacturer's specified range of 23–28 pCN^{-1}.

3.6. In Vitro Tests

Human adipose-derived stromal cells (ADSCs) were obtained according to established protocol as previously described [67] and cultured on the piezoelectric PVDF scaffolds electrospun with different collector rotational speeds (200, 1000, and 2000 rpm). First, PVDF samples were cut and sterilized by radiation. Next, for the cell viability test, piezoelectric scaffolds were placed in a 96-well culture plate (six samples for each type of material) and ADSCs were seeded directly on the surface of the scaffolds in a density of 4×10^3 cells per well. Cells seeded at the bottom of culture dish (6 wells) served as a control. For SEM observation, scaffolds were inserted into a 24-well culture plate (two samples per group) and seeded with a total of 5×10^4 cells per well. Cells were cultured in an osteogenic differentiation medium, composed of DMEM with 10% fetal bovine serum (FBS) and 1% antibiotic–antimycotic, supplemented with 10 nM dexamethasone, 3 mM NaH_2PO_4, and 50 µg/mL ascorbic acid 2-phosphate [68]. All specimens were incubated at 37 °C in 5% CO_2 for 21 days.

PrestoBlue assay (Thermo Fisher Scientific, Basingstoke, UK) for studying cellular metabolism activity was performed after 3, 14, and 21 days. First, the culture medium was removed, and cells were rinsed with PBS solution. Next, PrestoBlue working solution was applied and samples were placed in the incubator for 2 h. After incubation, solutions were transferred to new 96-well plate. Fluoroskan Ascent was used to measure the emission of the light at wavelengths 620 nm and 530 nm. Results were evaluated in comparison to the metabolic activity of the cells seeded on TCP (Tissue Culture Plastic, control 100%).

The observations of fibers and cell morphology were conducted using scanning electron microscopy (SEM, JSM-6010PLUS/LV InTouchScope™, JEOL, Tokyo, Japan) after 3 and 21 days. First, samples were properly prepared, washed with PBS, and next, were fixed with 2.5% glutaraldehyde in PBS overnight. The process of dehydration was conducted using water and ethanol (30, 40, 50, 60, 70, 80, 90, 100 (×2)% v/v). Then, ethanol/HDMS (Sigma Aldrich, Burlington, MA, USA) solutions were used (2:1 and 1:2 v/v). The last stage was to rinse samples with pure HDMS and leave them overnight.

3.7. Statistical Analysis

The data were additionally utilized to assess their statistical significance. The statistical analysis of viability data was conducted for $p < 0.05$ using GraphPad Prism 8.0.1 Software (GraphPad, Boston, MA, USA). A two-way ANOVA with Tukey's multiple comparisons test was conducted as necessary. A p-value below 0.05 was deemed statistically significant. Notations of "*" were assigned as $0.01 < p < 0.05$, "**" was assigned as $0.001 < p < 0.01$, and "***" was assigned as $p < 0.001$.

4. Conclusions

This study aimed to better understand to fundamental process of forming the polar phases in PVDF. The most important result is a demonstration of the effect of selected electrospinning parameters—rotational collector speed, the solution flow rate, and the applied voltage on polymorphs content of two PVDF types differing in molecular weight (180,000 g/mol and 530,000 g/mol). It is evident that in the case of rotational collector speed, there is a continuous increase in electroactive β and γ phase content, in addition to the rise of fiber orientation and reduction in fiber diameter. In the case of the applied voltage and solution flow rate, there is a maximum of electroactive phase content at a particular parameter's value. Therefore, the electroactive phase content is possible by optimizing the processing parameters. The maximum electroactive phase content equal to 92% was obtained at a rotational collector speed of 2000 rpm, voltage of 22 kV, and a flow rate of 0.8 mL/h. An increase in electroactive phase content is responsible for the observed increase in piezoelectric d_{33} coefficient, which could be crucial for cells considering the further perspective of using this kind of scaffold in regenerative medicine. Cell culture using human-adipose-derived stromal cells confirmed the non-cytotoxic nature of scaffolds. Additionally, it was observed that the cell viability increases not only with cultivation time

but also for fibers collected with the highest rotational speed, with the best fiber orientation and the largest content of electroactive phases.

Author Contributions: Conceptualization, A.Z., A.G. and P.Ł.S.; methodology, A.Z. (Angelika Zaszczyńska), A.G., A.Z. (Anna Ziemiecka), P.K.S., R.T., M.L.-S., U.S. and P.Ł.S.; software, A.Z. (Angelika Zaszczyńska), A.G., A.Z. (Anna Ziemiecka), and P.Ł.S.; validation, R.T., M.L.-S., U.S., P.K.S. and P.Ł.S.; formal analysis, A.Z. (Angelika Zaszczyńska), A.G., A.Z. (Anna Ziemiecka), P.K.S., R.T., M.L.-S., U.S. and P.Ł.S.; investigation, A.Z. (Angelika Zaszczyńska), A.Z. (Anna Ziemiecka), P.K.S., R.T., M.L.-S., U.S. and P.Ł.S.; writing—original draft preparation, A.Z. (Angelika Zaszczyńska), A.G. and P.Ł.S.; writing—review and editing, A.Z. (Angelika Zaszczyńska), A.G., A.Z. (Anna Ziemiecka), P.K.S., R.T., M.L.-S., U.S. and P.Ł.S.; software, A.Z. (Angelika Zaszczyńska), A.G., A.Z. (Anna Ziemiecka), and P.Ł.S.; visualization, A.Z. (Angelika Zaszczyńska), A.G. and P.Ł.S.; supervision, R.T., M.L.-S., U.S. and P.Ł.S. All authors have read and agreed to the published version of the manuscript.

Funding: This research received no external funding.

Institutional Review Board Statement: Not applicable.

Informed Consent Statement: Not applicable.

Data Availability Statement: Data are contained within the article.

Conflicts of Interest: The authors declare no conflicts of interest.

References

1. Zaszczyńska, A.; Niemczyk-Soczynska, B.; Sajkiewicz, P. A Comprehensive Review of Electrospun Fibers, 3D-Printed Scaffolds, and Hydrogels for Cancer Therapies. *Polymers* **2022**, *14*, 5278. [CrossRef]
2. Riggs, B.L.; Melton, L.J. The Worldwide Problem of Osteoporosis: Insights Afforded by Epidemiology. *Bone* **1995**, *17*, S505–S511. [CrossRef] [PubMed]
3. Lin, H.; Sohn, J.; Shen, H.; Langhans, M.T.; Tuan, R.S. Bone Marrow Mesenchymal Stem Cells: Aging and Tissue Engineering Applications to Enhance Bone Healing. *Biomaterials* **2019**, *203*, 96–110. [CrossRef] [PubMed]
4. Singh, J.; Rani, S.; Rohini; Parida, A. Generation of Piezoelectricity from the Human Body. In Proceedings of the 2014 Annual International Conference on Emerging Research Areas: Magnetics, Machines and Drives (AICERA/iCMMD), Kottayam, India, 24–26 July 2014; IEEE: Piscataway, NJ, USA, 2014; pp. 1–5.
5. Chorsi, M.T.; Curry, E.J.; Chorsi, H.T.; Das, R.; Baroody, J.; Purohit, P.K.; Ilies, H.; Nguyen, T.D. Piezoelectric Biomaterials for Sensors and Actuators. *Adv. Mater.* **2019**, *31*, 1802084. [CrossRef]
6. Dec, P.; Modrzejewski, A.; Pawlik, A. Existing and Novel Biomaterials for Bone Tissue Engineering. *Int. J. Mol. Sci.* **2022**, *24*, 529. [CrossRef]
7. Fukada, E.; Yasuda, I. On the Piezoelectric Effect of Bone. *J. Phys. Soc. Jpn.* **1957**, *12*, 1158–1162. [CrossRef]
8. Bassett, C.A.L. Biologic Significance of Piezoelectricity. *Calc. Tis Res.* **1967**, *1*, 252–272. [CrossRef] [PubMed]
9. Hammerick, K.E.; Longaker, M.T.; Prinz, F.B. In Vitro Effects of Direct Current Electric Fields on Adipose-Derived Stromal Cells. *Biochem. Biophys. Res. Commun.* **2010**, *397*, 12–17. [CrossRef] [PubMed]
10. Chiu, A.; Sharma, D.; Zhao, F. Tissue Engineering-Based Strategies for Diabetic Foot Ulcer Management. *Adv. Wound Care* **2023**, *12*, 145–167. [CrossRef]
11. Metwally, S.; Ferraris, S.; Spriano, S.; Krysiak, Z.J.; Kaniuk, Ł.; Marzec, M.M.; Kim, S.K.; Szewczyk, P.K.; Gruszczyński, A.; Wytrwal-Sarna, M.; et al. Surface Potential and Roughness Controlled Cell Adhesion and Collagen Formation in Electrospun PCL Fibers for Bone Regeneration. *Mater. Des.* **2020**, *194*, 108915. [CrossRef]
12. Metwally, S.; Stachewicz, U. Surface Potential and Charges Impact on Cell Responses on Biomaterials Interfaces for Medical Applications. *Mater. Sci. Eng. C* **2019**, *104*, 109883. [CrossRef] [PubMed]
13. Chackal-Roy, M.; Niemeyer, C.; Moore, M.; Zetter, B.R. Stimulation of Human Prostatic Carcinoma Cell Growth by Factors Present in Human Bone Marrow. *J. Clin. Investig.* **1989**, *84*, 43–50. [CrossRef] [PubMed]
14. Mokhtari, F.; Azimi, B.; Salehi, M.; Hashemikia, S.; Danti, S. Recent Advances of Polymer-Based Piezoelectric Composites for Biomedical Applications. *J. Mech. Behav. Biomed. Mater.* **2021**, *122*, 104669. [CrossRef] [PubMed]
15. Joo, S.; Gwon, Y.; Kim, S.; Park, S.; Kim, J.; Hong, S. Piezoelectrically and Topographically Engineered Scaffolds for Accelerating Bone Regeneration. *ACS Appl. Mater. Interfaces* **2024**, *16*, 1999–2011. [CrossRef] [PubMed]
16. Szewczyk, P.K.; Metwally, S.; Karbowniczek, J.E.; Marzec, M.M.; Stodolak-Zych, E.; Gruszczyński, A.; Bernasik, A.; Stachewicz, U. Surface-Potential-Controlled Cell Proliferation and Collagen Mineralization on Electrospun Polyvinylidene Fluoride (PVDF) Fiber Scaffolds for Bone Regeneration. *ACS Biomater. Sci. Eng.* **2019**, *5*, 582–593. [CrossRef] [PubMed]
17. Ura, D.P.; Rosell-Llompart, J.; Zaszczyńska, A.; Vasilyev, G.; Gradys, A.; Szewczyk, P.K.; Knapczyk-Korczak, J.; Avrahami, R.; Šišková, A.O.; Arinstein, A.; et al. The Role of Electrical Polarity in Electrospinning and on the Mechanical and Structural Properties of As-Spun Fibers. *Materials* **2020**, *13*, 4169. [CrossRef] [PubMed]

18. Jang, J.-W.; Min, K.-E.; Kim, C.; Shin, J.; Lee, J.; Yi, S. Review: Scaffold Characteristics, Fabrication Methods, and Biomaterials for the Bone Tissue Engineering. *Int. J. Precis. Eng. Manuf.* **2023**, *24*, 511–529. [CrossRef]
19. Sill, T.J.; Von Recum, H.A. Electrospinning: Applications in Drug Delivery and Tissue Engineering. *Biomaterials* **2008**, *29*, 1989–2006. [CrossRef] [PubMed]
20. Yoshimoto, H.; Shin, Y.M.; Terai, H.; Vacanti, J.P. A Biodegradable Nanofiber Scaffold by Electrospinning and Its Potential for Bone Tissue Engineering. *Biomaterials* **2003**, *24*, 2077–2082. [CrossRef]
21. Kitsara, M.; Agbulut, O.; Kontziampasis, D.; Chen, Y.; Menasché, P. Fibers for Hearts: A Critical Review on Electrospinning for Cardiac Tissue Engineering. *Acta Biomater.* **2017**, *48*, 20–40. [CrossRef]
22. Electroactive Biomaterials Regulate the Electrophysiological Microenvironment to Promote Bone and Cartilage Tissue Regeneration-Chen-Advanced Functional Materials-Wiley Online Library. Available online: https://onlinelibrary.wiley.com/doi/full/10.1002/adfm.202314079 (accessed on 8 April 2024).
23. Soliman, S.; Pagliari, S.; Rinaldi, A.; Forte, G.; Fiaccavento, R.; Pagliari, F.; Franzese, O.; Minieri, M.; Di Nardo, P.; Licoccia, S.; et al. Multiscale Three-Dimensional Scaffolds for Soft Tissue Engineering via Multimodal Electrospinning. *Acta Biomater.* **2010**, *6*, 1227–1237. [CrossRef]
24. Keirouz, A.; Chung, M.; Kwon, J.; Fortunato, G.; Radacsi, N. 2D and 3D Electrospinning Technologies for the Fabrication of Nanofibrous Scaffolds for Skin Tissue Engineering: A Review. *WIREs Nanomed. Nanobiotechnol.* **2020**, *12*, e1626. [CrossRef] [PubMed]
25. Saghati, S.; Akbarzadeh, A.; Del Bakhshayesh, A.R.; Sheervalilou, R.; Mostafavi, E. CHAPTER 6. Electrospinning and 3D Printing: Prospects for Market Opportunity. In *Soft Matter Series*; Kny, E., Ghosal, K., Thomas, S., Eds.; Royal Society of Chemistry: Cambridge, UK, 2018; pp. 136–155. ISBN 978-1-78801-100-6.
26. Bai, Y.; Liu, Y.; Lv, H.; Shi, H.; Zhou, W.; Liu, Y.; Yu, D.-G. Processes of Electrospun Polyvinylidene Fluoride-Based Nanofibers, Their Piezoelectric Properties, and Several Fantastic Applications. *Polymers* **2022**, *14*, 4311. [CrossRef] [PubMed]
27. Li, Y.; Liao, C.; Tjong, S.C. Electrospun Polyvinylidene Fluoride-Based Fibrous Scaffolds with Piezoelectric Characteristics for Bone and Neural Tissue Engineering. *Nanomaterials* **2019**, *9*, 952. [CrossRef]
28. Jun, I.; Han, H.-S.; Edwards, J.; Jeon, H. Electrospun Fibrous Scaffolds for Tissue Engineering: Viewpoints on Architecture and Fabrication. *Int. J. Mol. Sci.* **2018**, *19*, 745. [CrossRef]
29. Bhardwaj, N.; Kundu, S.C. Electrospinning: A Fascinating Fiber Fabrication Technique. *Biotechnol. Adv.* **2010**, *28*, 325–347. [CrossRef]
30. Farag, M.M. Recent Trends on Biomaterials for Tissue Regeneration Applications: Review. *J. Mater. Sci.* **2023**, *58*, 527–558. [CrossRef]
31. Wang, S.; Li, Q. Design, Synthesis and Processing of PVDF-based Dielectric Polymers. *IET Nanodielectrics* **2018**, *1*, 80–91. [CrossRef]
32. Salimi, A.; Yousefi, A.A. Analysis Method. *Polym. Test.* **2003**, *22*, 699–704. [CrossRef]
33. Huang, Y.; Zeng, J.; Li, S.; Dai, C.; Liu, J.; Liu, C.; He, Y. Conformational Regulation of Dielectric Poly(Vinylidene Fluoride)-Based Solid-State Electrolytes for Efficient Lithium Salt Dissociation and Lithium-Ion Transportation. *Adv. Energy Mater.* **2023**, *13*, 2203888. [CrossRef]
34. Yin, J.-Y.; Boaretti, C.; Lorenzetti, A.; Martucci, A.; Roso, M.; Modesti, M. Effects of Solvent and Electrospinning Parameters on the Morphology and Piezoelectric Properties of PVDF Nanofibrous Membrane. *Nanomaterials* **2022**, *12*, 962. [CrossRef] [PubMed]
35. Cui, Z.; Hassankiadeh, N.T.; Zhuang, Y.; Drioli, E.; Lee, Y.M. Crystalline Polymorphism in Poly(Vinylidenefluoride) Membranes. *Prog. Polym. Sci.* **2015**, *51*, 94–126. [CrossRef]
36. Cozza, E.S.; Monticelli, O.; Cavalleri, O.; Marsano, E. Preparation, Characterization, and Properties of Nanofibers Based on Poly(Vinylidene Fluoride) and Polyhedral Oligomeric Silsesquioxane. *Polym. Adv. Techs* **2012**, *23*, 1252–1257. [CrossRef]
37. He, Z.; Rault, F.; Lewandowski, M.; Mohsenzadeh, E.; Salaün, F. Electrospun PVDF Nanofibers for Piezoelectric Applications: A Review of the Influence of Electrospinning Parameters on the β Phase and Crystallinity Enhancement. *Polymers* **2021**, *13*, 174. [CrossRef] [PubMed]
38. Nayak, T.R.; Jian, L.; Phua, L.C.; Ho, H.K.; Ren, Y.; Pastorin, G. Thin Films of Functionalized Multiwalled Carbon Nanotubes as Suitable Scaffold Materials for Stem Cells Proliferation and Bone Formation. *ACS Nano* **2010**, *4*, 7717–7725. [CrossRef]
39. Ren, L.; Ozisik, R.; Kotha, S.P.; Underhill, P.T. Highly Efficient Fabrication of Polymer Nanofiber Assembly by Centrifugal Jet Spinning: Process and Characterization. *Macromolecules* **2015**, *48*, 2593–2602. [CrossRef]
40. Rošic, R.; Pelipenko, J.; Kocbek, P.; Baumgartner, S.; Bešter-Rogač, M.; Kristl, J. The Role of Rheology of Polymer Solutions in Predicting Nanofiber Formation by Electrospinning. *Eur. Polym. J.* **2012**, *48*, 1374–1384. [CrossRef]
41. Chakrabarty, B.; Ghoshal, A.K.; Purkait, M.K. Effect of Molecular Weight of PEG on Membrane Morphology and Transport Properties. *J. Membr. Sci.* **2008**, *309*, 209–221. [CrossRef]
42. Ghobeira, R.; Asadian, M.; Vercruysse, C.; Declercq, H.; De Geyter, N.; Morent, R. Wide-Ranging Diameter Scale of Random and Highly Aligned PCL Fibers Electrospun Using Controlled Working Parameters. *Polymer* **2018**, *157*, 19–31. [CrossRef]
43. Baji, A.; Mai, Y.-W.; Wong, S.-C.; Abtahi, M.; Chen, P. Electrospinning of Polymer Nanofibers: Effects on Oriented Morphology, Structures and Tensile Properties. *Compos. Sci. Technol.* **2010**, *70*, 703–718. [CrossRef]
44. Sajkiewicz, P.; Wasiak, A.; Gocłowski, Z. Phase Transitions during Stretching of Poly(Vinylidene Fluoride). *Eur. Polym. J.* **1999**, *35*, 423–429. [CrossRef]

45. Kalimuldina, G.; Turdakyn, N.; Abay, I.; Medeubayev, A.; Nurpeissova, A.; Adair, D.; Bakenov, Z. A Review of Piezoelectric PVDF Film by Electrospinning and Its Applications. *Sensors* **2020**, *20*, 5214. [CrossRef] [PubMed]
46. Ribeiro, C.; Sencadas, V.; Ribelles, J.G.; Lanceros-Méndez, S. Influence of Processing Conditions on Polymorphism and Nanofiber Morphology of Electroactive Poly(Vinylidene Fluoride) Electrospun Membranes. *Fac. Eng. Inf. Sci.-Pap. Part A* **2010**, *8*, 274–287. [CrossRef]
47. He, Z.; Rault, F.; Vishwakarma, A.; Mohsenzadeh, E.; Salaün, F. High-Aligned PVDF Nanofibers with a High Electroactive Phase Prepared by Systematically Optimizing the Solution Property and Process Parameters of Electrospinning. *Coatings* **2022**, *12*, 1310. [CrossRef]
48. Gebrekrstos, A.; Muzata, T.; Sinha Ray, S. Nanoparticle-Enhanced β-Phase Formation in Electroactive PVDF Composites: A Review of Systems for Applications in Energy Harvesting, EMI Shielding, and Membrane Technology. *ACS Appl. Nano Mater.* **2022**, *5*, 7632–7651. [CrossRef]
49. Wang, S.-H.; Wan, Y.; Sun, B.; Liu, L.-Z.; Xu, W. Mechanical and Electrical Properties of Electrospun PVDF/MWCNT Ultrafine Fibers Using Rotating Collector. *Nanoscale Res. Lett.* **2014**, *9*, 522. [CrossRef] [PubMed]
50. Leon-Valdivieso, C.Y.; Garcia-Garcia, A.; Legallais, C.; Bedoui, F. Electrospinning of Biomedically Relevant Multi-Region Scaffolds: From Honeycomb to Randomly-Oriented Microstructure. *Polymer* **2020**, *202*, 122606. [CrossRef]
51. Liu, K.; Wang, H.; Wu, Y.; Wang, Y.; Yuan, C. Preparation and Properties of Gamma-PVDF/Lead Zirconium Titanate Composites. *Polymer* **2023**, *281*, 126091. [CrossRef]
52. Wu, C.-M.; Chou, M.-H.; Zeng, W.-Y. Piezoelectric Response of Aligned Electrospun Polyvinylidene Fluoride/Carbon Nanotube Nanofibrous Membranes. *Nanomaterials* **2018**, *8*, 420. [CrossRef]
53. Donate, R.; Paz, R.; Moriche, R.; Sayagués, M.J.; Alemán-Domínguez, M.E.; Monzón, M. An Overview of Polymeric Composite Scaffolds with Piezoelectric Properties for Improved Bone Regeneration. *Mater. Des.* **2023**, *231*, 112085. [CrossRef]
54. Najjari, A.; Aghdam, R.M.; Ebrahimi, S.A.S.; Suresh, K.S.; Krishnan, S.; Shanthi, C.; Ramalingam, M. Smart Piezoelectric Biomaterials for Tissue Engineering and Regenerative Medicine: A Review. *Biomed. Eng./Biomed. Tech.* **2022**, *67*, 71–88. [CrossRef] [PubMed]
55. Tang, Y.; Wu, C.; Wu, Z.; Hu, L.; Zhang, W.; Zhao, K. Fabrication and in Vitro Biological Properties of Piezoelectric Bioceramics for Bone Regeneration. *Sci. Rep.* **2017**, *7*, 43360. [CrossRef] [PubMed]
56. Zhang, Y.; Chen, L.; Zeng, J.; Zhou, K.; Zhang, D. Aligned Porous Barium Titanate/Hydroxyapatite Composites with High Piezoelectric Coefficients for Bone Tissue Engineering. *Mater. Sci. Eng. C* **2014**, *39*, 143–149. [CrossRef] [PubMed]
57. Tandon, B.; Blaker, J.J.; Cartmell, S.H. Piezoelectric Materials as Stimulatory Biomedical Materials and Scaffolds for Bone Repair. *Acta Biomater.* **2018**, *73*, 1–20. [CrossRef] [PubMed]
58. Long, L.; Liu, W.; Hu, C.; Yang, L.; Wang, Y. Construction of Multifunctional Wound Dressings with Their Application in Chronic Wound Treatment. *Biomater. Sci.* **2022**, *10*, 4058–4076. [CrossRef] [PubMed]
59. Orkwis, J.A.; Wolf, A.K.; Shahid, S.M.; Smith, C.; Esfandiari, L.; Harris, G.M. Development of a Piezoelectric PVDF-TrFE Fibrous Scaffold to Guide Cell Adhesion, Proliferation, and Alignment. *Macromol. Biosci.* **2020**, *20*, 2000197. [CrossRef] [PubMed]
60. Cafarelli, A.; Marino, A.; Vannozzi, L.; Puigmartí-Luis, J.; Pané, S.; Ciofani, G.; Ricotti, L. Piezoelectric Nanomaterials Activated by Ultrasound: The Pathway from Discovery to Future Clinical Adoption. *ACS Nano* **2021**, *15*, 11066–11086. [CrossRef]
61. D'Alessandro, D.; Ricci, C.; Milazzo, M.; Strangis, G.; Forli, F.; Buda, G.; Petrini, M.; Berrettini, S.; Uddin, M.J.; Danti, S.; et al. Piezoelectric Signals in Vascularized Bone Regeneration. *Biomolecules* **2021**, *11*, 1731. [CrossRef]
62. Lei, T.; Zhu, P.; Cai, X.; Yang, L.; Yang, F. Electrospinning of PVDF Nanofibrous Membranes with Controllable Crystalline Phases. *Appl. Phys. A* **2015**, *120*, 5–10. [CrossRef]
63. Schindelin, J.; Arganda-Carreras, I.; Frise, E.; Kaynig, V.; Longair, M.; Pietzsch, T.; Preibisch, S.; Rueden, C.; Saalfeld, S.; Schmid, B.; et al. Fiji: An Open-Source Platform for Biological-Image Analysis. *Nat. Methods* **2012**, *9*, 676–682. [CrossRef]
64. Shehata, N.; Elnabawy, E.; Abdelkader, M.; Hassanin, A.; Salah, M.; Nair, R.; Ahmad Bhat, S. Static-Aligned Piezoelectric Poly (Vinylidene Fluoride) Electrospun Nanofibers/MWCNT Composite Membrane: Facile Method. *Polymers* **2018**, *10*, 965. [CrossRef] [PubMed]
65. Czwartos, J.; Zaszczyńska, A.; Nowak-Stępniowska, A.; Fok, T.; Budner, B.; Bartnik, A.; Wachulak, P.; Kołbuk, D.; Sajkiewicz, P.; Fiedorowicz, H. The Novel Approach to Physico-Chemical Modification and Cytocompatibility Enhancement of Fibrous Polycaprolactone (PCL) Scaffolds Using Soft X-Ray/Extreme Ultraviolet (SXR/EUV) Radiation and Low-Temperature, SXR/EUV Induced, Nitrogen and Oxygen Plasmas. *Appl. Surf. Sci.* **2022**, *606*, 154779. [CrossRef]
66. Zaszczyńska, A.; Sajkiewicz, P.; Gradys, A.; Tymkiewicz, R.; Urbanek, O.; Kolbuk, D. Influence of Process-Material Conditions on the Structure and Biological Properties of Electrospun Polyvinylidene Fluoride Fibers. *Bull. Pol. Acad. Sci. Tech. Sci.* **2020**, *68*, 627–633. [CrossRef]

67. Mrozikiewicz-Rakowska, B.; Szabłowska-Gadomska, I.; Cysewski, D.; Rudziński, S.; Płoski, R.; Gasperowicz, P.; Konarzewska, M.; Zieliński, J.; Mieczkowski, M.; Sieńko, D.; et al. Allogenic Adipose-Derived Stem Cells in Diabetic Foot Ulcer Treatment: Clinical Effectiveness, Safety, Survival in the Wound Site, and Proteomic Impact. *Int. J. Mol. Sci.* **2023**, *24*, 1472. [CrossRef] [PubMed]
68. Rumiński, S.; Kalaszczyńska, I.; Długosz, A.; Lewandowska-Szumieł, M. Osteogenic Differentiation of Human Adipose-Derived Stem Cells in 3D Conditions–Comparison of Spheroids and Polystyrene Scaffolds. *eCM* **2019**, *37*, 382–401. [CrossRef]

Micron 188 (2025) 103743

Contents lists available at ScienceDirect

Micron

journal homepage: www.elsevier.com/locate/micron

Poly(L-lactide)/nano-hydroxyapatite piezoelectric scaffolds for tissue engineering

Angelika Zaszczyńska [a], Arkadiusz Gradys [a], Dorota Kołbuk [a], Konrad Zabielski [a], Piotr K. Szewczyk [b], Urszula Stachewicz [b], Paweł Sajkiewicz [a,*]

[a] Institute of Fundamental Technological Research, Polish Academy of Sciences, Pawinskiego 5B, Warsaw 02-105, Poland
[b] Faculty of Metals Engineering and Industrial Computer Science, AGH University of Krakow, Krakow 30-059, Poland

ARTICLE INFO

Keywords:
Scaffolds
Tissue engineering
Bone tissue engineering
Smart medicine
Biodegradable polymers
Regenerative medicine

ABSTRACT

The development of bone tissue engineering, a field with significant potential, requires a biomaterial with high bioactivity. The aim of this manuscript was to fabricate a nanofibrous poly(L-lactide) (PLLA) scaffold containing nano-hydroxyapatite (nHA) to investigate PLLA/nHA composites, particularly the effect of fiber arrangement and the addition of nHA on the piezoelectric phases and piezoelectricity of PLLA samples. In this study, we evaluated the effect of nHA particles on a PLLA-based electrospun scaffold with random and aligned fiber orientations. The addition of nHA increased the surface free energy of PLLA/nHA (42.9 mN/m) compared to PLLA (33.1 mN/m) in the case of aligned fibers. WAXS results indicated that at room temperature, all the fibers are in an amorphous state indicated by a lack of diffraction peaks and amorphous halo. DSC analysis showed that all samples located in the amorphous/disordered alpha' phase crystallize intensively at temperatures just above the T_g and recrystallize on further heating, achieving significantly higher crystallinity for pure PLLA than for doped nHA, 70 % vs 40 %, respectively. Additionally, PLLA/nHA fibers show a lower heat capacity for PLLA in the amorphous state, indicating that nHA reduces the molecular mobility of PLLA. Moreover, piezoelectric constant d_{33} was found to increase with the addition of nHA and for the aligned orientation of the fibers. *In vitro* tests confirmed that the addition of nHA and the aligned orientation of nanofibers increased osteoblast proliferation.

1. Introduction

Over 1 million bone graft procedures are conducted annually in the United States (Huang et al., 2024; Wortham et al., 2024). Tissue engineering emerges as a potential avenue for effective bone repair (Zhang et al., 2024). Scaffolds intended for bone tissue engineering must have a structure similar to natural bone (Kennedy et al., 2024; Zaszczyńska et al., 2022) and be meticulously formed to facilitate osteogenic cell adhesion, proliferation, and differentiation (Bose et al., 2024; Pathak et al., 2023).

The requirements for cellular scaffolds in bone tissue engineering include several key aspects of effective bone growth, development, and regeneration (Bose et al., 2012). To provide adequate structural support, scaffolds can have a similar chemical composition and architecture similar to natural bone tissue (Chen et al., 2022). They must be biocompatible, meaning they should not cause negative immune reactions or toxicity when interfacing with surrounding cells (Fendi et al., 2024). This is crucial to avoid rejection and ensure safe use in living organisms. Additionally, the scaffold should gradually degrade, leaving space for the growth and regeneration of natural bone (Bauso et al., 2024; Manzini et al., 2021). Optimal scaffold microstructure and porosity allow nutrients, gases, and cells to diffuse through the scaffold. High porosity supports cell colonization and increases the effectiveness of regenerative processes (Liu et al., 2023). From the perspective of scaling from the laboratory to the industrial scale and widespread use, there should be the ease of fabrication of these scaffolds in a controlled manner, and the production process should be easy to scale to enable mass production for clinical applications (Norouzi et al., 2024; Zaszczyńska et al., 2024a).

PLLA exists in an amorphous or semi-crystalline form, exhibiting several desirable properties in tissue engineering (Khouri et al., 2024; Saurav et al., 2024; Srivastava et al., 2024). One of the possible applications is the area of bone tissue engineering, considering its favorable biocompatibility and biodegradability (Liu et al., 2024; Sethu et al.,

* Corresponding author.
E-mail address: psajk@ippt.pan.pl (P. Sajkiewicz).

https://doi.org/10.1016/j.micron.2024.103743
Received 17 October 2024; Received in revised form 7 November 2024; Accepted 7 November 2024
Available online 8 November 2024

2024). These features depend largely on the molecular conformation and the arrangement of polymer chains, which may vary depending on the PLLA crystal form (Hoogsteen et al., 1990; Zhang et al., 2010). PLLA shows complex polymorphism with three main crystalline forms: α (Eling et al., 1982; Puiggali et al., 2000), β (Eling et al., 1982; Puiggali et al., 2000; Glimcher, 1959), and γ (Cartier et al., 2000), depending on preparation conditions. Besides these three main crystal polymorphs, two disordered modifications of the α form, named α′ and α″, were observed in PLLA (Zhang et al., 2005, 2006; Wasanasuk and Tashiro, 2011; Wunderlich and Grebowicz, 1984; Liu et al., 2014). According to the literature, the α′ modification has a conformational disorder and a loose chain-packing manner, which makes this crystal modification a mesophase (condis crystal) (Liu et al., 2014; Pan et al., 2012; Barbosa et al., 2023; Zhang and Ma, 1999).

An ideal bone grafting material should exhibit osteoconductive, osteoinductive, and piezoelectric characteristics (Glimcher, 1959). Hydroxyapatite affects the piezoelectric properties of bone tissue. This is caused by shifts of ions in the crystal structure of nHA under mechanical stress, which leads to a change in the ionic balance and a dipole moment. Asymmetries in the structure allow the network to be polarized and an electrical signal generated. This piezoelectricity plays a key role in bone remodeling and tissue regeneration and is important for bone homeostasis (Barbosa et al., 2023). Hydroxyapatite is a crucial bioactive osteogenic inducer, playing a vital role in the adhesion of synthetic scaffolds to regenerating bone. The chemical integration between prosthetic biomaterials and bone tissue *in situ* can be accomplished by forming a layer of biologically active bone-like apatite on the surface of the scaffold (Zhang and Ma, 1999; Hong et al., 2008). Spherical nanoparticles exhibit the highest surface-to-volume ratio (Winey and Vaia, 2007). Due to their nanoscale dimensions, nearly spherical morphology, distinctive mechanical and physicochemical properties, surface chemistry, and excellent biocompatibility, nanoparticles integrated into a polymer matrix stand out as highly promising materials for multifunctional nanocomposites across diverse applications, including biomedical ones (Rancan et al., 2009; Rachmawati, 2016; Patel and Gundloori, 2023). The surface charges generated influence protein adsorption, affecting cell adhesion, migration, morphology, and proliferation. Polarized nHA accelerates protein adsorption, affecting cell adhesion, migration, morphology, proliferation, and the growth of bone-like apatite crystals in simulated body fluid (Saxena et al., 2019; Zhang et al., 2023a; Farag, 2023). Osteoblast cells exhibit enhanced proliferation on negatively polarized nHA surfaces, promoting new bone formation and enhanced osteobonding at injury sites. Furthermore, polarized nHA aids in the regeneration of blood vessels and epidermis during wound healing (Nagai et al., 2008; Okabayashi et al., 2009).

Considering the diverse range of potential applications for electrospun mats, including biomedical (Baniasadi et al., 2023), environmental (Zhou et al., 2023), and electronic applications (Li et al., 2024), one of the significant challenges in the electrospinning approach lies in preparing mats with adjustable properties (Xing et al., 2023). In this context, various modifications, both during the process and post-process of electrospun mats, have been suggested (Yang et al., 2023). These modifications encompass the use of multiple jets, fiber alignment, coaxial electrospinning, surface modifications, blending with other biopolymers, and/or incorporating micro or nanoparticles as fillers for the polymer matrix (Behroozi et al., 2023; Wang et al., 2023). Composite and nanocomposite materials have widespread applications across various fields, such as sensors, energy, anticorrosion, and catalysis. The ultimate properties of polymer-based composites are significantly influenced by various factors related to the interaction between the matrix and particles, including structure anisotropy and particle dimensions (Karbowniczek et al., 2022; Moradi et al., 2023; Szewczyk et al., 2023).

PLLA and nHA are materials widely used in tissue engineering, especially in the context of bone and nervous tissue regeneration. There are studies in the literature that analyze the effect of nHA on the properties of PLLA and its application in biomedicine. Li et al. investigated the properties of PLLA and nHA composites prepared by melt electrospinning (Li et al., 2012). Diaz et al. investigated the properties of materials made of PLLA/nHA in the form of polymer films (Díaz et al., 2019). *In vivo,* tests of printed materials made of PLLA with the addition of nHA were also carried out (Chen et al., 2019). However, only a few studies in the literature relate to PLLA nanofibers with the addition of nHA, e.g., (Tazibt et al., 2023; Davachi et al., 2016; Hwangbo et al., 2022). PLLA and nHA were selected for this study because of their complementary properties that make them suitable for tissue engineering applications, particularly for bone regeneration. The main advantage of this material system is thai it is a combination of biocompatibility and biodegradability, ability to mimic the natural composition of bone, and piezoelectric properties that is particularly crucial for bone tissue perspective. In our article, we propose an innovative approach to the electrospinning process, more precisely, the production of samples with random and aligned orientation of nanofibers. To summarize, the aim of the work was to investigate PLLA/nHA composites, particularly the effect of the fiber arrangements and the addition of nHA on the content of piezoelectric phases and piezoelectricity of PLLA samples. There are no works analyzing the piezoelectricity of PLLA materials with the addition of nHA in the context of piezoelectric properties occurring in natural bone. Our hypothesis was that even in the case of semicrystalline PLLA, nHA amplifies the piezoelectricity of the obtained fibers. Additionally, there is a lack of data on the influence of fiber arrangement on piezoelectricity in the context of cellular growth and viability. Osteoconductivity was examined using osteoblasts to evaluate the suitability of PLLA/nHA composites in bone tissue engineering.

2. Materials and methods

2.1. Materials

Poly(L-lactide) (PLLA, Purasorb PL 49, Corbion), with molecular weight Mw - 330 000 g/mol, was purchased from Purac, Netherlands. Nano-hydroxyapatite (nHA), a nanopowder <200 nm particle, was purchased from Sigma-Aldrich, Germany. 1,1,1,3,3,3, -hexafluoro-2-propanol (HFIP) was purchased from Iris Biotech GmbH, Germany. All chemical reagents were analytically pure.

Reagents for *in vitro* tests, such as amino acids, L-glutamine, fetal bovine serum (FBS), and antibiotics (penicillin/streptomycin), were purchased from Sigma Aldrich, Germany. Phosphate-buffered saline (PBS), Presto Blue, Trypsin EDTA, Dulbecco's Modified Eagle Medium, ActinGreen, and NucBlue were purchased from Thermo Fisher Scientific, United States. The cell line osteoblasts MG-63 were purchased from Sigma-Aldrich, Germany.

2.2. Preparation of PLLA solution, PLLA/nHA solution, and nanofibrous scaffold formation

PLLA fibers were formed using electrospinning. PLLA pellets were dissolved in HFIP at room temperature and left overnight. For electrospinning, 3.5 w/v % of PLLA solutions were prepared. Subsequently, the solution was doped with nHA at a 10 % w/v concentration. To prevent aggregation of the nHA nanoparticles, the solutions were treated with ultrasound (ultrasonic cleaner EMAG, EMMI-D60, Germany) for 20 min.

All PLLA solutions were loaded into a 3 ml syringe and positioned in an electrospinning chamber (Fluidnatek LE-50, Bioinicia, Valencia, Spain). The solutions were dispensed through 23-gauge stainless steel needles with an inner diameter of 0.337 mm at a flow rate of 1.5 ml/h. The distance from the needle tip to the collector was 110 mm. Fibers were gathered on a rotating drum collector (50 mm radius and 70 mm length) at rotation speeds of 200 rpm for random fibers and 2000 rpm for oriented fibers, with a linear velocity of 5.16 m/s. The process was conducted at temperatures between 21°C and 23°C and relative

humidity of 30 %. A positive voltage of 11 kV was applied to the needle while the collector was kept at a potential of −2 kV. After electrospinning, all materials were placed under a fume hood for 24 h to allow solvent residues to evaporate. The samples were named in analogy to the composition and speed of the collector during the manufacturing process; more precisely, PLLA formed at low rotational speed (100 rpm) was named PLLA_R (random orientation of fibers), and those formed at high rotational speed (2000 rpm) were named PLLA_A (aligned orientation of fibers). In the case of hydroxyapatite addition, nHA was added to the sample name; for example, PLLA/nHA_R means a hydroxyapatite-added sample formed at low collector speed (100 rpm), and PLLA/nHA_A means a hydroxyapatite-added sample formed at high collector speed (2000 rpm).

2.3. Characterization of PLLA/nHA nanofibrous scaffolds

2.3.1. Morphology analysis

Scanning electron microscopy (SEM) imaging was used to analyze the morphology using an accelerating voltage of 10 kV (SEM, JSM-6010PLUS/LV InTouchScope™, JEOL, Tokyo, Japan). Before imaging, each nonwoven underwent gold coating (approx. 10 nm) (Smart Coater, JEOL, Tokyo, Japan). Data analysis was conducted using ImageJ software (1.52q software version). The fiber diameter distribution was determined by employing a Gaussian approximation with 100 measurements per sample, and the goodness fit was also provided using ImageJ software

The impact of the collector's rotational speed on fiber orientation within the nanofibrous scaffold was analyzed using the directionality plugin in ImageJ software. Fourier Transform was applied to segments of the SEM images to determine the orientation patterns. The orientation distribution was then approximated with a Gaussian function using Origin 2021b software. The degree of fiber alignment was further evaluated by calculating the full width at half maximum (FWHM) of the Gaussian function used for the orientation distribution approximation. FWHM values were averaged across five images for each sample (Hotaling et al., 2015).

The orientation factor was determined using the anisotropy index α, where α equaling 1 indicates perfect alignment and α = 0 represents a random distribution (Eqs. (1),(2)) (Shehata et al., 2018):

$$\Omega = \frac{1}{I_{tot}}\sum I_i \begin{vmatrix} \cos^2\theta_i & \sin\theta_i\cos\theta_i \\ \sin\theta_i\cos\theta_i & \sin^2\theta_i \end{vmatrix} \quad (1)$$

$$\alpha = 1 - \lambda_1/\lambda_2 \quad (2)$$

where Ω represents the orientation matrix with eigenvalues of λ_1 and λ_2, I_{tot} - is the total length of the nanofiber (nm), I_i- is the length of the individual *i*-th nanofiber (nm), θ_i- angle between the nanofiber and the x-axis. The lengths and angles of the nanofibers were measured from SEM images using the Directionality plugin in ImageJ software.

Total average porosity *(p)* was determined from Eq. (3) (Zaszczyńska et al., 2024a):

$$p = \frac{V_t - V_f}{V_t} = \left(1 - V_f \times \frac{\rho}{m_t}\right) = \left(1 - \frac{m_f}{m_t}\right) \quad (3)$$

Where m_t is the theoretical mass of the solid sample, calculated as the product of the volume occupied by a patch V_t and the density of PLLA (1.25 g/cm^3) (Wang et al., 2007), while V_f and m_f denote the actual sample volume and mass, respectively.

The average pore size (*p*) was calculated from Eq. 4 (Zaszczyńska et al., 2024a):

$$P = \frac{2D}{(1-p)} \quad (4)$$

where, *p* is approximately the total porosity, *D* - the mean fiber diameter, $(1 - p)$ - average total area of fibers per unit area.

Energy Dispersive X-ray Spectroscopy (EDS) was used to confirm the presence of nHA (JSM-6010PLUS/LV InTouchScope™, JEOL, Tokyo, Japan). Samples were measured with the following parameters: accelerating voltage of 8 kV, working distance (WD) = 10 mm, probe current = 500 pA, and a collecting time of 30 min. The EDS analysis of the distribution of oxygen (O), phosphorus (P), calcium (Ca), and carbon (C) was performed.

2.3.2. Water contact angle measurements, surface tension energy, and water uptake determination

The water contact angle (WCA) of all nanofibrous samples was assessed using the static water contact angle method. Measurements were performed with a Data Physics OCA 15EC contact angle goniometer (Filderstadt, Germany). A distilled water droplet (2 μl) was placed on the nanofibrous scaffold surface at room temperature, and the water contact angle was recorded after 3 s. Each measurement was repeated 10 times for each type of material, and then the measurement was averaged.

The surface free energy (SFE) was specified using the Kaelble-Owens-Wendt method, which considers that the SFE consists of two main independent components: dispersion and polar interactions. Three liquids were used to calculate the surface free energy: diiodomethane, water, and formamide, according to the previously described procedure (Rudawska and Jacniacka, 2009; Kołbuk et al., 2022).

Components γ_s^p and γ_s^d of all samples can be calculated from Eq. 5 and Eq. 6:

$$\left(\gamma_s^d\right)^{0,5} = \frac{\gamma_d(\cos\theta_d + 1) - \sqrt{\left(\frac{\gamma_d^p}{\gamma_w^p}\right)}\gamma_w(\cos\theta_w + 1)}{2\left(\sqrt{\gamma_d^d} - \sqrt{\gamma_d^p - \left(\frac{\gamma_w^p}{\gamma_w^p}\right)}\right)} \quad (5)$$

$$\left(\gamma_s^p\right)^{0,5} = \frac{\gamma_w(\cos\theta_w + 1) - 2\sqrt{\gamma_s^d\gamma_w^d}}{2\sqrt{\gamma_w^p}} \quad (6)$$

where, γ_s^d is the dispersion element of Surface Free Energy of tested materials, and γ_s^p is the polar element of tested materials; γ^d Surface Free Energy of diiodomethane; γ_d^d the dispersive element of diiodomethane surface energy; γ_d^p the polar element of diiodomethane; γ_w Surface Free Energy of Water; $\gamma_w^d$the dispersive element of water Surface Free Energy; γ_w^ppolar element Surface Free Energy of water; θ_d and θ_w contact angle of diiodomethane and water.

Wu's method can be used to calculate the surface polarity (*X*p) (Eq. 7) (Kleintjens, 2012):

$$X_p = \frac{\gamma_s^p}{\gamma_s} \quad (7)$$

The absorption capacity of the scaffolds was assessed by measuring their ability to take in water, which is primarily influenced by the materials' hydrophilic properties (Rai et al., 2005). Each scaffold was sectioned into 2×1 cm pieces and submerged in deionized water. After specific time intervals (60 s), the scaffolds were retrieved, softly dried with tissue paper, and weighed (analytical balance, XA 52.R2, Radwag, Poland). This procedure was repeated over 10 min. The water absorption rate was calculated using equation (Kleintjens, 2012):

$$\%Water\ uptake = 100 \times \frac{W_{wet} - W_o}{W_0} \quad (8)$$

where W_o is the dry weight of the sample, and W_{wet} is the weight of the wet sample.

2.3.3. Fourier transform infrared spectroscopy (FTIR)

Molecular structure analysis, including hydroxyapatite addition, was conducted using Fourier Transform Infrared Spectroscopy (FTIR-ATR,

Bruker Vertex 70, Mannheim, Germany). The results were averaged from five independent samples and runs. The samples were scanned in the range of 400 cm^{-1} to 4000 cm^{-1} with a resolution of 2 cm^{-1} and a total of 32 scans.

2.3.4. Differential scanning calorimetry (DSC)

Thermal analysis of PLLA scaffolds, both pure and with nHA particles, was performed using a Differential Scanning Calorimeter Pyris 1 DSC (Perkin Elmer, Waltham, MA, USA) equipped with Intracooler 2 P under nitrogen atmosphere. Before DSC analysis, samples with masses 6–8 mg were loaded into standard aluminum pans and vacuum dried (vacuum dryer, Menmert, Spain) at ambient temperature for at least 24 hours to remove a solvent residue. DSC analysis consisted of two heating and cooling cycles at 10 K/min from −55°C to 220°C with 10 min fusion time. The scans were corrected for instrumental heat flow drift and curvature and are presented as apparent heat capacity, C_p, in $J/g_{PLLA}K$.

2.3.5. Wide angle X-ray scattering (WAXS)

Investigations were performed using a Bruker D8 Discover Diffractometer (Manheim, Germany). Measurements were conducted using Cu Kα radiation of wavelength $\lambda = 1.5406$ Å at a voltage of 40 kV and current of 40 mA. Measurements were conducted in reflection mode. Formation of the incident beam was performed using optics consisting of Göbel mirrors, a 1 mm linear slit, and a 2.5° n axial Soller. The WAXS profiles were recorded using a Lynxeye one-dimensional detector preceded by a Ni filter and a 2.5° axial Soller.

2.3.6. Piezoelectric coefficient measurements

The piezoelectric coefficient for electrospun PLLA membranes was evaluated using a specialized d_{33} meter (YE2730A d_{33} meter, Sinocera, China), tailored for precise measurements of d_{33} values in piezoelectric materials. Before the tests, electrodes of an 8 nm Au80–20Pd layer were sputter coated (Q150RS, Quorum Technologies, UK) on both sides of the PLLA fiber mats. Each sample was measured 5 times to obtain an average d_{33} value. A reference sample was integrated into the assessment process to ensure the instrument's accuracy and account for potential variations in piezoelectric values attributed to the high porosity of the materials (Sukumaran et al., 2023). This reference sample, obtained from PolyK (USA), was a piezoelectrically poled PVDF film measuring 110 μm in thickness, with a specified piezoelectric coefficient ranging from 23 to 28 pCN^{-1}. The 4 × 4 cm segment cut out from the reference sample was used for testing. The measurements were validated using the reference sample, yielding a value of 27.7 ± 1.5 pCN^{-1}, consistent with the manufacturer's reported range of 23–28 pCN^{-1}.

2.3.7. In vitro study

Biocompatibility tests were conducted using the human MG-63 cell line (86051601, Sigma Aldrich). The cells were cultured in a 25 cm^2 flask with a medium consisting of High Glucose Dulbecco's Modified Eagle's Medium (DMEM), 10 % fetal bovine serum (FBS), 1 % antibiotics, and 1 % glutamine. The cells were incubated in a 5 % CO2 environment at 37 ℃. To detach the cells from the flask, they were washed with PBS. Subsequently, 3 ml of 0.05 % trypsin solution was added to the cells, and the flask was placed in the incubator for a few minutes. After harvesting the cells, 10 ml of culture medium was added, and centrifugation was performed at room temperature. The pellet was resuspended in a culture medium to achieve the required cell density. Various studies were conducted to assess the cellular response to monolithic nanofibers, including cytotoxicity on direct contact and cellular morphology after 3 and 5 days of cultivation.

For cellular viability assessment, the MG-63 cell suspension was seeded on samples and Tissue Culture Plate TCP with a density of 1×10^4 cells/well and placed in an incubator according to the previously described protocol (Zaszczyńska et al., 2024b). After 3 and 5 days, the culture medium was removed, and each well was filled with 180 mL of PBS and 20 mL of Presto blue reagent. Afterward, the plate was returned to the incubator for 60 min. Fluorescence was measured using 530/620 nm excitation/emission filters by Fluorescent Accent FL Thermo Fisher Scientific. The results were compared with the Presto Blue fluorescence of blank samples, indicating no metabolic activity, and the control (Tissue Culture Plate TCP), which exhibited 100 % viability.

Fluorescence microscopy was employed to verify MG-63 morphology in direct contact. MG-63 cells were seeded on electrospun membranes, and after 3 and 5 days of cultivation, cells were fixed in 3 % formaldehyde for 20 min. Fixed cells were then treated with 0.01 % Triton X 100 for 5 min to permeabilize cell membranes.

Finally, cellular nuclei and the cytoskeleton were stained for 30 minutes with a combined solution of ActinGreen and NucBlue. ActinGreen binds to the cytoskeleton, while NucBlue targets nuclear DNA. Images were obtained using a Leica AM TIRF MC microscope (Germany).

2.4. Statistical analysis

The results were used to determine their statistical significance. The statistical analysis of viability data was performed for $p < 0.05$ using GraphPad Prism 8.0.1 software (GraphPad, Boston, MA, USA). Two-way ANOVA with Tukey's multiple comparisons was applied as necessary. Statistical significance was assessed by analyzing the p-values. A p-value below 0.05 was marked statistically significant. If the p-value fell between 0.01 and 0.05, it was marked with an "*".

3. Results and discussion

3.1. Morphology analysis

It is evident from Fig. 1 that fibers reveal a uniform morphology without bead formation in all scaffolds. Increasing the collector rotational speed reduces the fiber diameter in both pure samples and those with the addition of nHA. This reduction is from the average diameter of 125 ± 32 nm for pure PLLA_R and 123 ± 9 nm for PLLA/nHA_R at low collector rotation speed (100 rpm) to the value of 111 ± 7 nm for PLLA_A and 110 ± 6 nm for PLLA/nHA_A at higher collector rotation speed (2000 rpm). Based on the results, the inclusion of nHA does not cause changes in the average fiber diameter. This is consistent with previous literature, which suggests that the addition of hydroxyapatite does not affect fiber diameter (e.g., (Van Manen et al., 2014)). SEM images reveal a uniform distribution of nHA nanoparticles within the fibers without any visible agglomerations (see Fig. 1 C, D).

Fig. 2 shows that increasing the collector rotational speed improves the fiber orientation, leading to an orientation with a narrow distribution for fibers collected at 2000 rpm, contrary to randomly arranged fibers collected at 200 rpm. The fiber orientation distribution's full width at half maximum (FWHM) decreases from 87.90 at 100 rpm to 22.40 at 2000 rpm for both pure and doped PLLA. Higher rotational speeds increase tensile forces, enhancing the fibers' stretching and alignment (Obregon et al., 2016). The anisotropy index (α) confirms this tendency. As the rotational speed increased from 100 to 2000 rpm, the α value increased from 0.27 to 0.91 for pure PLLA and from 0.33 to 0.89 for PLLA with the addition of nHA. These results indicate an increase in the orientation of nanofibers with increasing collector rotation speed and no effect of the addition of nHA on the anisotropy index.

The analysis of porosity and mean pore size clearly indicates the effect of nHA addition. It leads to higher porosity of nonwovens and slightly lower pore size. In the case of PLLA_R samples, addition of nHA results in an increase of porosity from 82 ± 0.4 % to 89 ± 1.1 %, and for PLLA_A nonwovens from 85 ± 1.2 % to 94 ± 0.6 %. The mean pore size was reduced, irrespective of the fibers alignment from ~202 ± 6 nm to ~194 ± 9 nm after nHA addition. The effect of fiber alignment is negligible. Porosity is an important factor in tissue engineering because

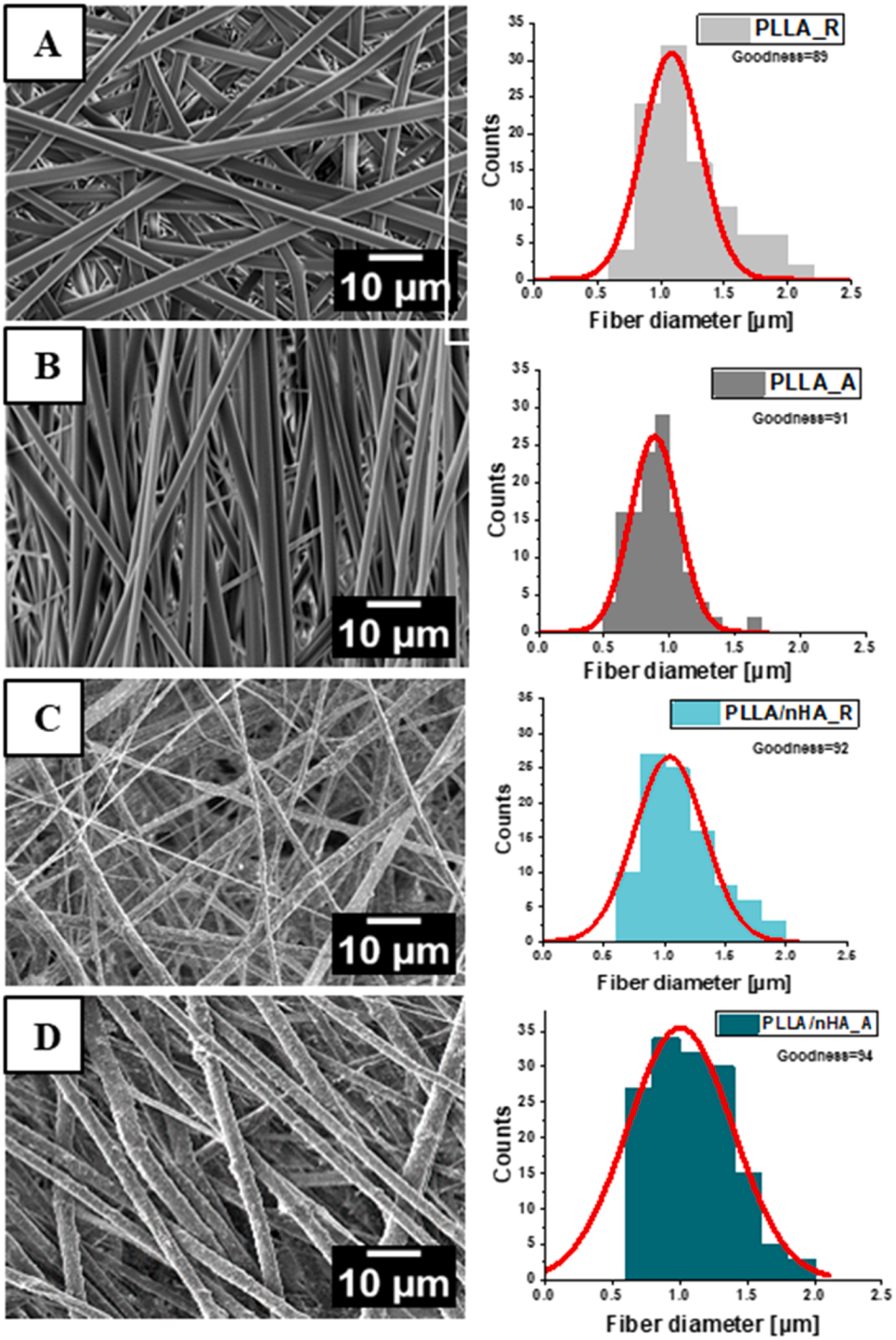

Fig. 1. SEM micrographs of A) PLLA_R, B) PLLA_A, C) PLLA/nHA_R, and D) PLLA/nHA_A nanofibrous scaffolds with corresponding diameter distributions approximated with Gaussian function.

it allows better penetration of nutrients and gases and promotes angiogenesis (Buitrago-Vásquez and Ossa-Orozco, 2018).

Verification of the presence of hydroxyapatite nanoparticles is shown in Table 1. Using the EsB detector, material contrasts were observed, which enabled the differentiation of individual components within the sample structure based on differences in the grayscale. In the case of doped samples, EDS analysis revealed the presence of key chemical elements characteristic of nHA nanoparticles, such as calcium (Ca) and phosphorus (P), in addition to the basic PLLA elements- carbon (C) and oxygen (O). This confirms that the hydroxyapatite nanoparticles were successfully added to the PLLA structure.

3.2. Water contact angle measurements, surface free energy, and water uptake determination

Fig. 3 shows the contact angle measurements, while Table 2 shows the SFEs and their components for all electrospun scaffolds. It is evident from Fig. 3 that the contact angles measured by using formamide are much lower compared with water and diiodomethane. Comparison of wettability within each group of fiber topography (random and aligned)

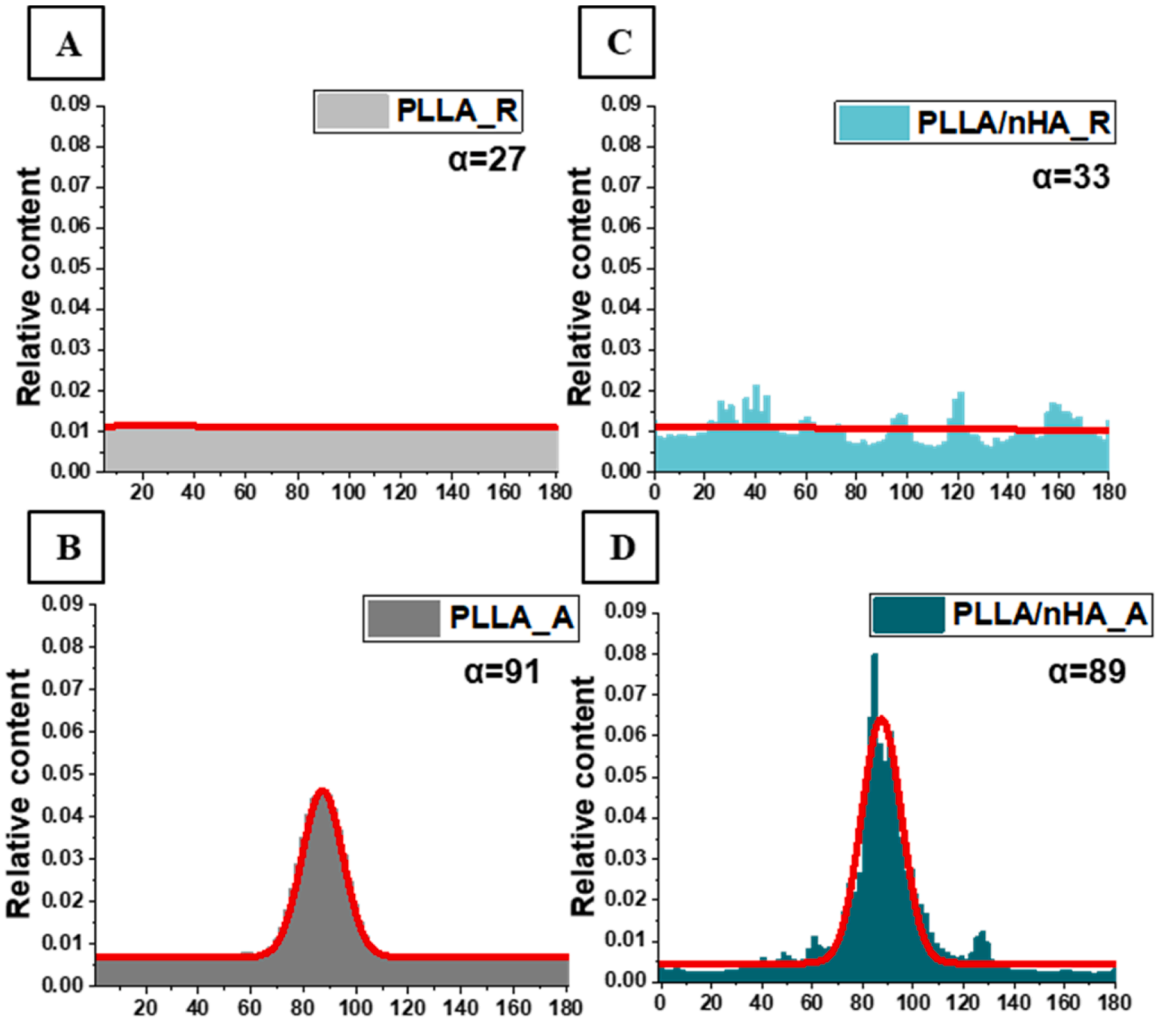

Fig. 2. Orientation distributions approximated with Gaussian function of all samples with anisotropy index α calculated from Eqs. (1) and (2) for samples A) PLLA_R, B) PLLA_A, C) PLLA/nHA_A and D) PLLA/nHA_A.

Table 1
PLLA scaffold elemental composition in wt% as measured using SEM-EDS.

Element	PLLA_R	PLLA_A	PLLA/nHA_R	PLLA/nHA_A
C	61.81 ± 0.7	61.97 ± 0.6	60.47 ± 0.3	60.13 ± 0.4
O	38.19 ± 0.3	38.03 ± 0.4	33.9 ± 0.7	33.81 ± 0.6
Ca	-	-	3.52 ± 0.4	3.79 ± 0.3
P	-	-	2.11 ± 0.2	2.27 ± 0.1
Other	-	-	-	-

clearly indicates the reduction of contact angle by addition of nHA being observed in all liquids. The effect of fiber arrangement on wettability is negligibly small if any. It is known from the literature that the wettability is strongly correlated with roughness which in turns depends on fibers arrangement, being higher for randomly arranged fibers (Szewczyk et al., 2019). Therefore, it can not be excluded that the slightly higher contact angle for randomly arranged fibers is at least partly due to the more rough surface of random nonwovens. The reduction in contact angle by nHA addition is important for cell adhesion to the nanofiber surface, which is beneficial in tissue engineering applications (Paragkumar N et al., 2006).

The SFE analysis reveals that aligned samples generally exhibit higher values (see Table 2), with SFE measured at 30 ± 2.2 mN/m and 33.4 ± 0.9 mN/m for random PLLA and PLLA/nHA, respectively, compared to 33.1 ± 0.3 mN/m for aligned PLLA, and 42.9 ± 1.9 for

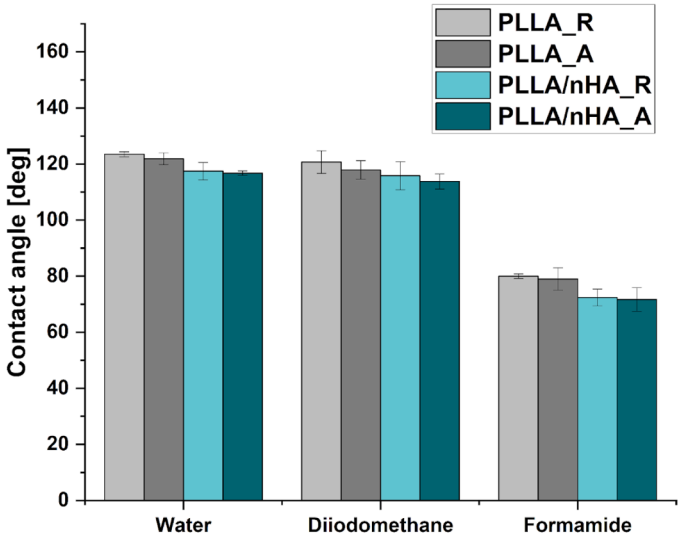

Fig. 3. Contact angle measurements for all electrospun scaffolds.

aligned PLLA with nHA addition. The ascending order of SFE is PLLA_R > PLLA_A > PLLA/nHA_R > PLLA/nHA_A. The Kaelble-Owens-Wendt method was used to calculate the total SFE, which combines the polar

Table 2
SFE, water contact angle (WCA), and their components for all nanofibrous scaffolds.

Sample ID	Water Contact Angle [°]	Dispersive Component [mN/m]	Polar component [mN/m]	Surface Free Energy [mN/m]	Surface Polarity [Xp]	Water Uptake [%]
PLLA_R	123 ± 0.3	27.3 ± 2.1	2.7 ± 0.4	30 ± 2.2	0.0989	140 ± 2
PLLA_A	121.7 ± 0.4	29 ± 2.1	4.1 ± 0.6	33.1 ± 0.3	0.1413	149 ± 5
PLLA/nHA_R	117 ± 0.3	29.8 ± 0.4	3.6 ± 0.5	33.4 ± 0.9	0.1208	215 ± 7
PLLA/nHA_A	116 ± 0.2	34.5 ± 1.1	8.4 ± 0.3	42.9 ± 1.1	0.2434	257 ± 4

component resulting from hydrogen bonds and dipole-dipole interactions with the dispersive component resulting from London and van der Waals forces (Rudawska and Jacniacka, 2009). Notably, the dispersion component was the main factor influencing the SFE of PLLA substrates. Moreover, the dispersion component showed an increasing trend in the following order: PLLA_R > PLLA_A > PLLA/nHA_R > PLLA/nHA_A.

PLLA_R indicated a lower polar component of the contact angle than PLLA_A. Therefore, the surface polarity (*Xp*) of PLLA_A was higher than PLLA_R. Additionally, polar components increased with the nHA additive, which was more effective for aligned fibers. Weak crystallinity and molecular order decide lower surface polarity (Kołbuk et al., 2022; Zaszczyńska et al., 2024b; Vijayendran, 1979), which was observed for PLLA_R. Adding nHA increases the surface polarity of PLLA/nHA_R and PLLA/nHA_A due to its low polar component γ_{sp} equal to c.a. 16.4 mN/m and related low WCA (Nasker et al., 2019). Surface polarity enhances protein adsorption, which was confirmed by using fibronectin (Barroca et al., 2018). From Fig. 4, it is evident that the highest water uptake was in samples with nHA addition. The PLLA/nHA aligned scaffold showed a lower percentage of water absorbed at the first minute. Still, it gradually increased till the second minute. The results showed that PLLA/nHA in random and aligned scaffolds exhibit better hydrophilicity than pure PLLA random or PLLA_A scaffolds. Also, it exhibits increased water uptake due to the hydrophilicity of nHA and its ionic exchange with water. According to the literature, this ionic exchange with the surrounding medium results in degradation and the formation of micro-porosities that enhance water uptake (Buitrago-Vásquez and Ossa-Orozco, 2018). Both the material's initial porosity and the fibers' porosity caused by nHA dissolution may play a significant role in water uptake. In summary, adding nHA increased samples' SFE and water uptake and is very important for porous materials dedicated to tissue engineering applications (Bhat et al., 2013).

3.3. Fourier transform infrared spectroscopy (FTIR)

FTIR spectra of all investigated electrospun fibers as well as PLLA before electrospinning (powder) and pure hydroxyapatite, are presented in Fig. 5. The main peaks of PLLA and nHA are summarized in Table 3 and assigned to the particular vibration data.

FTIR spectra of pure PLLA fibers formed at low and high rotational collector speed, do not show any differences. What is important is that there is no peak at 921 cm^{-1}, which is usually assigned to the crystalline form of PLLA, indicating that the samples do not contain crystals (Hambleton and Mele, 2024; Polak et al., 2023). The analysis of FTIR spectra of PLLA/nHA samples indicates the existence of all peaks related to PLLA and nHA. This observation leads to the conclusion that nHA is effectively loaded into PLLA fibers. Considering the partial overlapping of some of the PLLA and nHA peaks, we could not estimate the content of nHA in PLLA/nHA fibers. Additionally, there is no essential shift in the positions of the peaks of PLLA and nHA in PLLA/nHA fibers, indicating no molecular interactions between both components.

3.4. Wide angle X-ray scattering (WAXS)

Fig. 6 illustrates WAXS profiles for all fibers. It is evident after subtraction of the nHA profile of crystalline nature that all spun PLLA and PLLA doped with nHA fibers, both random and aligned, are amorphous. However, it is evident that the shape of the amorphous profile is not unimodal, requiring the approximation use of two Gaussian functions. This fact indicates that the amorphous structure in spun PLLA fibers is not completely disordered. It has two local maxima, indicated by peak deconvolution requiring two Gaussian peaks, suggesting the existence of some ordering with two most probable interatomic distances.

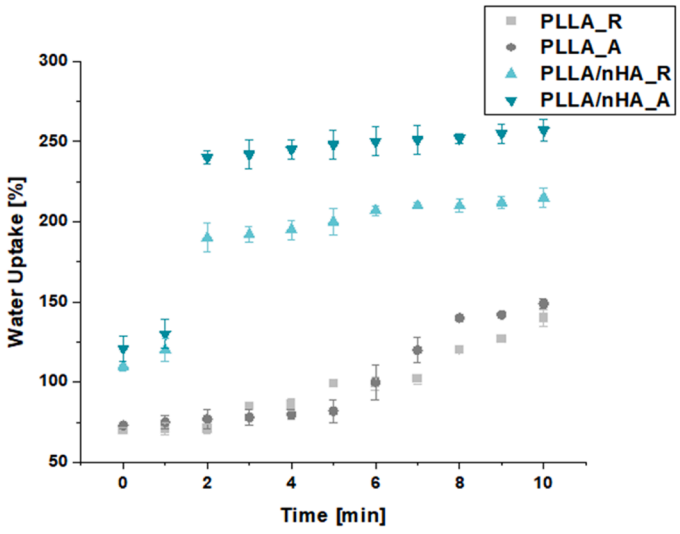

Fig. 4. Water uptake of the four kinds of scaffolds in deionized water over time calculated from Eq. (8).

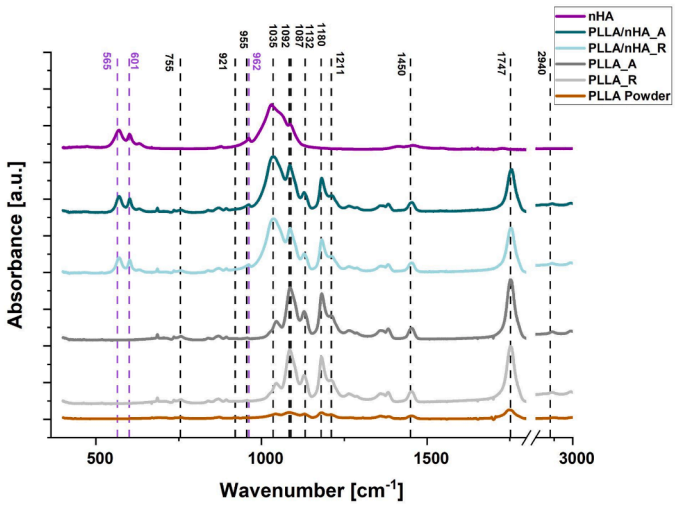

Fig. 5. FTIR spectra of hydroxyapatite particles, PLLA powder, electrospun pure PLLA, and PLLA/nHA scaffolds with random and aligned fiber orientation.

Table 3
Experimentally observed main FTIR peaks of PLLA and nHA.

Sample	Abbreviation	Vibrational mode	Position [cm^{-1}]	Ref.
nHA	ν_β PO_4	PO_4 bending (ν_β)	1092	(Stoch et al., 2000; Lopresti et al., 2020; Panda et al., 2022)
	ν_1PO_4	PO_4 stretching (ν_1)	962	(Panda et al., 2022)
	ν_4PO_4	PO_4 bending (ν_4)	601 555	
PLLA	ν(C-COO)	Stretching C-COO	868	(Leroy et al., 2017)
	ν_s(C-CH_3)	Symmetrical stretching C-CH_3	1035	(Leroy et al., 2017)
	ν_s(C-O-C)	Symmetrical stretching C-O-C	1092	(Pariy et al., 2022)
	ν_{as} (C-O) + τ (CH_3)	Symmetrical stretching and twisting	1180, 1211	(Pariy et al., 2022)
	δ_{as}(CH_3)	Asymmetrical scissoring	1450	(Scaffaro et al., 2023)
	ν(C═O)	Stretching	1747	(Scaffaro et al., 2017)
	ν(CH_2)	Symmetrical stretching	2940	(Nazir et al., 2021; Ribeiro et al., 2011)

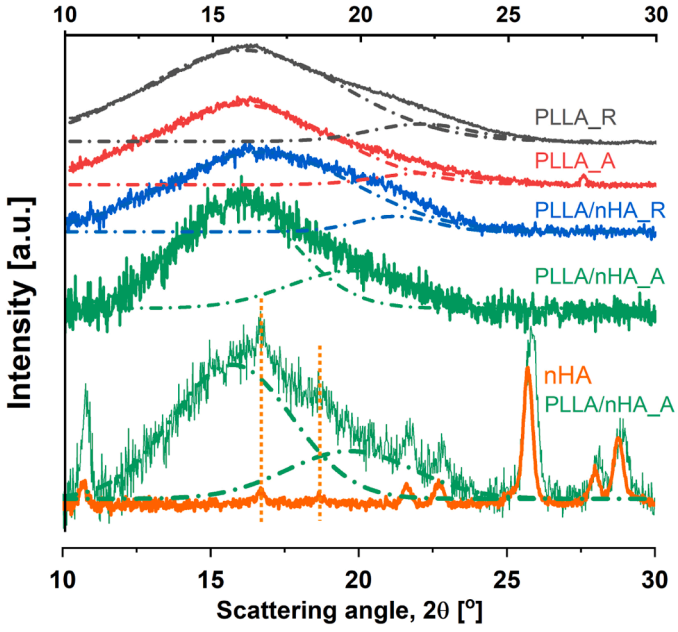

Fig. 6. WAXS profiles of analyzed fiber mats.The profiles at the bottom show a nHA profile, and the original profiles for the fibers doped with nHA display the nHA diffraction peaks; the upper curves show these profiles after subtraction of the nHA diffraction peaks, which were approximated with Gaussian function during peak deconvolution. For clarity, the upper profiles were shifted vertically. The vertical orange dashed lines indicate the positions of the most intense diffraction peaks of the α'phase of PLLA (Pan et al., 2007; Righetti et al., 2015), which overlap the small nHA diffraction peaks. Peak deconvolution of the asymmetric halo required two Gaussian function peaks.

3.5. Differential scanning calorimetry (DSC)

The curves in Fig. 7 represent the apparent heat capacity, C_p, normalized to PLLA mass, which were determined from the DSC heating scans registered at 10 K/min for as spun fibers. All the samples, which at ambient conditions are amorphous (as indicated by WAXS analysis),

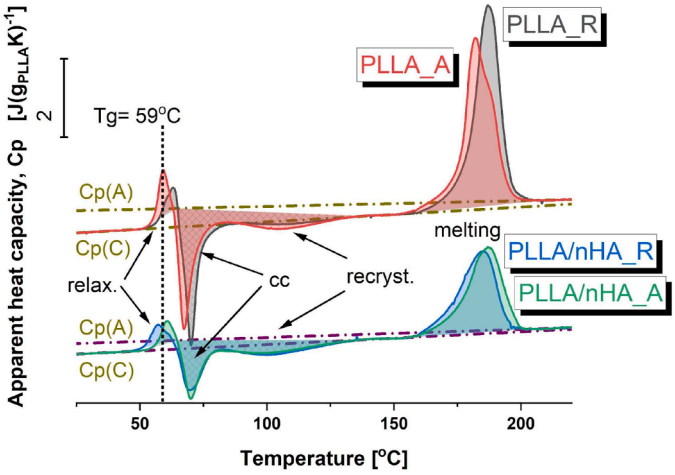

Fig. 7. Apparent heat capacity determined during 1st heating at 10 K/min for as-spun fibers. The curves for pure PLLA and doped with nHA are shifted along the y axis for clarity, and the scale bar is given. The exothermic effects of cc and recrystallization are indicated with grid-shaded areas; the endothermic enthalpy relaxation and melting are indicated with shaded areas. The linear approximation of temperature dependence of the heat capacity for amorphous and crystalline states (C_p(A), C_p(C)) determined by us are plotted as dash-dotted lines. The glass transition temperature, T_g, is indicated after (Pyda and Czerniecka-Kubicka, 2017).

show several transitions during heating. Generally, we see qualitatively similar behavior: below 50 °C, there is a linear increase in C_p with temperature. Between 50 °C and 80 °C there are two sharp thermal effects, where the endothermic one is seen to change abruptly into the exothermic one. Between 80 and 150 °C there is an additional broad exothermic effect. Above 160 °C starts a strong endothermic effect with a maximum at c.a. 180–190 °C. Above 200 °C there is a linear increase in C_p with temperature.

For pure PLLA fibers, the linear trend below 50 °C agrees with the behavior of PLLA Cp below the glass transition temperature, T_g, and reflects the C_p temperature dependence of PLLA at the glassy/crystal state (C). Above 200 °C, the linear trend agrees with the Cp behavior of PLLA in an amorphous state (A) (Pyda and Czerniecka-Kubicka, 2017). The respective lines for C_p(C) and C_p(A) were plotted as dash-dotted lines in Fig. 12 for reference.

The PLLA glass transition temperature, T_g, is expected at 59 °C (Pyda and Czerniecka-Kubicka, 2017). However, in this temperature range, we observe the abrupt sharp endothermic and exothermic effects, which cover the expected C_p change, ΔC_p, at T_g, making its determination difficult. The sharp endothermic effect at 55 °C is interpreted as an enthalpy relaxation (Pyda and Czerniecka-Kubicka, 2017), which is typical for PLLA and is known to depend on the thermal history. The sharp exothermic effect at 70 °C reflects crystallization from the glassy state (referred to as cold crystallization, cc), which is typically observed during heating for samples with reasonably high content of the mobile amorphous phase. However, it has to be noted that the temperature position and shape of the cc peak does not resemble the results found in the literature (Pyda and Czerniecka-Kubicka, 2017) for amorphous samples cooled from the melt. It is highly probable that this fast cold crystallization occurs in a highly disordered *α'* phase, as indicated by WAXS analysis.

The additional broad exothermic effect observed between 80 and 150 °C also does not resemble typical thermal effects reported in the literature for bulk PLLA samples cooled from melt and crystalizing during heating from the glassy state. However, it must be related to further recrystallization and/or polymorphic crystal-crystal transition (Di Lorenzo and Androsch, 2019). Assuming our hypothesis that the cold crystallization results in the formation of the *α'* phase, it is highly

probable that transitions in the temperature range between 80 and 160 ºC contain α'- α transition. This effect is followed by the final endothermic melting peak at c.a. 180–190 ºC, similar to the results in the literature.

A comparison of the curves in Fig. 7 shows that the thermal effects for the fibers doped with nHA are much smaller than for pure PLLA fibers. Moreover, for fibers doped with nHA, the PLLA heat capacity in an amorphous state, $C_p(A)$ at T>200 ºC, was lower than for pure PLLA fibers.

The enthalpies of the thermal effects observed during heating: relaxation, cold crystallization/recrystallization, and melting, are presented in Fig. 8. Enthalpy relaxation is seen as the strongest for aligned pure PLLA fibers (c.a. 5 J/g_{PLLA}) as compared to other samples (c.a. 3 J/g_{PLLA}). It indicates the highest orientation of the polymer chains and extended chain conformation in aligned pure PLLA fibers, which probably leads to higher crystallization enthalpy during further heating (c.a. 38 J/g_{PLLA}). It is, however, not reflected in the melting enthalpy, as the highest value is observed for pure random PLLA fibers (c.a. 65 J/g_{PLLA}), which corresponds to c.a. 71 % of crystallinity. This may be related to differences in polymorphic phase content indicated by a single melting peak for PLLA_R and a double melting peak for PLLA_A (Fig. 8).

For PLLA doped with nHA, we see much lower crystallization and melting enthalpies than for pure PLLA fibers (ΔHc= 25 and ΔHm= 36 J/g_{PLLA}, respectively), indicating 40 % crystallinity developed during heating. The collector rotational speed has no apparent effect on the PLLA/nHA fibers. It is clear that nHA reduces the crystallization ability of PLLA, most probably by affecting the polymer chain mobility as indicated by the lower heat capacity of the nHA doped vs pure PLLA samples.

3.6. Piezoelectric coefficient measurements

Piezoelectric coefficient measurements on fibers were carried out to examine how rotation speed and the addition of nHA affect the piezoelectric properties of prepared materials, see Fig. 9.

The results reveal significant differences in the piezoelectric coefficients between samples subjected to different collector rotation speeds. Specifically, PLLA_A exhibits a notably higher piezoelectric coefficient (4.58 ± 0.08 pCN^{-1}) than PLLA_R (4.04 ± 0.21 pCN^{-1}). This suggests that the increased rotation speed of the collector results in higher piezoelectric properties of the PLLA-based materials. Moreover,

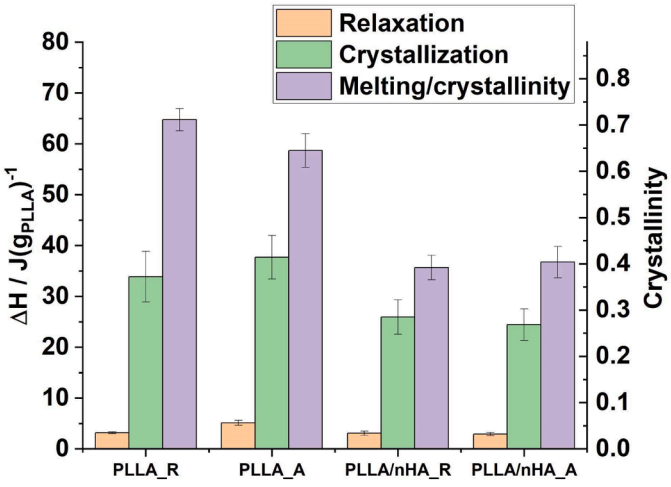

Fig. 8. The enthalpies of the thermal effects observed during the 1st heating scans are seen in Fig. 7 for enthalpy relaxation, cold crystallization/recrystallization, and melting. The right y scale indicates the crystallinity, which appeared during the 1st heating, calculated from the melting enthalpy, using the value of heat of fusion for the 100 % crystalline sample, Δh^0_m= 91 J/g (Pyda and Czerniecka-Kubicka, 2017).

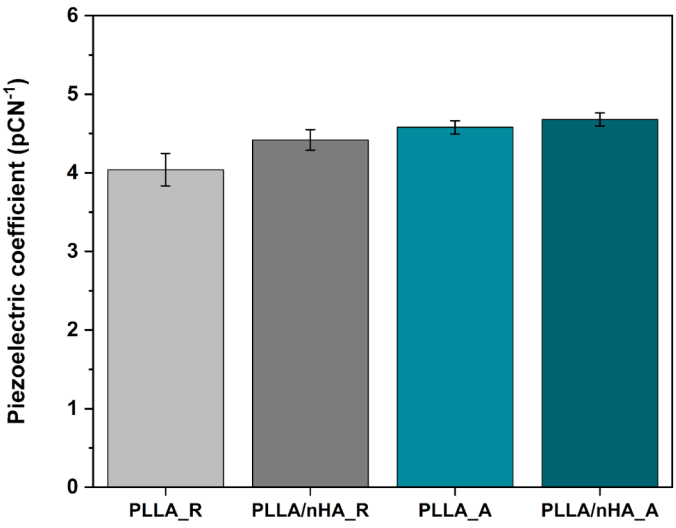

Fig. 9. Results from d_{33} piezoelectric coefficient measurement.

introducing hydroxyapatite nHA nanoparticles into the PLLA matrix influences the piezoelectric coefficient. PLLA/nHA_R and PLLA/nHA_A exhibit slightly higher coefficients (4.42 ± 0.13 pCN^{-1} and 4.68 ± 0.08 pCN^{-1}, respectively) than their non-nHA counterparts. Comparing the samples, PLLA/nHA_A demonstrates the highest piezoelectric coefficient, suggesting that the combination of higher collector rotation speed and nHA nanoparticles yields the most favorable piezoelectric response.

It is anticipated that the higher rotation rate forces a stretching of polymer chains. Although the polymer remains practically amorphous, with some traces of precrystalline local ordering (WAXS data), there is a change in molecular conformation, increasing polarization and piezoelectricity (Polak et al., 2023).

As for the PLLA with hydroxyapatite, our structure analysis results indicate that the increase of piezoelectric coefficient over the value of pure PLLA is most probably due to the contribution of higher nHA piezoelectricity compared to PLLA, only. The calculated piezoelectric coefficient for hexagonal phase d_{33} ~6.4 pm/V is consistent with the previously obtained value for monoclinic nHA (15.7 pm/V) (Polak et al., 2023).

3.7. In vitro study

Osteoblasts are fundamental for continuous bone remodeling and play an important role in evaluating materials for bone tissue engineering (Zhu et al., 2021a). Therefore, parallel to cellular viability, we determined osteoblasts nonwovens interaction.

Cell viability was assessed for MG-63 cultured on pure PLLA scaffolds and with the nHA addition, with random and aligned fiber orientation (Fig. 10). The in vitro analysis confirmed the non-toxic properties of all PLLA nanofibrous scaffolds. All scaffolds reached ≥ 70 % values of viability, which is in accordance with the ISO 10993–5 standard connected to the nontoxic materials for cells. Cell proliferation and attachment represent the initial stages of tissue regeneration and are essential for tissue regeneration (Jeznach et al., 2022). Hence, an assessment of cellular morphology was conducted. Following 3 and 5 days of cell cultivation directly seeded onto pristine PLLA scaffolds and PLLA/nHa, immunostained cells were analyzed using fluorescence microscopy (See Figs. 11 and 12). The morphology and spreading of osteoblasts in contact with the sample's surface closely resembled those observed on TCP, indicating cellular viability. The cells displayed well-spread morphology and demonstrated robust intercellular interactions. Effective osteoblasts-nonwoven interaction was confirmed by the elongation of cells, and notably, cell spreading was particularly pronounced on PLLA/nHA_A composite nanofibers. On aligned fibers

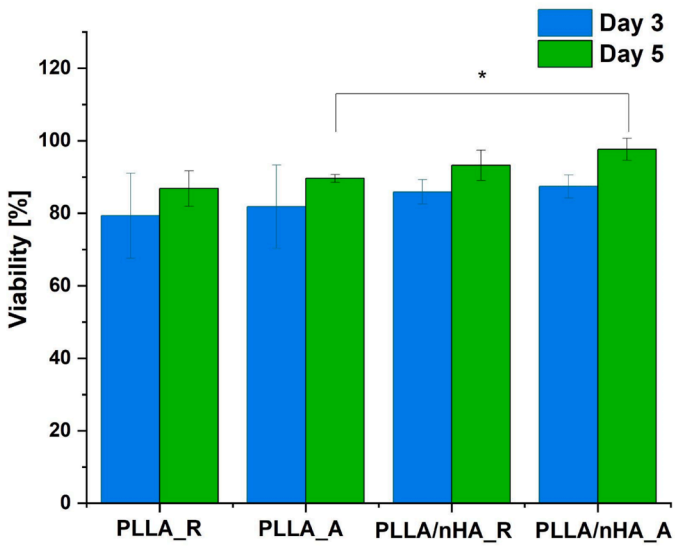

Fig. 10. Cell viability of MG-63 cells cultured on pristine and with nHA addition PLLA nanofibrous scaffolds as the rate of TCP (Tissue Culture Plastic, 100 %). Statistical significance: * $p < 0.05$.

cells align themselves and grow along the fibers more than they do on random meshes where they spread to a more round shapes. Previous studies have underscored the importance of integrating nanoscale components like nHA into engineered scaffolds to promote cell proliferation (Amarjargal et al., 2019). Consequently, the enhanced adhesion and proliferation of PLLA/nHA fibers can be attributed to the inclusion of nHA nanoparticles, which is related to reduced hydrophobicity (Table 2). An *in vitro* study substantiates that the PLLA/nHA nanofibrous scaffold exhibits increased bioactivity and holds promise for stimulating bone formation (Softas, 2022).

4. Discussion

In recent years, the growing demand for bone substitutes in clinical settings has fueled advances in bone tissue engineering (Koons et al., 2020). A major goal in this field is the replication of the bone extracellular matrix (ECM). In these efforts, the integration of bioceramic materials with biocompatible scaffolds has gained much interest (Salerno and Netti, 2023). Although PLLA scaffolds have properties similar to bone (ECM, their application in tissue engineering is hampered by inherent limitations (Capuana et al., 2022). In response to these limitations, in this paper, a piezoelectric cell scaffold composed of PLLA/nHA was spun as smart scaffolds dedicated to tissue engineering.

The fiber alignment in piezoelectric scaffolds is crucial in scaffold implantation material-cell response and plays a significant role in determining the final properties of the scaffolds. In our results, two types of fiber arrangements were produced: random and aligned. In randomly arranged fiber scaffolds, the fibers create a porous and complex structure, which is beneficial for cell adhesion and nutrient diffusion. The random arrangement of fibers can promote the formation of a more natural, complex spatial network that supports tissue growth in different directions (Tamayol et al., 2013). In contrast, oriented fibers are produced by increasing the collector speed during electrospinning (in our article, increasing from 100 rpm to 2000 rpm). The aligned fibers and the addition of nHA to the structure of nanofibrous scaffolds increased the SFE and water uptake of the samples, which are important for porous materials intended for tissue engineering applications (Bhat et al., 2013). The alignment of the fibers *per se* increased the effective contact area, which led to slightly greater SFE. The fiber orientation promotes the formation of structures that are more similar to natural tissue structures, leading to better tissue integration and regeneration (Fernandez-Yague et al., 2015).

The results of wettability measurements indicate hydrophilization of the nonwovens by adding nHA. This tendency is reflected by surface free energy measurements, particularly evident for the aligned fibers geometry (SFE determined with the Kaelble-Owens-Wendt method 42.9 mN/m for PLLA/nHA versus 33.1 mN/m for pure PLLA). The effect of nHA is not so evident in the case this type of random structures (SFE 33.4 mN/m vs. 30 mN/m for PLLA/nHA and PLLA nonwovens, respectively). for which the surface is more roughly with possible air bubbles trapped between the fibers, resulting in additional wettability deviation.

One of the reasons for an increase in piezoelectric response in samples formed with higher collector rotational speed can be attributed to fiber alignment.When the fibers are aligned, the piezoelectric dipoles are oriented in a uniform direction, even in practically amorphous material, resulting in a more efficient conversion of mechanical stress into electrical signals. This alignment may better mimic the anisotropic nature of natural bone tissue, potentially leading to improved tissue regeneration outcomes. Additionally, the increase in the piezoelectric coefficient d_{33} is caused by the higher fiber arrangement and uniform distribution of nHA nanoparticles in the PLLA matrix. These nanoparticles act as nucleating agents, leading to the ordering of PLLA chains (Zhang et al., 2023b). This structural ordering is key to enhancing the piezoelectric effect because it provides a more efficient conversion of mechanical stress into electrical signals (Zhao et al., 2023). Comparing the piezoelectric coefficients d_{33} for randomly arranged and aligned PLLA nanofibers with the literature data, significant differences are visible, which reflect the influence of fiber orientation on their piezoelectric properties. In the literature, d_{33} values for random PLLA nanofibers are usually lower because the orientation of molecular dipoles is random, which leads to a reduction of the total piezoelectric effect. Typical d_{33} values for randomly arranged PLLA nanofibers range from about 1–3 pCN^{-1} (Zhao et al., 2017), while in our studies a value of 4.04 ± 0.21 pCN^{-1} was obtained. For aligned PLLA fibers, where the fibers are regularly aranged in one direction, the d_{33} coefficient increases significantly to 4.58 pCN^{-1} and is higher than that obtained in the literature (Ren et al., 2024). The development of composite scaffolds with increased piezoelectric properties opens new possibilities in the field of bone and nervous tissue engineering (Li, 2019). The observed improvements in piezoelectricity are particularly noteworthy because they play a key role in mimicking the natural electrical environment of bone tissue, thereby promoting cellular activities necessary for tissue regeneration (Kapat et al., 2020).

Our *in vitro* studies are important due to the development of new scaffolds that improve osteoblast proliferation thanks to the addition of nHA. Confirmation of this can be found in FTIR-ATR spectral analysis, where characteristic nHA peaks were detected, confirming the successful modification of PLLA fibers. Our findings support the effective integration of nHA with PLLA, leading to increased proliferation of MG-63 cells on nHA-supplemented scaffolds compared to basic PLLA scaffolds. This highlights the potential of these advanced scaffolds in bone tissue engineering. Additionally, Yanagida's (Yanagida et al., 2009) research on PLLA coated with HAp nanocrystals showed promising properties of implant materials, such as reduced inflammation and improved cell adhesion, suggesting the possibility of creating soft tissue-compatible and biodegradable scaffolds. Similarly, Liao's work (Liao et al., 2006) on biodegradable PLLA/nHA/collagen composites highlighted increased neutrophil responsiveness, highlighting the need for further *in vivo* studies on the effectiveness of scaffolds in critical bone regeneration. These collaborative discoveries contribute to a better understanding of the potential applications of innovative biomimetic materials in tissue engineering. The initiation of osteogenesis in the presence of nHA coating on PLLA is complex and involves various factors such as biomineralization, osteoconductive properties, signals transmission, and optimized cell-material interactions. We note that nHA promotes the deposition of nHA crystals, mimicking natural mineralization (Ielo et al., 2022). Additionally, its osteoconductive

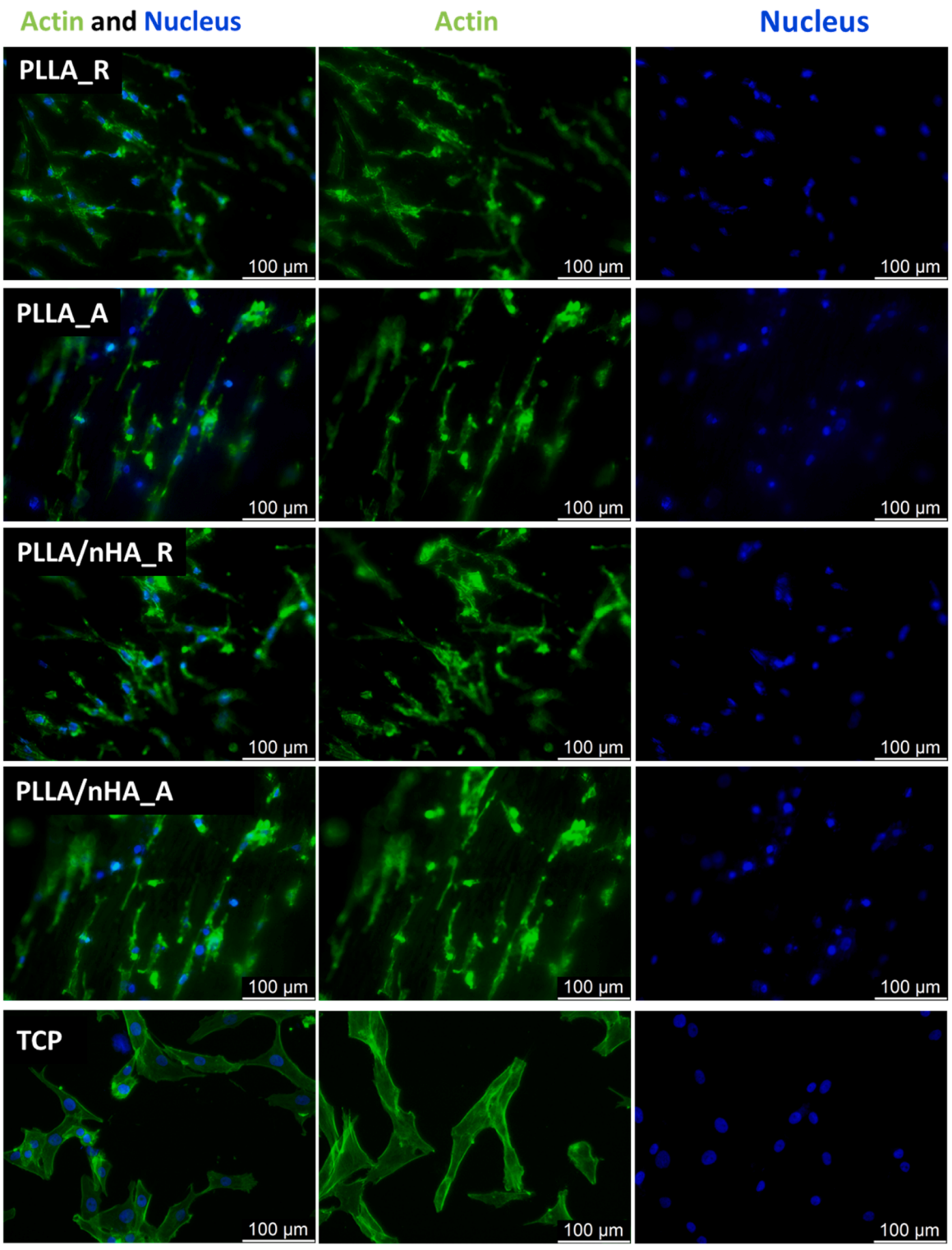

Fig. 11. FM images of MG-63 after immunofluorescent staining directly cultured on the nanofibrous scaffold for 3 days. Samples PLLA_R, PLLA_A, PLLA/nHA_R, and PLLA/nHA_A in comparison to TCP.

properties support the adhesion and migration of osteogenic cells (Zhu et al., 2021b), and the release of ions from nHA acts as important signals to catalyze osteogenic differentiation (Armiento et al., 2020).

5. Conclusions

The goal of this work was to develop an electrospun nanofibrous scaffold with PLLA and evaluate the effects of nHA addition on its properties for bone tissue engineering applications. The influence of changing the collector rotational speed on the properties of the scaffolds was determined. The electrospinning process was successful, and homogenous fibers were obtained with and without adding nHA. The presence of nHA showed no significant impact on the morphology of the fibers and their alignment for different rotational speeds. FTIR

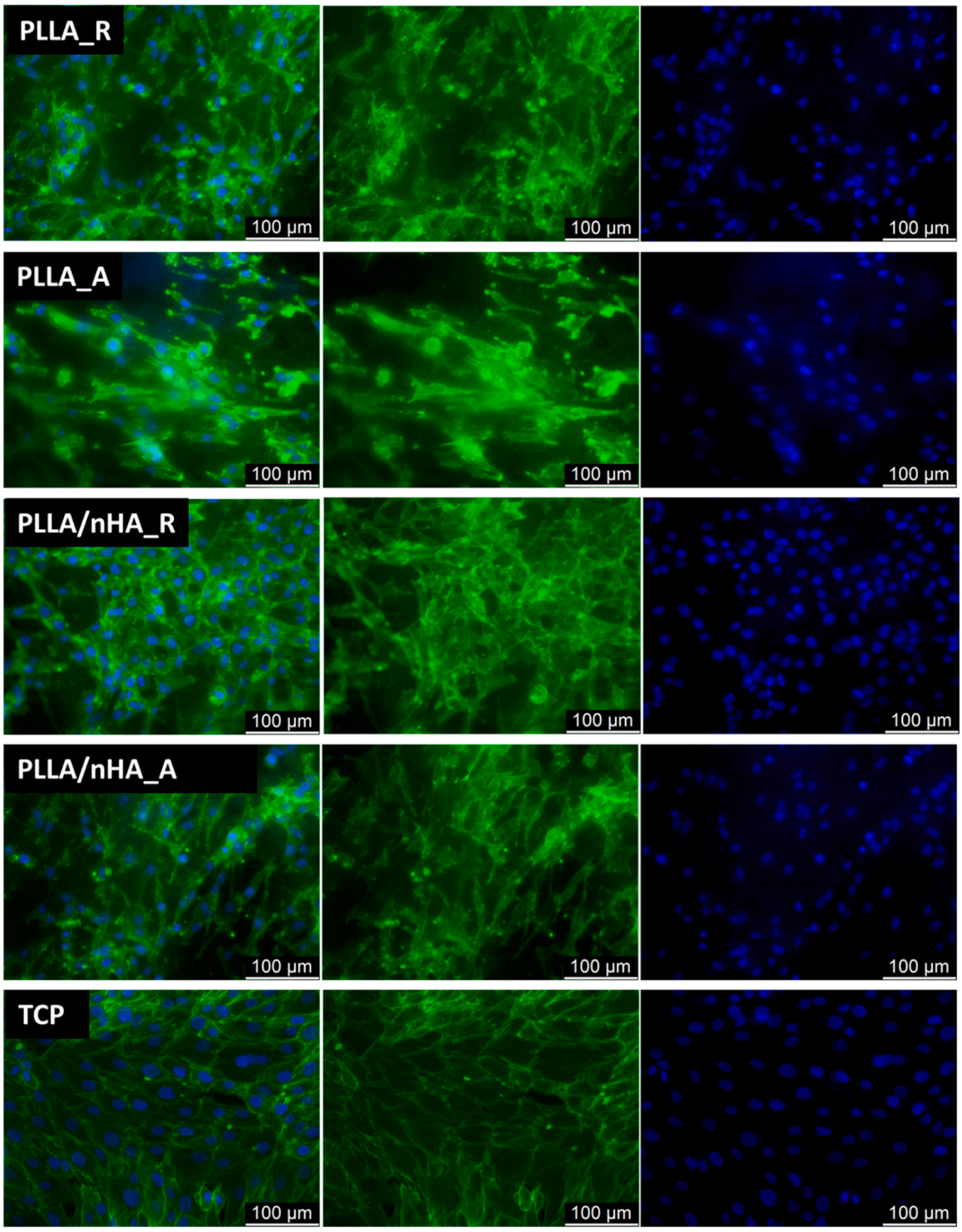

Fig. 12. FM images of MG-63 after immunofluorescent staining directly cultured on the nanofibrous scaffold for 5 days. Samples PLLA_R, PLLA_A, PLLA/nHA_R, and PLLA/nHA_A in comparison to TCP.

spectroscopy did not present any important changes in composition nor detect any interaction between constituents.

The hydrophilization of the nonwovens by adding nHA is clearly visible, being particularly evident for the aligned fibers geometry WAXS results show that all the fibers are in an amorphous state indicated by a lack of diffraction peaks. However, the presence of some disordered α' phase may be inferred from the asymmetric shape of the amorphous halo. DSC analysis revealed the presence of intense enthalpy relaxation effects at the glass transition temperature, the largest being for pure aligned PLLA fibers. All samples, being in the non-equilibrium (non-relaxed) amorphous/disordered α' phase state, intensively crystallize at temperatures just above T_g and recrystallize during further heating, developing much higher crystallinity for pure PLLA than for doped with nHA, 70 % vs 40 %, respectively. Additionally, PLLA/nHA fibers show lower heat capacity for PLLA in an amorphous state, indicating that nHA reduces PLLA molecular mobility.

Furthermore, PLLA fibers loaded with nHA showed increased porosity by 7–9 % compared to their counterparts, which is beneficial

for tissue engineering applications. Most importantly, the piezoelectric coefficient d_{33} was impacted by rotational speed and nHA presence. For the samples without nHA, obtained values were 4.04 pCN^{-1} for 100 rpm and 4.58 pCN^{-1} for 2000 rpm and increased further in its presence to 4.42 pCN^{-1} and 4.68 pCN^{-1}, respectively. Notably, our results show that the nHA can lead to the formation of more piezoelectric structure regardless of rotational speed. In addition, the nanoadditive improved osteoblast proliferation as reported by others.

The developed PLLA/nHA nanofibrous scaffold holds great promise for bone tissue engineering, offering biodegradability combined with reasonable piezoelectricity, porosity and slightly increased hydrophilicity due to nHA presence.

Ethical approval

Not applicable.

CRediT authorship contribution statement

Angelika Zaszczyńska: Writing – original draft, Visualization, Validation, Supervision, Software, Project administration, Methodology, Investigation, Formal analysis, Data curation, Conceptualization. **Dorota Kołbuk:** Writing – review & editing, Writing – original draft, Methodology, Investigation. **Arkadiusz Gradys:** Writing – review & editing, Writing – original draft, Supervision, Methodology, Investigation, Formal analysis, Conceptualization. **Konrad Zabielski:** Writing – review & editing, Writing – original draft, Methodology, Investigation. **Urszula Stachewicz:** Writing – review & editing, Writing – original draft, Supervision. **Piotr Szewczyk:** Writing – review & editing, Writing – original draft, Methodology, Investigation. **Paweł Sajkiewicz:** Writing – review & editing, Writing – original draft, Visualization, Validation, Supervision.

Declaration of Competing Interest

The authors declare that they have no known competing financial interests or personal relationships that could have appeared to influence the work reported in this paper.

Acknowledgments

The study was partially supported by the funding from the European Union's Horizon 2020 research and innovation programme under grant agreement No 958174, and within M-ERA.NET 3 funded by National Science Centre, Poland No 2021/03/Y/ST5/00231.

Appendix A. Supporting information

Supplementary data associated with this article can be found in the online version at doi:10.1016/j.micron.2024.103743.

Data availability

Data will be made available on request.

References

Amarjargal, A., Brunelli, M., Fortunato, G., Spano, F., Kim, C.S., Rossi, R.M., 2019. On-demand drug release from tailored blended electrospun nanofibers. J. Drug Deliv. Sci. Technol. 52, 8–14. https://doi.org/10.1016/j.jddst.2019.04.004.

Armiento, A.R., Hatt, L.P., Sanchez Rosenberg, G., Thompson, K., Stoddart, M.J., 2020. Functional biomaterials for bone regeneration: a lesson in complex biology. Adv. Funct. Mater. 30, 1909874. https://doi.org/10.1002/adfm.201909874.

Baniasadi, H., Madani, M., Seppälä, J., Zimmerman, J.B., Yazdani, M.R., 2023. Form-stable phase change electrospun nanofibers mat with thermal regulation and biomedical multi-functionalities. J. Energy Storage 68, 107660. https://doi.org/10.1016/j.est.2023.107660.

Barbosa, F., Garrudo, F.F.F., Alberte, P.S., Resina, L., Carvalho, M.S., Jain, A., Marques, A.C., Estrany, F., Rawson, F.J., Aléman, C., et al., 2023. Hydroxyapatite-filled osteoinductive and piezoelectric nanofibers for bone tissue engineering. Sci. Technol. Adv. Mater. 24, 2242242. https://doi.org/10.1080/14686996.2023.2242242.

Barroca, N., Marote, A., Vieira, S.I., Almeida, A., Fernandes, M.H.V., Vilarinho, P.M., Da Cruz E Silva, O.A.B., 2018. Electrically polarized PLLA nanofibers as neural tissue engineering scaffolds with improved neuritogenesis. Colloids Surf. B: Biointerfaces 167, 93–103. https://doi.org/10.1016/j.colsurfb.2018.03.050.

Bauso, L.V., La Fauci, V., Longo, C., Calabrese, G., 2024. Bone tissue engineering and nanotechnology: a promising combination for bone regeneration. Biology 13, 237. https://doi.org/10.3390/biology13040237.

Behroozi, A.H., Al-Shaeli, M., Vatanpour, V., 2023. Fabrication and modification of nanofiltration membranes by solution electrospinning technique: a review of influential factors and applications in water treatment. Desalination 558, 116638. https://doi.org/10.1016/j.desal.2023.116638.

Bhat, K.A., Leo Prakash, P., Manoharan, N., Lakshmibai, A., Sangeetha, D., 2013. Fabrication of polymethyl methacrylate/polysulfone/nanoceramic composites for orthopedic applications. J. Appl. Polym. Sci. 127, 2764–2775. https://doi.org/10.1002/app.37581.

Bose, S., Roy, M., Bandyopadhyay, A., 2012. Recent advances in bone tissue engineering scaffolds. Trends Biotechnol. 30, 546–554. https://doi.org/10.1016/j.tibtech.2012.07.005.

Bose, S., Sarkar, N., Jo, Y., 2024. Natural medicine delivery from 3D printed bone substitutes. J. Control. Release 365, 848–875. https://doi.org/10.1016/j.jconrel.2023.09.025.

Buitrago-Vásquez, M., Ossa-Orozco, C.P., 2018. Degradation, water uptake, injectability and mechanical strength of injectable bone substitutes composed of silk fibroin and hydroxyapatite nanorods. Rev. Fac. Ing. 27, 49–60. https://doi.org/10.19053/01211129.v27.n48.2018.8072.

Capuana, E., Lopresti, F., Ceraulo, M., La Carrubba, V., 2022. Poly-l-lactic acid (PLLA)-based biomaterials for regenerative medicine: a review on processing and applications. Polymers 14, 1153. https://doi.org/10.3390/polym14061153.

Cartier, L., Okihara, T., Ikada, Y., Tsuji, H., Puiggali, J., Lotz, B., 2000. Epitaxial crystallization and crystalline polymorphism of polylactides. Polymer 41, 8909–8919. https://doi.org/10.1016/S0032-3861(00)00234-2.

Chen, Y., Dong, X., Shafiq, M., Myles, G., Radacsi, N., Mo, X., 2022. Recent advancements on three-dimensional electrospun nanofiber scaffolds for tissue engineering. Adv. Fiber Mater. 4, 959–986. https://doi.org/10.1007/s42765-022-00170-7.

Chen, X., Gao, C., Jiang, J., Wu, Y., Zhu, P., Chen, G., 2019. 3D printed porous PLA/nHA composite Scaffolds with enhanced osteogenesis and osteoconductivity in vivo for bone regeneration. Biomed. Mater. 14, 065003. https://doi.org/10.1088/1748-605X/ab388d.

Davachi, S.M., Kaffashi, B., Torabinejad, B., Zamanian, A., 2016. In-vitro investigation and hydrolytic degradation of antibacterial nanocomposites based on PLLA/Triclosan/Nano-Hydroxyapatite. Polymer 83, 101–110. https://doi.org/10.1016/j.polymer.2015.12.015.

Di Lorenzo, M.L., Androsch, R., 2019. Influence of A′-/A-crystal Polymorphism on Properties of Poly(ʟ -lactic Acid). Polym. Int. 68, 320–334. https://doi.org/10.1002/pi.5707.

Díaz, E., Molpeceres, A.L., Sandonis, I., Puerto, I., 2019. PLLA/nHA composite films and scaffolds for medical implants: in vitro degradation, thermal and mechanical properties. J. Inorg. Organomet Polym. 29, 121–131. https://doi.org/10.1007/s10904-018-0972-y.

Eling, B., Gogolewski, S., Pennings, A.J., 1982. Biodegradable materials of poly(l-Lactic Acid): 1. Melt-spun and solution-spun fibres. Polymer 23, 1587–1593. https://doi.org/10.1016/0032-3861(82)90176-8.

Farag, M.M., 2023. Recent trends on biomaterials for tissue regeneration applications: review. J. Mater. Sci. 58, 527–558. https://doi.org/10.1007/s10853-022-08102-x.

Fendi, F., Abdullah, B., Suryani, S., Usman, A.N., Tahir, D., 2024. Development and application of hydroxyapatite-based scaffolds for bone tissue regeneration: a systematic literature review. Bone 183, 117075. https://doi.org/10.1016/j.bone.2024.117075.

Fernandez-Yague, M.A., Abbah, S.A., McNamara, L., Zeugolis, D.I., Pandit, A., Biggs, M. J., 2015. Biomimetic approaches in bone tissue engineering: integrating biological and physicomechanical strategies. Adv. Drug Deliv. Rev. 84, 1–29. https://doi.org/10.1016/j.addr.2014.09.005.

Glimcher, M.J., 1959. Molecular biology of mineralized tissues with particular reference to bone. Rev. Mod. Phys. 31, 359–393. https://doi.org/10.1103/RevModPhys.31.359.

Hambleton, A.R., Mele, E., 2024. Dimensional and structural instability of electrospun polylactic acid membranes in liquid environments: role of water, ethanol, and temperature. Fibers Polym. https://doi.org/10.1007/s12221-024-00564-x.

Hong, Z., Reis, R.L., Mano, J.F., 2008. Preparation and in vitro characterization of scaffolds of poly(l-lactic acid) containing bioactive glass ceramic nanoparticles. Acta Biomater. 4, 1297–1306. https://doi.org/10.1016/j.actbio.2008.03.007.

Hoogsteen, W., Postema, A.R., Pennings, A.J., Ten Brinke, G., Zugenmaier, P., 1990. Crystal structure, conformation and morphology of solution-spun poly(L-Lactide) fibers. Macromolecules 23, 634–642. https://doi.org/10.1021/ma00204a041.

Hotaling, N.A., Bharti, K., Kriel, H., Simon, C.G., 2015. DiameterJ: a validated open source nanofiber diameter measurement tool. Biomaterials 61, 327–338. https://doi.org/10.1016/j.biomaterials.2015.05.015.

Huang, X., Lou, Y., Duan, Y., Liu, H., Tian, J., Shen, Y., Wei, X., 2024. Biomaterial scaffolds in maxillofacial bone tissue engineering: a review of recent advances. Bioact. Mater. 33, 129–156. https://doi.org/10.1016/j.bioactmat.2023.10.031.

Hwangbo, H., Lee, J., Kim, G., 2022. Mechanically and biologically enhanced 3D-printed HA/PLLA/dECM biocomposites for bone tissue engineering. Int. J. Biol. Macromol. 218, 9–21. https://doi.org/10.1016/j.ijbiomac.2022.07.040.
Ielo, I., Calabrese, G., De Luca, G., Conoci, S., 2022. Recent advances in hydroxyapatite-based biocomposites for bone tissue regeneration in orthopedics. IJMS 23, 9721. https://doi.org/10.3390/ijms23179721.
Jeznach, O., Kołbuk, D., Reich, T., Sajkiewicz, P., 2022. Immobilization of gelatin on fibers for tissue engineering applications: a comparative study of three aliphatic polyesters. Polymers 14, 4154. https://doi.org/10.3390/polym14194154.
Kapat, K., Shubhra, Q.T.H., Zhou, M., Leeuwenburgh, S., 2020. Piezoelectric nano-biomaterials for biomedicine and tissue regeneration. Adv. Funct. Mater. 30, 1909045. https://doi.org/10.1002/adfm.201909045.
Karbowniczek, J.E., Ura, D.P., Stachewicz, U., 2022. Nanoparticles distribution and agglomeration analysis in electrospun fiber based composites for desired mechanical performance of poly(3-Hydroxybuty-rate-Co-3-hydroxyvalerate (PHBV) scaffolds with hydroxyapatite (HA) and titanium dioxide (TiO2) towards medical applications. Compos. Part B: Eng. 241, 110011. https://doi.org/10.1016/j.compositesb.2022.110011.
Kennedy, S.M., Vasanthanathan, A., Robert Rb, J., Amudhan, K., 2024. Advancements and prospects of polymer-based hybrid composites for bone plate applications. Polym. -Plast. Technol. Mater. 63, 68–87. https://doi.org/10.1080/25740881.2023.2274564.
Khouri, N.G., Bahú, J.O., Blanco-Llamero, C., Severino, P., Concha, V.O.C., Souto, E.B., 2024. Polylactic acid (PLA): properties, synthesis, and biomedical applications – a review of the literature. J. Mol. Struct. 1309, 138243. https://doi.org/10.1016/j.molstruc.2024.138243.
Kleintjens, L.A., 2012. Integration of Fundamental Polymer Science and Technology. Springer Science & Business Media. ISBN 978-94-009-4185-4.
Kołbuk, D., Ciechomska, M., Jeznach, O., Sajkiewicz, P., 2022. Effect of crystallinity and related surface properties on gene expression of primary fibroblasts. RSC Adv. 12, 4016–4028. https://doi.org/10.1039/D1RA07237D.
Koons, G.L., Diba, M., Mikos, A.G., 2020. Materials design for bone-tissue engineering. Nat. Rev. Mater. 5, 584–603. https://doi.org/10.1038/s41578-020-0204-2.
Leroy, A., Ribeiro, S., Grossiord, C., Alves, A., Vestberg, R.H., Salles, V., Brunon, C., Gritsch, K., Grosgogeat, B., Bayon, Y., 2017. FTIR microscopy contribution for comprehension of degradation mechanisms in PLA-based implantable medical devices. J. Mater. Sci: Mater. Med 28, 87. https://doi.org/10.1007/s10856-017-5894-7.
Li, Liao, 2019. Tjong electrospun polyvinylidene fluoride-based fibrous scaffolds with piezoelectric characteristics for bone and neural tissue engineering. Nanomaterials 9, 952. https://doi.org/10.3390/nano9070952.
Li, X., Liu, H., Wang, J., Li, C., 2012. Preparation and characterization of PLLA/nHA nonwoven Mats via laser melt electrospinning. Mater. Lett. 73, 103–106. https://doi.org/10.1016/j.matlet.2011.12.108.
Li, J., Zhao, Y., Zhai, W., Zhao, X., Dai, K., Liu, C., Shen, C., 2024. Highly aligned electrospun film with wave-like structure for multidirectional strain and visual sensing. Chem. Eng. J. 485, 149952. https://doi.org/10.1016/j.cej.2024.149952.
Liao, S., Tamura, K., Zhu, Y., Wang, W., Uo, M., Akasaka, T., Cui, F., Watari, F., 2006. Human neutrophils reaction to the biodegraded nano-hydroxyapatite/collagen and nano-hydroxyapatite/collagen/poly(L -lactic Acid) composites. J. Biomed. Mater. Res. 76A, 820–825. https://doi.org/10.1002/jbm.a.30582.
Liu, Y., Guo, Q., Zhang, X., Wang, Y., Mo, X., Wu, T., 2023. Progress in electrospun fibers for manipulating cell behaviors. Adv. Fiber Mater. 5, 1241–1272. https://doi.org/10.1007/s42765-023-00281-9.
Liu, X., Hua, X., Wu, H., 2024. Degradation behavior of poly (lactic acid) during accelerated photo-oxidation: insights into structural evolution and mechanical properties. J. Polym. Environ. https://doi.org/10.1007/s10924-024-03211-x.
Liu, J., Zhang, S., Zhang, L., Liu, L., Bai, Y., 2014. Uniaxial stretching of polylactide with different initial crystalline morphologies and temperature effect. Eur. Polym. J. 61, 83–92. https://doi.org/10.1016/j.eurpolymj.2014.08.021.
Lopresti, F., Carfì Pavia, F., Vitrano, I., Kersaudy-Kerhoas, M., Brucato, V., La Carrubba, V., 2020. Effect of hydroxyapatite concentration and size on morpho-mechanical properties of PLA-based randomly oriented and aligned electrospun nanofibrous mats. J. Mech. Behav. Biomed. Mater. 101, 103449. https://doi.org/10.1016/j.jmbbm.2019.103449.
Manzini, B.M., Machado, L.M.R., Noritomi, P.Y., Da Silva, J.V.L., 2021. Advances in bone tissue engineering: a fundamental review. J. Biosci. 46, 17. https://doi.org/10.1007/s12038-020-00122-6.
Moradi, A., Szewczyk, P.K., Stachewicz, U., 2023. Bridging a gap in thermal conductivity and heat transfer in hybrid fibers and yarns via polyimide and silicon nitride composites. Small 19, 2305104. https://doi.org/10.1002/smll.202305104.
Nagai, A., Yamashita, K., Imamura, M., Azuma, H., 2008. Hydroxyapatite electret accelerates reendothelialization and attenuates intimal hyperplasia occurring after endothelial removal of the rabbit carotid artery. Life Sci. 82, 1162–1168. https://doi.org/10.1016/j.lfs.2008.03.017.
Nasker, P., Samanta, A., Rudra, S., Sinha, A., Mukhopadhyay, A.K., Das, M., 2019. Effect of fluorine substitution on sintering behaviour, mechanical and bioactivity of hydroxyapatite. J. Mech. Behav. Biomed. Mater. 95, 136–142. https://doi.org/10.1016/j.jmbbm.2019.03.032.
Nazir, F., Iqbal, M., Khan, A.N., Mazhar, M., Hussain, Z., 2021. Fabrication of Robust Poly L-lactic acid/cyclic olefinic copolymer (PLLA/COC) blends: study of physical properties, structure, and cytocompatibility for bone tissue engineering. J. Mater. Res. Technol. 13, 1732–1751. https://doi.org/10.1016/j.jmrt.2021.05.073.
Norouzi, S., Saveh Shemshaki, N., Norouzi, E., Latifi, M., Azimi, B., Danti, S., Qiao, X., Miao, Y., Yang, S., Gorji, M., et al., 2024. Recent advances in biomaterials for tissue-engineered constructs: essential factors and engineering techniques. Mater. Today Chem. 37, 102016. https://doi.org/10.1016/j.mtchem.2024.102016.
Obregon, N., Agubra, V., Pokhrel, M., Campos, H., Flores, D., De La Garza, D., Mao, Y., Macossay, J., Alcoutlabi, M., 2016. Effect of polymer concentration, rotational speed, and solvent mixture on fiber formation using forcespinning®. Fibers 4, 20. https://doi.org/10.3390/fib4020020.
Okabayashi, R., Nakamura, M., Okabayashi, T., Tanaka, Y., Nagai, A., Yamashita, K., 2009. Efficacy of polarized hydroxyapatite and silk fibroin composite dressing gel on epidermal recovery from full-thickness skin wounds. J. Biomed. Mater. Res 90B, 641–646. https://doi.org/10.1002/jbm.b.31329.
Pan, P., Kai, W., Zhu, B., Dong, T., Inoue, Y., 2007. Polymorphous crystallization and multiple melting behavior of poly(L -Lactide): molecular weight dependence. Macromolecules 40, 6898–6905. https://doi.org/10.1021/ma071258d.
Pan, P., Yang, J., Shan, G., Bao, Y., Weng, Z., Cao, A., Yazawa, K., Inoue, Y., 2012. Temperature-variable FTIR and solid-state ^{13}C NMR investigations on crystalline structure and molecular dynamics of polymorphic poly(L -Lactide) and poly(L -Lactide)/poly(D -Lactide) stereocomplex. Macromolecules 45, 189–197. https://doi.org/10.1021/ma201906a.
Panda, A.K., Sitaramgupta, V.S.N., Pandya, H.J., Basu, B., 2022. Electrical stimulation waveform-dependent osteogenesis on PVDF/$BaTiO_3$ composite using a customized and programmable cell stimulator. Biotech. Bioeng. 119, 1578–1597. https://doi.org/10.1002/bit.28076.
Paragkumar N, T., Edith, D., Six, J.-L., 2006. Surface characteristics of PLA and PLGA films. Appl. Surf. Sci. 253, 2758–2764. https://doi.org/10.1016/j.apsusc.2006.05.047.
Pariy, I.O., Chernozem, R.V., Chernozem, P.V., Mukhortova, Y.R., Skirtach, A.G., Shvartsman, V.V., Lupascu, D.C., Surmeneva, M.A., Mathur, S., Surmenev, R.A., 2022. Hybrid biodegradable electrospun scaffolds based on poly(l-Lactic Acid) and reduced graphene oxide with improved piezoelectric response. Polym. J. 54, 1237–1252. https://doi.org/10.1038/s41428-022-00669-1.
Patel, P.R., Gundloori, R.V.N., 2023. A review on electrospun nanofibers for multiple biomedical applications. Polym. Adv. Techs 34, 44–63. https://doi.org/10.1002/pat.5896.
Pathak, R., Punetha, V.D., Bhatt, S., Punetha, M., 2023. Multifunctional role of carbon dot-based polymer nanocomposites in biomedical applications: a review. J. Mater. Sci. 58, 6419–6443. https://doi.org/10.1007/s10853-023-08408-4.
Polak, M., Berniak, K., Szewczyk, P.K., Karbowniczek, J.E., Marzec, M.M., Stachewicz, U., 2023. PLLA Scaffolds with controlled surface potential and piezoelectricity for enhancing cell adhesion in tissue engineering. Appl. Surf. Sci. 621, 156835. https://doi.org/10.1016/j.apsusc.2023.156835.
Puiggali, J., Ikada, Y., Tsuji, H., Cartier, L., Okihara, T., Lotz, B., 2000. The frustrated structure of poly(l -Lactide). Polymer 41, 8921–8930. https://doi.org/10.1016/S0032-3861(00)00235-4.
Pyda, M., Czerniecka-Kubicka, A., 2017. Thermal Properties and Thermodynamics of Poly(l-Lactic Acid) (Advances in Polymer Science). In: Di Lorenzo, M.L., Androsch, R. (Eds.), Synthesis, Structure and Properties of Poly(lactic acid), 279. Springer International Publishing, Cham, pp. 153–193 (Advances in Polymer Science).
Rachmawati, H., 2016. Curcumin-loaded PLA nanoparticles: formulation and physical evaluation. Sci. Pharm. 84, 191–202. https://doi.org/10.3797/scipharm.ISP.2015.10.
Rai, B., Teoh, S.H., Ho, K.H., 2005. An in vitro evaluation of PCL–TCP composites as delivery systems for platelet-rich plasma. J. Control. Release 107, 330–342. https://doi.org/10.1016/j.jconrel.2005.07.002.
Rancan, F., Papakostas, D., Hadam, S., Hackbarth, S., Delair, T., Primard, C., Verrier, B., Sterry, W., Blume-Peytavi, U., Vogt, A., 2009. Investigation of polylactic acid (PLA) nanoparticles as drug delivery systems for local dermatotherapy. Pharm. Res 26, 2027–2036. https://doi.org/10.1007/s11095-009-9919-x.
Ren, K., Shen, Y., Wang, Z.L., 2024. Piezoelectric properties of electrospun polymer nanofibers and related energy harvesting applications. Macro Mater. amp; Eng. 309, 2300307. https://doi.org/10.1002/mame.202300307.
Ribeiro, C., Sencadas, V., Costa, C.M., Gómez Ribelles, J.L., Lanceros-Méndez, S., 2011. Tailoring the morphology and crystallinity of poly(L-Lactide Acid) electrospun membranes. Sci. Technol. Adv. Mater. 12, 015001. https://doi.org/10.1088/1468-6996/12/1/015001.
Righetti, M.C., Gazzano, M., Di Lorenzo, M.L., Androsch, R., 2015. Enthalpy of melting of A′- and α-crystals of poly(l-Lactic Acid). Eur. Polym. J. 70, 215–220. https://doi.org/10.1016/j.eurpolymj.2015.07.024.
Rudawska, A., Jacniacka, E., 2009. Analysis for determining surface free energy uncertainty by the owen–wendt method. Int. J. Adhes. Adhes. 29, 451–457. https://doi.org/10.1016/j.ijadhadh.2008.09.008.
Salerno, A., Netti, P.A., 2023. Review on bioinspired design of ECM-mimicking scaffolds by computer-aided assembly of cell-free and cell laden micro-modules. JFB 14, 101. https://doi.org/10.3390/jfb14020101.
Saurav, S., Mohan, A., Tabassum, Z., Girdhar, M., 2024. Recent trends in polymer-based nanocomposites and its application in bone tissue engineering. Hyderabad, India, 030138.
Saxena, A., Pandey, M., Dubey, A.K., 2019. Induced electroactive response of hydroxyapatite: a review. J. Indian Inst. Sci. 99, 339–359. https://doi.org/10.1007/s41745-019-00117-9.
Scaffaro, R., Lopresti, F., Botta, L., 2017. Preparation, characterization and hydrolytic degradation of PLA/PCL Co-Mingled nanofibrous mats prepared via dual-jet electrospinning. Eur. Polym. J. 96, 266–277. https://doi.org/10.1016/j.eurpolymj.2017.09.016.
Scaffaro, R., Settanni, L., Gulino, E.F., 2023. Release profiles of carvacrol or chlorhexidine of PLA/graphene nanoplatelets membranes prepared using

electrospinning and solution blow spinning: a comparative study. Molecules 28, 1967. https://doi.org/10.3390/molecules28041967.
Sethu, S., Kalimuthu, M., Nagarajan, R., Krishnan, K., Mohammad, F., Arul Kumar, M., 2024. Hybrid fabrication and characterization of biocompatible bamboo/PLA composites. J. Mater. Res. Technol. 29, 2656–2666. https://doi.org/10.1016/j.jmrt.2024.01.265.
Shehata, N., Elnabawy, E., Abdelkader, M., Hassanin, A., Salah, M., Nair, R., Ahmad Bhat, S., 2018. Static-aligned piezoelectric poly (vinylidene fluoride) electrospun nanofibers/MWCNT composite membrane: facile method. Polymers 10, 965. https://doi.org/10.3390/polym10090965.
Softas, C., 2022. Selective Laser Sintering of Hydroxyapatite-Based Materials for Tissue Engineering. In: Narayan, R.J. (Ed.), In *Additive Manufacturing in Biomedical Applications*. ASM International, pp. 92–105. ISBN 978-1-62708-392-8.
Srivastava, A., Bhati, P., Singh, S., Agrawal, M., Kumari, N., Vashisth, P., Chauhan, P., Bhatnagar, N., 2024. A review on polylactic acid-based blends/composites and the role of compatibilizers in biomedical engineering applications. Polym. Eng. Sci. 64, 1003–1044. https://doi.org/10.1002/pen.26626.
Stoch, A., Jastrzębski, W., Brożek, A., Stoch, J., Szaraniec, J., Trybalska, B., Kmita, G., 2000. FTIR absorption–reflection study of biomimetic growth of phosphates on titanium implants. J. Mol. Struct. 555, 375–382. https://doi.org/10.1016/S0022-2860(00)00623-2.
Sukumaran, S., Szewczyk, P.K., Knapczyk-Korczak, J., Stachewicz, U., 2023. Optimizing piezoelectric coefficient in PVDF fibers: key strategies for energy harvesting and smart textiles. Adv. Electron. Mater. 9, 2300404. https://doi.org/10.1002/aelm.202300404.
Szewczyk, P.K., Taşlı, A.E., Knapczyk-Korczak, J., Stachewicz, U., 2023. Steering triboelectric and mechanical properties of polymer fibers with carbon black. Compos. Sci. Technol. 243, 110247. https://doi.org/10.1016/j.compscitech.2023.110247.
Szewczyk, P.K., Ura, D.P., Metwally, S., Knapczyk-Korczak, J., Gajek, M., Marzec, M.M., Bernasik, A., Stachewicz, U., 2019. Roughness and fiber fraction dominated wetting of electrospun fiber-based porous meshes. Polymers 11, 34. https://doi.org/10.3390/polym11010034.
Tamayol, A., Akbari, M., Annabi, N., Paul, A., Khademhosseini, A., Juncker, D., 2013. Fiber-based tissue engineering: progress, challenges, and opportunities. Biotechnol. Adv. 31, 669–687. https://doi.org/10.1016/j.biotechadv.2012.11.007.
Tazibt, N., Kaci, M., Dehouche, N., Ragoubi, M., Atanase, L.I., 2023. Effect of filler content on the morphology and physical properties of poly(lactic acid)-hydroxyapatite composites. Materials 16, 809. https://doi.org/10.3390/ma16020809.
Van Manen, E.H.C., Zhang, W., Walboomers, X.F., Vazquez, B., Yang, F., Ji, W., Yu, N., Spear, D.J., Jansen, J.A., Yelick, P.C., 2014. The influence of electrospun fibre scaffold orientation and nano-hydroxyapatite content on the development of tooth bud stem cells in vitro. Odontology 102, 14–21. https://doi.org/10.1007/s10266-012-0087-9.
Vijayendran, B.R., 1979. Polymer polarity and surfactant adsorption. J. Appl. Polym. Sci. 23, 733–742. https://doi.org/10.1002/app.1979.070230308.
Wang, X., Kumar, V., Li, W., 2007. Low density sub-critical CO_2 -blown solid-state PLA foams. Cell. Polym. 26, 11–35. https://doi.org/10.1177/026248930702600102.
Wang, P., Lv, H., Cao, X., Liu, Y., Yu, D.-G., 2023. Recent progress of the preparation and application of electrospun porous nanofibers. Polymers 15, 921. https://doi.org/10.3390/polym15040921.
Wasanasuk, K., Tashiro, K., 2011. Crystal structure and disorder in poly(l-Lactic Acid) δ Form (A′ Form) and the phase transition mechanism to the ordered α form. Polymer 52, 6097–6109. https://doi.org/10.1016/j.polymer.2011.10.046.
Winey, K.I., Vaia, R.A., 2007. Polymer nanocomposites. MRS Bull. 32, 314–322. https://doi.org/10.1557/mrs2007.229.
Wortham, J.M., Haddad, M.B., Stewart, R.J., Annambhotla, P., Basavaraju, S.V., Nabity, S.A., Griffin, I.S., McDonald, E., Beshearse, E.M., Grossman, M.K., et al., 2024. Second nationwide tuberculosis outbreak caused by bone allografts containing live cells — United States, 2023. MMWR Morb. Mortal. Wkly. Rep. 72, 1385–1389. https://doi.org/10.15585/mmwr.mm725253a1.
Wunderlich, B., Grebowicz, J., 1984. Thermotropic Mesophases and Mesophase Transitions of Linear, Flexible Macromolecules (Advances in Polymer Science). In: Platé, N.A. (Ed.), Liquid Crystal Polymers II/III, 60/61. Springer Berlin Heidelberg, Berlin, Heidelberg, pp. 1–59 (Advances in Polymer Science).
Xing, J., Zhang, M., Liu, X., Wang, C., Xu, N., Xing, D., 2023. Multi-material electrospinning: from methods to biomedical applications. Mater. Today Bio 21, 100710. https://doi.org/10.1016/j.mtbio.2023.100710.
Yanagida, H., Okada, M., Masuda, M., Ueki, M., Narama, I., Kitao, S., Koyama, Y., Furuzono, T., Takakuda, K., 2009. Cell adhesion and tissue response to hydroxyapatite nanocrystal-coated poly(l-lactic acid) fabric. J. Biosci. Bioeng. 108, 235–243. https://doi.org/10.1016/j.jbiosc.2009.04.003.
Yang, X., Chen, Y., Zhang, C., Duan, G., Jiang, S., 2023. Electrospun carbon nanofibers and their reinforced composites: preparation, modification, applications, and perspectives. Compos. Part B: Eng. 249, 110386. https://doi.org/10.1016/j.compositesb.2022.110386.
Zaszczyńska, A., Gradys, A., Ziemiecka, A., Szewczyk, P.K., Tymkiewicz, R., Lewandowska-Szumieł, M., Stachewicz, U., Sajkiewicz, P., 2024a. Enhanced electroactive phases of poly(vinylidene fluoride) fibers for tissue engineering applications. IJMS 25, 4980. https://doi.org/10.3390/ijms25094980.
Zaszczyńska, A., Kołbuk, D., Gradys, A., Sajkiewicz, P., 2024b. Development of poly (Methyl methacrylate)/nano-hydroxyapatite (PMMA/nHA) nanofibers for tissue engineering regeneration using an electrospinning technique. Polymers 16, 531. https://doi.org/10.3390/polym16040531.
Zaszczyńska, A., Niemczyk-Soczynska, B., Sajkiewicz, P., 2022. A comprehensive review of electrospun fibers, 3D-printed scaffolds, and hydrogels for cancer therapies. Polymers 14, 5278. https://doi.org/10.3390/polym14235278.
Zhang, J., Duan, Y., Domb, A.J., Ozaki, Y., 2010. PLLA mesophase and its phase transition behavior in the PLLA−PEG−PLLA copolymer as revealed by infrared spectroscopy. Macromolecules 43, 4240–4246. https://doi.org/10.1021/ma100301h.
Zhang, J., Duan, Y., Sato, H., Tsuji, H., Noda, I., Yan, S., Ozaki, Y., 2005. Crystal modifications and thermal behavior of poly(L -Lactic Acid) revealed by infrared spectroscopy. Macromolecules 38, 8012–8021. https://doi.org/10.1021/ma051232r.
Zhang, R., Ma, P.X., 1999. Porous poly(L-Lactic Acid)/apatite composites created by biomimetic process. J. Biomed. Mater. Res. 45, 285–293. https://doi.org/10.1002/(SICI)1097-4636(19990615)45:4<285::AID-JBM2>3.0.CO;2-2.
Zhang, J., Tashiro, K., Domb, A.J., Tsuji, H., 2006. Confirmation of disorder α form of poly(L -lactic Acid) by the x-ray fiber pattern and polarized IR/Raman spectra measured for uniaxially-oriented samples. Macromol. Symp. 242, 274–278. https://doi.org/10.1002/masy.200651038.
Zhang, Y., Wang, W., Chen, Z., Shi, H., Zhang, W., Zhang, X., Hua, X., 2023b. An artificial bone filling material of poly L-lactic acid/collagen/nano-hydroxyapatite microspheres: preparation and collagen regulation on the property. Int. J. Biol. Macromol. 229, 35–50. https://doi.org/10.1016/j.ijbiomac.2022.12.200.
Zhang, M., Xu, F., Cao, J., Dou, Q., Wang, J., Wang, J., Yang, L., Chen, W., 2024. Research advances of nanomaterials for the acceleration of fracture healing. Bioact. Mater. 31, 368–394. https://doi.org/10.1016/j.bioactmat.2023.08.016.
Zhang, M., Xu, S., Wang, R., Che, Y., Han, C., Feng, W., Wang, C., Zhao, W., 2023a. Electrospun nanofiber/hydrogel composite materials and their tissue engineering applications. J. Mater. Sci. Technol. 162, 157–178. https://doi.org/10.1016/j.jmst.2023.04.015.
Zhao, G., Huang, B., Zhang, J., Wang, A., Ren, K., Wang, Z.L., 2017. Electrospun poly(l -Lactic Acid) nanofibers for nanogenerator and diagnostic sensor applications. Macro Mater. amp; Eng. 302, 1600476. https://doi.org/10.1002/mame.201600476.
Zhao, H., Liang, K., Wang, S., Ding, Z., Huang, X., Chen, W., Ren, Y., Li, J., 2023. A stress self-adaptive silicon/carbon “ordered structures” to suppress the electro-chemo-mechanical failure: piezo-electrochemistry and piezo-ionic dynamics. Adv. Sci. 10, 2303696. https://doi.org/10.1002/advs.202303696.
Zhou, W., Yu, J., Zhang, S., 2023. Environmentally friendly waterproof and breathable membranes via electrospinning. J. Text. Inst. 1–23. https://doi.org/10.1080/00405000.2023.2201061.
Zhu, Y., Goh, C., Shrestha, A., 2021b. Biomaterial properties modulating bone regeneration. Macromol. Biosci. 21, 2000365. https://doi.org/10.1002/mabi.202000365.
Zhu, G., Zhang, T., Chen, M., Yao, K., Huang, X., Zhang, B., Li, Y., Liu, J., Wang, Y., Zhao, Z., 2021a. Bone physiological microenvironment and healing mechanism: basis for future bone-tissue engineering Scaffolds. Bioact. Mater. 6, 4110–4140. https://doi.org/10.1016/j.bioactmat.2021.03.043.

molecules

MDPI

Article

On the Structural and Biological Effects of Hydroxyapatite and Gold Nano-Scale Particles in Poly(Vinylidene Fluoride) Smart Scaffolds for Bone and Neural Tissue Engineering

Angelika Zaszczyńska [1], Marzena Zychowicz [2], Dorota Kołbuk [1], Piotr Denis [1], Arkadiusz Gradys [1,*] and Paweł Ł. Sajkiewicz [1,*]

[1] Institute of Fundamental Technological Research, Polish Academy of Sciences, Pawinskiego 5B, 02-106 Warsaw, Poland; azasz@ippt.pan.pl (A.Z.); dkolbuk@ippt.pan.pl (D.K.); pdenis@ippt.pan.pl (P.D.)
[2] Department of Stem Cell Bioengineering, Mossakowski Medical Research Institute, Polish Academy of Sciences, Pawinskiego 5, 02-106 Warsaw, Poland; mzychowicz@imdik.pan.pl
* Correspondence: argrad@ippt.pan.pl (A.G.); psajk@ippt.pan.pl (P.Ł.S.)

Abstract: Piezoelectric materials, due to their ability to generate an electric charge in response to mechanical deformation, are becoming increasingly attractive in the engineering of bone and neural tissues. This manuscript reports the effects of the addition of nanohydroxyapatite (nHA), introduction of gold nanoparticles (AuNPs) via sonochemical coating, and collector rotation speed on the formation of electroactive phases and biological properties in electrospun nanofiber scaffolds consisting of poly(vinylidene fluoride) (PVDF). FTIR, WAXS, DSC, and SEM results indicate that introduction of nHA increases the content of electroactive phases and fiber alignment. The collector rotational speed increases not only the fiber alignment but also the content of electroactive phases in PVDF and PVDF/nHA fibers. Increased fiber orientation and introduction of each of additives resulted in increased SFE and water uptake. In vitro tests conducted on MG-63 and hiPSC-NSC cells showed increased adhesion and cell proliferation. The results indicate that PVDF-based composites with nHA and AuNPs are promising candidates for the development of advanced scaffolds for bone and neural tissue engineering applications, combining electrical functionality and biological activity to support tissue regeneration.

Keywords: scaffolds; tissue engineering; bone tissue engineering; smart medicine; biodegradable polymers; regenerative medicine; poly(vinylidene fluoride)

Academic Editors: Dimitrios Bikiaris and Hua Wei

Received: 2 January 2025
Revised: 27 January 2025
Accepted: 19 February 2025
Published: 25 February 2025

Citation: Zaszczyńska, A.; Zychowicz, M.; Kołbuk, D.; Denis, P.; Gradys, A.; Sajkiewicz, P.Ł. On the Structural and Biological Effects of Hydroxyapatite and Gold Nano-Scale Particles in Poly(Vinylidene Fluoride) Smart Scaffolds for Bone and Neural Tissue Engineering. *Molecules* **2025**, *30*, 1041. https://doi.org/10.3390/molecules30051041

1. Introduction

In recent times, nanoscale materials, especially Smart Materials (SM), have the potential to enhance tissue engineering and stem cell therapy [1,2]. Tissue engineering presents an exciting avenue for the development of functional constructs that mimic the structural organization of native tissues, aiming to enhance or replace biological functions, thus potentially obviating the need for organ transplantation. In tissue engineering, the main goal is successful formation of three-dimensional (3D) tissues, which may be achieved by seeding of the biological cells into specially designed manufactured scaffolds [3]. The ideal scaffold for tissue engineering applications should perfectly imitate the functional properties of the extracellular matrix (ECM) of the target tissues for regeneration [4]. However, the intricate chemical and architectural composition of the bone and neural systems pose additional challenges to engineering tissue, necessitating specific criteria in scaffold design, especially in bone and neural tissue engineering.

One of the responses to such requirements is the use of SM, among which poly(vinylidene fluoride) (PVDF) is very well-known due to its high piezoelectric properties [5]. In this context, various approaches, such as conductive polymers, aligned polymers, and both exogenous and endogenous electrical stimulation, have demonstrated promising outcomes [6]. Figure 1 shows schematic illustration of SM for bone and neural tissue applications.

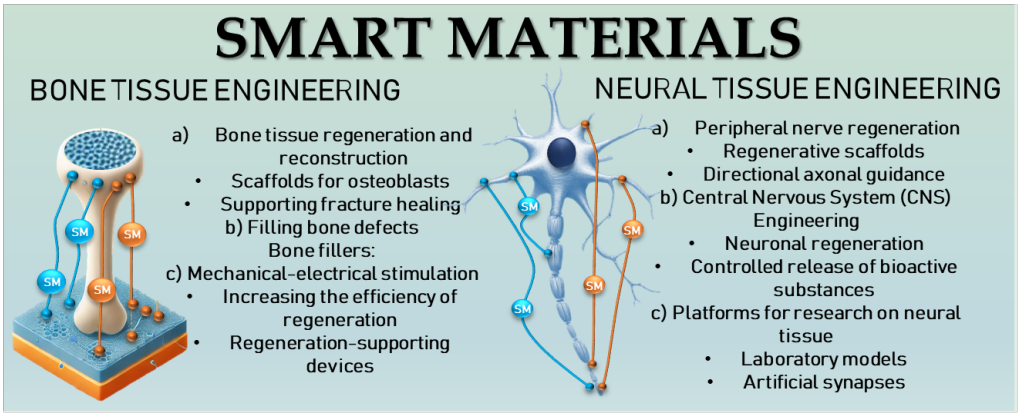

Figure 1. Schematic illustration of electroactive biomaterials for bone and neural tissue regeneration.

PVDF is a synthetic polymer known for its high piezoelectric properties and electrospinning ability [7]. PVDF exhibits five distinct crystalline phases, named as, α, β, γ, δ, and ε [8]. Among these, the piezoelectric phases (β, γ, δ) are characterized by a polar crystal structure, where the dipoles align in parallel, resulting in a non-zero dipole moment [9]. The β-phase is particularly significant due to its outstanding piezoelectric, pyroelectric, and ferroelectric properties [10]. In this phase, all dipole moments align in a single direction, producing the strongest piezoelectric response. Polar γ-phase has lower piezoelectricity compared to β-phase, this is due to the presence of *gauche* bond in C-C repeating unit [11].

This thermoplastic polymer has high chemical resistance, and biocompatibility, rendering it indispensable in various electro-optical [12], electromechanical [13], and biomedical applications [14]. Piezoelectric PVDF holds significant promise for advanced applications in cell biology and tissue engineering, particularly in piezoelectric sensing and actuation of cellular activities [15]. Notably, PVDF and its copolymers have emerged as highly promising materials in the realm of biological and biomedical applications [16]. These materials lend themselves readily to processing, yielding well-defined nanofibers that find application in cell culture. PVDF is a non-toxic material with great potential for applications. However, it is important to control the production and modification processes to avoid introducing harmful additives or by-products that could negatively affect the safety of biomedical applications [17]. Given the burgeoning interest in tissue engineering scaffolds with piezoelectric capabilities, PVDF assumes a prime position as an excellent candidate for fabricating bioscaffolds endowed with piezoelectric properties. While the piezoelectric properties of PVDF hold potential applications for neuronal and osteogenic cell outgrowth, thorough demonstrations of this aspect remain rare in the current literature [18,19].

Piezoelectric materials have the unique ability to generate electric charges in response to mechanical deformation, which is particularly useful in the regeneration of neural tissue [20]. In nerve regeneration, electrical signals play a key role because they promote the growth, guidance, and differentiation of nerve cells [21]. Electrical signals generated by piezoelectric materials can activate ion channels in nerve cell membranes, which in turn promotes the release of growth factors and other cellular signals necessary for regeneration. This can lead to increased proliferation and differentiation of nerve cells [22].

Additionally, piezoelectricity is found in bones [23]. Piezoelectric materials play an important role in the regeneration of bone tissue due to their ability to generate electric charges under the influence of mechanical deformations [24]. Bone tissue, similar to nervous tissue, responds to electrical signals that can support regenerative processes. Electrical signals can activate osteoblasts, promoting their proliferation (increase in cell number) and differentiation (transformation into mature bone cells). Increased osteoblast activity leads to faster formation of new bone tissue [25].

Scientists have long been interested in the use of nanohydroxyapatite (nHA) in bone tissue engineering due to its chemical similarity to the natural bone matrix. In the study conducted by Yang et al. [26], nHA was incorporated into poly(lactide-co-glycolide) (PLGA) to enhance the bioactivity of the scaffolds. Their study showed that these composites promoted adhesion, proliferation, and increased expression of osteogenic-related genes, suggesting their potential for use in bone regeneration. Other studies, such as those conducted by Akbari et al. [27], focused on piezoelectric PVDF/PCL/HA composites. They demonstrated that these composites could generate electrical pulses in response to mechanical stress, which could stimulate bone regeneration via mechanotransduction. The results showed that the piezoelectric properties of PVDF combined with the bioactivity of nHA could accelerate the bone healing process. Furthermore, gold nanoparticles (AuNPs) have been widely studied due to their excellent conductive properties and biocompatibility [28]. For example, Motamedi et al. [6] studied PVDF and gold nanoparticle composites, showing that their combination can improve the electrical conductivity of scaffolds, which may be suitable for use as a scaffold in neural tissue engineering. Other studies have also been conducted on electrospun PVDF fibers [29] with additives [30] but without orientation. Still, there are only a few studies on aligned fibers and their effects on the material structure and biological properties. To the authors' knowledge, studies on the orientation of piezoelectric nanofibrous scaffolds with additives for bone and neural cell regeneration applications are lacking in the literature. All these studies emphasize the growing interest and potential of piezoelectric PVDF, nHA, and AuNPs composites in bone and neural tissue regeneration, indicating their innovativeness and multifaceted impact on developing advanced biomedical scaffolds.

Therefore, our goal was to design piezoelectric scaffolds with random and aligned fiber orientation. Studying various nanofiber orientations and their influence on properties is a new approach that can lead to optimizing the functionality of these materials in multi-biomedical applications. Oriented nanofibers can better simulate the structure of natural tissues and induce the formation of piezoelectric phases, which can be crucial for effective regeneration. On the other hand, the addition of piezoelectric nHA and AuNPs can also increase piezoelectric phase content, material-cell interactions, promoting osseointegration, and can support repair processes in nerve cells. In the context of current advances in the field of SM and their importance for tissue engineering applications, selecting the most optimal method for manufacturing PVDF fibers with strong piezoelectric response is crucial to increase the efficiency of these materials applications while reducing production costs.

2. Results and Discussion

2.1. Morphology Analysis

From Figure 2, it is clear that the fibers in all scaffolds exhibit uniform and bead-free morphology. Increasing the collector rotation speed reduces the fiber diameter in all samples. This reduction ranges from an average diameter of 903 ± 54 nm for PVDF_R, 847 ± 70 nm for PVDF/nHA_R, and 890 ± 81 nm for PVDF/AU_R at low collector rotation speed (100 rpm) to values of 347 ± 14 nm for PVDF_A, 290 ± 30 nm for PVDF/nHA_A, and 354 ± 30 nm for PVDF/AU_A at higher collector rotation speed (2000 rpm). Increasing

the collector rotation speed leads to the fibers being stretched with greater force along their length. As a result of this stretching, the fibers become thinner, which means that their diameter decreases [31]. High rotation speed leads to increased molecular orientation along the fiber axis (e.g., [32]). SEM images revealed a uniform distribution of nanoparticles in the fibers without visible agglomerations (see Figure 2C–F). The addition of nHA increases the dielectric properties and electrical conductivity of the solution [33]. This causes an increase in repulsive interactions in the solution, which in turn increases the jet pulling force (reduces Rayleigh instabilities) which led to a slight decrease in the fiber diameter (903 ± 54 nm, 847 ± 70 nm for PVDF_R, PVDF/nHA_R and 347 ± 14 nm and 290 ± 30 nm for PVDF_A and PVDF/nHA_A, respectively) (Figure 3) [34].

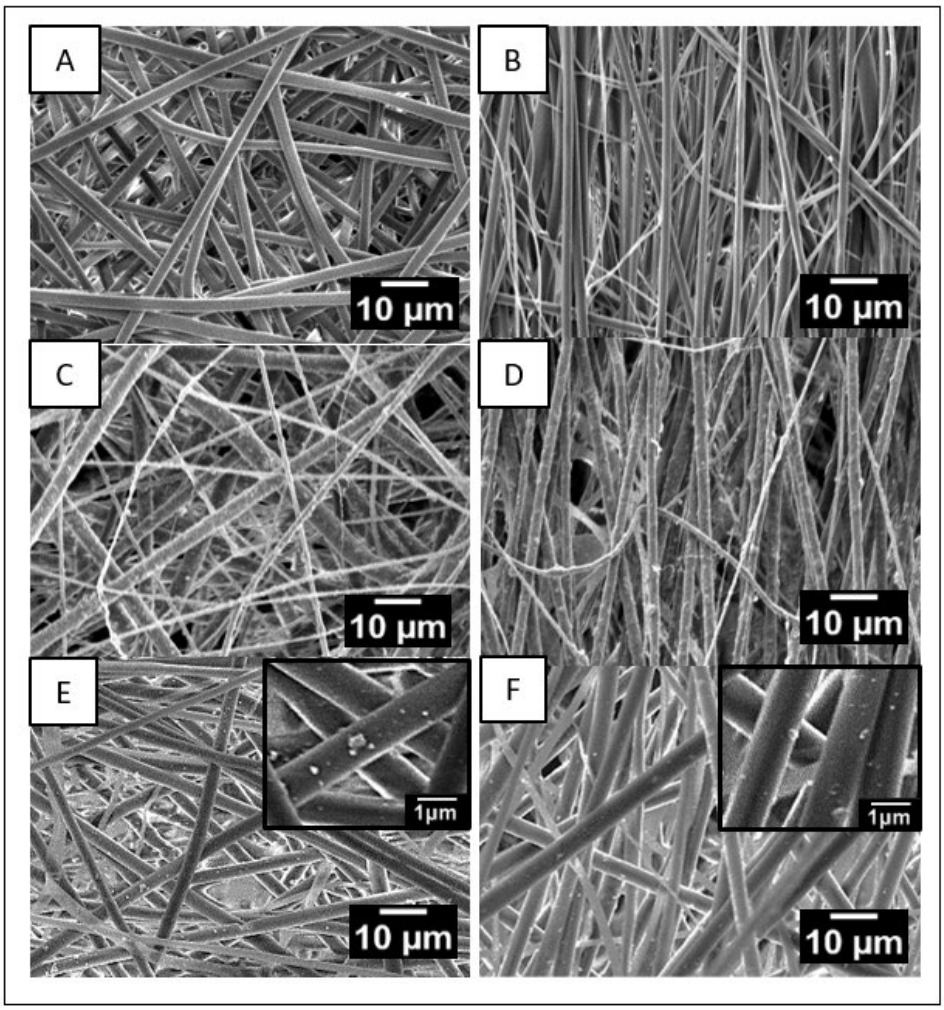

Figure 2. SEM micrographs of (**A**) PVDF_R, (**B**) PVDF_A, (**C**) PVDF/nHA_R, and (**D**) PVDF/nHA_A, (**E**) PVDF/AU_R, (**F**) PVDF/AU_A nanofibrous scaffolds.

Figure 4 shows that increasing the collector rotational speed improves the fiber orientation, leading to an orientation with a narrow distribution for fibers collected at 2000 rpm, contrary to randomly arranged fibers collected at 100 rpm. The fiber orientation distribution's full width at half maximum (FWHM) decreases from 87.90 at 100 rpm to 22.40 at 2000 rpm for pure PVDF. Higher rotational speeds increase tensile forces, enhancing the fibers' stretching and alignment. The anisotropy index (α) confirms this tendency. As the rotational speed increased from 100 to 2000 rpm, the α value increased from 0.29 to 0.78 for pure PVDF, from 0.40 to 0.92 for PVDF with the addition of nHA, and from 0.27 to 0.87 for PVDF with AuNPs addition. It is worth mentioning that the addition of nHA influenced the slight orientation already in the sample with random fiber orientation, which

may be caused by a higher electrical charge in material (PVDF/nHA_R, Figure 4C) [35]. PVDF contains molecular dipoles, and the addition of nHA increases dielectric constant, leading to stronger repulsive interactions in solution, and hence promoting their directionality [36]. In the case of pure PVDF and with AuNPs addition, there is practically no preferred orientation in nonwovens collected at 100 rpm.

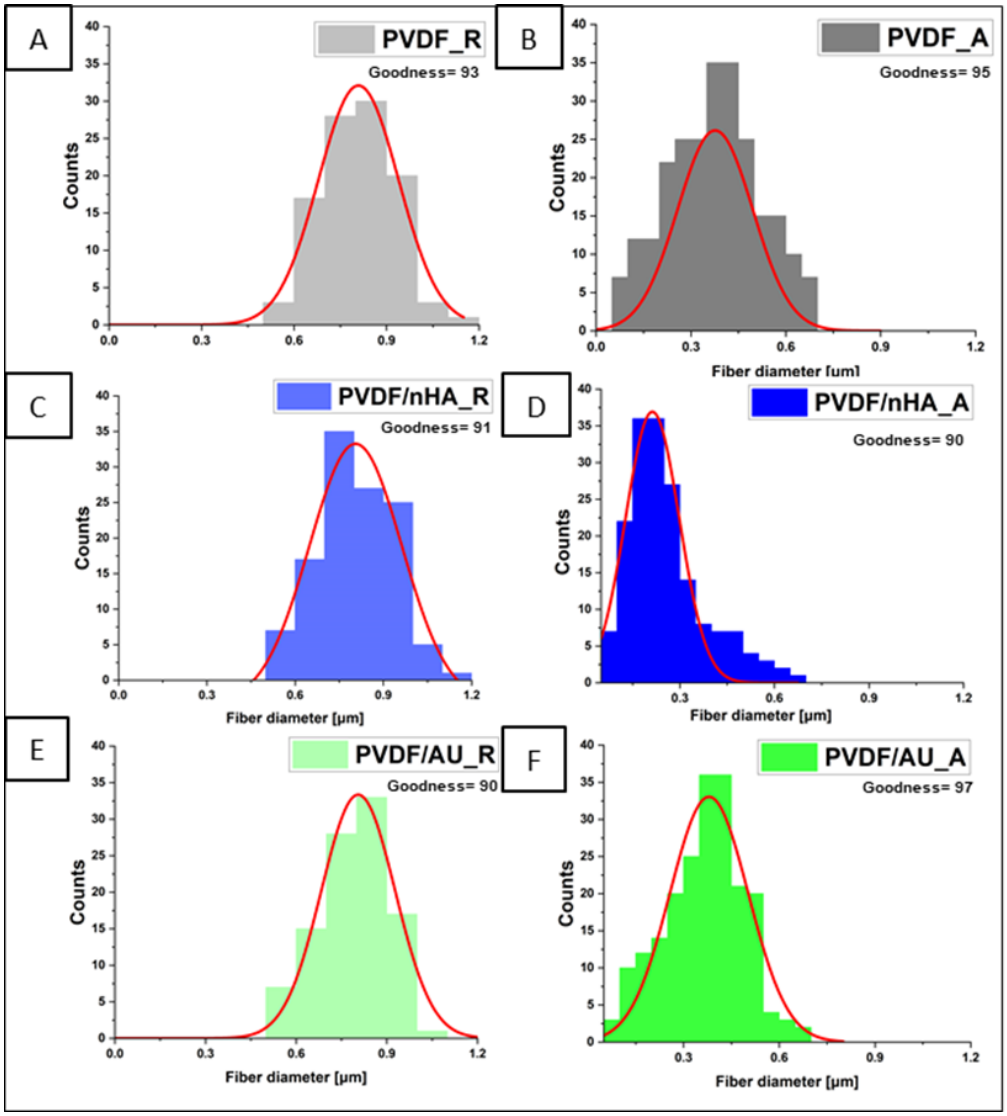

Figure 3. Diameter distributions approximated with Gaussian function of nanofibrous scaffolds (**A**) PVDF_R, (**B**) PVDF_A, (**C**) PVDF/nHA_R, and (**D**) PVDF/nHA_A, (**E**) PVDF/AU_R (**F**) PVDF/AU_A.

The analysis of porosity and average pore size shows the influence of collector rotation speed as well as nHA and AuNPs addition (Table 1). Increasing collector rotation speed leads to lower porosity of nonwovens and slightly lower pore size. Porosity increases slightly with the addition of nHA and AuNPs but is still lower in the aligned fiber orientation. The addition of nHA and AuNPs increases porosity in PVDF/nHA_R and for PVDF/nHA_A (analogously for samples with AuNPs addition), but still the porosity in aligned samples is lower. Thus, the influence of collector rotation speed on fiber porosity can be observed for pure PVDF samples and for samples with nHA and AuNPs additions. The average pore size was reduced with the introduction of a higher collector rotation speed for all samples. The largest difference was observed for samples with nHA addition.

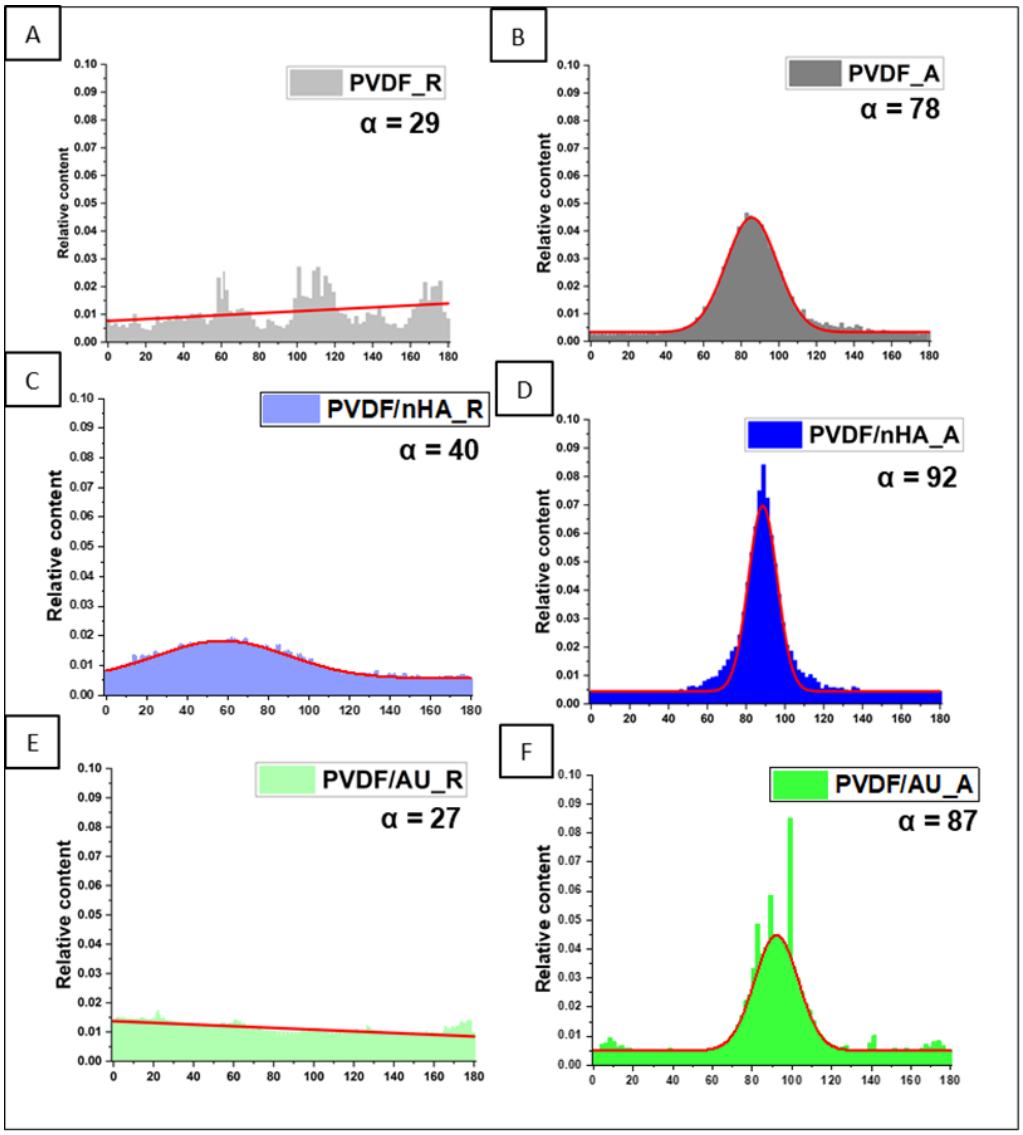

Figure 4. Orientation distributions and anisotropy index α of all nanofibrous scaffolds (**A**) PVDF_R, (**B**) PVDF_A, (**C**) PVDF/nHA_R, and (**D**) PVDF/nHA_A, (**E**) PVDF/AU_R (**F**) PVDF/AU_A.

Table 1. Porosity and pore size values for all nanofibrous scaffolds.

	PVDF_R	PVDF_A	PVDF/nHA_R	PVDF/nHA_A	PVDF/AU_R	PVDF/AU_A
Porosity [%]	87 ± 1.1	83 ± 0.9	93 ± 1.1	87 ± 0.6	90 ± 0.4	85 ± 0.3
Pore size [nm]	202 ± 7	195 ± 3	204 ± 9	198 ± 8	203 ± 6	200 ± 4

The presence of nHA and AuNPs as additives to PVDF has been verified by SEM-EDS (Table 2). In the case of samples with nHA and AuNPs, analysis confirmed the presence of elements of nHA nanoparticles, such as phosphorus (P) and calcium (Ca), in addition to the basic PVDF elements carbon (C) and oxygen (O). Additionally, the presence of gold was confirmed in both samples PVDF/AU_R and PVDF/AU_A.

Table 2. Piezoelectric scaffold composition in wt% as measured using SEM-EDS.

Element	PVDF_R	PVDF_A	PVDF/nHA_R	PVDF/nHA_A	PVDF/AU_R	PVDF_AU_A
C	61.81 ± 0.7	61.97 ± 0.6	60.47 ± 0.3	60.13 ± 0.4	60.75 ± 0.5	60.84 ± 0.7
O	38.19 ± 0.3	38.03 ± 0.4	33.9 ± 0.7	33.81 ± 0.6	38.9 ± 0.3	38.83 ± 0.4
Ca	-	-	3.52 ± 0.4	3.79 ± 0.3	-	-
P	-	-	2.11 ± 0.2	2.27 ± 0.1	-	-
Au	-	-	-	-	0.35 ± 0.5	0.33 ± 0.2
Other	-	-	-	-	-	-

2.2. Water Uptake, Contact Angle Measurements, and Surface Free Energy Determination

Figure 5 illustrates the contact angle measurements, and additionally Table 3 shows the surface free energy values and their components. The overall effect of the addition of nHA, AuNPs, and fiber configuration on the contact angle is visible. The higher collector rotational speed during the electrospinning process, the addition of nHA and AuNPs causes a decrease in the contact angle. A similar phenomenon is observed for aligned fibers arranged compared to randomly oriented fibers. The Figure 5 shows that the contact angles measured with formamide are lower than those obtained with water and diiodomethane. However, the influence of nHA, AuNPs, and fiber configuration is similar for all liquids. The reduction in contact angle in nHA- and AuNPs-doped PVDF samples may also indicate improved cell adhesion to the nanofiber surfaces, which is beneficial in tissue engineering, where it is crucial to ensure adequate cell adhesion to scaffolds to improve tissue regeneration [37].

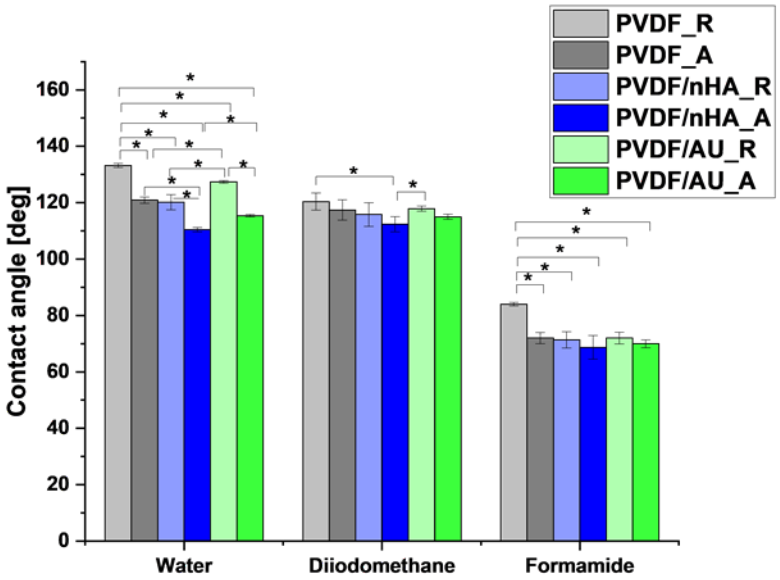

Figure 5. Contact angle measurements for all nanofibrous scaffolds ("*" means p-value ≤ 0.05).

It is evident from Figure 6 that the highest water uptake was in scaffolds with nHA in both random and aligned orientation. Pure samples PVDF_R and PVDF_A samples showed lower water absorption in all cases. After 10 min, the water absorption in the PVDF_R sample was about 140%, compared to 194% for PVDF_A. Such low water absorption capacity is consistent with the hydrophobic nature of PVDF, which does not exhibit strong interactions with water. The random arrangement of fibers did not favor increasing the contact surface with water, which additionally limited the ability of the samples to absorb moisture [38]. In the case of oriented PVDF fibers, the higher result can be explained by the more ordered fiber structure, which increases the surface availability for water, resulting

in a slightly higher level of absorption. However, the water absorption of pure PVDF still remained low, due to its nonpolar nature [39].

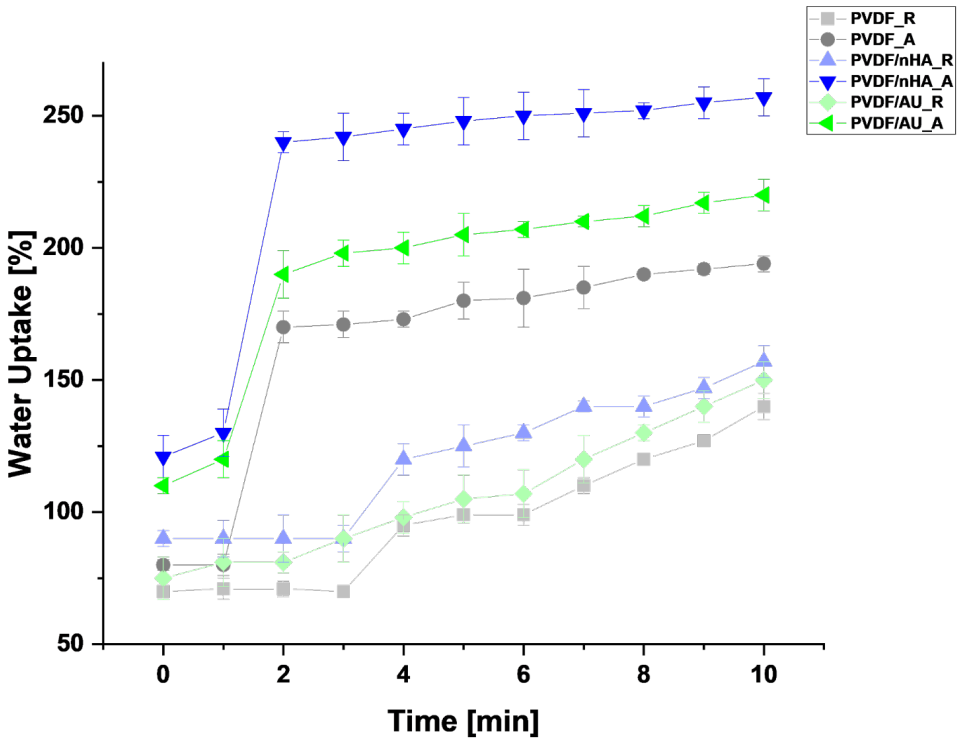

Figure 6. Water uptake of all piezoelectric scaffolds calculated from Equation (8).

The introduction of nHA and AuNPs increased the ability of the samples to absorb water. The samples with nHA showed significantly higher water absorption capacity. For the PVDF/nHA_R the water absorption was about 157% after 10 min. Hydroxyapatite promoted moisture retention and increased the sample's ability to absorb water. However, the random arrangement of the fibers limited the full use of this potential, which is why water absorption was lower than in the case of an aligned structure. On the other hand, in the aligned structure, PVDF/nHA_A showed the highest level of water absorption among all the tested samples—about 257% after 10 min. The combination of nHA, AuNPs and the organized structure of the fibers promoted maximization of the contact surface with water, which resulted in significantly better moisture absorption. Such high water absorption capacity could be beneficial in the context of applications in bone/neural tissue engineering, where good moisture retention and stimulation of biological regenerative processes are required [40]. In summary, fiber orientation has a clear effect on the results, with aligned fibers promoting higher water uptake in all samples, suggesting that the topography of the material may be an important factor influencing its hydrophilic properties [41]. The SFE was calculated using the Kaelble-Owens-Wendt method [42]. SFE measurements confirm that the samples with aligned fiber orientation exhibit higher values (see Table 3). More precisely, SFE measured at 35 ± 0.8 mN/m and 45 ± 0.5 mN/m and 38 ± 1.3 mN/m for random PVDF_R and PVDF/nHA_R, and PVDF/AU_R, respectively, compared to 37 ± 0.2 mN/m for aligned PVDF_A, 47 ± 1.1 mN/m for PVDF/nHA_A, and 42.9 ± 1.9 for aligned PVDF/AU_A. The growing order of SFE is PVDF_R > PVDF_A > PVDF/AU_R > PVDF/AU_A > PVDF/nHA_R > PVDFA/nHA_A. In all samples, the dispersive component was higher compared to the polar component and was the main factor influencing the SFE. Moreover, the polar components increased with the addition of nHA and AuNPs, which was more effective in the case of aligned fibers. Thus, the surface polarity (*Xp*) of PVDF/nHA_A was higher and was *Xp* = 0.271 compared to PVDF_A

Xp = 0.156. Low crystallinity and molecular ordering lead to lower surface polarity [43–45], which was observed in the samples with random fiber orientation. The addition of nHA and AuNPs increases the surface polarity in PVDF/nHA_A and PVDF/AU_A samples due to the low polar component γ_s^p of about 8 mN/m and the associated lower WCA [46]. The surface polarity promotes protein adsorption, which has been shown for fibronectin [47]. According to available studies, this ion exchange with the surrounding environment leads to material degradation and the formation of microporosity, which in turn increases the water absorption capacity [48]. Both the material porosity and the fiber porosity resulting from the addition of nHA and AuNPs can have a significant impact on moisture absorption. In summary, the addition of nHA and AuNPs significantly increased the SFE of the samples and their water absorption capacity (see Figure 6), which is crucial for porous biomaterials used in tissue engineering [49–51].

Table 3. SFE, water contact angle (WCA), and their components for all nanofibrous scaffolds.

Sample ID	Water Contact Angle [°]	Dispersive Component [mN/m]	Polar Component [mN/m]	Surface Free Energy [mN/m]	Surface Polarity (*Xp*)	Water Uptake [%]
PVDF_R	133 ± 0.7	32 ± 0.7	3 ± 0.4	35 ± 0.8	0.093	140 ± 5
PVDF_A	120 ± 1.1	32 ± 0.4	5 ± 0.7	37 ± 0.2	0.156	194 ± 3
PVDF/nHA_R	120 ± 2.7	37 ± 0.1	8 ± 0.3	45 ± 0.5	0.216	157 ± 6
PVDF/nHA_A	110 ± 0.7	37 ± 0.6	10 ± 1.2	47 ± 1.1	0.271	257 ± 7
PVDF/AU_R	127 ± 0.5	34 ± 1.2	4 ± 0.6	38 ± 1.3	0.117	150 ± 7
PVDF/AU_A	115 ± 0.4	35 ± 0.9	7± 0.9	42 ± 0.9	0.211	120 ± 6

2.3. Determination of the Crystallinity and the Phase Content

2.3.1. Fourier Transform Infrared Spectroscopy (FTIR)

It is evident from Figure 7A,B that both additives nHA and AuNPs were successfully added to PVDF nanofibrous scaffolds. Figure 7A shows the spectra of PVDF samples with nHA added in random and aligned fiber orientation, as well as the measurement of nHA. In PVDF samples, there are three characteristic peaks, 565 cm^{-1} and 601 cm^{-1}, corresponding to PO_4 bending (ν_4) and PO_4 stretching (ν_1), 962 cm^{-1} corresponding to PO_4 stretching (ν_1) and 1092 cm^{-1} which can be assigned to PO_4 bending (ν_β) [52,53]. This confirms the presence of nHA in the structure of PVDF samples. Figure 7B shows the FTIR spectra of PVDF samples with AuNPs. An observed peak at around 525 cm^{-1} and 612 cm^{-1} is relative to the Au-O stretching vibration [54–56] and confirms the presence of AuNPs in the nanofibrous scaffolds.

Figure 8 exhibits the FTIR spectra of all samples. The bands from α-phase (490, 766, 1402, 1432 cm^{-1}), β-phase (510, 600, 840, 1280 cm^{-1}) and γ-phase (812, 840, 1234 cm^{-1}) are present [57]. Some of the α and β bands are overlapped with the bands coming from the γ-phase, for instance, with the band at 840 cm^{-1}. Multiple phases such as α, β, and γ phases coexist with partially overlapped bands (Figure 8A). Additionally, the peak at 1407 cm^{-1} attributes ν_{as}(CC) and $_{\omega}$(CH_2) modes of vibration because of the electronegativity difference of fluorine atoms in PVDF and the surface charge of AuNPs, and nHA. This interaction of PVDF with nHA minimizes the potential energy of stereochemical conformation and induces β, and γ-phases. These particular characteristics have been observed by slight shifts of FTIR spectra corresponding to piezoelectric phases by the addition of nHA to the PVDF matrix [58,59]. Attention was focused on the spectrum in the range of 760 cm^{-1} to 880 cm^{-1}, where α- and β-phase peaks are illustrated in detail (Figure 8B) [60]. The differences between the heights of these peaks were used to

calculate the piezoelectric phases using Equations (5)–(7). In Figure 8C, peaks of polar β-phases are observed at 3019 and 2980 cm^{-1}. These peaks are due to $\nu_{as}(CH_2)$ and $\nu_s(CH_2)$ vibrational bands. AuNPs and nHA cause the minor shifting towards higher wavelength corresponding to lower energy states. This is evidence for the strong interactions of nHA, AuNPs with PVDF [61].

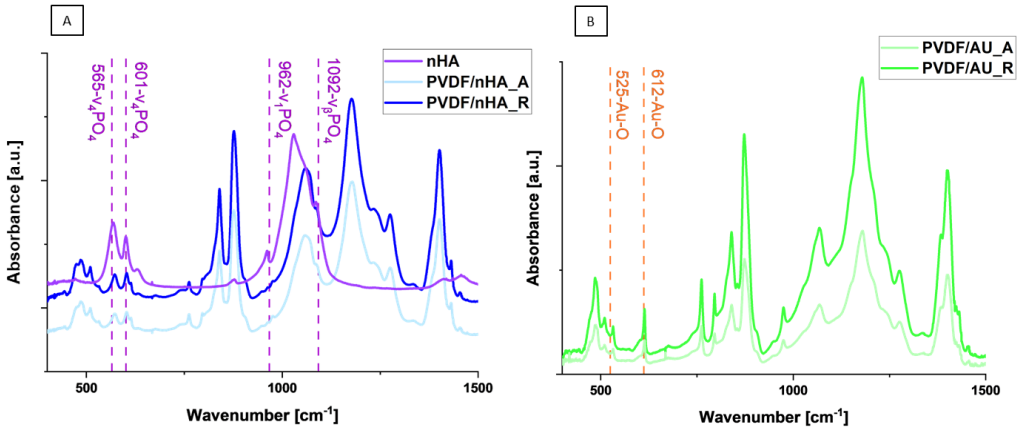

Figure 7. (**A**) FTIR spectra of hydroxyapatite powder and PVDF samples with nHA addition in random and aligned fiber orientation; (**B**) FTIR spectra of AuNPs and PVDF samples with AuNPs addition in random and aligned fiber orientation.

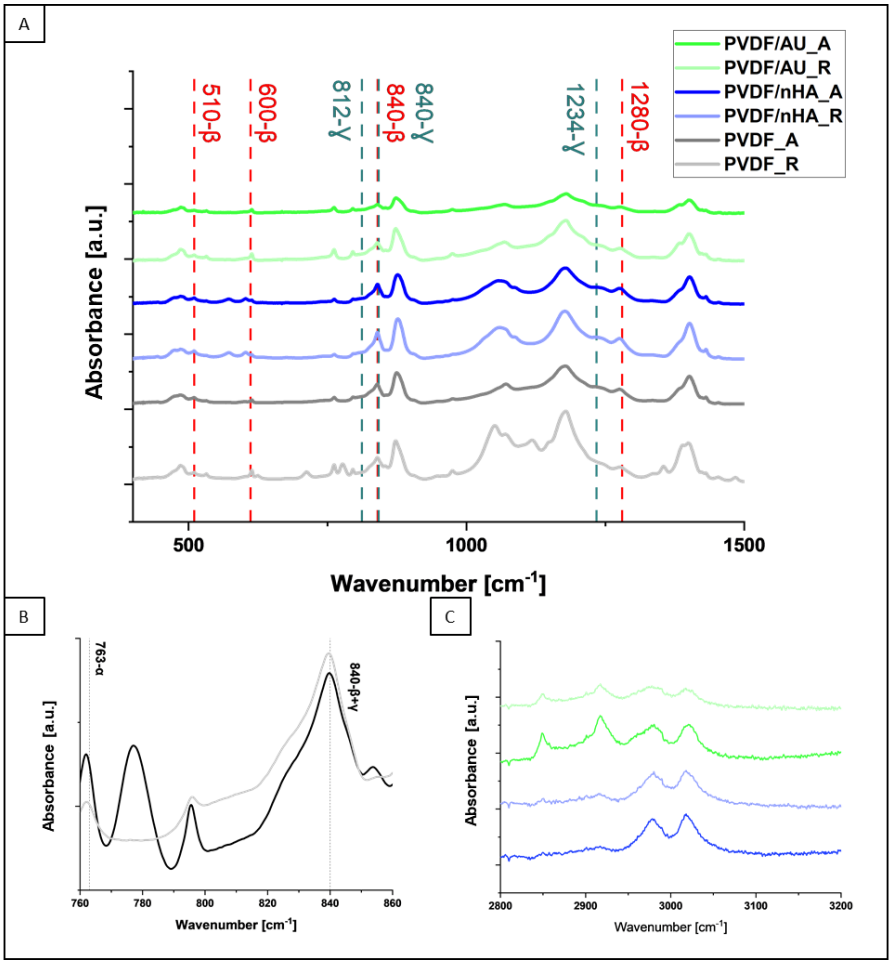

Figure 8. FTIR spectra of PVDF samples with nHA and AuNPs addition in random and aligned samples (**A**) with focus on 760 cm^{-1} to 880 cm^{-1} region (**B**), and 3200 cm^{-1} to 2800 cm^{-1} region (**C**). The graph shows the occurrence of piezoelectric β and γ phases, omitting the bands of non-piezoelectric α phase.

The relative amount of β-phase in each sample was estimated from absorption bands at 840 cm^{-1} and 766 cm^{-1} (corresponding to β and α phases, respectively) using Equations (3)–(5) (Table 4, Figure 9). For pure PVDF scaffolds, it is obvious that the β-phase content is higher for the fibers formed at a collector speed of 2000 rpm than for the fibers formed at a collector speed of 100 rpm. Therefore, it can be concluded that the piezoelectric effect will show higher values for the fibers formed at a collector speed of 2000 rpm. The calculated β + γ phase content for the pure PVDF samples is 55.3 ± 2.4 for PVDF_R and 79.8 ± 0.1 for PVDF_A. These calculations confirm the increased amount of β and γ phases in the sample spun at higher collector speeds similar to our previous results [62]. Moreover, it was observed that the addition of nHA increased the amount of piezoelectric phases, in both, random and aligned piezoelectric scaffolds. The strongest effect was exerted by the addition of nHA, with the piezoelectric phase content of 81.9 ± 0.8 for the PVDF/nHA_A sample (including 0.901 ± 1.1 γ-phase), followed by 81 ± 0.5 (including 0.9003 ± 0.4 γ-phase) for the PVDF/nHA_R sample. The addition of nHA can modify the local PVDF matrix, promoting the formation of an ordered chain structure, which favors the occurrence of the β-phase. According to Islam et al. [63] nHA leads to stabilization of β structure, reducing the tendency of its transformation into non-piezoelectric phases. The decrease in the content of piezoelectric phases in PVDF/AU_R (34 ± 1.9) and PVDF/AU_A (53 ± 7.3) may be due to some heating during the sonication, which could lead to a partial transformation of the β and γ phases into the α phase [64]. This issue needs further studies.

Table 4. Phase content in nanofibrous scaffolds from FTIR.

Sample ID	F(α) (%)	F(β) + F(γ) (%)	F(β) (%)	F(γ) (%)
PVDF_R	44.7 ± 0.3	55.3 ± 2.4	52.3 ± 1.1	3 ± 2.2
PVDF_A	13 ± 0.6	88 ± 0.1	80.8 ± 3.1	7.2 ± 2.3
PVDF/nHA_R	19 ± 1.7	81 ± 0.5	80.997 ± 2.2	0.003 ± 0.4
PVDF/nHA_A	18.1 ± 0.8	81.9 ± 0.8	80.999 ± 0.2	0.901 ± 1.1
PVDF/AU_R	66 ± 0.9	34 ± 1.9	32.97 ± 0.9	1.03 ± 1.3
PVDF/AU_A	47 ± 1.2	53 ± 7.3	50.96 ± 2	2.04 ± 2.6

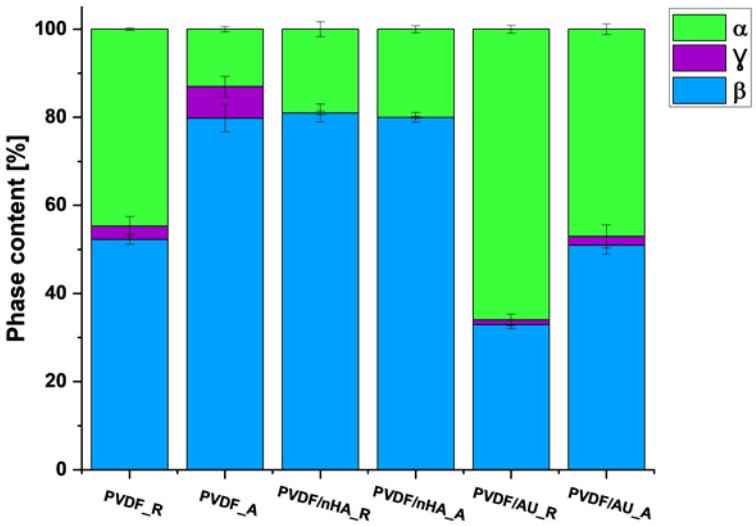

Figure 9. Phase content from FTIR analysis.

Figure 10A demonstrates the relationship between the degree of fiber alignment (expressed as FWHM values), the average fiber diameter, and the piezoelectric phases (β and γ) content. Such a strong increase in the piezoelectric phases content with increasing collector rotation speed, with a simultaneous lower fiber diameter, is associated with an increase in tensile forces, which leads to better alignment and orientation of molecules

in nanofibers [65]. It is known from the literature that the orientation of molecules induced by an external field, such as a mechanical one [66], promotes the formation of piezoelectric phases. Similarly, Figure 10B shows that lower porosity in the samples causes an increase in the amount of piezoelectric phases, with a simultaneous lower average fiber diameter. In materials with lower porosity, a higher compactness of the structure promotes the stabilization of the piezoelectric phases, which have higher piezoelectricity compared to the α phase (non-piezoelectric). The β and γ phases are more stable in more ordered and less porous materials because this limits the migration and deformation of the polymer chains [67].

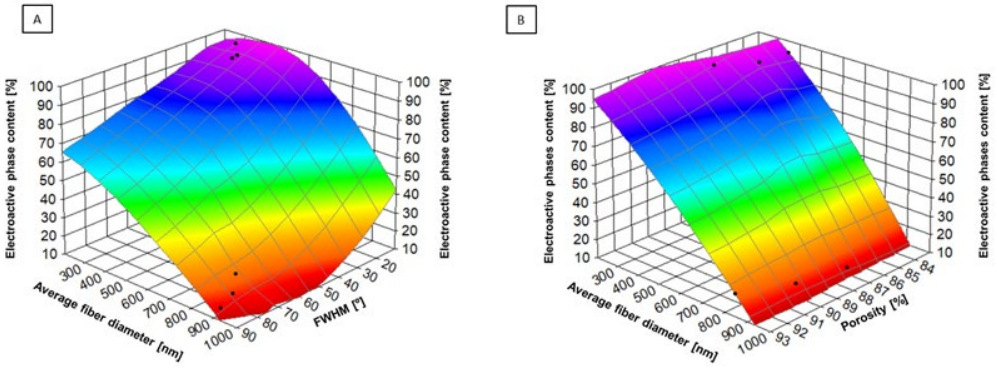

Figure 10. (**A**) The relation between fiber alignment (expressed as FWHM values), average fiber di-ameter, and piezoelectric phases content. (**B**) The relation between average fiber diameter, porosity, and piezoelectric phases con-tent.

2.3.2. Wide Angle X-Ray Scattering (WAXS)

Figure 11 illustrates WAXS profiles for all scaffolds. It is supplemented with the profile registered for PVDF pellets crystalized from melt at 10 K/min for comparison. The *hkl* indices of the α and β crystal planes reflections of PVDF at observed diffraction peaks are provided according to the literature [68], and indicated by extended dark grey and red, respectively, vertical dash-dotted lines for guidance: α100, α020, α110 and α021 for the α phase evidenced at c.a. 17.7°, 18.4°, 20° and 26.6° and β200/110 for the β phase evidenced at c.a. 20.8°. Additionally, the profile registered for pure nHA is shown (without *hkl* indices) with indications of the positions of eight diffraction peaks by vertical blue dash-dotted lines. No reflections for Au in PVDF/Au fibers were noticed in the range studied.

The strongest reflections from the α and β phases: α110 and β200/110 are expected at very similar diffraction angles: 2θ = 20.13° and 20.8°, respectively. Additionally, they are superimposed with a broad amorphous halo, with a maximum expected at c.a. 18–19°. This makes analysis of the profiles registered for the scaffolds quite difficult. However, it is more reasonable to judge the α phase content from the intensity of the diffraction peaks at higher diffraction angles, 2θ > 25°, expected to come from three reflections: the α120, α021 and α111 planes, which are clearly resolved on the profile registered for PVDF pellet crystalized at 10 K/min. The positions of those three diffraction peaks, according to the literature [68], are expected at 2θ = 25.77°, 26.73° and 27.97°, respectively. On the other hand, the profiles registered for the scaffolds show only one broad diffraction peak and based on its position, this peak was assigned to the reflection from the α021 plane. According to the intensity of the α021 peak, it may be judged from Figure 12 that the highest α phase content may be expected in ultrasonicated PVDF/Au random fibers. Furthermore, decreasing content of α phase may be expected in the order: PVDF/Au aligned > PVDF random > PVDF aligned > PVDF/nHA random and aligned.

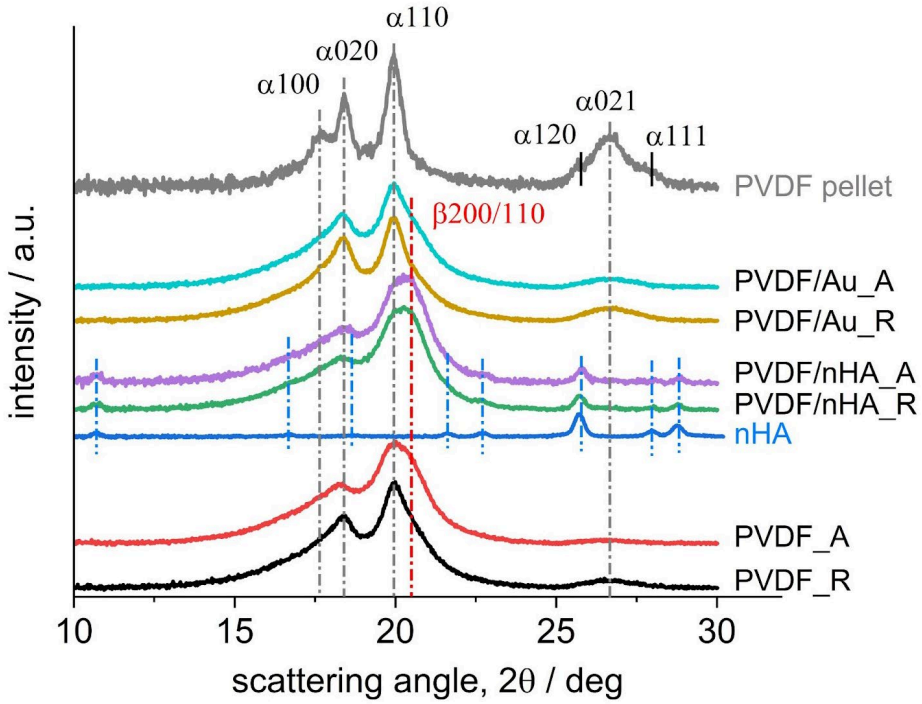

Figure 11. WAXS profiles registered for the scaffolds. Profiles for PVDF pellet melt-crystallized at 10 K/min and for pure nHA, provided for comparison, were used during the peak deconvolution analysis. Profiles registered at room temperature.

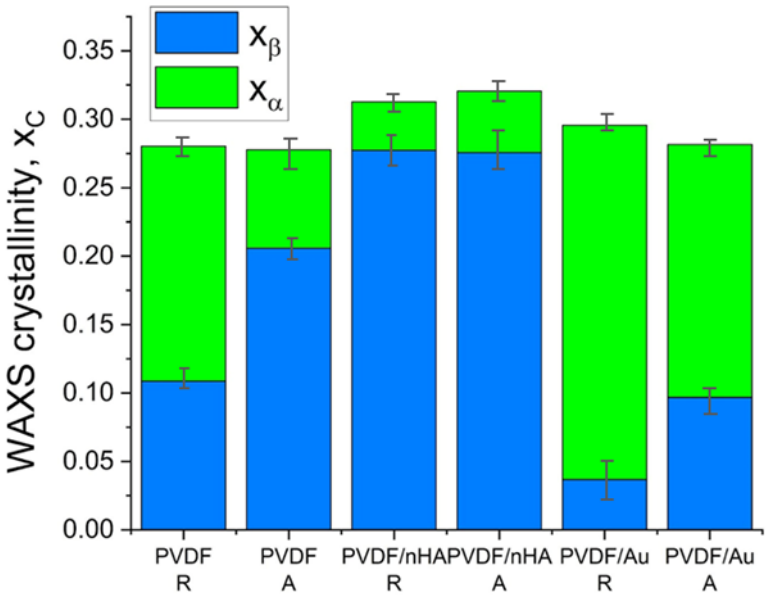

Figure 12. Phases content results obtained from WAXS analysis.

In order to determine the scaffolds' crystallinity and the contents of the α and β phases as well as of nHA, deconvolution of the diffraction peaks was performed by using the non-linear least-square fitting method using Gauss function. It was necessary to start with determination of the interrelations between the intensities of the α phase peaks. For this, the profile registered for PVDF pellet was used, as it shows very high content of the α phase only. Then, according to the data provided in [68], indicating that the structure factors for the α020 reflection are the same for the antipolar and polar forms of the α phase, the α020 peak intensity was taken as the reference. According to our deconvolution results for the PVDF pellet (see Supplementary Materials), the intensity of the strongest α phase reflection, i.e., α110 was assumed as 2.55 times of the α020 intensity. Moreover, according

to the literature [68], the structure factor for the α120 reflection in the polar form of α phase was assumed as equal to zero, while the structure factors for the reflections from the α021 and α111 planes for antipolar and polar α phases were assumed equal. In deconvolution analysis of the scaffolds' profiles, presence of only the α021 reflection was assumed for simplicity, without resolving the α111 reflection.

Figure 12 presents the results of the overall crystallinity and the phase content for the scaffolds. The overall crystallinity was determined as c.a. 30% (see Supplementary Materials for details). It may be seen that addition of nHA strongly increases the β phase content in PVDF from 10 to 27% in random fibers and from 20 to 27% in aligned fibers. On the other hand, ultrasonication leads to increase in the α phase content, from 17 to 25% in the PVDF/Au random fibers and from 7 to 17% in the PVDF/Au aligned fibers. It may also be concluded that higher rotation speed of the collector (aligned fibers) increases the β phase content in PVDF and PVDF/Au fibers but does make no change in PVDF/nHA fibers.

As regards the α and β phase content, the WAXS results generally agree with the FTIR results. It has to be noted that in the diffraction angle range applied in the WAXS methodology, we could not reveal the presence of the γ phase. The indication of the presence of the γ phase was found by DSC method, what is reported in next section.

2.3.3. Differential Scanning Calorimetry (DSC)

Figure 13 shows the DSC scans registered during 1st heating for all the samples. On the curves characteristic features are marked: two endothermic peaks with apparent maxima and one shoulder denoted as P1, P2, and P3, respectively, where the peak P1 appears around 60 °C, the peak P2 around 166 °C and the shoulder P3 around 171 °C. It has to be noted that for samples doped with nHA the peak P2 occurs without the shoulder P3.

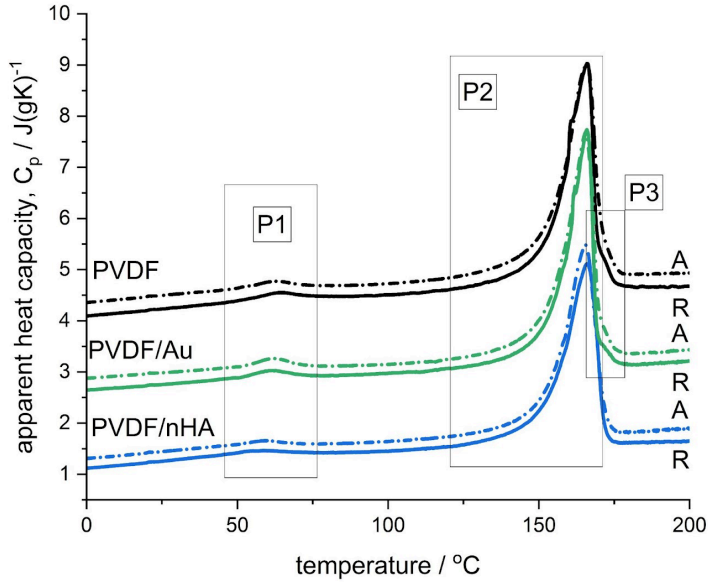

Figure 13. DSC scans registered during the 1st heating shown as the apparent heat capacity. The curves were shifted for clarity.

The peak P1, which is usually detected in PVDF samples after storing at ambient conditions, is attributed to disruption of very defective secondary crystals. The peak temperature range and size was found comparable to the results reported for PVDF samples casted from DMF solution at various temperatures [69] and to the results from the studies on the effect of storage and annealing in PVDF [70].

As regards the high-temperature melting thermal effect consisting of the peaks P2 and P3, observed only in PVDF and PVDF/Au samples, these thermal effects were subjected to a peak deconvolution analysis using Asymetric Double Sigmoid (ADS) function, which resulted in determination of the contribution of each peak (P2 and P3). The temperature position and the melting enthalpy, ΔH, of each peak (P1, P2, P3) are presented in Figure 14. Moreover, the deconvolution analysis examples are provided in the Supplementary Materials, also for PVDF/nHA samples, where approximation of the melting thermal effect was done with a single ADS function.

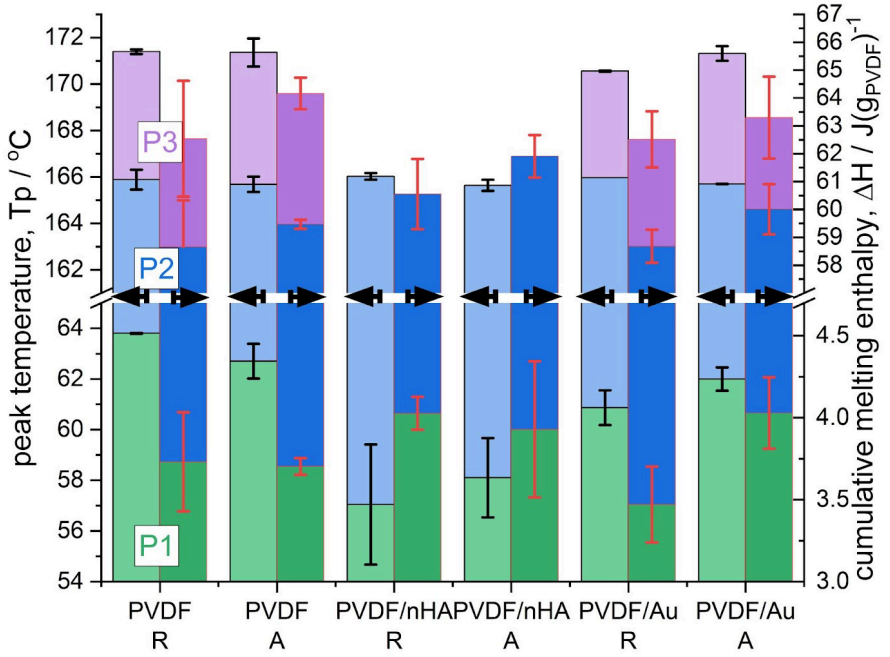

Figure 14. Characteristics of the peaks P1, P2 and P3 determined after deconvolution of the DSC scans (see Figure 13): maximum of the peak temperature, *Tp*, (left axis), and the cumulative melting enthalpies normalized to the PVDF content, ΔH (J/g$_{PVDF}$) (right axis).

Figure 14 shows that the temperature position of the P1 peak, which is attributed to disruption of very defective secondary crystals, depends on the fiber composition or post-processing (sonication). Pure PVDF fibers show the highest temperature positions of the P1 peak, c.a. 64 and 63 °C, for random and aligned fibers, respectively. The lowest temperature positions of the P1 peak are seen for PVDF/nHA fibers, c.a. 57 and 58 °C, for R and A fibers, respectively. For sonicated PVDF/Au fibers, the positions of the P1 peak were found lower than for pure PVDF, at temperatures c.a. 61 and 62 °C, for R and A fibers, respectively.

The temperature position of the P2 peak is seen at c.a. 166 °C for all the samples, while of the P3 peak c.a. 171 °C, observed for PVDF and PVDF/Au fibers only. As revealed by our FTIR and WAXS analysis (see the previous Section 2.3.2) showing always the presence of the α and β phases, the P2 peak was assigned to the simultaneous melting of the α and β crystals. On the other hand, the P3 peak was assigned to the melting of the γ crystals as revealed by our FTIR analysis, which is also supported by data in the literature [71].

For PVDF/nHA fibers the size of the peak P1 was found slightly higher than for pure PVDF, c.a. 4 J/gPVDF, along with the highest size of the peak P2, 57 and 58 J/gPVDF for random and aligned fibers, respectively.

Ultrasonication of PVDF/Au fibers led to slight decrease in the size of the P1 peak for random fibers, from 3.7 to 3.4 J/gPVDF, and to slight increase in the size of the P1 peak for aligned fibers, from 3.7 to 4 J/gPVDF. The size of the P2 was found to increase for

random fibers without a change in the size of the P3 peak. On the other hand, for aligned fibers the size of the P3 peak decreased without a change in the size of the P2 peak. It may be concluded that ultrasonication of aligned fibers led to a slight decrease in γ phase while increasing the amount of very defective secondary crystals, indicated by increase in the size of the P1 peak. For random fibers, ultrasonication led to a slight increase in the α crystals from the very defective secondary crystals, manifested by a decrease in the size of the P1 peak. Both conclusions are supported by our FTIR results (see Section 2.3.1, Table 4 and Figure 9).

Assuming the theoretical value of the equilibrium fusion enthalpy, ΔH^0 = 104.5 J/g [72], crystallinities for the scaffolds were determined as c.a. 60%, which is two-fold higher than the values obtained by WAXS analysis (c.a. 30% in Figure 13). Such a huge discrepancy is highly unexpected and the presumed difference should not exceed a few percent in favor of DSC values. This has been confirmed for PVDF pellet showing 53.5% WAXS and 55.8% DSC crystallinity (see Supplementary Materials). Similarly small differences in crystallinity as determined by WAXS and DSC for various PVDF samples can be found in the literature [73]. Much larger difference between DSC and WAXS crystallinity is usually observed in fibers formed by electrospinning technique (e.g., [74]). Such a difference can be easily explained by the highly defective crystal structure of electrospun fibers, formed during extremely fast solvent evaporation. This structure with relatively low crystallinity is registered by WAXS experiment, contrary to the DSC analysis where crystallinity is deduced from melting of crystals formed both during electrospinning as well as during heating. Taking into account that the structure of electrospun fibers is very far from the thermodynamic equilibrium, the process of additional crystallization/recrystallization is naturally expected during DSC heating, resulting in apparently high crystallinity. The process of growing of small and imperfect crystals during heating is unresolved in the heat flow since it is stretched out on a relatively long time (temperature range). According to the literature [75], for polymer fibers there exists the effect of the crystal melting point depression with decreasing fiber diameter below the bulk melting point. Contrary to this, we found slightly higher melting temperatures, *Tp*, for the fibers than for the pellet (165 °C), which might be another indication of the crystals' growing/perfecting upon heating.

Additional reason of higher melting enthalpies could be related to the fact of using the same value of the equilibrium melting enthalpy (ΔH^0 = 104.5 J/g [72]), irrespectively of the phase content. Assumption of this value for α phase only, and a much higher value, for example $\Delta H^0{}_\beta$ = 219.7 J/g [69] for the β phase, could provide better, however, still limited approximation of the DSC and WAXS results. In such an approach, good approximation was obtained only for the β phase-rich PVDF/nHA fibers but not for the samples with low content of the β phase (pure PVDF and PVDF/Au fibers).

2.4. In Vitro Study on Osteoblasts Human MG-63 Cell Line

Osteoblasts are crucial for ongoing bone remodeling and play a significant role in assessing materials used in bone tissue engineering [76]. In addition to evaluating cellular viability, we investigated the interaction between osteoblasts and nonwoven scaffolds. Cell viability was measured for MG-63 cells cultured on pure PVDF scaffolds, as well as those with nHA and AuNPs additives, with both random and aligned fiber orientations (Figure 15). The in vitro analysis confirmed the non-toxic nature of all PVDF nanofibrous scaffolds, with all samples achieving cell viability levels $\geq$ 70%, meeting the ISO 10993-5 standard [77] for non-toxic materials.

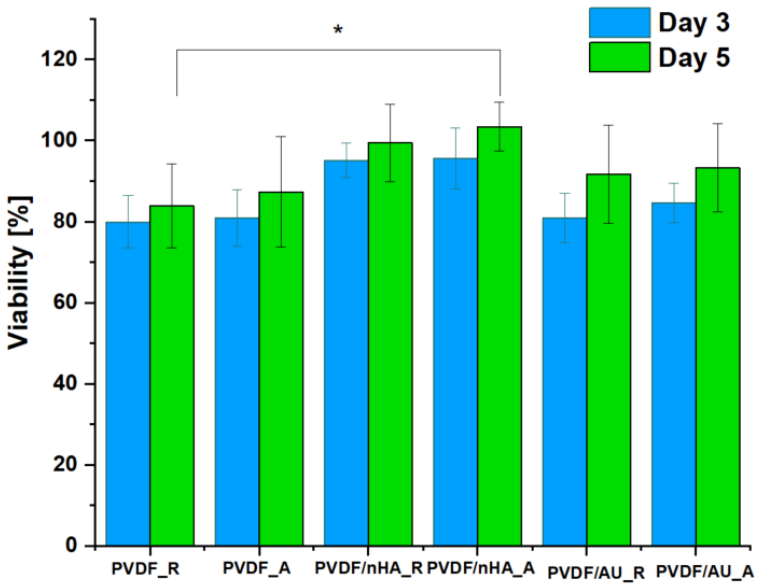

Figure 15. Cell viability of MG-63 cells cultured on pristine and with nHA and AuNPs addition PVDF nanofibrous scaffolds as the rate of TCP (Tissue Culture Plastic, 100%). Statistical significance: * $p < 0.05$.

Experiments on piezoelectric scaffolds made of pure PVDF, PVDF/nHA and PVDF/AU showed interesting relationships between nanofiber orientation, piezoelectric phase content (mainly β phase) and MG-63 cell viability after 5 days of cell culture (Figure 16). The influence of fiber alignment (expressed as FWHM), and piezoelectric phase content on MG-63 cell viability was significant. The highest MG-63 cell viability was observed in the the sample with nHA addition and aligned fiber orientation (lowest FWHM), which were additionally characterized by the highest β phase content. Hydroxyapatite, due to its bioactivity, promoted better bone cell deposition and growth [78]. Moreover, aligned PVDF fibers with high β phase content additionally enhanced biological processes, promoting piezoelectric activity, which in turn stimulated MG-63 cells. The alignment of the fiber with the cell growth direction promoted more organized proliferation and better cell attachment to the scaffold surface. On the contrary, on PVDF_R samples, MG-63 cells showed moderate viability, which can be attributed to the lower β-phase content and less favorable structure for cell adhesion and proliferation. The random fiber orientation limits the mechanical and electrical stimuli that affect the cells. The addition of AuNPs promoted an increase in the piezoelectric phase. AuNPs supported the stabilization of the β-phase through surface interactions, which contributed to the increased piezoelectric phase content. Samples with AuNPs showed better results in terms of cell viability compared to pure PVDF, regardless of the fiber orientation. Both AuNPs and nHA could act as an additional factor supporting cell adhesion and proliferation by improving the electrical conductivity and supporting the piezoelectric properties of PVDF. In the case of aligned samples, cell growth was even more noticeable, indicating the synergistic effect of fiber orientation and additives.

In summary, there is a relationships between nanofiber orientation (expressed as FWHM), piezoelectric phase content, and MG-63 cell viability (Figure 16). Oriented fibers (lower FWHM) favor higher β-phase content, which in turn improves MG-63 cell viability and proliferation. Modification of PVDF with gold or hydroxyapatite further enhances these effects, making such materials more suitable for bone tissue engineering applications. However, this issue is very complex and requires more detailed research. Analysis of these relationships allows for a better understanding of the influence of the structure and surface modification of materials on their bioactivity and application potential in bone tissue engineering [79].

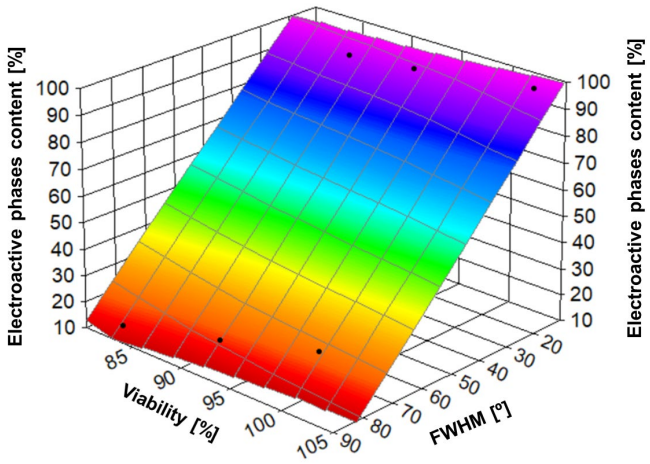

Figure 16. The relation between porosity, piezoelectric phase content, and MG-63 viability after day 5.

Cell proliferation and attachment are critical for tissue regeneration, representing the early stages of the process [80]. To further evaluate this, cellular morphology was assessed. After 3 and 5 days of culture on pure PVDF scaffolds, PVDF/nHA, and PVDF/AuNPs, immunostained cells were analyzed using fluorescence microscopy (Figures 17 and 18). The morphology and spreading of osteoblasts on the scaffold surfaces closely resembled those on tissue culture plastic (TCP), corresponding with good cell viability. The cells exhibited a well-spread morphology and strong intercellular connections. Effective interaction between osteoblasts and the nonwoven scaffolds was confirmed by the elongation and spreading of the cells, which was especially pronounced on PVDF_A, PVDF/nHA_A and PVDF/Au_A composite nanofibers. Fluorescence microscopy images clearly show different cell growth patterns depending on the nanofiber orientation-cell elongation due to contact guidance is seen on aligned nonwovens. The cells tended to elongate in the direction of the fiber orientation, suggesting that PVDF nanofibers affect the direction of osteoblast migration and proliferation. This behavior may be due to the mechanical interaction of the piezoelectric properties of PVDF, which can generate electric charges, thus promoting cell elongation along the fibers. These effect was observed previously on nonvowens formed from PCL [81], PMMA [44] etc. In the case of scaffolds with a random nanofiber structure, osteoblast cells showed a more dispersed morphology, which is characteristic of an irregularly arranged surface.

Previous research has highlighted the importance of incorporating nanoscale components like nHA and AuNPs into scaffolds to enhance cell proliferation [82,83]. The improved adhesion and proliferation observed on PVDF/nHA and PVDF/Au fibers are likely due to the inclusion of nHA and AuNPs, which contribute to reduced porosity (Table 1) and hydrophobicity (Table 3). In vitro studies support the conclusion that PVDF/nHA and PVDF/Au nanofibrous scaffolds demonstrate increased bioactivity and hold significant potential for promoting bone formation.

2.5. In Vitro Study on Human Induced Pluripotent Stem Cell-Derived Neural Stem Cell Culture (hiPSC-NSC)

In vitro preliminary experiments using Human Induced Pluripotent Stem Cell-Derived Neural Stem Cell (hiPSC-NSC), were conducted to evaluate cell differentiation and behavior on electrospun nanofibrous mats made from pure PVDF and PVDF doped with nHA, with fibers oriented in both random and aligned configurations (Figure 19). These nanofibers served as scaffolds, supporting the growth of iPSC-derived neural stem cells. YAP/TAZ staining used to visualize mechanosensitive molecules that shuttle between the nucleus and cytoplasm in response to environmental conditions was mainly observed throughout the cells, similar to what is typically seen on soft hydrogels or 3D scaffolds. Cells at the surface of the nanofibers

differentiated into neurons, displaying long, interconnected projections (as indicated by beta-tubulin III staining). A slight effect of fiber orientation on cell alignment was observed. This may be attributable to an additional extracellular matrix (ECM) protein coating applied to the nanofibrous mats, which is necessary for adequate cell adhesion. In aligned samples, higher directional differentiation of neuronal cells can be observed compared to random orientation. However, whether aligned fibers better support the formation of neuronal networks and axonal growth compared to random scaffolds requires more detailed studies.

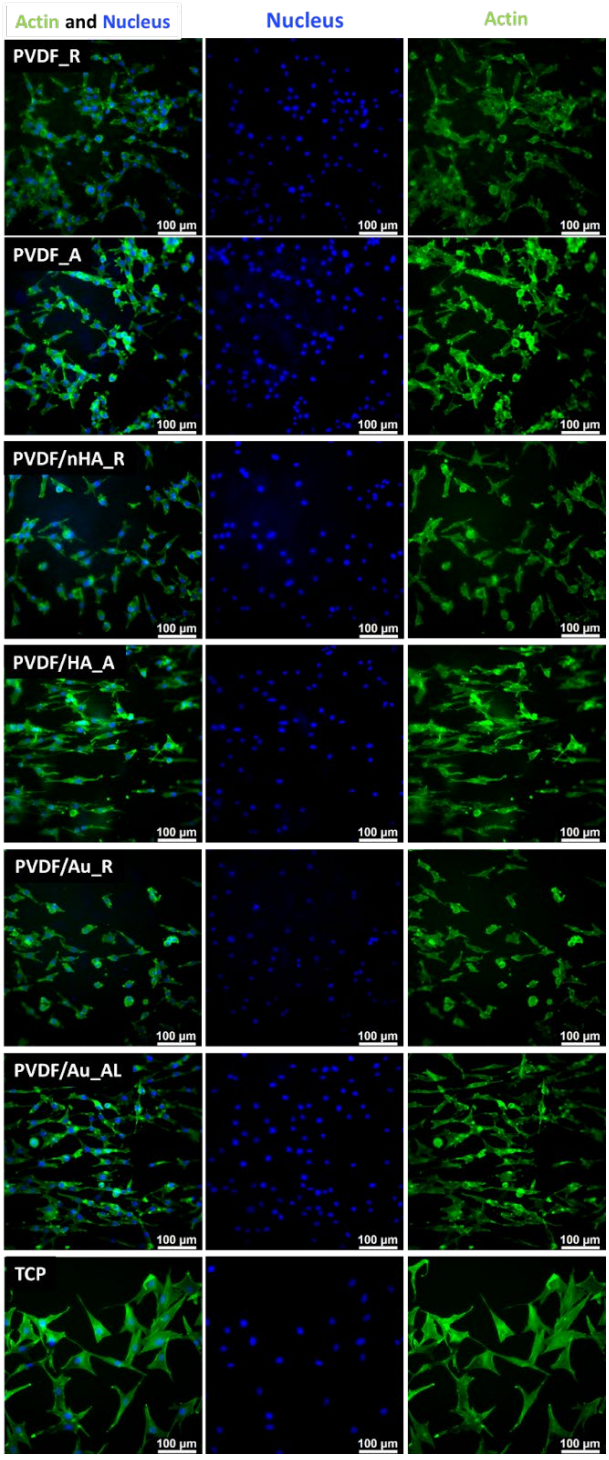

Figure 17. FM images of stained MG-63 directly cultured on the specimen substrate for 3 days. Samples PVDF_R, PVDF_A, PVDF/nHA_R, PVDF/nHA_A, PVDF/AU_R and PVDF/AU_A in comparison to TCP.

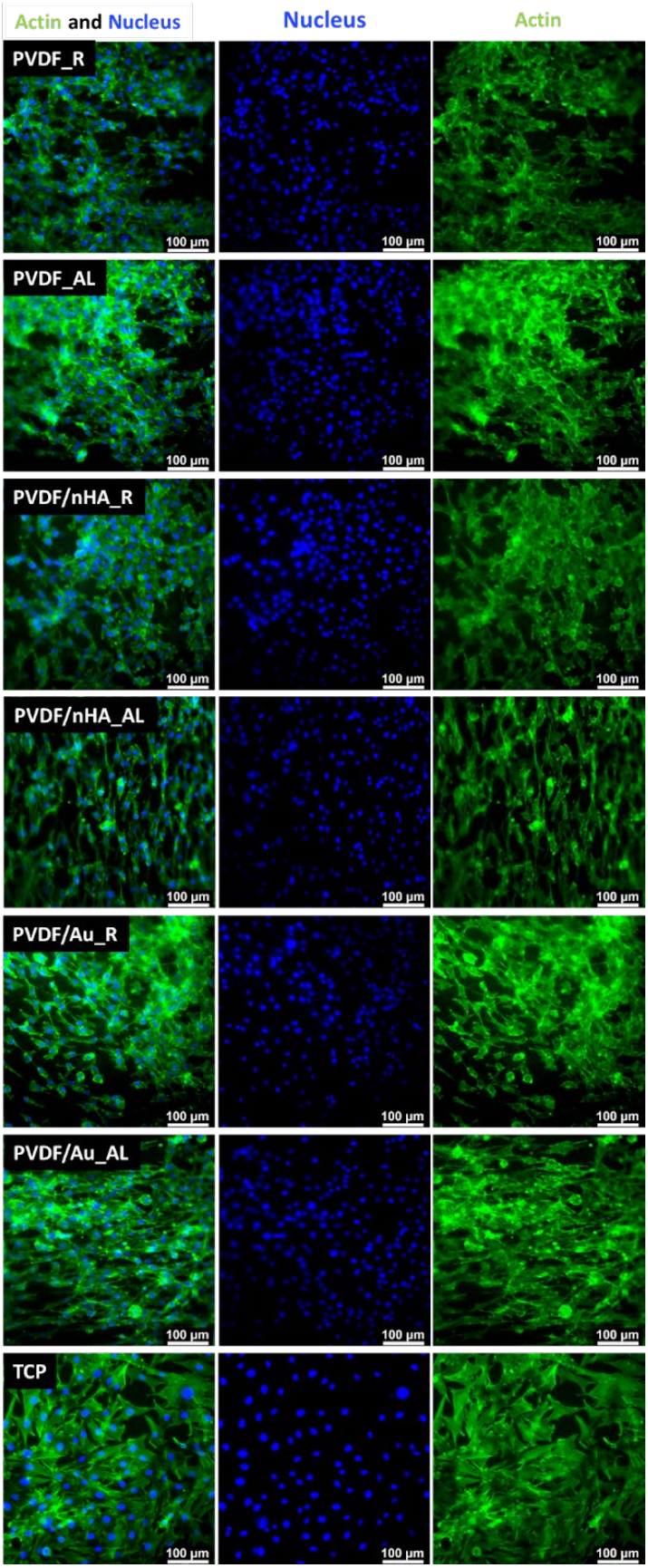

Figure 18. FM images of stained MG-63 directly cultured on the specimen substrate for 5 days. Samples PVDF_R, PVDF_A, PVDF/nHA_R, PVDF/nHA_A, PVDF/AU_R and PVDF/AU_A in comparison to TCP.

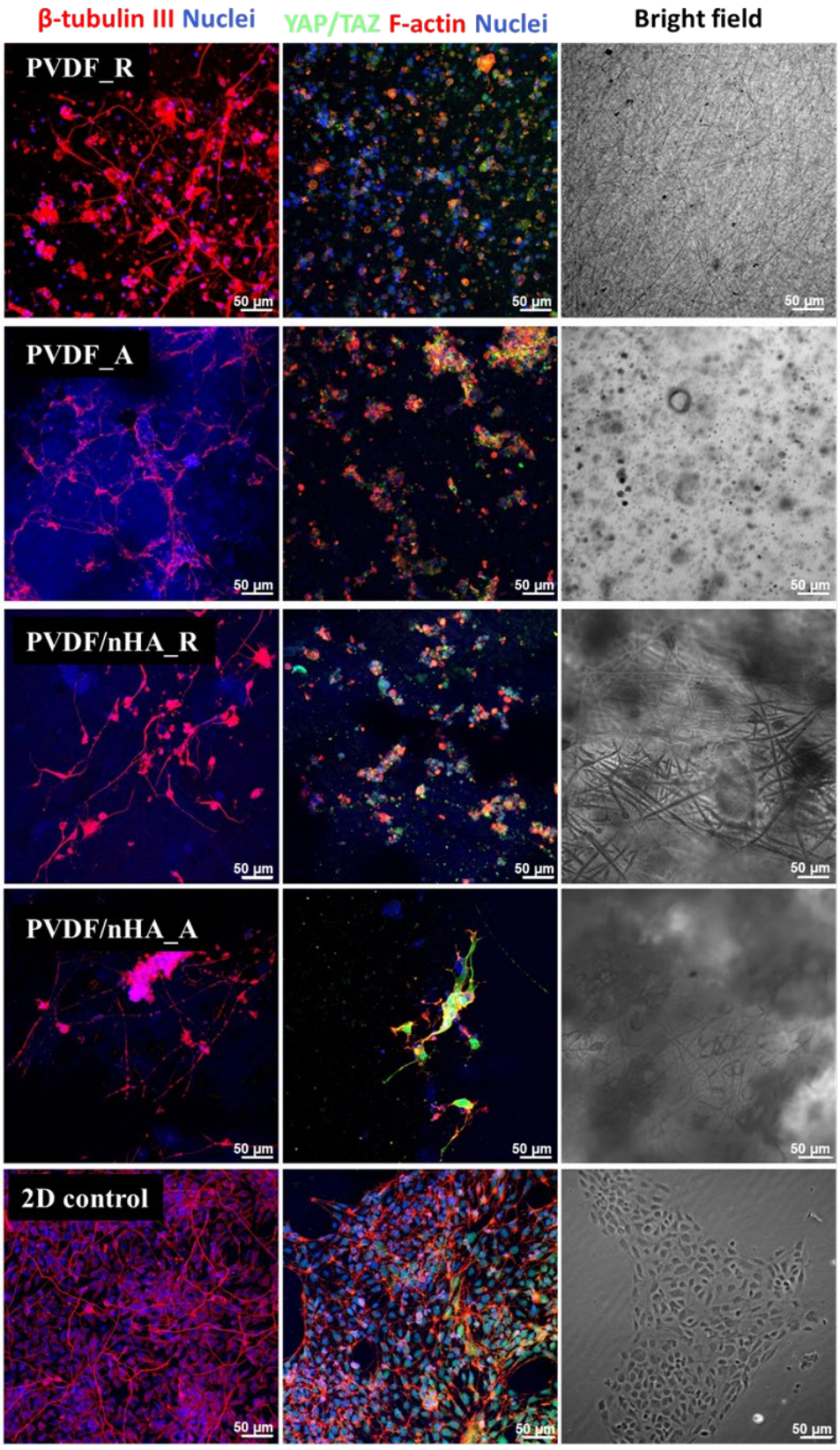

Figure 19. Immunocytochemical analysis of hiPSC-derived NSC cultured for 5 days on the PVDF scaffolds. After 5 days of culture, cells were stained for a neuronal marker (β-tubulin III, red) or mechanotransduction mediating factors YAP/TAZ (green) together with f-actin staining (Alexa546-conjugated Phalloidin, red). Extracellular matrix-coated (diluted geltrex) glass coverslips served as 2D control. Cell nuclei are contra-stained with Hoechst (blue).

3. Experimental Part

3.1. Materials and Methods

Poly(vinylidene fluoride) (PVDF) with a molecular weight of Mw = 530,000 g/mol was purchased from Sigma-Aldrich, Steinheim, Germany. Hydroxyapatite (nHA) nanopowder, with particles smaller than 200 nm, was also obtained from Sigma-Aldrich, Germany, as well as dimethylformamide (DMF) and acetone. A solution of citrate-stabilized gold nanoparticles (AuNPs, 40 nm in size, 99.99% purity, optical density of 8.7) was obtained from Nano Flow, Liège, Belgium. Reagents used were of analytical grade.

Reagents for in vitro tests on osteoblasts, such as amino acids, L-glutamine, fetal bovine serum (FBS), and antibiotics (penicillin/streptomycin), were purchased from Sigma Aldrich (Gillingham, UK). Phosphate-buffered saline (PBS), Presto Blue, Trypsin EDTA, Dulbecco's Modified Eagle Medium, ActinGreen, and NucBlue were purchased from Thermo Fisher Scientific (Waltham, MA, USA). The human osteoblast cell line MG-63 was also purchased from Sigma-Aldrich (86051601, London, UK).

Reagents for in vitro tests on hiPSC-NSC (Thermo Fisher Scientific, USA), such as, Essential 8 Medium, Vitronectin (VTN-N) Recombinant Human Protein, Truncated, UltraPure™ 0.5 M EDTA, pH 8.0, Geltrex™ LDEV-Free hESC-qualified Reduced Growth Factor Basement Membrane Matrix, Neurobasal™ Medium, Gibco™ PSC Neural Induction Medium, Advanced DMEM, Goat serum, Alexa Fluor™ 546 Phalloidin, Alexa Fluor™ 546 goat anti mouse IgG2aAlexa Fluor™ 488 goat anti rabbit H + L were purchased from Thermo Fisher Scientific (USA). Dulbecco's Phosphate Buffered Saline, Modified, without calcium chloride and magnesium chloride, Accutase® solution, PFA, Triton X-100, Anti-β-Tubulin III (neuronal) antibody, Hoechst 33258, Mouse monoclonal were purchased from Sigma-Aldrich (UK). Rabbit polyclonal anti YAP/TAZ antibody was purchased from Cell Signaling Technology, Danvers, MA, USA, and Fluorescent Mounting Medium was purchased from Dako, Santa Clara, CA, USA.

3.2. Preparation of PVDF/nHA Solution and Scaffold Fabrication via Electrospinning Technique and Sonochemical Coating

PVDF pellets were dissolved in DMF/acetone (4:1 ratio) at 60 °C for 6 h. For pure PVDF 20 wt.% of PVDF solutions were prepared. For samples with nHA addition, an appropriate amount of nHA nanoparticles was added to obtain 10 (*w*/*v*%) solution and stirrer for 2 h. To avoid nHA aggregation, the solutions were sonificated for 30 min (ultrasonic cleaner EMAG, EMMI-D60, Salach, Germany).

All the PVDF solutions were loaded into a 5 mL syringe and placed into a Bioinicia horizontal setup (Fluidnatek LE-50, Bioinicia, Valencia, Spain). Based on previous studies [62,84], the process parameters leading to the formation of the higher amount of piezoelectric phases in samples were selected. A 23 G needle was used with an inner diameter of 0.337 mm. A flow rate during process was 0.8 mL/h. The distance between the collector and the needle was 190 mm. The fibers were collected on a rotating drum collector rotating at 100 (to obtain random fibers), and 2000 rpm (to obtain aligned fibers). The process was carried out at the temperature range of 21 °C and humidity of 25%. The positive voltage applied to the needle was 22 kV, and the collector electric potential was −2 kV. After electrospinning, all materials were placed under a fume hood for 48 h in order to evaporate the solvent. The pure PVDF samples were marked as PVDF_R for random and PVDF_A for aligned fiber orientation of the sample. Also, samples with addition of nHA were marked PVDF/nHA_R for random fiber orientation and PVDF/nHA_A for aligned fiber orientation in the sample. For samples with AuNPs, the sonochemical coating was used according previously developed method [85]. The ultrasonic treatment of pure PVDF samples with gold (AuNPs) nanoparticles was carried out in a citric acid bath containing

the Au component. Ultrasonic fiber functionalization was achieved with an efficiency of 80% using a pulse cycle on a Hielscher UP200Ht device (Teltow, Germany). The coating process took place at specific time intervals (2 × 2 min). Then, the samples were thoroughly rinsed with water and dried. These samples were marked as PVDF/Au_R for random and PVDF/Au_A for aligned fiber orientation with AuNPs addition.

3.3. Characterization of Piezoelectric Nanofibrous Composites

3.3.1. Morphology Analysis

The morphological analysis of piezoelectric scaffolds was performed using Scanning Electron Microscopy imaging (SEM, JSM-6010PLUS/LV InTouchScope™, JEOL, Tokyo, Japan), operated at an accelerating voltage of 11 kV. Before imaging, each nonwoven sample was double-coated with a thin layer of gold (2–3 nm). After imaging, analysis of microstructures was conducted using ImageJ software (1.52q software version, Washington, DC, USA). Fiber diameter distribution was determined by applying a Gaussian approximation, with 100 measurements taken for each sample.

The alignment of the fibers analyzed using ImageJ software with the directionality plugin was quantified by calculating the full-width at half maximum (FWHM) of the Gaussian function used to approximate the orientation distribution. FWHM values were averaged across six images for each sample.

Analysis of the fiber orientation in all specimens was determined using the anisotropy index α, ranging between 1 for the ideal alignment of fibers and 0 for the random distribution of fibers (Equations (1) and (2)) [86,87].

$$\Omega = \frac{1}{I_{tot}} \sum I_i \begin{vmatrix} cos^2\theta_i & sin\theta_i cos\theta_i \\ sin\theta_i cos\theta_i & sin^2\theta_i \end{vmatrix} \quad (1)$$

$$\alpha = 1 - \lambda_1/\lambda_2 \quad (2)$$

More precisely, Ω is a matrix with λ_1 and λ_2 values, I_{tot}—the sum of individual nanofiber lengths (nm), I_i—the length of the nanofiber (nm), θ_i—the angle between the x-axis and the axis of the nanofiber oriented perpendicular to the collector axis.

Porosity (p) was determined from Equation (3) [88]:

$$p = \frac{V_t - V_f}{V_t} = \left(1 - V_f \times \frac{\rho}{m_t}\right) = (1 - \frac{m_f}{m_t}) \quad (3)$$

where, V_f is the volume of the tested sample, mf is the mass of the tested sample, m_t is the theoretical mass of the solid sample as the product of the PVDF density (1.75 g/cm^3 [89]) and the volume V_t.

Pore size (P) was estimated from Equation (4) [88]:

$$P = \frac{2D}{(1-p)} \quad (4)$$

where, D is the mean fibers diameter in each specimen, $(1 - p)$ is the area of fibers per unit and p is the porosity.

The presence of nHA and AuNPs was confirmed through Energy Dispersive X-ray Spectroscopy (EDS) (JSM-6010PLUS/LV InTouchScope™, JEOL, Tokyo, Japan). Samples were measured with the following parameters: working distance (WD) = 10 mm, accelerating voltage of 8 kV, probe current of 500 pA, and a collecting time of 30 min.

3.3.2. Water Uptake, Water Contact Angle Measurements and Surface Free Energy Determination

Piezoelectric samples was divided into a 2 × 1 cm rectangle and immersed in demineralized water every 60 s for 10 min and weighed (XA 52.R2 analytical balance, Radwag, Radom, Poland).

The water uptake capacity of the samples was determined using Equation (5) [90].

$$\%\ Water\ uptake = 100 \times \frac{W_{wet} - W_o}{W_o} \quad (5)$$

where, W_o and W_{wet} is the weight of dry and wet samples, respectively.

The wettability of nanofibrous scaffolds was tested using the Data Physics OCA 15EC contact angle goniometer (Filderstadt, Germany). A drop of liquid (volume 2 µL) was deposited on the surface of the nanofibrous scaffolds. The contact angle was calculated after 3 s at 21 °C.

Surface Free Energy (SFE) was calculated using the Kaelble-Owens-Wendt method. This method assumes that SFE is the sum of two main independent components related to polar and dispersion interactions. Three liquids were used to evaluate SFE-water, highly dispersible diiodomethane, and formamide, as described [87] (Equations (6) and (7)).

$$\left(\gamma_s^d\right)^{0.5} = \frac{\gamma_d(cos\theta_d + 1) - \sqrt{\left(\frac{\gamma_d^p}{\gamma_w^p}\right)}\gamma_w(cos\theta_w + 1)}{2\left(\sqrt{\gamma_d^d} - \sqrt{\gamma_d^p - \left(\frac{\gamma_w^p}{\gamma_w^p}\right)}\right)} \quad (6)$$

$$\left(\gamma_s^p\right)^{0.5} = \frac{\gamma_w(cos\theta_w + 1) - 2\sqrt{\gamma_s^d\gamma_w^d}}{2\sqrt{\gamma_w^p}} \quad (7)$$

where, γ_s^d—dispersion component of SFE, γ_s^p—polar component, γ_d—SFE of diiodomethane; γ_d^d—dispersive component of diiodomethane, γ_d^p—polar element of diiodomethane, γ_w—SFE of water; γ_w^d—the dispersive element of water, γ_w^p—polar element of water; θ_d and θ_w contact angle of diiodomethane and water, respectively.

Surface polarity (Xp) was determined using the Wu's method (Equation (8)) [91]:

$$X_p = \frac{\gamma_s^p}{\gamma_s} \quad (8)$$

3.3.3. Determination of the Crystallinity and the Phase Content Fourier Transform Infrared Spectroscopy (FTIR)

Molecular structure analysis, determination of piezoelectric phase content and presence of nHA and AuNPs was conducted using Fourier Transform Infrared Spectroscopy with ATR technique (Bruker Vertex 70, Mannheim, Germany). The results are data from measurements of five samples. Investigations of the nanofibrous scaffolds was provided in the range of 400 cm^{-1} to 4000 cm^{-1} with a resolution of 2 cm^{-1} and a total of 32 scans.

The amount of piezoelectric phases (F_{EA}), β and γ, was calculated from Equation (9) [36,92]:

$$F_{EA} = \frac{I_{840*}}{\left(\frac{K_{840*}}{K_{763}}\right) \times I_{763} + I_{840*}} \times 100\% \quad (9)$$

where, intensities from bands 763 cm^{-1} and 837–841 cm^{-1} were calculated. According to the Beer-Lamber law, absorption coefficients K_{840} and K_{763} are 7.7 × 10^4 cm^2 mol^{-1} and

6.1 × 10, respectively. Absorbance from bands 1234 cm^{-1} and 1275 cm^{-1} was used to calculate the β-phase (F(β)) and γ-phase (F(γ)) [36,92].

$$F(\beta) = F_{EA} \times \left(\frac{\Delta H_{\beta'}}{\Delta H_{\beta'} + \Delta H_{\gamma'}} \right) \times 100\% \quad (10)$$

$$F(\gamma) = F_{EA} \times \left(\frac{\Delta H_{\gamma'}}{\Delta H_{\beta'} + \Delta H_{\gamma'}} \right) \times 100\% \quad (11)$$

where $\Delta H\beta'$ is the absorbance difference between the peaks (1275 cm^{-1} and 1260 cm^{-1}), whereas $\Delta H\gamma'$ is the peak 1234 cm^{-1} and the nearest valley, around 1225 cm^{-1}.

Wide Angle X-Ray Scattering (WAXS)

Bruker D8 Discover diffractometer (Manheim, Germany) was used. Coupled theta-2theta geometry with divergent beam optic (1 mm slit) was used in reflective mode with Cu lamp X-ray source (power was set to nominal 1600 W). Scans were done at 10–30 deg. 2theta angular range, with 1 s signal record time per step (0.02°. increment step size).

The WAXS profiles were analysed using the non-linear least-square fitting method with the Gauss function resulting to deconvolution of the diffraction peaks, enabling determination of the overall crystallinity, X_C, and the α and β phase contents, X_α and X_β as:

$$X_c = \frac{\sum I_i}{I_{tot}},\ X_\alpha = \frac{\sum I_{i\alpha}}{I_{tot}},\ X_\beta = \frac{\sum I_{i\beta}}{I_{tot}} \quad (12)$$

where I_i represents integral intensity of an *i*-th diffraction peak, $I_{i\alpha}$ and $I_{i\beta}$ are the intensities of the α or β phase diffraction peaks, respectively, and I_{tot} represents the total integral intensity of the registered WAXS profile.

Differential Scanning Calorimetry (DSC)

Thermal analysis of PVDF scaffolds was performed using a Differential Scanning Calorimeter (DSC, Pyris 1, Perkin Elmer, Waltham, MA, USA) equipped with Intracooler 2P under nitrogen atmosphere. Oriented and random fibrous samples (7–10 mg) as well as a pellet sample for comparison were loaded into standard aluminum pans.

Thermal analysis consisted of determination of the melting temperatures and enthalpies as well as calculation of the crystallinity after a deconvolution analysis of the melting endotherms using Asymmetric Double Sigmoid (ADS) function.

3.3.4. In Vitro Study on Human Osteoblasts MG-63 Cell Line

In vitro research was evaluated using the human MG-63 cell line. The cells were grown in 25 cm^2 flasks containing medium made from 10% fetal bovine serum (FBS), High-Glucose Dulbecco's Modified Eagle's Medium (DMEM), 1% glutamine and antibiotics. Incubation was carried out at 37 °C in an atmosphere containing 5% CO_2. To detach the cells, the flask was rinsed with PBS, followed by the addition of 3 mL of a 0.05% trypsin solution. The flask was then returned to the incubator for a few minutes. After cell detachment, 10 mL of fresh culture medium was added, and the suspension was centrifuged at room temperature. The resulting pellet was re-suspended in culture medium to obtain the desired cell density. Several experiments were performed to evaluate the cellular response to monolithic nanofibers, including cytotoxicity tests using extracts and analysis of cellular morphology.

To evaluate cellular viability, MG-63 cells were seeded onto the test samples and Tissue Culture Plate (TCP) at a density of 1 × 10^4 cells per well, followed by incubation. On days 3 and 5, the culture medium was carefully removed, and each well was filled with

180 µL of PBS and 20 µL of Presto Blue reagent. The plate was then incubated for 60 min. Fluorescence readings were obtained using excitation/emission filters of 530/620 nm with a Fluorescent Accent FL device from Thermo Fisher Scientific. The results were analyzed by comparing the Presto Blue fluorescence of blank samples, which served as a baseline for no metabolic activity, and the control (TCP), which represented 100% cell viability.

Fluorescence microscopy was used to examine the morphology of osteoblasts in direct contact with the material. MG-63 cells were cultured on electrospun membranes, and after 3 and 6 days of incubation, the cells were fixed using 3% formaldehyde for 20 min. To permeabilize the cell membranes, the fixed cells were treated with 0.01% Triton X-100 for 5 min. Subsequently, the cellular nuclei and cytoskeleton were stained for 30 min using a solution containing ActinGreen and NucBlue, which specifically bind to the cytoskeleton and nuclear DNA, respectively. Microscopic images were acquired using a Leica AM TIRF MC microscope (Wetzlar, Germany).

3.3.5. In Vitro Study on Human Induced Pluripotent Stem Cell-Derived Neural Stem Cell Culture (hiPSC-NSC)

Neural stem cells were derived from a human induced pluripotent stem cell (hiPSC) line following the protocol described by Buzanska et al. [93], with some modifications. Briefly, cells from a human episomal iPSC line (Gibco, Thermo Fisher Scientific) were routinely cultured on vitronectin-coated culture dishes in Essential 8 Medium (Thermo Fisher Scientific). For neural induction, the cells were washed in PBS without calcium and magnesium (PBS−/−) and passaged using EDTA. The cells were then transferred to Geltrex-coated (Thermo Fisher Scientific) culture vessels in Essential 8 Medium. After 24 h, the medium was replaced with PSC Neural Induction Medium (Thermo Fisher Scientific), and the cells were cultured for up to 7 days, with daily medium changes. On day 7 of neural induction, the confluent cultures were washed with PBS−/− and passaged using Accutase into new Geltrex-coated (1:100 in Neurobasal Medium) 6-well plates at a density of 1×10^5 cells/cm^2 in neural expansion medium (a 1:1 mixture of PSC Neural Induction Medium and Advanced DMEM, Thermo Fisher Scientific). The cells were maintained under these conditions and passaged weekly. Cells from passage 6 were used for further experiments.

Cell Culture on Biomaterials and Immunofluorescent Staining

To culture hiPSC-NSCs on biomaterials, PVDF scaffolds were sterilized by exposure to UV light for 30 min on each side, then rinsed with 70% ethanol, washed three times with PBS for 10 min each, and incubated with a Geltrex solution (1:100 in Neurobasal Medium) for 1 h at 37 °C. The hiPSC-NSCs were seeded onto the PVDF scaffolds at a density of 1×10^5 cells/cm^2 in neural expansion medium. An uncoated scaffold was used to assess the adhesion of the neural stem cells directly to the PVDF biomaterial. The next day, the scaffolds were transferred to a new culture dish and cultured for up to 7 days. On day 7, the cells on the PVDF scaffolds were washed with PBS, fixed with 4% paraformaldehyde (PFA), washed again with PBS, and permeabilized with 0.5% Triton X-100 for 15 min. After removing the permeabilization solution, the samples were blocked with 10% goat serum for 1 h at room temperature. The cells were then incubated overnight at 4 °C with the following primary antibodies: monoclonal mouse anti-neuronal beta III tubulin (1:1000, Sigma-Aldrich), polyclonal rabbit anti-YAP/TAZ (1:500, Stem Cell Signaling), and Alexa-546-conjugated Phalloidin (1:500, Thermo Fisher Scientific). The next day, after washing with PBS, the samples were incubated for 1 h at room temperature with the appropriate secondary antibodies: Alexa-546 goat anti-mouse IgG2a and Alexa-488 goat anti-rabbit polyclonal antibody (both 1:500, Thermo Fisher Scientific). After washing with PBS, the samples were counterstained with Hoechst (1:100, Sigma) for 15 min to visualize the

nuclei. Following a final PBS wash, the samples were mounted in fluorescent mounting medium (Dako, Glostrup, Denmark) and imaged using a confocal microscope (LSM510, Zeiss, Oberkochen, Germany) at the Laboratory of Advanced Microscopy Techniques, Mossakowski Medical Research Institute, PAS.

3.4. Statistical Analysis

All results were analyzed to determine statistical significance. Viability results were evaluated using GraphPad Prism 8.0.1 software, applying a threshold of $p < 0.05$. As needed, a two-way ANOVA followed by Tukey's multiple comparisons test was performed. Statistical significance was assessed based on *p*-values, with values below 0.05 considered significant. *p*-values in the range of 0.01 to 0.05 were marked with an asterisk ("*") to indicate significance.

4. Conclusions

It was presented that higher collector rotational speed or nHA addition to PVDF electrospun fibers increases not only the fibers' alignement but also promotes formation of the piezoelectric phases. The β phase content was found the highest in PVDF/nHA fibers, being 80–90% of the total crystallinity and was found independent on the collector rotational speed. The lowest β phase content was determined for ultrasonicated PVDF/Au random fibers, being 12–33% of the total crystallinity. For pure PVDF and ultrasonicated PVDF/Au fibers, higher β phase content was observed for higher collector rotational speed. Additionally, low content of the γ phase in pure and with AuNPs addition, being 3–7% of the total crystallinity, was found in FTIR analysis and confirmed using DSC analysis as a small high temperature melting peak. Moreover, addition of nHA or coating of the fibers with AuNPs improved scaffolds' surface properties (SFE) and water absorption.

According to WAXS analysis, the fibers were c.a. 30% crystalline, only, which is much lower than the crystallinity of a pellet (c.a. 53%). During DSC heating, high metastability of electrospun structure led to intense growth of the defective small crystals resulting in twice higher melting enthalpy and slightly higher melting temperature than for the pellet samples.

In vitro results using MG-63 results showed that aligned fibers favor higher β-phase content, which in turn improves MG-63 cell viability and proliferation. Modification of PVDF with nHA or AuNPs further enhances these effects, making such materials more suitable for bone tissue engineering applications [94]. Whereas, in vitro results using hiPSC-NSC showed that in aligned samples, higher directional differentiation of neuronal cells can be observed. This is due to that aligned fibers better support the formation of neuronal networks and axonal growth compared to random scaffolds [95].

The piezoelectric composites demonstrated a high degree of adaptability in their fiber orientation (random vs. aligned), offering flexibility in their applications. Randomly oriented fibers may better mimic the structural complexity of a natural bone matrix, while aligned fibers are particularly suited for guiding nerve regeneration, highlighting the material's multifunctionality.

The conducted studies on piezoelectric nanofibrous composites with nHA and AuNPs confirmed the value of these innovative composites as promising candidates for advancing tissue engineering solutions, particularly in challenging regenerative contexts like bone and nervous system repair.

Supplementary Materials: The following supporting information can be downloaded at: https://www.mdpi.com/article/10.3390/molecules30051041/s1, Figure S1: DSC deconvolution; Figure S2: WAXS deconvolution.

Author Contributions: Conceptualization, A.Z., A.G. and P.Ł.S.; methodology, A.Z., A.G., M.Z., P.D. and D.K.; validation, A.Z., A.G. and P.Ł.S.; formal analysis, A.Z., A.G. and P.Ł.S.; investigation, A.Z., A.G., M.Z., P.D. and D.K.; resources, A.Z., A.G. and P.Ł.S.; data curation, A.Z., A.G. and P.Ł.S.; writing—original draft preparation, A.Z., A.G., M.Z., P.D. and D.K.; writing—review and editing, A.Z., A.G. and P.Ł.S.; visualization, A.Z., A.G. and P.Ł.S.; supervision, A.G., P.Ł.S. and D.K.; project administration, A.Z.; funding acquisition, P.Ł.S. All authors have read and agreed to the published version of the manuscript.

Funding: This research received no external funding.

Institutional Review Board Statement: Not applicable.

Informed Consent Statement: Not applicable.

Data Availability Statement: Raw data will be made available by the corresponding author upon reasonable request.

Acknowledgments: A.Z. would like to acknowledge Nano Flow Company (Belgium) for providing research materials (gold nanoparticles, AuNPs) and Statutory Found IFTR PAS. M.Z. would like to acknowledge Statutory Found to MMRI PAS (in vitro tests on hiPSC-NSC).

Conflicts of Interest: The authors declare no conflicts of interest.

References

1. Zaszczynska, A.; Sajkiewicz, P.; Gradys, A. Piezoelectric Scaffolds as Smart Materials for Neural Tissue Engineering. *Polymers* **2020**, *12*, 161. [CrossRef] [PubMed]
2. Zaszczyńska, A.; Zabielski, K.; Gradys, A.; Kowalczyk, T.; Sajkiewicz, P. Piezoelectric Scaffolds as Smart Materials for Bone Tissue Engineering. *Polymers* **2024**, *16*, 2797. [CrossRef]
3. Yu, S.; Tai, Y.; Milam-Guerrero, J.; Nam, J.; Myung, N.V. Electrospun Organic Piezoelectric Nanofibers and Their Energy and Bio Applications. *Nano Energy* **2022**, *97*, 107174. [CrossRef]
4. Li, S.; Dan, X.; Chen, H.; Li, T.; Liu, B.; Ju, Y.; Li, Y.; Lei, L.; Fan, X. Developing Fibrin-Based Biomaterials/Scaffolds in Tissue Engineering. *Bioact. Mater.* **2024**, *40*, 597–623. [CrossRef]
5. Percival, K.M.; Paul, V.; Husseini, G.A. Recent Advancements in Bone Tissue Engineering: Integrating Smart Scaffold Technologies and Bio-Responsive Systems for Enhanced Regeneration. *Int. J. Mol. Sci.* **2024**, *25*, 6012. [CrossRef] [PubMed]
6. Motamedi, A.S.; Mirzadeh, H.; Hajiesmaeilbaigi, F.; Bagheri-Khoulenjani, S.; Shokrgozar, M.A. Piezoelectric Electrospun Nanocomposite Comprising Au NPs/PVDF for Nerve Tissue Engineering. *J. Biomed. Mater. Res* **2017**, *105*, 1984–1993. [CrossRef]
7. Ali, M.; Bathaei, M.J.; Istif, E.; Karimi, S.N.H.; Beker, L. Biodegradable Piezoelectric Polymers: Recent Advancements in Materials and Applications. *Adv. Healthc. Mater.* **2023**, *12*, 2300318. [CrossRef]
8. Kalimuldina, G.; Turdakyn, N.; Abay, I.; Medeubayev, A.; Nurpeissova, A.; Adair, D.; Bakenov, Z. A Review of Piezoelectric PVDF Film by Electrospinning and Its Applications. *Sensors* **2020**, *20*, 5214. [CrossRef]
9. Mohammadi, B.; Yousefi, A.A.; Bellah, S.M. Effect of Tensile Strain Rate and Elongation on Crystalline Structure and Piezoelectric Properties of PVDF Thin Films. *Polym. Test.* **2007**, *26*, 42–50. [CrossRef]
10. Kabir, E.; Khatun, M.; Nasrin, L.; Raihan, M.J.; Rahman, M. Pure β-Phase Formation in Polyvinylidene Fluoride (PVDF)-Carbon Nanotube Composites. *J. Phys. D Appl. Phys.* **2017**, *50*, 163002. [CrossRef]
11. Mokhtari, F.; Latifi, M.; Shamshirsaz, M. Electrospinning/Electrospray of Polyvinylidene Fluoride (PVDF): Piezoelectric Nanofibers. *J. Text. Inst.* **2016**, *107*, 1037–1055. [CrossRef]
12. Khonina, S.N.; Voronkov, G.S.; Grakhova, E.P.; Kazanskiy, N.L.; Kutluyarov, R.V.; Butt, M.A. Polymer Waveguide-Based Optical Sensors—Interest in Bio, Gas, Temperature, and Mechanical Sensing Applications. *Coatings* **2023**, *13*, 549. [CrossRef]
13. Mohammadpourfazeli, S.; Arash, S.; Ansari, A.; Yang, S.; Mallick, K.; Bagherzadeh, R. Future Prospects and Recent Developments of Polyvinylidene Fluoride (PVDF) Piezoelectric Polymer; Fabrication Methods, Structure, and Electro-Mechanical Properties. *RSC Adv.* **2023**, *13*, 370–387. [CrossRef] [PubMed]
14. Zaszczyńska, A.; Niemczyk-Soczynska, B.; Sajkiewicz, P. A Comprehensive Review of Electrospun Fibers, 3D-Printed Scaffolds, and Hydrogels for Cancer Therapies. *Polymers* **2022**, *14*, 5278. [CrossRef] [PubMed]
15. Andrey, V.; Koshevaya, E.; Mstislav, M.; Parfait, K. Piezoelectric PVDF and Its Copolymers in Biomedicine: Innovations and Applications. *Biomater. Sci.* **2024**, *12*, 5164–5185. [CrossRef]
16. Hazarika, G.; Jadhav, S.V.; Ingole, P.G. Exploring the Potential of Polymeric Membranes in Cutting-Edge Chemical and Biomedical Applications: A Review. *Mater. Today Commun.* **2024**, *39*, 109022. [CrossRef]

17. Deshmukh, S.; Kathiresan, M.; Kulandainathan, M.A. A Review on Biopolymer-Derived Electrospun Nanofibers for Biomedical and Antiviral Applications. *Biomater. Sci.* **2022**, *10*, 4424–4442. [CrossRef]
18. Zhang, Y.-Q.; Geng, Q.; Li, C.; Wang, H.-C.; Ren, C.; Zhang, Y.-F.; Bai, J.-S.; Pan, H.-B.; Cui, X.; Yao, M.-X.; et al. Application of Piezoelectric Materials in the Field of Bone: A Bibliometric Analysis. *Front. Bioeng. Biotechnol.* **2023**, *11*, 1210637. [CrossRef]
19. Nain, A.; Chakraborty, S.; Barman, S.R.; Gavit, P.; Indrakumar, S.; Agrawal, A.; Lin, Z.-H.; Chatterjee, K. Progress in the Development of Piezoelectric Biomaterials for Tissue Remodeling. *Biomaterials* **2024**, *307*, 122528. [CrossRef]
20. Das, K.K.; Basu, B.; Maiti, P.; Dubey, A.K. Interplay of Piezoelectricity and Electrical Stimulation in Tissue Engineering and Regenerative Medicine. *Appl. Mater. Today* **2024**, *39*, 102332. [CrossRef]
21. Domingues, J.M.; Miranda, C.S.; Homem, N.C.; Felgueiras, H.P.; Antunes, J.C. Nanoparticle Synthesis and Their Integration into Polymer-Based Fibers for Biomedical Applications. *Biomedicines* **2023**, *11*, 1862. [CrossRef] [PubMed]
22. Shlapakova, L.E.; Surmeneva, M.A.; Kholkin, A.L.; Surmenev, R.A. Revealing an Important Role of Piezoelectric Polymers in Nervous-Tissue Regeneration: A Review. *Mater. Today Bio* **2024**, *25*, 100950. [CrossRef]
23. Tandon, B.; Blaker, J.J.; Cartmell, S.H. Piezoelectric Materials as Stimulatory Biomedical Materials and Scaffolds for Bone Repair. *Acta Biomater.* **2018**, *73*, 1–20. [CrossRef] [PubMed]
24. Li, J.; Yin, J.; Wee, M.G.V.; Chinnappan, A.; Ramakrishna, S. A Self-Powered Piezoelectric Nanofibrous Membrane as Wearable Tactile Sensor for Human Body Motion Monitoring and Recognition. *Adv. Fiber Mater.* **2023**, *5*, 1417–1430. [CrossRef]
25. Ribeiro, T.P.; Flores, M.; Madureira, S.; Zanotto, F.; Monteiro, F.J.; Laranjeira, M.S. Magnetic Bone Tissue Engineering: Reviewing the Effects of Magnetic Stimulation on Bone Regeneration and Angiogenesis. *Pharmaceutics* **2023**, *15*, 1045. [CrossRef]
26. Yang, X.; Li, Y.; He, W.; Huang, Q.; Zhang, R.; Feng, Q. Hydroxyapatite/Collagen Coating on PLGA Electrospun Fibers for Osteogenic Differentiation of Bone Marrow Mesenchymal Stem Cells. *J. Biomed. Mater. Res.* **2018**, *106*, 2863–2870. [CrossRef]
27. Akbari, N.; Khorshidi, S.; Karkhaneh, A. Effect of Piezoelectricity of Nanocomposite Electrospun Scaffold on Cell Behavior in Bone Tissue Engineering. *Iran. Polym. J.* **2022**, *31*, 919–930. [CrossRef]
28. Fu, S.; Zhao, X.; Yang, L.; Qin, G.; Zhang, E. A Novel Ti-Au Alloy with Strong Antibacterial Properties and Excellent Biocompatibility for Biomedical Application. *Biomater. Adv.* **2022**, *133*, 112653. [CrossRef] [PubMed]
29. Pisarenko, T.; Papež, N.; Sobola, D.; Ţălu, Ş.; Částková, K.; Škarvada, P.; Macků, R.; Ščasnovič, E.; Kaštyl, J. Comprehensive Characterization of PVDF Nanofibers at Macro- and Nanolevel. *Polymers* **2022**, *14*, 593. [CrossRef] [PubMed]
30. Chen, C.; Bai, Z.; Cao, Y.; Dong, M.; Jiang, K.; Zhou, Y.; Tao, Y.; Gu, S.; Xu, J.; Yin, X.; et al. Enhanced Piezoelectric Performance of BiCl3/PVDF Nanofibers-Based Nanogenerators. *Compos. Sci. Technol.* **2020**, *192*, 108100. [CrossRef]
31. Edwards, M.D.; Mitchell, G.R.; Mohan, S.D.; Olley, R.H. Development of Orientation during Electrospinning of Fibres of Poly(ε-Caprolactone). *Eur. Polym. J.* **2010**, *46*, 1175–1183. [CrossRef]
32. Kiselev, P.; Rosell-Llompart, J. Highly Aligned Electrospun Nanofibers by Elimination of the Whipping Motion. *J. Appl. Polym. Sci.* **2012**, *125*, 2433–2441. [CrossRef]
33. Duta, L.; Grumezescu, V. The Effect of Doping on the Electrical and Dielectric Properties of Hydroxyapatite for Medical Applications: From Powders to Thin Films. *Materials* **2024**, *17*, 640. [CrossRef]
34. Mokhtari, F.; Azimi, B.; Salehi, M.; Hashemikia, S.; Danti, S. Recent Advances of Polymer-Based Piezoelectric Composites for Biomedical Applications. *J. Mech. Behav. Biomed. Mater.* **2021**, *122*, 104669. [CrossRef]
35. Lopresti, F.; Carfì Pavia, F.; Vitrano, I.; Kersaudy-Kerhoas, M.; Brucato, V.; La Carrubba, V. Effect of Hydroxyapatite Concentration and Size on Morpho-Mechanical Properties of PLA-Based Randomly Oriented and Aligned Electrospun Nanofibrous Mats. *J. Mech. Behav. Biomed. Mater.* **2020**, *101*, 103449. [CrossRef]
36. Li, Y.; Liao, C.; Tjong, S.C. Electrospun Polyvinylidene Fluoride-Based Fibrous Scaffolds with Piezoelectric Characteristics for Bone and Neural Tissue Engineering. *Nanomaterials* **2019**, *9*, 952. [CrossRef] [PubMed]
37. Kołbuk, D.; Ciechomska, M.; Jeznach, O.; Sajkiewicz, P. Effect of Crystallinity and Related Surface Properties on Gene Expression of Primary Fibroblasts. *RSC Adv.* **2022**, *12*, 4016–4028. [CrossRef]
38. Prasad, G.; Liang, J.-W.; Zhao, W.; Yao, Y.; Tao, T.; Liang, B.; Lu, S.-G. Enhancement of Solvent Uptake in Porous PVDF Nanofibers Derived by a Water-Mediated Electrospinning Technique. *J. Mater.* **2021**, *7*, 244–253. [CrossRef]
39. Saxena, P.; Shukla, P. A Comprehensive Review on Fundamental Properties and Applications of Poly(Vinylidene Fluoride) (PVDF). *Adv. Compos. Hybrid Mater.* **2021**, *4*, 8–26. [CrossRef]
40. Khan, M.U.A.; Aslam, M.A.; Bin Abdullah, M.F.; Hasan, A.; Shah, S.A.; Stojanović, G.M. Recent Perspective of Polymeric Biomaterial in Tissue Engineering—A Review. *Mater. Today Chem.* **2023**, *34*, 101818. [CrossRef]
41. EL-Ghoul, Y.; Alminderej, F.M.; Alsubaie, F.M.; Alrasheed, R.; Almousa, N.H. Recent Advances in Functional Polymer Materials for Energy, Water, and Biomedical Applications: A Review. *Polymers* **2021**, *13*, 4327. [CrossRef]
42. Rudawska, A.; Jacniacka, E. Analysis for Determining Surface Free Energy Uncertainty by the Owen–Wendt Method. *Int. J. Adhes. Adhes.* **2009**, *29*, 451–457. [CrossRef]

43. Kolbuk, D.; Guimond-Lischer, S.; Sajkiewicz, P.; Maniura-Weber, K.; Fortunato, G. The Effect of Selected Electrospinning Parameters on Molecular Structure of Polycaprolactone Nanofibers. *Int. J. Polym. Mater. Polym. Biomater.* **2015**, *64*, 365–377. [CrossRef]
44. Zaszczyńska, A.; Kołbuk, D.; Gradys, A.; Sajkiewicz, P. Development of Poly(Methyl Methacrylate)/Nano-Hydroxyapatite (PMMA/nHA) Nanofibers for Tissue Engineering Regeneration Using an Electrospinning Technique. *Polymers* **2024**, *16*, 531. [CrossRef]
45. Vijayendran, B.R. Polymer Polarity and Surfactant Adsorption. *J. Appl. Polym. Sci.* **1979**, *23*, 733–742. [CrossRef]
46. Nasker, P.; Samanta, A.; Rudra, S.; Sinha, A.; Mukhopadhyay, A.K.; Das, M. Effect of Fluorine Substitution on Sintering Behaviour, Mechanical and Bioactivity of Hydroxyapatite. *J. Mech. Behav. Biomed. Mater.* **2019**, *95*, 136–142. [CrossRef] [PubMed]
47. Ribeiro, C.; Panadero, J.A.; Sencadas, V.; Lanceros-Méndez, S.; Tamaño, M.N.; Moratal, D.; Salmerón-Sánchez, M.; Gómez Ribelles, J.L. Fibronectin Adsorption and Cell Response on Electroactive Poly(Vinylidene Fluoride) Films. *Biomed. Mater.* **2012**, *7*, 035004. [CrossRef] [PubMed]
48. Buitrago-Vásquez, M.; Ossa-Orozco, C.P. Degradation, Water Uptake, Injectability and Mechanical Strength of Injectable Bone Substitutes Composed of Silk Fibroin and Hydroxyapatite Nanorods. *Rev. Fac. Ing.* **2018**, *27*, 49–60. [CrossRef]
49. Bhat, S.; Uthappa, U.T.; Altalhi, T.; Jung, H.-Y.; Kurkuri, M.D. Functionalized Porous Hydroxyapatite Scaffolds for Tissue Engineering Applications: A Focused Review. *ACS Biomater. Sci. Eng.* **2022**, *8*, 4039–4076. [CrossRef] [PubMed]
50. Gupta, A.; Singh, S. Multimodal Potentials of Gold Nanoparticles for Bone Tissue Engineering and Regenerative Medicine: Avenues and Prospects. *Small* **2022**, *18*, 2201462. [CrossRef] [PubMed]
51. Dreanca, A.; Muresan-Pop, M.; Taulescu, M.; Tóth, Z.-R.; Bogdan, S.; Pestean, C.; Oren, S.; Toma, C.; Popescu, A.; Páll, E.; et al. Bioactive Glass-Biopolymers-gold Nanoparticle Based Composites for Tissue Engineering Applications. *Mater. Sci. Eng. C* **2021**, *123*, 112006. [CrossRef] [PubMed]
52. Wang, S.; Tong, W.; Li, Y.; Zhang, P.; Liu, Y.; Chen, Y.; Zhang, Y. Contributions of Piezoelectricity and Triboelectricity to a Hydroxyapatite/PVDF–HFP Fiber-Film Nanogenerator. *Nano Energy* **2023**, *105*, 108026. [CrossRef]
53. Cai, X.; Lei, T.; Sun, D.; Lin, L. A Critical Analysis of the α, β and γ Phases in Poly(Vinylidene Fluoride) Using FTIR. *RSC Adv.* **2017**, *7*, 15382–15389. [CrossRef]
54. Shaikh, S.F.; Jadhav, B.V.; Patil, R.P. Photocatalytic Activity of Zn-CO-Ferrite Nanoparticle Synthesized Using Lemon as Green Binding Agent by SOL-GEL Method. *Indo Am. J. Pharm. Sci.* **2018**, *5*, S89–S93.
55. Barnawi, N.; Allehyani, S.; Seoudi, R. Biosynthesis and Characterization of Gold Nanoparticles and Its Application in Eliminating Nickel from Water. *J. Mater. Res. Technol.* **2022**, *17*, 537–545. [CrossRef]
56. Gurunathan, S.; Han, J.; Park, J.H.; Kim, J.-H. A Green Chemistry Approach for Synthesizing Biocompatible Gold Nanoparticles. *Nanoscale Res. Lett.* **2014**, *9*, 248. [CrossRef] [PubMed]
57. Liu, Y.; Lu, J. Research Trends of Piezoelectric Biomaterials in Osteochondral Tissue Engineering. *Mater. Today Commun.* **2024**, *41*, 110264. [CrossRef]
58. Magdy, G.; Hassanin, A.H.; Kandas, I.; Shehata, N. PVDF Nanostructures Characterizations and Techniques for Enhanced Piezoelectric Response: A Review. *Mater. Chem. Phys.* **2024**, *325*, 129760. [CrossRef]
59. Kushwah, M.; Sagar, R.; Rogachev, A.A.; Gaur, M.S. Dielectric, Pyroelectric and Polarization Behavior of Polyvinylidene Fluoride (PVDF)—Gold Nanoparticles (AuNPs) Nanocomposites. *Vacuum* **2019**, *166*, 298–306. [CrossRef]
60. Kaspar, P.; Sobola, D.; Částková, K.; Dallaev, R.; Šťastná, E.; Sedlák, P.; Knápek, A.; Trčka, T.; Holcman, V. Case Study of Polyvinylidene Fluoride Doping by Carbon Nanotubes. *Materials* **2021**, *14*, 1428. [CrossRef]
61. Meesaragandla, B.; García, I.; Biedenweg, D.; Toro-Mendoza, J.; Coluzza, I.; Liz-Marzán, L.M.; Delcea, M. H-Bonding-Mediated Binding and Charge Reorganization of Proteins on Gold Nanoparticles. *Phys. Chem. Chem. Phys.* **2020**, *22*, 4490–4500. [CrossRef] [PubMed]
62. Zaszczyńska, A.; Gradys, A.; Ziemiecka, A.; Szewczyk, P.K.; Tymkiewicz, R.; Lewandowska-Szumieł, M.; Stachewicz, U.; Sajkiewicz, P.Ł. Enhanced Electroactive Phases of Poly(Vinylidene Fluoride) Fibers for Tissue Engineering Applications. *Int. J. Mol. Sci.* **2024**, *25*, 4980. [CrossRef] [PubMed]
63. Islam, A.; Khan, A.N.; Shakir, M.F.; Islam, K. Strengthening of β Polymorph in PVDF/FLG and PVDF/GO Nanocomposites. *Mater. Res. Express* **2020**, *7*, 015017. [CrossRef]
64. Martins, P.; Lopes, A.C.; Lanceros-Mendez, S. Electroactive Phases of Poly(Vinylidene Fluoride): Determination, Processing and Applications. *Prog. Polym. Sci.* **2014**, *39*, 683–706. [CrossRef]
65. Isaac, B.; Taylor, R.M.; Reifsnider, K. Mechanical and Dielectric Properties of Aligned Electrospun Fibers. *Fibers* **2021**, *9*, 4. [CrossRef]
66. Leon-Valdivieso, C.Y.; Garcia-Garcia, A.; Legallais, C.; Bedoui, F. Electrospinning of Biomedically Relevant Multi-Region Scaffolds: From Honeycomb to Randomly-Oriented Microstructure. *Polymer* **2020**, *202*, 122606. [CrossRef]

67. Nunes-Pereira, J.; Ribeiro, S.; Ribeiro, C.; Gombek, C.J.; Gama, F.M.; Gomes, A.C.; Patterson, D.A.; Lanceros-Méndez, S. Poly(Vinylidene Fluoride) and Copolymers as Porous Membranes for Tissue Engineering Applications. *Polym. Test.* **2015**, *44*, 234–241. [CrossRef]
68. Davis, G.T.; McKinney, J.E.; Broadhurst, M.G.; Roth, S.C. Electric-Field-Induced Phase Changes in Poly(Vinylidene Fluoride). *J. Appl. Phys.* **1978**, *49*, 4998–5002. [CrossRef]
69. Gradys, A.; Sajkiewicz, P. Determination of the Melting Enthalpy of β Phase of Poly(Vinylidene Fluoride). *e-Polymers* **2013**, *2013*, 203–216. [CrossRef]
70. Neidhöfer, M.; Beaume, F.; Ibos, L.; Bernès, A.; Lacabanne, C. Structural Evolution of PVDF During Storage or Annealing. *Polymer* **2004**, *45*, 1679–1688. [CrossRef]
71. Gregorio, R. Determination of the α, β, and γ Crystalline Phases of Poly(Vinylidene Fluoride) Films Prepared at Different Conditions. *J. Appl. Polym. Sci* **2006**, *100*, 3272–3279. [CrossRef]
72. Nakagawa, K.; Ishida, Y. Annealing Effects in Poly(Vinylidene Fluoride) as Revealed by Specific Volume Measurements, Differential Scanning Calorimetry, and Electron Microscopy. *J. Polym. Sci. Polym. Phys. Ed.* **1973**, *11*, 2153–2171. [CrossRef]
73. Purushothaman, S.M.; Tronco, M.F.; Ponçot, M.; Chitralekha, C.S.; Guigo, N.; Malfois, M.; Kalarikkal, N.; Thomas, S.; Royaud, I.; Rouxel, D. Quantifying the Crystalline Polymorphism in PVDF: Comparative Criteria Using DSC, WAXS, FT-IR, and Raman Spectroscopy. *ACS Appl. Polym. Mater.* **2024**, *6*, 8291–8305. [CrossRef]
74. Enayati, M.S.; Behzad, T.; Sajkiewicz, P.; Bagheri, R.; Ghasemi-Mobarakeh, L.; Łojkowski, W.; Pahlevanneshan, Z.; Ahmadi, M. Crystallinity Study of Electrospun Poly (Vinyl Alcohol) Nanofibers: Effect of Electrospinning, Filler Incorporation, and Heat Treatment. *Iran. Polym. J.* **2016**, *25*, 647–659. [CrossRef]
75. Arinstein, A.; Zussman, E. Electrospun Polymer Nanofibers: Mechanical and Thermodynamic Perspectives. *J. Polym. Sci. B Polym. Phys.* **2011**, *49*, 691–707. [CrossRef]
76. Kitsara, M.; Blanquer, A.; Murillo, G.; Humblot, V.; De Bragança Vieira, S.; Nogués, C.; Ibáñez, E.; Esteve, J.; Barrios, L. Permanently Hydrophilic, Piezoelectric PVDF Nanofibrous Scaffolds Promoting Unaided Electromechanical Stimulation on Osteoblasts. *Nanoscale* **2019**, *11*, 8906–8917. [CrossRef] [PubMed]
77. *ISO 10993-5:2009*; Biological Evaluation of Medical Devices—Part 5: Tests for In Vitro Cytotoxicity. International Organization for Standardization: Geneva, Switzerland, 2009. Available online: https://www.iso.org/standard/36406.html (accessed on 18 February 2025).
78. Braga, F.J.C.; Rogero, S.O.; Couto, A.A.; Marques, R.F.C.; Ribeiro, A.A.; Campos, J.S.D.C. Characterization of PVDF/HAP Composites for Medical Applications. *Mater. Res.* **2007**, *10*, 247–251. [CrossRef]
79. Zhang, X.; Lang, W.-Z.; Xu, H.-P.; Yan, X.; Guo, Y.-J. The Effects of Hydroxyapatite Nano Whiskers and Its Synergism with Polyvinylpyrrolidone on Poly(Vinylidene Fluoride) Hollow Fiber Ultrafiltration Membranes. *RSC Adv.* **2015**, *5*, 21532–21543. [CrossRef]
80. Costa, R.; Ribeiro, C.; Lopes, A.C.; Martins, P.; Sencadas, V.; Soares, R.; Lanceros-Mendez, S. Osteoblast, Fibroblast and In Vivo Biological Response to Poly(Vinylidene Fluoride) Based Composite Materials. *J. Mater. Sci. Mater. Med.* **2013**, *24*, 395–403. [CrossRef] [PubMed]
81. Kołbuk, D.; Guimond-Lischer, S.; Sajkiewicz, P.; Maniura-Weber, K.; Fortunato, G. Morphology and Surface Chemistry of Bicomponent Scaffolds in Terms of Mesenchymal Stromal Cell Viability. *J. Bioact. Compat. Polym.* **2016**, *31*, 423–436. [CrossRef]
82. Zaszczyńska, A.; Gradys, A.; Kołbuk, D.; Zabielski, K.; Szewczyk, P.K.; Stachewicz, U.; Sajkiewicz, P. Poly(L-Lactide)/Nano-Hydroxyapatite Piezoelectric Scaffolds for Tissue Engineering. *Micron* **2025**, *188*, 103743. [CrossRef]
83. Mousa, N.; El-Hosainy, H.; Shoueir, K.; El-Kemary, M. Photoluminescence Sensing of Pb^{2+} Using Cellulose Acetate Nanofiber Decorated with Au Nanoparticles. *J. Alloys Compd.* **2023**, *931*, 167481. [CrossRef]
84. Zaszczyńska, A.; Sajkiewicz, P.Ł.; Gradys, A.; Tymkiewicz, R.; Urbanek, O.; Kołbuk, D. Influence of process-material conditions on the structure and biological properties of electrospun polyvinylidene fluoride fibers. *Bull. Pol. Acad. Sci. Tech. Sci.* **2020**, *68*, 627–633. [CrossRef]
85. Kołbuk, D.; Urbanek, O.; Denis, P.; Choińska, E. Sonochemical Coating as an Effective Method of Polymeric Nonwovens Functionalization. *J. Biomed. Mater. Res.* **2019**, *107*, 2447–2457. [CrossRef] [PubMed]
86. Ivars, J.; Labanieh, A.R.; Soulat, D. Effect of the Fibre Orientation Distribution on the Mechanical and Preforming Behaviour of Nonwoven Preform Made of Recycled Carbon Fibres. *Fibers* **2021**, *9*, 82. [CrossRef]
87. Shehata, N.; Elnabawy, E.; Abdelkader, M.; Hassanin, A.; Salah, M.; Nair, R.; Ahmad Bhat, S. Static-Aligned Piezoelectric Poly (Vinylidene Fluoride) Electrospun Nanofibers/MWCNT Composite Membrane: Facile Method. *Polymers* **2018**, *10*, 965. [CrossRef]
88. Kanak; Yogita; Singh, P.; Manori, A.; Kumar, A.; Chandra, R.; Raina, K.K.; Shukla, R.K.; Manori, S. Photocatalytic Degradation of Malachite Green Using PVDF Membranes Doped with Fe_3O_4 Nanoparticles: Role of Porosity and Surface Roughness. *Phys. Scr.* **2023**, *98*, 105953. [CrossRef]
89. Li, Y.; Li, R.K.Y.; Tjong, S.C. Fabrication and Properties of PVDF/Expanded Graphite Nanocomposites. *e-Polymers* **2009**, *9*, 019. [CrossRef]

90. ElBakry, H.A.; Ammar, M.M.; Moussa, T.A. Effect of Nanodiamonds Surface Deposition on Hydrophilicity, Bulk Degradation and In-Vitro Cell Adhesion of 3D-Printed Polycaprolactone Scaffolds for Bone Tissue Engineering. *Biomed. Mater.* **2024**, *19*, 055016. [CrossRef]
91. Kleintjens, L.A. *Integration of Fundamental Polymer Science and Technology*; Springer Science & Business Media: Berlin/Heidelberg, Germany, 2012; ISBN 978-94-009-4185-4.
92. Ghobeira, R.; Asadian, M.; Vercruysse, C.; Declercq, H.; De Geyter, N.; Morent, R. Wide-Ranging Diameter Scale of Random and Highly Aligned PCL Fibers Electrospun Using Controlled Working Parameters. *Polymer* **2018**, *157*, 19–31. [CrossRef]
93. Buzanska, L. The Collagen Scaffold Supports hiPSC-Derived NSC Growth and Restricts hiPSC. *Front. Biosci.* **2019**, *11*, 105–121. [CrossRef] [PubMed]
94. Kapat, K.; Shubhra, Q.T.H.; Zhou, M.; Leeuwenburgh, S. Piezoelectric Nano-Biomaterials for Biomedicine and Tissue Regeneration. *Adv. Funct. Mater.* **2020**, *30*, 1909045. [CrossRef]
95. Sirkkunan, D.; Pingguan-Murphy, B.; Muhamad, F. Directing Axonal Growth: A Review on the Fabrication of Fibrous Scaffolds That Promotes the Orientation of Axons. *Gels* **2021**, *8*, 25. [CrossRef]

OŚWIADCZENIA DOKTORANTA O UDZIALE W PUBLIKACJACH NAUKOWYCH

INSTYTUT PODSTAWOWYCH PROBLEMÓW TECHNIKI

POLSKIEJ AKADEMII NAUK

IPPT PAN

02-106 Warszawa, ul. A. Pawińskiego 5B, Fax (+48)22 8269815, Telefon centr. (+48)22 8261281, Dyrektor (+48)22 8268911
NIP:525 000 89 79 REGON: 326026 http://www.ippt.pan.pl

Oświadczenie doktoranta o udziale w publikacji naukowej

Niniejszym potwierdzam, że mój wkład w przygotowanie **publikacji nr 1**, tj. Zaszczynska, A.; Sajkiewicz, P.; Gradys, A. Piezoelectric Scaffolds as Smart Materials for Neural Tissue Engineering. *Polymers*, Vol.12, No.1, pp.161-1-25, **2020**, obejmował koncepcję, zgromadzenie i analizę danych obejmujących 270 pozycji literaturowych. Dodatkowo, odpowiedzialna byłam za napisanie artykułu naukowego w formie przeglądowym, wykonanie rysunków występujących w tekście, przygotowanie odpowiedzi dla recenzentów i wprowadzenie odpowiednich poprawek. Pełniłam funkcję autora korespondencyjnego.

Podpis doktorantki
Mgr inż. Angelika Zaszczyńska

Angelika Zaszczyńska

Podpis promotora
Prof. dr hab. inż. Paweł Ł. Sajkiewicz

Podpis współautorów:
- Dr inż. Arkadiusz Gradys

Arkadiusz Gradys

INSTYTUT PODSTAWOWYCH PROBLEMÓW TECHNIKI

POLSKIEJ AKADEMII NAUK

02-106 Warszawa, ul. A. Pawińskiego 5B, Fax (+48)22 8269815, Telefon centr. (+48)22 8261281, Dyrektor (+48)22 8268911
NIP:525 000 89 79 REGON: 326026 http://www.ippt.pan.pl

Oświadczenie doktoranta o udziale w publikacji naukowej

Niniejszym potwierdzam, że mój wkład w przygotowanie **publikacji nr** 2 tj. Zaszczyńska A., Zabielski K., Gradys A. D., Kowalczyk T., Sajkiewicz P. Ł., Piezoelectric Scaffolds as Smart Materials for Bone Tissue Engineering, *Polymers*, ISSN: 2073-4360, DOI: 10.3390/polym16192797, Vol.16, No.19, pp.2797-1-30, **2024**, obejmował koncepcję, zgromadzenie i analizę danych obejmujących 214 pozycji literaturowych. Dodatkowo, byłam współodpowiedzialna za napisanie artykułu naukowego w formie przeglądowym, wykonanie rysunków występujących w tekście, przygotowanie odpowiedzi dla recenzentów i wprowadzenie odpowiednich poprawek.

Podpis doktorantki
Mgr inż. Angelika Zaszczyńska

Angelika Zaszczyńska

Podpis promotora
Prof. dr hab. inż. Paweł Ł. Sajkiewicz

Podpisy współautorów:
- Dr inż. Arkadiusz Gradys
- Mgr inż. Konrad Zabielski
- Dr hab. inż. Tomasz Kowalczyk

INSTYTUT PODSTAWOWYCH PROBLEMÓW TECHNIKI

POLSKIEJ AKADEMII NAUK

02-106 Warszawa, ul. A. Pawińskiego 5B, Fax (+48)22 8269815, Telefon centr. (+48)22 8261281, Dyrektor (+48)22 8268911
NIP:525 000 89 79 REGON: 326026 http://www.ippt.pan.pl

Oświadczenie doktoranta o udziale w publikacji naukowej

Niniejszym potwierdzam, że mój wkład w przygotowanie **publikacji nr 3**, tj. Zaszczyńska A., Sajkiewicz P.Ł., Gradys A., Tymkiewicz R., Urbanek O., Kołbuk D., Influence of process-material conditions on the structure and biological properties of electrospun polyvinylidene fluoride fibers, *BULLETIN OF THE POLISH ACADEMY OF SCIENCES: TECHNICAL SCIENCES*, Vol.68, No.3, pp.627-633, **2020**, obejmował dyskusję i określenie koncepcji badań, wykonanie przeglądu literatury, wytworzenie za pomocą procesu elektroprzędzenia nanowłóknistych mat z poli(fluorku winylidenu) o różnym stężeniu i ułożeniu włókien, przeprowadzenie badań lepkości, przeprowadzenie badań morfologii próbek z użyciem skaningowej mikroskopii elektronowej (SEM), badanie próbek z użyciem metody spektoskopii ATR-FTIR i kalkulację zawartości faz piezoelektrycznych w próbkach, wykonanie obrazowania komórek metodą skaningowej mikroskopii elektronowej (SEM). Dodatkowo, brałam czynny udział w analizie i dyskusji wyników. Byłam odpowiedzialna za napisanie i redagowanie manukryptu, przygotowanie rysunków oraz wykresów występujących w tekście, przygotowanie odpowiedzi dla recenzentów i wprowadzenie odpowiednich poprawek do manuskryptu. Pełniłam funkcję autora korespondencyjnego.

Podpis doktorantki
Mgr inż. Angelika Zaszczyńska

Angelika Zaszczyńska

Podpis promotora
Prof. dr hab. inż. Paweł Ł. Sajkiewicz

Sajkiewicz

Podpis współautorów:
- Dr inż. Arkadiusz Gradys
- Ryszard Tymkiewicz
- Dr inż. Olga Urbanek-Świderska Olga Urbanek-Świderska
- Dr hab. inż. Dorota Kołbuk-Konieczny Dorota Kołbuk-Konieczny

INSTYTUT PODSTAWOWYCH PROBLEMÓW TECHNIKI

POLSKIEJ AKADEMII NAUK

IPPT PAN

02-106 Warszawa, ul. A. Pawińskiego 5B, Fax (+48)22 8269815, Telefon centr. (+48)22 8261281, Dyrektor (+48)22 8268911
NIP:525 000 89 79 REGON: 326026 http://www.ippt.pan.pl

Oświadczenie doktoranta o udziale w publikacji naukowej

Niniejszym potwierdzam, że mój wkład w przygotowanie **publikacji nr 4** tj. Zaszczyńska A., Gradys A.D., Ziemiecka A., Szewczyk P., Tymkiewicz R., Lewandowska-Szumieł M., Stachewicz U., Sajkiewicz P.Ł., Enhanced Electroactive Phases of Poly(vinylidene Fluoride) Fibers for Tissue Engineering Applications, *International Journal of Molecular Sciences*, Vol.25, No.9, pp.4980-1-25, **2024**, obejmował dyskusję i określenie koncepcji badań, wykonanie przeglądu literatury, wytworzenie za pomocą procesu elektroprzędzenia nanowłóknistych mat z poli(fluorku winylidenu) o małej i dużej masie cząsteczkowej i ułożeniu włókien, przeprowadzenie badań morfologii próbek z użyciem skaningowej mikroskopii elektronowej (SEM), wykonanie badań orientacji i porowatości włókien, badanie próbek z użyciem metody spektoskopii ATR-FTIR i kalkulację zawartości faz piezoelektrycznych w próbkach, wykonanie obrazowania ludzkich komórek macierzystych metodą skaningowej mikroskopii elektronowej (SEM). Wykonałam analizę statystyczną przeprowadzonych badań. Dodatkowo, brałam czynny udział w analizie i dyskusji wyników. Byłam odpowiedzialna za napisanie i redagowanie manukryptu, przygotowanie rysunków oraz wykresów występujących w tekście, przygotowanie odpowiedzi dla recenzentów i wprowadzenie odpowiednich poprawek do manuskryptu.

Podpis doktorantki
Mgr inż. Angelika Zaszczyńska
Angelika Zaszczyńska

Podpis promotora
Prof. dr hab. inż. Paweł Ł. Sajkiewicz

Podpisy współautorów:

- Dr inż. Arkadiusz Gradys
- Mgr inż. Anna Ziemiecka
- Dr inż. Piotr K. Szewczyk
- Ryszard Tymkiewicz
- Prof. dr hab. inż. Małgorzata Lewandowska-Szumieł
- Prof. dr hab. inż. Urszula Stachewicz

INSTYTUT PODSTAWOWYCH PROBLEMÓW TECHNIKI

POLSKIEJ AKADEMII NAUK

IPPT PAN

02-106 Warszawa, ul. A. Pawińskiego 5B, Fax (+48)22 8269815, Telefon centr. (+48)22 8261281, Dyrektor (+48)22 8268911
NIP:525 000 89 79 REGON: 326026 http://www.ippt.pan.pl

Oświadczenie doktoranta o udziale w publikacji naukowej

Niniejszym potwierdzam, że mój wkład w przygotowanie **publikacji nr 5** tj. Zaszczyńska A., Gradys A. D., Kołbuk-Konieczny D., Zabielski K., Szewczyk P., Stachewicz U., Sajkiewicz P. Ł., Poly(L-lactide)/nano-hydroxyapatite piezoelectric scaffolds for tissue engineering, *Micron*, ISSN: 0968-4328, DOI: 10.1016/j.micron.2024.103743, Vol.188, pp.103743-1-15, **2025**, obejmował dyskusję i określenie koncepcji badań, wykonanie przeglądu literatury, wytworzenie za pomocą procesu elektroprzędzenia nanowłóknistych mat z poli(L-laktydu) z dodatkiem nanohydroksyapatytu o różnym ułożeniu włókien, przeprowadzenie badań morfologii próbek z użyciem skaningowej mikroskopii elektronowej (SEM) i SEM-EDS, wykonanie badań orientacji i porowatości włókien, wykonanie badań zwilżalności próbek, wykonanie badań energii swobodnej próbek, wykonanie badań próbek z użyciem metody spektoskopii ATR-FTIR, przeprowadzenie pomiarów z wykorzystaniem skaningowej kalorymetrii różnicowej (DSC) i udział w ich analizie, uczestniczyłam w przeprowadzeniu badań szerokokątowego rozpraszania rentgenowskiego (WAXS) i brałam udział w ich analizie, uczestniczyłam w przeprowadzeniu badań komórkowych z linii osteoblastopodobnych komórek ludzkich MG-63 i brałam udział w ich analizie. Wykonałam analizę statystyczną przeprowadzonych badań. Dodatkowo, brałam czynny udział w analizie i dyskusji wyników. Byłam odpowiedzialna za napisanie i redagowanie manukryptu, przygotowanie rysunków oraz wykresów występujących w tekście, przygotowanie odpowiedzi dla recenzentów i wprowadzenie odpowiednich poprawek do manuskryptu.

Podpis doktorantki
Mgr inż. Angelika Zaszczyńska
Angelika Zaszczyńska

Podpis promotora
Prof. dr hab. inż. Paweł Ł. Sajkiewicz

Podpisy współautorów:

- Dr inż. Arkadiusz Gradys
- Mgr inż. Konrad Zabielski
- Dr hab. inż. Dorota Kołbuk-Konieczny
- Dr inż. Piotr K. Szewczyk
- Prof. dr hab. inż. Urszula Stachewicz

INSTYTUT PODSTAWOWYCH PROBLEMÓW TECHNIKI

POLSKIEJ AKADEMII NAUK

02-106 Warszawa, ul. A. Pawińskiego 5B, Fax (+48)22 8269815, Telefon centr. (+48)22 8261281, Dyrektor (+48)22 8268911
NIP:525 000 89 79 REGON: 326026 http://www.ippt.pan.pl

Oświadczenie doktoranta o udziale w publikacji naukowej

Niniejszym potwierdzam, że mój wkład w przygotowanie **publikacji nr 6** tj. Zaszczyńska, A., Zychowicz, M., Kołbuk, D., Denis, P.; Gradys, A.; Sajkiewicz, P.Ł. On the Structural and Biological Effects of Hydroxyapatite and Gold Nano-Scale Particles in Poly(Vinylidene Fluoride) Smart Scaffolds for Bone and Neural Tissue Engineering. *Molecules*, DOI: 10.3390/molecules30051041, 30, 1041, **2025**, obejmował dyskusję i określenie koncepcji badań, wykonanie przeglądu literatury, wytworzenie za pomocą procesu elektroprzędzenia nanowłóknistych mat z poli(fluorku winylidenu) o różnym ułożeniu włókien i ich ukierunkowaniu, przeprowadzenie badań morfologii próbek z użyciem skaningowej mikroskopii elektronowej (SEM), wykonanie badań orientacji i porowatości włókien, wykonanie badań zwilżalności próbek i energii swobodnej próbek, badanie próbek z użyciem metody spektoskopii ATR-FTIR i kalkulację zawartości faz piezoelektrycznych w próbkach, przeprowadzenie pomiarów z wykorzystaniem skaningowej kalorymetrii różnicowej (DSC) i udział w ich analizie, uczestniczyłam w przeprowadzeniu badań szerokokątowego rozpraszania rentgenowskiego (WAXS) i brałam udział w ich analizie, uczestniczyłam w przeprowadzeniu badań komórkowych z linii osteoblastopodobnych komórek ludzkich MG-63 i brałam udział w ich analizie. Dodatkowo, brałam czynny udział w analizie i dyskusji zebranych wyników. Byłam odpowiedzialna za napisanie i redagowanie manukryptu, przygotowanie rysunków oraz wykresów występujących w tekście, przygotowanie odpowiedzi dla recenzentów i wprowadzenie odpowiednich poprawek do manuskryptu.

Podpis doktorantki
Mgr inż. Angelika Zaszczyńska

Angelika Zaszczyńska

Podpis promotora
Prof. dr hab. inż. Paweł Ł. Sajkiewicz

Podpisy współautorów:

- Dr inż. Arkadiusz Gradys
- Dr hab. inż. Dorota Kołbuk-Konieczny Dorota Kołbuk-Konieczny
- Mgr inż. Piotr Denis Piotr Denis
- Dr n. med. Marzena Zychowicz Marzena Zychowicz